THE UNIVERSITY *of* EDINBURGH

Evaluating the geological, geomorphic and geophysical evidence for the re-location of Odysseus' homeland, "Ancient Ithaca"

Kirsten L. Hunter

A thesis submitted in fulfilment of the requirements
for the degree of Doctor of Philosophy
to the
University of Edinburgh
2013

Declaration

This thesis has been composed solely by myself. The work presented is my own unless otherwise specified and contributions have been acknowledged. The work has not been submitted for other degree or professional qualification

K. L. Hunter

Acknowledgements

Firstly and most importantly, great thanks to my supervisor Professor John Underhill for his dedicated support to the project and this thesis, being always on hand for useful geo-advice, confident-boosting comments and help.

Thank you to Robert Bittlestone, John Underhill and James Diggle for establishment of the Odysseus Unbound project.

The Seismic Possee, members past and present: Ryan, Rachel, Gustavo, Susannah, Nik Lykakis, Nick Roberts, Jaume, Marta. Extra thanks to Ryan Williams for his geological fieldwork expertise and Suzie for her driving during field-mapping.

At the University of Edinburgh: Roger Hipkin (for Fortran and the flat), the late John E. Dixon, Kathy Whaler, former undergraduate Susanna Ebmeier (for use of her final year dissertation regarding Gravmag), Chris Place (for IT). Thank you to the late Barry Dawson for encouragement. Further PhD funding was supplied by the Hayward Fund which supplies funding for Eastern Mediterranean geo-studies.

Thanks to Fugro (in particular Steve Poulter, Steve Thomson for release of additional funds, Dave Kilcoyne for technical support, Anthony, Eduard, Stewart, Ray, Greg Hodges) and their affiliates (Fugro Oceansismica, Fugro Airborne Surveys, Fugro Aperio (Rod Eddies), Fugro Robertson, Fugro Geotechnique) for kindly providing partial sponsorship for this PhD under the NERC (Natural Environment Research Council's Co-operative Awards in Science & Engineering) CASE scheme and provided technical support throughout course of the project and for underpinning finance for the geophysical methods deployed.

In Greece, the following provided support: Vasilis Rouhatas (for use of Hotel Palatino, emergency translator, local workers and support), Nelly Konstandaki, Maria (Greek Ministry of Archaeology), John Crawshaw (core photographs).

The project also benefited from the cooperation and support of the Institute of Geology and Mineral Exploration (IGME).

To my friends and family.

Contents

Abstract

The application of geological and geophysical methods on the Ionian Island of Kefalonia has provided a new-found basis by which to test the hypothesis that Ancient Ithaca, the home of Odysseus as described in Homer's epic the *Odyssey*, a subject which has perplexed academics for centuries. Although popular belief places Odysseus' homeland on Ithaki, a small mountainous island lying to the east of Kefalonia, its location does not fit Homer's descriptions of Ancient Ithaca since it is described as a "low-lying" island lying "furthest to the west" (facing dusk not dawn). Being land-locked and connected to the rest of Kefalonia by a narrow (6 km x 2 km) isthmus called the Thinia valley, the Paliki Peninsula of Western Kefalonia provides a better geographical fit. However, it has generally been dismissed as a candidate for Ancient Ithaca since it is not an island today and the topography of the connecting isthmus rises to a height of c. 200 m along the centre of the Thinia valley. Despite these obstacles and based on a quote by the ancient geographer Strabo made around 1 BC, Bittlestone et al. (2005) proposed that during the Mycenaean Era an ancient seaway ("Strabo's Channel") could have existed where Thinia stands today and the valley's present topography is due to landslide deposition which eventually closed the seaway.

This thesis presents the results of a 3-year geological, geomorphological and geophysical investigation of "Strabo's Channel". The investigation was carried out using a survey programme of complimentary non-invasive geophysical techniques calibrated by 17 shallow sedimentary cores and combined with surface geological mapping and geomorphological observations. In addition to a helicopter-mounted electromagnetic (HEM) survey acquired for Northern Paliki, gravity measurements were taken across the Thinia isthmus, and resistivity and seismic refraction surveys were carried out at strategic sites. Marine shallow seismic reflection surveys were also undertaken in the coastal areas adjacent to the isthmus to chart postglacial transgression into these shallow coastal areas and to reconstruct the paleo-geography of Northern Paliki since the Last Glacial Maximum (LGM) (c. 21 500 BP).

The survey area is sited in the Pre-Apulian isopic zone of the Hellenide thrust belt which represents a structurally-inverted passive continental margin subsequently affected by foreland contraction and overprinted by neotectonic (outer-arc) deformation resulting from African-Eurasian plate collision. The results showed that the geology and geomorphology of Thinia was far more complicated than originally believed. The bedrock geology records the Cretaceous-Quaternary evolution of an extensional-compressional regime brought about through the foreland-migration of the Hellenide fold-and-thrust deformation in the Early Miocene which reactivated earlier south-easterly-dipping extensional faults. The peninsula was affected by further Late Quaternary, Holocene and recent neotectonic deformation caused by the formation of the dextral Kefalonia Transform Fault (KTF) and slope failure resulting from the generation of steep slopes.

The shallow marine seismic reflection survey showed clear differentiation between the tectonised "pre-Holocene" and onlapping postglacial sediments separated by a prominent erosional surface associated with the LGM sea level lowstand of -120 m. The survey detected a buried drainage valley deeply-incised into the pre-Holocene of the Gulf of Argostoli indicating that a major glacial river drained from Thinia during this lowstand. During postglacial sea level rise this valley was infiltrated by marine waters to form a ria, flooding two large glacial lakes which acted as depocentres for postglacial sediments.

While the prevalence of slope collapse of the steep valley sides in Thinia favoured the idea that "Strabo's Channel" was infilled through repeated deposition of landslide debris, the presence of bedrock at the surface of Thinia ruled out the possibility that the present valley topography was built-up through Late Holocene deposition of landslide material between Kefalonia and Paliki. The onshore tests confirmed the presence of a thick deposit of steeply-dipping and tectonised marine sediments within the valley. Biostratigraphic analysis of core samples dated these as Early Miocene to Early Pleistocene (Gelasian) indicating marine waters existed along the valley until at least 1.80 million years ago, an order of magnitude younger than previously reported in the area. However, no new independent sediment younger

than Early Pleistocene was retrieved in the cores obtained for this study despite the findings of an earlier borehole which appeared to contain Late Quaternary and Holocene marine fauna (*Ehux*). The geophysical surveys and cores failed to detect the sides or bottom of a channel or evidence of substantial clastic debris within the proposed channel route thus ruling out the possibility that a buried marine-level channel which extended from "sea-to-sea" had existed during the Late Bronze Age.

One strategic area of investigation was the upland site of a suspected paleo-lake (Lake Katachori) which overlapped the proposed route of Strabo's Channel at ~170 m elevation. Although the presence of freshwater algae within the upper few metres confirmed a lacustrine environment, the geophysical and core evidence showed it was shallow (6 m thick) and was sited on steeply easterly-dipping Plio-Pleistocene sediments uplifted to ~170 m above sea level. The occurrence of freshwater algae admixed with uppermost Plio-Pleistocene sediments probably represents a basal reworked basal lag deposit thus, implying departure from marine depositional setting occurred in Thinia sometime after the Gelasian (1.80 Ma).

Coring at Livadi Marsh suggested that while the marsh was flooded during the Bronze Age to a depth of c. 1.2 m, making it a candidate for Ancient Ithaca's harbour, no significant coseismic uplift appears to have occurred since the Late Bronze Age. Current coastal position was due to progradation and aggradation of marsh sediments with no more than 1.2m of coseismic uplift.

The lack of Holocene-Late Quaternary sediment relating to an uplifted marine channel and the presence of Lake Katachori may tentatively be explained through the uplift and westwards translation of the sediments of central Thinia through establishment of a contractional-extensional linked gravity driven rotational slip linking the listric "Agia Ioanni Fault" with the Atheras Thrust. The boreholes detected shear-thrusting and steep dips within the Miocene and Plio-Pleistocene marl sediments demonstrating that the area experienced strong tectonic dislocation which is in favour of this model however further tests are required to investigate this and whether it could feasibly have occured in the required timescale.

CHAPTER 1: Background and Rationale

1.1 Introduction

The search for the ancient civilisations of the Greek world has been a long-held quest. Before the advent of reliable geoscientific methods, such investigations relied entirely upon what was written in historic literature. However, this often meant having to differentiate between what was fact and fiction. The development of geoarchaeology has allowed the investigation of these ancient sites using geo-scientific means. The convention Before Present (BP) will be used throughout unless otherwise stated. Because "present" time changes standard practise is to use 1950 as the arbitrary origin of the age scale.

1.1.1 Geoarchaeology: The Role of Geophysics and Other Geo-techniques in an 'Archaeological' Setting

Geoarchaeology is the scientific discipline in which an archaeological problem is investigated by means of geoscientific methods, using the past and present landscape and shallow subsurface of the Earth to make inferences about the past (Van Andel, 1994; Rapp and Hill, 1998; Pollard, 1999; Ghilardi and Desruelles, 2009). Its multi-disciplinary nature means it has a wide-range of techniques at its disposal and expertise can be drawn from many sources making it an incredibly versatile investigative tool. In particular, the crucial role played by near-surface, non-invasive geophysical surveys in the preliminary stages of a geoarchaeological investigation, especially when calibrated through direct sampling of the subsurface (e.g. shallow sedimentary coring), are becoming increasingly important with such surveys now considered standard tools within such a setting.

Sometimes included under the subheading of 'archaeological prospection', geophysical methods work by measuring variations of key physical properties (e.g.

density, resistivity, magnetic susceptibility) and characteristics of lithologies within the shallow Earth. Geophysical surveys are referred to as ‘non-invasive’ because they can be undertaken with minimal or no physical infiltration of the ground. A wide range of geophysical techniques have been developed to allow different qualities of the subsurface to be measured. The survey type chosen is dependent on the imaging target and the conditions in which that target sits. For example, detecting buried anthropogenic remains requires a survey type which images the very shallow subsurface (first few metres of depth) with high resolution (e.g. resistivity, ground penetrating radar (GPR)). If the ground is very wet, resistivity is better suited than GPR since this survey technique is a measure of pore fluid conductivity.

Geophysical surveys are attractive in a geoarchaeological investigation for several reasons. Their non-destructive nature minimises disturbance to the local environment which is useful on sites where intrusive investigations are not permissible. Surveys are fairly low-cost (running a survey usually only requires a few people) and can cover very large areas rapidly (e.g. airborne surveys). They can also help define with relative precision the optimal location for expensive ‘proof of concept’ archaeological excavations and intrusive tests. However, because geophysical surveys do not directly sample the subsurface, a wide range of results are possible for a single lithology which in turn may overlap with several different rock types. This leads to data non-uniqueness i.e. data from a single survey type cannot uniquely define an underlying geological feature or give definitive answers on rock types. This problem is mitigated by using a series of complementary geophysical tests rather than just a single approach which allows cross-referencing of results and also by providing all important and much needed ‘ground-truth’ of the geophysical data through direct sampling of the subsurface (e.g. shallow sedimentary coring), essential for aiding modelling of the data towards a unique solution.

1.1.2 Application to Ancient Greece

The history of geoarchaeology and Greece are deeply entwined since this country offers a diverse landscape, a coastline populated by ancient civilisations and a rich history being the meeting point between the cultures of Europe and Asia Minor (Figure 1.1) (Zangger, 2001). The list of historically significant Greek targets successfully investigated using geoarchaeological means, in particular those of which used non-invasive geophysical techniques as a primary method of investigation coupled with sedimentary coring, is becoming increasingly long and varied. These methods are particularly useful in the recreation of Holocene paleo-geographies and at sites where archaeological remains are scarce or absent.

A notable investigation by Jones et al. (2000) saw the deployment of geophysical techniques in the investigation of Xerxe's Canal. The site of this canal, reputedly built on orders by the Persian King Xerxes around 500 BC (Before Christ) to allow the Persian invasion fleet access to the Aegean, is located across a narrow 2 km long isthmus in Thessaloniki, north-eastern Greece. Little surface evidence for Xerxe's Canal was apparent at the time of investigation. The primary objective was to locate and map the marine-level canal within the isthmus now largely buried through siltation and slope collapse. There were also no striking archaeological remains associated with what must have been a dramatic feature which brought the investigation away from conventional archaeology into the field of geoscience. To tackle this problem a series of complementary non-invasive geophysical survey techniques were used (resistivity soundings, refraction seismic profiles and ground-penetrating radar) to successfully image the sides of the Canal. These techniques were coupled with a highly-detailed topographic survey and analysis of sedimentary cores to ascertain the fullest view of this buried feature (Figure 1.2).

Further examples show how these techniques and other geoarchaeological tests can be used in the reconstruction of Holocene shorelines. Vafidis et al. (2003) used a shallow seismic refraction survey and high resolution aerial photography to locate

and map the ancient port of Itanos in Crete while a complimentary resistivity survey was used to detect anthropogenic anomalies.

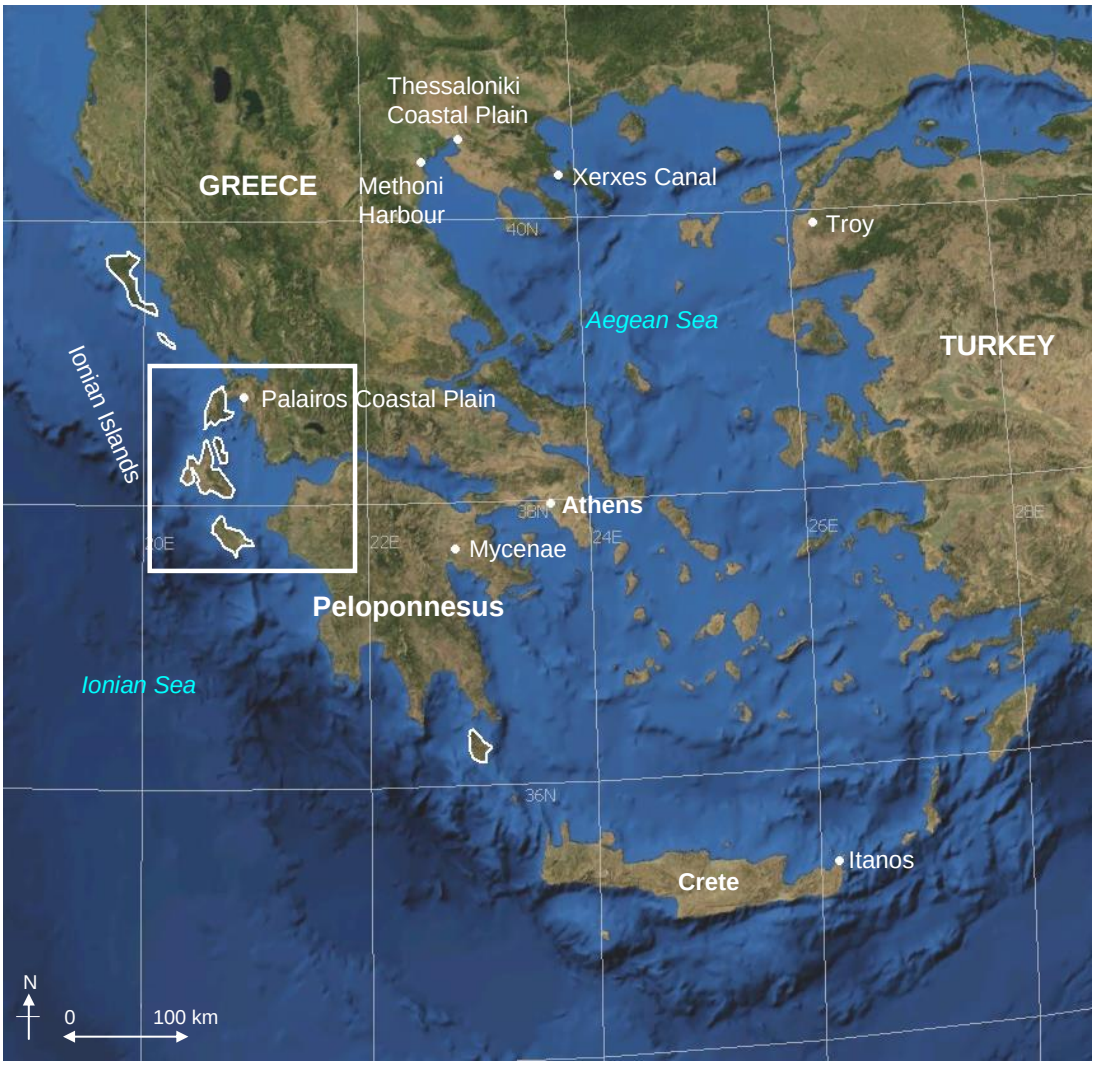

Figure 1.1 Map of Greece and the Aegean showing the locations of historically significant Mycenaean (Late Bronze Age) sites mentioned in the text which were investigated using geoarchaeological techniques. The Ionian Islands are outlined in white. The location of Figure 1.6 is indicated by the white box. Satellite image source: NASA World Wind.

Vött et al (2006) demonstrated that sediments sampled by shallow cores can serve as important geological achieves for Holocene sea-level change in near coastal environments as demonstrated during the reconstruction of the Palairos paleo-coastal plain in NW Greece. The investigation of the ancient harbour at Methoni used a selection of complimentary techniques which included digital elevation maps, bathymetric data and historical manuscripts (Kraft and Aschenbrenner, 1977;

Hatzopoulos, 1990; Ghilardi et al., 2007). Similar investigations by Ghilardi et al. (2007; 2008; 2008b) enabled the reconstruction of the coastal configuration of Thessaloniki Plain, over the last 6000 years.

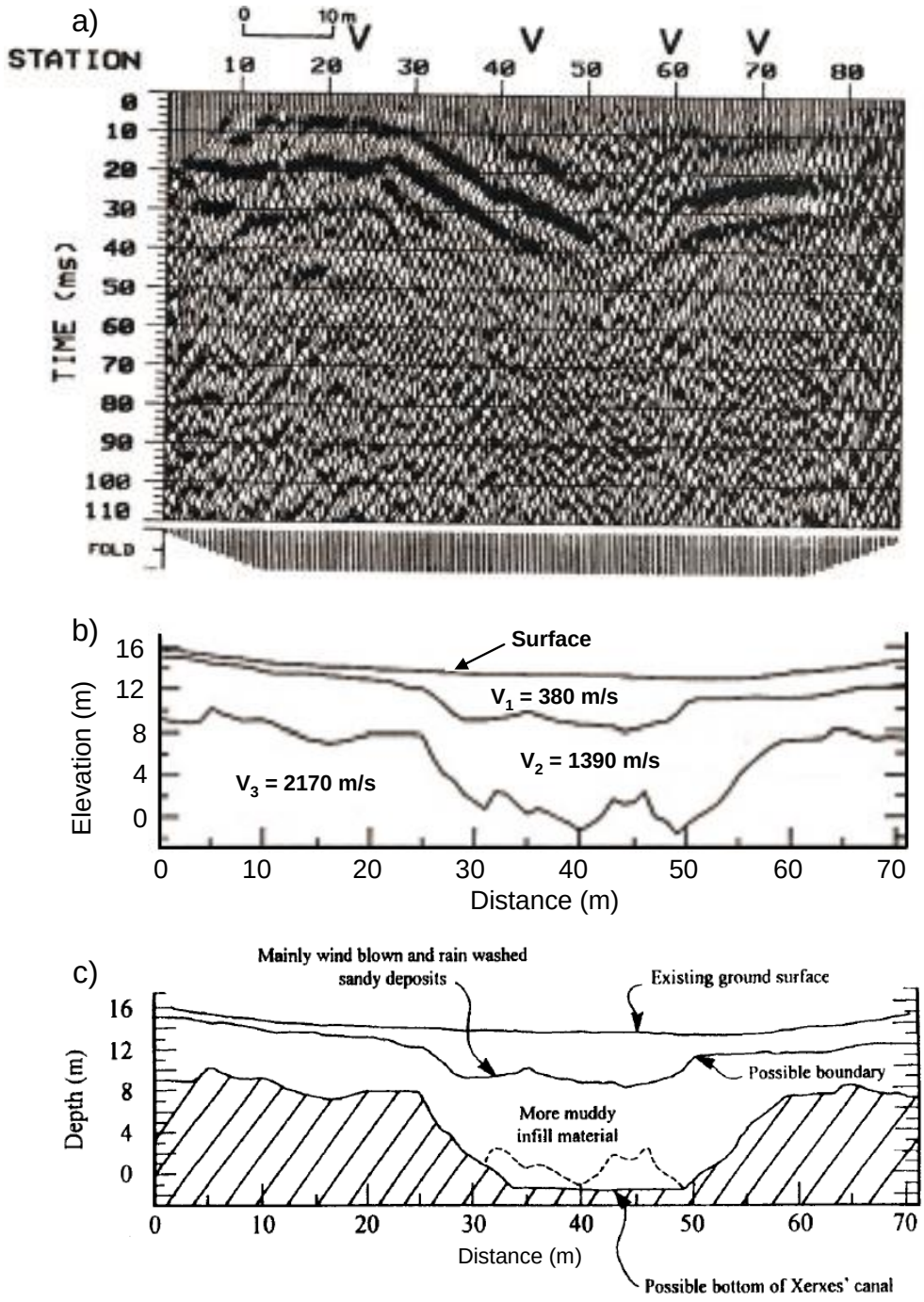

Figure 1.2 Results of the seismic investigation of the central sector of Xerxe's Canal: a) High resolution seismic reflection profile in wiggle trace format; b) High resolution seismic refraction profile following velocity analysis of same profile and representation of the Canal at this location based on the seismic data. From Jones et al. (2000).

1.1.3 The Late Bronze (Mycenaean) Age of Greece

The Bronze Age of Greece took place between 3000 BC and 1200 BC (4950 to 3150 BP) (Zangger, 2001). The *Odyssey* and *Iliad* are two of the oldest and most popular pieces of Western European literature, attributed to the poet Homer. The poems are set during the Mycenaean Golden Age of Greece which occurred in the Late Bronze Age and spanned between 1450 and 1100 BC (Zangger, 2001). The *Iliad* opens a few weeks before the end of the Trojan War (c. 3250 BP according to Luce (1998)). Troy is coming to the end of its ten-year siege at the hands of a coalition of Greek states led by King Agamemnon. The events of the *Odyssey* take place ten years after the siege of Troy (c. 3240 BP using the convention used by Luce (1998)). The poem recounts the exploits of King Odysseus during his ten-year journey from the battlefield back to his homeland of Ancient Ithaca and his subsequent successful retaking of his kingdom.

Because of their great historical significance the locations featured in the poems have become key archaeological targets over the centuries. Homer's detailed geographical descriptions of locations like Agamemnon's Palace at Mycenae and the battlefields of the Trojan plain strongly suggested they were based on real places. However, despite extensive searching, these locations remained elusive. In particular, the true location of Ancient Ithaca, the island home of King Odysseus of the "Cephalonians", is a subject which has caused debate and controversy amongst academics for centuries due to discrepancies between Homer's description of Ithaca and the possible locations available for this island.

The discrepancies between the Homeric text and actual geology of the Aegean and Ionian areas have typically been put down to Homer being unfamiliar with the locations he was depicting or that he was a poor geographer. This is an unfair accusation especially when other authors make efforts to get geography correct be they Shakespeare or Ian Rankin. The strong supernatural content of the poems have, in fact, led some to dismiss the events and places in the *Odyssey* and *Iliad* as entirely

fictitious until the discovery of a significant Late Bronze-aged settlement at Hissarlik in the 1870s believed to be the *Iliad's* city-under-siege, Troy.

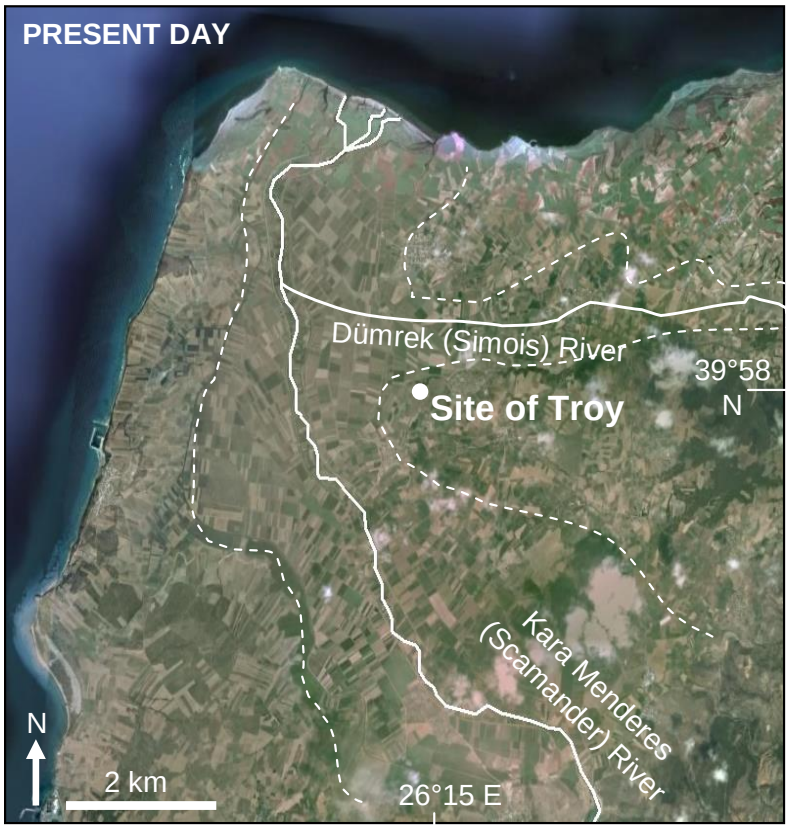

Figure 1.3 Satellite image of present-day north-western Turkey coast showing extensive flood-control and irrigation canals have within the Scamander and Simois River floodplains (dotted white lines). Satellite image source: Google Earth.

1.1.4 Schliemann's Troy

Troy was said to stand near a "high mound…which men call Thorn Hill [Batieia]" overlooking where the Trojan armies were emplaced "on the swelling of the [Trojan] plain" within sight of the Greek camp and ship station which "filled the long mouth of the shore [of Troia Bay] between the enclosing headlands". The Homeric text describes a battle which took place in front of Troy which involved crossing the "fair-flowing river Xanthos (Scamander). The Scamander (today the Kara Menderes) exists in north-western Turkey forming a broad flood plain however the present coastal configuration does not fit the Homeric description (Figure 1.3).

The ancient Greek geographer, Strabo, offered a possible solution to this problem. Believing that Homer was the "founder of geography" and harbouring a strong conviction that the locations in the *Iliad* and *Odyssey* were all based on real locations, Strabo attempted to resolve the descriptions of Homer's world in his work, *Geographica*. *Geographica* is a 17-volume encyclopaedia written early in the first century AD and contains observations of a geographical and cultural nature around the Mediterranean Basin, northern Europe and the Middle East both made and collected by Strabo (Bittlestone et al., 2005). The key observation in *Geographica* was as follows:

"The Simois and Scamander affect a confluence in the plain, and since they carry down a great quantity of silt they advance the coastline and create a blind mouth, and saltwater lagoons and marshes…"

Geographica 13.1.31 (Strabo, c.1 in Kraft et al., 2003).

This observation suggested that the alluvial plain below the ruins at Hissarlik may not have been there at the time of the events of the *Iliad* (Luce, 1998). In 1822, based on Homer's geographical description of the city and this quote by Strabo, Scottish journalist Charles Maclaren published 'A Dissertation on the Topography of the Plain of Troy'. Maclaren suggested the city lay at Hissarlik under the ruins of the Augustine Roman city of Ilium, some 15 km inland rather than on the edge of a bay, and suggested that the mouths of the Scamander and Simois Rivers may have been further inland during the events of the *Iliad* (Maclaren, 1822).

The first investigative trenches were dug by English archaeologist Frank Calvert in 1865 followed by a more extensive campaign by Heinrich Schliemann (Bittlestone et al., 2005). Schliemann led two campaigns at Hissarlik in the 1870's which led to the excavation of several building phases of a substantial Bronze Age settlement which appeared to fit the building plan of Troy as described by Homer (Bittlestone et al., 2005). After this success, Schliemann went on to find the city of Mycenae and, famously, Agamemnon's golden mask.

In order to provide conclusive evidence as to whether or not these ruins could indeed be Troy, a systematic drilling and radiometric dating investigation of sediments in the area was undertaken (Kraft et al., 1980; Kayan, 1991; 1995; 1996; 1997) (Figure 1.4). Using the results of that study, texts from the *Iliad* and evidence from historical sources Kraft at al. (2003) created a series of paleo-coastline reconstructions from ca. 3250 BP illustrating how the north-western Turkish coast had been altered as the Scamander and Simois had advanced seaward due to massive flood control and drainage through irrigation canals eventually resulting in the siltation of Troia Bay (Figure 1.5). The data proved decisively that during the events of the Trojan War the mouth of the Scamander would have been approximately 5 km inland of its present position and would have formed a wide flood plain below the city as described by Homer (Kraft at al., 2003).

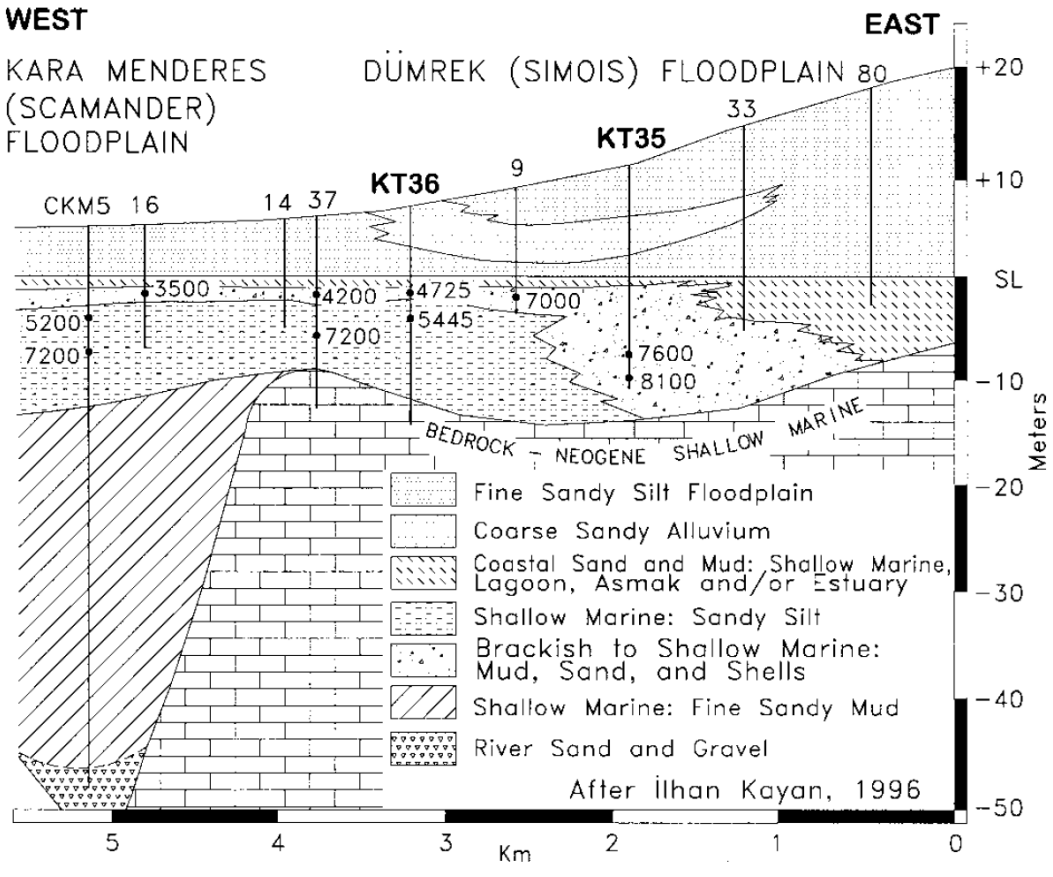

Figure 1.4 Axial cross-section of Simois River floodplain to the north of Troy labelled "W-E" in Figure 1.5, lower right, showing the positions of boreholes drilled during the extensive drilling campaign to investigate the flooding history of the floodplains and to determine whether this area once held a marine bay (Troia Bay) during the time of the *Iliad*. From Kraft et al. (2003).

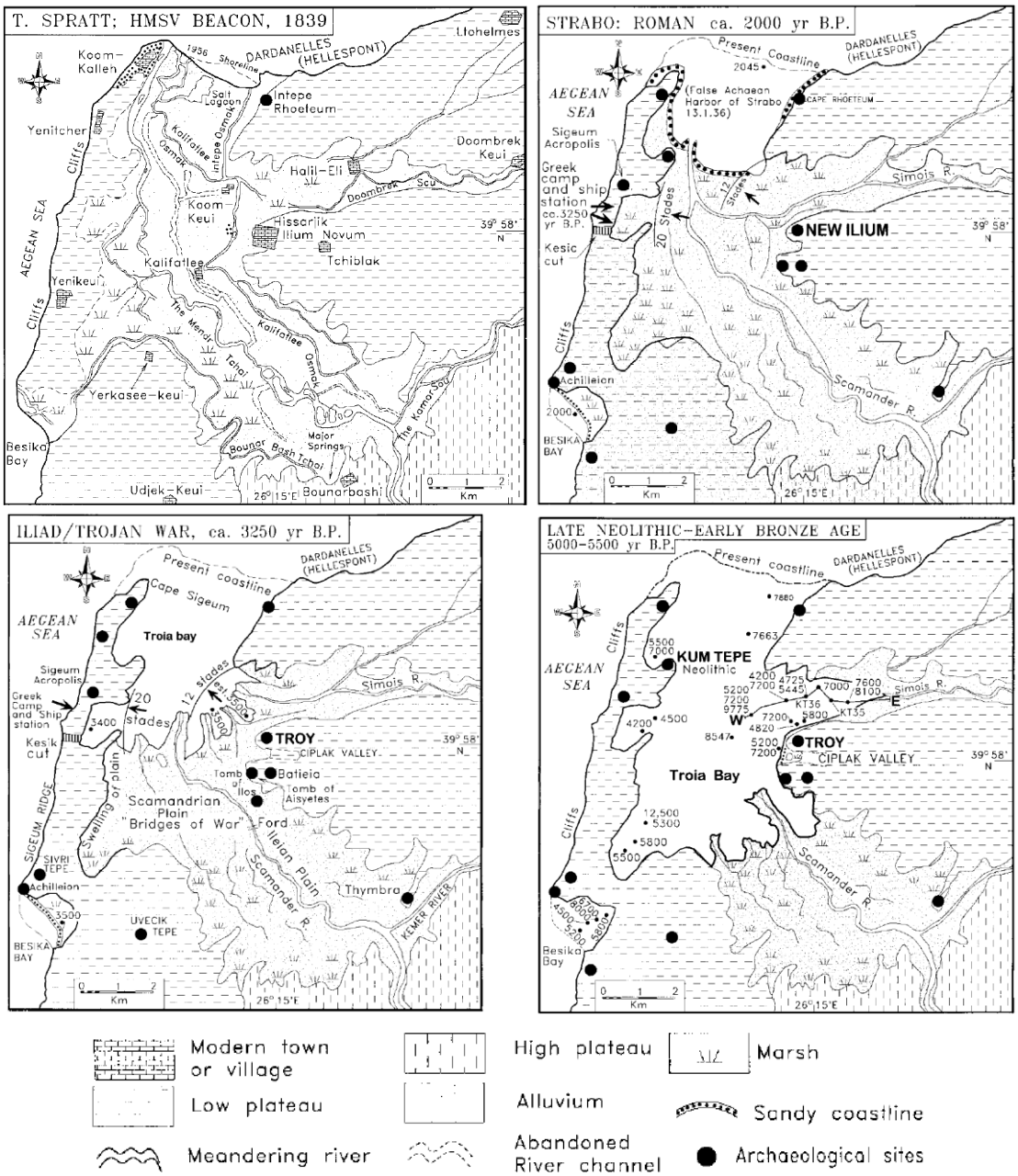

Figure 1.5 Spratt (1839) map of the configuration of the Kara Menderes (Scamander) and Dumrek (Simois) River flood plains during investigations of the Bronze Age ruins at Hissarlik (top left). Paleo-geographic reconstructions and marine embayment of north-western Turkey from the time of Strabo's observations, the Trojan War and Late Neolithic-Early Bronze Age (top right to lower left). These maps clearly show a dramatic advancement of the coastline due to siltation of around 9 km which has taken place over the last 7450 years. From Kraft et al. (2003).

The findings of this investigation not only showed that Schliemann's ruins were both historically and geographically compatible with the Homeric description but also that Troy was indeed based on a real place i.e. Homer's description was geographically

accurate. Dramatic changes in the coastline of north-western Turkey over the last ~3300 years had led to a settlement on the coast being completely land-locked and the marine inlet which serviced the city becoming silted and dry. It also showed that while some of the historic references (e.g. Strabo's third hand observations) could be disputed, the results of the geoscientific survey were reliable and repeatable thus reducing the reliance on disputed writings of antiquity.

Kraft et al. (2003) underpinned the importance of combining modern geoarchaeological techniques with verifying the location of Homer's Troy in the following quote:

"Only a classicist can translate and interpret correctly the nuances of ancient Greek literature. Yet it takes a sedimentologist – geomorphologist to correlate the scholarship of the classicist with the geologic data and develop reasonably precise ancient landscapes."

The success at Hissarlik meant that a new solution to Homer's "missing" locations could be explored rather than simply dismissing them as fiction or branding Homer a poor geographer. Homer's geographical description of places like Ancient Ithaca may still be accurate if the ancient landscape had undergone similarly dramatic and rapid changes in morphology at other contentious locations. This meant that a geoarchaeology approach could be used to investigate these sites where simply relying upon conventional archaeology and historic sources had failed to produce conclusive evidence.

1.1.5 The Search for Ancient Ithaca

The search for Homer's Ancient Ithaca has been long and varied with investigations spanning several centuries and focusing on several locations across the Ionian Islands (Bittlestone et al., 2005). In lines 19-26 of the *Odyssey*, Odysseus gives a detailed description of his Ancient Ithaca home in the following key statement:

I am Odysseus, Laertes' son, world-famed
For stratagems: my name has reached the heavens.
Bright Ithaca is my home: it has a mountain,
Leaf-quivering Neriton, far visible.
Around are many islands, close to each other,
Doulichion and Same and wooded Zakynthos.
Ithaca itself lies low, furthest to sea
Towards dusk; the rest, apart, face dawn and sun.

Odyssey 9, 19-26 (trans. James Diggle, in Bittlestone et al., 2005).

Homer's geographical description places Ithaca somewhere in the Ionian Islands of Western Greece as the name "Zakynthos" can be equated to a modern island with that name (Figure 1.6). The Ionian Islands comprise of seven principle members which are Kefalonia, Zakynthos (Zante), Lefkada (Lefkas), Ithaki, Corfu (Kerkyra), Paxi and Kythira and several smaller islands. The largest islands are predominately mountainous with vertiginous, rugged coastlines deeply-incised with shallow bays and have limited flattish alluvial plains at the base of valleys and coastal areas.

The name "Same" can be linked with reasonable confidence to the modern island Kefalonia. While no longer a modern island name, "Same" is a modern coastal port on the east coast which was the site of Greco-Roman city-state settlement and hence can be linked with the historic name for Kefalonia (Bittlestone et al., 2005). This name still appears as the island's third largest and ancient town of Sami, and before the 2011 local governmental elections it was the name of a large municipality composing the central and eastern part of the island (Samos). At 760 km^2 in area, Kefalonia is largest of the Ionian Islands (Souyoudzoglou Haywood, 2000) and dominated by the dramatic, high elevation topography of the Ainos mountain range whose highest peak, Mega Soros, stands 1628 m above sea level. The island "Doulichion" is a mystery as, like Ancient Ithaca, no island by that name currently exists.

According to the Homer's description, Ancient Ithaca itself "lies low" which implies an island of low elevation or gentle topography relative to the surrounding islands. "Furthest to sea" and "towards dusk" while the rest "face dawn and sun" suggests an island which sits furthest to the west and seaward of an island group. Popular belief and historic searches place Ancient Ithaca on modern-day Ithaki, a small mountainous island which lies to the northeast of Kefalonia, whose very similar name and abundance of Mycenaean-age artefacts has made it the focus of numerous theories throughout the search for Ancient Ithaca (Figure 1.7).

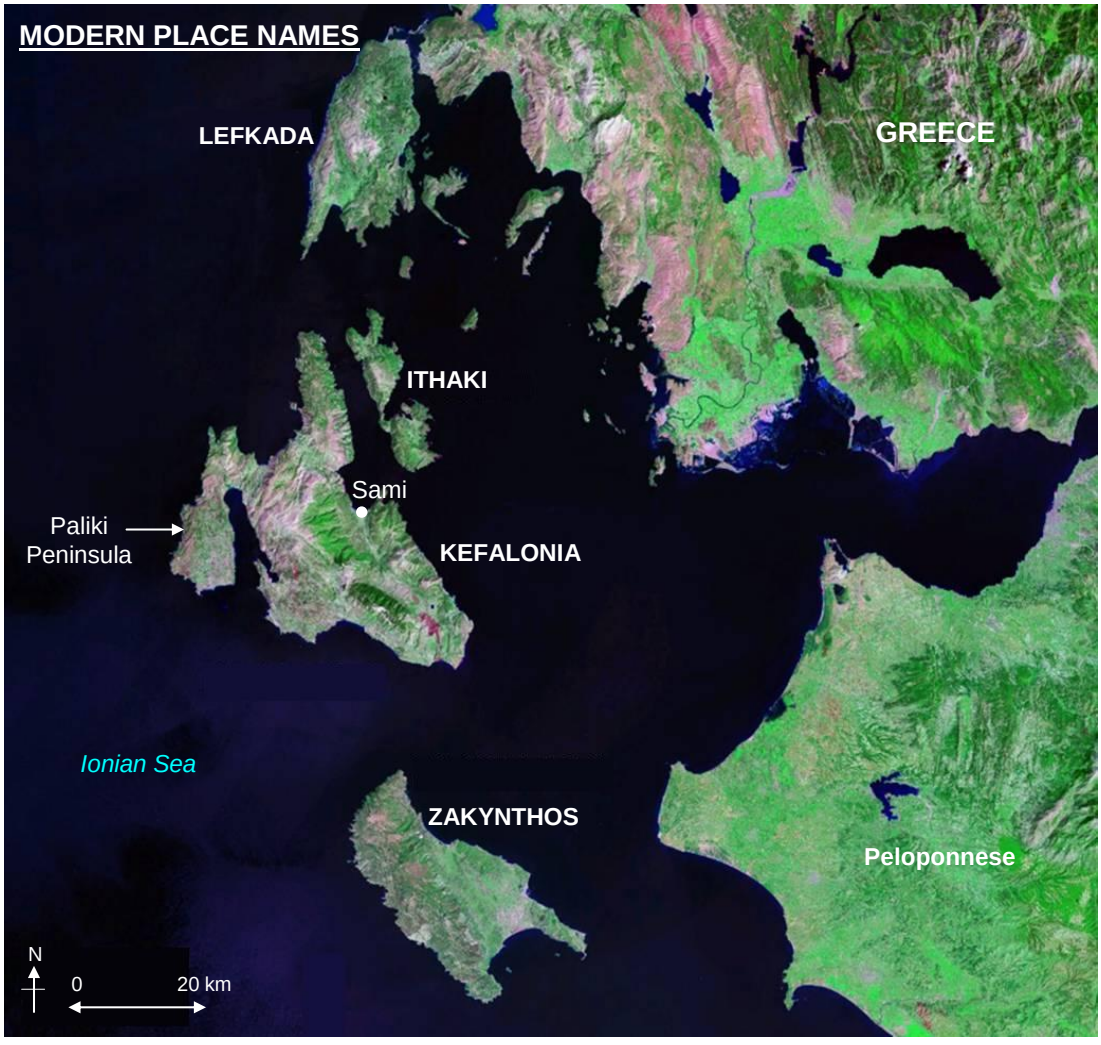

Figure 1.6 The Ionian Islands (Kefalonia, Zakynthos, Lefkada and Ithaki). Satellite image source: Landsat-7 false colour satellite mosaic (SWIR 7,4,2) courtesy of NASA Applied Sciences Directorate – John C. Stennis Space Centre (website: https://zulu.ssc.nasa.gov/mrsid/mrsid.pl). Modified from Underhill (2006).

However Ithaki's physical geography completely contradicts the Homeric description. It is not low-lying but very mountainous, the highest being Nirito (809 m) and Nerovoulo (669 m), with a vertiginous cliff line and it does not lie to the west of the island group but closest to the mainland and the east.

To qualify as a candidate for Ancient Ithaca, the location must not only fit Homer's description of Ithaca but must also offer possible geographical locations for the key places encountered by Odysseus from his arrival on Ithaca to reaching his palace such as Ithaca's deep harbour, the Arethusa Spring and the distinct headland-within-a-headland of Phorcys Bay under Neriton Mountain where Odysseus first made landfall. Until recently no satisfactory theory has been put forward on the location of Ancient Ithaca.

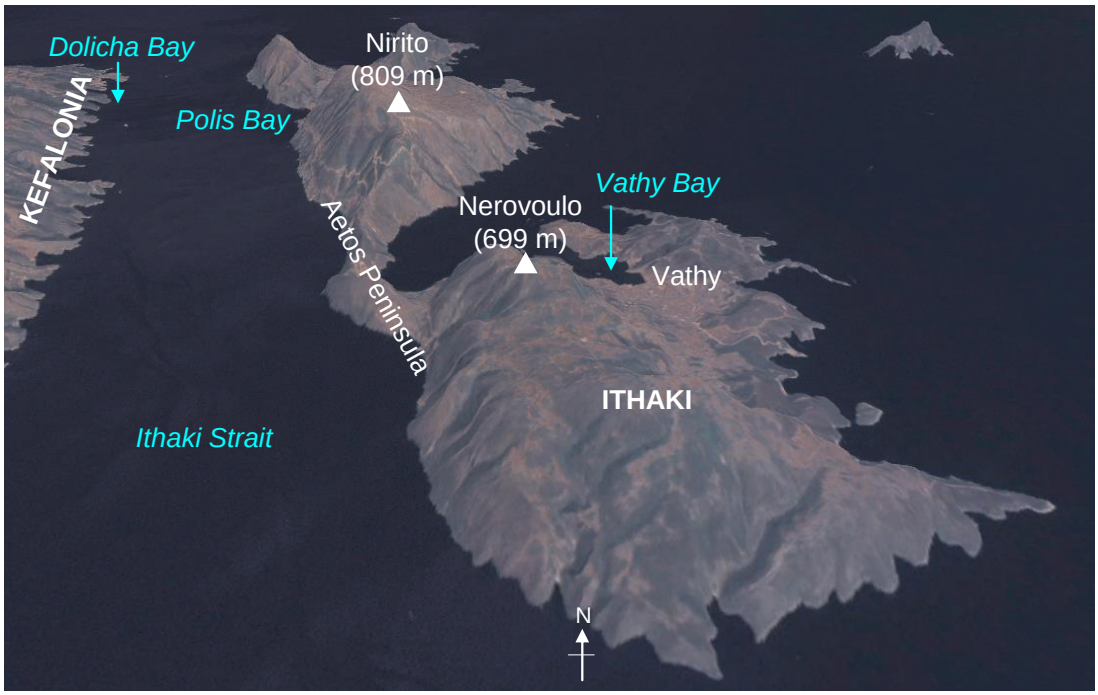

Figure 1.7 The small island of Ithaki popularly believed to be Ancient Ithaca however its steep mountainous topography and geographical location to the east of the central Ionian Island group contradicts Homer's description of Ithaca. Satellite image source: NASA.

1.1.6 "Strabo's Channel": A Geoarchaeological Solution to an Ancient Problem

G. Volterras (1903), a resident of Paliki with strong local knowledge of the local geography, the author le Noan (2001, 2003, 2004) and, most recently, Bittlestone et al. (2005) noticed the similarities between Homer's Ithaca and Paliki, the westerly-most peninsula of Kefalonia. Paliki provides a far more convincing geographical fit to Homer's description of Ancient Ithaca than the island of Ithaki. The peninsula is around 120 km^2 in area. Its highest peak is Lachties hill (518 m) therefore it is some 600 m lower in elevation than modern Ithaki with an average elevation of around 220 m. Figure 1.8 illustrates the contrast between the high elevation mountains of Kefalonia and Ithaki and the low elevation "low-lying" land of Paliki. Being on the western side of Kefalonia, it also forms the "furthest out" to sea part of the Ionian Islands all of which lie between it and the mainland in the east.

As well as providing geographical matches to the Homeric description, places that Odysseus encountered during his journey to his palace could be equated with locations in Paliki (Bittlestone et al., 2005) (Figure 1.9). For example, Phorcys Bay could be equated with Atheras Bay in Northern Paliki which shares a similarly distinct pair of headlands and safe anchorage within the sheltered waters of its inner bay (Volterras, 1803). There is a Mount Neriton overlooking this bay as described in the text which can be seen from afar and forms the first substantial topography observed when approaching from the north-west by boat. Further south is a possible candidate for the city of Ithaca itself situated on a conical fortified hill (Kastelli Hill) across which high quantities of pottery shards believed to date to the Late Bronze Age were found (Bittlestone et al., 2005). Lying at the foot of this hill is a low-lying, boggy area, called Livadi Marsh, which may have once served as Ithaca's deep harbour if sea levels had been higher or if the land was lower during the time of Odysseus, a strong possibility given the tectonic instability of the region.

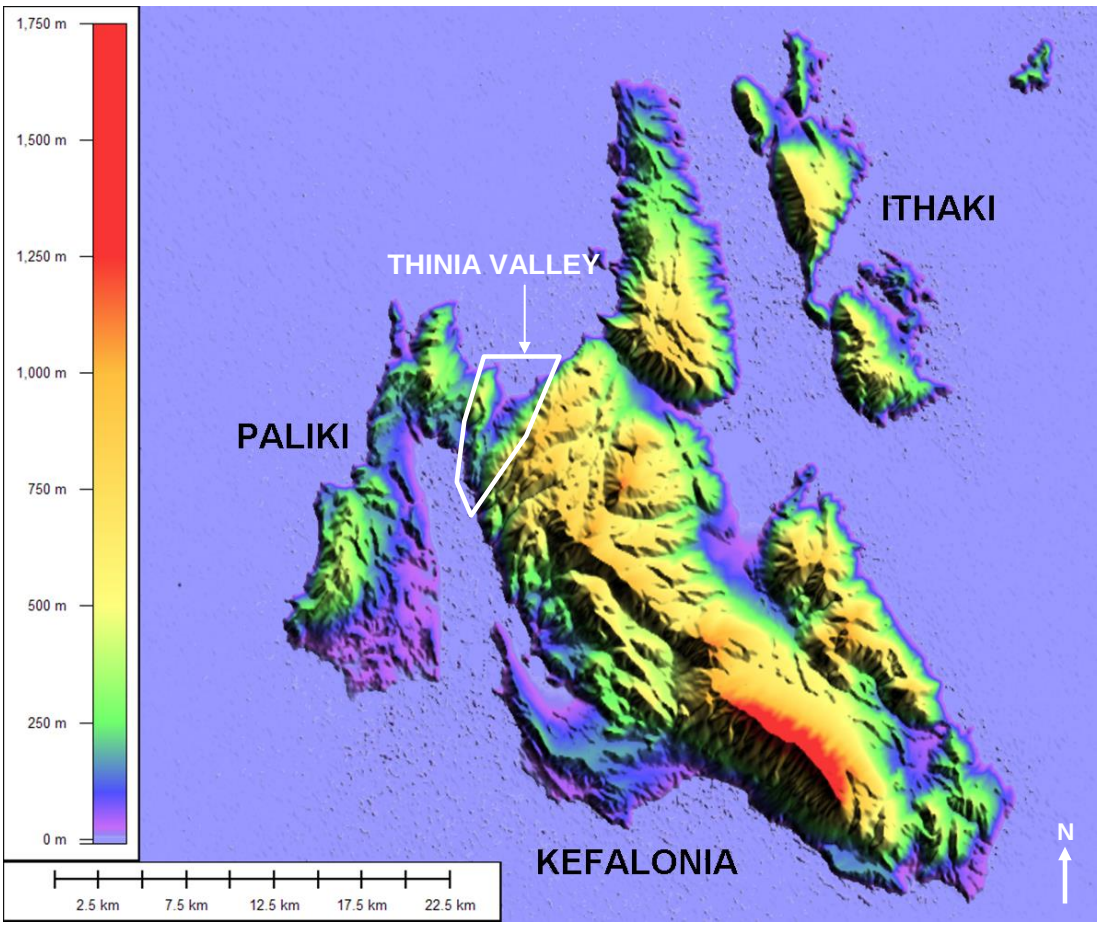

Figure 1.8 Digital Elevation Model (DEM) of Kefalonia and Ithaki illustrating the difference in topography between mountainous Kefalonia and Ithaki and the low-lying Paliki peninsula where high elevation = hot colours, low elevation = cold colours. The highest elevation (red area) corresponds to the Ainos Range. The Thinia valley is outlined in white. DEM data obtained from the NASA Shuttle Radar Topography Mission (SRTM-90) and processed by Global Mapper. Modified from Underhill (2006).

After Kefalonia, Paliki also contains the richest variety of Mycenaean-age artefacts of the islands. In 1921, a Late Bronze Age tomb was found at Oikopeda close to Kontogenada as well as vases and shards from large jars which included some of the earliest Late Bronze Age pottery uncovered on the island and finely-worked metal finds (Souyoudzoglou Haywood, 2000). Four tholos chamber tombs of the same age were found to the south of Kontogenada and a further two were found to the north-east of Parisata. Despite this rich evidence, Paliki has been generally dismissed as a candidate for Ancient Ithaca since it is land-locked and connected to the rest of Kefalonia by a narrow land-bridge called the Thinia valley (Figure 1.10).

Figure 1.9 Map of Paliki showing the locations mentioned in the text of this chapter. The locations of the Roman towns Pali (or Paleis) and Cranioi are indicated in red. Satellite image credits as for Figure 1.6.

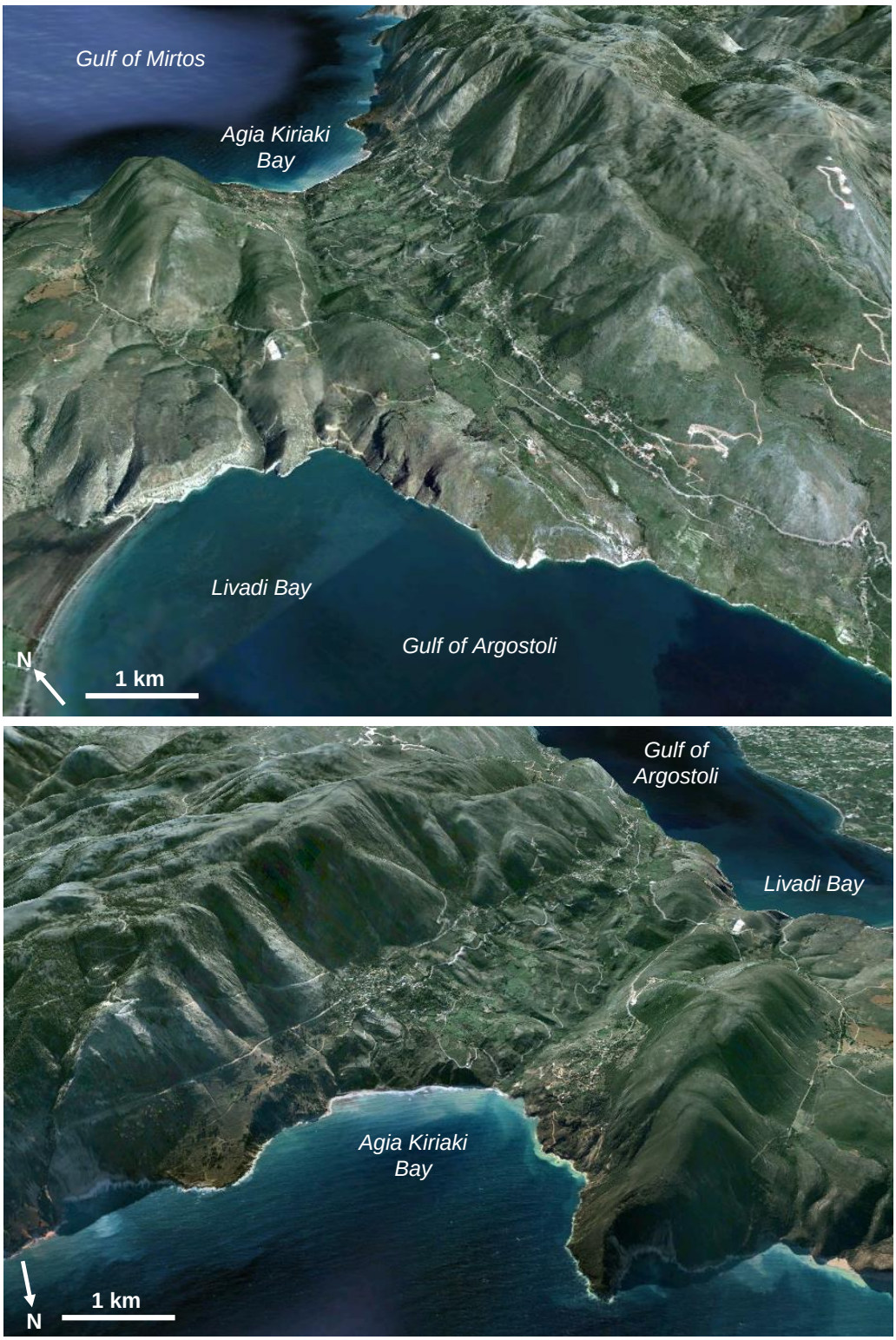

Figure 1.10 The Thinia valley looking northeast (top) and southeast (bottom). Satellite image source: Google Earth.

However, an interesting quote from Strabo's *Geographica* dated around 1 AD offers a possible solution:

"The largest mountain upon it is Ainos, whereon is the temple of Zeus Aenesius; and where the island is narrowest it forms an isthmus so low-lying that it is often submerged from sea to sea. Both Paleis [Pali] and Cranioi are on the gulf near the narrows."

Geographica 10, 2-15 (Bittlestone et al., 2005)

While Ainos can be identified on the island of Kefalonia (red peak on Figure 1.8), the location of the frequently submerged narrows is a problematic description as nowhere on Kefalonia is there such a feature. This quote suggested that at Strabo's time Kefalonia was dissected by a narrow seaway into two discrete landmasses. The term "isthmus" however comes from the ancient Greek for "neck" and refers to a narrow strip of land connecting two greater areas of land usually bounded on either side by water (Encyclopædia Britannica). The remains of the Roman towns of Pali (or Paleis) and Cranioi can be identified on either side of the Gulf of Argostoli. Pali is positioned to the north of Lixouri (giving the Paliki peninsula its name) while Cranioi lies close to the capital (indicated in red on Figure 1.9).

In 2003, a team composed of economist Robert Bittlestone, geologist Professor John Underhill of Edinburgh University and classist James Diggle of Cambridge University proposed a new theory on the relocation of Ancient Ithaca. Their published work Odysseus Unbound (Bittlestone et al., 2005) proposed that given the position of these ancient towns on either side of the Gulf of Argostoli the most likely location which fulfils the definition of an "isthmus" is the Thinia land-bridge (Figure 1.10). Thinia forms a NNE-SSW striking valley approximately 6 km long and 4 to 0.5 km wide bounded by steep, high elevation mountains. The eastern valley side is defined by the Imerovigli mountain range (994 m). The north-western valley side forms a NNE-SSW orientated anticlinal mountain (Agrilias hill, 517 m). To the north of the valley lies the crescent-shaped Agia Kiriaki Bay while to the south is the Gulf

of Argostoli, a narrow (~4 km wide) north-south orientated stretch of water which almost separates Paliki from Kefalonia.

Locating Strabo's "narrows" at Thinia implies that around 2000 years ago during the periods of marine inundation from "sea to sea" the Paliki peninsula would become cut off from the rest of Kefalonia effectively forming a temporary island. Bittlestone et al. (2005) proposed that Strabo's "narrows" were the remains of a more substantial channel-like feature which existed where the Thinia valley stands today. Dubbed "Strabo's Channel" this feature may have been more navigable during the time of Odysseus (~3240 BP) so around 1300 years prior to Strabo's observation and substantial enough for Paliki to have been considered a free-standing island and, as such, a valid candidate for Ithaca.

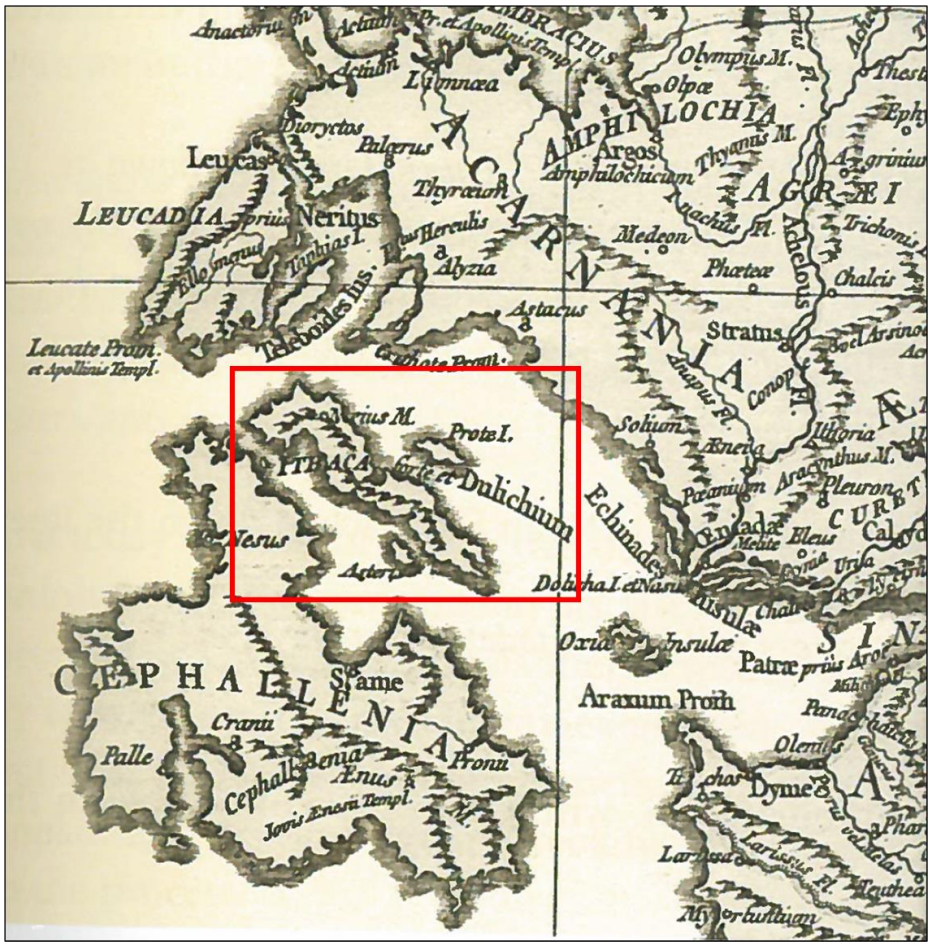

Figure 1.11 Eighteenth century map of Kefalonia by D'Anville (1978) showing Ithaki as Doulichion ("Dulichium") outlined in a red box. Modified from le Noan (2001).

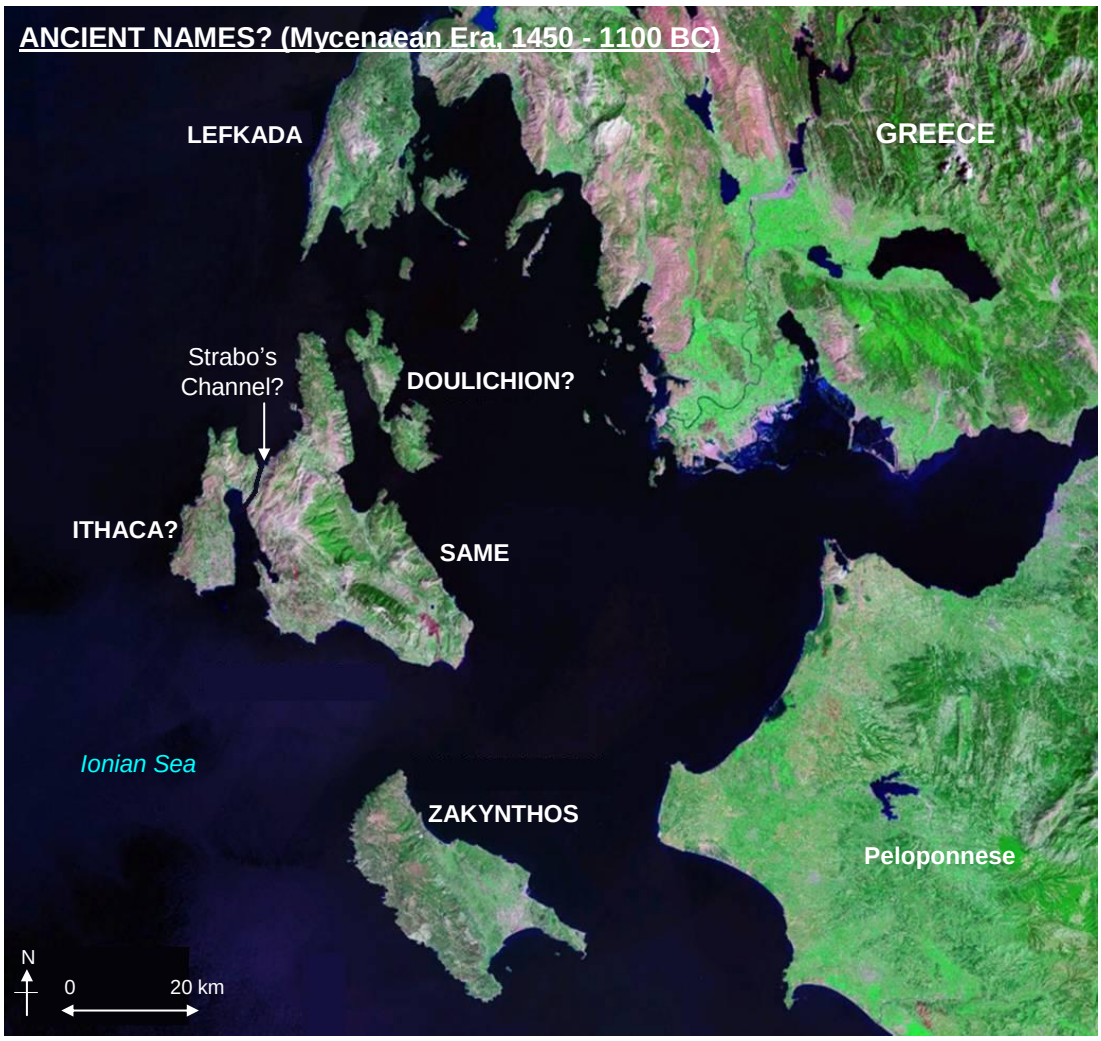

Figure 1.12 Possible ancient names applied to the Ionian Islands as a result of the "Strabo's Channel" theory. Satellite image source: As for Figure 1.6. Modified from Underhill (2006).

A further consequence of this new island configuration was a possible location for Doulichion which can tentatively be attributed to modern-day Ithaki. The name "Dulichium" tentatively appears in a 14th century Venetian map referring to the island of Ithaki (Figure 1.11). In 1678, Jacob Spon suggested that the primary town of Ithaki, Vathi, was once known as Dolicha "…because there is in front a large port with the hovels of a town still called Dolicha…" (Spon, 1678). There is also some evidence of this in nearby modern place names e.g. Dolicha Bay which overlooks Ithaki (Bittlestone et al., 2005). The resulting map of the Ionian Islands with ancient names applied is presented in Figure 1.12.

However, it is clear that no such channel exists in Thinia today. Parts of the valley stand well above sea level (up to 210 m at its central saddle) and there is little indication that marine waters could ever have washed from "sea to sea". The relocation of Ancient Ithaca to the Paliki peninsula therefore depends upon the Thinia valley having undergone dramatic geomorphological changes since the Late Bronze Age, going from a marine seaway to a land-bridge. It also depended upon these changes occurring over a very short geological timescale since if Strabo's observation of a frequently-submerged "narrows" was made around 1 BC then disappearance of the Channel must have taken place over 2000 years or less. This immediately puts strain on the theory, raising questions as to how likely such a change could happen so rapidly, geologically-speaking.

However, the extensive sedimentary coring investigation at Troy undertaken by Kraft et al. (2003) provides crucial evidence that such a dramatic and rapid change in the Late Holocene landscape had taken place elsewhere in the Eastern Mediterranean, in this case the out-building of the NW Turkish coast by around 5 km over around 3300 years. It was therefore feasible to consider that a similarly dramatic change may have changed Paliki from an island into a peninsula in a similar timescale. The key testable idea is therefore whether or not the Thinia valley was once a marine seaway during the time of Odysseus.

Despite the dependency of the relocation of Ancient Ithaca primarily on a single ancient source (Strabo) whose authenticity could be disputed, the "Strabo's Channel" theory provides an attractive "Occam's Razor" solution to the relocation of Homer's Ancient Ithaca reducing a complicated classical problem with a long history of conflicting theories into a simple test rooted in the field of geoscience which can be investigated using a geoarchaeological approach.

1.1.7 Thesis Rationale and Aims

The aim of this thesis is to test the "Strabo's Channel" theory as proposed by Bittlestone et al. (2005) using geoarchaeological techniques namely the application of non-invasive geophysical tests "ground-truthed" with shallow sedimentary coring and combined with geological and geomorphological observations. A directly archaeological investigation at this point is beyond the scope of this thesis however the results, if positive, may justify future archaeological investigation. For now, there are three key testable possibilities to the "Strabo's Channel" theory:

1. No marine channel existed in Thinia during the Late Bronze Age (Strabo's "narrows" were an erroneous second hand observation) and the topography of the Thinia isthmus was the same as it is today, dismissing the possibility that Paliki was an island at the time of Odysseus.

2. Paliki was connected to the rest of Kefalonia by a narrow causeway (Thinia was only partially flooded i.e. a "sea-girt" island) in a similar way that the island of Lefkada (to the north of Kefalonia) is connected to mainland Greece today.

3. The Thinia land-bridge did not exist at all during the Late Bronze Age and a marine channel ("Strabo's Channel") completely separated the Paliki peninsula from the rest of Kefalonia forming an island.

1.1.8 Thesis Structure

Chapter 1: Background and Rationale

This chapter presents the background to the "Strabo's Channel" theory and is split into three parts. The first part introduces the concept of the channel and the historical

background to the search for Homer's Ancient Ithaca. The second part of the chapter concerns the geological background of the area. The third part will then describe the possible mechanisms by which "Strabo's Channel", if it existed, might have disappeared to form the Thinia valley as it stands today.

Chapter 2: Data and Methods

The Data and Methods chapter presents the geoarchaeological methods used to investigate the "Strabo's Channel" theory. It presents the results of the preliminary tests carried out as "reconnaissance" for this theory before commencement of the surveys covered by this thesis, the results of which were deemed positive enough to justify further testing through a complimentary series of non-invasive geophysical tests and sedimentary coring presented in this study. The second part of the chapter describes the tests carried out and the reasoning behind the locations where they were undertaken as well as detailed explanations of the acquisition and processing stages for these tests.

Chapter 3: Surface Geology and Geomorphology

Chapter 3 presents the results of the detailed geological and geomorphological field mapping campaigns of the Thinia valley and lists the results of the biostratigraphic analysis of surface samples collected to improve the resulting geological map.

Chapter 4: Onshore Geophysics

Chapter 4 presents the results of the non-invasive onshore geophysical tests. The first part of the chapter presents a conductivity and magnetic overview of Northern Paliki and the Thinia valley before focusing on the ground-based tests (resistivity and seismic refraction) at the sites of Atheras and Livadi Marsh. The second part of the chapter presents the results of the Thinia ground-based tests (gravity, resistivity and seismic refraction).

Chapter 5: Onshore Subsurface Calibration

The first part of this chapter describes the shallow sedimentary coring survey undertaken at sites in Northern Paliki (Atheras valley and Livadi Marsh) and in the Thinia valley aimed at providing crucial surface calibration ("ground-truthing") of the non-invasive geophysical results. The second part presents the three cross-sections and five core-ties produced from the borehole data and resulting stratigraphic columns.

Chapter 6: Offshore Geophysics

This chapter presents the results of the shallow marine seismic reflection surveys undertaken across the coastal areas of Northern Paliki: Gulf of Argostoli, Agia Kiriaki Bay and Atheras Bay.

Chapter 7: Discussion and Conclusion

The first part of Chapter 7 presents the discussion of the results including an evaluation of the structural evolution of Thinia and how this relates to the wider geo-tectonic setting of Western Greece and the implications of the results of this thesis on the "Strabo's Channel" theory. The second part of the chapter proposes locations for future investigation in light of these findings. The third part of the chapter presents the conclusions of the thesis.

1.2 Regional Geological and Tectonic Setting

To better contextualise and understand the geology of Thinia, its geological and tectonic setting relative to the wider region of Western Greece must be considered. Thinia represents a microcosm of the region's geological evolution. The geological history of Western Greece is a complex one which has been the subject of numerous detailed studies (e.g. McKenzie, 1972; 1978; Dewey and Şengör, 1979; Le Pichon and Angelier, 1981; Kahle and Müller, 1996; Clarke et al., 1998).

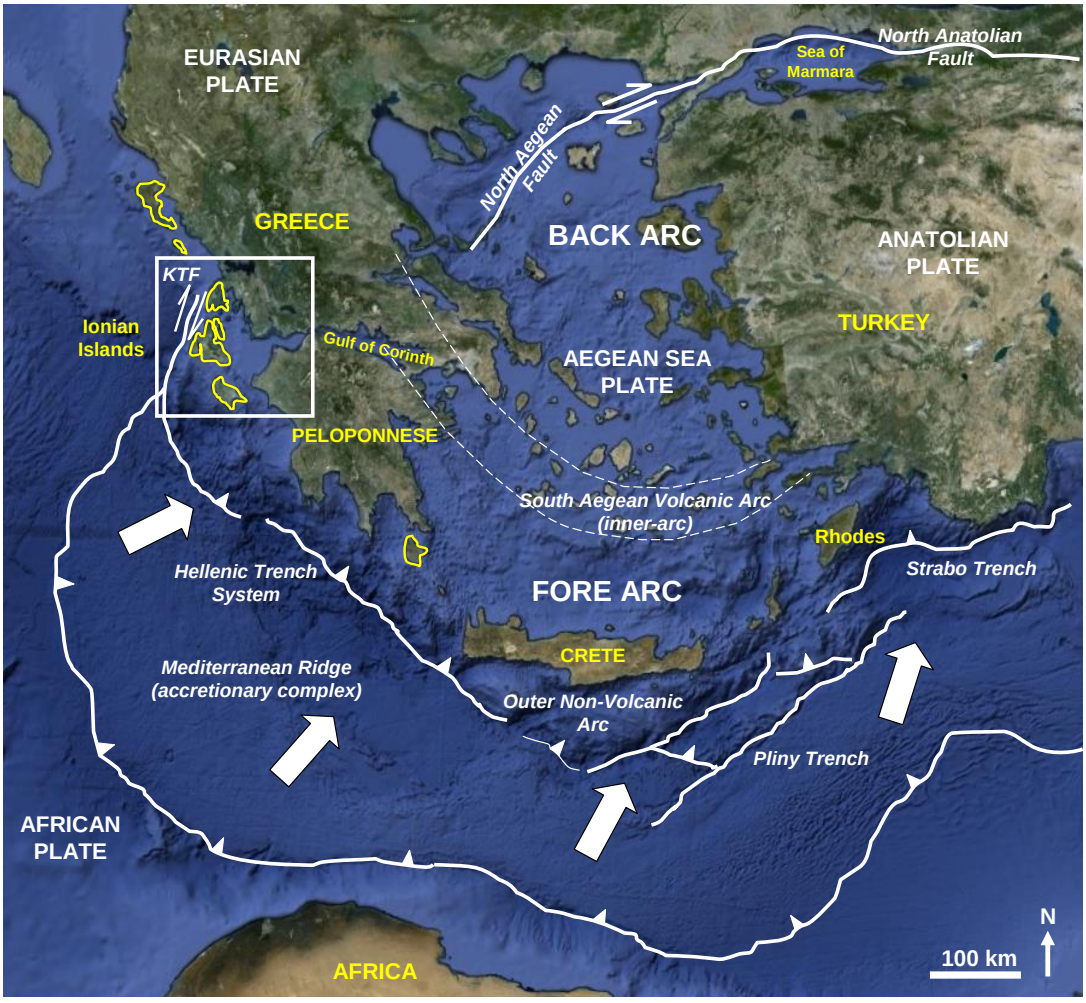

Figure 1.13 The current plate tectonics of the Eastern Mediterranean. The location of Figure 1.6 is outlined by a white box. The Ionian Islands are highlighted in yellow. KTF = Kefalonia Transform Fault. Modified from Chamot-Rooke et al. (2005) and Underhill (1989). The large white arrows along the Hellenic Trench indicate direction of Africa-Hellenic arc relative motion inferred from focal mechanisms of earthquakes (from Pichon et al., 1981). Satellite image credits: Google Earth.

Because of the sheer volume of literature available on this subject, this part of the chapter will only focus on the relevant aspects of geology within this complex regime in order to provide a reasonable geological background upon which to build the research covered by this study. A brief geological history of the External Hellenides of Western Greece will be given. Kefalonia's position in the outer arc region of an active subduction zone will be explained with a more detailed description of the tectonic structures which affect the island, including the Kefalonia Transform Fault and Hellenic Arc-Trench subduction zone before focusing on Western Kefalonia and the Thinia valley itself.

The Ionian Islands occupy the shallow continental shelf of Western Greece in the compression-dominated outer arc zone to the NW of the Hellenic arc-trench system (Underhill, 1989) (Figure 1.13). The Eastern Mediterranean is one of the most tectonically active areas in the world. The current tectonic-stratigraphy of Western Greece is the result of the collision between the African and Eurasian plates (Le Pichon et al., 1995; Papazachos and Kiratzi, 1996). Convergence between these two plates initiated ~80 Ma ago in the Late Cretaceous as increased sea-floor spreading in the South Atlantic relative to that of the North caused rotation of the African Plate relative to the Eurasian (Institut Français du Pétrole, 1966; Mercier et al., 1979; Kamberis et al., 1996; Kokinou et al., 2006). This collision led to the formation of the Hellenic arc-trench, a major arcuate subduction zone which runs from the Ionian Islands, below Crete and Rhodes to western Turkey (Papazachos and Comninakis, 1971; Underhill, 1989; Clarke et al., 1998; Kokinou et al., 2006). At this subduction zone, the northward-moving oceanic lithosphere of the African plate is consumed at a rate of almost 40 mm/yr (McKenzie, 1972; Le Pichon et al., 1995; Papazachos and Kiratzi, 1996). This tectonic configuration results in the Eastern Mediterranean being one of the most tectonically active areas in the world.

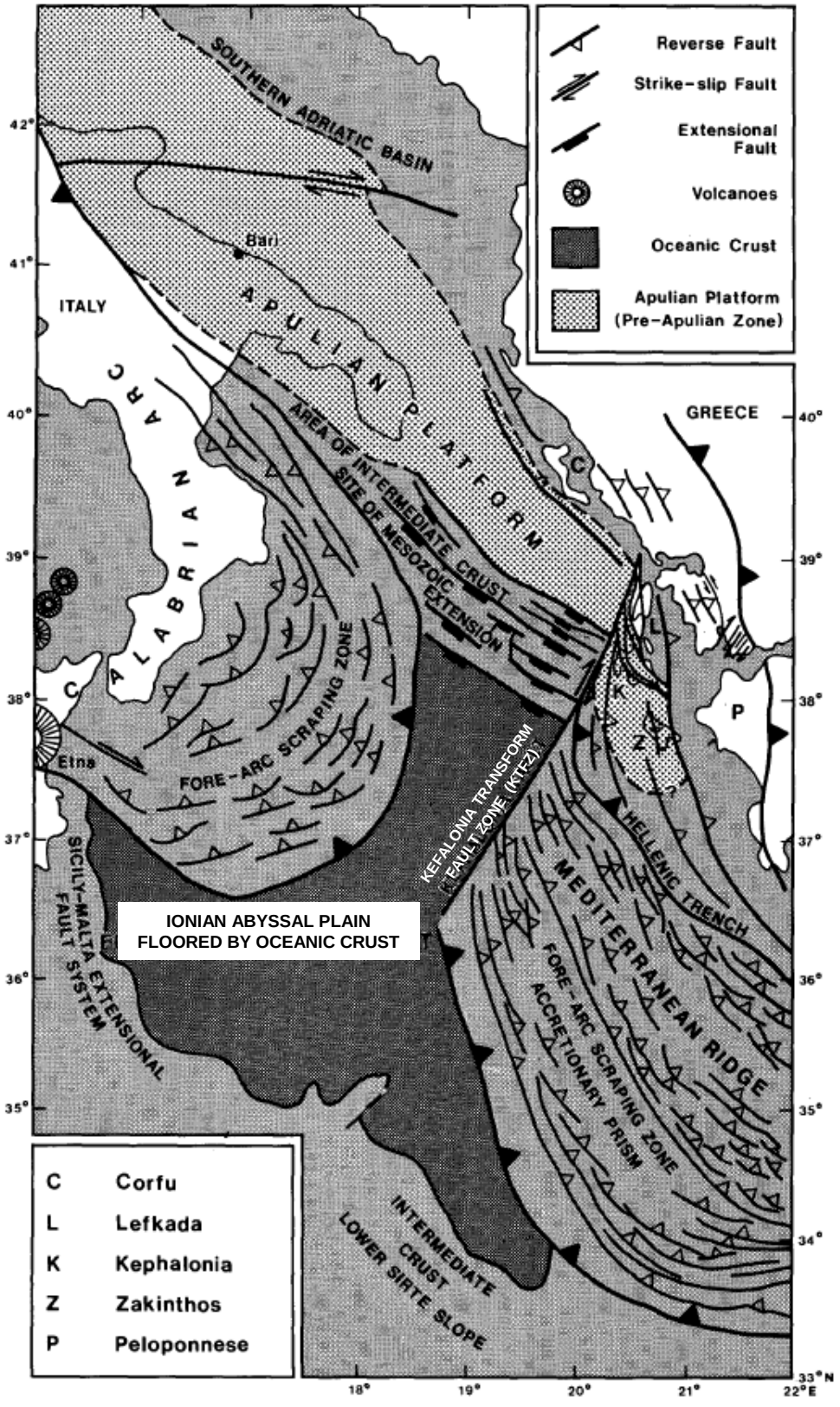

Figure 1.14 Structural configuration of the Ionian Sea showing the Apulian Platform's relationship with the Kefalonia Transform Fault (KTF). After Underhill (1989) and Finetti (1982).

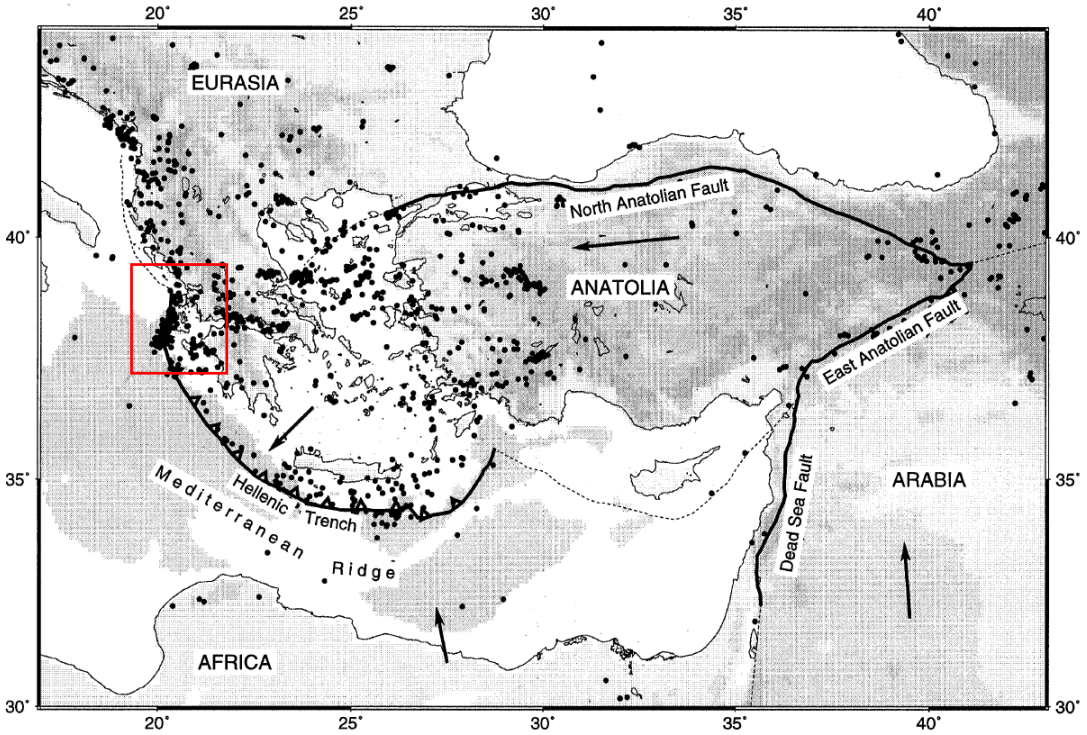

Figure 1.15 Tectonic setting of the Eastern Mediterranean. Approximate plate motions relative to the Eurasian plate are indicated by arrows. Shallow (<40 km) earthquakes of magnitude M>4.5 from are shown as dots (earthquake data from the ISC catalogue 1964-1993). Topographic shading increases at 500 m vertical intervals and the sea floor below 2500 m is shaded. The location of the Ionian Islands is indicated by a red box. After Clarke et al. (1998).

The north-western tip of the Hellenic subduction zone terminates at the Kefalonia Transform Fault (KTF): a seismically highly active dextral strike-slip fault which runs along the north-western coast of Kefalonia and Lefkas for around 200 km (Lagios et al., 2007; Finetti, 1982; Underhill, 1989). The NNE-strike of the KTF parallels the slip vector for subduction along the Hellenic trench and slip rate varies from 7 to 30 mm/yr based on DGPS measurements (Anzidei et al., 1996; Hollenstein et al., 2006). The surface trajectory of the KTF can be inferred through collation of large earthquake epicentres and detailed bathymetry (Louvari et al., 1999). It lies in a deep bathymetric trough of more than 3000 m which strikes at N20E (EERI Special Earthquake Report, 2003; Kokinou et al., 2006). The presence this major seismic discontinuity was first identified by Scordilis et al. (1985) who suggested that the 1983 Kefalonia earthquake (magnitude 7.0) located in the vicinity of the discontinuity had a dextral strike-slip mechanism. The KTF links the Hellenic subduction zone with an east-moving "pseudo" continent to continent collision

between the Apulian platform and Hellenic foreland in the north and separates the oceanic crust of the Ionian abyssal plain from Ionian Islands on the wedge-end of the Mediterranean ridge forming a "triple junction" like configuration (Figure 1.14) (Finetti, 1982; Underhill, 1989; Sachpazi et al., 2000).

Counter-clockwise rotation of the African plate during collision has caused right-lateral motion of the Aegean and Anatolia continental lithosphere relative to the stable Eurasian plate towards the west-southwest driven by a combination of Anatolia being squeezed out westwards and roll-back of the subducting African plate to the south (Le Pichon and Angelier, 1979; Kahle and Müller, 1996) (Figure 1.15). The Aegean/Anatolian block is bounded to the north-east by the North Aegean fault and Marmara Sea, to the NW by Anatolia, in the south by the Hellenic Arc and in the west by the Kefalonia Transform Fault (Kahle and Müller, 1996).

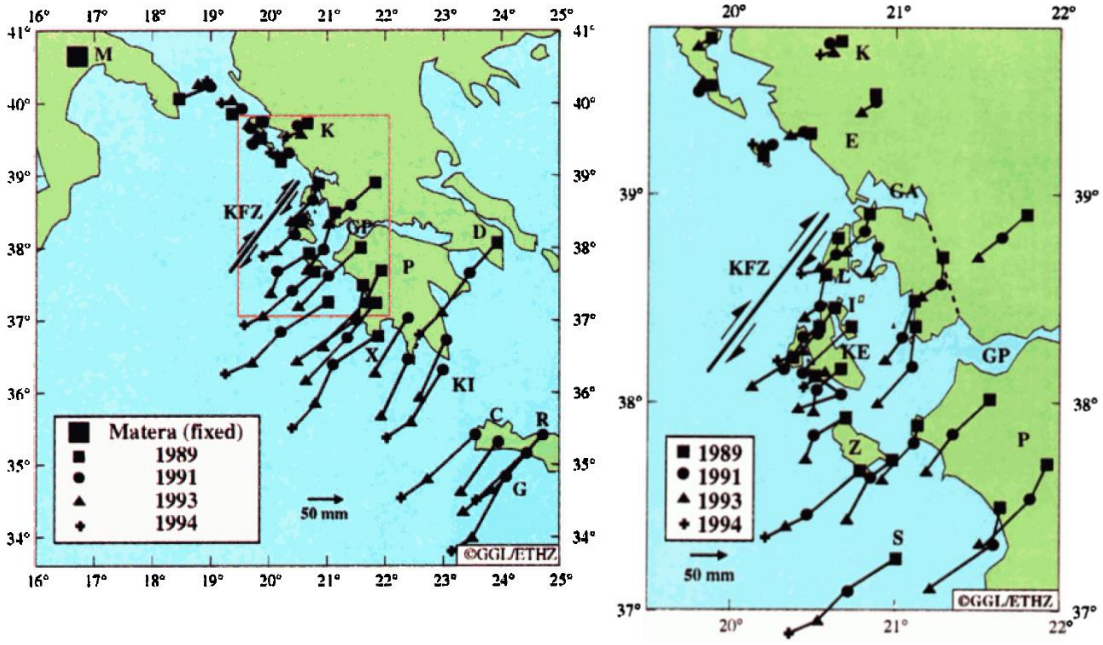

Figure 1.16 GPS recorded crustal motion between 1989 and 1994 of Western Greece relative to Matera, SE Italy. The motion vectors show that the Kefalonia Transform Fault Zone (KTZ) forms the boundary between relatively stable crustal and the SW-orientated rapid movement (almost 40 mm per year) of the Aegean sea plate and SW Greece (left). Close-up of central Ionian Islands (right) which sit right at the edge of these two kinematic regimes. Where M=Matera, D=Dionysos, X=Xrisokellaria, K=Karitsa, GP=Gulf of Patras, A=Atiki, KI=Kithira, C=Crete, R=Roumeli, G=island of Gavdhos, P=Peloponnesus. K=Karitsa, E=Epiros, L=Lefkada, GA=Gulf of Amvrakia, I=Ithaki, KE=Kephalonia, Z=Zakinthos, GP=Gulf of Patras, S=Strofades and P =Peloponnesus. From Kahle and Müller (1996).

GPS studies of Western Greece undertaken by Kahle and Müller (1996) between 1989 and 1994 involving 46 observation sites located between Matera in SE Italy and Gavdhos, the southernmost island in Europe indicated two distinct kinematic patterns relative to a Europe-fixed reference (Matera) (Figure 1.16). To the north of Lefkada and the Gulf of Amvrakia there was minimal motion. Ionian Islands of Lefkada, Ithaki, Kefalonia, Zakynthos, Strofades, Crete and Gavdhos and Peloponnesus, on the other hand, showed rapid south-westerly orientated motion with a maximum displacement of around 200 mm per year at the southern tip of Peloponnesus and Crete. The boundary between these patterns was the KTF demonstrating that this fault system took up the motion of the Hellenic arc-trench subduction zone (Le Pichon et al., 1979; Anderson and Jackson, 1987).

1.2.1 Hellenide (Alpine) Deformation and Formation of Isopic Zones

The Hellenides are an Alpidic orogen which comprise mainland Greece formed by the Eurasian-Apulian (African) plate collision (Figure 1.17). They consist of a series of tectono-stratigraphically similar Mesozoic sedimentary facies isopic zones believed to have formed as a result of the development, foundering and subsequent shortening of a passive continental margin associated with the early Mesozoic opening and late Mesozoic-early Cenozoic (Eocene) closure of the Neotethys Ocean (Dewey et al., 1973; Jackson, 1994; Jones and Robertson, 1991; Mountrakis, 1986; Sotiropoulos et al., 2003; Underhill, 1985; Underhill, 1989). Under the compression of plate collision, these Mesozoic belts were rifted and a series of thrust sheets developed, thrusting onto one another sequentially from the site of the Neotethys and migrating progressively towards the foreland during the Late Eocene and Early Oligocene (Dewey et al., 1973; Smith and Moores, 1974; Clew, 1989; Underhill, 1989).

The External Hellenides are those isopic zones which lie to the west of the Pindos Thrust, a major north-south striking, easterly-dipping thrust fault which runs the

length of Greece (from west to east): Gavrovo-Tripolitza zone, Ionian Zone and the Pre-Apulian or Paxos zone (Aubouin, 1959; 1965; Dercourt, 1959; Aubouin and Dercourt, 1962; Aubouin et al., 1976; Temple, 1968; Jenkins, 1972; Smith and Moores, 1974; Underhill, 1989). The Mesozoic and Paleocene sequences of these zones are believed to represent the rifted extensional passive continental margin of the rigid Apulian platform onlapped by Neogene sediments formed during foreland basin subsidence ahead of the westwards-migrating Hellenide fold-and-thrust belt (Underhill, 1989) (Figure 1.18).

Between the Oligocene and Early Miocene, lithospheric down-bending due to the thrust load of the Pindos thrust sheet (Allen et al., 1986; Homewood et al., 1986; Ricci Lucchi, 1986) led to the development of a foreland basin (Ionian-Gavrovo basin) which ran parallel to the Pindos Zone. This basin contained the Gavrovo and Ionian Zones with the Pre-Apulian Zone occurring at the distal margin while extensional faulting within this zone formed to accommodate this movement (Underhill, 1989). Clastic sediments derived from the Pindos Mountains flooded the foreland basin from east to west with the Gavrovo Zones containing more proximal sediments and the Pre-Apulian Zone representing the tapered distal "feather-edge" of these onlapping sediments (Clews, 1989). Formation of a peripheral bulge ahead of the Ionian basin caused erosion of the Oligocene and basal sediments of the Pre-Apulian Zone. At the end of the Early Miocene, the active front of the Hellenide fold-and-thrust system jumped from the Pindos thrust to invert the discontinuity which became the Ionian Thrust, the major easterly-dipping thrust which defines the western boundary of the Ionian Zone (Underhill, 1989; Sachpazi et al., 2000; Hatzfeld et al., 1990).

Continued westwards migration of the deformation front during the Early Pliocene led to reactivation of the Pre-Apulian extensional faults as reverse faults in Kefalonia and Zakynthos (Sorel, 1976; Sorel et al., 1976; Mercier et al. 1976; 1979; Underhill, 1985; 1989; Stiros et al., 1994), the creation of new thrust faults and west-verging folds. Generally these thrust faults show flattening at the top with folded hangingwall

block edges and contain small-scale low or high angle faulting, orientated subparallel to the strike of the primary thrust (Sorel, 1976; Cushing, 1985; Underhill, 1989).

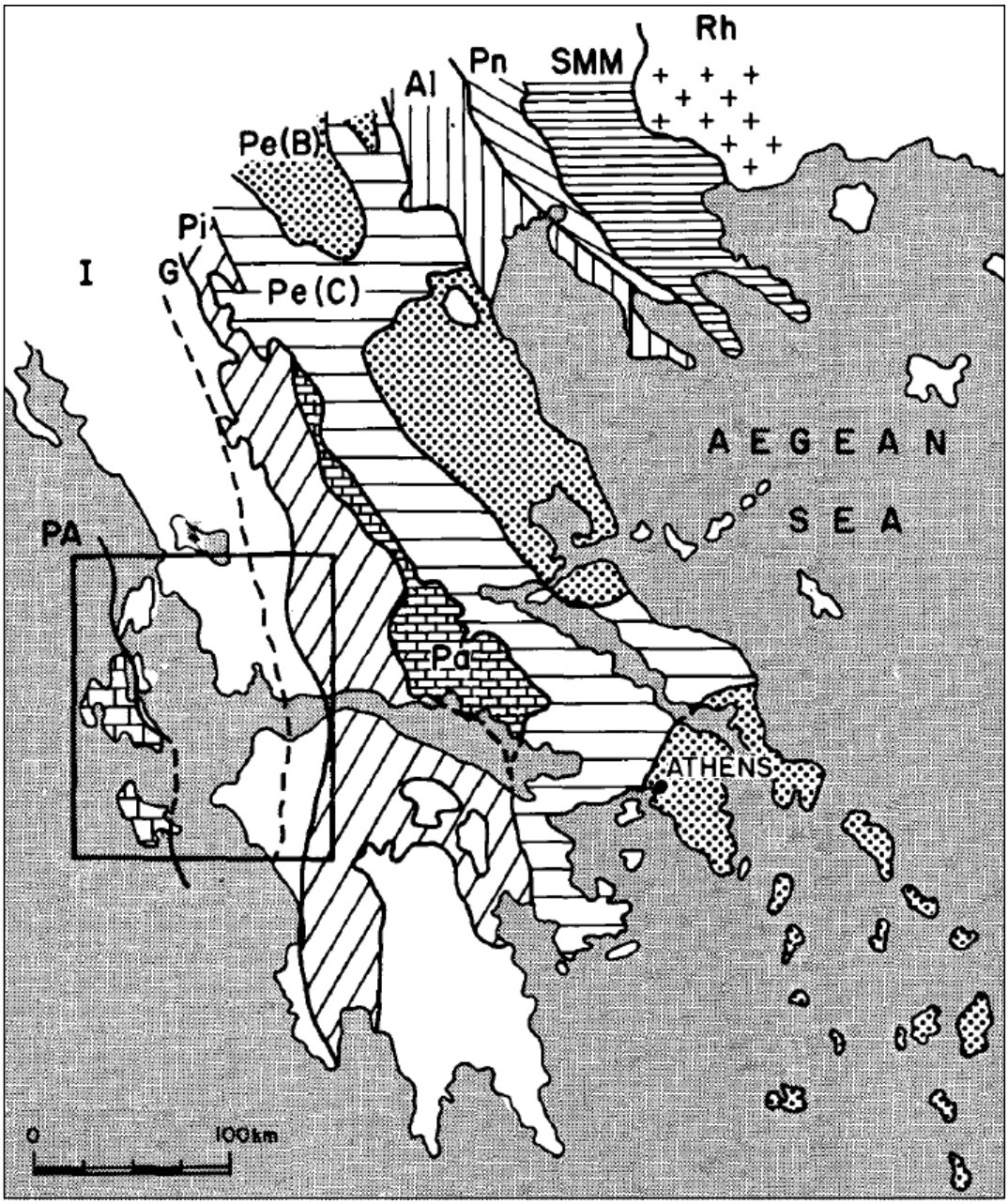

Figure 1.17 The isopic zones of Hellenides (as defined by their unique tectonostratigraphic histories): Rh = Rhodope Massif, SMM = Serbo-Macedonian Massif, Pn = Peonias, Al = Almopias and Paikon, Pe = Pelagonian (B = basement, C = cover), Pa = Parnassos and Beotians, Pi = Pindos, G = Gavrovo-Tripolitza, I = Ionian, PA = Pre-Apulian. The location of the Ionian Islands and Figure 1.6 is indicated by the black box. From Aubouin (1965) and Underhill (1989).

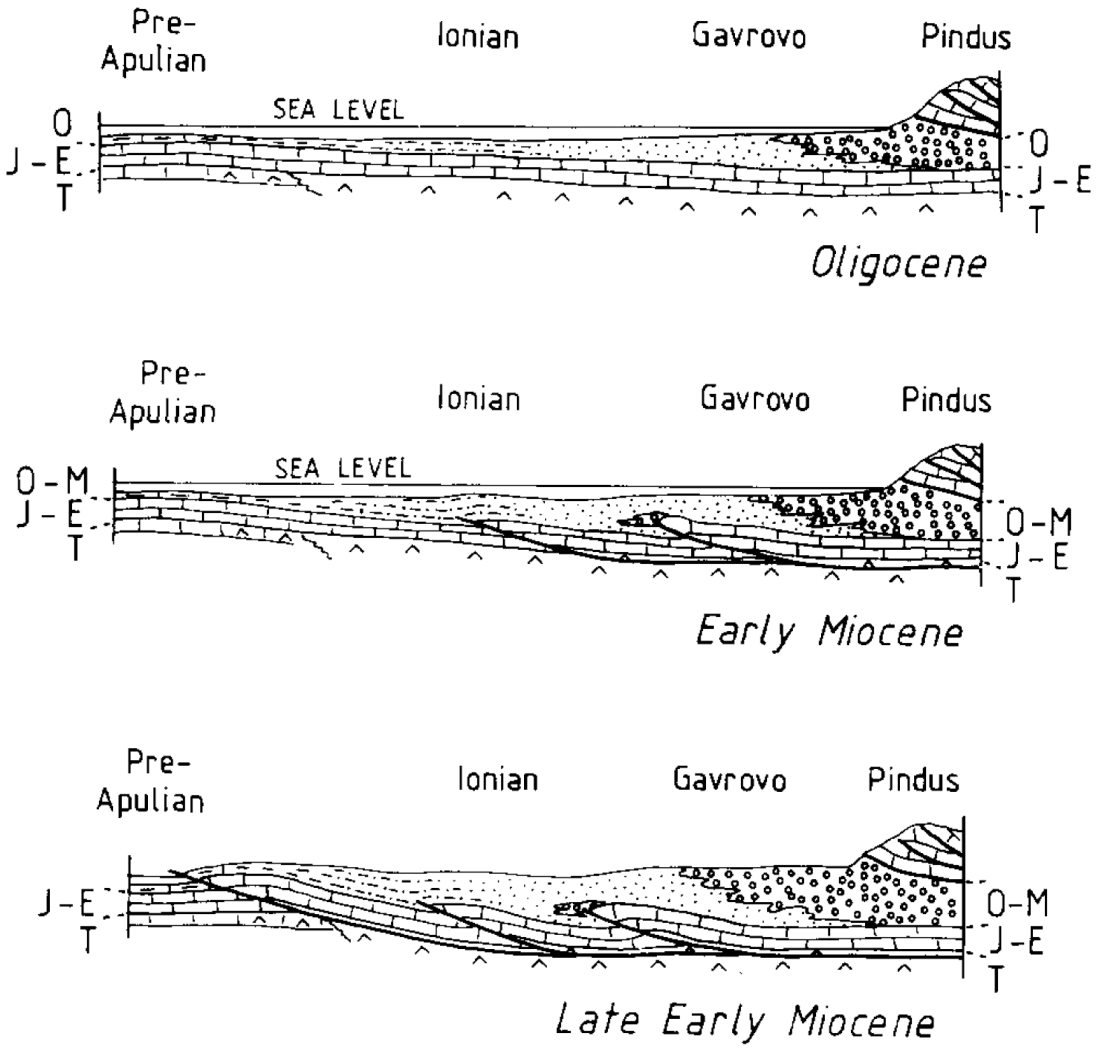

Figure 1.18 Schematic sections across the External Hellenides showing westwards migration of the deformation front: a) Oligocene; b) Early Miocene; c) Late-Early Miocene. T = Triassic evaporites acting as décollement for faults west of the Pre-Apulian Zone, J-E = Jurassic to Eocene inclusive, O = Oligocene and M = Miocene. From Clews (1989).

Present convergence is ongoing to the west offshore Zakynthos where the Pre-Apulian zone is overthrusting the Ionian Sea marine basin (Lagios et al., 2007).The Pre-Apulian Zone represents a structurally-inverted passive continental margin (for the Apulian platform) affected by foreland contraction and (outer-arc) tectonic deformation. This zone was once believed to represent the undeformed, extensional autochthonous foreland of the Hellenides with the Ionian Thrust marking the western limit of the compressional deformation (Aubouin, 1965; Jones, 1968; British Petroleum Co. Ltd., 1971; Smith and Moores, 1974). However, detailed geological

investigations conducted by Underhill (1985; 1989) across Kefalonia, Zakynthos and Lefkada proved definitively that some of the faults previously marked in published maps as extensional were, in fact, compressional and demonstrated that the Pre-Apulian Zone of these islands had experienced significant late Neogene and Quaternary crustal shortening. The locus of current deformation is believed to be the western margin of the Pre-Apulian Zone (Underhill, 1989).

1.2.2 Neotectonic Overprinting

Superimposed on this foreland propagating fold-and-thrust system was neotectonic deformation due to continued south-westwards motion of the Aegean in response to the westwards moving Anatolia and onset of subduction along the Hellenic Trench (Le Pichon and Angelier, 1979; 1981) (Figure 1.19). The exact timing onset of subduction along the Hellenic trench (i.e. when oceanic lithosphere was first overridden by continental crust) is a matter for debate since subduction appears to have initiated at different times along its length. The crustal loading and resulting lithospheric down-bending caused by the piling up of the Hellenide thrust sheets is believed to have initiated subduction in the Late Miocene south of Crete and in the southern Ionian Sea approximately 10-15 Ma after it had begun in Crete when the Pre-Apulian zone overrode oceanic crust (Underhill, 1989). The subduction zone may initially have been located in the outer Ionian zone but jumped to the present position at the western margin of the Pre-Apulian Zone during the Early Pliocene due to difficulties subducting the quasi-continental crust (Underhill, 1989; Crew, 1989).

The initiation of subduction led to the establishment of an island-arc (Northern Greece volcanoes, Turkey volcanoes). Establishment of an inner island-arc has caused back-arc extension behind the island-arc and the creation of a marginal sea (Aegean Sea) (Le Pichon and Angelier, 1979, 1981; Ninkovich and Hays, 1972; McKenzie, 1972, 1978; Fytikas et al., 1976, 1984; Innocenti et al., 1981, 1982; Underhill, 1989). Southern migration of the subduction zone due to "roll-back" motion (as oceanic crust to the south-west is easier to subduct than continental crust) has led to the development of a new, active, island arc (the South Aegean Volcanic

Arc) containing volcanic islands like Santorini (Ninkovich and Hays, 1972; Fytikas et al., 1976; 1984; Innocenti et al., 1981; 1982). Fore-arc scraping above the subduction zone has created an accretionary shield complex (Mediterranean Ridge) which takes the form of a broad bathymetric high between the deeper waters of the Hellenic Trench and the Ionian Abyssal Plain and compressional deformation and low-angle thrust faults dominate here (Kokinou et al., 2006). From Zakynthos to Crete these faults strike NW-SE and dip NE and from Crete to Rhodes they strike WNW-ESE and dip NNE (Papazachos, 1996; Underhill, 1989; Kokinou et al., 2006). The northern boundary of the Mediterranean Ridge is defined from the trench by a series of backstop wedge backthrusts (Chamot-Rooke et al., 2005).

While the Hellenide deformation generally behaves as a foreland propagating fold-and-thrust system where the deformation front migrations into undeformed rock (Butler, 1982; Boyer and Elliott, 1982), deviations from the this model occur in the form of Plio-Quaternary out-of-sequence thrust movements and reactivation of thrust faults (Eisenstadt and De Paor, 1987; Underhill, 1989). This may have been triggered and exenterated by the Hellenic subduction neotectonism (Underhill, 1989)

The Ionian Islands, located in the compressional outer-arc, experience clockwise rotation in response to this subduction roll-back and expulsion of the Aegean region (Lagios et al., 2007). Compressional deformation dominates within the outer arc zone, separated from the extensional region of the inner island-arc by a zone of aseismicity (Underhill, 1989). The KTF is believed to have formed to accommodate the clockwise rotation experienced by this part of the outer-arc as constraint on movement to the NW and the re-establishment of NE-SW compression in western Greece resulted in only the southern margin of the region being free to move westwards as it was bounded by denser oceanic crust which was more easily overridden than the continental crust occurring to the north (Underhill, 1989).

This tectonic setting has led to the Ionian Islands, occurring in the transitional zone between active subduction in the southwest and continental collision in the north, experiencing the highest shallow seismicity in Europe with over 50 large (magnitude

5.0 and greater) earthquakes occurring over the last ~100 years, six of those being significant events (magnitude 6.3 or greater) (Papazachos and Papazachou, 1989; Papazachos, 1990; Papazachos and Papazachou, 1997). The last strong earthquake (magnitude 6.3) occurred on 14 August, 2003 along the Lefkada segment of the KTF and which affected much of the Lefkada island municipality (EERI Special Earthquake Report, 2003; Papathanassiou et al., 2005).

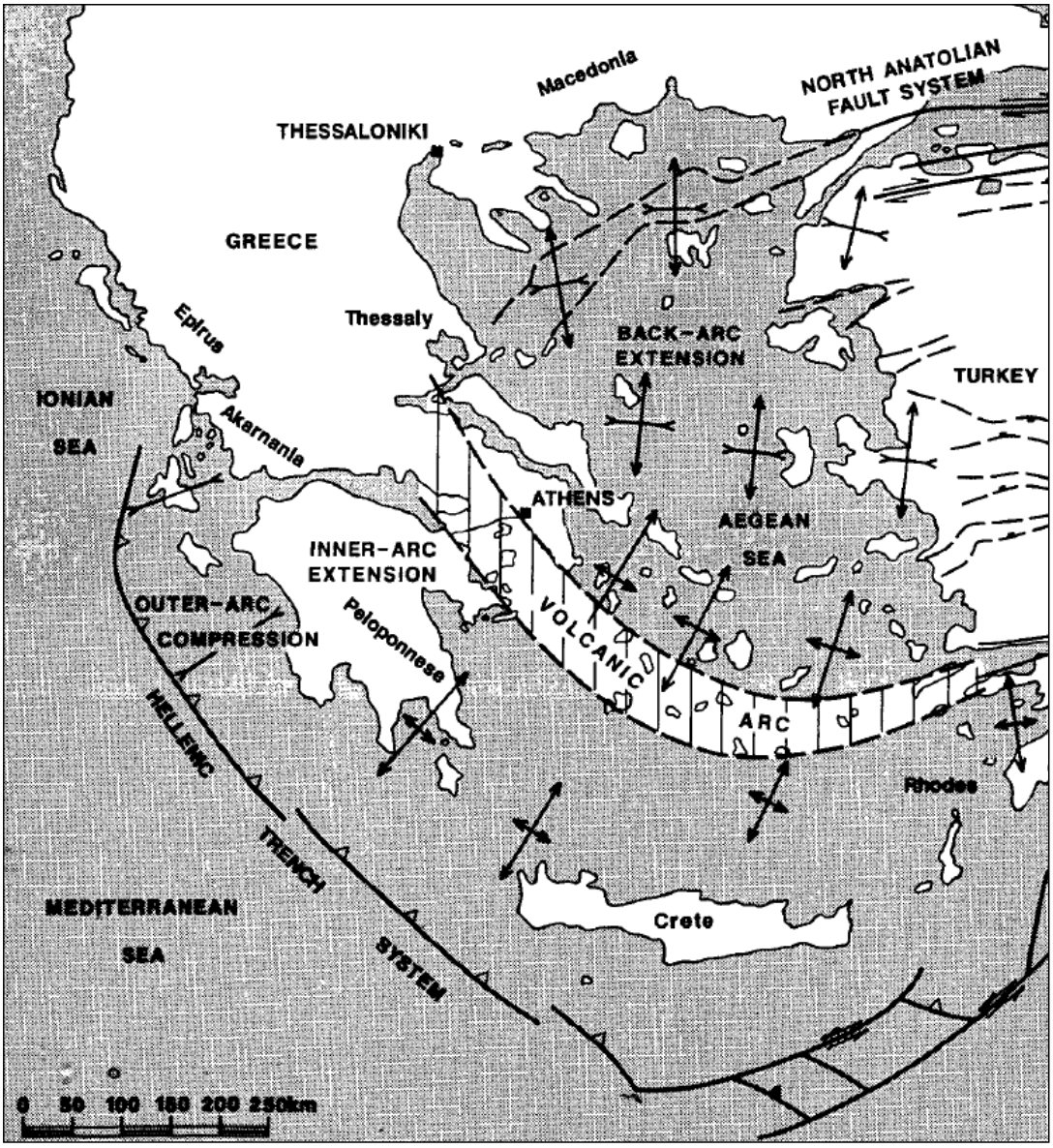

Figure 1.19 Neotectonic setting of the Aegean domain showing the configuration of island-arcs which have led to the development of back-arc extension and formation of a marginal sea (Aegean Sea) while compressional tectonics occur in the outer-arc. From Underhill (1989).

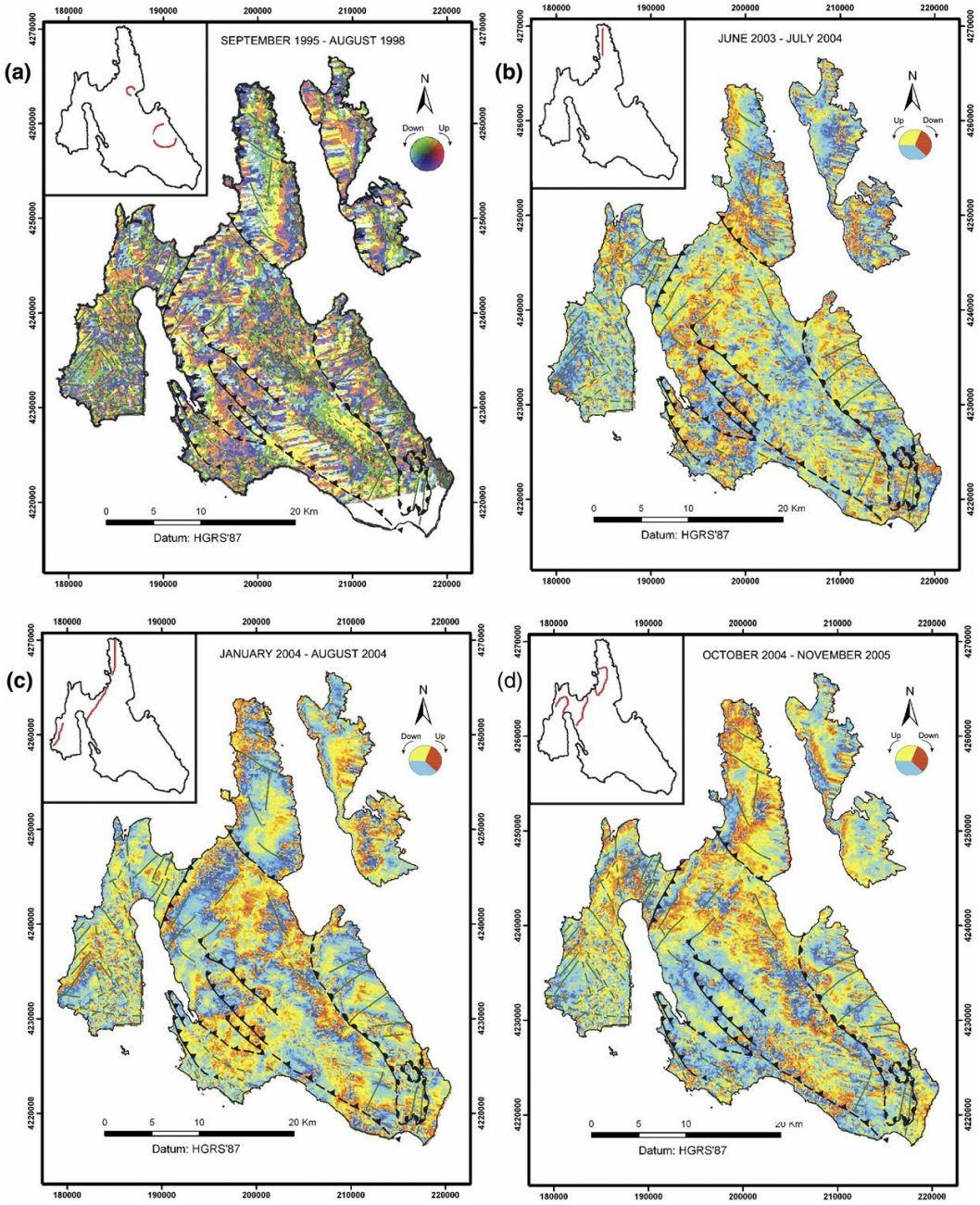

Figure 1.20 DInSAR images of Kefalonia Island for the periods: (a) Sept. 1995 to Aug. 1998; (b) June 2003 to July 2004; (c) Jan. 2004 to Aug. 2004; (d) Oct. 2004 to Nov. 2005. Insets indicate position of fringes. From Lagios et al. (2007).

Detailed short-term studies of land movement by Lagios et al. (2007) using data gathered from Differential Global Positioning (DGPS) stations and Differential Interferometric Synthetic Aperture Radar (DInSAR) demonstrated that Kefalonia experiences complicated small-scale (millimetres) vertical and horizontal

displacement from year to year (Figure 1.20). Between 1995 and 2006 Kefalonia underwent several phases of differential uplift totalling around 20 cm, focused in the northern and western parts of the island. Analyses which ran from 2003 to 2004, a period which covered the Lefkada Earthquake of 14 August 2003, showed that the northern part of the island experienced 28 mm of uplift possibly in relation to this earthquake event. As well as vertical uplift, DGPS revealed that from 2001 to 2006 the island underwent clockwise rotation relative to a centrally located station on Mt Ainos with a horizontal component of 6 to 34 mm and a vertical component of 50 mm focused on Paliki (Figure 1.21).

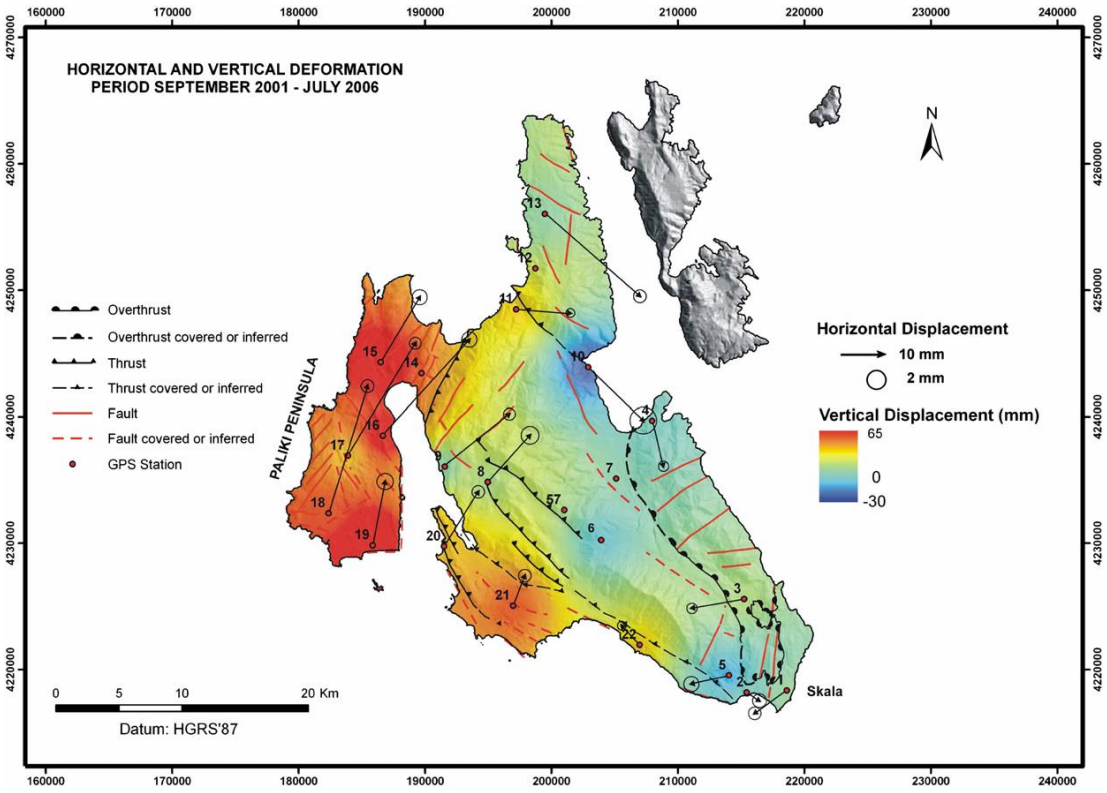

Figure 1.21 Vertical and horizontal deformation of Kefalonia deduced from DGPS measurements for the total period 2001 to 2006, relative to station No. 06 (Mt. Ainos). From Lagios et al. (2007).

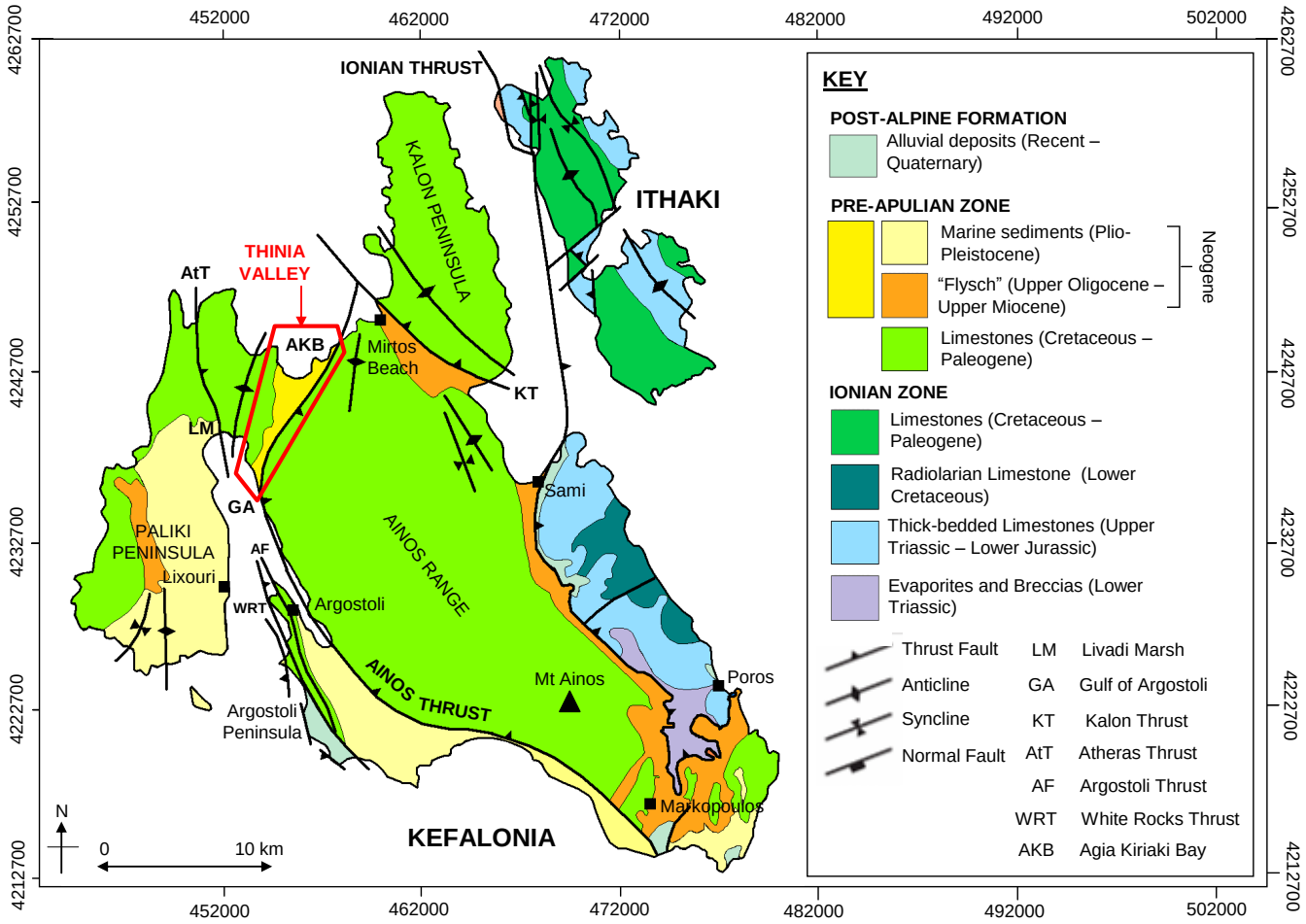

Figure 1.22 Sketch showing the Pre-Apulian and Ionian stratigraphy of Kefalonia and Ithaki. Thinia valley is outlined by the red polygon. Modified from Lagio et al. (2007) and Underhill (2009).

Figure 1.23 The Ionian Thrust viewed from Poros bringing Jurassic limestone over Triassic evaporates and Miocene marl. Photo credits: J. Underhill.

1.2.3 Kefalonia

The majority of Kefalonia lies within the Pre-Apulian or Paxos Zone, the outermost isopic zone of the Hellenide thrust belt. In the south-eastern part of the island the Ionian thrust sheet emplaces Ionian Zone sediments over the Pre-Apulian stratigraphy (Figure 1.22). The western boundary of the Ionian Zone is defined by the Ionian Thrust, a major sub-horizontal thrust which forms a distinct scarp in south-eastern Kefalonia bringing Mesozoic carbonates and sheared Triassic evaporites onto easily-eroded Miocene marls (Sorel, 1976; Underhill, 1989) (Figure 1.23). The Triassic stratigraphy, which dies out in the Pre-Apulian zone, served a crucial role during the Hellenide compression acting as a décollement horizon for thrust faulting (Underhill, 1988; Clews, 1989).

A possible zone of décollement can be observed along the in the form of a complex series of sheared very dark Triassic evaporites separating the Jurassic carbonates

from the Miocene marl (Underhill, 1989). This thrust represents a major reactivation of a normal fault that separated the deep water "basinal" facies of the Ionian Zone and shallow water "platform" facies of the Pre-Apulian Zone (Underhill, 1989). The Ionian Thrust follows a "ramp-and-flat", staircase geometry (Figure 1.24) with a well-defined, northward-plunging hanging-wall anticline paralleling the thrust fault trace (Boyer and Elliot, 1982; Suppe, 1983; Underhill, 1989).

Pre-Apulian Kefalonia is predominately composed of Hellenide (Alpine) Mesozoic and Cenozoic sedimentary rocks. The stratigraphy consists of a thick succession of Upper Cretaceous to Paleogene carbonates overlain by folded Oligocene to earliest Tortonian deep-marine "flysch" marls and interbedded turbiditic calcareous sandstones (British Petroleum Co. Ltd., 1971; Mercier et al., 1972). These are unconformably overlain by Plio-Quaternary sediments which are particularly prevalent around southern Paliki and Argostoli Peninsula. The Pre-Apulian stratigraphy of Kefalonia is dissected by five major easterly-dipping thrust faults (from east to west): Kalon, Ainos, Argostoli, White Rocks and Atheras Thrust (Underhill, 2006). These thrust faults divide Kefalonia into four sections: Erissos (Kalon) Peninsula (northern), Paliki peninsula (western), the Ainos block (central and western) and the Argostoli block (southern western).

Western Kefalonia is defined as the area lying to the west of the Ainos Thrust (Figure 1.25). The Ainos Thrust ascribes a ~40 km arc which runs from Agia Kiriaki Bay to Markopoulos bounding the western margin of the Ainos Range and emplaces deep marine Cretaceous and Paleogene limestones over Mio-Pliocene marls (Underhill, 1989; 2006; 2008; 2009). The Ainos Range is a major west-verging, asymmetric, NW-SE to N-S trending anticline which can be traced for around 20 km running from Mirtos Bay in the north to Markopoulos in the southeast (Underhill, 1989). This thrust runs along the eastern side of Thinia and the Gulf of Argostoli where it was visible in places at the shoreline (Figure 1.26, A).

Three major thrust faults ran to the west of the Ainos Thrust: the Atheras Thrust (which ran from Atheras Bay to Livadi Marsh and two thrusts (the Argostoli Fault

and White Rocks Thrust) which ran along the Argostoli Peninsula. The Atheras Thrust was formed during the Late Quaternary (Sorel, 1976) and emplaces Paleogene limestone over Miocene marl (Figure 1.26, B). Formation of a hangingwall anticline and "flat-ramp" geometry can be seen above Livadi Marsh (Figure 1.27, A and B). The hangingwall also contains numerous small-scale normal faults (Figure 1.27, C). Without better exposures or subsurface data it is not clear where the Atheras Thrust goes after reaching Livadi Marsh. There is a conspicuous gap between where the Atheras Thrust reaches the marsh and where the visible hangingwall stands and the vertically-tilted beds which should appear above the fault plane are absent.

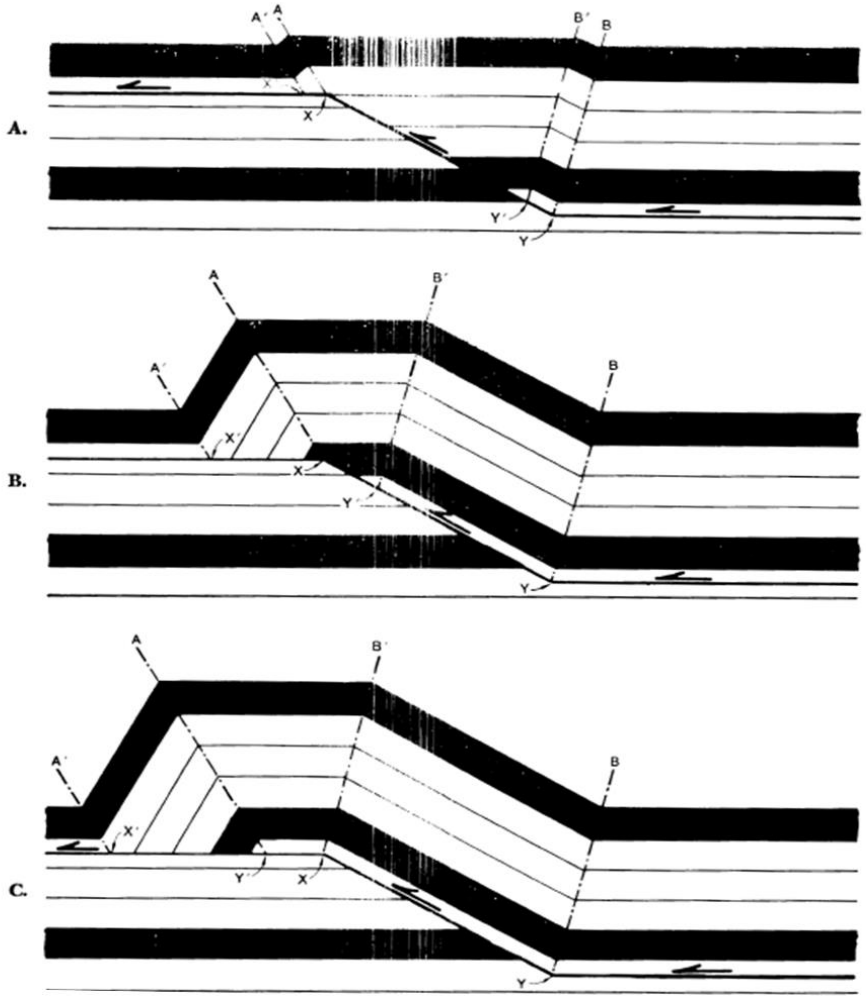

Figure 1.24 Series of sketches showing the kinematic development of fault-bends folds in response to a simple step in décollement illustrating the process which may have resulted in the ramp-flat geometry observed in the Ionian Thrust hangingwall (after Suppe and Namson, 1979; Suppe, 1983).

A. Argostoli Peninsula

The southern part of the Gulf of Argostoli is split into two by the NNW-SSE trending Argostoli Peninsula. The geology and topography of the peninsula is affected by at two major NW-SE striking thrust faults: the White Rocks Thrust (WRT) and the Argostoli Fault formed through structural inversion (Underhill, 1989; Sorel, 1976). The Argostoli fault enters the Gulf at the tip of the Argostoli peninsula while the WRT enters the Gulf earlier at the coastline at Lassi. These faults bring a wedge of Cretaceous limestone over Plio-Calabrian (Lower Pleistocene) rotated downlapping fan delta sediments. This fault appears to have formed as an easterly-dipping, extensional growth fault, initiated in the Mesozoic and reactivated in the late Miocene in response to lithospheric down-bending associated with initiation of subduction along the Hellenic trench (Underhill, 1989).

This fault acted as an olistolith source for the adjacent sub-basin (Mercier et al., 1976; Sorel, 1976; Underhill, 1985). An early Pliocene angular unconformity separating the Miocene sequences from gently-dipping middle Pliocene delta-fan sequences occurs within the hangingwall of this fault representing the resulting uplift and tilting of this area due to emplacement of the Ionian Thrust (Underhill, 1989). Significant exposures of Messinian age also occur within the hangingwall of this fault at Cape Liakka. Onlapping sequences indicate thrust reactivation occurred after the Calabrian (0.78 Ma) (Underhill, 1989).

The WRT forms an easterly-dipping, low-angle, reverse fault which runs sub-parallel to the west of the Argostoli Fault and brings Cretaceous and Palaeogene limestones over Plio-Pleistocene sediments Underhill (1989). The position of the WRT relative to the Argostoli fault and apparent lack of synsedimentary movement on it suggests the WRT developed as a consequence of thrust splay in the footwall to the reactivated Argostoli fault (Underhill, 1989).

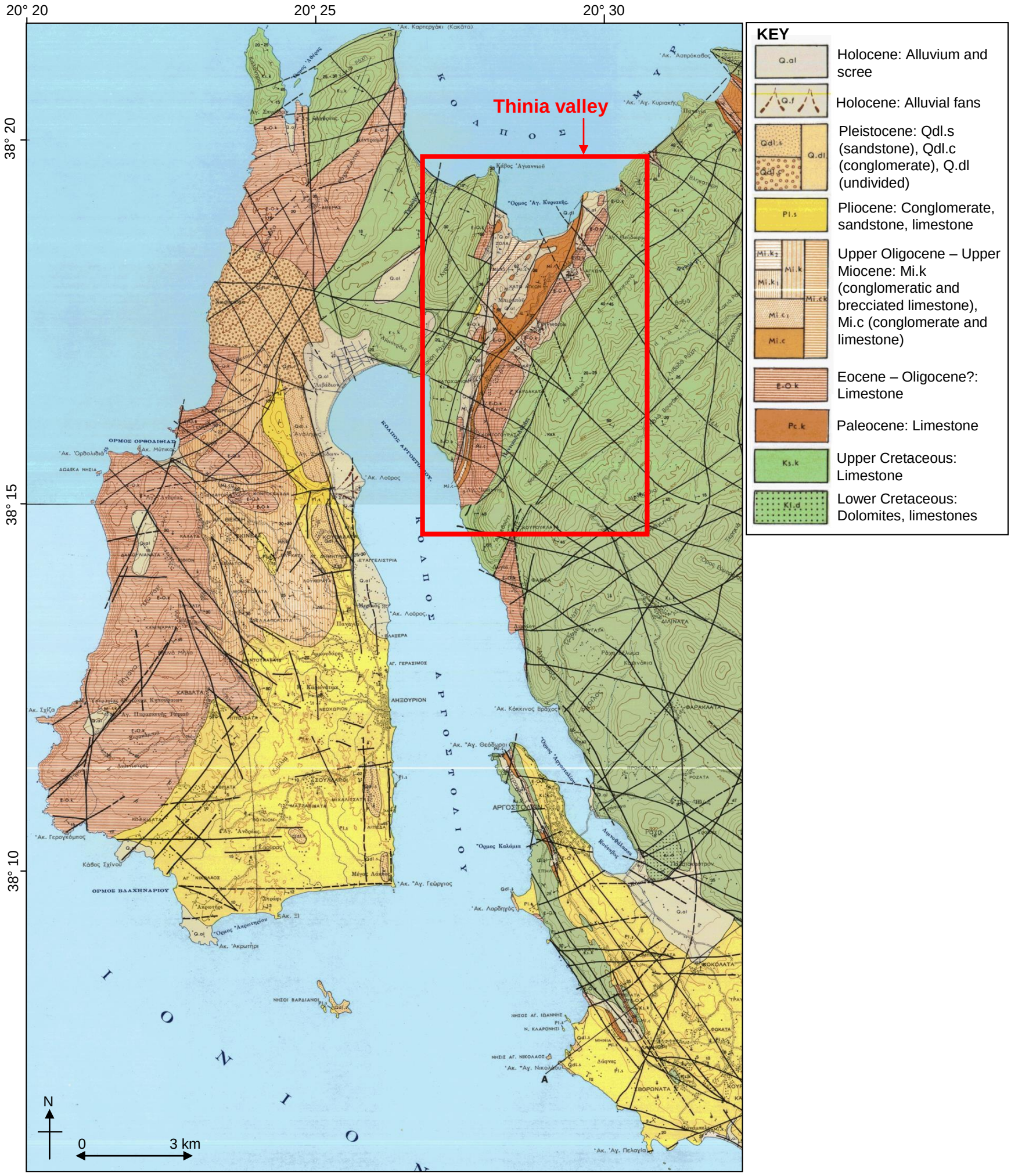

Figure 1.25 Geological map produced by British Petroleum Co. Ltd et al. (1985) and the Institute of Geological and Mineral Exploration (IGME) showing the main stratigraphic boundaries of Western Kefalonia and possible fault interpretations.

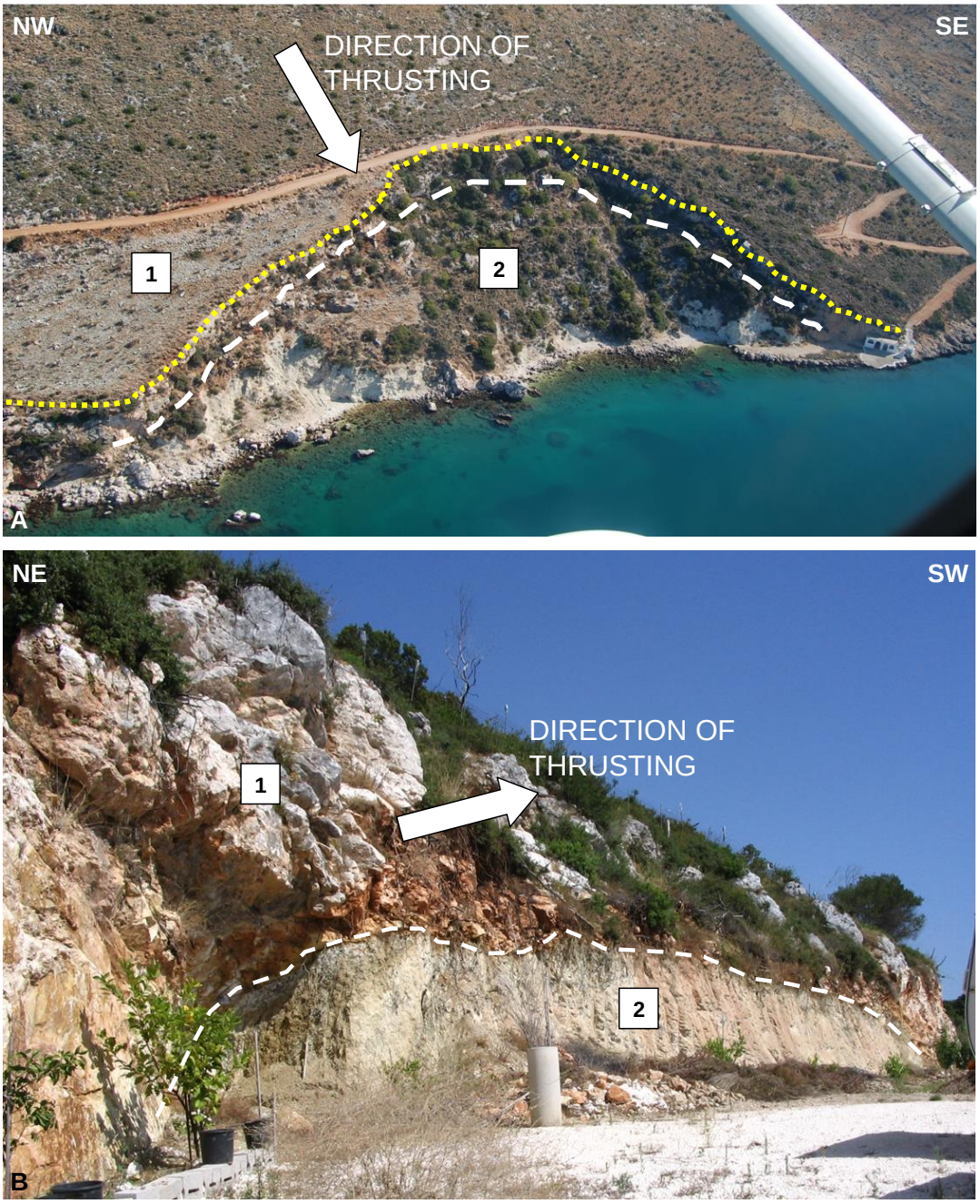

Figure 1.26 Thrust-faulting of Western Kefalonia: A. The Ainos Thrust (fault plane indicated by a white dashed line) between limestone (1) and marl (2) is visible here due to an old fan-shaped collapse (yellow dotted line). Otherwise it runs below or close to the shoreline down the eastern coast of the Gulf of Argostoli; B. The Atheras Thrust (white dashed line) emplacing Paleogene limestone (1) onto Miocene marl (2).

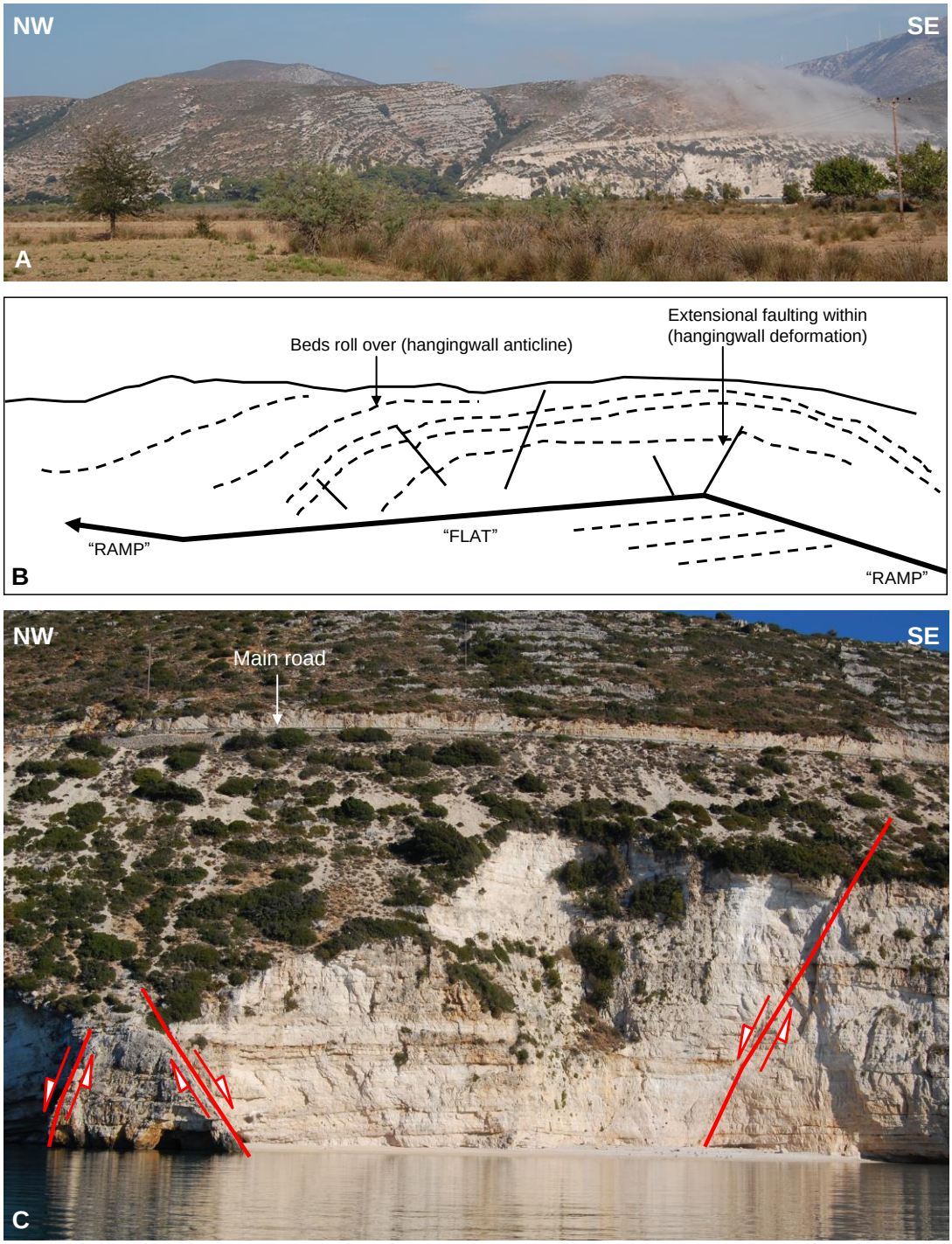

Figure 1.27 Hangingwall deformation within the Atheras Thrust: A. Formation of a roll-over anticline within the visible portion of the thrust hangingwall to the east of Livadi Marsh; B. Interpretation of A in terms of "flat-ramp" geometry; C. Close-up of normal faulting within the deformed hangingwall.

The cross-bedded Calabrian and Plio-Pleistocene sediments within the footwall of this thrust are orange in colour, sandy and tilted to vertical and locally overturned and contain complex micro-faulting and bedding-parallel slip indicating they have been strongly deformed by the local thrust faults (Figure 1.28, A). The presence of a gently-dipping "Paleomilazzien" (roughly equivalent to the onset of the Mindel-Riss interglacial, 300 to 380 ka) raised beach unconformably overlying these overturned sediments suggests that fault movement along the White Rocks Thrust can be dated to between ~1 Ma and ~500 ka (Sorel, 1976; Bousquet et al., 1976).

Both faults can be traced southwards to the a branch point where the displacement associated with the faults dies out leaving a southwest-verging anticline along the trace of the Argostoli fault and a west-verging fold along that of the WRT (Underhill, 1989). Underhill (1989) observed numerous examples of post-Paleomilazzien (after 450 000 BP) shortening to the west of the White Rocks Thrust in the form of steep, SW-dipping backthrusts thrusting Eocene limestone and Plio-Quaternary sediments over raised beach deposits. A notable example is the Cape Lardigos backthrust in which dark brown upper Calabrian cross-sets overthrust the Paleomilazzien raised beach sediments which, in turn, unconformably overlies lower Calabrian sediments (Sorel, 1976; Underhill (1989) (Figure 1.28, B). These backthrusts form a series of little "triangle zones", structures which typically form at the deformation front of a mountain belt by two upward-converging thrusts within the hanging wall of a thrust (Gordy et al., 1977; Butler, 1982; Jones, 1982).

B. Paliki Peninsula

The sediments of the Paliki Peninsula were composed of easterly-dipping marine Plio-Pleistocene sediments and reddish Pleistocene conglomerates and sandstones which overlay Upper Oligocene-Upper Miocene "flysch". This stratigraphy unconformably overlay Eocene limestones which defined much of the western coast. Recent alluvium deposits were prevalent along the eastern shore where streams emptying into the Gulf created alluvial fans which extended the shoreline eastwards.

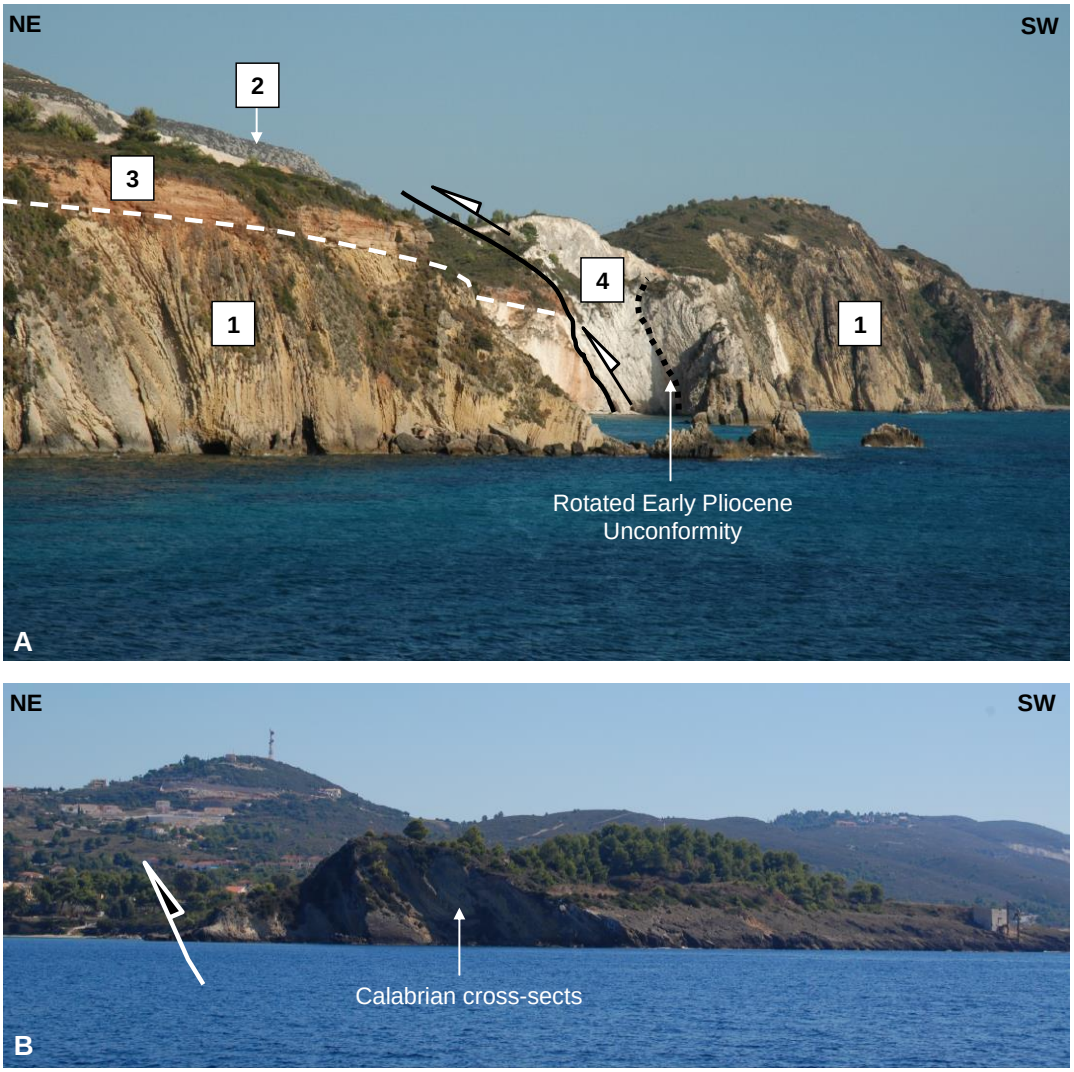

Figure 1.28 Argostoli Peninsula geology: A. The Plio-Calabrian sediments (1) on the western coast of Argostoli Peninsula which are overthrust by the White Rocks and Argostoli Thrust (2). These sediments are reddish-orange, harder and sandier and westerly-dipping. A backthrust of Paleogene limestone emplaced onto c.20 m raised beach (4) unconformably overlain by Plio-Calabrian sediments occurs within this cliff. These sediments are all overlain by a raised Paleomillazien raised beach (3) (Photo credit: J. Underhill). B. Westerly-dipping backthrust at Cape Lardigos emplacing Calabrian cross-sets over the Paleomilazzien raised beach sediments which, in turn, unconformably overlies lower Calabrian sediments (Sorel, 1976; Underhill, 1989).

Figure 1.29 Plio-Quaternary "badlands" which cover the south-eastern part of the Peninsula. Facies change from the fine-grained pale silty sediments (1) to the harder, red sediments (2) of equivalent age observed along the western coast of Argostoli Peninsula. 3) Beach rocks representing submerged ancient shorelines.

The Plio-Quaternary hills (Figure 1.29, 1) were eroded at the top suggesting marine immersion during the Pliocene and Calabrian (Sorel, 1976). The sediments are a similar age to those in Figure 1.28 but are finer-grained and paler implying a facies change occurs somewhere between the two peninsulas. At the south-eastern tip of the peninsula the beginning of this change may occur where reddish sandier sediment begins to intercalate with the paler sediment (Figure 1.29, 2).

There is some evidence of folding within the sediments of Paliki Peninsula (Underhill, 1989) which dates to the Hellenide deformation however the most striking deformation occurs in the form of numerous NNE-SSW to NE-SW striking normal faults which dissect the Eocene and Miocene stratigraphy of the western coast of Paliki. In Northern Paliki (Atheras Bay) these normal faults orientate more towards the NE-SW and dipped both NW and SE (Figure 1.30). These faults do not extend as far as the Thinia valley. These features appear in some locations to offset the Atheras Thrust indicating they post-dated this Late Quaternary thrust. This

suggests they may have formed to accommodate movement along the Kefalonia Transform Fault or due to late-stage activity of pre-existing Hellenide structures.

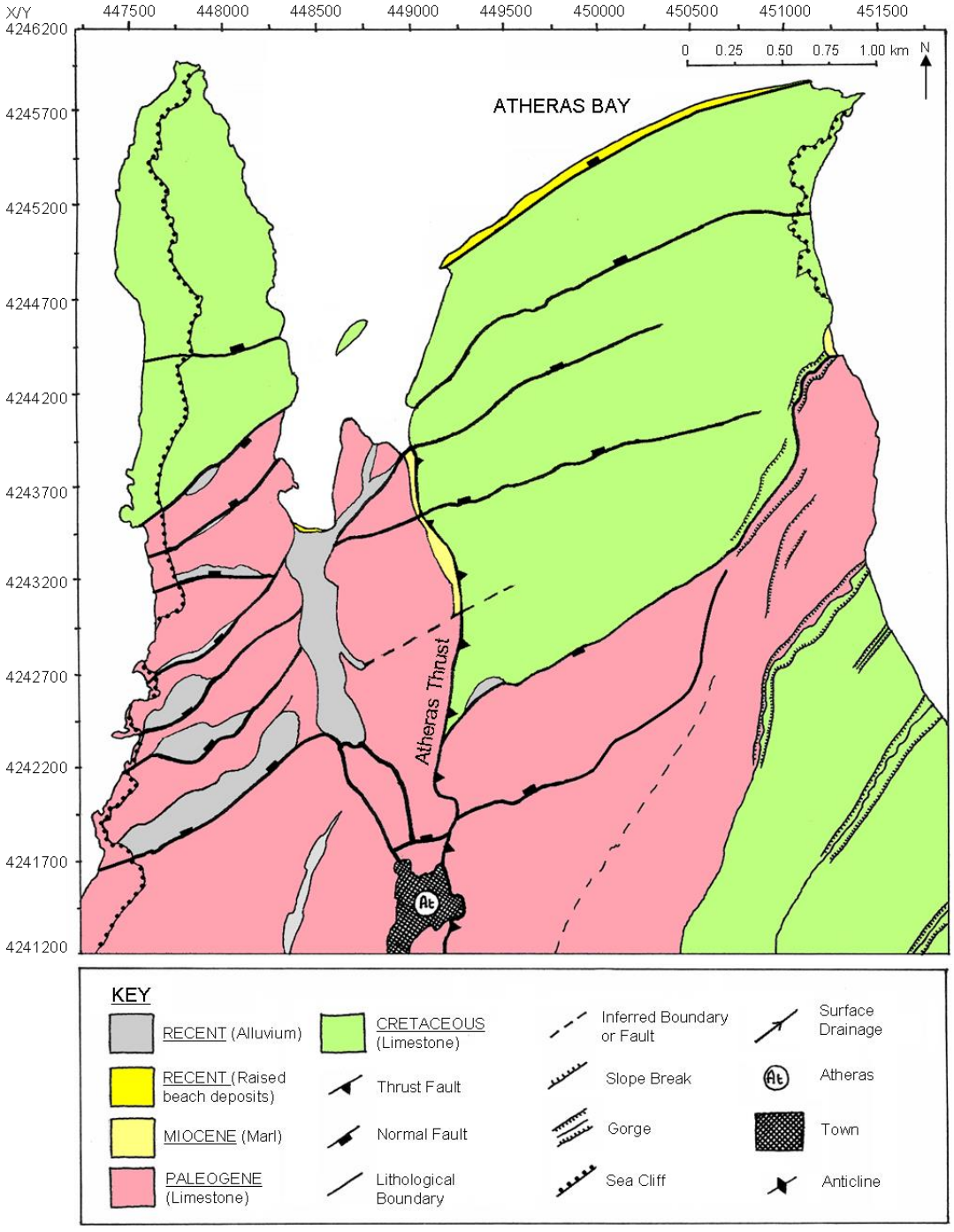

Figure 1.30 Geological sketch map of Atheras Bay showing the numerous NE and SW dipping normal faults cross-cutting the Atheras Thrust (based on map by British Petroleum Co. Ltd et al. (1985) and the Institute of Geological and Mineral Exploration (IGME), Figure 1.25).

C. Thinia Valley

The topography of the Thinia land-bridge can be separated into two parts: a c. 4 km long, NNE-SSW striking asymmetric northern valley and a shorter (c. 2.2 km) topographically-dramatic southern end separated by a high elevation central flattish "saddle" region surrounded by limestone hills (Figure 1.31). Figure 1.32 presents a north-south topographic profile along the valley axis. The highest part of the valley coincides with a small limestone quarry (Petrikata Quarry). At 195 to 210 m elevation, this outcrop acted as watershed for the two deeply-incised drainage systems: one draining SW to NE into Agia Kiriaki Bay and one draining southwards NE to SW into the Gulf of Argostoli.

The northern part of Thinia is visually the most convincing for the existence of "Strabo's Channel" given its deeply-incised valley morphology (Figure 1.33, A). The orientation of this valley appeared to be controlled by the presence of a large, easterly-dipping NNE-SSW striking normal fault and anticlinal axis defining the western valley side in the northern half of the valley. The mouth of the valley is flat-bottomed and very low elevation (1 to 2 m above sea level) and alluvium-filled suggesting it may have formed a shallow marine inlet during the late Holocene (Figure 1.33, B). The topography to the east of this stream is composed of low elevation hills which are sharply-incised by seasonally active streams which drain from the steep west-facing slope of Imerovigli (Figure 1.34, A).

The morphology of the high elevation central saddle region meant it was much less easy to visualise a marine-level channel in this part of the valley. The region was characterised by a flattish, elliptical area (around 36 000 m^2) of heavily-farmed alluvium surrounded by steep, high elevation hills (Figure 1.34, B, and 1.35). This area was believed to have once enclosed a small, freshwater lake dubbed "Lake Katachori" which has since drained or silted up. While there is no longer permanent standing water here, the site still accumulates temporary standing water during the heavy, prolonged winter rains as the clay-rich surface soils become waterlogged from the surface run-off from the surrounding hills.

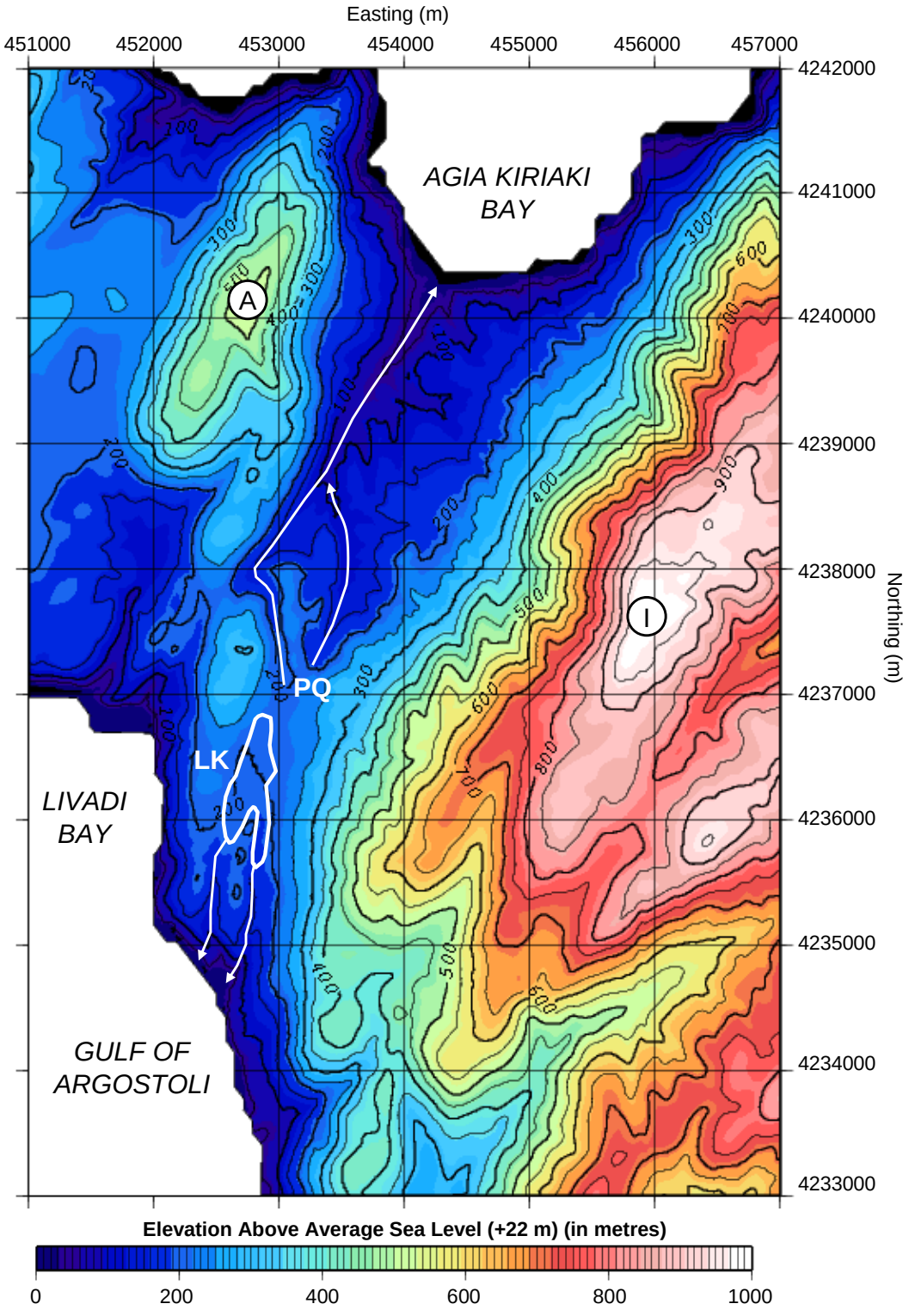

Figure 1.31 Topographic map of Thinia indicating the contrast between the high topography defining the eastern side of the valley associated with the Imerovigli (I) and Agrilias (A) mountains and the predominately low elevation valley, dominated by NNE-SSW trending drainage patterns. LK = Lake Katachori, PQ = Petrikata Quarry. The resolution of this digital elevation model (DEM) is 15 cm (horizontal) and 10 cm (vertical) to 2 sigma (95% confidence). DEM plotted using technique described in Section 2.6.1, B.

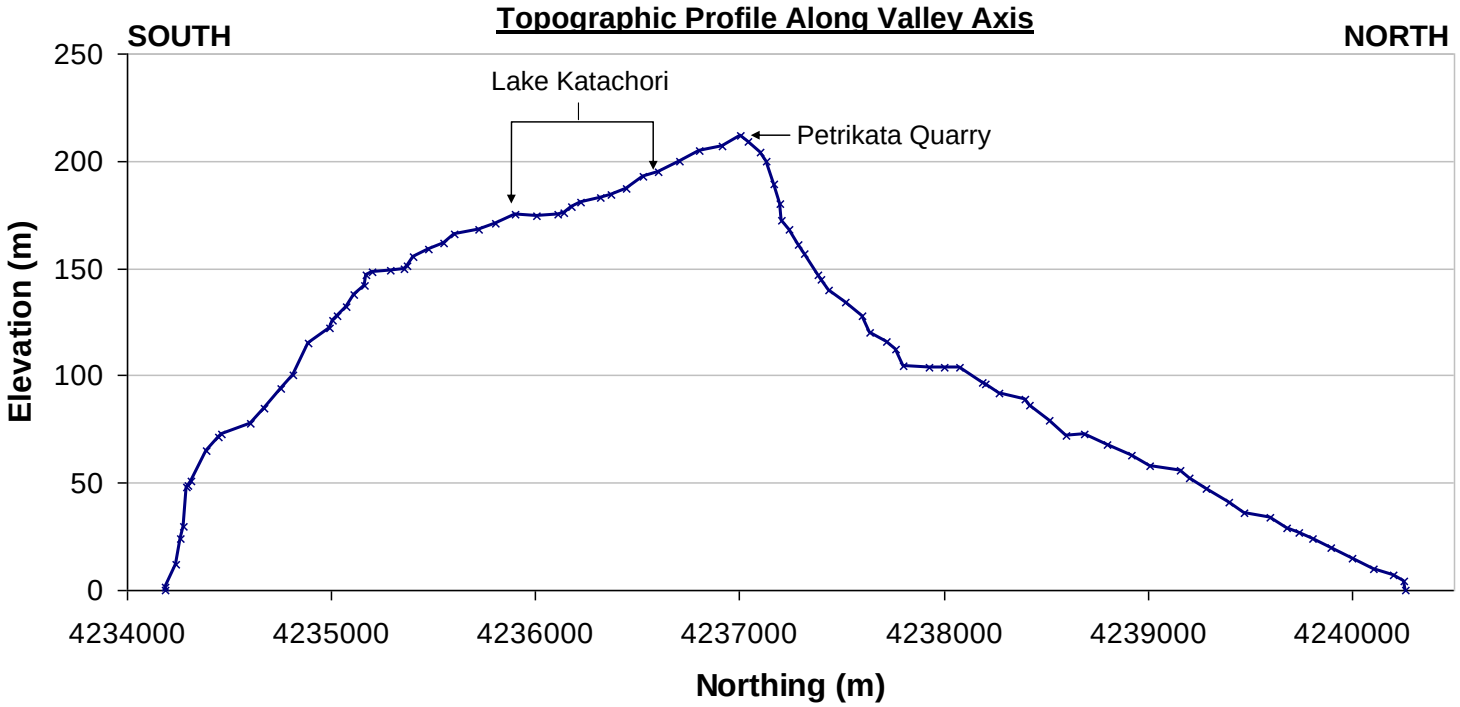

Figure 1.32 Vertically-exaggerated surface topography cross-section taken along the axis of the Thinia valley. The locations of Lake Katachori and Petrikata Quarry are indicated. A slight "kink" at the northern end of the cross-section indicates the 6 m beach terrace which occurs at Agia Kiriaki Bay. The 1.2 m terrace at the southern end of the cross-section is too small to be resolved at this scale.

Figure 1.33 The valley morphology of northern Thinia: A. The asymmetric, NNE-SSW striking northern valley viewed from the raised saddle region (taken beside the church of Petrikata village); B. The flat valley exit below Zola.

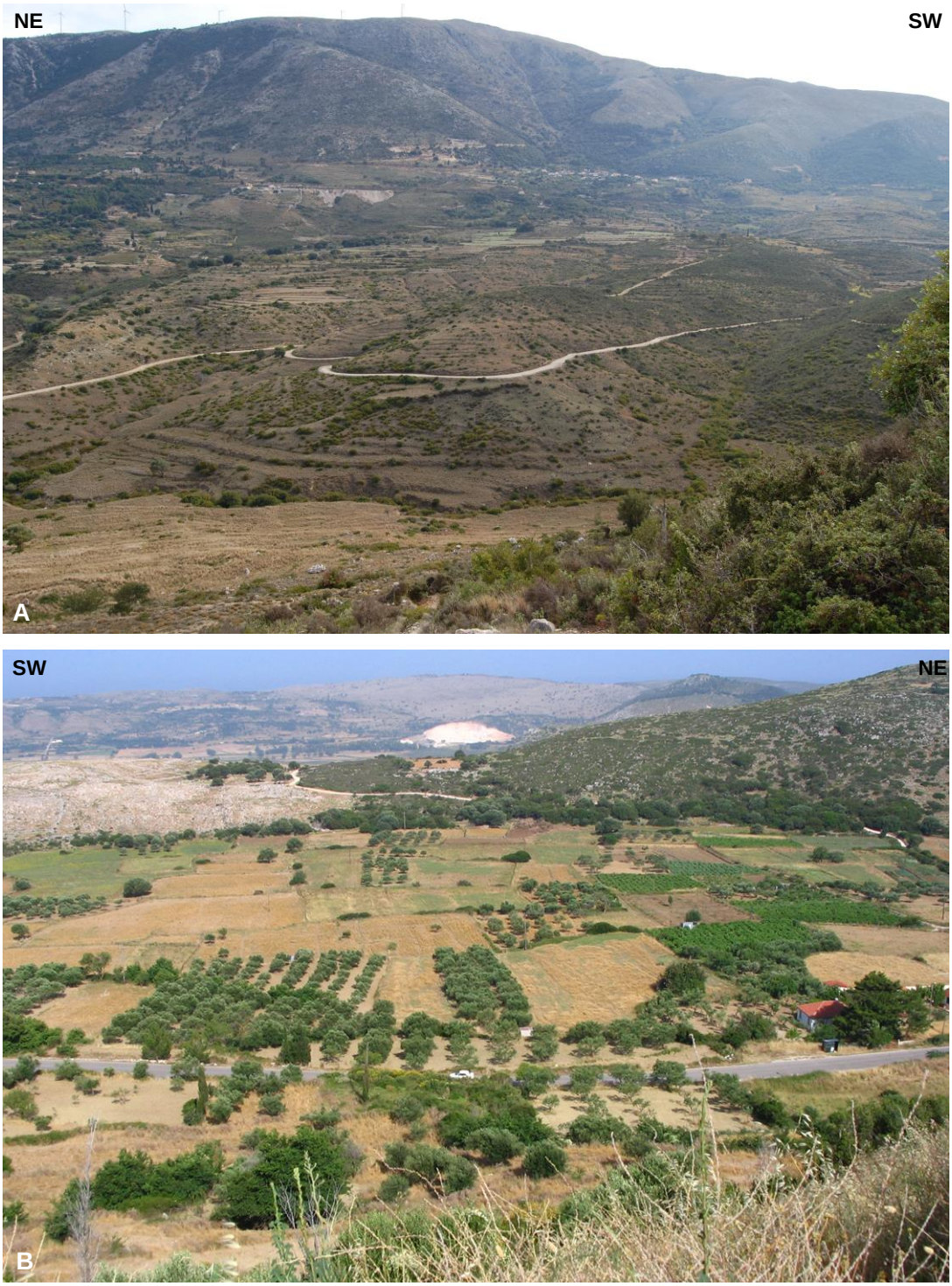

Figure 1.34 View from Zola looking eastwards towards the stream-incised foothills of Imerovigli (A); The suspected paleo-lake Lake Katachori which occupies the flat central saddle region (B). The location of the lake is indicated in Figure 1.31.

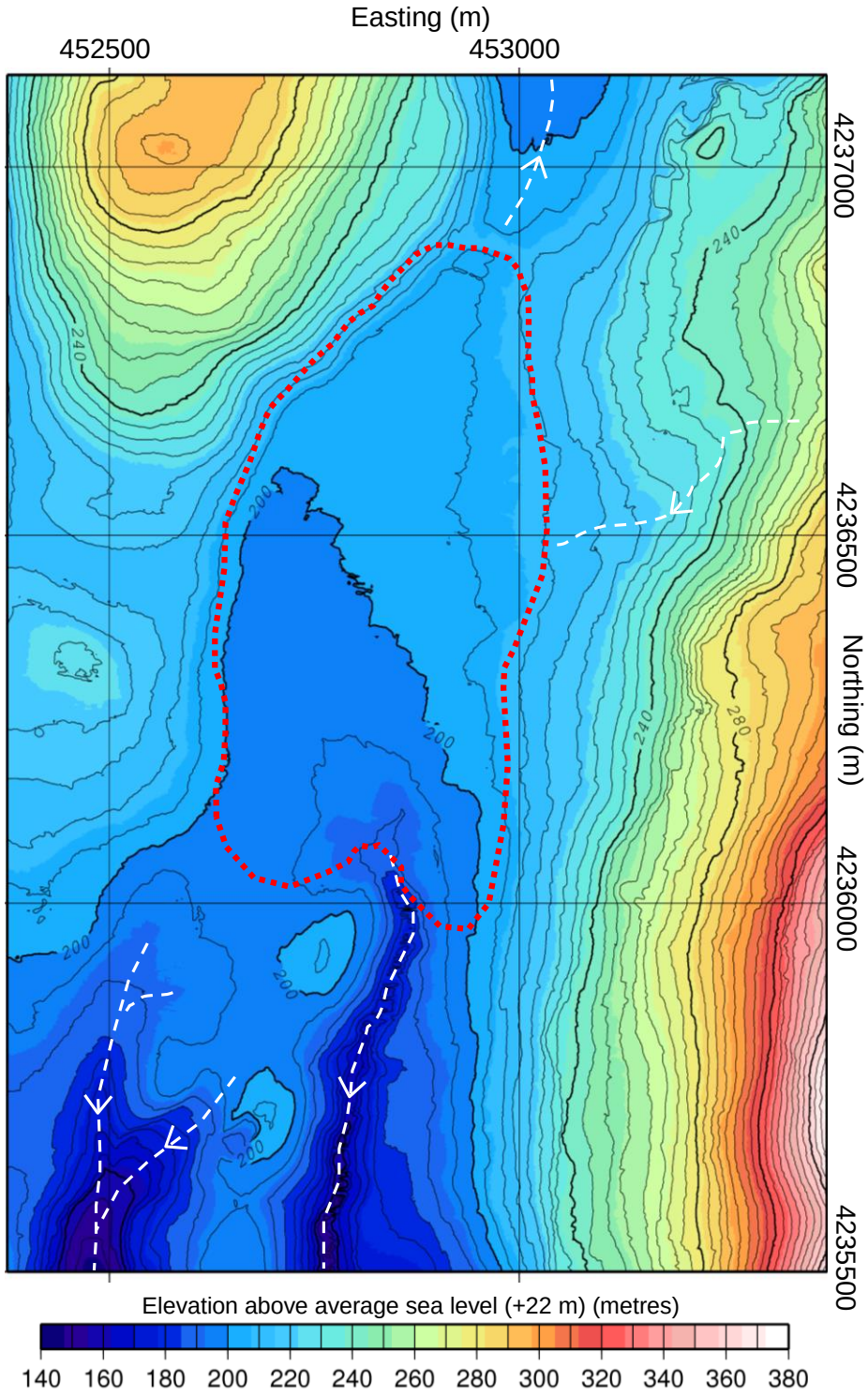

Figure 1.35 Topographic map of Lake Katachori (proposed boundaries of the lake are outlined with a red dotted line). The lake occupies a flat basin surrounded by steep, high elevation limestone hills prone to water-logging in the rainy months as it serves as a focus for drainage from these mountains. The map shows that the key drainage (white dashed lines) direction is southwards. Location of Lake Katachori relative to the rest of the valley is indicated in Figure 1.31. The resolution of this digital elevation model (DEM) is 15 cm (horizontal) and 10 cm (vertical) to 2 sigma (95% confidence). DEM plotted using technique described in Section 2.6.1, B.

Figure 1.36 Southern Thinia: A. Boulder-strewn slopes of southern Thinia (red and white truck in centre of photograph for scale); B. Very large limestone breccia boulder with author for scale.

The southern part of Thinia was deeply-incised by two SW-draining stream gullies which formed deeply incised ravines around 60 to 70 m deep creating three ridges

and the steep slopes which were extensively scattered with landslide debris (Figure 1.36, A). The shoreline itself was defined by a high (70 to 100 m) vertiginous sea cliff so it was far less easy to visualise the course of a marine-level channel given its high elevation above present sea level. Some of the clasts were very large (lorry-sized) including the remains of buildings which had been transported down the slope during landslide activity (Figure 1.36, B). The paucity of vegetation on this slope suggested slope collapses were frequent.

The surface geology map produced by J. Underhill in Bittlestone et al. (2005) (Figure 1.37) showed that Thinia could be resolved into two parts: an easterly-dipping sequence of folded and locally faulted shallow marine Paleogene-Cretaceous limestones onlapped by Neogene marls (Accordi et al., 1998) and a westerly-dipping succession of deeper marine Paleogene-Cretaceous limestones emplaced upon this succession by the Ainos Thrust (Bizon, 1967) (Figure 1.38).

The steep (45 to 60°) westerly-dip of the limestones within the hangingwall of the thrust occurred at the western limb of a major hangingwall anticline established above the Ainos Thrust (Underhill, 2006). This configuration of deep water limestones emplaced upon shallow water limestones of an equivalent age indicates that, like the Ionian Thrust, the Ainos Thrust signifies a major reactivation of an easterly-dipping normal fault. The presence of slicken sides along these bedding planes caused by down-dip flexural slip (Underhill, 2006) led to the misidentification of this thrust as a extensional rather than compressional fault with a throw of more than 1500 m (British Petroleum Co. Ltd., 1971).

The geological map suggested that the valley is dominated by recent sediment deposits. These took the form of alluvium (*terra rossa*) (grey on Figure 1.37) which accumulated across the saddle region and down stream gullies and colluvial deposits (purple on Figure 1.37) which covered the eastern side of the valley. *Terra rossa* or "red earth" is the name given to the soil typically found in a Mediterranean carbonate setting and consists of clay particles and other non-soluble material left behind from the weathering of limestone (Zangger, 2001). These sediments typically accumulate

down stream gullies, within valleys or flat coastal areas. The high iron oxide content of this soil accounts for its strong brick-red colour. Such soils are generally fragile and deep deposits (metres) represent not only thousands of years of accumulation but a stable environment (Zangger, 2001).

Colluvium refers to deposits of loose sediment (of grain size ranging from clays to boulders) which have been deposited at the bottom of a low-gradient slope, axis of a valley or against a barrier on that slope usually through landsliding where it forms fan-shaped deposits (similar to alluvial fans) or a series of small hills (Madigan, 2007). Fine-grained colluvium (alluvium) can be moved downslope by means of river and stream channels to form "outfingers" (Knepper et al., 1995). Coarse colluvium (scree, talus breccias when lithified) containing angular, poorly-sorted clasts is usually indicative of having been formed through slope collapse, debris flow etc. and is generally found at the base of a cliff face or fault scarp. The geological map of Thinia suggests the landslide coverage from east to west is around 2 km, covering much of the valley floor, and is sourced from "scalloped" embayments within the west-facing slope of Imerovigli. The presence of this material makes tracing the course of the Ainos Thrust difficult.

The marls of the valley were disrupted by several prominent marl-enclosed limestone ridges trending roughly parallel to the valley axis, one of which (dubbed the "Agia Sotira" Thrust) was identified as a thrust fault emplacing limestone over the marl (Bizon, 1967; Bittlestone et al., 2005; Underhill, 2006). Its unusually steep dip (45 to 60°) had led to this fault being classed as extensional in earlier maps (e.g. British Petroleum and Co. Ltd, 1971). It is possible that some of these alluvium-enclosed limestone ridges might represent large coherent clasts derived from the steep valley sides.

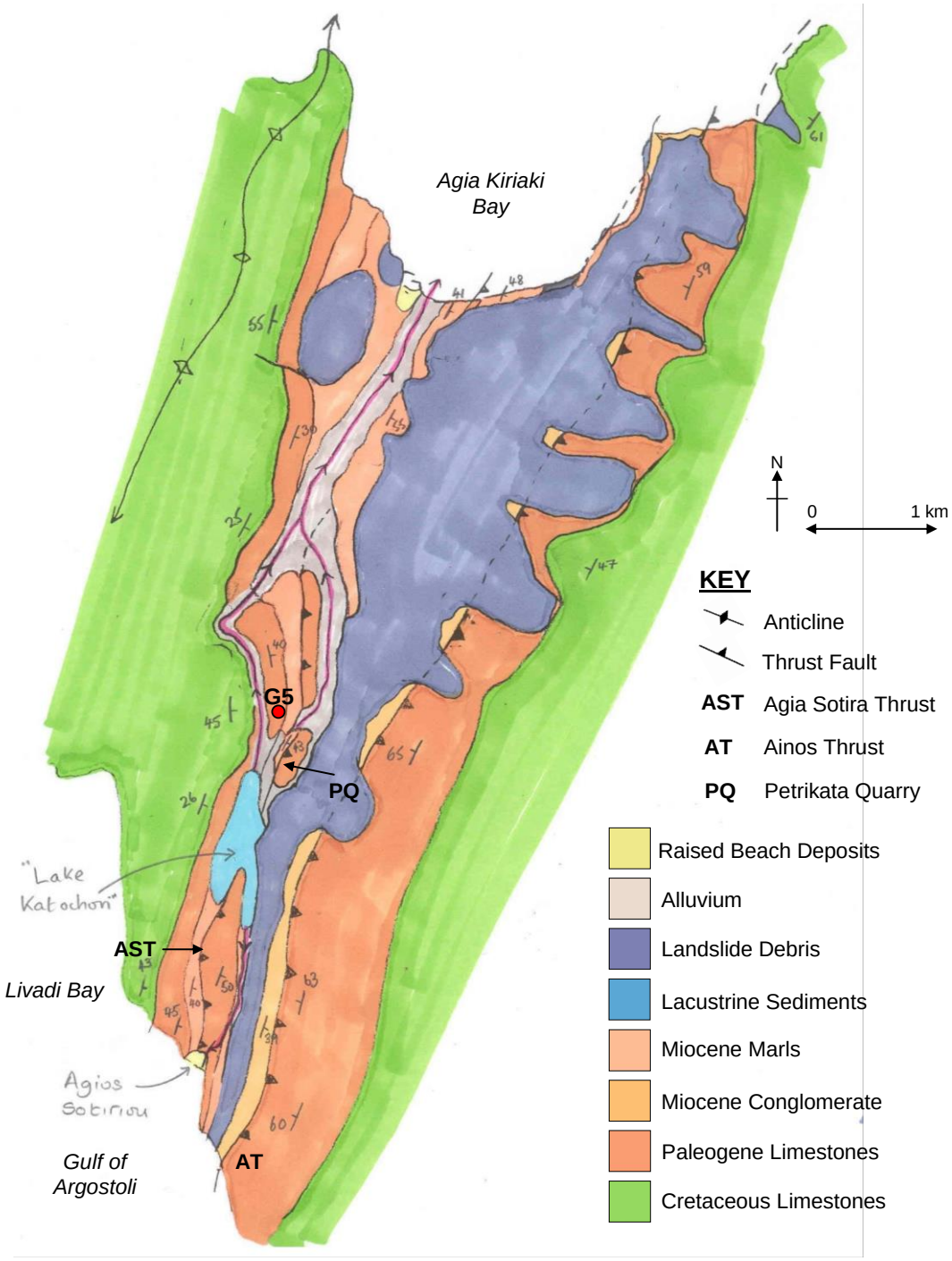

Figure 1.37 Geological map of the Thinia valley produced by J. Underhill for Bittlestone et al. (2005). Much of the eastern part of the valley and west-facing slope of Imerovigli is covered by colluvial or landslide deposits (purple). Alluvium (grey) is concentrated down the primary drainage gullies along the valley axis. Lake Katachori is indicated by the light blue area in the central saddle region. The location of the brine-bearing borehole (G5) is marked by a red circle.

Figure 1.38 A. Headland defining the eastern shore of Agia Kiriaki Bay where the Ainos Thrust (white dashed line) emplaces limestone-conglomerate (1) over marl (2). B. Ainos Thrust plane above Petrikata village. This part of the thrust experienced lateral coseismic movement of around 8 m during the 1953 earthquake destroying the old village of Petrikata which used to be situated at this location (B. credits: J. Underhill).

A study by Koumantakis and Mimides (1989) offered insight into the ancient history of Thinia. This borehole (labelled G5 in Figures 1.37 and 1.39) was drilled as part of an extensive hydro-geological research programme which began in 1985 to search for untapped aquifers to ease local water shortages. This borehole was drilled at a height of 191.62 m to a depth of 260 m into a pyramidal hill of Eocene limestone roughly 20 000 m^2 in area detached from the western valley side by Miocene marls. This apparent detachment made this hill attractive for well boring as it suggested the aquifer would also be detached from the surrounding geology, disconnected from any flushing action of the local groundwater system.

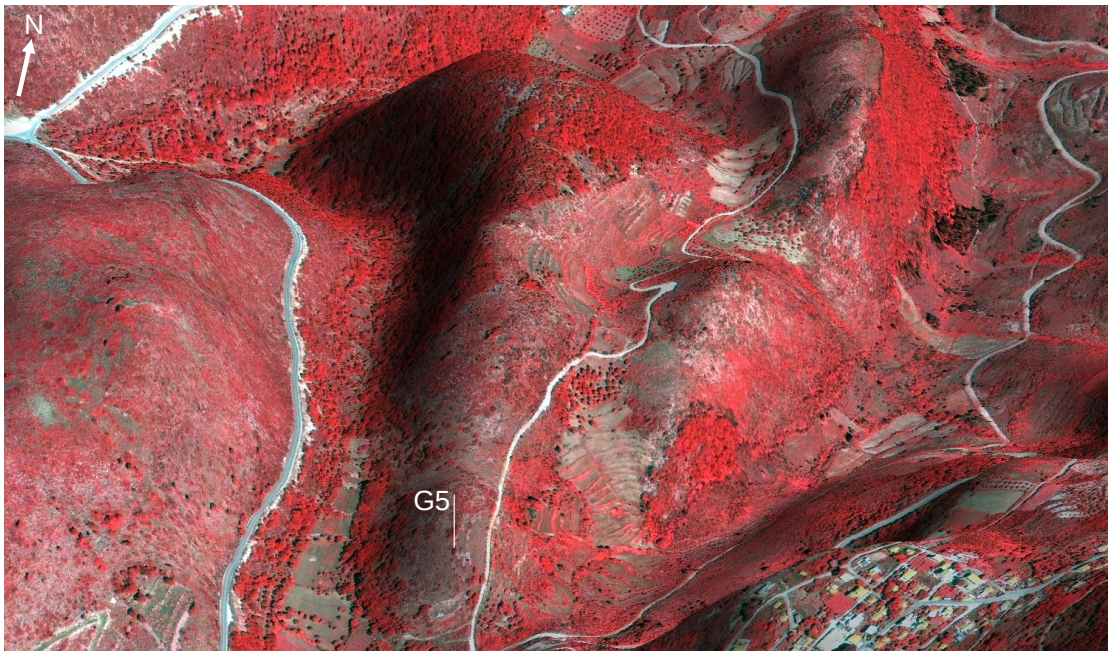

Figure 1.39 3D map of the limestone hill in which the brine-bearing borehole G5 was sited. Map produced on the OziExplorer3D mapping visualization software using the 100 pc false colour Quickbird satellite map draped over a 3-dimensional grid. Vertical exaggeration is 1.5.

At a depth of 258 m (-66.38 m below sea level), hypersaline water or brine (characterised as containing higher concentrations of sodium, calcium or magnesium in combination with chlorine and sulphates than normal sea water) was encountered. The concentration of these salts suggested the brine had been enclosed within the Eocene limestone for millions of years and had not come into contact with the surface nor had hydraulic connection with groundwaters (Koumantakis and Mimides, 1989). The composition of the brine was indicative of the initial stages of

evaporation of sea water within moderate temperatures and may have been caused by the presence of localised evaporites within the subsoil possible created during the Messinian Salinity Crisis (Hsu, 1983) through which the groundwater percolated, dissolving these salts creating hypersaline groundwater. These brines may also be evidence of an ancient (Neogene-aged) seaway which existed where the Thinia valley now stands representing trapped marine waters (Bittlestone et al., 2005).

1.3 Testing of "Strabo's Channel"

Given the geomorphological and geological background of Thinia, it is difficult today to see how a continuous marine channel could have occurred where the valley, which reaches a maximum elevation of 210 m above present sea level, now stands. To be a valid contender for "Strabo's Channel", the channel must fulfil the following criteria:

1. The channel must be marine i.e. deep enough to have reached Mycenaean sea level along its entire length.

2. It must have been continuous from "sea to sea" i.e. connecting Agia Kiriaki Bay in the north to the Gulf of Argostoli in the south.

3. It must have been in existence and substantial enough to have allowed the Paliki peninsula to be considered a free-standing island during the time of Odysseus (Late Bronze Age).

The testing of "Strabo's Channel" must therefore take into consideration the processes which might have led to its destruction and whether these processes could feasibly account for the disappearance of what would have been a dramatic feature in such a rapid timescale in geological terms. Given the tectonic and geological setting of Thinia there are four possible mechanisms by which this could have occurred:

1. **Eustatic sea level change (Section 1.3.1):** Were Mycenaean sea levels high enough to have covered the Thinia land-bridge at its present elevation?

2. **Earthquake-driven coseismic uplift (Section 1.3.2):** The land bridge was uplifted through earthquake-driven positive coseismic land movement.

3. **Burial (Section 1.3.3)**: "Strabo's Channel" was infilled through collapse of the channel gorge and deposition of landslide material.

1.3.1 Eustatic Sea Level Change

A much higher relative sea level (up to 210 m higher than present levels) during the Late Bronze Age would make fitting "Strabo's Channel" hypothesis easier as it would mean land seen many metres above sea level today may have been beneath or at sea level during the time of Odysseus. A subsequent major fall in sea level to present day levels could have left the remains of a marine channel "high and dry".

Global sea levels for the last 250 Ma show numerous fluctuations (Haq et al., 1987). Within the Mediterranean basin there is a deviation from the global mean during the Late Miocene (upper Messinian) due to the tectonic isolation and desiccation of the Mediterranean basin (the Messinian Salinity Crisis). During this time, the Mediterranean and former Paratethys seas (a large shallow sea which extended from the Northern Alps to the Aral Sea in Central Asia) experienced a brief, very large sea-level drop of c. 1500 m below sea level from 5.64 to 5.48 Ma causing subaerial erosion, the formation of fluvial canyons and progradation of fan deltas which infilled Early Pliocene rias to form coastal shelves (Suc et al., 2008). In low-lying basinal areas massive salt deposits occurred while at higher elevations this event was represented by an unconformity ("Messinian Unconformity") caused the major drawdown of sea level resulting in the removal of the Lower to Lower Uppermost Pliocene and Upper Miocene (Messinian) and (Bache et al., 2009). This extreme lowstand was followed by a sea level highstand of +70 m above sea level (the "Zanclean Flood") from 5.33 to 4.00 Ma during the lower Zanclean and deposition of pelagic sediments (Suc et al., 2008).

Sea levels for the last 2.5 million years have been strongly affected by the repeated expansion and retreat of the Northern Hemisphere Ice Sheets which has resulted in numerous sea level falls (glacials) and rises (interglacial) (Van Andel, 1994). During the sea level highstand of the Last (Tyrrhenian) Interglacial (125 000 years ago) sea levels were around 80 m higher than present day resulting in many low-lying areas being flooded (Figure 1.40, A and Figure 1.41, top).

During Last Glacial Maximum (LGM) (which lasted between 26 500 and 18 000 BP (Van Andel, 1994)) sea levels dropped to a major lowstand of around 120 m below present day levels (Perissoratis and Conispoliatis, 2003; Shackleton et al., 2003; Tzedakis et al., 2002). At this time large areas of coastal land extended further out to sea than they do today (Figure 1.42). The Western Greece coastline was up to 10 km further offshore and the Peloponnesus coastline extended to between 5 and 8 km (Perissoratis and Conispoliatis, 2003). Many near-shore islands becoming connected to the mainland via land-bridges and formation of deep lakes through trapped sea waters behind these islands e.g. Corfu, Amvrakikos Gulf (Papatheodorou et al., 1993). Islands within the Ionian Sea grew as sea levels fell lower than the shallow bathymetric surrounding their coasts. Kefalonia and Zakynthos were connected via land-bridge which now lies around 80 m below present sea levels (Braune, 1973).

The most continuous and detailed record of postglacial sea level rise comes from C14 dates taken from the Barbados corals (Figure 1.40, B) and show that sea levels have risen steadily after the glacial lowstand (Shackleton, 1987; Fairbanks, 1989; Bard et al., 1990; Lambeck and Chappell, 2001; Mix et al., 2001; Lambeck et al., 2003). As the rate of sea level change slowed towards the late Holocene, sea level underwent numerous small-scale fluctuations (dotted lines in Figure 1.40, B) which oscillated ~1 to 2 m above and below the steadily rising mean (Van Andel, 1994).

A key point to define is when (Holocene) eustatic postglacial sea level rise actually ended. By 8000 BP ice coverage in the northern hemisphere had reduced to close to what it is today and sea level was approximately 25 m below present day levels (Van Andel, 1994). Flat coastal plains were flooded to create embayments upon which human settlement proliferated since these flat areas were more favourable for agriculture and habitation than the usually mountainous land interiors (Perissoratis and Conispoliatis, 2003).

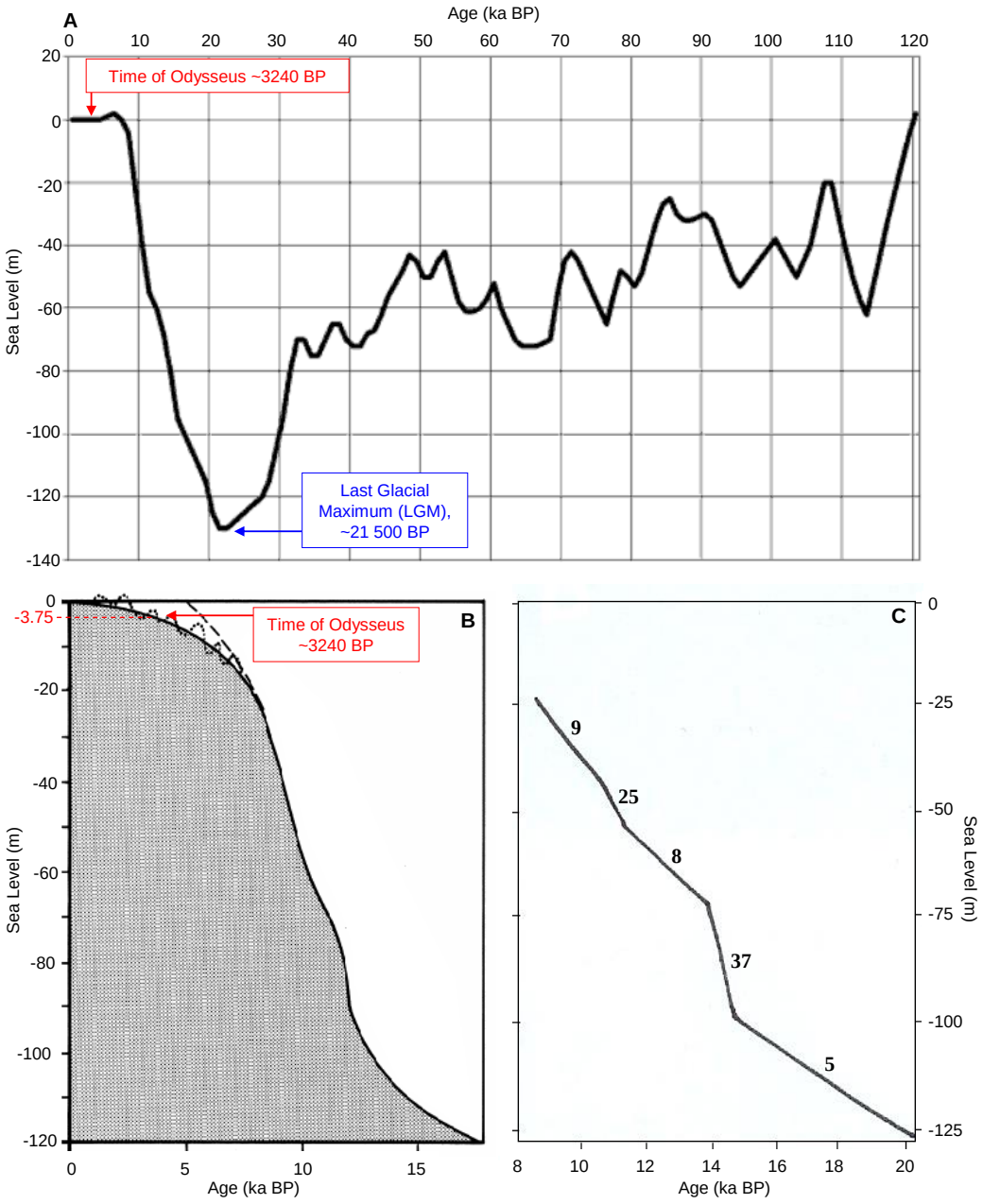

Figure 1.40 Eustatic sea level curves for the Late Quaternary and Holocene: A. Modified from Lambeck and Chappell (2001), Mix et al. (2001) and Lambeck et al. (2003). B. Barbados postglacial sea level curve. The dotted lines indicate possible curves for the last 8000 years. Modified from Fairbanks (1989) and Van Andel (1994). C. Postglacial sea level curve modified from Bard et al. (1990). The numbers in bold indicate the rate of sea-level rise (in mm/yr).

NASA World Wind: Sea levels at Last (Tyrrhenian) Interglacial (125 000 years ago) [c. +80 m]

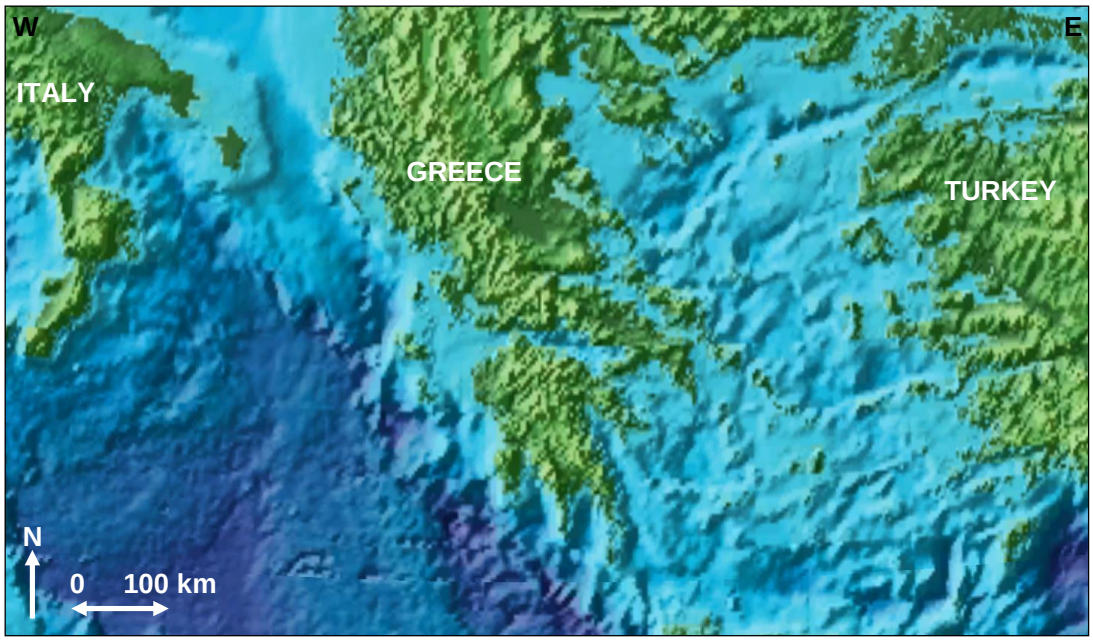

NASA World Wind: Sea levels at present day [0 m]

Figure 1.41 Maps constructed using the NASA World Wind data depicting different sea levels in the Aegean and Ionian Seas: Sea levels during the Last (Tyrrhenian) Interglacial (125 000 years ago) [c. +80 m] (top) and sea levels at present day (bottom).

In the last 8000 years, these embayments and lowlands have undergone dramatic morphological changes as postglacial rise stabilised (Flemming, 1978; Flemming and Webb, 1986) and a phase of increased alluvial deposition between 5000 and 2000 BP

caused siltation of river plains and out-building of coastal deltas (Vita-Finzi, 1972; Kraft et al., 1975) leaving several sites of historical interest many miles inland of their previous positions e.g. as demonstrated by studies at Troy (Kraft et al., 2003), Axios Plain (Kraft et al., 1977). A further rise of +3 m above has been proposed between 6000 and 3000 BP in relation to minor melting of the Antarctic ice sheet however no clear evidence of this has been forthcoming (Nakada and Lambeck, 1988; 1989; Lambeck, 2002). The Fairbanks (1989) curve showed that global sea levels during the Late Bronze Age were around 3.75 m below sea level. A eustatic sea level of between -3.75 m and 0 m is therefore assumed for Mycenaean Kefalonia.

As such eustatic sea levels of the Late Bronze Age were never high enough to submerge the Thinia valley as it stands today (up to 210 m above sea level) and a significant drop in sea level (like that which accompanied the Messinian Salinity Crisis) has not taken place since the time of Odysseus which might have left the remains of a Late Holocene marine channel "high and dry".

NASA World Wind: Sea levels at Last Glacial Maximum (21 500 years ago) [c. -120 m]

Figure 1.42 Map constructed using the NASA World Wind data depicting different sea levels in the Aegean and Ionian Seas: Sea levels during the Last Glacial Maximum (21 500 years ago) [c. -121 m].

1.3.2 Earthquake-driven Coseismic Uplift

The second possibility, given the tectonic setting of Kefalonia and high degree of seismicity experienced by Western Greece annually, is that the Thinia valley (and remains of "Strabo's Channel") was uplifted to its present elevation through earthquake-driven "coseismic" uplift. Coseismic uplift is the name given to the rapid, localised tectonically-driven vertical land movement (in the order of centimetres to metres) which can accompany an earthquake of magnitude 6.0 or greater (Pirazzoli et al., 1994).

Such land movement will cause apparent fluctuations in local sea level so tectonically-active areas will often have relative sea level curves which deviate from the global mean e.g. Akarnania and NW Peloponnesus, Vött (2007). This type of uplift can be charted in the field by dating ancient shorelines which have been lifted above the existing shoreline. Such shorelines can be identified through marine erosion (wave-cut notches, "benches", raised beaches, intertidal pools and elevated mollusc borings), submerged archaeological remains and marine deposits such as "beachrock" (Pirazzoli et al., 1994). Beachrock is sedimentary rock consisting of lithified beach deposits (gravel, sands) cemented by carbonate minerals which form parallel layers along a shoreline and extends up to 300 m offshore (a good example occurs in Figure 1.29, labelled 3) (Neuendorf et al., 2005).

A key historic location which illustrates the affects of shoreline movement affects apparent sea level are the ruins of the Roman Temple of Serapis (Figure 1.43) located at Pozzuoli in the Bay of Naples (Lyell, 1830; Babbage, 1847). The temple at Pozzuoli is highly significant in the history of geology as it featured as a key example in the famous publication by Charles Lyell (1797-1875) "The Principles of Geology: Being an Attempt to Explain the Former Changes of the Earth's Surface, by Reference to Causes now in Operation" (3 vol., 1830-1833). This work marked a crucial stage in the geology discipline as it introduced the concept that some processes affecting the Earth occur rapidly – a deviation from gradualism which believed that geological processes occur in very slow stages.

Figure 1.43 Temple of Serapis. The three upright columns show encrustations from boring *Modiola lithophaga* bivalves several metres above sea level, a species which occurs at the water line, indicating that sea levels were once high enough to flood the temple to this level before falling to the present level. As this temple had presumably originally been built well above sea level (around 2000 years ago), these encrustations and the current partial submergence suggested that significant changes in relative sea level had occurred. Photo credits: J. Underhill.

Today, the Temple of Serapis lies partially submerged at the modern shoreline. The three remaining upright pillars each have a zone of dark encrustations around 2.7 m above the temple floor which is caused by the boring clam species *Modiola lithophaga* (Figure 1.44). As this species only occurs at the water line, the presence of these encrustations implied that at some point since the building of the temple around 2000 years ago, sea levels were at this level. Presuming that the Temple was originally built well above sea level, Lyell deduced that this change in sea level was not caused by a eustatic change but related to the rise and fall of the land on which the Temple of Serapis was built. The land movement along the coast of Naples is caused by the filling and emptying of pockets of magma associated with the Campi Flegrei caldera (De Natale et al., 2006).

Strabo's observation that the narrows were often "submerged from sea-to-sea" may refer to a location like the Temple of Serapis in which the shoreline experienced

repeated coseismic uplift bringing it above sea level only to be overtaken during the intervening periods of tectonic quiescence by postglacial sea level rise resulting in the observed repeated uplifts and submersions.

Braune (1973) and British Petroleum Co. Ltd et al. (1985) identified evidence of positive Quaternary land movement in the form of Pleistocene-aged fossil shorelines around the southern coast of Kefalonia characterised by partial wave-cut notches and mollusc borings between 6 and 200 m (Figure 1.45). These occurred at 6-11 m (?Flandrien, ?Neorthotyrrhenien), 18-22 m (?Tyrrhenien = Last Interglacial (Eemian) 125 000 BP), 35-55m (Milazzien), 80-100 m (Sicilien), 140-160 m (?) and 180-200 m (?Calabrian).

Figure 1.44 Close-up of the three upright columns showing bivalve encrustations around 3 m above present sea level. Photo credits: J. Underhill.

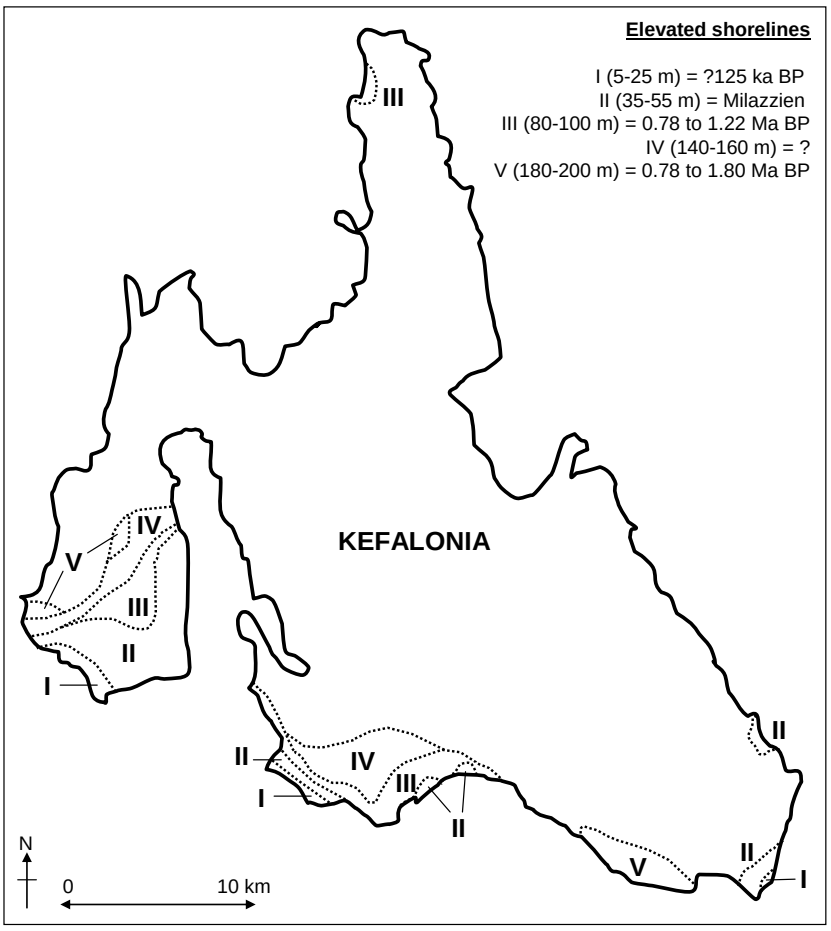

Figure 1.45 Elevated shorelines (schematic) on Kefalonia at heights 5-25 m (I) (?Flandrien, ?Neorthotyrrhenien to ?Tyrrhenien = Last Interglacial (Eemian) 125 000 BP), 35-55 m (II) (Milazzien), 80-100 m (III) (Sicilien), 140-160 m (IV) (?) and 180-200 m (V) (Calabrian) above sea level. Modified after Braune (1973).

The timings in brackets in are partly after Woldstedt (1958; 1969) however the terrace at 140-160 m remained uncorrelated as it did not tie with Quaternary Mediterranean sea level highstands (Braune, 1973). The presence of upper Pliocene sediments at 100 m to the south-east of Argostoli suggested that the terraces above +100 m should be assigned a Pliocene age and the variation in height may have come about through folding (Braune, 1973; Sorel, 1976; Stiros et al., 1994).

However, only two historic incidents of coseismic uplift have been confirmed on Kefalonia: one between 350 to 710 AD and the second associated with the 1953 Great Ionian Earthquake, the last major earthquake to affect Kefalonia (Papazachos and Papazachou, 1989; Pirazzoli et al., 1994) (marked in red on Figure 1.46). The

most studied of these coseismic episodes in that which occupied the 1953 earthquake.

The Great Ionian Earthquake occurred on 12 August 1953 and registered as 7.2 with an epicentre located in the south-eastern part of the island (indicated by a red star in Figure 1.57, a). This devastating seismic event and its affects on the apparent shoreline of Kefalonia were studied in detail by Galanopoulos (1955), Mueller-Miny (1957), Papazachos and Papazachou (1989), Pirazzoli et al. (1994) and Stiros et al. (1994). While this earthquake caused massive damage to the entire island, the highest seismic intensity appeared confined to the central part of the island (Figure 1.57, b) Stiros et al. (1994). A focal mechanism for this event (Figure 1.57, a) showed that it was compressional with a NNW strike suggesting this earthquake was associated with out-of-sequence activity along a thrust fault (McKenzie, 1972). The main shock was preceded by two magnitude 6+ foreshocks (6.4 occurring on 9 August and 6.8 on 11 August) and at least one major aftershock on the same day measuring 6.3 (Bittlestone et al., 2005).

Date	Magnitude (Ms)
14.08.2003	6.3
17.09.1983	7.0
17.09.1972	6.3
12.08.1953	7.2
20.09.1939	6.3
24.01.1912	6.8
04.02.1867	7.2
14.03.1862	6.6
22.07.1767	7.2
24.07.1766	6.7
22.06.1759	6.5
28.08.1714	6.4
20.02.1743	7.0
??.??.1688	6.5
??.??.1661	?
24.08.1658	6.8
30.09.1636	7.1
??.??.1469	7.2

Figure 1.46 Major earthquakes which have occurred on Kefalonia over the last 500 years from historical data. Only main shocks of seismic sequences are included. The data highlighted in red indicates the only instance of recorded coseismic uplift. Source: Papazachos and Papazachou (1989) with the addition of the Lefkada Earthquake (top), the 1661 earthquake after Vogt and Albini (1992).

The 1953 earthquake caused coseismic uplift and westward tilting of central Kefalonia creating a coastal terrace between 0.3 and 0.7 m above sea level. Around Paliki, instance of uplift relating to this event were harder to identify although this may have been due to the lithology around these coastlines (the soft Neogene and Quaternary "badlands") being unfavourable for preserving uplift (Galanopoulos, 1955).

The effects of earthquakes on the island is further complicated by the large thrust faults cross-cutting the Pre-Apulian Zone. The pattern of seismic intensities suffered by various segments of the island during major historic earthquakes indicates the presence of seismic discontinuities which coincide with these faults (Figure 1.48). In other words, earthquake-driven coseismic uplift may occur in some parts of the island but not in others, depending on the location of the earthquake.

Distribution of seismic intensities and coastal uplift associated with the 1953 event led some authors (e.g. Stiros et al., 1994) to propose that coseismic uplift associated with this event was confined to the central part of the island and performed a piston-like motion facilitated by two sub-parallel extensional faults (the "Livadi Fault" and "Agia Ephemia Fault") occurring roughly where the Atheras Thrust and Kalon Thrust occur however the lack of significant recent scarps along these fault planes makes this unlikely. The Ainos Thrust, however, appears to have taken up some of the movement of the 1953 earthquake. During the earthquake, the hangingwall of the fault behind the old village of Petrikata (a name which significantly translates roughly as the "place of fallen rocks") (Figure 1.38, B) experienced a rapid lateral movement of 8 m using the soft marl as a slip plane. This movement destroyed the original village of Petrikata which was rebuilt further down the slope.

The 1953 coseismic uplift and further instances of coseismic uplift was dramatically illustrated by a mushroom-shaped rock which lay around 50 m offshore within the harbour of Poros at the south-eastern part of the island (Figure 1.49). This rock preserved several wave-cut notches relating to coseismic uplift events totalling 3.2 m (Bittlestone et al., 2005).

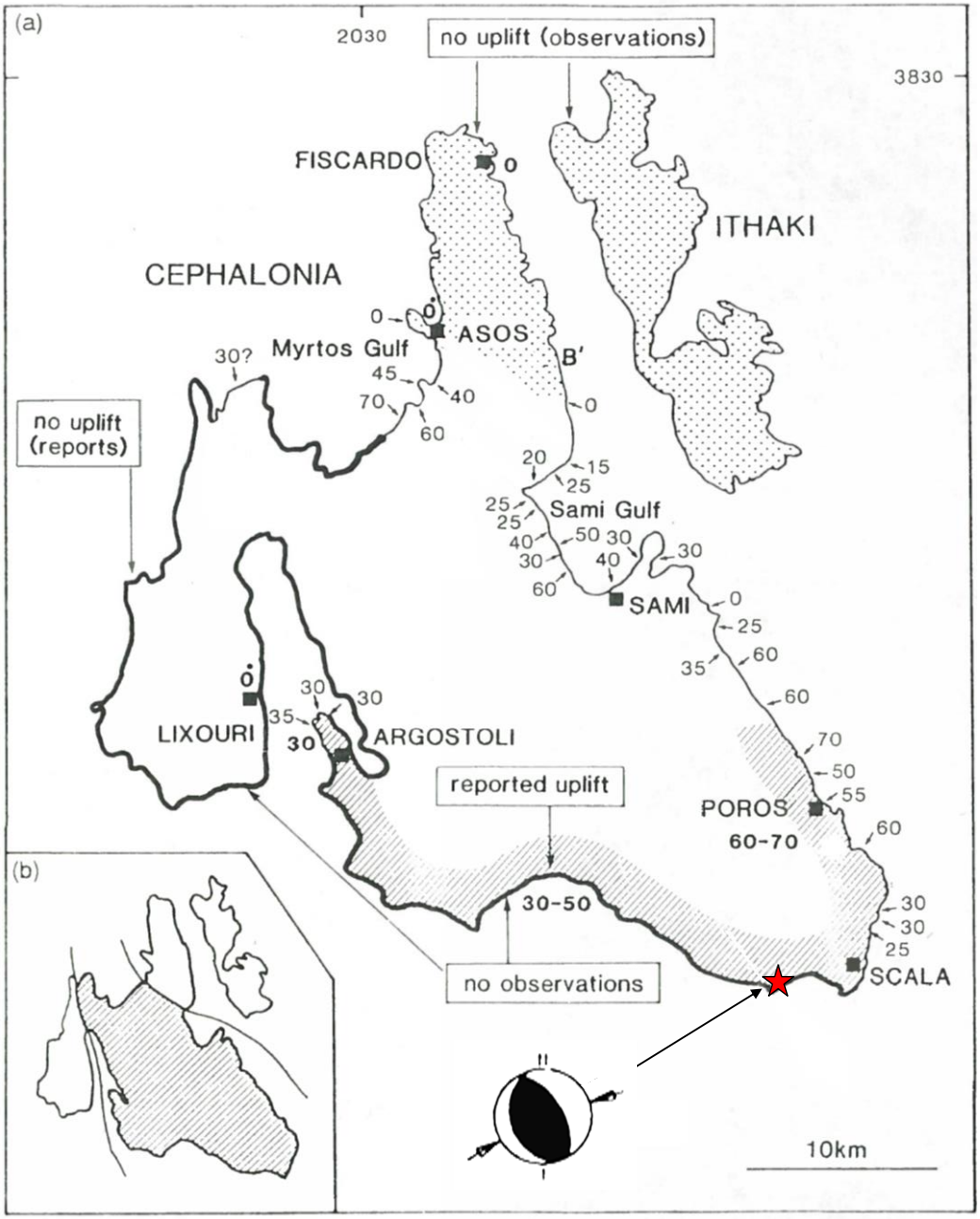

Figure 1.47 The 1953 Great Ionian Earthquake: a) Summary of the coastal uplift associated with the 1953 Great Ionian Earthquake (in cm) (from Stiros et al., 1994). Numbers with arrows = Stiros et al. (1994); bold numbers = estimations from reports by Galanopoulos (1955). The red star marks the epicentre of the main shock. Focal mechanism from McKenzie (1972). The solid black coastline indicates unfavourable geology for determining coseismic movement. Hatched areas indicate where coastal movement in relation to the 1953 event has occurred; b) Summary of 1953 uplift (hatched).

A clear double "bench" and fossil notches occurred around the edge of this rock at around +0.6 m (marked A to C in Figure 1.49) and around +1.2 m (marked D in Figure 1.49). While the lower bench corresponded to the 1953 earthquake uplift, the

upper bench correlated with a much older event dating between 350 to 710 AD (Pirazzoli et al., 1994). This event was also centred on the south-eastern part of the island and was tentatively correlated with the Early Byzantine tectonic paroxysm, a period of regional tectonic intensity characterised by coseismic uplift around the eastern Mediterranean probably due to temporary acceleration of subduction along the Hellenic arc-trench (Pirazzoli, 1986). A large wave-cut notch occurred at +2.1 m (E in Figure 1.49) believed to represent a time of relative sea level stability which occurred between 3060 to 2570 cal. BC and cal. AD 350 to 710 prior to the Early Byzantine uplift (Pirazzoli et al., 1994).

Undated instances of (possible Late Holocene) positive coseismic land movement were identified around Thinia. Surrounding Livadi Marsh, the possible contender for Ithaca's harbour, is a clear beach terrace around 6 m present sea levels indicating sea levels were once high enough to completely flood this marsh area.

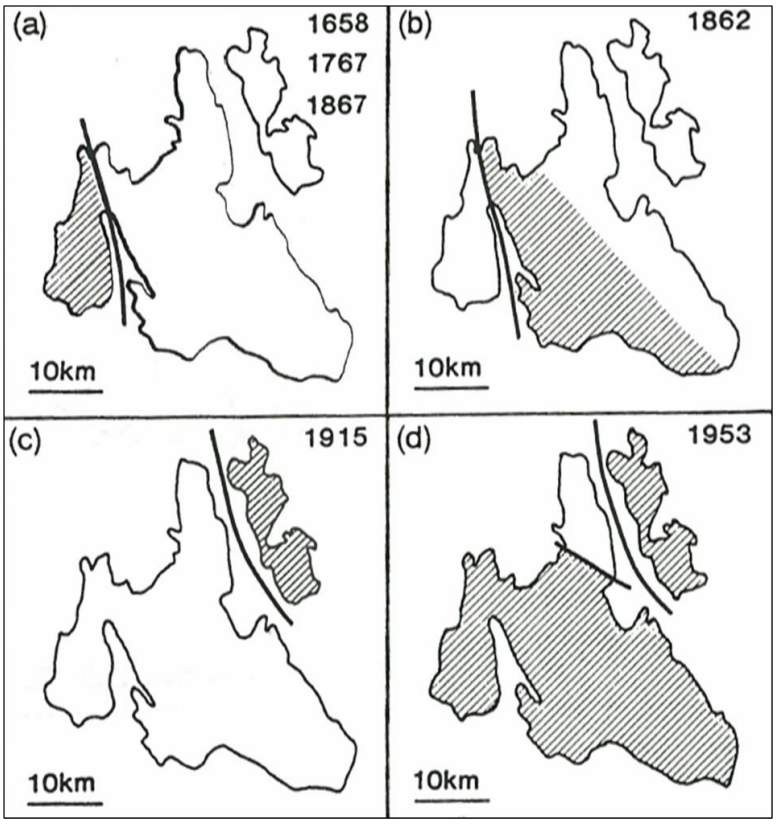

Figure 1.48 Maps showing the location of damage (hatched areas) relating to historic earthquakes (from Stiros et al., 1994). The discontinuity running through the Gulf of Argostoli in (a) and (b) was interpreted as the "Gulf of Argostoli Thrust" by Stiros et al. (1994).

While this terrace may relate to Braune's (1973) Late Pleistocene (Tyrrhenien, 125 ka) shoreline given its elevation above sea level (Figure 1.45) it may also be evidence of recent sea level change caused by coseismic movement. Raised beach terraces around 1-2 m occurred at Agia Sotira (Figure 1.50, A) and at the north-eastern tip of Agia Kiriaki Bay (Figure 1.50, B) which took the form of an angular unconformity separating easterly-dipping conglomerates from horizontally-bedded raised beach conglomerates with a wave-cut platform at ~6 m (Underhill, 2009). Wave-cut notches were observed at c. 50-100 cm above sea level along the base of the vertiginous limestone shore of southern Thinia extending from Agia Sotira southwards along the eastern side of the Gulf of Argostoli (Figure 1.51). Given their magnitude, these instances of uplift were probably linked to the 350 to 710 AD uplift event recorded by Pirazzoli et al. (1994) and the later 1953 Great Ionian Earthquake.

Even if these various instances of coseismic movement had occurred in the last 3300 years then the Thinia valley has potentially experienced only around 6 m of uplift since the Late Bronze Age. This falls largely short of the necessary 210 m of uplift required for the Thinia valley to reach the levels seen today.

Figure 1.49 Mushroom-shaped rock in Poros harbour indicating possible instances of coseismic uplift (marked in red). From Bittlestone et al. (2005).

Figure 1.50 Possible instances of "Late Holocene" coseismic uplift within Thinia: A. The raised beach at Agia Sotira inlet, southern Thinia. Beach pebbles can be found 1- 2 m above sea level; B. Angular unconformity separating easterly-dipping conglomerates from horizontally-bedded raised beach conglomerate with a wave-cut platform at ~ 6 m at north-eastern tip of Agia Kiriaki Bay (photo credits J. Underhill) (Underhill, 2009).

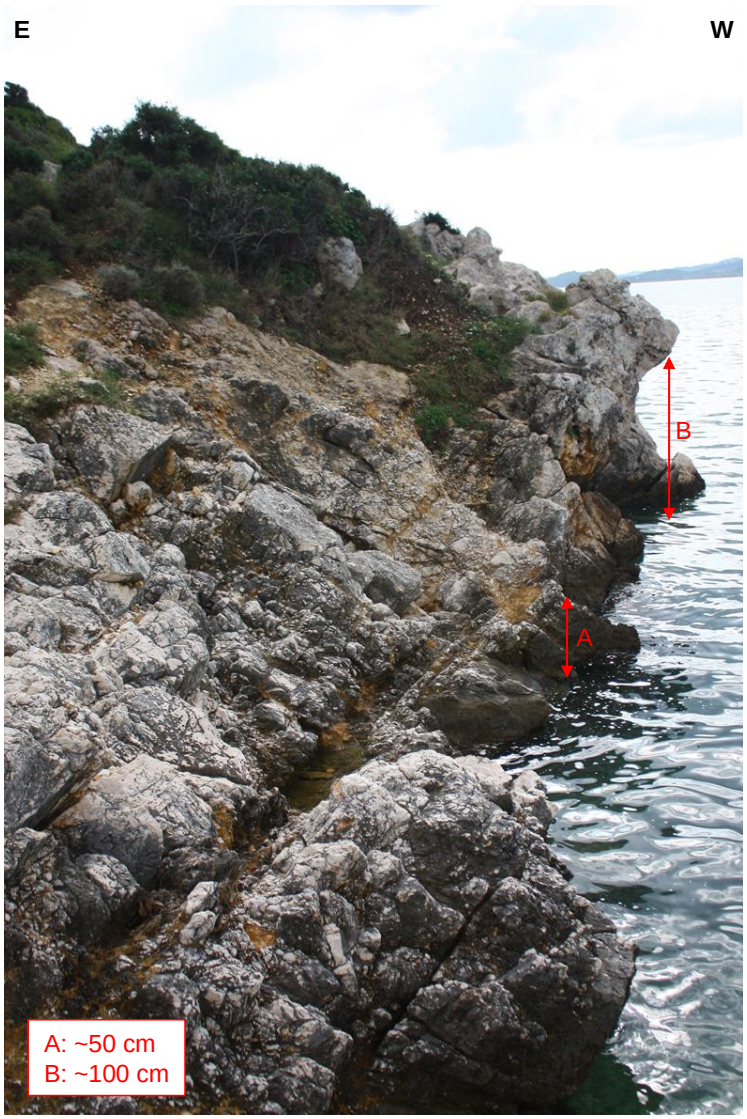

Figure 1.51 Wave-cut notches within easterly-tilted limestone sea cliff at Agia Sotira Bay.

1.3.3 Burial

An alternative possibility is that "Strabo's Channel" was infilled through deposition of landslide material into the Channel axis sourced from the catastrophic collapse of the steep-sided, high elevation mountains bounding the seaway. In this scenario the base of the Channel remains at Late Bronze Age sea level while repeated pulses of landslide material are deposited into the seaway between Paliki and Kefalonia, progressively closing the gap between landmasses and raising the topography of the valley (Figure 1.52). Strabo's observation of an "often submerged" narrows favours

this process since it may refer to a marine channel where partial infilling had already resulted in it being no longer entirely navigable. There were two possibilities:

1. The present topography of the Thinia valley was formed entirely through the built-up of landslide material deposited into a 1 to 4 km wide marine seaway lying between Paliki and Kefalonia.

2. "Strabo's Channel" formed a narrow gorge incised into the bedrock which was continuous from north to south of the land-bridge and reached below Mycenaean sea level (-3.75 m below present day levels to 0 m). This scenario is favourable because it reduces the amount of landslide material needed to infill the channel; however, it raised questions as to whether such a narrow gorge was "substantial" enough for Paliki to be considered an island.

The presence of *in situ* limestone and marl bedrock at the valley surface (as shown in Figure 1.37) immediately rules out scenario 1 and greatly restricts the route that a channel gorge could take in scenario 2. The proposed route of "Strabo's Channel" by Bittlestone et al. (2005) (presented in Figure 1.53 as a dark blue shaded area) is situated within a very narrow (70 to 200 m wide) band of recent alluvial material and follows the axis of the valley. The north-south elevation profile for "Strabo's Channel" therefore matches Figure 1.32. At the highest elevation part of the valley (Petrikata Quarry), "Strabo's Channel" would have to form a narrow, vertiginous gorge around 210 m deep in order to reach sea level. Resolving the proposed "Strabo's Channel" gorge into an inverted triangular prism of average height 100 m, a 125 m wide base and a length of 6300 m, the volume of landslide material required to fill it would be in the region of 4×10^4 km^3.

Landslides are defined as the (usually rapid) mass-movement of clastic and soil material travelling downslope under the effects of gravity. Most landslides are shallow-seated slope failures (mechanical deformation of the sediments occurs up to 5 m in depth) which move across "shear surfaces" (Petley and Allison, 1997). The average landslide can transport material of the order 1 to 10 km^3 in volume. This falls

far short of the volume required to fill the proposed wedge of "Strabo's Channel" and raises questions about whether burial method could be a feasible mechanism of destruction which would require thousands of large landslides.

A possible solution is the "sturzstrom". Sturzstroms are classed as deep-seated landslides (i.e. those with mechanical deformation occurring up to depths of 250 m). They are much rarer and are capable of transporting clastic debris 10 to 100 km^3 in volume (Hsü, 1975). Other than containing a large volume of material, sturzstroms can also travel up to several kilometres in less than a few minutes even on low gradient surfaces due to their flow-like behaviour (Hsü, 1975). This fluid-like movement may be due to the generation of unconsolidated attrition breccias as the high forces generated by the enormous volume of material within the sturzstrom continually shatter the clasts creating as fine powder which fills the pore spaces in between the larger clasts, a process which lowers the friction coefficient and shearing resistance (Prager et al., 2006).

There are several well-documented examples of these "super" landslides. The most notable event occurred at the Vaiont Reservoir in Northern Italy in 1963 (Petley and Petley, 2006; Kilburn and Petley, 2003). During the filling of the Vaiont Reservoir, 270 Mm^3 of mountain side catastrophically collapsed into the lake displacing ~30 Mm^3 of water and caused a wave which topped the reservoir dam by 245 m (Figure 1.54). The collapse occurred in less than a minute travelling around 500 m down-dip entirely filling the reservoir gorge to a depth of almost 400 m.

The landslide travelled to 140 m up the opposite bank. The resulting flood in the valley below caused around 2500 deaths. The morphology of the dam sides were susceptible to collapse, characterised by a very deep, very narrow gorge interbedded with Jurassic-Cretaceous limestones and soft, weak clays which dipped towards the axis of the gorge. The effect of increasing water levels in the reservoir and persistent rainfall immediately prior to the collapse increased pore pressure within the clay layers reducing effective normal strength and initiating slow creep (Kilburn and Petley, 2003; Hendron and Patton, 1987). Water levels in the reservoir were then

reduced in an attempt to stabilise the slopes reducing hydraulic pressure within the rock causing collapse.

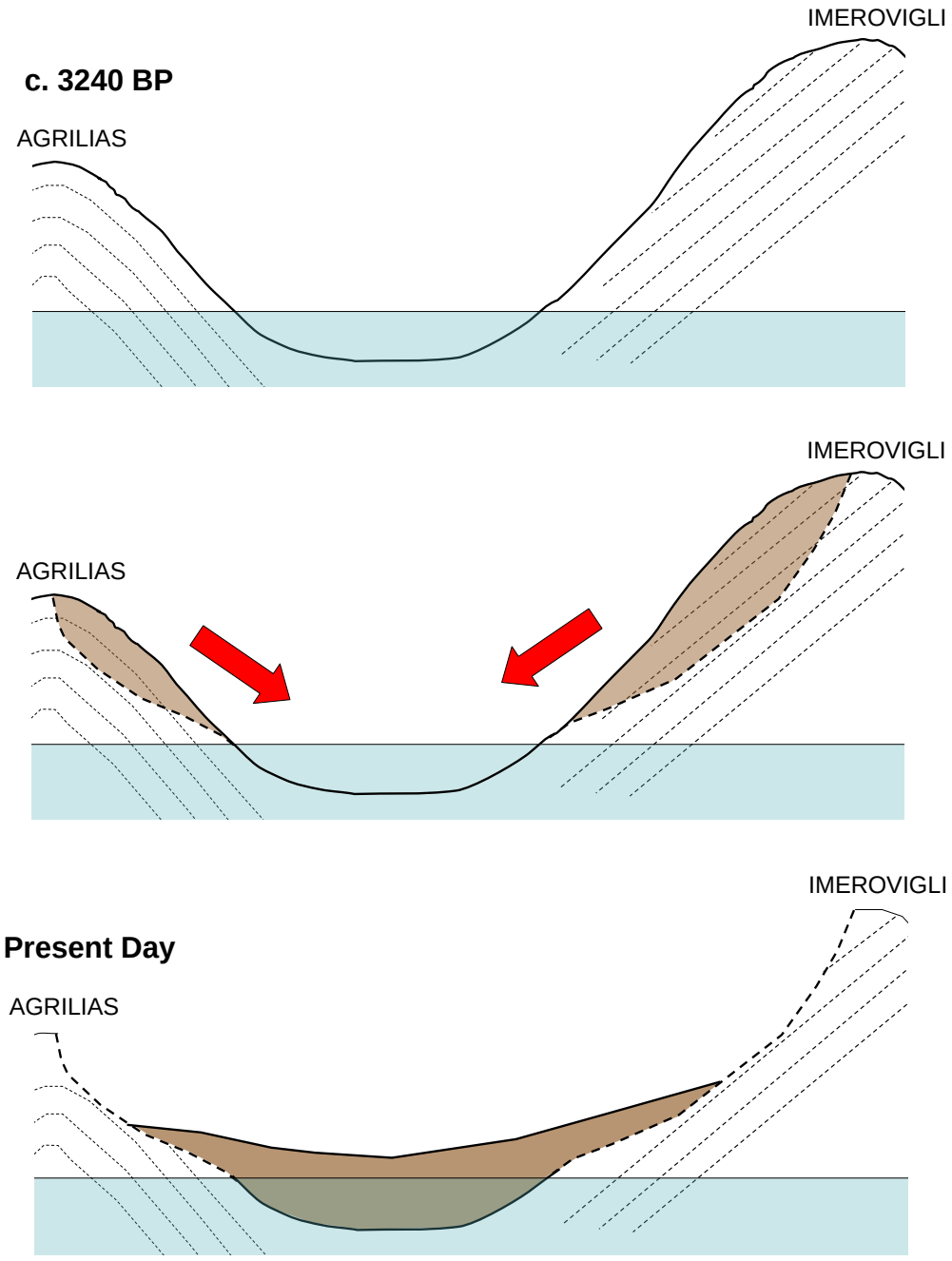

Figure 1.52 Series of block diagrams showing how a Mycenaean age marine channel might have been buried through collapse of the steeply-dipping valley sides of Thinia which accounts for the scalloped embayments observed in the limestone of the steep valley sides.

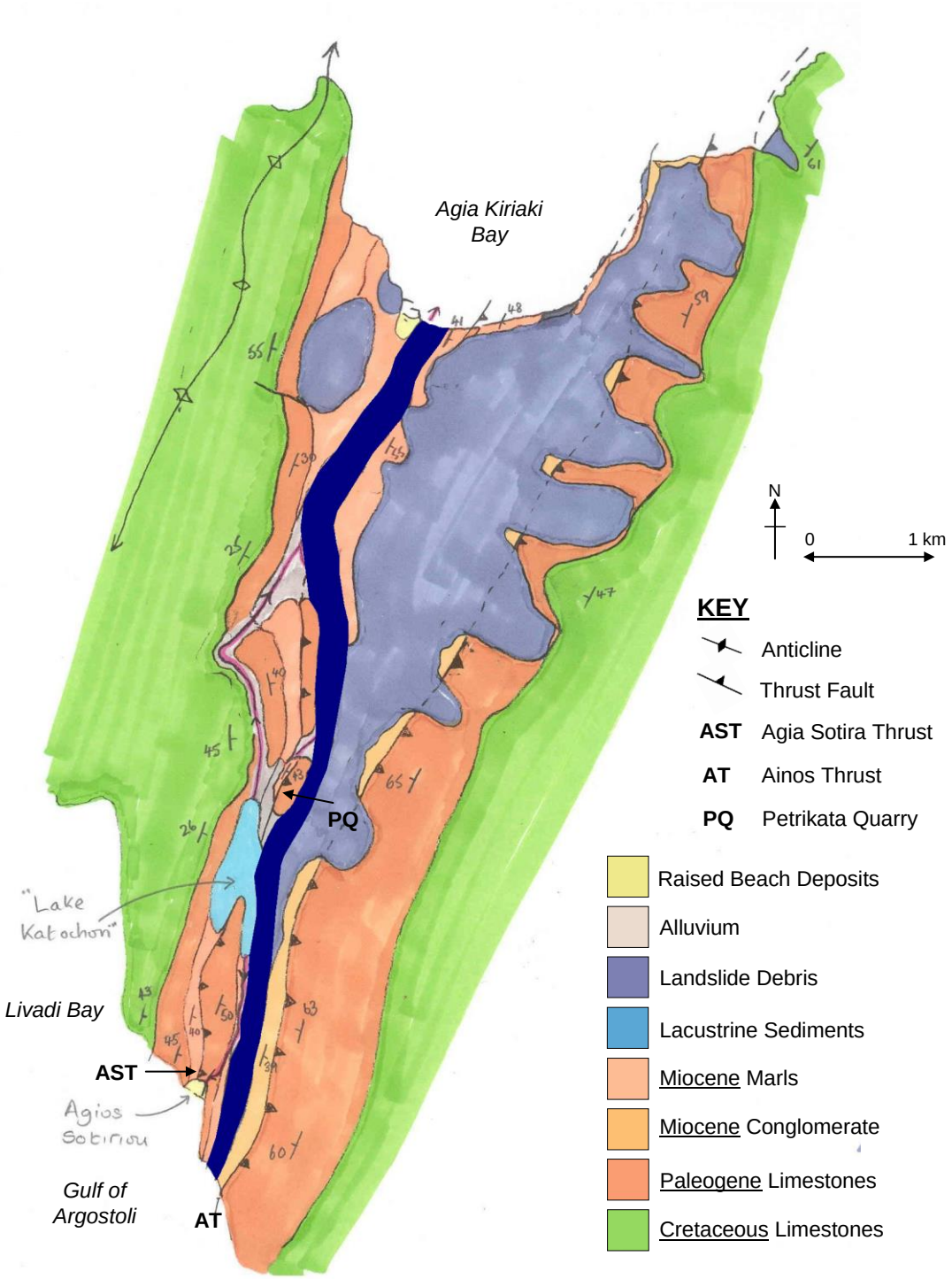

Figure 1.53 Geological sketch map of the Thinia valley produced by J. Underhill for Bittlestone et al. (2005) indicating the proposed route of "Strabo's Channel" (dark blue) in the case that the Channel forms an infilled narrow gorge. This is the most likely route as it follows the valley axis. A topographic section taken along this route is presented in Figure 1.32.

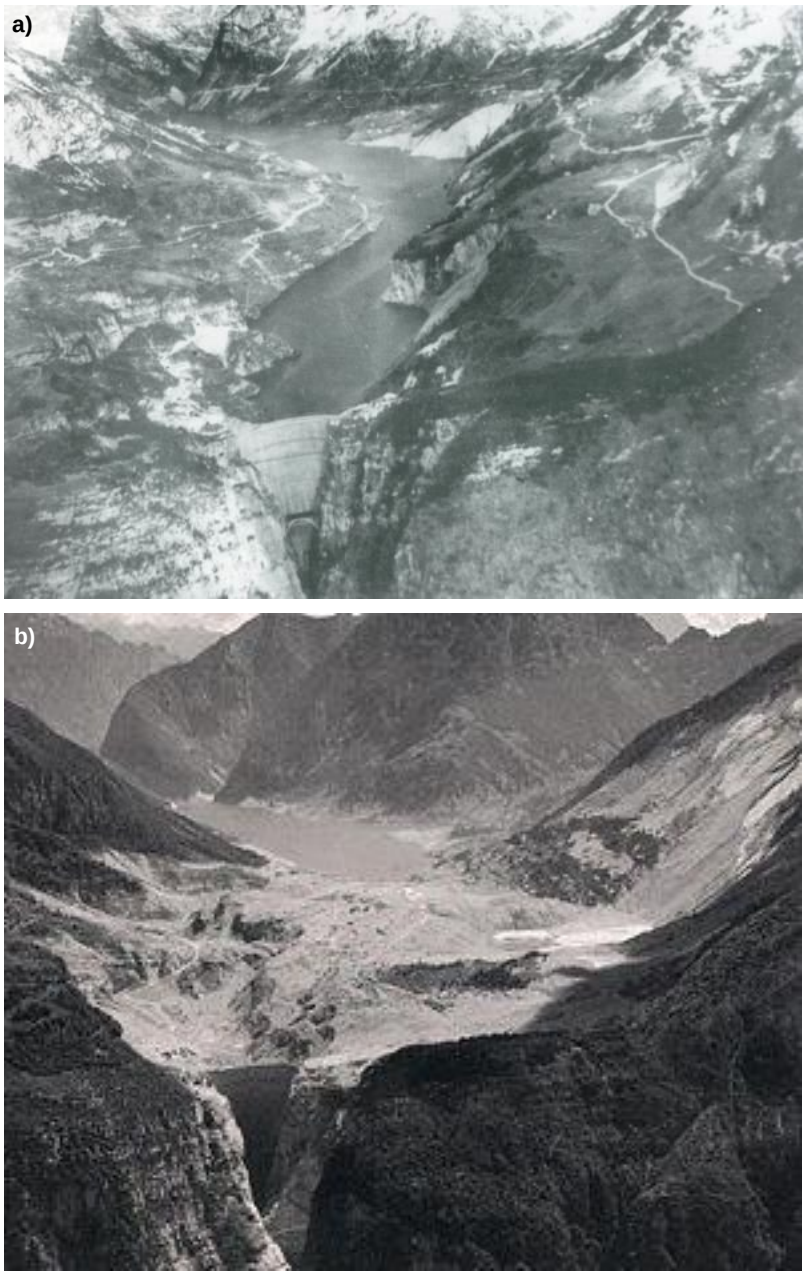

Figure 1.54 Vaiont Reservoir before (a) and after (b) failure. Source: The Landslide Blog.

Sturzstrom deposits can been several kilometres in extent and tens of metres in thickness and are typically chaotic forming small hills containing clasts of varying sizes and fragmentation with large angular blocks ranging from a few metres in diameter to slabs many metres in length. These large clasts are bound in a fine-grained matrix created from pulverised rock. The deposits can have sharply-defined limits with a distal rim a few metres above the existing topography (1881 Elm

sturzstrom, Hsü (1975)). A borehole-calibrated GPR and seismic investigation of the Holocene-aged Fernpass sturzstrom of Tyrol, Austria by Prager et al. (2006) detected several distinct discontinuities of varying intensities and geometries which were attributed to individual prograding debris flows onlapping the hummocky rockslide relief and undulating basal reflectors.

Given the volume and far-travelling nature of material which can be transported within a single event, sturzstroms offer a feasible mechanism as to how such a large volume of material might have accumulated within the Thinia valley in such a short geological timescale. In favour of the burial mechanism of destruction are examples of large-scale slope detachments around other locations in western Kefalonia where the steeply-dipping topography lends itself to slope failure. Within the steep sea cliffs surrounding Mirtos Beach to the north-east of Thinia is a massive rhombohedral limestone clast tens of metres across which has become detached from the slope and is moving slowly down the cliff (Figure 1.55). Substantial slope collapse occurred in and around Thinia during the Great Ionian Earthquake storm of 1953. Achieve footage from this earthquake showed massive scallop-shaped collapses of the vertiginous sea cliffs of the island which occurred in a few hours (Figure 1.56, B). More recent slope collapses are visible along the eastern coast of the Gulf of Argostoli (Figure 1.56, A).

However, this mechanism of destruction also caused issues relating to the valley morphology. Of particular challenge to the "Strabo's Channel" hypothesis is the site of the suspected paleo-lake Lake Katachori as described earlier (pale blue in Figure 1.53) which occupies the saddle region. The presence of the paleo-lake creates an unavoidable issue for the hypothesis as the lake sediments partially overlap the proposed channel route in Figure 1.53 at a height of around 170 m above sea level. If the lake is dated as being older than the Late Bronze Age then it rules out the possibility that a buried, untranslated marine channel existed here during the time of the *Odyssey*.

Figure 1.55 Detached rhombohedral clast at Mirtos Bay. Photo credits: J. Underhill.

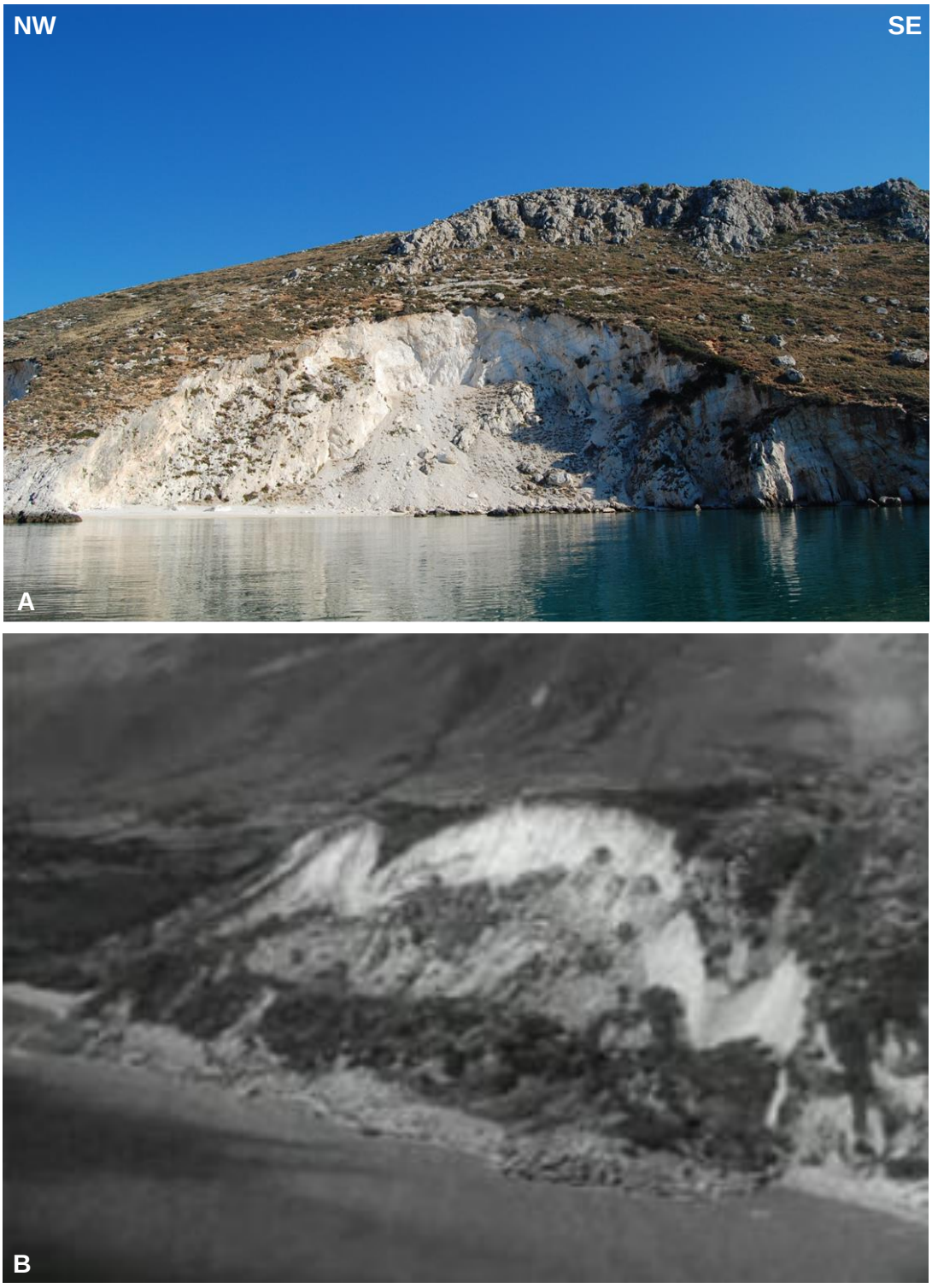

Figure 1.56 Photographs depicting fan-shaped collapse of the vertiginous limestone cliffs which bound the shoreline of Kefalonia: A. Aerial photograph of slope collapse taken after the 1953 earthquakes (source: British Pathe news clip); B. Recent slope collapse on the southern shore of Thinia.

1.4 Summary

The application of geological and geophysical methods on the Ionian Island of Kefalonia has provided a new-found basis by which to test the re-location of the island of Ancient Ithaca, the island stronghold of King Odysseus as described in Homer's epic the *Odyssey*, a subject which has perplexed academics for centuries.

The "Strabo's Channel" theory provides a feasible means by which the Paliki peninsula, the best geographical fit to Homer's description of Ancient Ithaca, could have been considered an island during the time of Odysseus (around 3300 years ago) despite being land-locked and connected to the rest of Kefalonia by a 6 km long isthmus, which can be tested using geoarchaeological means.

Three possible processes by which "Strabo's Channel" might have disappeared to leave the current morphology of the Thinia valley were presented: eustatic sea level change, earthquake-driven coseismic uplift and burial (through collapse of the channel gorge and valley sides). Of these, the most likely cause of destruction was burial.

CHAPTER 2: Data and Methods

2.1 Introduction

The "Strabo's Channel" theory is an attractive solution to the mystery surrounding the re-location of Ancient Ithaca as it reduces a complicated problem into a simple test which can be investigated using geoscientific means.

The investigation was carried out using a survey programme of complimentary non-invasive geophysical techniques calibrated by 17 shallow sedimentary cores and combined with surface geological mapping and geomorphological observations designed to confirm and expanded upon the tentatively positive results of the preliminary "reconnaissance" tests. In addition to a helicopter-mounted electromagnetic (HEM) survey taken across Northern Paliki, ground-based surveys resistivity and seismic refraction were undertaken at strategic sites in Northern Paliki (Atheras, Livadi Marsh) and Thinia (Northern and Southern Thinia, Lake Katachori). Gravity was undertaken across the whole of the Thinia isthmus. Shallow marine seismic reflection surveys were also undertaken in the coastal areas adjacent to the isthmus. This chapter will be structured in the following way:

1. **Preliminary (reconnaissance) surveys (Section 2.2):** Summary of the tests conducted before commencement of this study whose results justified further, large-scale testing of the "Strabo's Channel" theory.

2. **Data collection (Section 2.3):** Introducing the survey techniques used and the order of data collection in the field.

3. **Onshore non-invasive surveys (Section 2.4):** Description of the locations of the onshore surveys and reasons behind these locations.

4. **Offshore non-invasive survey (Section 2.5):** Description of the locations of the offshore surveys and reasons behind these locations.

5. **Survey methodology (Section 2.6):** Description of the survey techniques in more detail including how the surveys were carried out and what processing steps were applied to the acquired data.

6. **Summary (Section 2.7).**

2.2 Preliminary (Reconnaissance) Surveys

The following tests of the "Strabo's Channel" theory were conducted before commencement of this thesis. The results of these early surveys were deemed sufficient "proof of concept" and provided enough encouragement to justify the need for further testing of this hypothesis through the application of industrial-scale geophysical tests and initiation of this PhD. In all three tests Professor John Underhill (University of Edinburgh) led the investigative campaign.

2.2.1 Sub-bottom profiling (SBP) survey of Gulf of Argostoli and Mirtos, Sept-Oct 2005

A preliminary sub-bottom profiling (SBP) survey was undertaken in the Gulfs of Argostoli and Mirtos (including Agia Kiriaki Bay) between the dates of 31st Aug and 3rd Sept 2005 before commencement of this thesis. The purpose of this survey was to examine evidence for and against a channel incision on the shelf either end of Thinia by imaging the sea bed morphology of these coastal regions and Holocene to Upper Quaternary (postglacial) sedimentary record beneath. The survey was carried out using an ORE 3.5 kHz "pinger" suspended by a towfish and EPC 3200 recorder with a sweep rate of 0.25 s (provided by UOE) installed in a local fishing boat and was located using the vessel's onboard GPS. Acquisition was limited due to the shallow water depth restrictions of the equipment (the towfish needed a water depth of at least 2 m to operate efficiently and data collected close to this limit were susceptible to interference from the proximity to the sea bed). Around 200 km of good quality seismic was acquired.

The results indicated differentiation of the sediments in these coastal areas and hinted at the presence of a buried drainage system beneath the recent sediment fill of the Gulf. A distinct facies change within the upper sediment unit was detected around the proposed southern exit which might have related to alluvial fan deposits.

2.2.2 Single gravity profile taken across northern Lake Katachori, June 2006

A single, ~800 m long gravity profile was undertaken by a small supervised team of University of Edinburgh undergraduates (including the author) from 21st to 24th June 2006 as a "rough and ready" preliminary investigation into the gravity response of the saddle region and the suspected paleo-lake, Lake Katachori. As explained in Section 1.3.3, the site of Lake Katachori caused issues for the "Strabo's Channel" theory in the case of a buried, untranslated channel as the lake sediments overlapped the proposed route of the channel presented in Figure 1.53 at a height of ~170 m above sea level. The investigation and dating of this site was therefore crucial for testing the validity or disproval of the theory so investigation of this site was considered a high priority and the findings of this investigation were expected to have a major impact on the hypothesis.

Measurements were taken every 10 m using a LaCoste and Romberg Gravity Meter and the relative elevation of each measurement point was recorded using a theodolite and hand-held reflector. The results showed a marked drop in gravity from west to east, which had been predicted in the case that the lake fill sat on top of a low density colluvium-filled channel wedge relative to the denser surrounding bedrock. Although there were limitations in this survey (only a single profile was taken and there were mechanical problems with equipment) the results were still deemed positive enough to plan for further geophysical tests.

2.2.3 Borehole drilled (Cephalonia-Thinia 001) and mud samples acquired, proposed southern exit of "Strabo's Channel", Oct 2006

In October 2006, an exploratory deep borehole was drilled at the proposed southern exit of "Strabo's Channel" at an elevation of 107.5 m above mean sea level (using a locally acquired water-well drilling rig) with the intention of penetrating the Channel axis at this contentious high elevation location and quantifying the depth of the

observed landslide debris. Mud samples were acquired to a depth of 121 m (13.5 m below mean sea level). Analysis of these samples was undertaken by Dr. Kristalina Stoykova of the Bulgarian Academy of Science. The results of this analysis are presented in Appendix A.

The core consisted of Late Quaternary to Late Miocene sediments which limestone clasts of ?Oligocene age mixed into Late Miocene and Pliocene material. The crucial marker nannofossil which led to a Late Quaternary age being assigned to these sediments was a coccolith species believed to be *Emiliania huxleyi* (*Ehux*) found in mud samples at 7 m [core], 10 m [core], 13 m [core] and 26 m [core]. *Ehux* is a ball-shaped species of coccolithophore, a type of single-celled phytoplankton, approximately 5 microns in diameter, consisting of a coccosphere covered with calcium carbonate scale-like plates called coccoliths. *Ehux* is very abundant, globally distributed from the tropics to the sub-Arctic, and is most well known for its ability to create massive milky turquoise blooms (probably due to the reflectivity of individually shed coccolith scales) up to 100 000 km^2 and extensive enough to be viewed from space. Blooms occur in the upper water column and its spores are prone to being transported great distances (hundreds of km) by the wind.

The *Ehux* spores in the Oct 2006 borehole were questionably small (only around 2 to 3 microns) but their presence within the top 44 m (107.5 m to 63.5 m above sea level) of the core as well as other reworked assemblages (of Miocene to Oligocene age) suggested this part of the core represented recent (Late Holocene) valley “fill”.

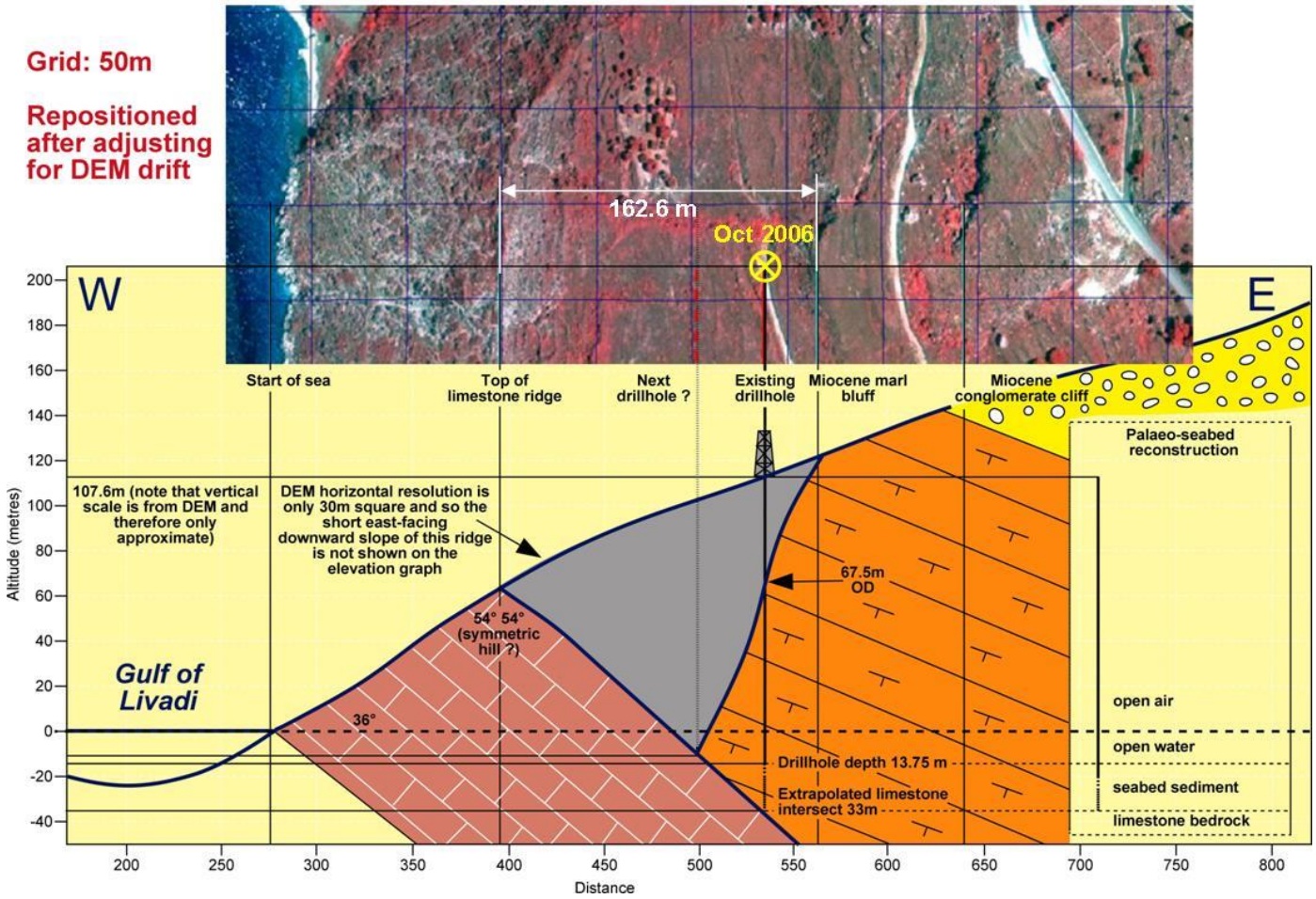

Figure 2.1 Preliminary interpretation of cuttings from the Oct 2006 borehole drilled into the proposed southern exit of "Strabo's Channel" by J. Underhill.

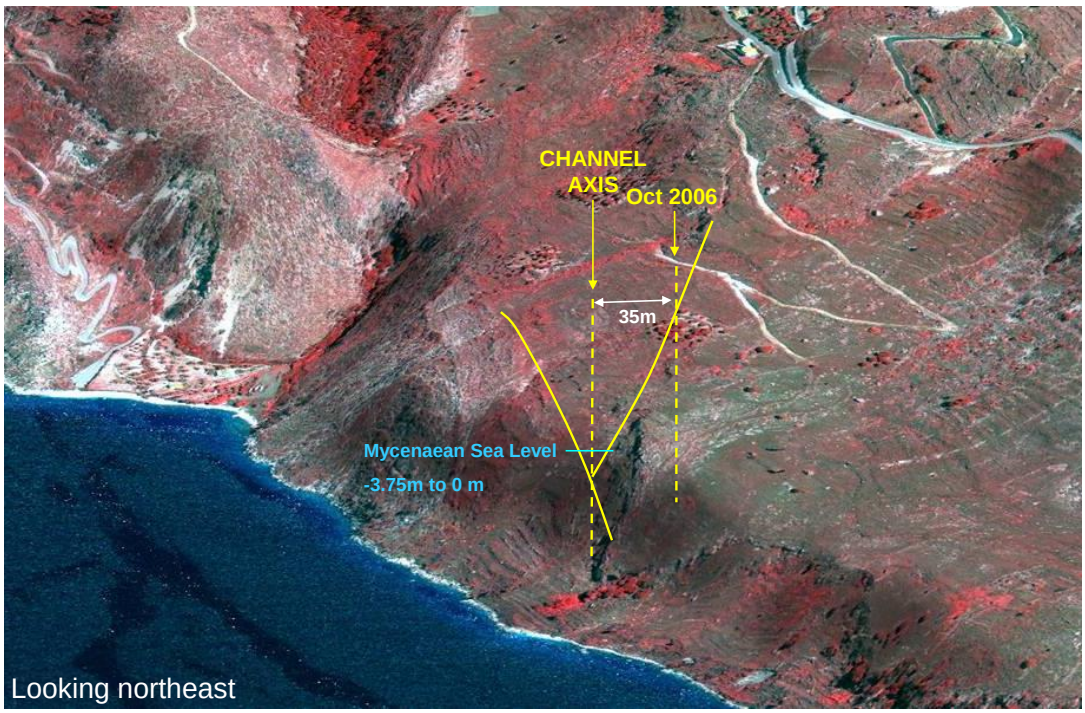

Figure 2.2 Proposed axis of "Strabo's Channel" at southern exit deduced from Oct 2006 borehole data plotted on OziExplorer3D using Digital Globe Quickbird satellite – false infra-red imagery.

The presence of marine spores within the colluvial deposits may represent a windblown deposit which is likely given the borehole's coastal location. These spores might also be the result of tsunami action contaminating the Holocene deposits with marine waters and offering a possible trigger to the sudden and rapid infilling of "Strabo's Channel". The spores may also have mixed into the mud sample through collapse of the core during extraction and may not be *in situ*. From 44 m [core] to 121 m [core] the core consisted of suspected *in situ* Late Miocene bedrock. A preliminary interpretation by J. Underhill based on mud cuttings (no solid rock core ground truth) is presented in Figure 2.1 and Figure 2.2. In this model, the borehole misses the Channel axis and, instead, penetrates the Channel's westerly-dipping eastern side at 40 m [core] to 44 m [core] (67.5 m to 63.5 m above sea level). These results were considered crucial evidence for the presence of a buried channel at this location and incentive for further coring tests to confirm the presence of *Ehux* and whether similar deposits could be found elsewhere in the valley.

2.3 Data Collection

Following the encouraging results of preliminary "reconnaissance" tests, a partnership between the authors of Bittlestone et al. (2005) and the geotechnical company Fugro was established in March 2007 to enable a more comprehensive investigation of "Strabo's Channel". This arrangement allowed the application of industrial-scale geophysical survey techniques to investigate the theory including the establishment of a PhD, primarily sponsored by Natural Environment Research Council (NERC). In addition, Fugro provided Council for Advancement and Support of Education (CASE) sponsorship of the PhD. Additional funds were acquired via the Hayward Trust, established for Eastern Mediterranean based research.

The geo-techniques carried out for this thesis were aimed at confirming and expanding upon the tentatively positive results of the preliminary tests. The following techniques were employed (the brackets indicate the locations where the technique methodologies are described):

1. **Geological fieldmapping (Chapter 3)**
2. **Topographic survey (Section 2.6.1)**
3. **Helicopter-mounted electromagnetometry (HEM) (Section 2.6.2)**
4. **Gravity (Section 2.6.3)**
5. **Resistivity (Section 2.6.4)**
6. **Seismic refraction (Section 2.6.5)**
7. **Shallow marine seismic reflection (Section 2.6.6)**
8. **Shallow sedimentary coring (Chapter 5)**

Data collection was carried out in the following stages:

1. **Logistics Week (18th to 27th June 2007):** Investigation of suitable vessels for the marine shallow seismic reflection survey, meetings with local mayors, IGME in Athens, municipalities and landowners for permits and permissions. Initial field observations in order to plan for survey lines.

2. **"Phase I" Data Collection Campaign (19th Sept to 25th Dec 2007):** Acquisition of helicopter-mounted electromagnetic (HEM) survey, and ground-based gravity, resistivity and seismic refraction surveys at specific sites in Northern Paliki (Atheras and Livadi Marsh) and Thinia (Northern and Southern Thinia and Lake Katachori). The results of these onshore surveys will be presented in Chapter 4. Shallow marine seismic reflection surveys were undertaken in the Gulf of Argostoli, Atheras Bay and Agia Kiriaki Bay (the results of which are presented in Chapter 6). An aerial "sortie" was undertaken to acquire aerial photographs of Thinia and Northern Paliki (18th Oct 2007). Geological field-mapping was undertaken between 17th Sept and 30th Oct 2007 (results presented in Chapter 3).

3. **"Phase II" Data Collection Campaign (17th Nov to 19th Dec 2008):** Further gravity acquisition. The results of these surveys will be presented in Chapter 4.

4. **"Phase III" Data Collection Campaign (19th June 2009 to 8th July 2009):** Further gravity acquisition. The results of these surveys will be presented in Chapter 4.

5. **Drilling of Onshore Shallow Sedimentary Cores (27th Sept 2010 to 28th Jan 2011):** Seventeen continuous shallow sedimentary cores were drilled based on the results of these non-invasive surveys. The results of the coring are presented in Chapter 5. Further geological field-mapping was undertaken between 17th and 24th Oct 2010.

2.4 Onshore Non-invasive Surveys

2.4.1 "Phase I"

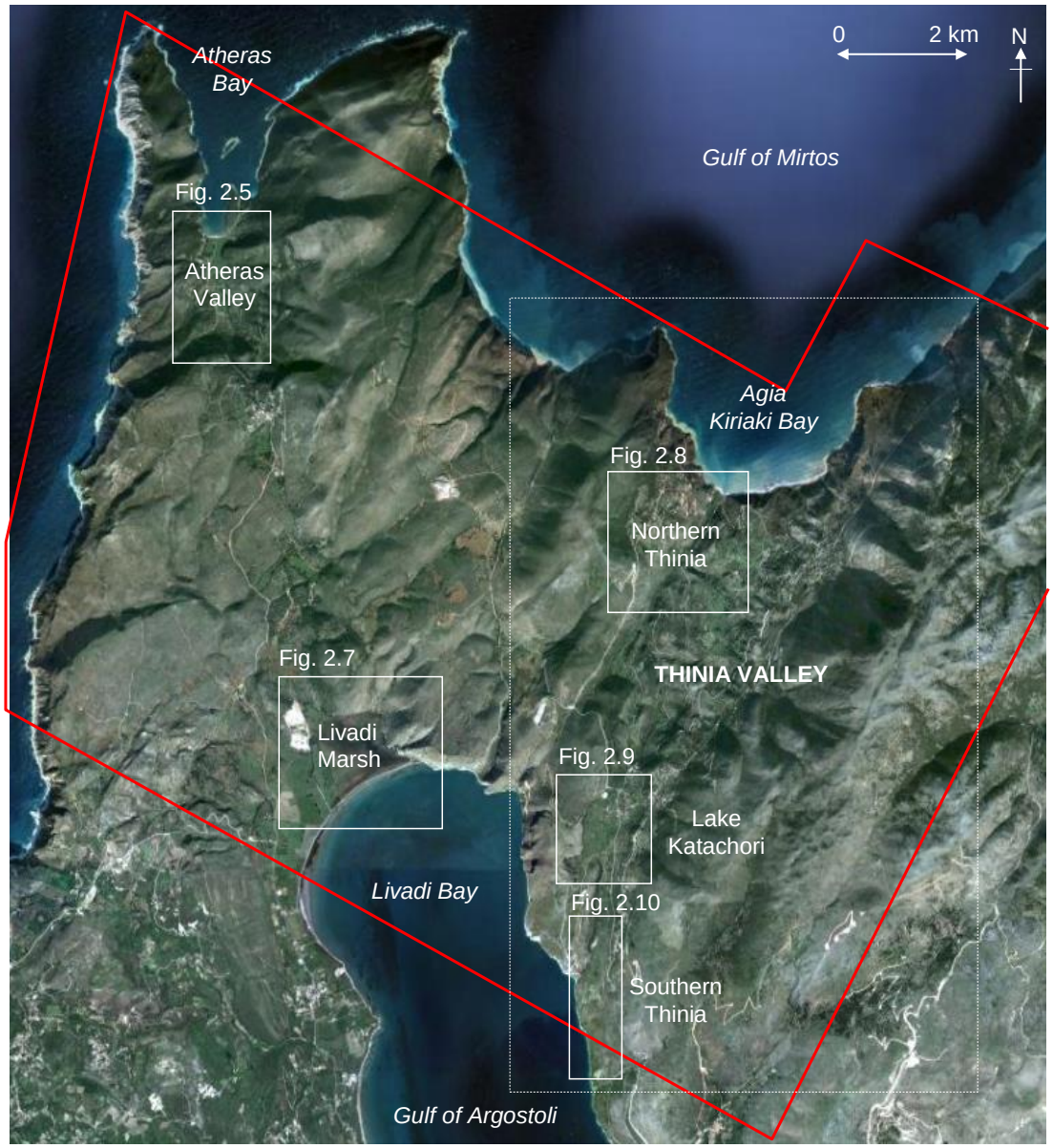

Figure 2.3 Google Earth satellite map showing the locations of the Phase I onshore surveys (outlined in white). The area covered by the airborne survey is indicated by a red line.

The helicopter-mounted electromagnetic (HEM) survey (outlined in red in Figure 2.3) was undertaken across Northern Paliki and Thinia and was aimed at acquiring a "semi-regional" overview of the ground conductivity and surface magnetic properties within a 10 x 10 km area. It was hoped that this survey would image the recent valley

fill (alluvial, landslide) within Thinia to a depth of ~100 m and aim to resolve the base of this fill. In addition to the HEM survey, ground-based surveys of gravity, resistivity and seismic refraction were also undertaken during the Phase I data collection campaign which focused upon the following regions (outlined in white on Figure 2.3):

1. **Atheras (A)**
2. **Livadi Marsh (B)**
3. **Thinia Valley (C)**

A. Atheras

Atheras Bay lies at the northerly-most tip Paliki and consists of two mountainous headlands which enclose a further smaller pair of headlands within the inner bay, a configuration most clearly illustrated looking northwards out to sea (Figure 2.4, A) and is reminiscent of Homer's description of Phorcys Bay, Odysseus' first land-fall after returning to Ithaca (Volterras, 1903; Bittlestone et al., 2005).

The bay encloses a low elevation (between 0 and 21 m above sea level), low-gradient valley floored by *terra rossa* alluvial sediment and cross-cut by numerous terraces running parallel to the shoreline (Figure 2.4, B) some of which have been used for field demarcation and some of which are clearly man-made. These terraces were of interest to the investigation as they might represent beach terraces uplifted through positive coseismic land movement affecting Northern Paliki thus potentially tying into the beach terraces detected around Thinia and Livadi Marsh (Section 1.3.2).

The onshore geophysical surveys were aimed at determining the depth of the bay-fill within the valley. Five resistivity and seismic refraction profiles were acquired across Atheras Bay (labelled ABL1 to ABL5 on Figure 2.5) between 3rd and 5th Oct. ABL1 to ABL4 were orientated W-E while ABL5 was orientated N-S providing a cross-line linking the four E-W lines.

Figure 2.4 Atheras Bay: A. The distinct "headland-within-a-headland" of Atheras Bay viewed from Atheras town which might represent Odysseus's first landfall on Ancient Ithaca, Phorcys Bay; B. Aerial photograph of the possible raised beach terraces cross-cutting the valley representing raised postglacial (Holocene) sea levels or instances of positive coseismic land movement affecting Northern Paliki.

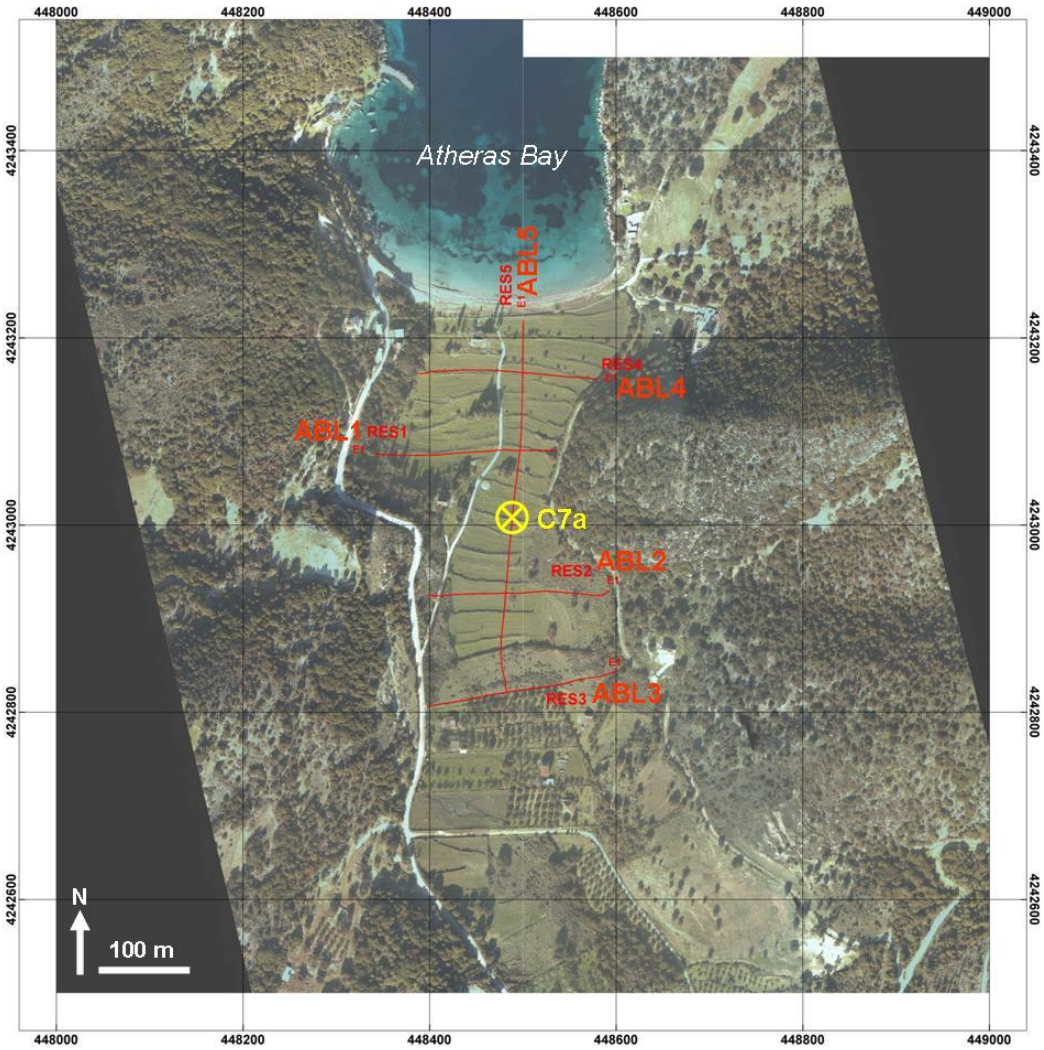

Figure 2.5 Satellite map showing the location of the Atheras Bay resistivity and seismic refraction surveys (marked in red and labeled ABL1 to ABL5) and the calibrating borehole C7a (described in Section 5.2.1).

B. Livadi Marsh

Livadi Marsh occupies the flat land at the head of the Gulf of Argostoli (Livadi Bay). It comprises of a very flat, very low elevation (a metre or less above sea level) boggy area approximately 3 km^2 in area (Figure 2.6). Given the very low elevation of the marsh relative to the present shoreline it is likely the area has been inundated by the sea in recent (Late Holocene) times. Because of its location beneath the Kastelli hill fort the marsh was well-placed to serve as a possible deep harbour for Ancient Ithaca if this flooding occurred during the Late Bronze Age (Bittlestone et al., 2005).

This site was investigated to determine if relative sea level could have been high enough to flood Thinia during the Late Bronze Age. Today a raised spit upon which the modern-day road is built runs across the mouth of the marshland protecting it from inundation from the sea. For Livadi Marsh to be a likely contender for Ancient Ithaca's "deep harbour" marine inundation of this area would need to have occurred within the last ~3300 years. The subsequent "drying out" of the marsh may have been caused by the ~6 m of Late Holocene coseismic uplift which is speculated by some to have affected Northern Paliki.

The Livadi Marsh surveys were aimed at determining the depth of the recent "harbour fill" sediment. These surveys were also aimed at detecting the course of the Atheras Thrust which wasn't clear after it reaches Livadi Marsh. It appears that a portion of the hangingwall is missing and has presumably collapsed into marsh, a process, if proven, is favourable evidence for large-scale mass-wasting in this area.

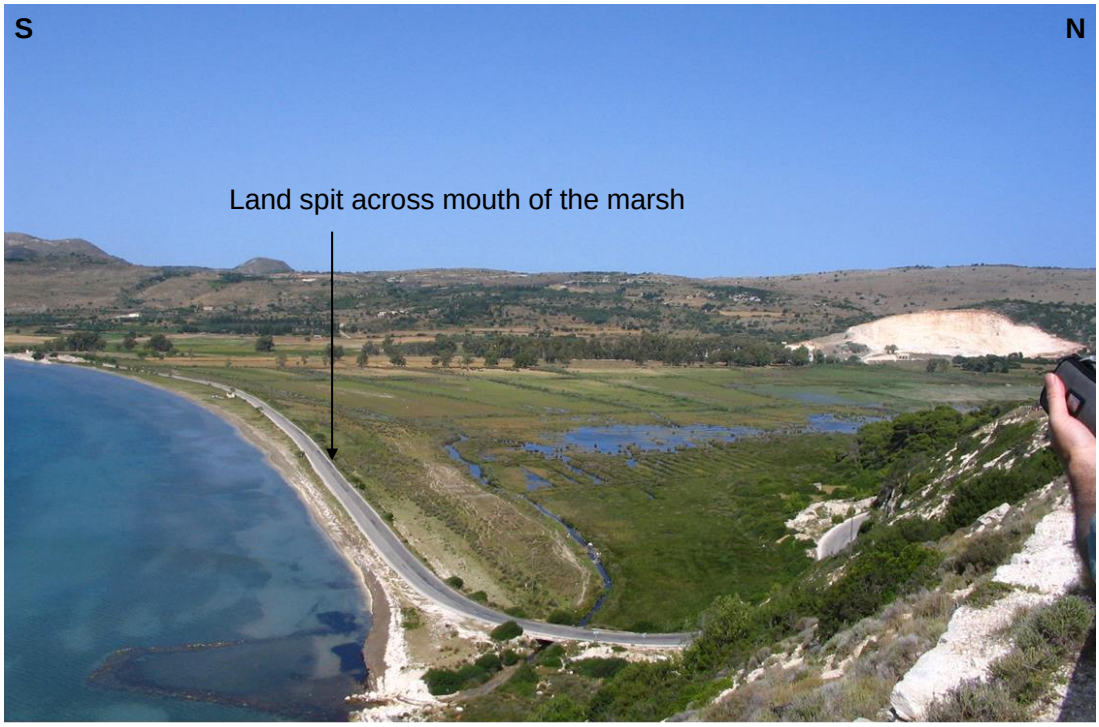

Figure 2.6 View of Livadi Marsh from Atheras Thrust hangingwall indicating the position of the raised land spit which protects this low-lying boggy area from further marine inundation.

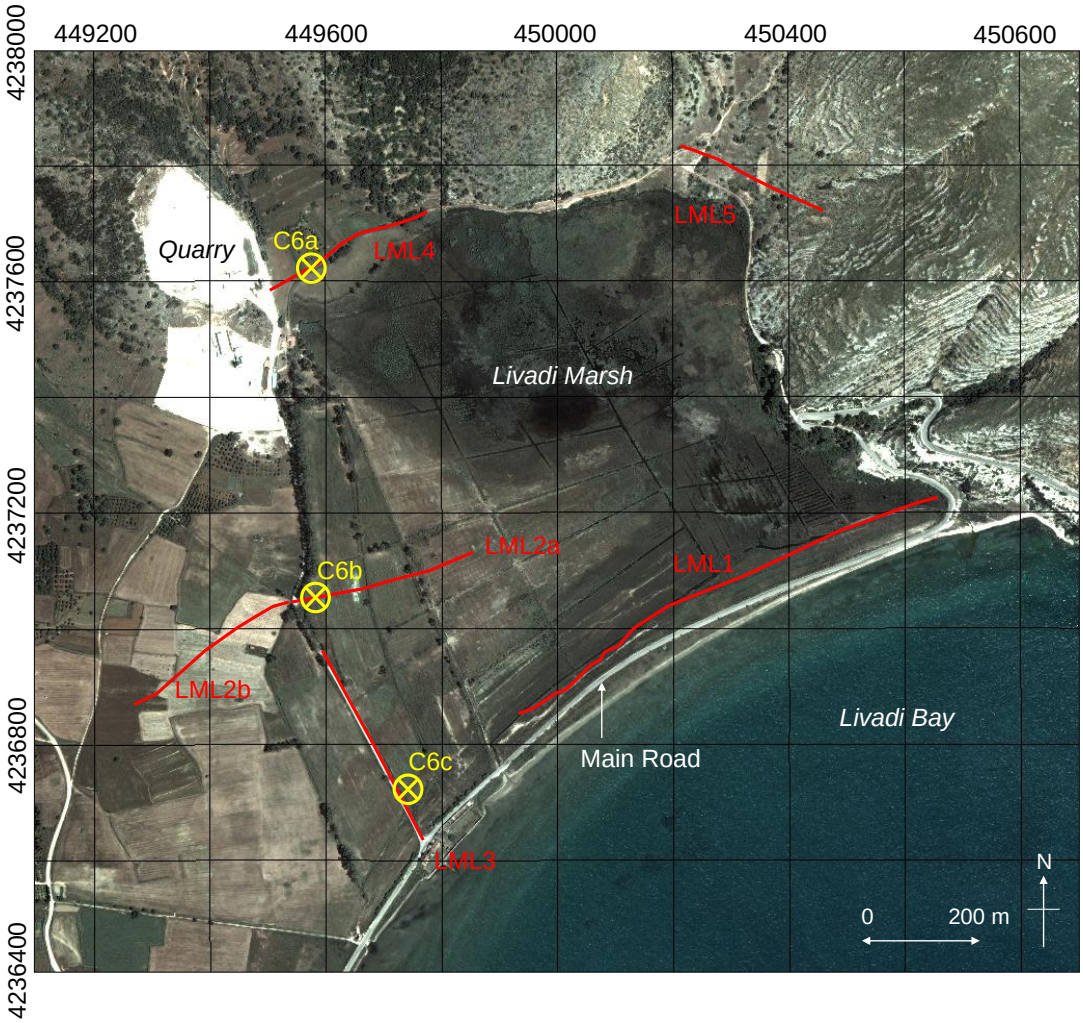

Figure 2.7 Satellite map of Livadi Marsh showing the location of the six resistivity and seismic refraction lines (red, labeled LML1 to LML5) and boreholes (C6a, C6b and C6bc) in yellow. Map produced by OziExplorer using natural (100 pc) colour satellite image.

Six resistivity and seismic refraction lines (labelled LML1 to LML5 on Figure 2.7) were conducted across the marsh between 6th Oct and 19th Oct 2007. Concerns were raised about excessive salt deposits in the sediments (and saline water table) in this near coastal location interfering with the resistivity survey. The locations of the lines were restricted due to waterlogged marshland and deep standing water. LML1 was positioned along the land spit along the shoreline. Lines LML2a and LML2b cross-cut the western edge of the marsh. LML3 provided a north-south line. LML4 was positioned across narrow inlets to the northwest of the marsh to investigate possible small harbour areas for the settlement at Kastelli Hill, the most likely location of Odysseus palace (Bittlestone et al., 2005). For the same reason, LML5 was placed to

investigate another narrow inlet to the northeast of the marsh. This line was positioned across the base of the deeply-incised gullies within the limestone slope which the magnetic map identified as a source of the strongly magnetised marsh sediments.

C. Thinia Valley

The Thinia valley tests were aimed at directly investigating the "Strabo's Channel" hypothesis and determining whether or not a marine channel existed here during the Late Bronze. The Phase I land-based surveys focused on three key areas:

1. **Northern Thinia**
2. **Lake Katachori**
3. **Southern Thinia**

1. Northern Exit

The proposed northern exit of "Strabo's Channel" was located along the axis of the NNE-SSW striking stream valley beneath Zola to the east of Zola's harbour (Figure 2.8). The aims of the survey here were to determine the depth of the landslide deposits and thickness of the Zola talus deposits.

The northern exit electrical resistivity survey consisted of seven lines (labelled NTL0 to NTL6 in Figure 2.8) and was undertaken between 26th Sept and 2nd Oct 2007. Six lines (NTL0 and NTL2 to NTL6) were orientated roughly perpendicular to the existing outwash channel. NTL0, NTL2, NTL3 and NTL4 were located within the boulder field immediately to the east of the Zola talus fan. NTL5 and NTL6 were positioned further southwest. The surface terrain of this area was a mixture of agricultural land and dense scrubland with boulder debris and steep topography. The survey lines were located along the incised gullies of the numerous paleo-streams which drained from the eastern side of the valley into the modern outwash stream as

the topography was less extreme. Gravity profiles were taken at the same locations as the E-W orientated resistivity profiles (labelled NTG1 to NTG6 in blue on Figure 2.8) between 28th Sept and 16th Oct 2007 with the aim of detecting the low density zone expected from a rubble-filled channel wedge relative to surrounding bedrock in the case of a buried, untranslated channel.

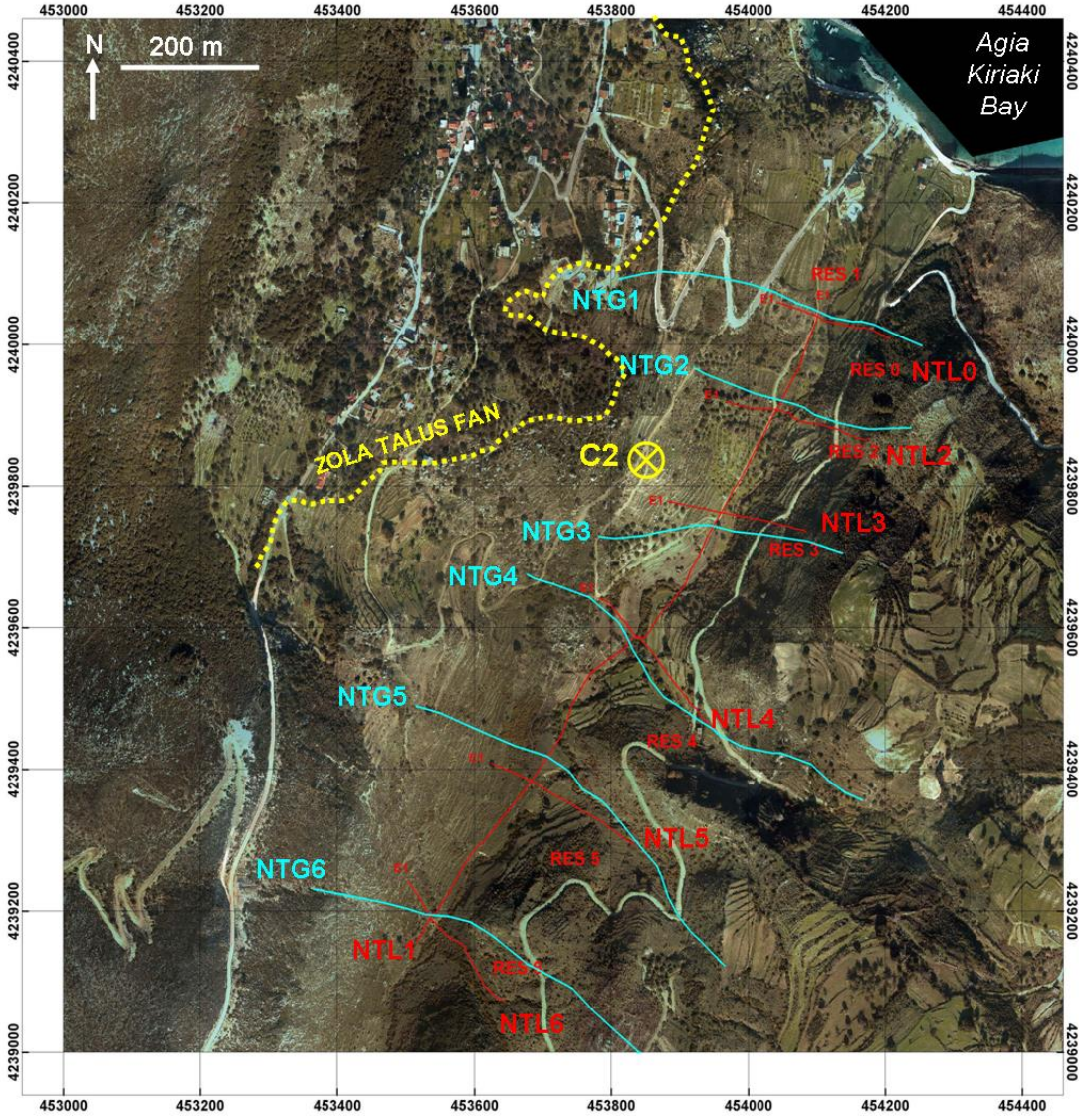

Figure 2.8 Satellite map of northern Thinia showing the locations of the seven resistivity and seismic refraction lines (red, labeled NTL0 to NTL6) and six "Phase I" gravity lines (blue, NTG1 to NTG6). The location of the borehole C2 is indicated in yellow.

2. Lake Katachori

Following the encouraging results from the single gravity profile taken across Lake Katachori in June 2006 (Section 2.2.2) which detected a low gravity anomaly across the paleo-lake area, a more extensive gravity survey was undertaken. Five E-W orientated gravity profiles were taken across the lake (labelled LKG1 to LKG5 on Figure 2.9). LKG5 followed the location of the June 2006 profile (Section 2.2.2).

Seven resistivity and seismic refraction lines were also acquired (labelled LKL1 to LKL7 in Figure 2.9). Five E-W orientated profiles (LKL1 to LKL5) measuring between 224 m and 373 m long were run perpendicular to the long axis of the lake. Two lines (LKL6 and LKL7) measuring around 470 m long were placed roughly parallel to the lake's long axis. These long lines were located on the basis of a rough on site inversion of the resistivity data (basic least squares inversion with no altering of the default RES2DINV software parameters) in order to identify the thickest parts of the lake fill. For this rough interpretation "lake fill" was classed as the very low resistivity material detected by the E-W lines, the base of which was not resolved by these shorter lines. LKL6 and LKL7 were thus made longer to increase the imaging depth of the profiles (up to 40 m) and resolve the base of the lake fill material.

The key outcomes of investigation were to firstly determine whether Lake Katachori was a lake at all and, if so, when it formed and why in a region where no lakes currently occur. The flatter terrain of the paleo-lake allowed ease of resistivity and refraction cable deployment and transportation between measurements. Because the paleo-lake formed one of the most intensively-farmed agricultural areas in the valley, ongoing farming activities caused occasional obstruction. Dense olive groves reduced the efficiency of the GPS rover to get a clear signal to take topographic readings. The occurrence of private land presented restrictions on the locating of profile locations. Fencing surrounding the small land-holdings presented obstacles to the resistivity and seismic refraction cable however this was less of a problem with the gravity survey which did not require a cable.

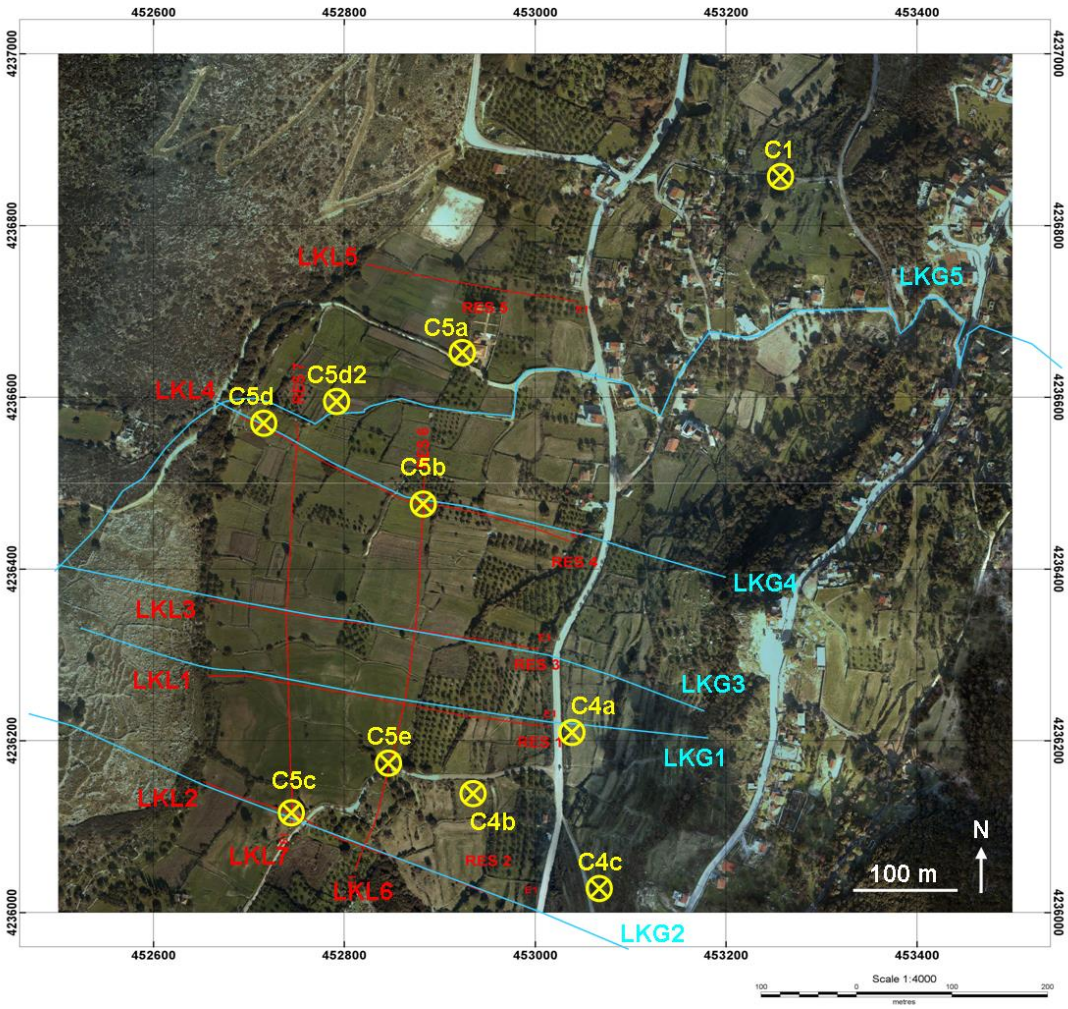

Figure 2.9 Satellite map of Lake Katachori showing the locations of the seven resistivity and seismic refraction lines (red, labeled LKL1 to LKL7) and five "Phase I" gravity lines (blue, LKG1 to LKG5). Borehole locations are indicated in yellow.

3. Southern Thinia

Resistivity, seismic refraction and gravity surveys were undertaken to investigate the boulder-strewn area proposed to be the southern exit of "Strabo's Channel". These surveys were aimed at detecting the interface between the backfill and underlying bedrock to determine whether the surface colluvium of this region formed only a thin veneer or represented the top of a ~180 m high, vertiginous wedge of backfill. To be a valid contender for the southern exit, this wedge of colluvial material would need to reach sea level. These tests were also aimed at determining the age of this material.

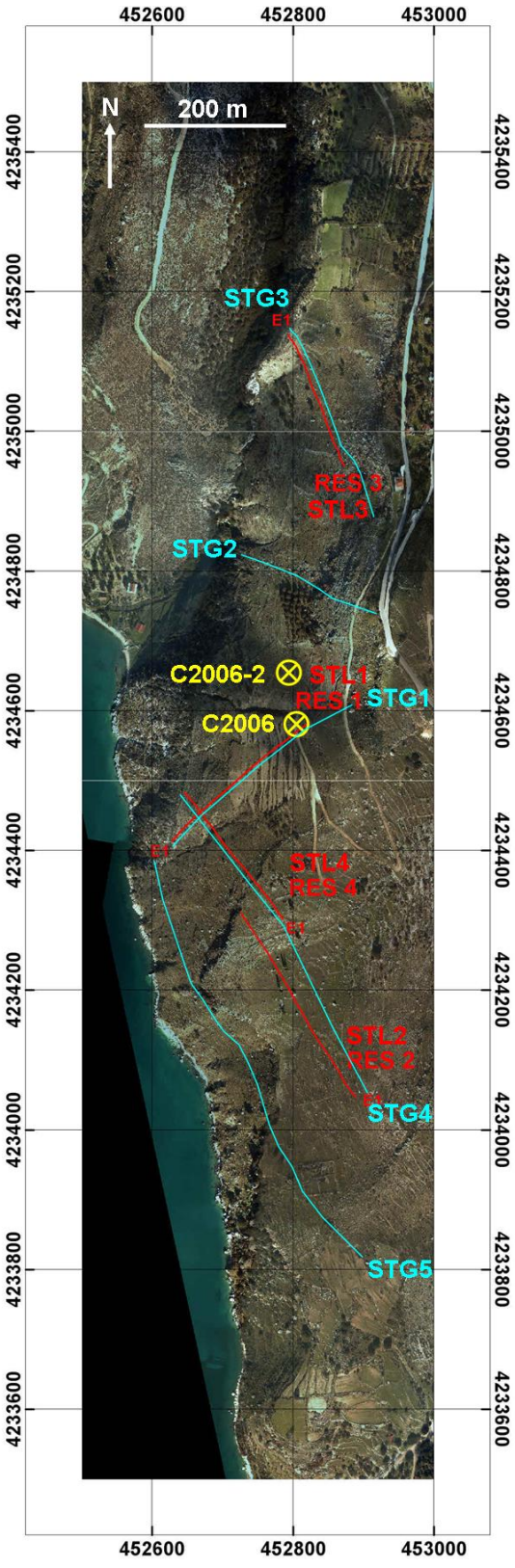

Figure 2.10 Satellite map of southern Thinia showing the locations of the four resistivity and seismic refraction lines (red, labeled STL1 to STL4) and five Phase I gravity lines (blue, STG1 to STG5). Borehole locations are indicated in yellow.

The southern exit electrical resistivity survey consisted of four lines (labelled STL1 to STL4 in Figure 2.10). STL1, STL3 and STL4 were positioned to cross-cut the southern Channel exit proposed in Figure 1.53. STL2 was aimed at investigating the area to the south of this location. The surface terrain of the slumped area was a mixture of agricultural land and low scrub with steep topography and scattered boulder debris. Gravity profiles were taken across the resistivity lines (labelled STG1, STG3 and STG4 in blue on Figure 2.10). Two further gravity lines (STG2 and STG5) were taken separately.

2.4.2 "Phase II"

Preliminary views of the "Phase I" gravity data from Lake Katachori gravity survey imaged a low gravity anomaly to the east of the paleo-lake, in the region where "Strabo's Channel" was expected to cross. This was consistent with the preliminary June 2006 gravity profile which also imaged a lowering of gravity in this zone. The Phase II survey was deployed to better image this low gravity anomaly and to investigate whether this key response was a local anomaly or if it could be detected at other locations along the proposed channel route suggesting it was part of a larger anomaly, reducing the chances of misinterpretation. Phase II extended the gravity survey coverage further across Thinia and tied the Phase I surveys together relative to the rest of the valley. To be a valid contender for "Strabo's Channel", this response should be continuous from Agia Kiriaki Bay to the Gulf of Argostoli and modelling of the gravity data should show this low density material reaching sea level.

2.4.3 "Phase III"

This survey involved the collection of gravity data in the gaps left by the previous two phases (particularly in NE Thinia where colluvial debris covered much of the land surface) ensuring a good coverage of data points across the valley.

2.5 Offshore Surveys

Shallow marine seismic reflection data was acquired across the coastal areas immediately to the north and south of the Thinia isthmus (Agia Kiriaki Bay and the Gulf of Argostoli respectively) and in Atheras Bay between 15th and 30th Oct 2007. The 2007 survey was aimed at acquiring seismic data of a greater volume, greater depth and quality than the 2005 survey.

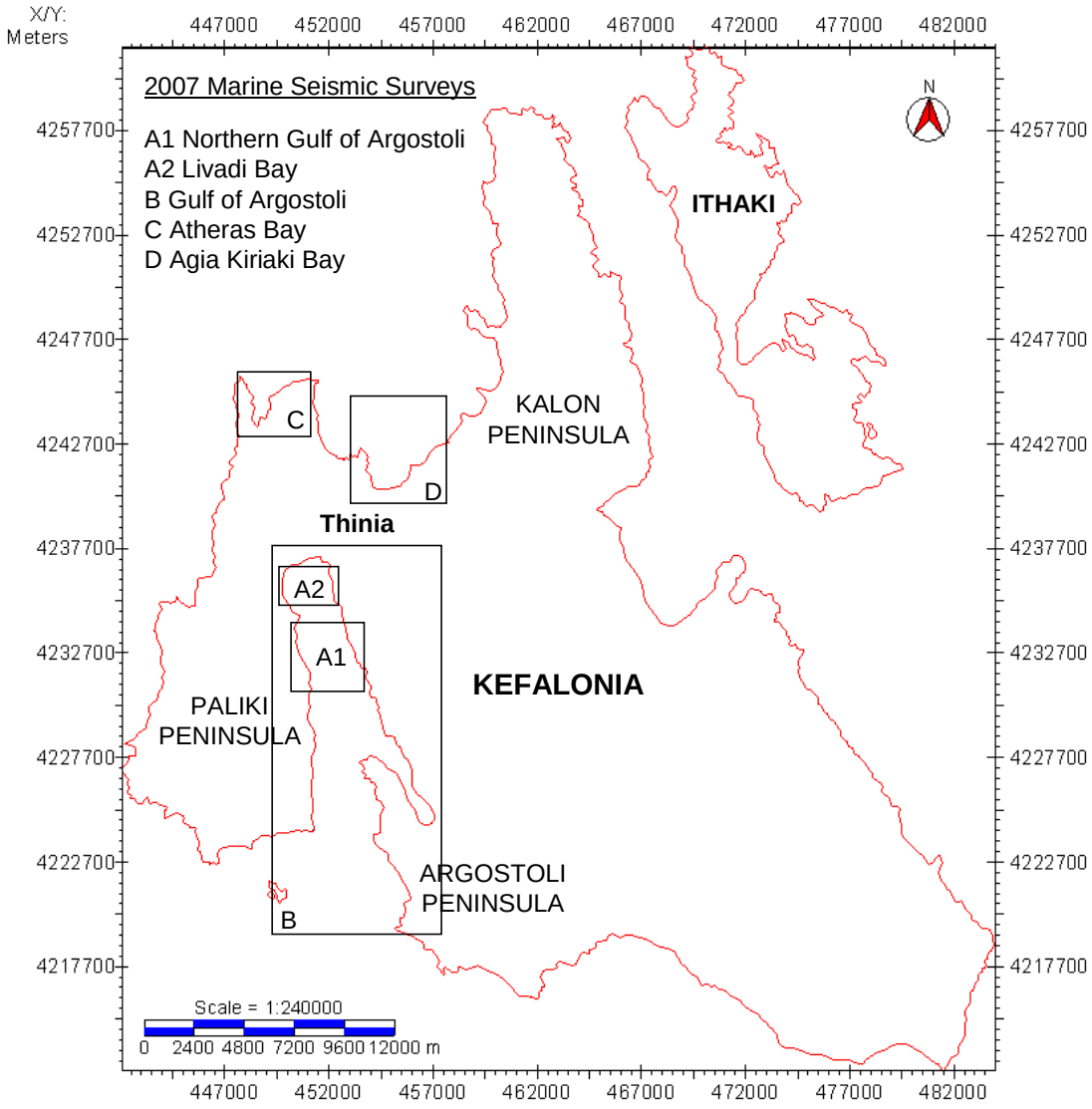

Figure 2.11 Kingdom base map showing the locations of the Oct 2007 shallow marine seismic reflection surveys.

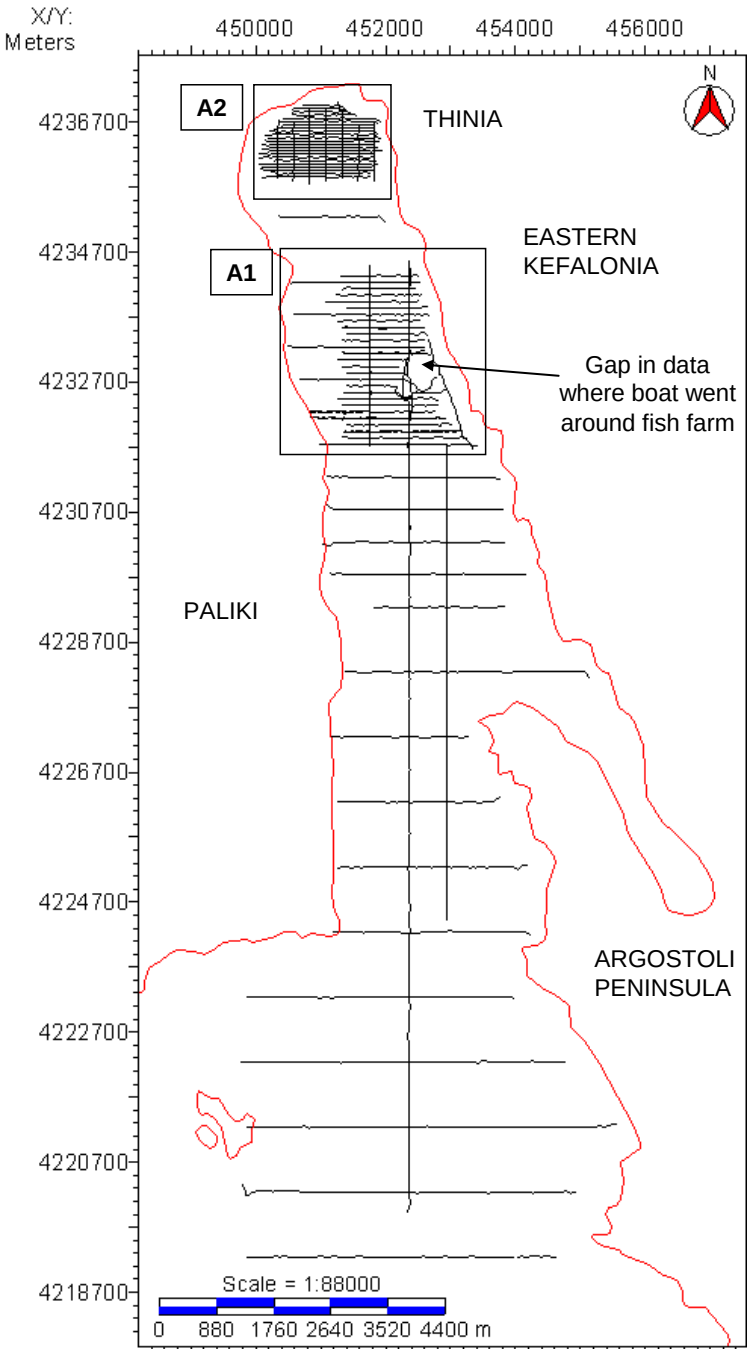

Figure 2.12 Kingdom base map showing the locations of the Gulf of Argostoli marine seismic reflection surveys.

Five volumes of data were acquired: Gulf of Argostoli (A1, A2 and B), Atheras Bay (C) and Agia Kiriaki Bay (D) (Figure 2.11). The primary targets of investigation were the sea-floor morphology and the recent sedimentation record particular around the proposed exits of "Strabo's Channel" as evidence for the Channel was expected

to be evident in this uppermost unit e.g. the presence of alluvial fans or colluvial debris or evidence of a channel incised into the sea bed. The surveys were also aimed at investigating evidence for (and against) neotectonic (coseismic) activity on offshore "Alpine" (Hellenide) structures and determining the relationship between faulted geology offshore and similar structures onshore.

2.5.1 A1: Northern Gulf of Argostoli

The A1 volume (Figure 2.12) formed 2.8 km x 2.4 km grid of line-spacing around 110 m located offshore of the southern exit of "Strabo's Channel" (Figure 2.10). This volume contained a total of 29 profiles: 26 east-west orientated lines, two north-south lines and one NW-SE line running along the coast.

2.5.2 A2: Livadi Bay

The A2 volume (Figure 2.12) formed the smallest (1.9 km by 1.3 km) and northerly-most grid with line-spacing of < 60 m between E-W lines and approximately 260 m between the N-S lines. This volume contained a total of 30 lines (23 E-W lines and 7 N-S lines). This survey was established to detect onlapping marine sediments into the shallow northern part of the Gulf charting the later stages of postglacial sea level rise.

2.5.3 B: Middle and Lower Gulf of Argostoli

Volume B spanned most of the Gulf of Argostoli and comprised of 18 lines (Figure 2.12). The middle Gulf (between the northern tip of the Argostoli peninsula and the A1 seismic volume) contained 7 east-west lines with spacing of 0.5 km. The lower Gulf (the region which extends south between the northern tip of Argostoli Peninsula and Lixouri) contained 9 east-west lines of ~1 km spacing. These lines were all linked by two north-south lines. A single line (KEF-B-33) was located between A1 and A2

2.5.4 C: Atheras Bay

The Atheras Bay survey (Volume C) was a small roughly triangular survey spanning around 2 km x 2.5 km (Figure 2.13). The aim of the survey was enable a better understanding of the structural geology of the region and map the progression of postglacial sea level rise into the Bay.

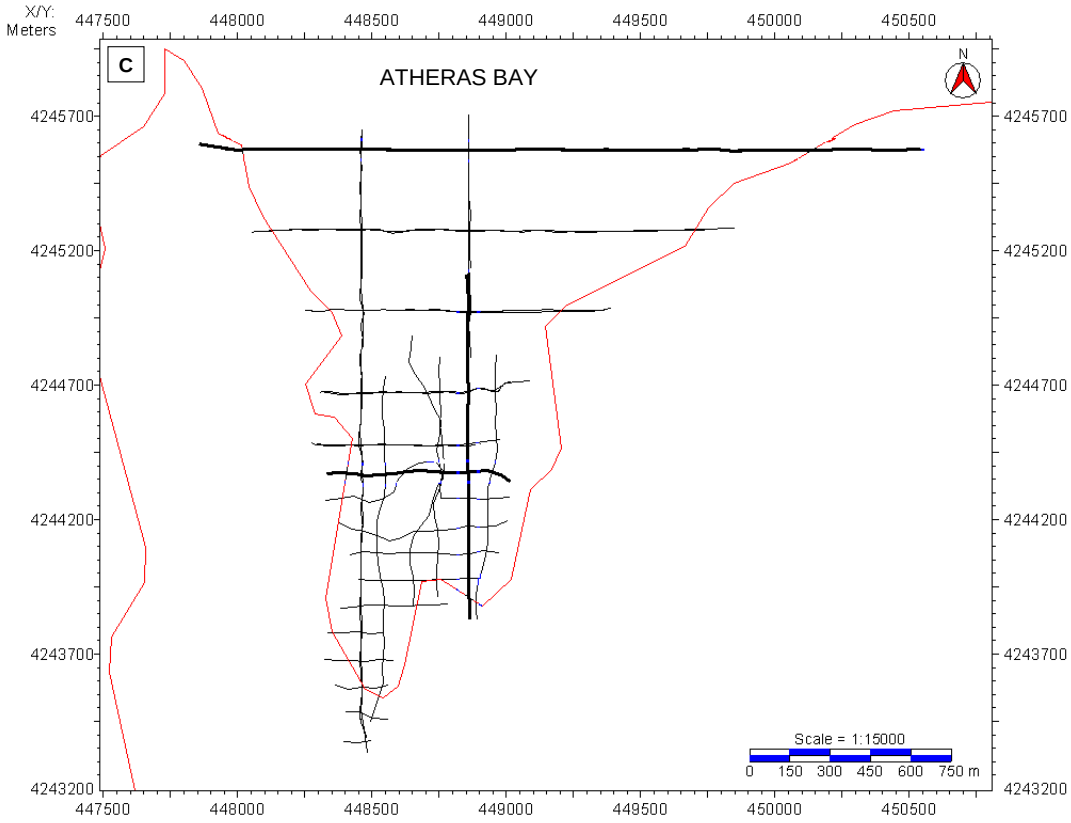

Figure 2.13 Kingdom base map showing the location of the Atheras Bay marine seismic reflection surveys.

2.5.5 D: Agia Kiriaki Bay

The Agia Kiriaki Bay volume consisted of one large survey measuring roughly 4.6 km x 3.8 km with total of 35 lines (30 E-W lines and 5 N-S lines) and line-spacing of 50 m to 100 m (Figure 2.14). The survey was placed to look for offshore evidence of "Strabo's Channel" to the north of the Thinia land-bridge. The grid extended out into the Gulf of Mirtos with spacing between E-W lines of approximately 0.4 km and around 1 km between the N-S lines.

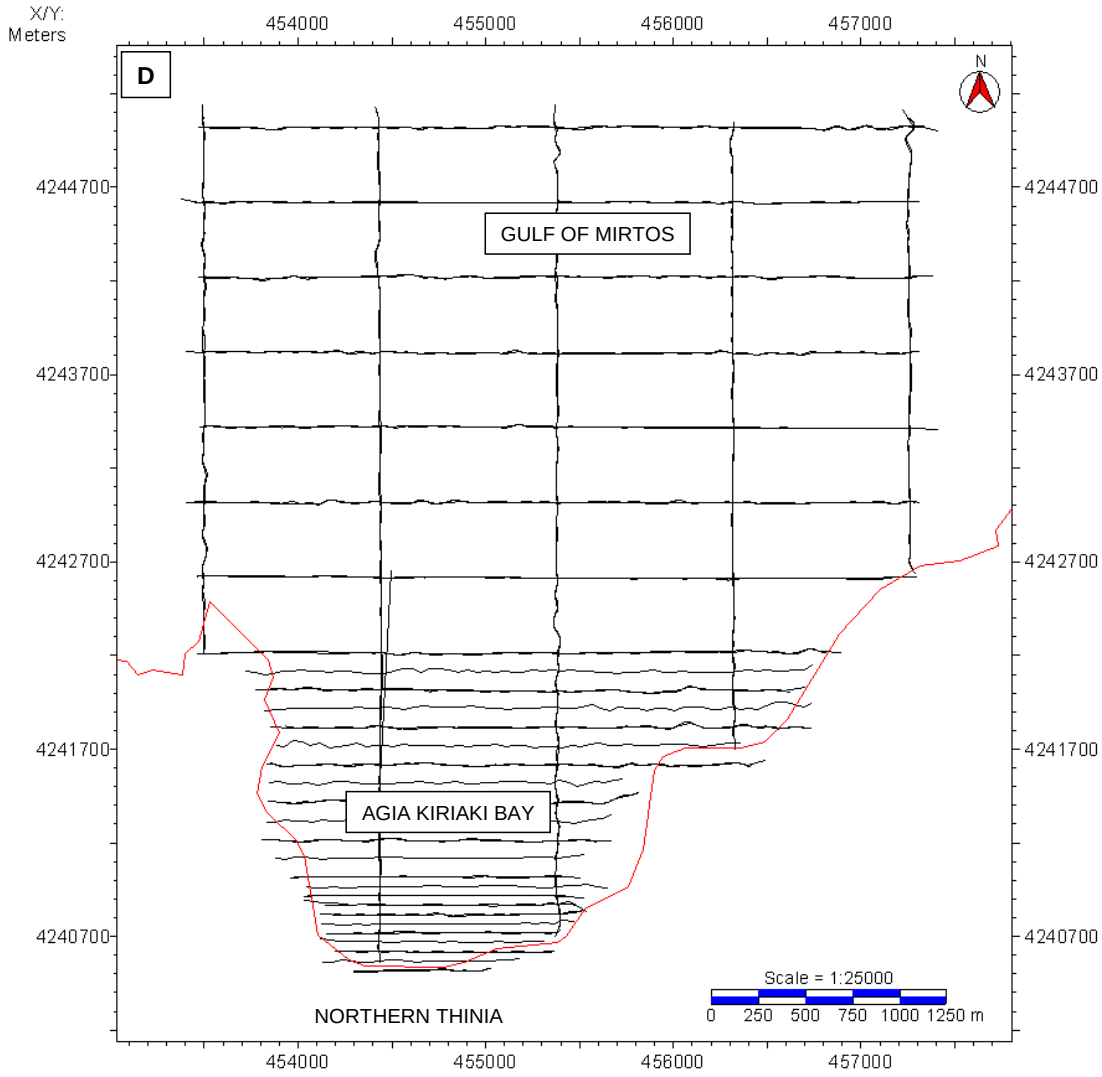

Figure 2.14 Kingdom base map showing the location of the Agia Kiriaki Bay marine seismic reflection surveys.

Survey	Type (A = Airborne, L = Land-based, M = Marine)	Survey Technique	Equipment	Details
Preliminary (Reconnaissance) Surveys	M	Sub-bottom profiling (SBP) survey (Section 2.2.1)	ORE 3.5 kHz "pinger", EPC 3200 recorder	Approximately 200 km of good quality seismic acquired for Gulf of Argostoli and Gulf of Mirtos.
	L	Gravity (Section 2.2.2)	LaCoste and Romberg Gravity Meter	Single profile taken across Lake Katachori, gravity stations taken every 10 m. Locations of stations measured using theodolite and hand-held reflector.
	L	Shallow sedimentary coring (Section 2.2.3)	Water well drilling rig	121 m deep borehole taken in Southern Thinia, mud samples acquired and biostratigraphically analysed.
Non-invasive Surveys	A	Helicopter-mounted electromagnetometry survey (Chapter 4)	RESOLVE "bird" suspended from helicopter	Depth slices of Northern Paliki taken at frequencies 400 Hz, 1800 Hz, 8200 Hz, 40 kHz and 140 kHz. RTP Magnetic map.
	L	Gravity survey (Chapter 4)	Scintrex CG-5 "AutoGrav" relative gravity meter	Gravity stations 10 m apart; survey encompassed the whole of Thinia valley.
	L	Resistivity survey (Chapter 4)	Campus Tigre resistivity meter	Wenner alpha array with electrode spacing of 5 m; total of 29 profiles taken; North (7) and South Thinia (4), Lake Katachori (7), Atheras Bay (5) and Livadi Marsh (6).
	L	Seismic refraction survey (Chapter 4)	Geometrix Geode 24 seismic meter	Geophone spacing of 5 m; total of 29 profiles taken along same lines as resistivity survey.
	M	Shallow marine seismic reflection survey (Chapter 6)	A single 100 m hydrophone streamer and electric sparker source	Five volumes acquired: Gulf of Argostoli (A1, A2 and B), Atheras Bay (C) and Agia Kiriaki Bay (D).
	M	Sub-bottom profiling (SBP) survey (Chapter 6)	Ship's sonar	SBP survey taken along some of the sparker profiles in all five volumes.
Intrusive Surveys	L	Shallow sedimentary coring (Chapter 5)	6 ton Ecofore CE-603	17 continuous cores with soil sample collection taken at Atheras Bay, Livadi Marsh and Thinia. Paleontological studies were undertaken of the soil samples; age-dated using a biostratigraphic or nannofossil method.

Table 2.1 Summary of the non-invasive geophysical and invasive survey techniques applied to investigate the "Strabo's Channel" theory. The reference within the brackets in the survey technique column refers to the section of this thesis which presents the results of these surveys.

2.6 Survey Methodology

This section will describe in brief terms the techniques employed to investigation "Strabo's Channel" (topographic survey, non-invasive onshore and offshore), the equipment used to collect the data and the methods used to handle the data. A full summary of all the surveys undertaken is presented in Table 2.1.

2.6.1 Topographic Survey

A. Trimble Survey

The ground-based (gravity, resistivity and seismic refraction) geophysical survey data points were measured by an independent topographic survey in terms of Universal Transverse Mercator (UTM) i.e. easting (X) and northing (Y). This survey used a Trimble 5700 differential global positioning system (DGPS) which consisted of a base station and a portable "rover" linked by radio signal. The DGPS base station was set up in a prominent location (in order to get a clear view of the sky and greatest number of satellites to make an accurate reading on its location) and left for an hour in order to get a good average location on its position. In optimal conditions this set-up should give an ideal position accuracy of ± 6 mm however accuracy was probably in the region of ± 1 to 2 cm. The main source of uncertainty was due to dense tree cover. The reference ellipsoid used by the DGPS evaluated average sea level to ~+22 m above sea level (0 m).

B. Digital Elevation Model (DEM)

A high resolution digital elevation model (DEM) data for Thinia and Northern Paliki was acquired by Fugro Airborne Surveys in December 2007. In the valley where LIDAR was acquired, resolution was in the order of 15 cm (horizontal) and 10 cm vertical) to 2 sigma (95% confidence). The reference ellipsoid used by the DEM took

an average sea level of ~+22 m above sea level (0 m). The positions taken by the Trimble survey were compared to the equivalent points extracted from the DEM using the *grdtrack* command in Fortran and were found to be within ± 10 cm of one another which was considered of reasonable accuracy.

Preparation of the raw DEM data was carried out by the author under supervision using a series of programmes constructed using the imperative language Fortran 95. Fortran 95 was mounted on the university server and accessed using Hummingbird Exceed Freeware and the NX Client interface. Plotting of the DEM in terms of easting, northing and elevation was undertaken using the command-line programme Generic Mapping Tools (GMT). GMT is described as an open-source collection of approximately 60 command-line operated Unix tools designed to allow the manipulation of multi-dimensional (x,y and x,y,z) geographic and Cartesian data sets and the display of them in the form of PostScript (PS) or Encapsulated Postscript Files (EPS) (Wessel and Smith, 1991; 1995; 1998; 2009).

C. Satellite Maps (Digital Globe Quickbird, Google Earth)

The key satellite maps used were high resolution (~60 cm) false colour infra-red Digital Globe Quickbird satellite images. The images were false colour with near infra-red appearing as red, red appearing as green and green as blue. Blue colours did not appear. Well-watered lush vegetation appears rich red since chlorophyll reflects light in the near infra-red so the Quickbird images gave a measure of vegetation density. The vegetation along the routes of active and seasonal watercourses appeared the most vivid red thus enabling springs, often the sign of a lithological contact was close-by, to be identified and tracked from a distance. 1:5000 scale versions were used for field-mapping because their resolution allowed the location to be identified with precision. These maps were viewed and manipulated using OziExplorer GPS Mapping Software (3.95.4q) created by Des Newman of D&L Software Pty Ltd Australia (www.oziexplorer.com).

2.6.2 Helicopter-mounted electromagnetic (HEM) survey

HEM surveys work by detecting and measuring the electrical conductivity (the reciprocal of resistivity) and magnetic susceptibility of the ground through electromagnetic induction and detection of the total magnetic field respectively (Knepper et al., 1995).

The survey was carried out by Fugro Airborne Surveys using the RESOLVE frequency-domain and magnetometer system. This set-up used a transmitting coil and receiving coil housed within a cylindrical rigid boom or "bird" around 10 m long slung by cable beneath the helicopter which was towed over the survey area at a height of around 800 m (Figure 2.15). The RESOLVE bird contained a six-frequency system consisting of five horizontal "co-planar" coils (being equivalent to both transmitting and receiving coils lying flat on the ground) one "co-axial" coil pair (where an axis normal to the plane of the coils passes through the centre of the pair) (Fugro Airborne Surveys, 2011). Data points were collected every 10 metres and calibrated automatically for phase and gain while airborne, using internal calibration coils removing noise from recorded data. The location of the surveys was measured using global positioning system (GPS) and the survey helicopter's altimeter.

The HEM data was provided in a series of pre-processed (reduced) colour contoured maps of TIFF image format and corresponding Oasis Montaj viewer GRD files produced using Fugro Airborne Survey's in-house processing, Geosoft and Profile Analyst software. Apparent resistivity maps were produced for five different frequencies (140 kHz, 40 kHz, 8200 Hz, 1800 Hz and 400 Hz). The natural filtering ability of the Earth (Sheriff, 1973) mean the lowest frequencies are good for detecting large-scale deep features and high frequencies can pick up small shallow targets. As a rough guide, the highest frequencies (140 kHz, 40 kHz) imaged between ≤20 m and 40 m. The lowest frequency (400 Hz) imaged between 80 and 100 m. The magnetic data was reduced-to-pole (RTP), a filter which reconstructs the total magnetic intensity field at its observed inclination as if it were situated at the north magnetic pole (GeoExplo, 2011).

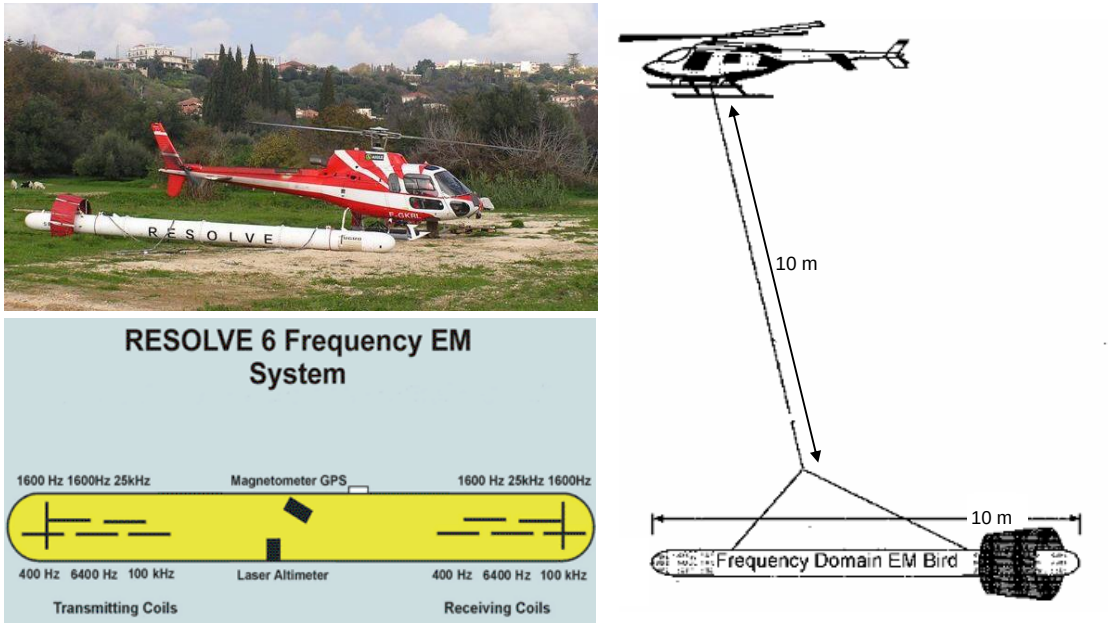

Figure 2.15 Helicopter-mounted electromagnetic (HEM) and magnetic survey equipment set-up (clockwise from top left): The chartered survey helicopter with RESOLVE bird, sketch showing typical HEM survey in action (modified from GeoExplo, 2011), diagnostic sketch of Fugro Airborne Survey's RESOLVE bird (from Fugro Airborne Surveys, 2011).

2.6.3 Gravity Survey

Gravity surveys measure the variation of gravitational acceleration (g) (i.e. the changing "gravitational field") over an area of interest using a gravimeter. These variations in g appear as "gravity anomalies" which are caused by the density contrast ($\Delta\rho$) between objects of different density within the subsurface. Gravity anomalies are direct indications of density contrasts between vertical columns of rock which extend from the surface to depths between 10 m to over 100 km (Nabighian et al., 2005). A gravity survey encompasses the sum of all lateral density contrasts at all depths within these columns of rock.

Systematic acquisition of the gravity data occurred in three parts (Phase I, II and III). The surveys were conducted in a series of profiles with gravity stations established every 10 m using a Scintrex CG-5 Autograv relative gravimeter (Figure 2.16). Spacing between profiles was chosen to attain a high resolution grid of data while maintaining a reasonable speed of acquisition. Over 3980 useable measurements

were collected. The location of each gravity station was recorded using the Trimble DGPS rover.

The Autograv gravity sensor had took 6 raw samples per second. An accumulative average of this output was displayed graphically (Scintrex, 2006). This was helpful in observing if the meter had been disturbed by external events during the taking of a measurement such as natural seismic activity. Measurement times were between 45 and 60 seconds producing a total of 270 or 360 raw relative gravity readings which were averaged continuously to produce an averaged relative gravity reading. Readings were repeated at each station until at least three averaged readings matched to within 0.005 mGal. Their accompanying time of measurement (also accurately recorded by the gravimeter to the second) was noted down.

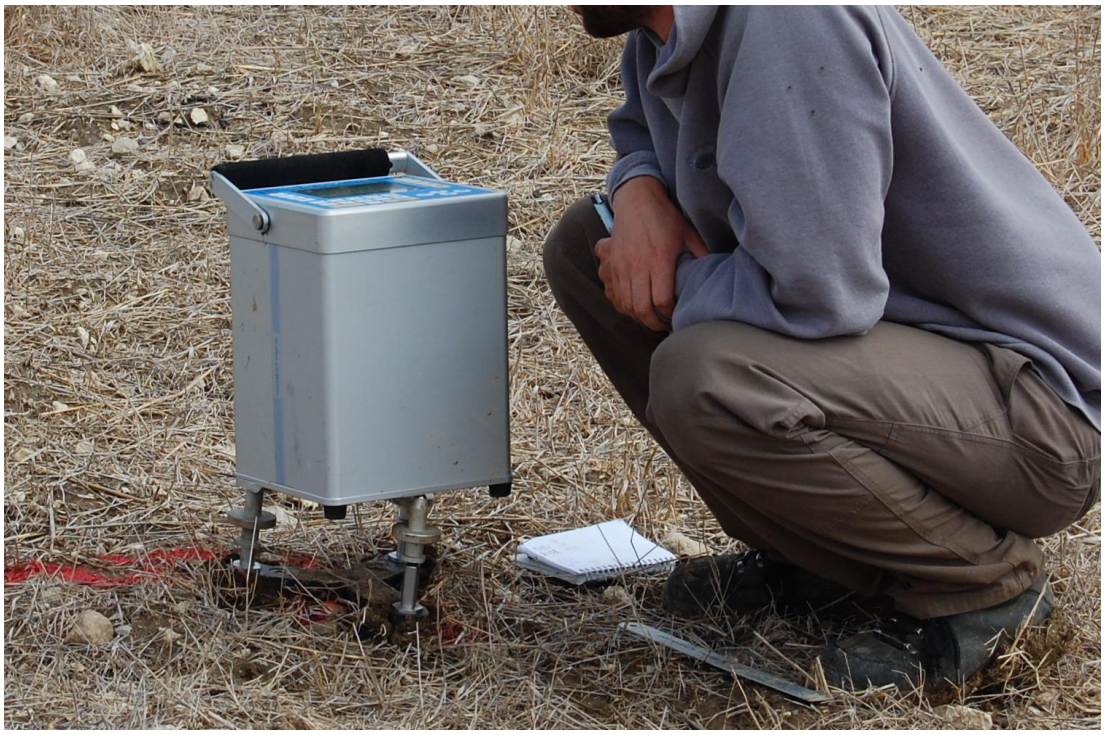

Figure 2.16 Gravity survey within the Lake Katachori paleo-lake bed using the Autograv gravity meter during the "Phase I" data collection.

A. Processing of the Gravity Data

The raw gravity data required a series of corrections or "reductions" to remove all but those signals due to local geology before they could be used to make inferences about the subsurface of Thinia. "Noise" is classed as tiny perturbations to the weighted spring within the gravimeter mechanism which are superimposed on the measured gravity results. Noise can be random (passing traffic, quarry works) or fall into predictable patterns. Predictable disturbances include instrumental drift and tidal effects. These deviations can often overwhelm the subtle variations in g caused by underlying geology therefore correction for predictable noise is crucial however because of their predictability there are good methods available to mitigate their effects.

The measured gravity response at each station consists of several gravity signals superimposed upon one another including those of the bulk Earth itself such as the planet's oblate spheroidal shape as well as variations in the Earth's topography. Only variations in the measured gravity field due to local geology were desired therefore the objective of these reductions is to remove all temporal, spatial, elevation and topography-related anomalies in order to enhance information about the density variations within the upper crust. The reduced gravity data (the "Local" or "Residual Gravity Anomaly") represents the gravity response after the various reductions have been made and subtracted from the original measured signal. For in depth descriptions refer to Rasmussen and Pederson (1979) (for gravity calculation), Smith (1959) (anomaly depth) and Boyd 1999[1] (general concept of gravity).

Processing of the raw gravity data was undertaken using a series of programmes constructed using Fortran 95. Using Fortran 95 to write these programs from relative scratch rather than using specialised software was advantageous as the programmes could be written to personal preference. The resulting output files were in ASCII format thus ensuring a high degree of compatibility with other applications and avoiding the file format constraints which often occur with using particular software. It was important to preserve the raw data in its original format and not to manually

manipulate the data in anyway as far as possible to save time and error. The processing stages of the raw gravity data were as follows:

1. **Tidal Correction.**
2. **Instrumental Drift Correction.**
3. **Latitude Variations.**
4. **Elevation Variations.**
5. **Bouguer Slab Adjustment.**
6. **Removal of Regional Gravitational Trend.**
7. **Terrain Correction.**

1. Tidal Correction

Tidal drift is the oscillatory variation of gravity observations caused by the direct gravitational attraction of the moon and sun upon the sensor. Gravity readings uncorrected for tidal drift plot as a sinusoidal line. This effect can have a magnitude of 0.2 mGals. Tidal correction was not carried out by the Autograv but was eliminated during calculation of the instrumental drift correction.

2. Instrumental Drift Correction

Instrumental drift causes deviations in readings due to the workings of the gravimeter itself. These are generally related to stretching of the spring mechanism which occurs during the course of the survey (on average by 0.5 ppm per day) and the magnitude of spring stretch can be in the order of 0.5 mGals per day. This drift appears as a linear increase on the gravity values with time. This effect is reduced by adopting a "loop" survey procedure (Figure 2.17). In this procedure a base station (labelled blue in Figure 2.17) is established along each profile. The survey is initiated and ended by taking a measurement at that base station thus completing the "loop". The base station is returned to at regular intervals during the survey. This records "parts" of the drift curve at different times. Linear interpolation can be used to interpolate within the gaps and the resulting model can be removed from the data later. Because

of the need to make repeated returns, the location of the base station was chosen for its easy of accessibility from the other stations along the profile. They were located away from large objects (large boulders, houses etc.) whose gravitational effect may cause deviation of readings.

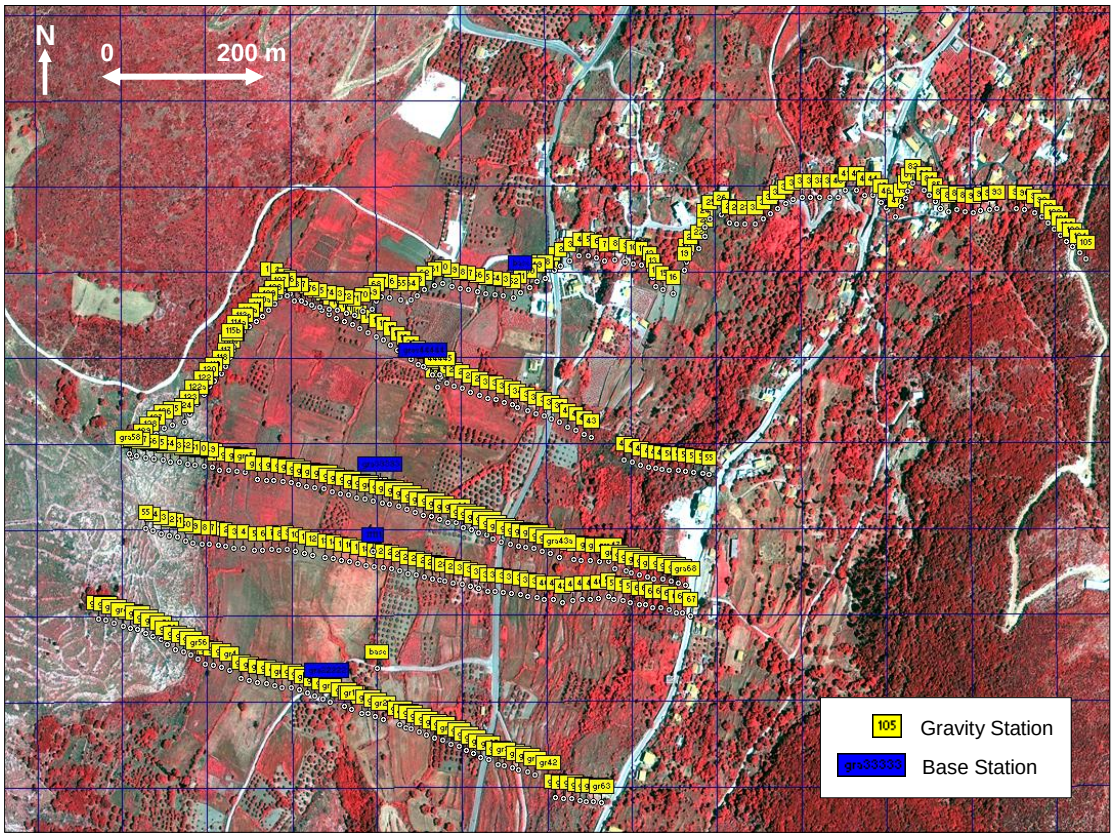

Figure 2.17 Quickbird satellite image showing the locations of the gravity base stations (blue) established during the Phase I Lake Katachori gravity survey designed to reduce the affects of instrumental drift on the recorded gravity readings.

For this method to retain a reasonable level of accuracy, returns to the base station have to be regular otherwise the interpolation would be too inaccurate. The Thinia base stations were returned to around every 2 hours. Within these 2 hour loops several repeat readings were taken at stations along the profile (~10% repeats per loop) in particular those stations for which repeat readings had given less than 0.005 mGal accuracy. To link the survey profiles for each site, a “base station loop” was performed and repeated at least six times. The Phase I sites were linked by forming a loop consisting of a chosen base station from each survey.

3. Latitude Variations

After being corrected for drift, the observed gravity values have to be corrected for spatial variations i.e. those which are not related to the local geology such as Earth's rotation around its polar axis and its degree of oblateness. Effects of rotation are removed by calculating the gravitational acceleration expected from a model Earth (i.e. making the assumption that the Earth is elliptical, rotating at an appropriate rate and contains no lateral variations in mass distribution) and subtracting this from the drift-correction gravity values. The calculated gravitational acceleration for this model Earth is the "theoretical" or "normal" gravity (γ).

4. Elevation Variations

Typically gravitational acceleration decreases by 0.3086 mGal for every metre of elevation, a number which can easily overwhelm a small density contrast in the local geology. The Free-Air Correction mathematically adjusts the gravity values to the "same" elevation or "datum elevation" (which is usually sea-level) by multiplying the elevation of each gravity station by the vertical gradient of gravity (0.3086 mGal/m).

5. Bouguer Slab Adjustment

The Bouguer Slab Adjustment corrects measurements for the gravitational effect caused by the excess mass of topography directly below gravity stations located above the elevation datum (mean sea level) and accounts for mass deficiency for stations below the elevation datum. This correction assumes that a simple slab of infinite horizontal extent, uniform estimated bulk density and thickness (h) can be used to represent the excess mass effectively cancelling out its effect on the measured gravitational acceleration. The chosen crustal density (ρ) is aimed at resolving the dramatic parts of the topography sticking up above the ground surface which, in the case of Thinia, were the limestone ridges and mountains associated with thrust faults within the valley. These ridges are harder and therefore more

resistant to erosion which has removed the marl around them. As limestone has a density range of 2.5 to 2.8 g/cm^3, the standard Bouguer anomaly correction density of 2.67 g/cm^3 was considered a good approximation of these parts of elevation.

6. Removal of Regional Gravitational Trend

Once all known reduction parameters were applied, it was necessary to distinguish what part of the gravity signal represented the regional geology (the "Regional Gravity Anomaly"), and what is caused by the immediate local subsurface i.e. the "Residual Gravity Anomaly". Regional Gravity Anomalies have a long wavelength representing a slowly changing anomaly spatially and tend to represent deep (long wavelength) or large-scale features such as deep crustal density variations or topography along the crust-mantle boundary. Local gravity anomalies have a much shorter, sharper wavelength. The Regional Gravity Anomaly can be subtracted from the Bouguer Gravity Field computationally either using a database of known regional trends or by subtracting an observed visible trend to the data. This will produce a (first degree) Residual Gravity Field.

7. Terrain Correction

A further terrain correction can be applied in topographically dramatic areas where Bouguer Anomaly approximation is not accurate enough through numerical integration of the gravity effect of a digital elevation model (DEM). The terrain correction for Thinia didn't make a great difference except where the topography was extreme. While some of the topographic anomalies (around the Petrikata quarry and southern Thinia) were resolved, instances of dramatic topography on a very small scale (particularly the sharp valleys within northern Thinia) were not entirely removed. Some anomalies may also have been due to gravity stations being assigned to wrong base stations, a factor which cannot at this point be mitigated further.

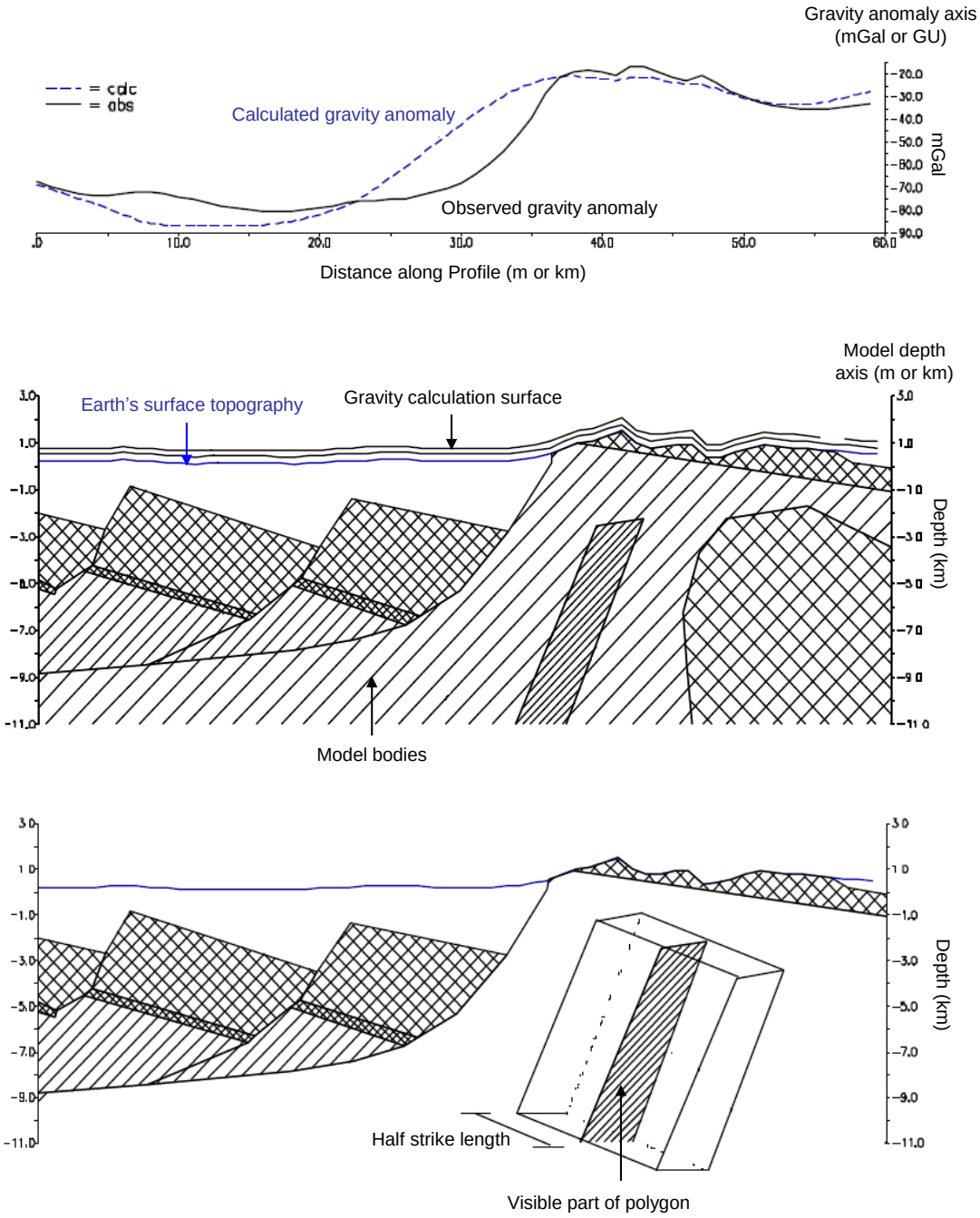

Figure 2.18 Series of schematic cross-sections illustrating the Gravmag modelling software. Half-strike length is defined as a length according to a 2-D polygon in the third dimension which is perpendicular to the defined profile direction and symmetrically placed about it. Modified from Pedley et al., 1993.

B. Modelling of the Bouguer-corrected Residual Gravity Data

In order to resolve the anomalies observed in the gravity map it was necessary to model the gravity response in terms of what underlying geological structures might be causing the changes in local gravity. Modelling of a gravity anomaly is relatively straightforward as the shape of a gravity anomaly is primarily a function of density. Generally the more tightly-contoured the anomaly, the closer it is to the surface. Deeper features are more gradual.

Modelling was undertaken using the Windows-based British Geological Survey 1997 software Gravmag (version 1.7c): an interactive programme for modelling gravity which allows the user to construct and edit a modelled geological cross-section in the form of a layered density model whose calculated gravity anomaly matches that of the observed gravity response (Figure 2.18) (Pedley et al., 1993). Models are constructed by drawing interlocking polygons defined by a set of vertices in the X, Z plane. These polygons are assigned a finite strike length in the third dimension by entering the "half-strike" length when initially creating polygons. Half-strike length is defined as a length according to a 2D polygon in the third dimension which is perpendicular to the defined profile direction and symmetrically placed about it (Pedley et al., 1993). The modelled gravity response is altered by changing the shape and density of the polygons.

There will be numerous possible geological solutions which could explain this anomaly due to unknown variations in the size and shape of the object causing the anomaly, the density of the surrounding rocks and the object's depth. The profiles chosen to be modelled were sketched as geological cross-sections based on surface dip measurements and coincided with boreholes. This enabled the gravity models to be improved and brought to a more likely solution. The following models should therefore be considered as likely solutions of the data since gravity, like other non-invasive tests, suffers from data non-uniqueness.

2.6.4 Resistivity Survey

Resistivity surveys measure lateral variations in the electrical resistivity, the property of a material which resists electrical current flow, of the subsurface by passing an artificially generated low-level current into the ground and measuring the response of the subsurface to this current in the form of potential difference. A resistivity survey produces data in terms of "apparent resistivity" which is defined as a weighted average of the true resistivities sampled by the survey equipment (Vickery, 2000).

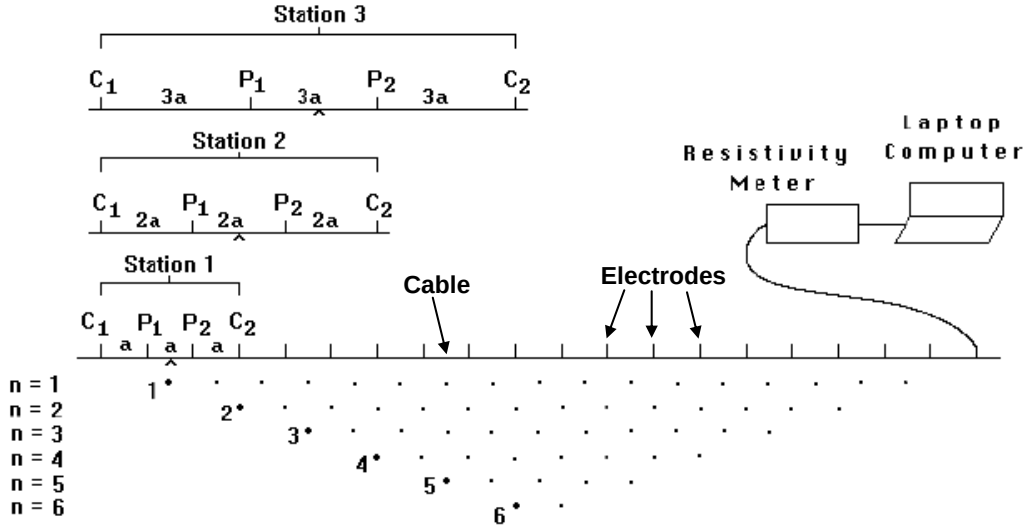

Figure 2.19 Sketch showing the sequence of measurements required to build up a pseudosection using a computer-controlled multi-electrode survey (top). All measurements along n=1 are made before all measures along n=2 etc. Layer numbers (n = 1, 2, etc.) are converted into a modeled depth scale in the pseudosection. Modified from RES2DINV ver. 3.4.

The surveys used a constant (electrode) separation (5 m) traversing method (CST) and a Wenner alpha array set-up which meant when the end of the profile was reached, the entire survey cable was moved along to the next part of the survey line to achieve longer lines than cable length allowed until the limit of the profile was reached (Figure 2.19). Data was collected and stored in DAT file form, e.g**.** L1.dat using a 12-channel Campus International Tigre electrical resistivity meter which was automatically set-up to work through a large number of different electrode combinations to order to build up a pseudosection of measured apparent resistivity.

The survey lines were made to be as straight as possible however this was limited by tarmac roads or rocky locations where the electrodes could not infiltrate the surface and the presence of private land-holdings in which the profile could not continue. Because of these land restriction there was an element of on-the-spot flexibility in the positioning of lines in order to comply with these restrictions yet still yield useful results. The position of the beginning and end of each profile was located using the Trimble rover as were the positions of the electrodes. Anomalously high surface readings (i.e. close to the resistivity of air, 10^{12} Ωm) occurred frequently during the Thinia surveys due to poor electrode contact with the ground due to very dry soil conditions. The storing of such data anomalies was avoided by telling the resistivity meter to test the quality of each electrode's ground contact automatically. An electrode with an abnormally high response was either hammered in further or the ground around it was made wet to improve its contact with the ground.

A. Processing of the Resistivity Data

Data was inverted using the RES2DINV software, designed to automatically determine a 2D distance-depth cross-section showing how resistivity varied continuously with depth for the subsurface for the data obtained from electrical imaging surveys (Griffiths and Barker, 1993). This software uses a 2D model which divides the subsurface into a series of rectangular blocks then uses a forward-modelling subroutine is used to calculate an apparent resistivity value for each block in order to produce a pseudosection that resembles the actual measured resistivity (Figure 2.20) (RES2DINV ver. 3.4 manual). A non-linear least-squares optimisation technique is used for the inversion routine based on the smoothness-constrained least-squares method (deGroot-Hedlin and Constable, 1990; Loke and Barker, 1996a). The optimisation method aims at trying to reduce the difference between the calculated and measured apparent resistivity values by adjusting the resistivity of the model blocks. The measure of this "fit" is given by the root mean squared error (RMSE).

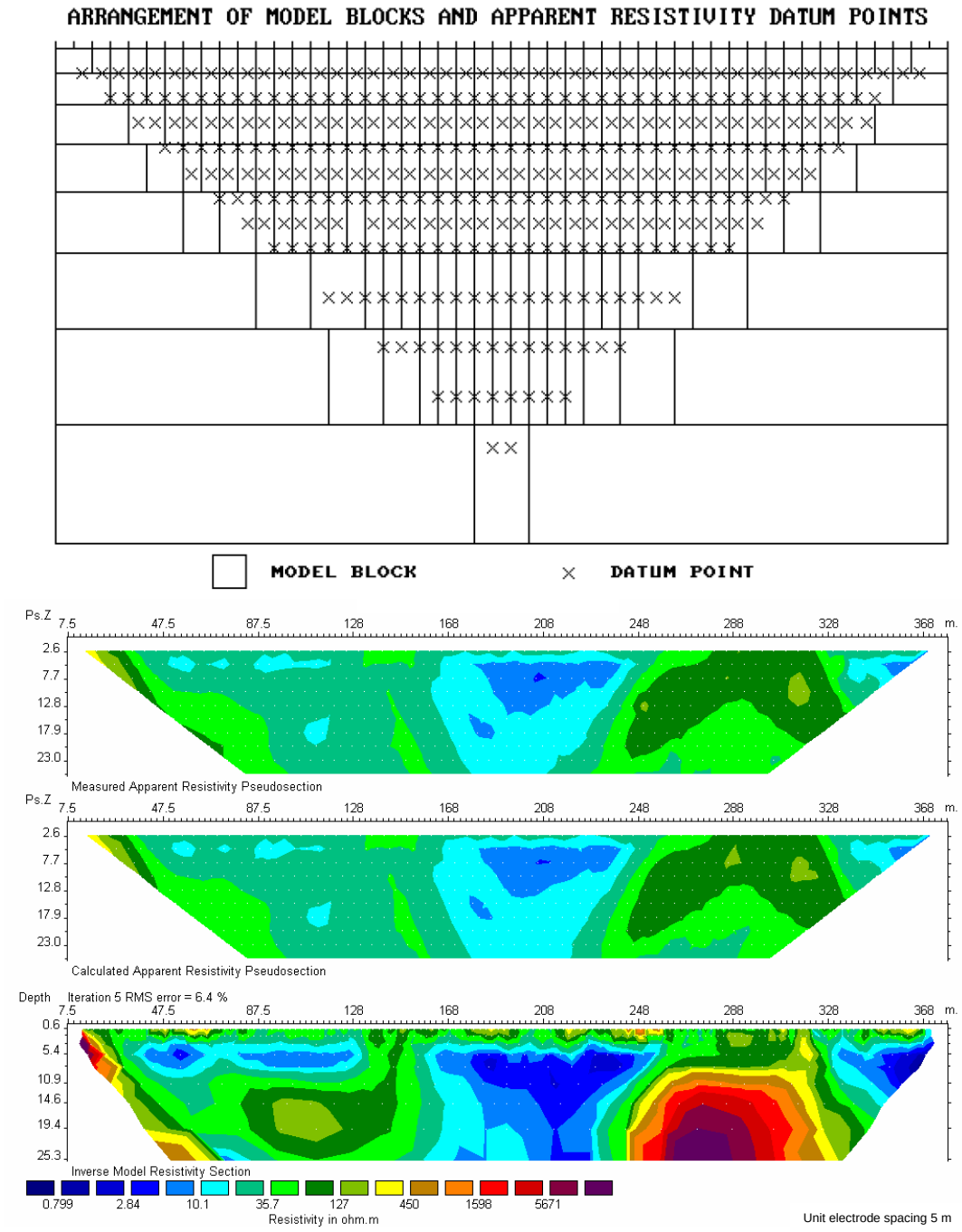

Figure 2.20 Arrangement of the blocks used in a model together with the datum points in the pseudosection (bottom). Modified from RES2DINV ver. 3.4. Example of output produced by RES2DINV with simple least-squares inversion (LKL1): Measured apparent resistivity pseudosection (top), calculated apparent resistivity pseudosection (middle) and inverse model resistivity section (bottom) all without adjustment for topography. The root mean squared (RMS) error for this particular inversion is given as 6.4% (the 5th iteration of the data was chosen).

Running a simple least-squared inversion on the survey data produced two pseudosections (measured apparent resistivity and calculated apparent resistivity) an inverse model resistivity section in the 2-D plane with corresponding RMSE value. Automatic smoothing of the modelled resistivity values was applied directly by the software if the maximum apparent resistivity was 300 times greater than the minimum. Due to data non-uniqueness, repeated inversions produced slightly different results. The resistivity contours produced were therefore considered approximations rather than exact resistivity contrast boundaries.

Generally, the aim of repeated inversions is to reduce this value as much as possible however caution has to be applied as the model with the lowest RMSE isn't always the most realistic from a geological perspective (particularly in noisy data sets) as it may contain large and unrealistic variations in model resistivity values (RES2DINV ver. 3.4 manual). The best model to choose is the one after which the RMSE does not change significantly (usually between the 3rd and 5th iteration).

2.6.5 Seismic Refraction Survey

Seismic refraction images the structure of the subsurface by introducing surface-sourced seismic waves into the ground and measuring the travel time of the critically refracted seismic waves (direct or head waves) represented by the initial returning ground motion at varying distances from the source (Vafidis et al., 2003; Boyd, 1999[3]). Later wave arrivals (the reflected wave component) are discarded.

The seismic refraction data was collected using a Geometrics Geode 24 with a 24-channel spread. Surveys were undertaken by replacing the resistivity electrodes with geophones maintaining a spacing of 5 m. The shot source was a plastic plate struck by a hammer blow. This source was chosen because of its repeatability and the force and duration of the impact was kept as constant as possible. The hammer was wired to the seismic computer so that data collection was initiated at the time contact was made between the hammer and plastic plate. This meant there would be no offset

between the initiation of the seismic pulse and the head wave's arrival at the geophone array.

The seismic pulse was initiated at each end of the geophone profile to produce forward and reverse wave arrivals along the profile and at 10 m intervals along the line enabling dipping reflectors to be resolved. The raw refraction seismic data was acquired as a series of shot records in SEG-2 (DAT) format. Survey lines were broken into sections (halves, thirds, quarters or fifths depending on the length of the line) with about ten shots taken for each section.

A. Processing of the Raw Seismic Refraction Data

Processing of the raw seismic refraction data was undertaken in two stages using the Pickwin and Plotrefa modules of the Geometrics software SeisImager/2D:

1. **Picking of head wave arrivals (first "breaks") (Pickwin).**
2. **Inversion of travel time data using tomographic or time-term inversion method (Plotrefa).**

1. The Pickwin Module

The Pickwin module allowed the display of each wiggle trace. After manipulation of the display parameters to achieve the optimum scale and vertical exaggeration for ease of interpretation, the picking of the headwave arrival or "first break" in each wiggle trace was undertaken (Figure 2.21). The first "break" was interpreted as the initiation of the major wave motion representing the arrival of the initial ground disturbance associated with the striking of the hammer. Some of the seismic lines were slightly "hairy" due to interfering vibrations from traffic in close proximity to roads particularly in Livadi Marsh and Lake Katachori, where the fine-grained alluvial sediments carried the vibration further. The traces containing poor or no data were deleted. After picking first breaks for each wiggle trace, the picks were

connected and saved as a travel time (VS) file which listed each geophone positions in metres versus corresponding first break arrival time (in msec) for that geophone.

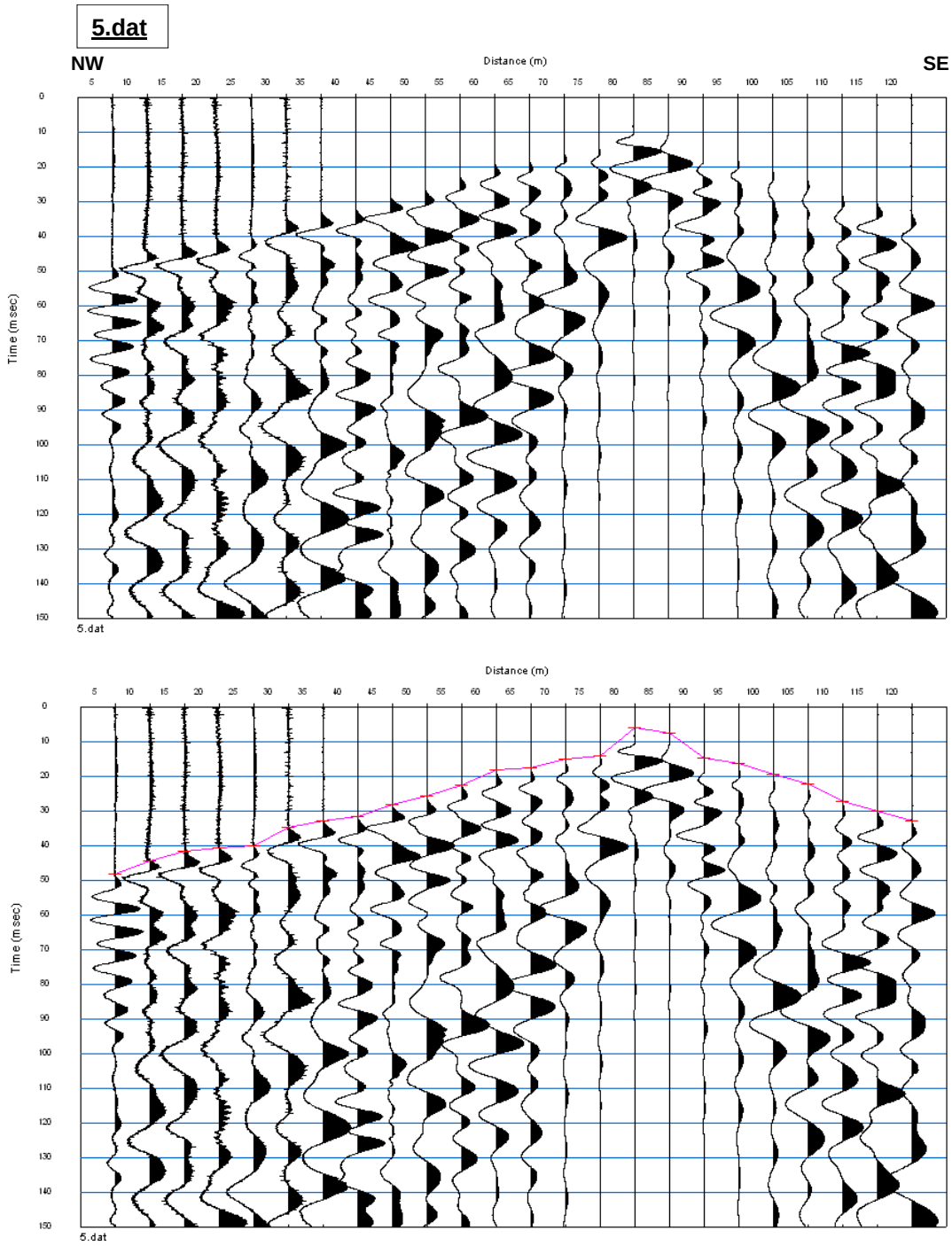

Figure 2.21 Shot record for 5.dat from LKL1, Lake Katachori (top) viewed using the SeisImager/2D Pickwin™ software with first arrivals picked (pink line) (bottom).

2. The Plotrefa Module

Plotrefa is the interpretation module of SeisImager/2D which takes as its input the appended travel time files (Figure 2.22, top) constructed in the previous section. Once the travel time curves for each line had been appended and corrected for reciprocal time, the resulting traveltime data was inverted to produce a series of topographically-adjusted multi-layered velocity models. The result was a series of 2D profiles of depth versus distance showing how velocities varied with depth. The boundaries between layers approximated stratigraphic interfaces.

Time-term Inversion: The Time-term inversion technique uses a combination of linear least squares and delay time analysis to invert the first break files of a velocity section creating an (up to) three-layered velocity model.

Tomographic Inversion: Tomographic inversion method involves the creation of an initial 10 to 15 layer velocity model (Figure 2.22, bottom). This process then iteratively traces rays through the model. This inversion method works best in areas of extreme topography, when strong horizontal velocity variations exist and when velocity contrasts are more gradational (SeisImager/2D™ Manual, 2006). The minimum velocity for the model was usually chosen as 0.34 km/s, the velocity of air. The maximum velocity was chosen through trial and error. The inversion process is repeated (about 5 to 6 times) with the aim of reducing the RMSE between theoretical and observed traveltimes as much as possible. RMSE can be improved by modifying the initial model i.e. altering the maximum and minimum velocities then repeating the inversion process. The chosen model represented the RMSE after it did not change beyond 0.1 msec. If necessary, the first break picks can be returned to and adjusted in the Pickwin module and the inversion and ray-tracing process can then repeated.

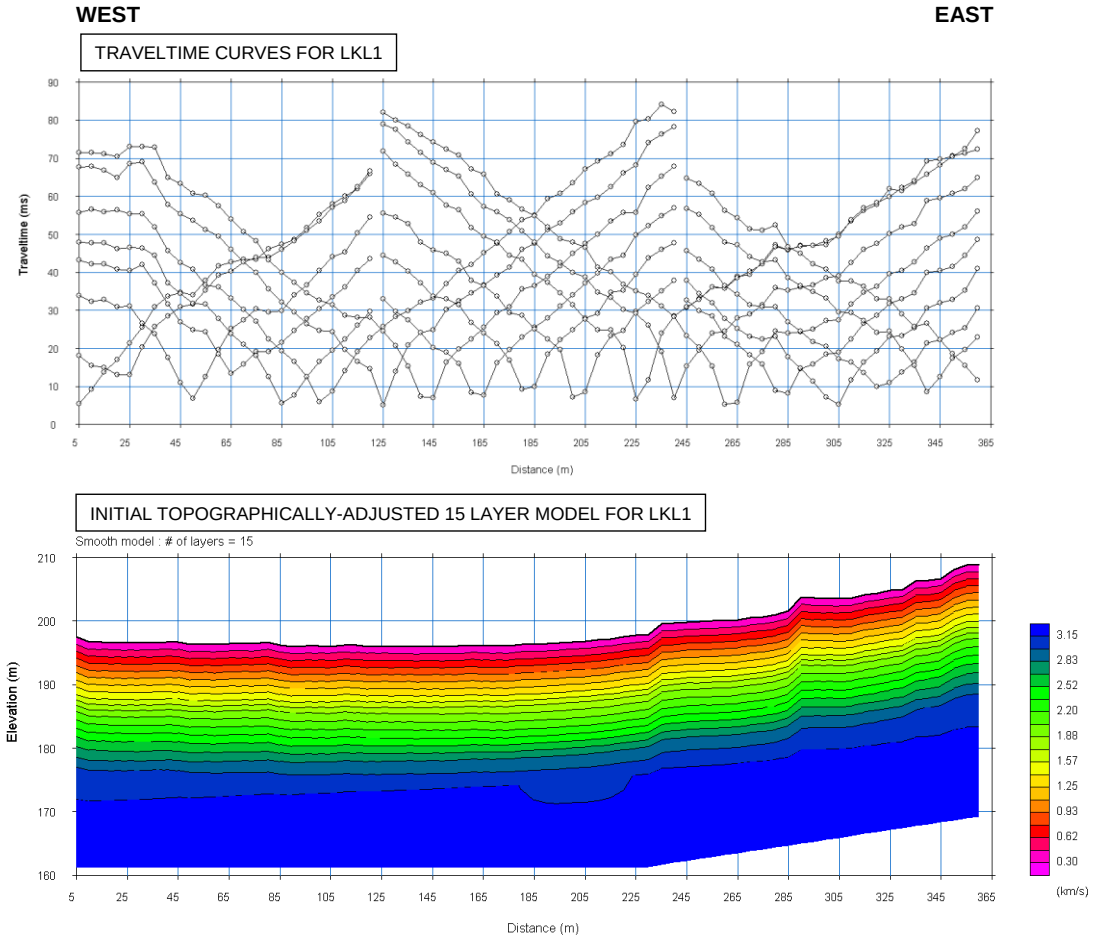

Figure 2.22 The stages of building up a velocity model in Plotrefa™: Reciprocal time corrected traveltime curves for refraction seismic line LKL1, Lake Katachori (top). The white circles represent individual travel times. Initial "smoothed" 15 layer model with topographic adjustment generated for this line with manually defined bottom layer (bottom). Vertical exaggeration of the traveltime curves is 1.5 and 2.5 for the model.

2.6.6 Shallow Marine Seismic Reflection Survey

The shallow marine seismic reflection surveys were undertaken by Fugro Oceansismica S.p.A. (part of Fugro's Offshore Survey Division) and used a locally-chartered diving boat rigged with Fugro equipment (Figures 2.23 and 2.24). Seismic reflection data was collected using a single 100 m hydrophone streamer and electric sparker source. The position of the streamer was maintained using a "towfish". Data was stored in a series of high resolution, distance versus two-way travel time (TWTT) (seconds) profiles set out in 2-dimensional grids. The position of the boat was determined by onboard GPS. Bathymetric data was also gathered using the

vessel's GPS and sonar. The raw data was processed by Fugro Oceansismica. High resolution sub-bottom profiling (SBP) was also acquired along some of the sparker survey profiles to image the upper 10 to 30 m of the sub-seabed.

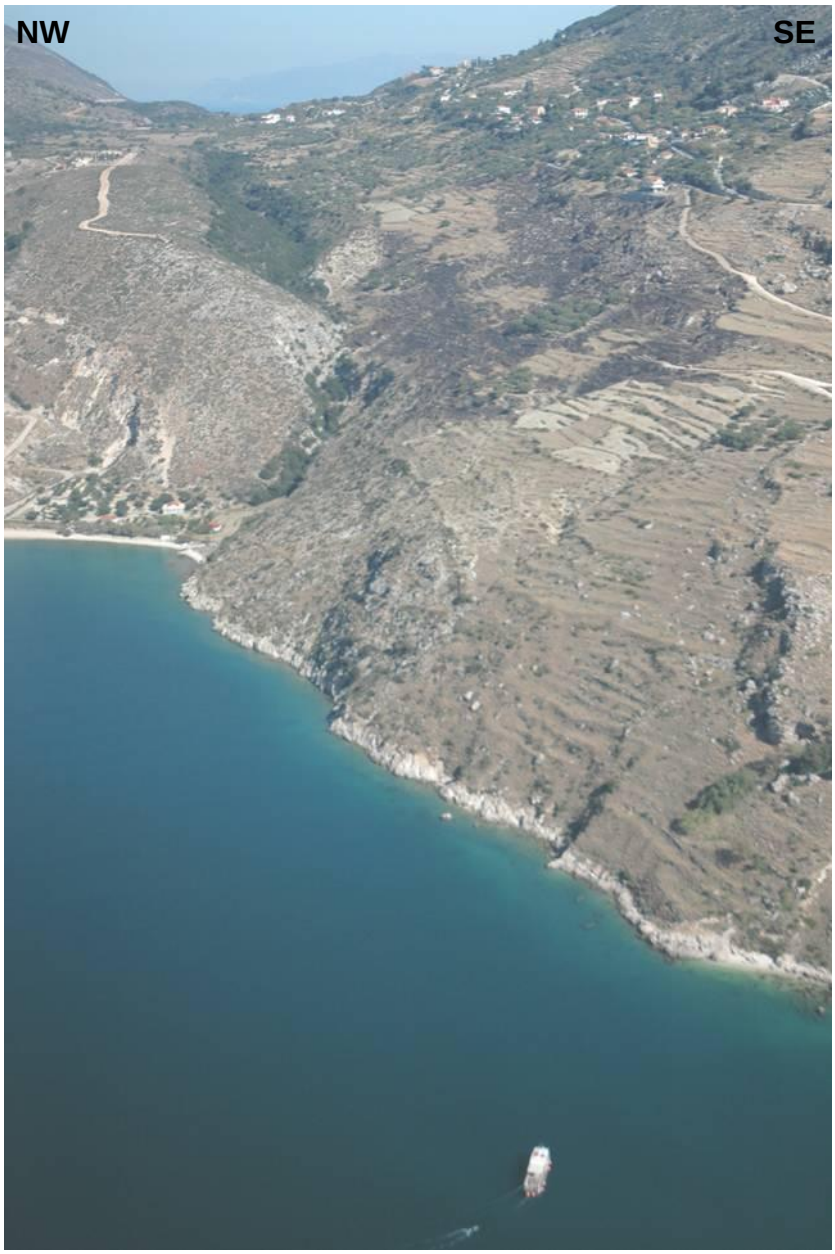

Figure 2.23 The survey vessel with streamer deployed below southern Thinia. Image credits: J. Underhill.

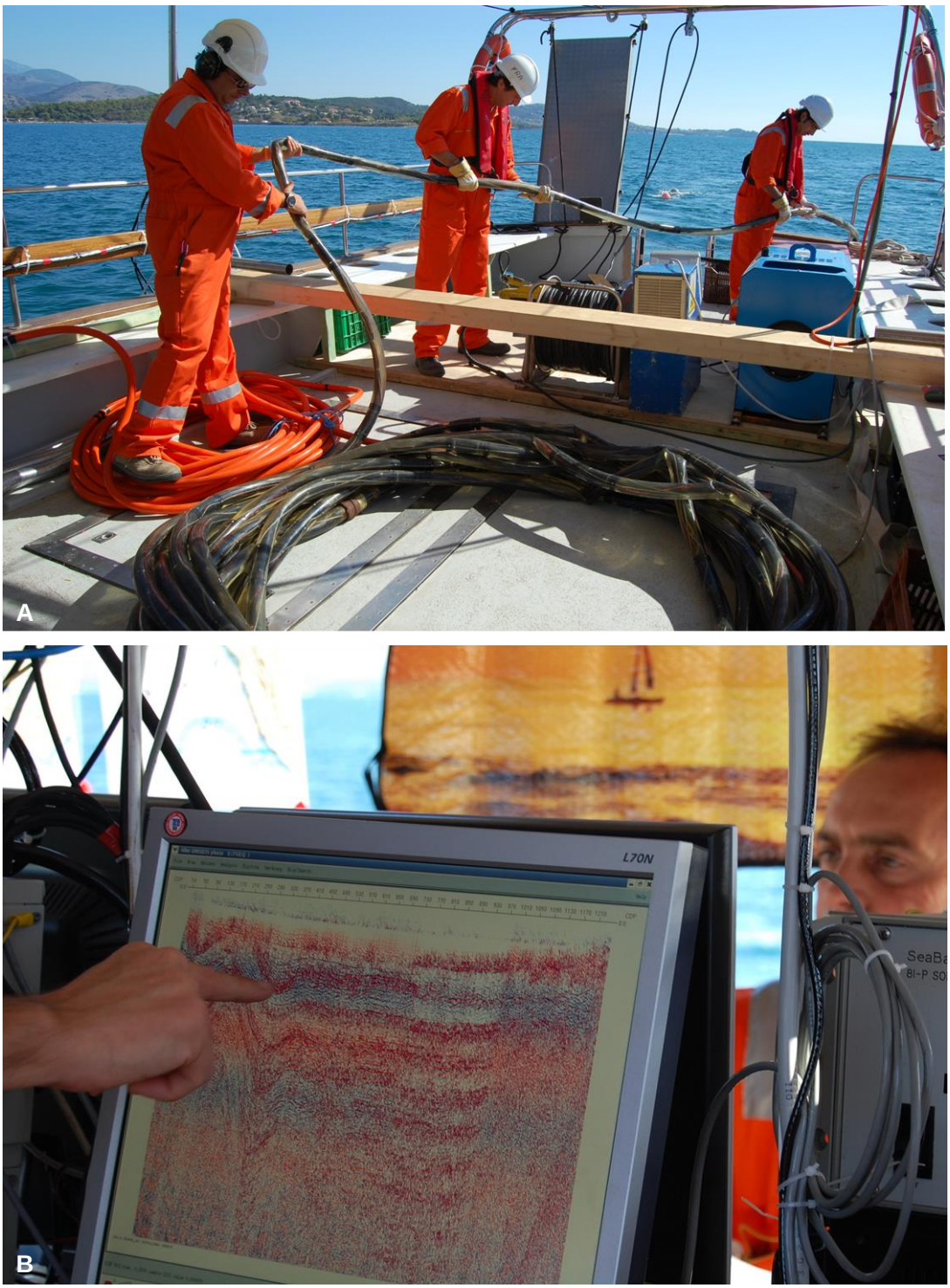

Figure 2.24 Photographs showing aspects of the Oct 2007 shallow marine seismic surveys undertaken by Fugro Oceansismica in the Gulf of Argostoli: A. Deployment of the hydrophone streamer; B. Collection of raw seismic.

2.7 Summary

The promising results of the preliminary surveys carried out in the early stages of the investigation into "Strabo's Channel" justified the commencement of this PhD and the application of industrial-scale geophysical techniques to test this hypothesis. A series of complimentary techniques targeting both onshore and offshore locations were chosen in order to acquire the fullest view of the Thinia valley and the surrounding area.

In addition to a helicopter-mounted electromagnetic (HEM) survey, land-based tests of gravity, resistivity and seismic refraction were deployed across sites in Northern Paliki (Atheras Bay and Livadi Marsh) and Thinia (Northern Thinia, Lake Katachori and Southern Thinia). Shallow marine seismic reflection surveys were undertaken in the coastal areas of Thinia (Gulf of Argostoli and Agia Kiriaki Bay) and Atheras Bay. An extensive onshore coring campaign was also undertaken.

CHAPTER 3: Surface Geology and Geomorphology

3.1 Introduction

The geology of Thinia has been mapped in detail by previous authors. However, these maps have produced conflicting results, particularly regarding the locations and types of faults present within the valley. Two field-mapping campaigns were conducted across Thinia between 17th September to 30th October 2007 and 17th to 24th October 2010. Detailed field-mapping notebooks were kept.

The key aim of the field-mapping was to produce a new surface geology map of the valley building upon and, if necessary, revising existing geological maps. As explained in Section 1.3.3, the mechanism of channel destruction favoured by Bittlestone et al. (2005) was infilling and burial of "Strabo's Channel" through collapse of its gorge-like sides and deposition of landslide material into the channel. One of the key outcomes of this fieldmapping campaign was to quantify the surface extent of existing colluvial material within Thinia and, secondly, to investigate where erosion was currently occurring and how voluminous and frequent this was in order to estimate the timescales required to produce the historic deposits. Mapping would also identify key locations for further investigation during the non-invasive geophysical surveys and sedimentary coring.

In addition to field-mapping, surface outcrop samples were collected from strategic sites relevant to important areas within the valley and used to supplement the geological knowledge of the area and the boreholes. These samples were dispatched to Fugro Robertson Limited in North Wales to deduce their age and biostratigraphy and are listed from pages 131 to 138 in Appendix B. Those samples labelled numerically (e.g. 9, 10, 11) were collected by members of Fugro Géotechnique. Those labelled non-numerically (e.g. 1_Oct11) were collected by the author and J. Underhill. The locations of these samples are shown on the geological map (Figure 3.29).

3.2 Geology and Geomorphological Observations

The investigation of the geology of Thinia will work from north to south and cover the following areas:

1. **Northern Thinia (Section 3.2.1)**
2. **Central saddle region (Section 3.2.2)**
3. **Southern Thinia (Section 3.2.3)**

3.2.1 Northern Thinia

The coastal cliff at Agia Kiriaki Bay provided a cross-section through the northern valley sediments. The sediments within this cliff ascribed a series of asymmetric NNE-SSW striking, east-dipping folds (Figure 3.1, A). The top of these folds was truncated by the surface topography. These folded deposits were composed of thinly-bedded, fine-grained bluish-grey to brownish muddy clays and marls which were easily crumbled which alternated with layers (up to 50 cm in thickness) of a harder, paler lithology (Figure 3.1, B).

Beach deposits worn smooth by wave-action showed that the grey marls had an undulating texture (Figure 3.2, A) and were imbedded with ~10 cm long rounded clasts of coarser-grained material (Figure 3.2, B). Within this marl were dark, finely-bedded, crumbling organic-rich layers (>50 cm in thickness) flecked with coal (Figure 3.3, A). The harder layers were moderately-fine to fine-grained sandstone, limestone or recrystallised (altered) marl with orange, cream and yellow laminations, calcite-filled fractures and shell fragments. These harder layers had a purplish-reddish cast like iron oxide staining. There was possible evidence of cross-bedding within these layers (Figure 3.3, B). These folds were broken by numerous small easterly-dipping shear faults and fine calcite-filled fractures indicating these deposits had undergone post-depositional deformation. The underside of the anticlinal folds of these hard layers appeared rusty and displayed NW-SE trending glassy striations caused by movement of the harder layer over the more ductile soft marl (Figure 3.4,

A). The upper surface of these layers showed evidence of shell-fragments, fossilised ripples and bioturbation (worm casts, burrows) (Figure 3.4, B). The harder layers were more resistive to erosion than the grey marls so the tips of the folds protruded from the surface topography to form a series of NE-SW orientated "ribs" running along the eastern side of the asymmetric northern valley for at least 2.3 km indicating the folded sediments were prevalent in the northern valley.

Moving closer to the Ainos Thrust, these marly deposits became harder and paler and the bedding became strongly deformed and convoluted making it difficult to determine overall bedding plane dip (Figure 3.5, A). This deformed marl also contained a few very rare clasts of conglomerate composed of well-cemented rounded pebbles (Figure 3.5, B).

Notably absent within the Agia Kiriaki Bay sea cliff were the large-scale landslide deposits (boulders, jumbled bedding, etc.) expected if the valley fill had been built upon from major repeated rockslides filling a seaway between Paliki and Kefalonia which suggested that Channel route may be restricted to one of the zones of slumped material where no bedding plane structures could be determines (Zola harbour or beneath Agon village). Extensive slumping occurred along the length of Agia Kiriaki Bay where a combination of the undercutting action of the sea, erosion of streams draining off the land and the strongly-deformed sediments had made the sea cliff very unstable.

Determination of the age of folding within the Agia Kiriaki sea cliff was of importance and whether it had occurred recently in response to tectonism or collapse of the western valley side or if it tied into the westwards compression affecting the Pre-Apulian zone. These sediments might date to the Neogene but deformation occurred post-deposition and could have occurred much more recently. Similar-looking dark grey marls to those in the Agia Kiriaki Bay sea cliff occurred along close of the axis of the northern valley as far south as the Petrikata Quarry greatly restricting the route a Channel may have taken.

Figure 3.1 Sandstone or hard marl and clay sediments visible in the Agia Kiriaki Bay sea cliff: A. View of the easterly-dipping folds formed by the sediments and alternating hard (pale) and soft (darker) layers; B. Close-up photo illustrating the contrast between the layers of fine-grained blue-grey clays and red-stained sandstone.

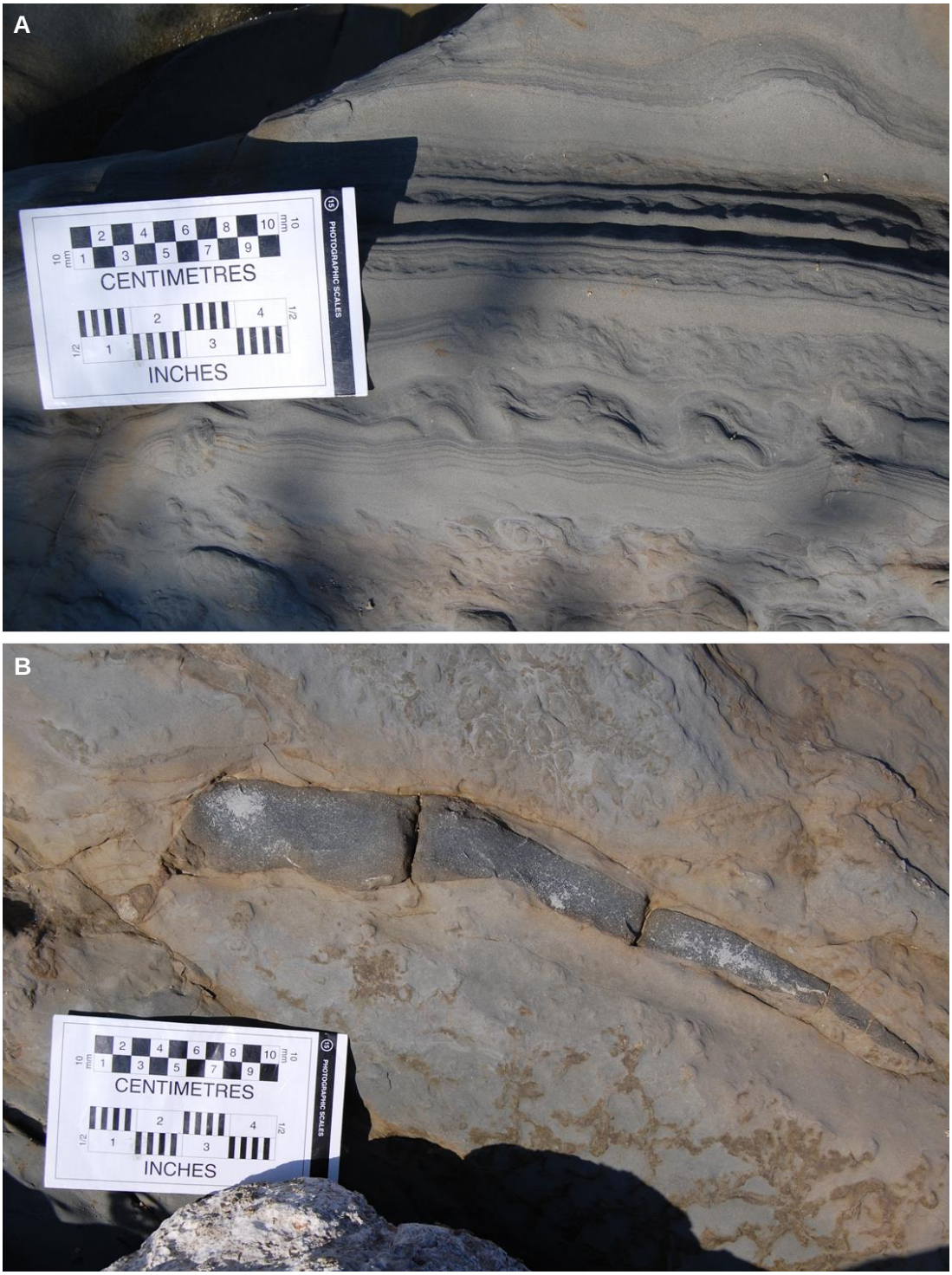

Figure 3.2 Sea-worn beach deposits of the Agia Kiriaki Bay sediments: A. Undulating beds within the grey marl; B. Coarse-grained clast within same exposure.

Figure 3.3 Sea-worn beach deposits of the Agia Kiriaki Bay sediments: A. Coal-flecked layer between sandstone and clay layers; B. Close-up of lineations (possible cross-bedding) in hard sandstone layer within the soft marl.

Figure 3.4 Photographs illustrating features of the sandstone layers: A. Part of a fold's anticlinal axis still intact showing "baked" appearance surrounded by grey, softer marl with striations on its underside (indicated by white dashed lines) with the same strike as the folds; B. Worm casts and ripples within harder layers.

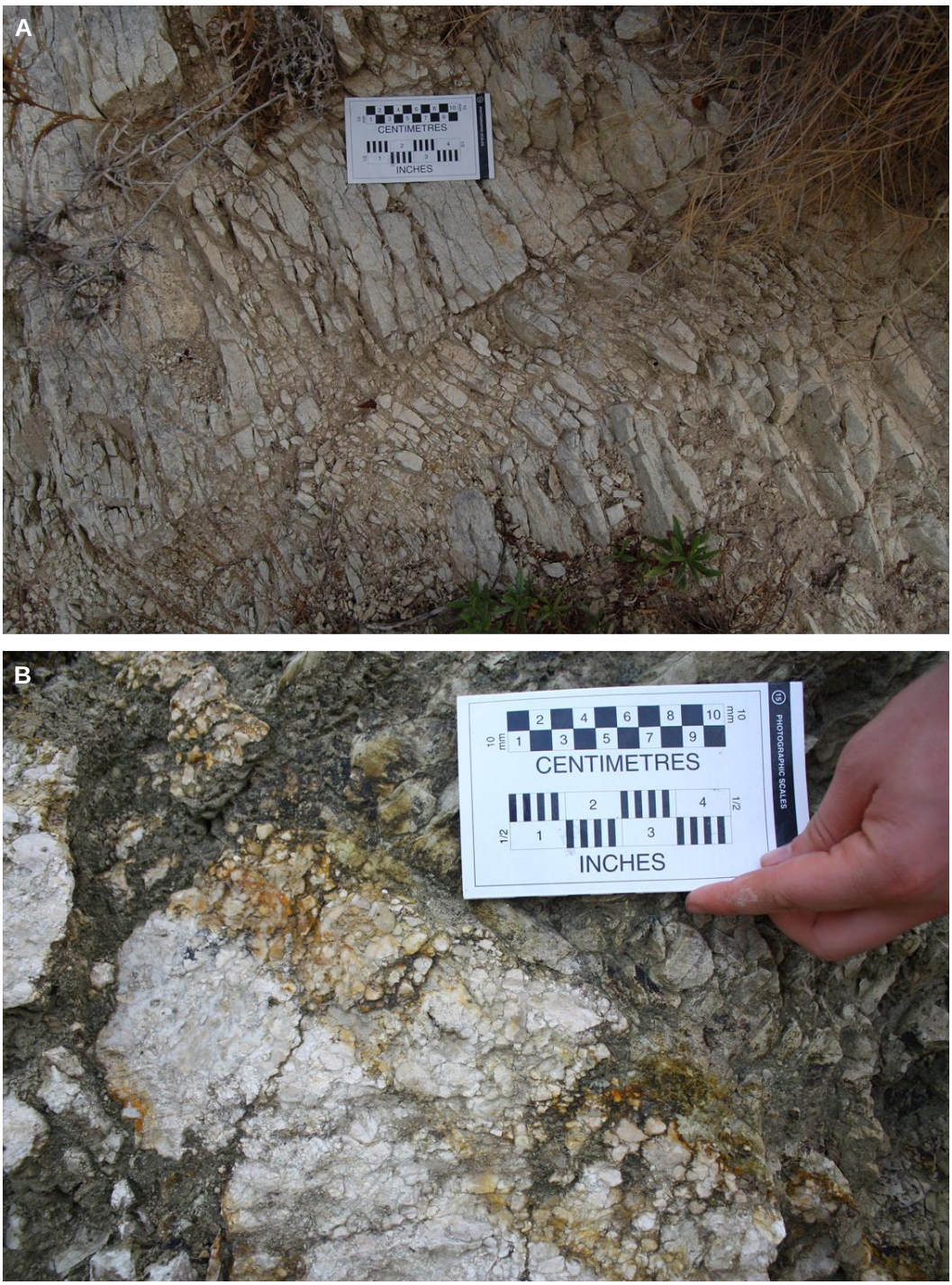

Figure 3.5 Marl deposits in Agia Kiriaki Bay: A. Deformed marl beds in Ainos Thrust footwall; B. Clast of fine-grained conglomerate within the deformed marl.

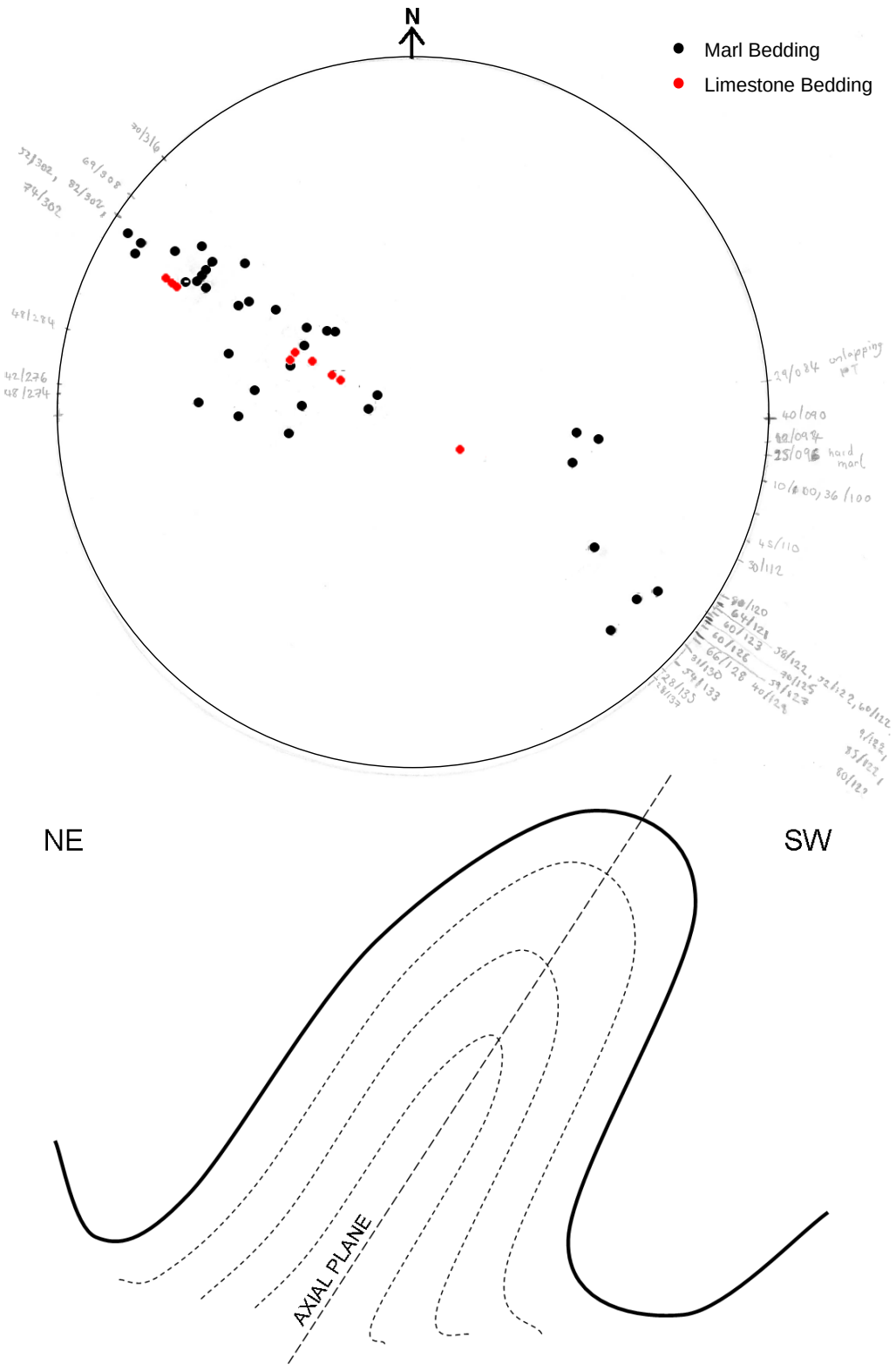

Figure 3.6 Lambert lower-hemisphere equal-area stereonet constructed for the marl (black dots) and limestone (red dots) in the northern part of Thinia valley (top) and sketch of asymmetric loops within the marl observed in the Agia Kiriaki Bay sea cliff (bottom).

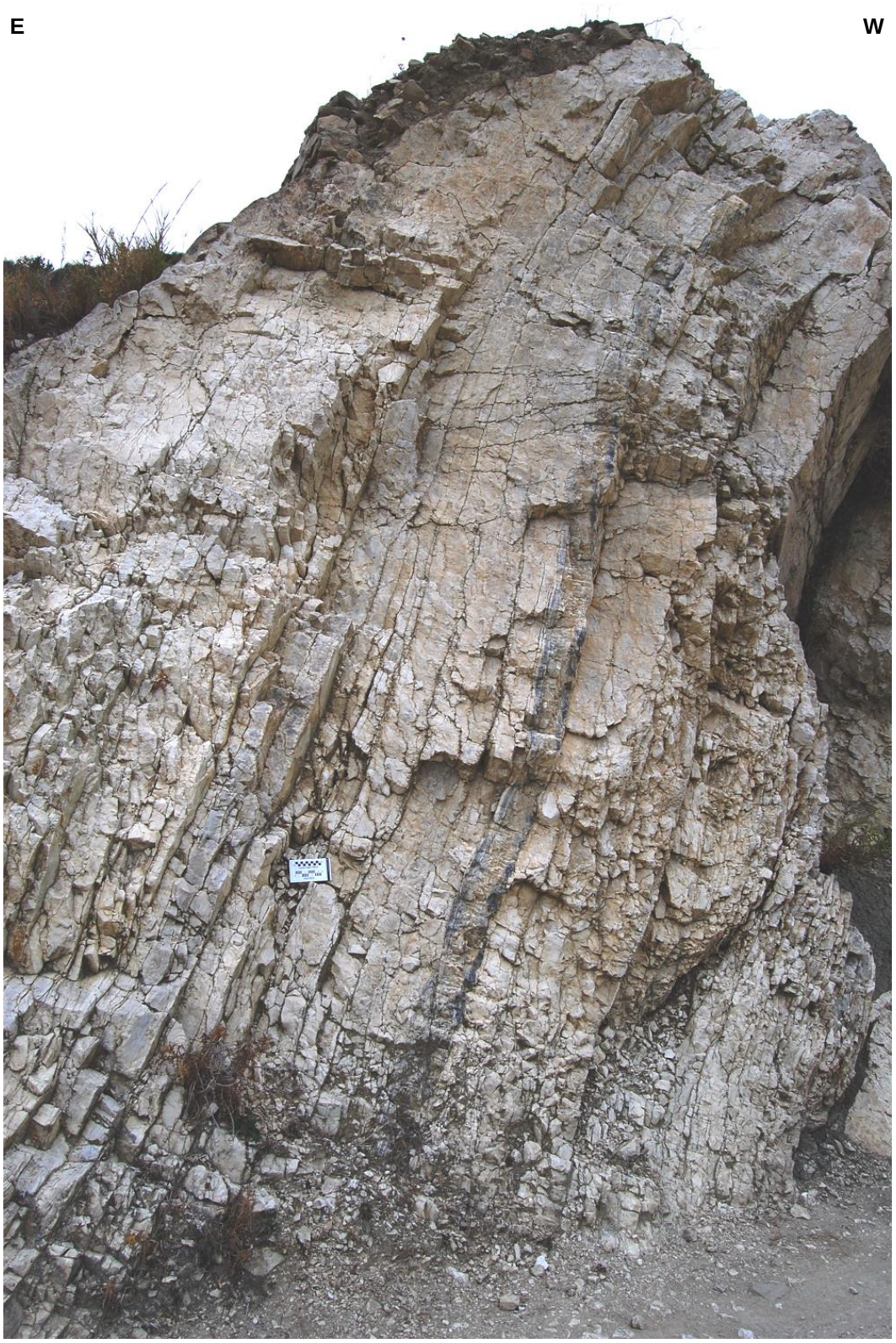

Figure 3.7 Limestone outcrop within the marl sea cliff at Agia Kiriaki Bay which might represent an olistolith derived from higher up the stratigraphy or an easterly-dipping thrust fault.

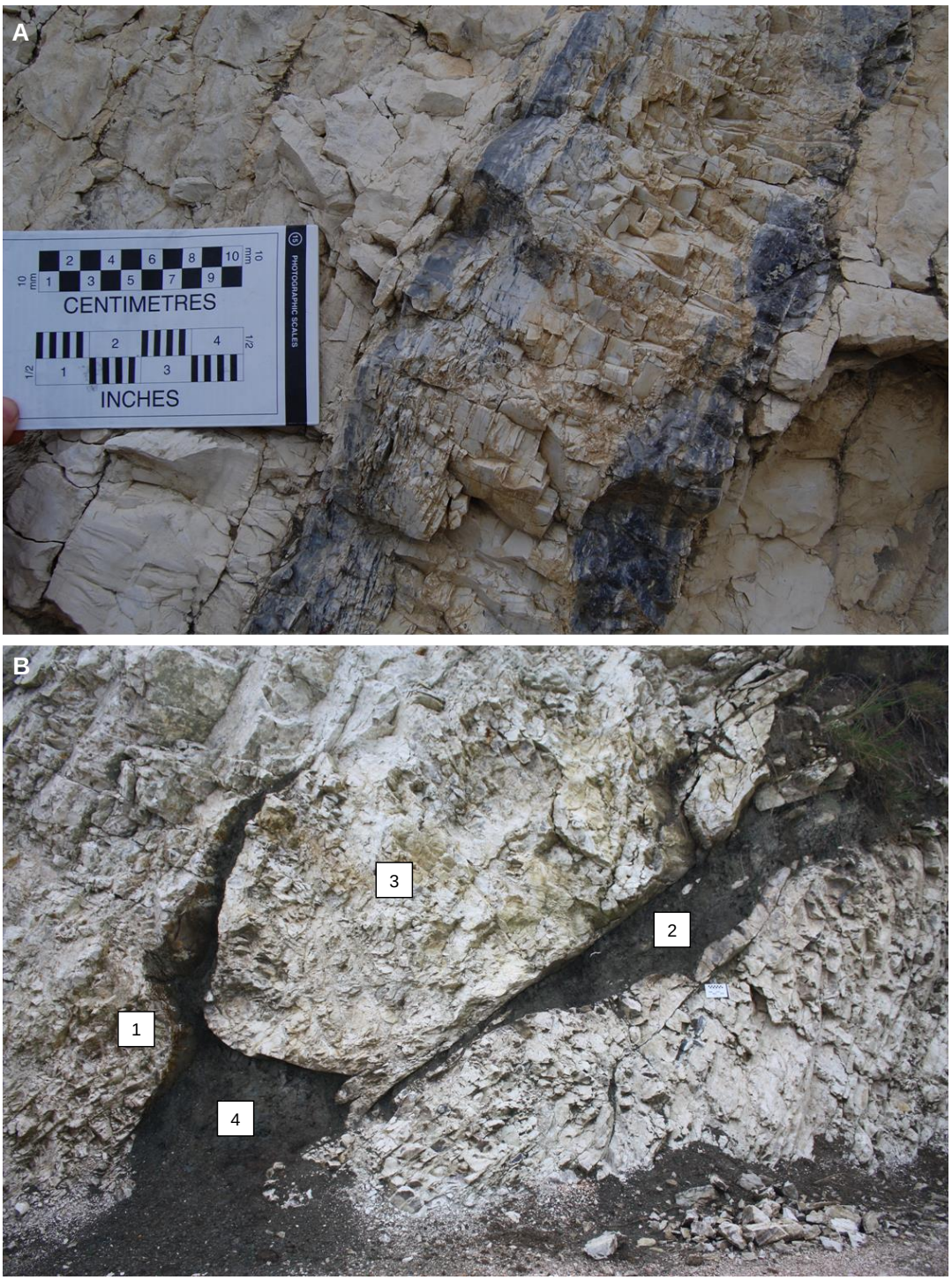

Figure 3.8 Deformation within the limestone outcrop in the Agia Kiriaki Bay beach cliff. A: Elongated flint nodules following the steeply-dipping bedding planes; B: Close-up of thrusting within the outcrop - failed thrust (1); thrust (2); partial rip-up clast (3); fault gouge (4).

The softness of the sediments made it difficult to tell how old they were. These deposits may have represented recent mudflows, an interpretation supported by the slump prone nature of these sediments and their presence down-dip of the marl hills

making up the northern valley. While folding in soft clays could have formed relatively recently (thousands or hundreds of years) the folding of the harder sandy layers may have taken hundreds of thousands to millions of years, although in some circumstances (eogenesis, early diagensis) sandstone can be created in only a few to tens of years (Boggs, 2006). A stereonet of bedding plane dip of the marls of Thinia showed that these folds formed a series of NE-SW to NNE-SSW striking open folds which were NE-dipping indicating a compressional force from the SE (Figure 3.6). This would point towards compression relating to Hellenide thrusting or collapse of the west-facing slope of Imerovigli. The surface geomorphology of the northern valley appeared to be controlled through surface drainage from Imerovigli rather than build up through deposition of landslide material.

A. Possible olistolith within Agia Kiriaki Bay sea cliff

Roughly 496 m along the shoreline road from Zola harbour at the base of the sea cliff was a small (~12 m across) limestone exposure (Figure 3.7). As this feature was harder than the surrounding marl it is being naturally excavated through differential erosion and with more of the limestone being visible in Oct 2010 than during the 2007 field-mapping campaign. The limestone in this exposure resembled the limestone within Petrikata Quarry being very pale grey to whitish, very well-cemented and heavily-fractured.

The bedding within the outcrop dipped steeply (60 to 70°) eastwards forming a dramatic wave-like structure. Some of the beds contained elongated 5 to 20 thick nodules of blue flint ranging from pebble-size to several metres long whose long axis matched that of the bedding planes (Figure 3.8, A). The “stretching” of these nodules suggested that this limestone had undergone strong post-deposition deformation. The presence of flint within this limestone suggested a similar depositional environment to that of the limestone observed within the Petrikata Quarry.

The outcrop showed numerous examples of eastwards orientated shear thrusting and production of a possible partial rip-up clast. Figure 3.8, B, illustrates these features.

The shear thrust initially tried to propagate along the steep bedding planes (1) however failed to break through the outcrop completely. A second shear thrust (2) of shallower angle (20°) had successfully broken through the limestone. Between these shear thrusts was a partially formed rip-up clast (3). Filling the ruptures caused by the shear thrusts around the rip-up clast was very soft, muddy dark grey fault gouge which contained small, angular clasts of limestone (4).

The presence of limestone in the middle of marls and clays raised questions as to the origin of this outcrop. This outcrop may represent an olistolith within a Plio-Miocene submarine gravity flow derived from the valley sides (Bizon, 1967). Its apparent detachment from other limestone ridges within the valley supported this idea. However, plotting of the bedding planes onto Figure 3.6 (red crosses) indicated that this limestone had the same SSE dip as the marl folds which suggested it formed part of the same deformation that caused this folding. This outcrop might be another easterly-dipping thrust (e.g. the northern continuation of the Agia Sotira Thrust).

3.2.2 Central Saddle Region

A. Lake Katachori

The sediments of the suspected paleo-lake were characterised as being chestnut-red, clay-rich *terra rossa* alluvium which onlapped the surrounding limestone hills. The southern part of the Lake was dissected by the Agia Sotira Thrust. The lake was presumed to be a very young feature based on the presence of a tongue of talus material (Figure 3.9) which onlapped the easterly-dipping limestone of the western lake "shore". This material formed the slightly raised topography at the south-western part of the lake (Figure 1.35). While dating of this material was not undertaken, the tongue partially buries the walls of an undated ruined settlement which occurred on the lake shore and therefore pre-dated the settlement (tens to thousands of years old). This material was onlapped by the lake sediments and therefore pre-dated formation of the lake i.e. the lake was ~4000 years old or less.

Figure 3.9 Suspected tongue of talus material at the south-western end of Lake Katachori onlapping the upward-sloping limestone ridge defining the western lake "shore".

B. Petrikata Quarry

Petrikata Quarry lay to the north of Lake Katachori and was contained within a limestone outcrop which measured roughly 80 x 353 m (Figure 3.10). Dense vegetation, road infrastructure and slope collapse isolated this outcrop from other limestone hills in the central part of the valley which made determining the origin of this outcrop impossible through surface observations alone.

The position of the outcrop within the proposed route of "Strabo's Channel" (labelled PQ on Figure 1.53) created a problematic bottleneck at the northern end of the saddle region restricting the Channel route to around 100 m across. The limestone making up this outcrop was very well-cemented, very pale grey to cream in colour and contained football-sized crystals of wine-red chert. It was strongly brecciated with easterly-dipping (32 to 38°), 1 to 0.5 m thick layers of breccia bound in a fine-grained pale matrix of powdered limestone (gouge from minor normal faults and shear faults within the limestone?) alternating with heavily fractured limestone (Figure 3.11, A). This fracturing suggested this limestone had undergone strong deformation since deposition. The quarry outcrop appeared to overthrust the

underlying marl. This limestone-marl contact was most clearly seen to the north of the quarry (Figure 3.11, B) where it had an easterly dip of 40°. This was a shallower dip than the Agia Sotira Thrust however there was shear thrusting within the quarry itself which showed a steeper dip (~45°) suggesting this outcrop was related to thrust faulting within the valley.

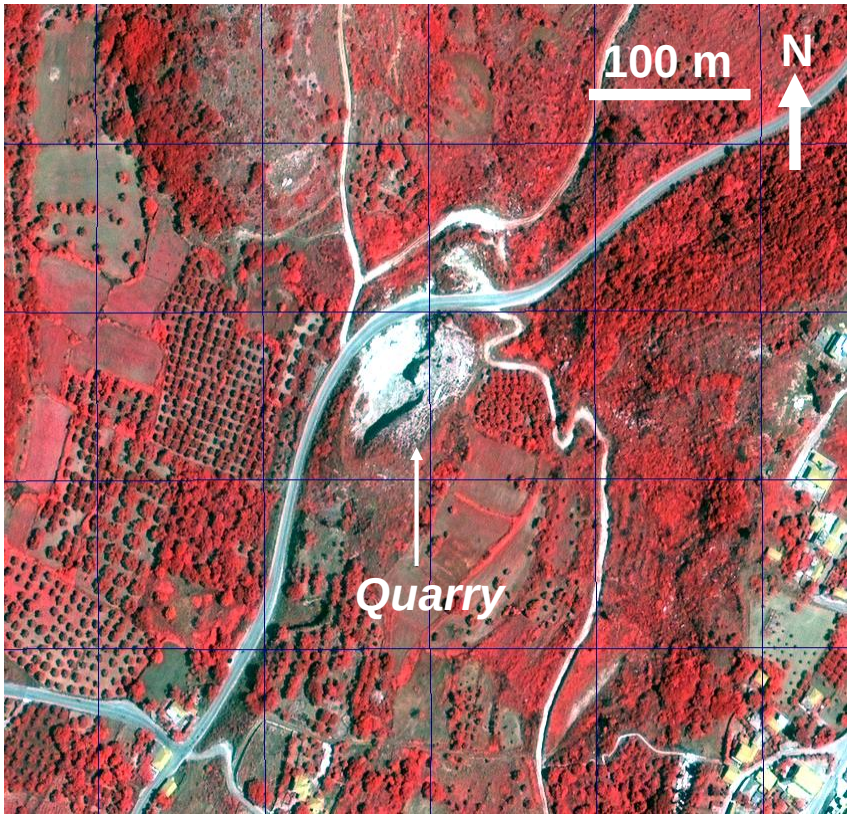

Figure 3.10 High resolution false colour Quickbird satellite image of Petrikata Quarry to the north of Lake Katachori plotted using the OziExplorer mapping software.

Another possibility is that this outcrop represents a large coherent clast detached from along the Ainos Thrust and transported down under gravity into the valley axis. The marl-limestone contact running around the base of the quarry may have been the base of the clast. The heavily fractured nature of the limestone would support this. The presence of a large clast embedded in the sediment here would be supportive of the theory that "Strabo's Channel" was infilled by large slumps of landslide material (i.e. evidence of sturzström activity) however it was very questionable whether such a collapse could have occurred so recently (within the last hundred or thousands of years). Biostratigraphic analysis of the surface samples suggested the limestone was

shallow marine Upper Cretaceous linking it with the Agia Sotira Thrust and western valley side rather than the deep water limestone of the Ainos Thrust hangingwall.

Figure 3.11 Photos from Petrikata Quarry: A. The layers of breccia alternating with fractured limestone, indicating a breccia layer of 50 cm; B. Thrust plane exposed at Petrikata Quarry.

3.2.3 Southern Thinia

The presence of bedrock ruled out the Agia Sotira inlet itself (Figure 1.50, A) as being a possible exit for “Strabo’s Channel”. The only route “Strabo’s Channel” could have taken is restricted to a 75 m to 200 m wide NNE-SSW orientated slope covered with alluvium and natural terracing. The eastern side of the route formed a 2 to 6 m high scarp of loosely-consolidated conglomerate sitting on top of a marl bluff. The western side of the route was defined by the limestone hangingwall of the Agia Sotira Thrust onlapped by very steeply dipping (sub-vertical) marl (dated to Early-Middle Miocene [Serravallian to Burdigalian] by Outcrop Sample 2).

Figure 3.12 was taken from the base of the sea cliff looking towards the proposed southern exit. There were two possible exit options for the Channel from the isthmus. The most obvious exit location lay around 500 m south of the Agia Sotira inlet in a gap between outcrops of bedrock. The route here formed a slumped zone in the cliff which consists of a series of small-scale slope collapses containing powdered pale marl, soil and a loose consolidation of poorly-sorted clasts of limestone, marl and conglomerate. The second exit point was located around 200 m further south and on the eastern side of the conglomerate scarp. The surface of this area was largely obscured by colluvial debris consisting of consisted of a broad boulder field with some very large limestone clasts in excess of 10 m across. The issue with both of these locations was the presence of limestone running along the base of the cliff 1 to 2 m above sea level onto which the slumped material onlapped.

This conglomerate terrace above the route was composed of rounded to sub-rounded limestone pebbles in a calcareous pinkish matrix (Figure 3.13). The contact between marl and conglomerate is undercut and possibly represents a relic wave-cut notch and therefore a raised shoreline. The elevation of this possible shoreline was also similar to the Zola talus edge and suggested could be Pliocene in age (Braune, 1973).

Figure 3.12 The proposed southern exits of "Strabo's Channel" with labeled version in lower image.

There was no clear scarp indicating the thrust plane of the Ainos Thrust. Instead there were several 2- 3 m high terraces and at the turn-off for Kondogourata was a well-cemented conglomerate which dated to Paleogene forming a possible link between the limestone of the thrust hangingwall and the more loosely consolidated

limestone along the Channel route (Samples 14 to 16). This conglomerate was composed of rounded limestone clasts of a similar colour to the matrix which had a very fine-grained marble-like quality (Figure 3.14, B). This outcrop also contained a weathered "channel" infilled with angular limestone clasts and a pale calcareous matrix interpreted as a lithified debris flow (Figure 3.15 and Figure 3.14, A). This "channel" formed part of a larger slump which could be seen on the high resolution false colour satellite image extending from the valley side to the shoreline (Figure 3.16). This debris flow obscures part of the possible route "Strabo's Channel" could take and the degree of lithification suggests it is thousands to millions of years old. Samples taken from this location (Samples 49, 50, 51) could not determine a biostratigraphic age of the sediments although a possible Neogene age was put forward.

Figure 3.13 Photograph taken at the base of the slump at proposed southern exit. Angular pebbles of limestone, marl and limestone conglomerate within muds. The slump material sits on top of eroded limestone around 1 m above sea level. During Mycenaean times this limestone may have been up to 6 m below present-day sea level.

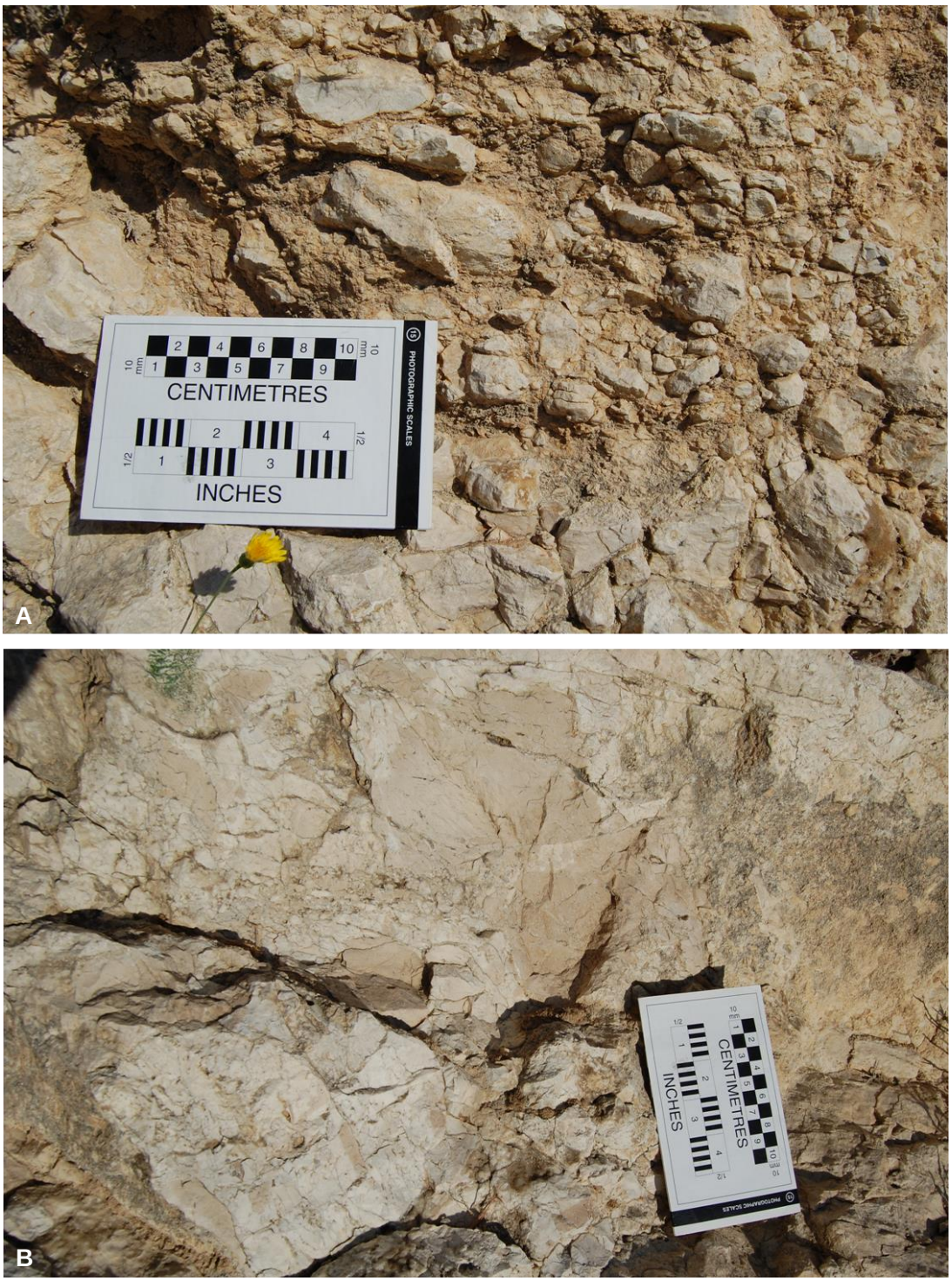

Figure 3.14 A: Close-up of lithified clastic material from above Figure. B. Close-up of well-cemented marble-like limestone conglomerate forming the bedrock outside of the clastic material. This rock is almost entirely composed of rounded limestone clasts of varying shades from white to dark grey-blue. There is no clear contact between bedded "true" limestone and this conglomerate at this location so no clear route of Ainos Thrust.

Figure 3.15 Example of a major debris flow cut into the Paleogene conglomerate within the hangingwall of the Ainos Thrust (top) – indication of major erosion of bedrock (at turn-off to Kondogourata). The boundaries of this debris flow are indicated by the black dashed line in interpreted version at the bottom.

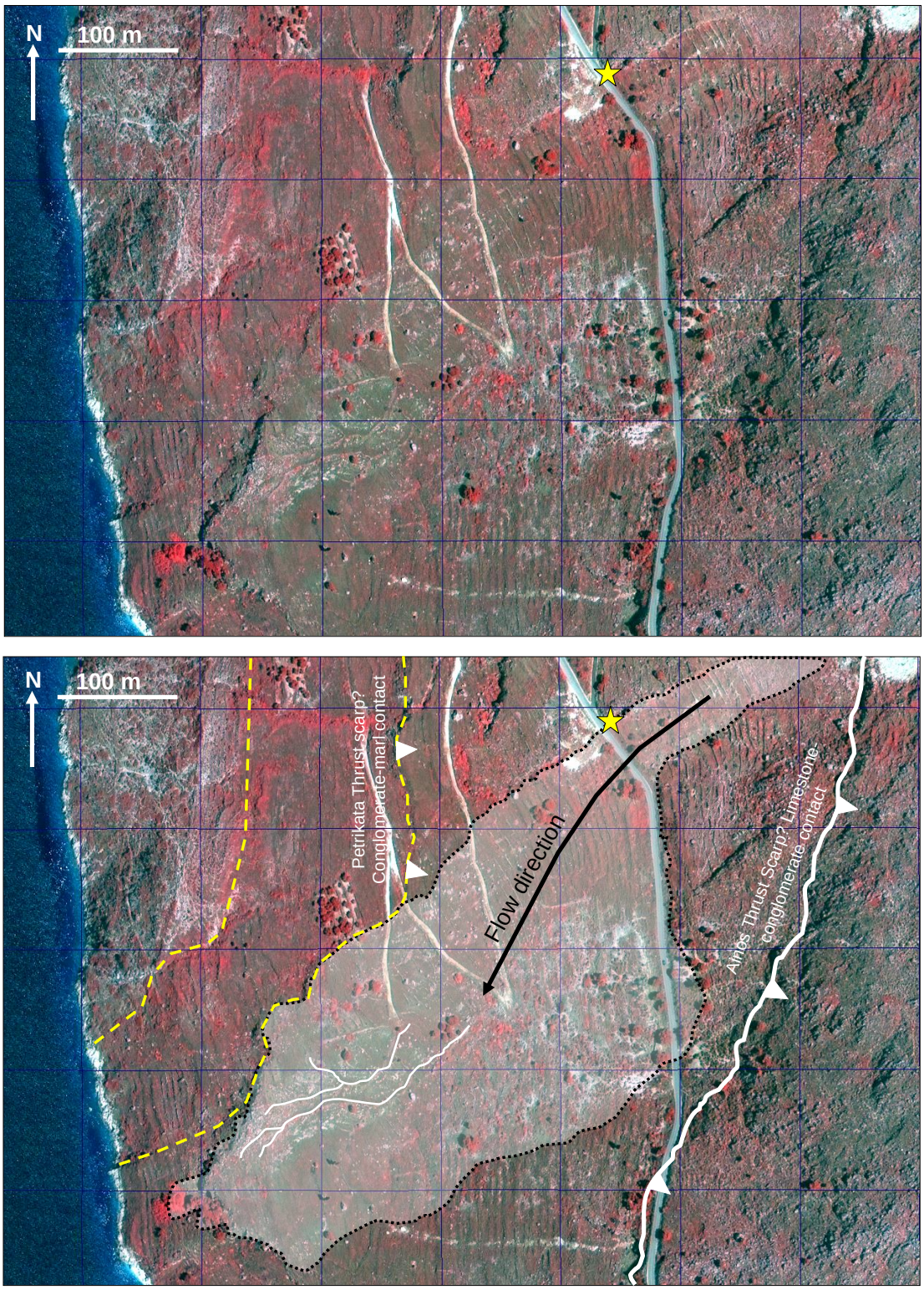

Figure 3.16 Evidence of debris flow at southern exit in false colour Quickbird satellite image (shaded in white). Dendric surface run-off patterns are marked in white. Location of Figure 3.14 and 3.15 is indicated by a yellow star. This debris flow may partially obscure the proposed southern exit of "Strabo's Channel" (indicated by yellow dashed lines).

.

3.3 Faulting in Thinia

The Thinia valley was dominated by Hellenide fold-and-thrust structures. The Ainos Thrust (Figure 1.38) defined the eastern valley side. In addition to the Agia Sotira Thrust (AST), an easterly-dipping thrust fault disrupting the marl sediments down the central part of the valley previously mapped by J. Underhill (Figure 1.37), one other previously-unidentified thrust fault (the "Petrikata Thrust") was mapped. However, the results of the fieldmapping showed that the structural geology of the valley was far more complicated than previously believed. There was clear indication of an underlying easterly-dipping extensional structure which existed prior to he Hellenide deformation migration into Pre-Apulian Zone. As well as the Ainos Thrust, which is known to represent a reactivated easterly-dipping normal fault, some of the thrusted structures within the valley (e.g. Agia Sotira Thrust) appeared to be reactivated normal faults due to their steep dip (45 to 60°) and smooth east-facing slopes. The western valley side was also bounded by a steep (25 to 30°), smooth scarp interpreted as a NNE-SSW striking, southeasterly-dipping normal fault.

This extensional-compressional regime was further complicated by at least three faulted offsets which occurred to the west of the Ainos Thrust and post-dated emplacement of the thrust faults. These offset the valley sediments and western valley side in a NW-SE direction. The most striking example occurred at Zola where the normal fault defining the western valley side was offset to the NW by around 700 m and some vertical displacement to the north. These offsets were not believed to be related to the series of normal faults visible along the western coast of Paliki (Figure 1.30) as displacement along the Paliki faults died out long before reaching the valley.

Displacement of the Ainos Thrust by around 150 m also occurred in southern Thinia and suggested that the pronounced curvi-linear valley along which this displacement occurred represented a north-westerly-dipping listric normal fault ("Agia Ioanni Fault") affecting this portion of the Ainos Thrust hangingwall. This fault may be youngest in the valley and generated through slope collapse due to the high-angle bedding dips caused through the complicated faulting history of the valley.

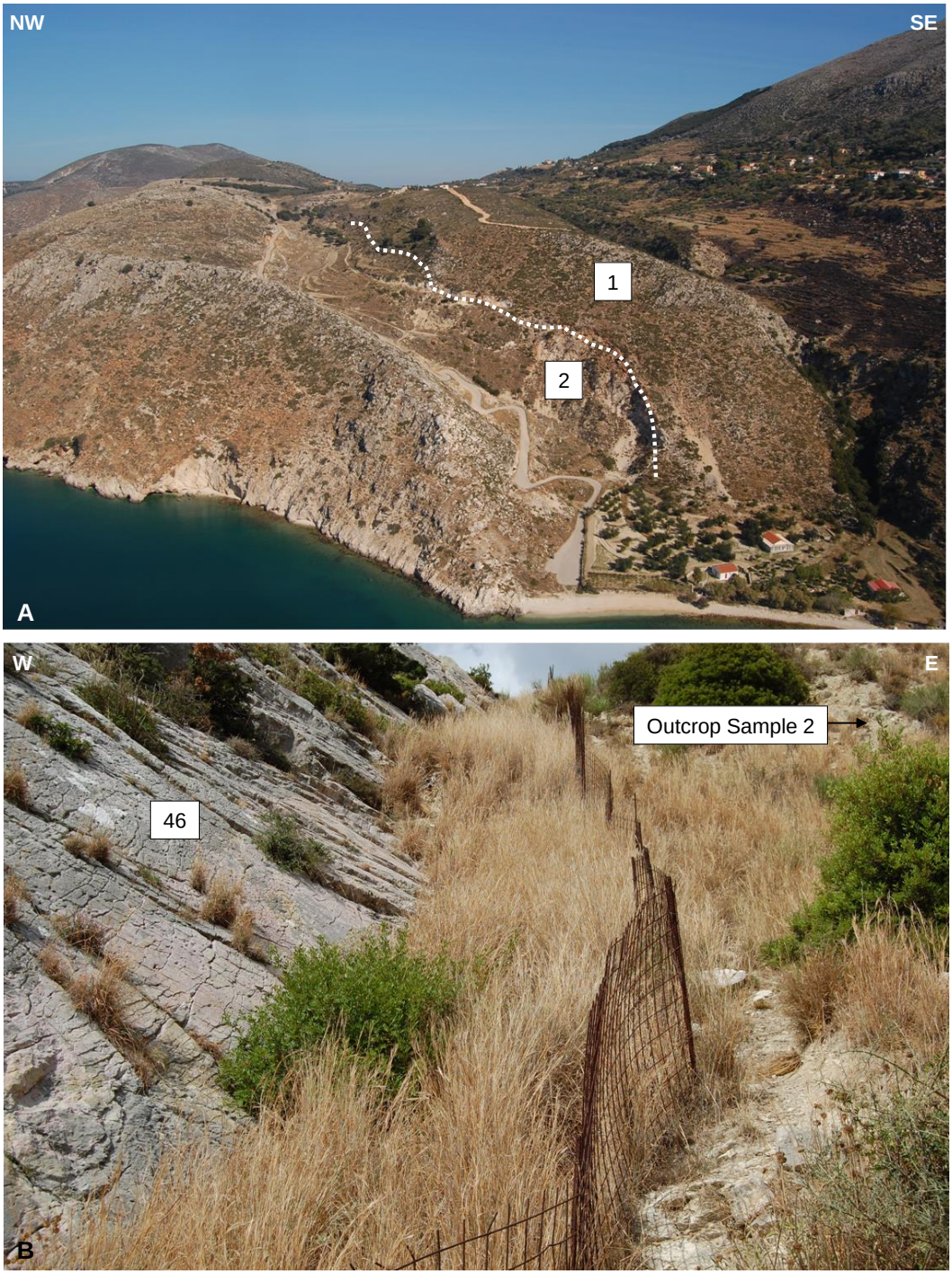

Figure 3.17 Agia Sotira Thrust (AST): A. Aerial view of the AST ridge taken looking northeastwards where 1 = limestone and 2 = marl. The thrust plane is indicated by a dotted white line; B. Marl onlapping the limestone of the AST. The limestone of the thrust is very smooth, steep with evidence of slicken sides suggesting it had its origins as an extensional fault. Outcrop sample 2 was taken from the marl here and yielded a Lower-Middle Miocene (Burdigalian – Serravalian) age. Sample 46 yield an Eocene age.

3.3.1 Agia Sotira Thrust (AST)

The Agia Sotira Thrust formed a very steep, NNE-SSW striking narrow ridge which ran from the Agia Sotira inlet to Lake Katachori. This thrust emplaced very steeply-dipping (45 to 55°) limestones over Neogene marls (sample 35) (Figure 3.17, A). Samples taken from the hangingwall immediately above the hangingwall at Agia Sotira inlet (samples 23, 33, 21) were Cretaceous in age and shallow marine. Limestone at the base of the visible portion of hangingwall yielded an Eocene age (sample 46). The thrust plane could be identified most clearly above the Agia Sotira inlet as an eroded scarp of pale marl beneath limestone. The Agia Sotira Thrust appears again to the north of the saddle region in similar form.

With a dip of 45 to 55° the AST was unusually steep for a thrust fault. The east-facing slope of the thrust ridge had a very smooth, "polished" appearance and seemed to display slicken sides (Figure 3.17, B). These features and angle of dip had led to past misidentification of this fault as an easterly-dipping normal fault in some maps. However, the development of a hangingwall anticline and the clear emplacement of limestone over marl on the western side of the ridge classed this as a thrust fault. Given that this thrust had the same orientation and dip to the large normal fault defining the western side of the valley, it was possible that this thrust was originally an easterly-dipping normal fault which was re-activated as a thrust fault under compression. Determining the timing of this re-activation was of key importance as this would help identify the source of the compression which caused this re-activation.

3.3.2 "Petrikata" Thrust

The "Petrikata" thrust was an easterly-dipping thrust fault identified running between the Ainos Thrust and Agia Sotira Thrust within the saddle region (Figure 3.18). Prior to the field-mapping campaign this thrust had been identified as a normal fault in earlier maps (British Petroleum and Co. Ltd., 1966).

This thrust formed a well-defined scarp between 2 and 25 m high which ran along the Divaraton-Katochoriou main road from the north of Petrikata Quarry below the villages built along the central part of the valley. The scarp was composed of brecciated limestone with lenses of very well-cemented limestone conglomerate tilted to subvertical. The limestone was heavily-fractured with small-scale faulting (shear and normal) in a similar way to the limestone at Petrikata Quarry indicating this limestone had undergone strong deformation. An accumulation of large boulders marked the length of this scarp. Bedding plane dip measurements taken from the marl immediately onlapping this thrust to the north of Petrikata showed a steeper dip (~70 to 90°) like the marl onlapping Agia Sotira Thrust suggesting this thrust had a similar steep dip. Samples (32, 43, 44) taken from the thrust yielded a Paleogene age. This scarp had previously been attributed to normal faulting, differential erosion due to changes in the hardness of the marl or out-building of talus deposits sourced from the eastern slope. This "new" thrust scarp was an important discovery due to its location beneath settlement and its restrictive effects on the proposed route of "Strabo's Channel".

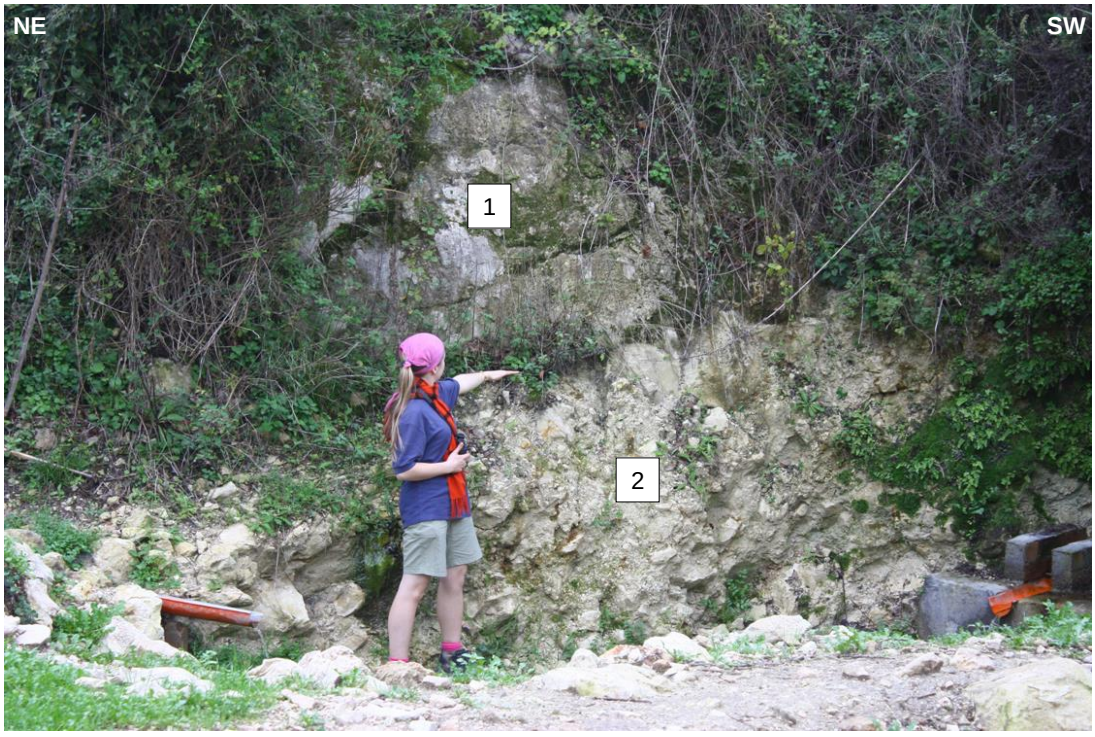

Figure 3.18 The "Petrikata" Thrust at its last confirmed location down an incised gully beneath Nifi village with limestone (1) overthrusting marl (2). The position of the thrust plane is indicated.

3.3.3 Backthrust at Agia Sotira Bay

A thrusted contact was observed along the steep road running up from Agia Sotira Bay which emplaced limestone and limestone breccia over marl (Figure 3.19). The limestone here dipped westwards indicating the formation of a backthrust. This backthrust may indicate the formation of a "triangle zone" at the front of the easterly-dipping thrusting deformation front. The most well-known example of a triangle zones is in the Canadian Rockies (Morley, 1986; Vann et al., 1986). Triangle zones tend to form at the foreland margins of thrust-and-fold belts and are defined as the structure formed by two upward-converging thrusts within the hangingwall of a thrust (in this case the Atheras Thrust) (Butler, 1982). A similar series of backthrusts occurred along the west coast of Argostoli Peninsula marking the western limit of the two thrust faults along the Argostoli Peninsula (Section 1.2.3, B).

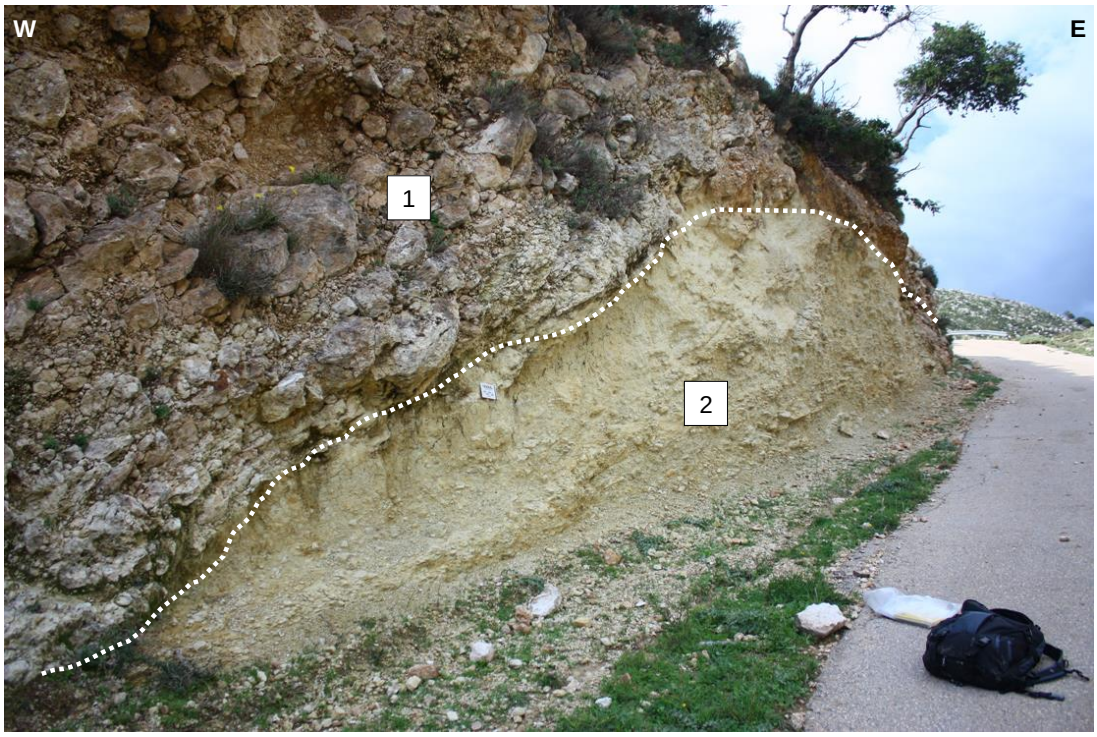

Figure 3.19 Westerly-dipping backthrust above Agia Sotira Bay where limestone overthrusts marl (2). The limestone above the marl is heavily brecciated and rubbled in sections. The thrust plane is marked by a white dotted line.

3.3.4 The "Agia Ioanni Fault" (possible rotational slump within Ainos Thrust hangingwall)

In southern Thinia above Agia Ioanni Bay the Ainos Thrust is visibly displaced by around 150 m along a pronounced curvi-linear valley which extended around the top of a large portion of the thrust's hangingwall to Nifi. At the top of the mountainside, the valley forms a smooth, NW-dipping slip plane with a throw of around 560 m (dubbed the "Agia Ioanni Fault"). This displacement and scarp suggested this valley forms a major listric normal fault (Figure 3.20, 3.21). The "detached" portion of Ainos Thrust hangingwall (a lens-shaped hill measuring around 1 km x 4 km) may represent a massive coherent slump (Figure 3.22). Independent movement of this block would explain the 8 m of lateral displacement of the Ainos Thrust plane which occurred during the 1953 earthquake at Petrikata but nowhere else along the eastern side of Thinia. This fault then dives below the Gulf of Argostoli so presumably the displacement along this fault extends further westwards of the Ainos Thrust plane. The key question was, if this block did represent a rotational slump, could this slip have occurred recently (in the last ~3300 years) and therefore be partially responsible for infilling or even displacement of a Mycenaean age marine channel through the formation of toe-thrusting ahead of the slump within the marl?

Figure 3.20 View of Thinia from Lixouri harbour with the possible north westerly-dipping listric fault ("Agia Ioanni Fault") occurring within the Ainos Thrust hangingwall. Photo credits: J. Underhill.

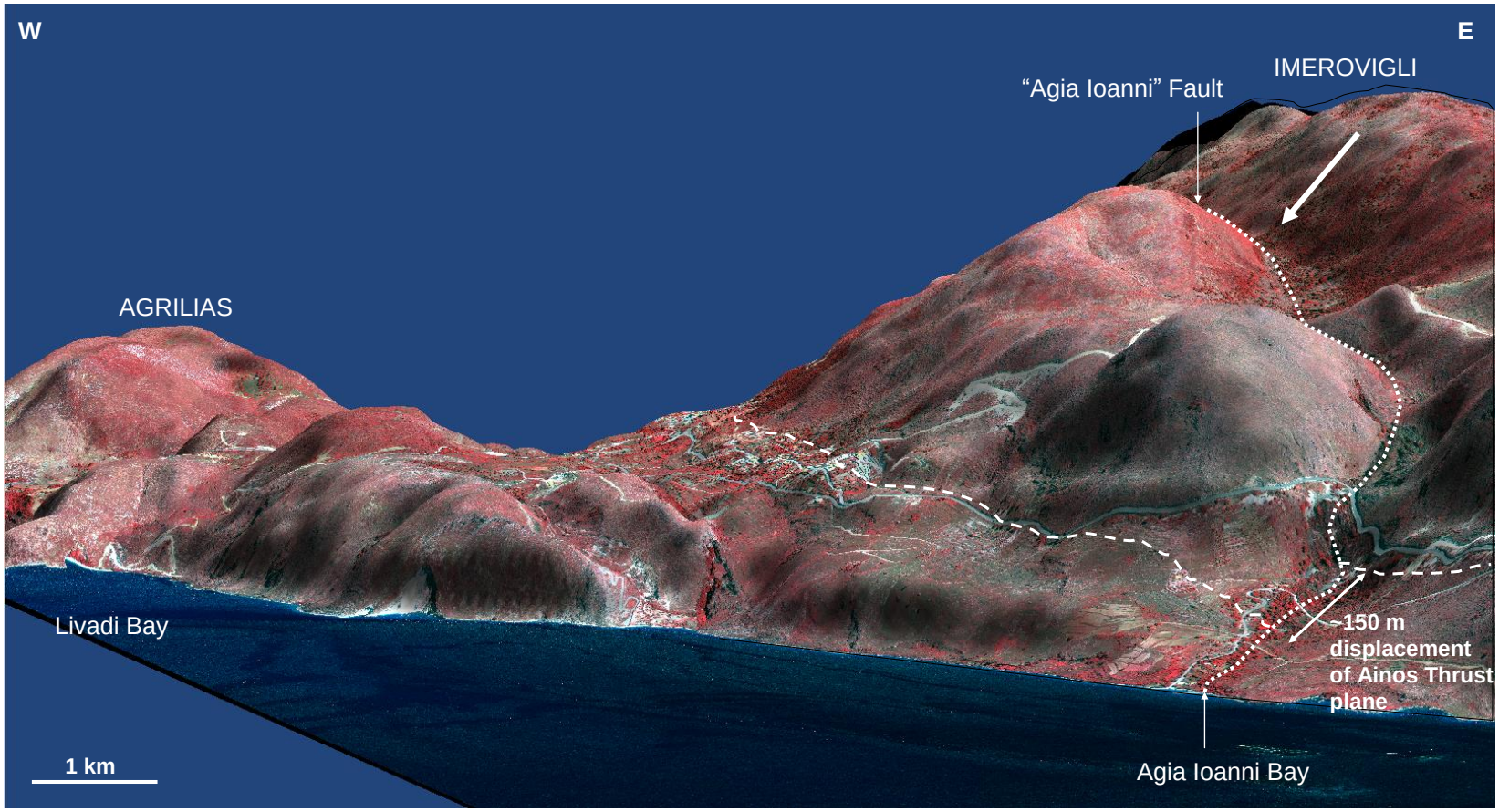

Figure 3.21 Possible massive rotational slump within Ainos Thrust hangingwall affecting southern portion of Thinia viewed from the northern Gulf of Argostoli. The slip plane above the slump white dotted line) extends from Nifi to Agia Ioanni Bay in the Gulf of Argostoli and displaces the Ainos Thrust plane (white dashed line) by around 150 m. Produced on the OziExplorer3D mapping visualization software using the 100 pc false colour Quickbird satellite map draped over a 3-dimensional grid. Vertical exaggeration is 1.5.

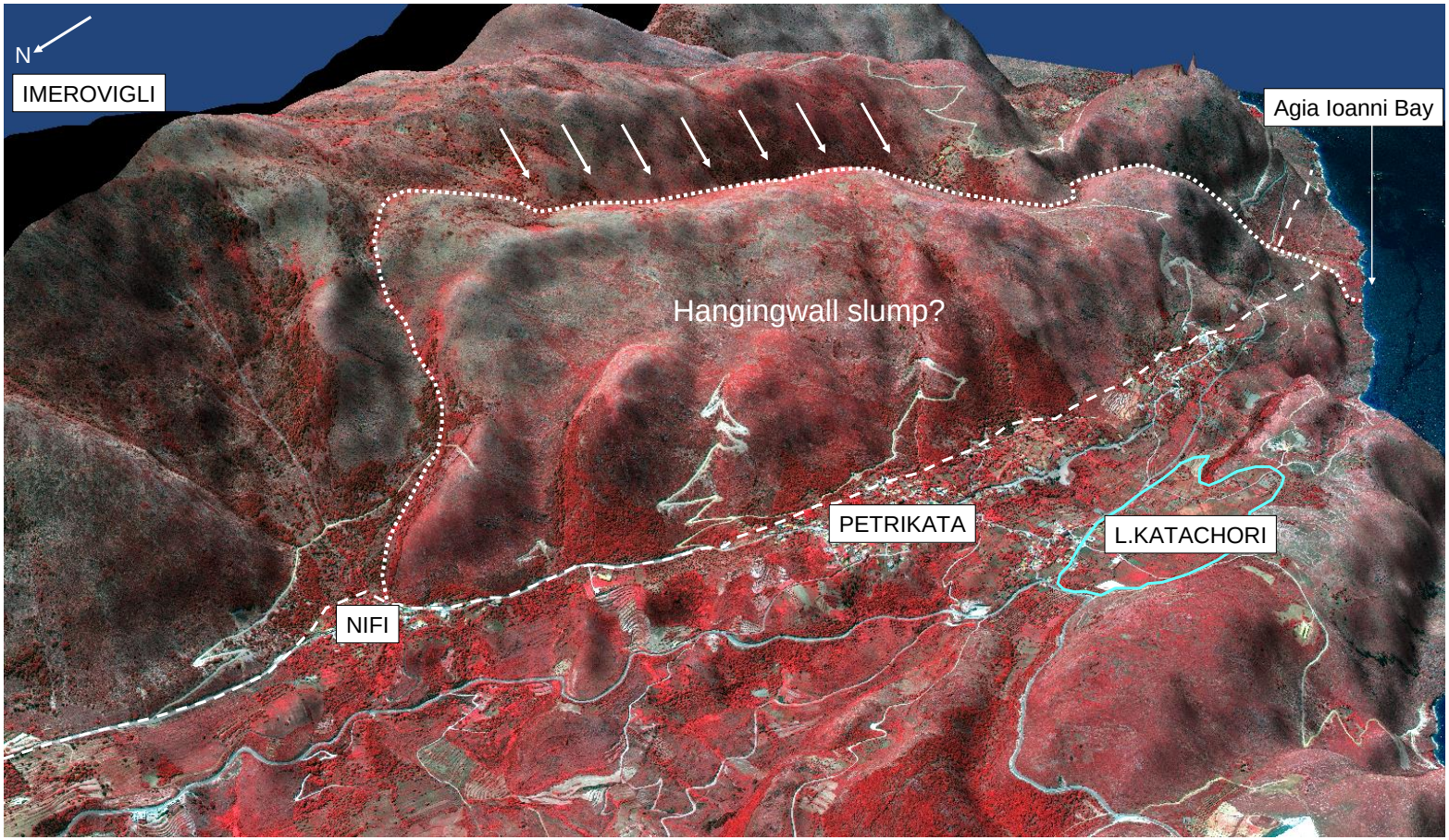

Figure 3.22 Possible detached coherent block within the Ainos Thrust hangingwall. The slip plane above the slump extends from Nifi to Agia Ioanni inlet in the Gulf of Argostoli and displaces the Ainos Thrust plane (white dashed line). Lake Katachori is outlined in light blue. Map information as for Figure 3.21.

3.4 Extent of Colluvial Deposition

The surface of Thinia was predominately covered with a rubble-rich (*terra rossa*) alluvium with significant accumulations of colluvial material at the base of Imerovigli beneath the villages of Angon (Figure 3.23, A), Nifi (Figure 3.23, B) and Petrikata and beneath Zola (Figure 3.24) on the west. These were fed by scalloped embayments incised by dendric streams which cut back into the mountainside.

These took the form of topographically-raised "megabreccia" aprons or fans which spread out across the low foothills of the valley floor. These fans typically had a lithified edge 2 to 10 m high consisting of limestone breccia bound in a pinkish-red calcareous cement and were surrounded by a broad boulder fields which extended up to a kilometre away from the lithified deposit (all the way to the shoreline in the case of Zola and Angon). These boulder fields were composed of limestone blocks several tens of cubic metres in volume which were angular and brecciated and occasionally coated with a layer of limestone or calcite stalactiforme concretion. The material within these fans was heterometric with clast size diminishing with higher elevation. Near the top of the talus deposits the clast are less than 20 cm, angular and bound in an argillaceous brownish-red cement (Figure 3.25, A). Figure 3.25, B, shows a close-up of the conglomeritic material defining the lithified edge of the talus. Sorel (1967) estimated that the average thickness of these deposits was at least 30 m.

Determining an age for these talus aprons was difficult. The absence of an established surface drainage network on the Zola fan led Gaki-Papanastassiou et al. (2011) to suggest this deposit was geologically very young and may actually be only a few thousand or hundreds of years old. Sorel (1976), however, saw similarities in the morphology of the Zola talus and the Mindel breccias of Epire and Akarnaria in Western Greece and speculated that the talus represented Plio-Calabrian sediments sealed with Mindel cement. In this case the Zola talus formed in response to Calabrian movement of the NNE-SSW anticlinal axis running above Zola causing collapse along the NNE-SSW striking fault plane defining the western valley side.

Figure 3.23 The talus deposits at Nifi (A) and Angon (B) (outlined by a dashed line). Drainage from Imerovigli is indicated. The scalloped slope break above these deposits is indicated by a white dotted line. The Ainos Thrust is indicated by a white straight dashed line.

Figure 3.24 The talus deposit at Zola (outlined by a white dashed line).

There was indication that the Zola fan may have extended further eastwards in the form of fragments of easterly-dipping limestone breccia scarp clinging to the western valley side at an elevation of around 136 m (Figure 3.26) and a similar deposit on the other side of the drainage valley. Both deposits had been undercut and suggested part of the Zola fan had been eroded away by the northwards draining stream. In the case of Figure 3.26 this would amount to around 70 m of down-cutting of the marl (Figure 3.27). This amount of down-cutting was comparable to the incision of the streams above Agia Sotira inlet and could not have occurred in recent history which would agree with Sorel's (1976) speculation that the Zola talus is millions rather than thousands of years old.

No age-dates exist for the fans along the eastern side of the valley. The talus deposits beneath Imerovigli show a much higher degree of surface drainage where the numerous streams draining into the valley had eaten down into the bedrock and carried "outfingers" of finer material up to 1.5 km away from the main fan deposit. The greater amount of erosion experienced by these deposits suggested they were much older than the Zola fan (thousands to millions of years) however this increased

erosion may be due to more surface drainage from the mountainous eastern valley side and they could still be of a comparable age.

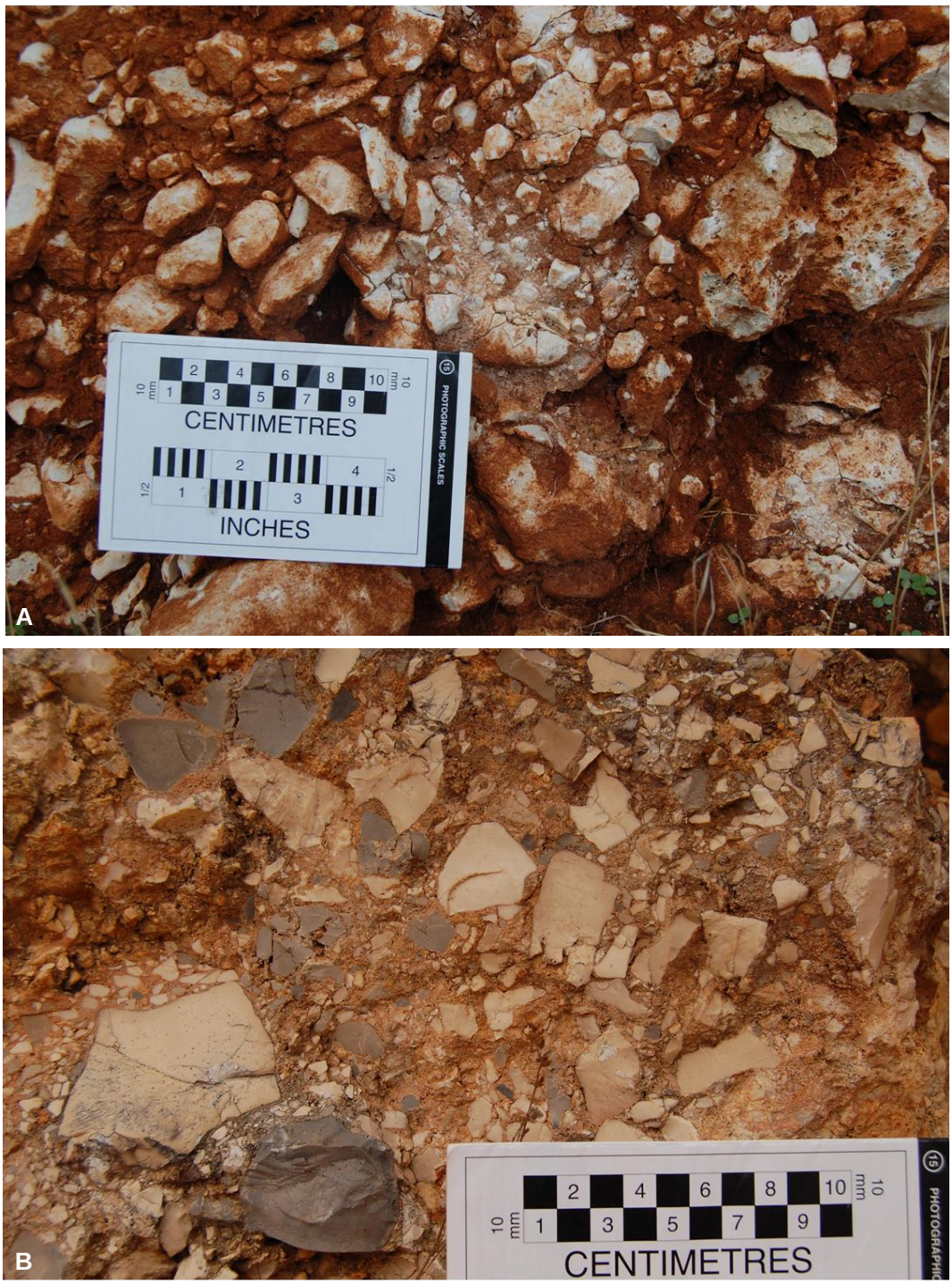

Figure 3.25 Zola talus fan: A. Near the top of the fan, the colluvial debris forms a loosely-consolidated breccia of angular limestone fragments mostly less than 10 cm with the occasional large boulder bound in a brownish-red argillaceous matrix; B. Conglomerate at edge of the talus fan.

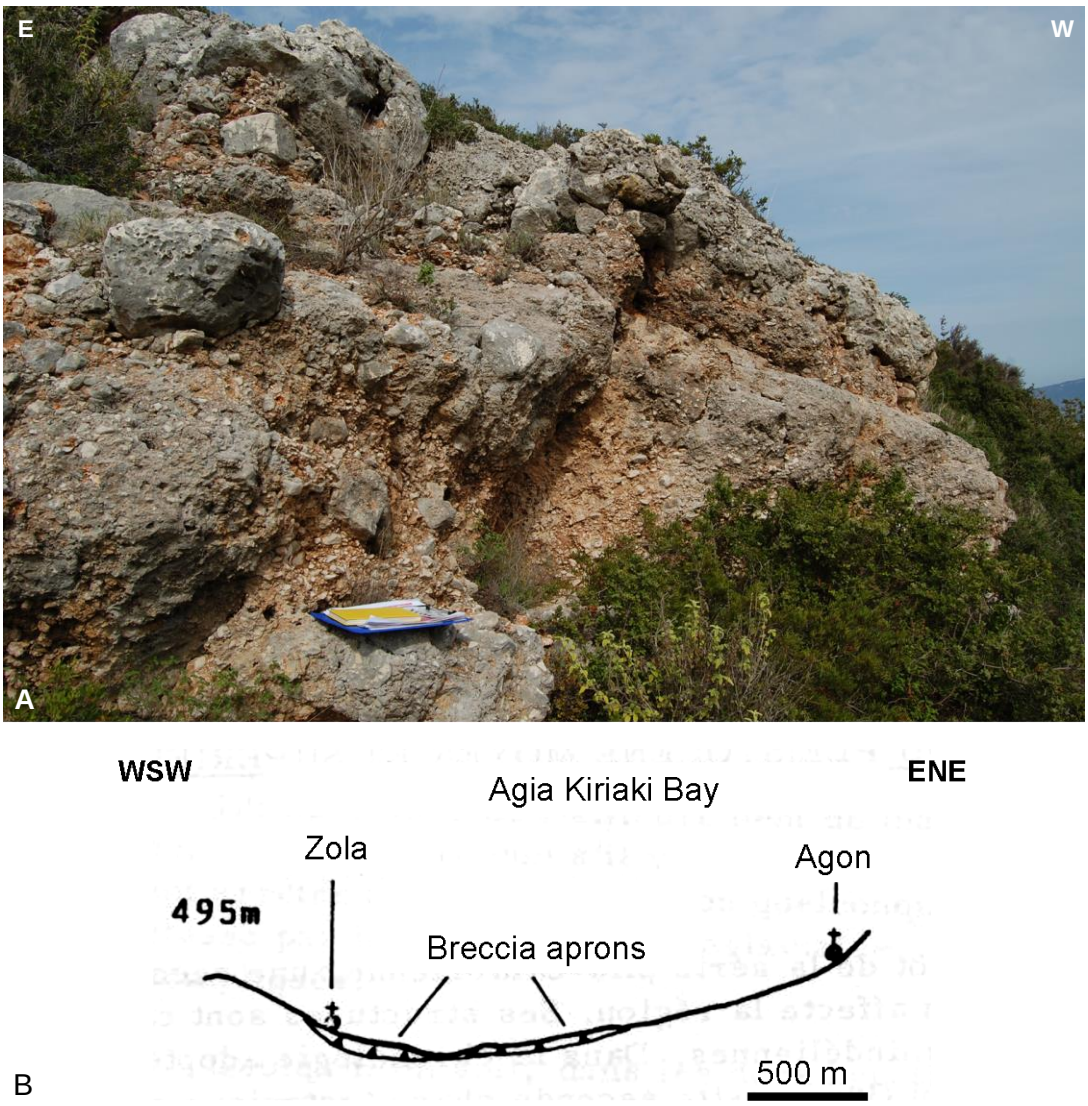

Figure 3.26 Easterly-dipping limestone conglomerate scarp attached to the western valley side close to Zola (A). A similar scarp occurs on the opposite side of the valley, illustrated (B) by Sorel (1976).

Because of this significant erosion, the coverage of colluvium was not as extensive as previously mapped by Bittlestone et al. (2005). The processes which formed the Zola talus apron are still actively ongoing at the top of the fan where newly-deposited limestone rubble from the steeply-dipping slip plane continue to supply the apron with fresh clastic material (Figure 3.28). However, no significant volume of landslide material had been deposited within the valley between the initial fieldmapping campaign and the final visit three years later. There was some evidence of small-scale slope collapse from higher up the valley sides in the form of large (car-sized) boulders. Between the first and second fieldmapping campaigns (three

years), several newly fallen boulders were discovered. Smaller-scale undercutting of the marls (within stream gullies and along Agia Kiriaki Bay coastline) was much more prevalent.

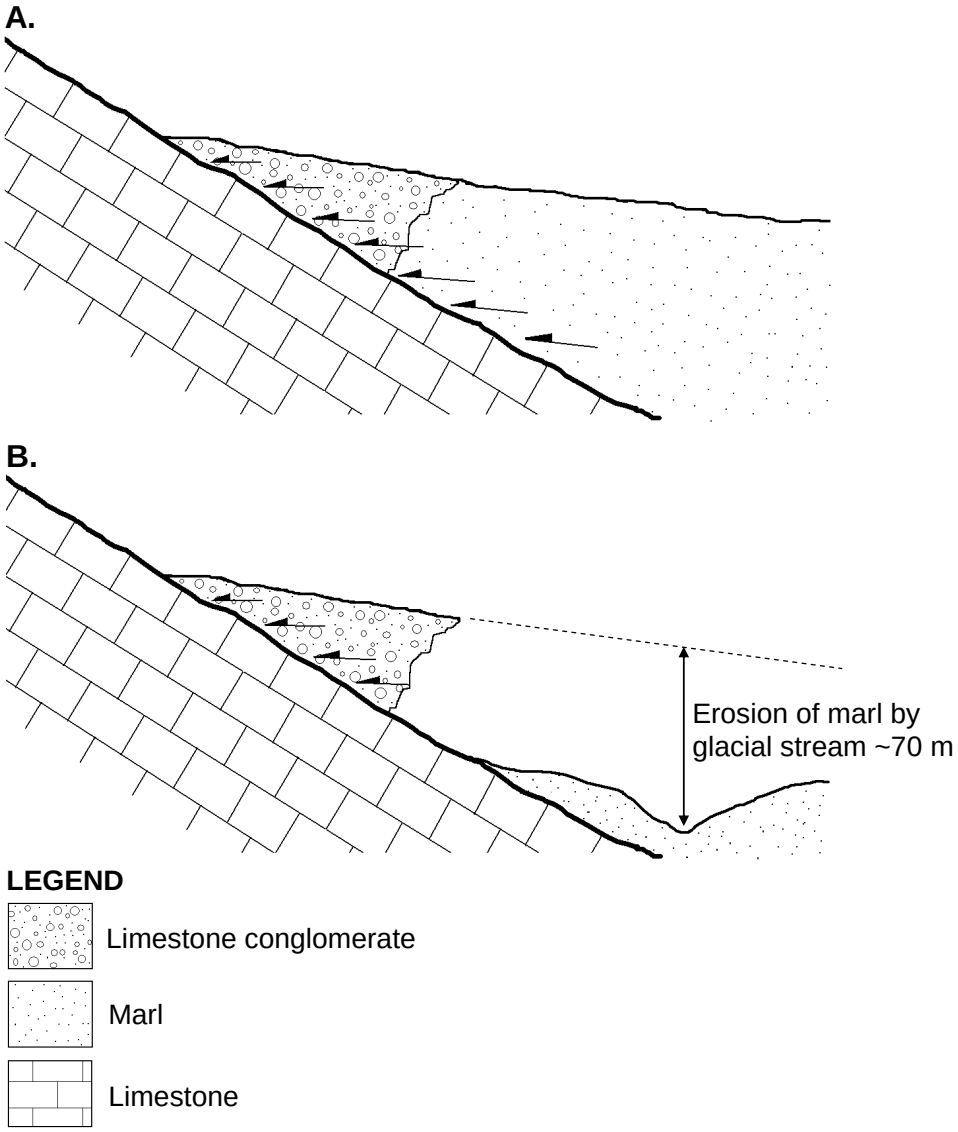

Figure 3.27 Sketch of Figure 3.26 depicting the conglomerate scarp on western valley side and down-cutting of marl.

Figure 3.28 Steeply-dipping limestone conglomerate beds above the Zola talus which are actively fracturing and adding fresh clasts to the fan below.

3.5 Surface Geology and Geomorphology Summary

The results of the geological and geomorphological study of the Thinia valley are presented in Figure 3.29. The fieldmapping campaign undertaken in this chapter confirmed the findings of the earlier geological map produced by J. Underhill for Bittlestone et al. (2005) (Figure 1.37). Thinia was predominately composed of marls and clays disrupted by limestone thrust faults. The marls varied in appearance in different parts of the valley and had undergone strong post-depositional deformation. In the northern part of Thinia, the marls ascribed a series of easterly-dipping folds of alternating hard and dark, soft strata. In the central and southern sectors these marls were paler with convoluted bedding and a wide range of (predominately easterly) dips (25 to 90°).

The campaign also investigated previously unmapped features. A newly-identified easterly-dipping thrust fault was mapped ("Petrikata Thrust", described in Section 3.3.2). This thrust formed a clear scarp in the topography running beneath the villages on the eastern side of the valley in the central sector.

The colluvial deposits were not as extensive as first believed and had experienced significant erosion suggesting they were much older than a few thousands of years. The short-term rates of further colluvial deposition (three years) were very low.

The structural geology of Thinia was more complicated that initially thought with an underlying easterly-dipping extensional structure overthrust by Hellenide compressional deformation. This in turn was faulted by NW-SE striking offsets which post-dated the extensional-compressional regime. There was indication of shear-thrusting within the marls and limestone suggesting strong post-depositional deformation. The steeply-dipping, deformed marl sediments were prone frequent slope failure and slumping was prevalent particularly on the northern coast and down stream gullies.

On the basis of this map, five E-W orientated cross-sections were constructed (labeled I-I' to V-V' on Figure 3.29 and presented in Figures 3.30 to 3.34) using surface measurements of bedding plane dip to project the strata into the sub-surface. A dip of ~45-60° was proposed for the Ainos Thrust. A similar dip was chosen for the Petrikata Thrust as it was assumed this thrust had similar origins to the Agia Sotira Thrust.

These cross-sections cut the NNE-SSW to NE-SW orientated stratigraphic trend observed within the valley roughly perpendicular to its strike. While the configuration of the northern cross-sections (I-I' and II-II') made fitting a "Strabo's Channel" relatively easy, the presence of thrust faults within the central and southern sectors of the valley greatly reduced the amount of space required to accommodate a buried marine channel.

This was particular clear in cross-section III-III' which cross-cut the most contentious part of the valley. This was where the route of "Strabo's Channel" was restricted by Lake Katachori and the Petrikata Quarry outcrop. This section followed a similar route to the original 2006 gravity survey (Section 2.2.2) and cross-cut the gravity low detected by this and the Phase I gravity results for Lake Katachori. The presence of the Petrikata Thrust and the Agia Sotira Thrust reduced the width of the channel route to only around 100 m requiring a near-vertiginous gorge to ensure the channel reached sea level.

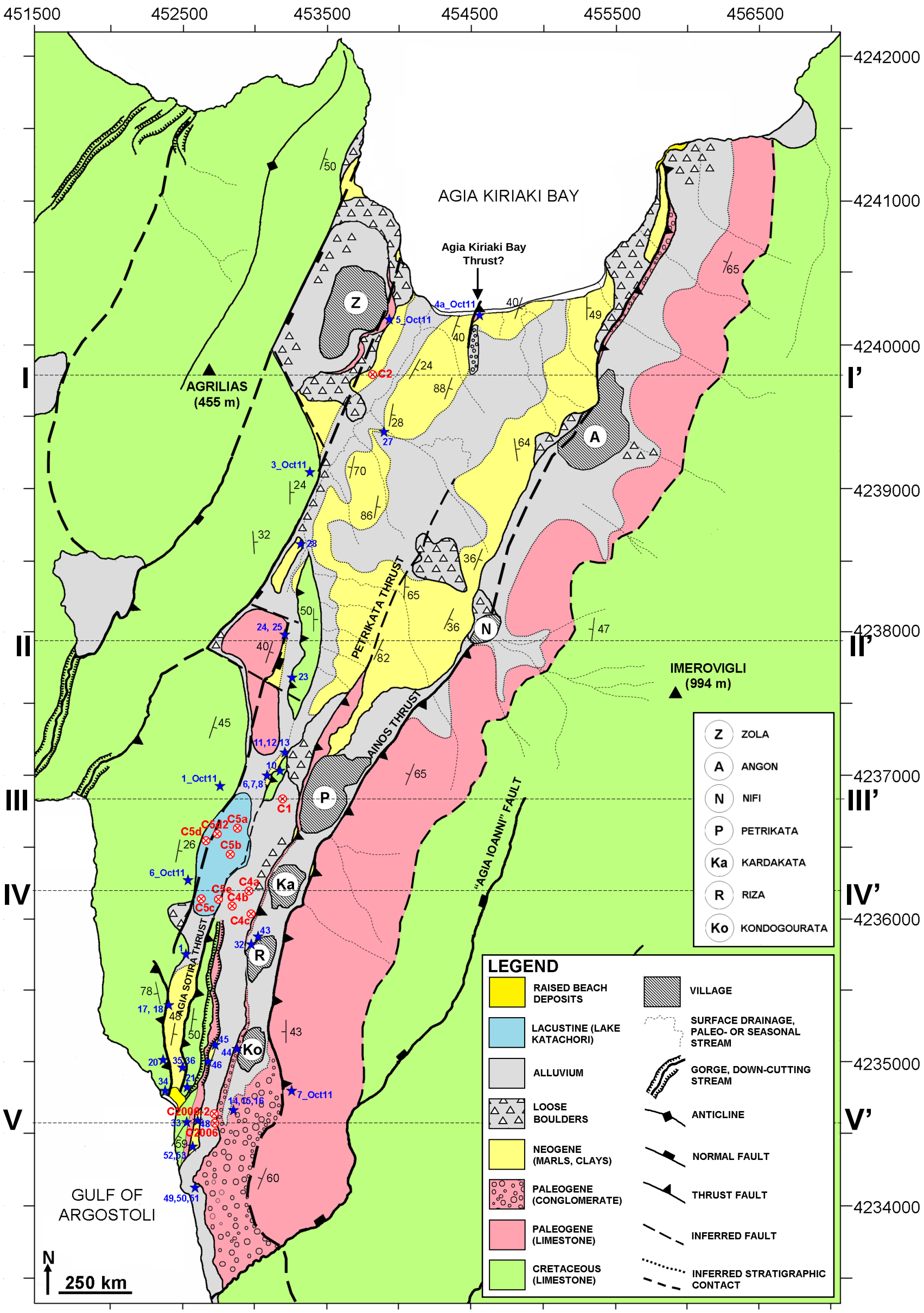

Figure 3.29 Geological map for Thinia produced from detailed field-mapping. Blue stars indicate the locations of surface samples which are listed in Appendix B. Boreholes are indicated in red. The locations of the five geological cross-sections I-I' to V-V' (Figures 3.30 to 3.34) are indicated. The position of the Cretaceous-Paleogene boundary is from the geological map produced by J. Underhill for Bittlestone et al. (2005).

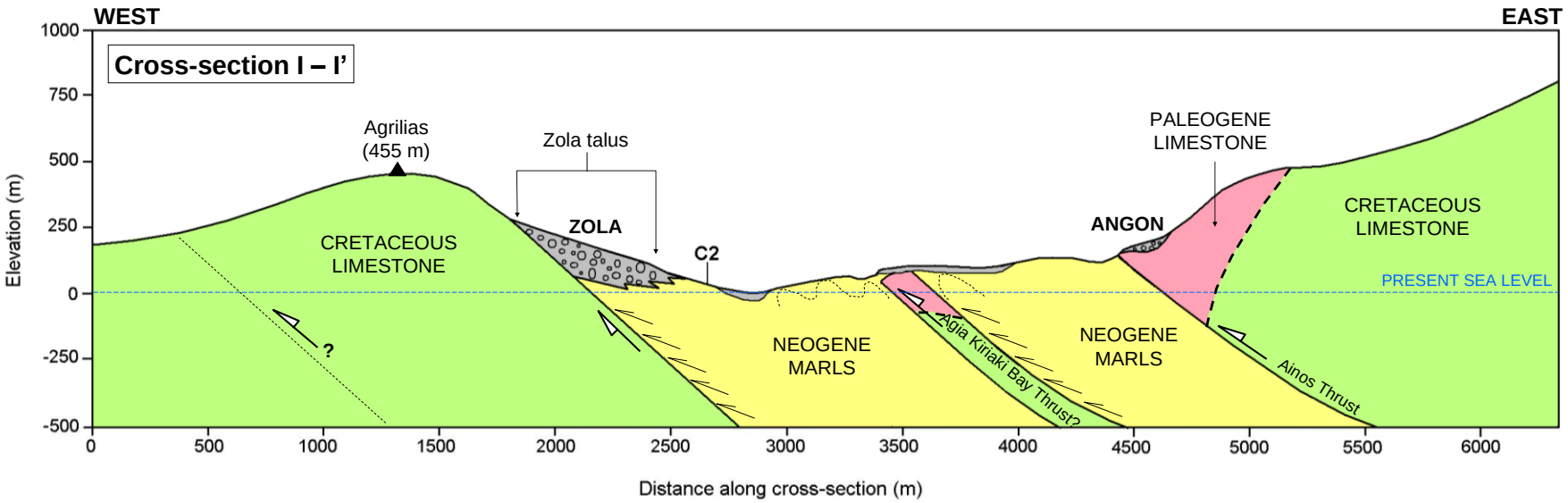

Figure 3.30 Geological sketch cross-section I-I' produced from the fieldmapping campaigns (location indicated on Figure 3.29). Dashed lines indicate the inferred positions of lithological boundaries and faults. The undulating dashed lines within the Neogene marls indicate the presence of asymmetric folds. The location of borehole C2 is indicated.

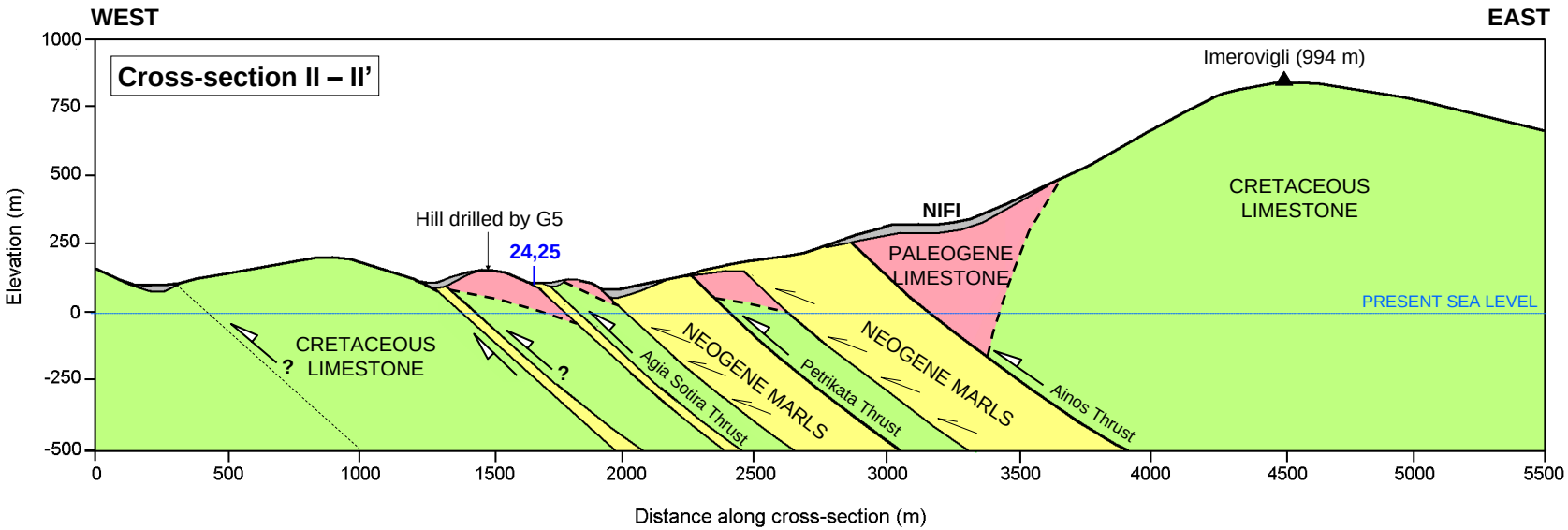

Figure 3.31 Geological sketch cross-section II-II' produced from the fieldmapping campaigns (location indicated on Figure 3.29). Dashed lines indicate the inferred positions of lithological boundaries and faults. The location of the brine-bearing hill drilled by G5 (located in Figure 1.37) is indicated. The blue numbers refer to surface samples listed in Appendix B.

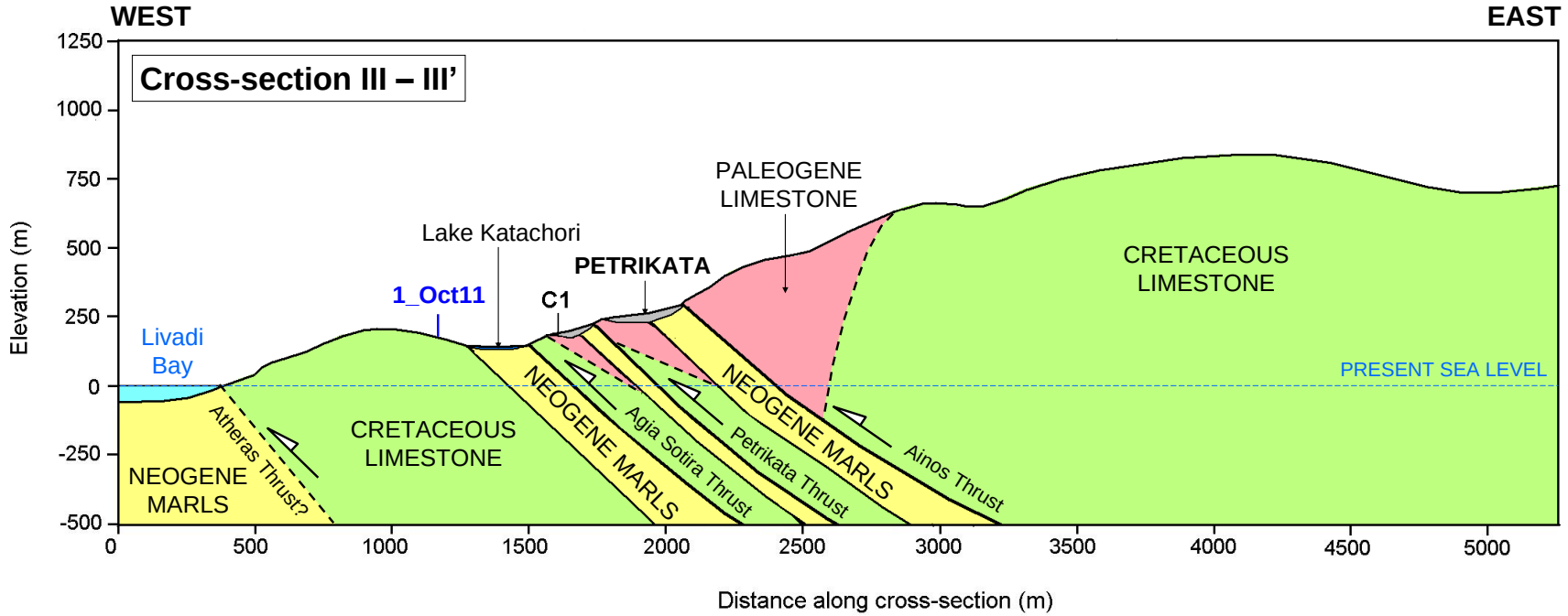

Figure 3.32 Geological sketch cross-section III-III' produced from the fieldmapping campaigns (location indicated on Figure 3.29). Dashed lines indicate the inferred positions of lithological boundaries and faults. The location of borehole C1 is indicated. The blue numbers refer to surface samples listed in Appendix B.

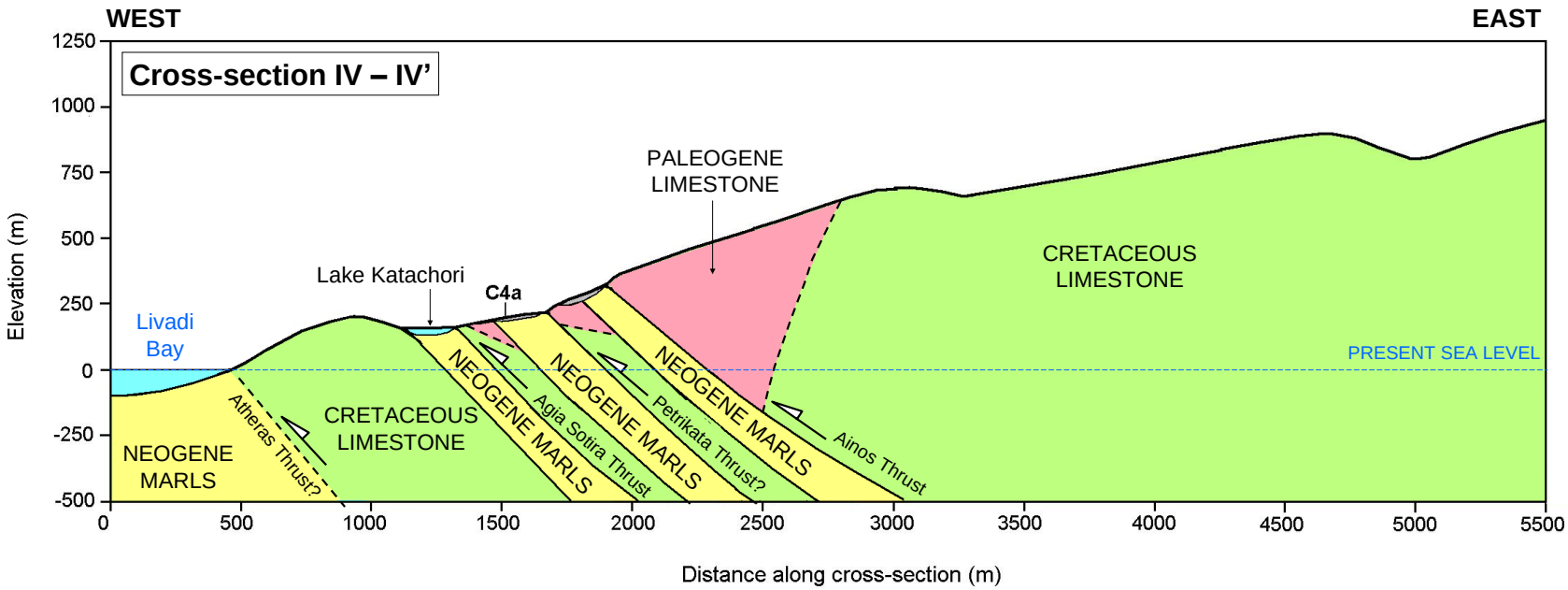

Figure 3.33 Geological sketch cross-section IV-IV' produced from the fieldmapping campaigns (location indicated on Figure 3.29). Dashed lines indicate the inferred positions of lithological boundaries and faults. The location of borehole C4a is indicated. The blue numbers refer to surface samples listed in Appendix B.

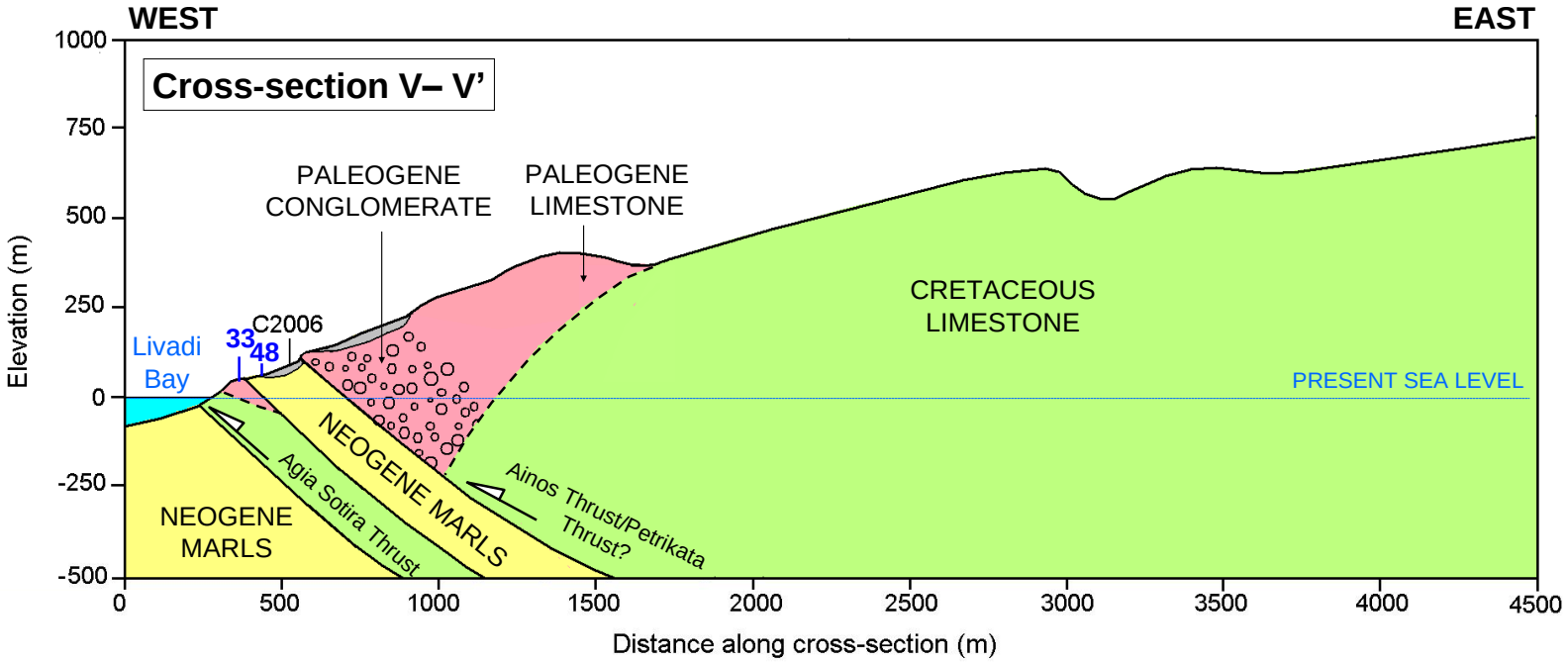

Figure 3.34 Geological sketch cross-section V-V' produced from the fieldmapping campaigns (location indicated on Figure 3.29). Dashed lines indicate the inferred positions of lithological boundaries and faults. The location of borehole C2006 is indicated. The blue numbers refer to surface samples listed in Appendix B.

CHAPTER 4: Onshore Geophysics

4.1 Introduction

This chapter presents the complete results of the non-invasive geophysical tests conducted onshore across Northern Paliki and at strategic sites. The onshore geophysics was aimed at producing a thorough image of the subsurface of the survey area using a complimentary series of survey types. These surveys either tested the "Strabo's Channel" theory directly (e.g. the proposed northern and southern exits) or were aimed at locations out with the Thinia valley (e.g. Livadi Marsh, Atheras Bay) which were deemed necessary in understanding the geological history of the area. The resistivity and corresponding seismic refraction lines are presented together to allow direct correlation between them with accompanying map to show their location. The chapter is structured as follows:

1. **Northern Paliki (Section 4.2).**
2. **Atheras Bay (Section 4.3).**
3. **Livadi Marsh (Section 4.4).**
4. **Thinia (Section 4.5).**

Elevations above sea level in the digital elevation model (DEM) and resistivity and seismic refraction profiles are in terms of mean sea level (+22 m above sea level) due to the approximation of the ellipsoid used by the Trimble GPS device and Fugro Airborne Surveys.

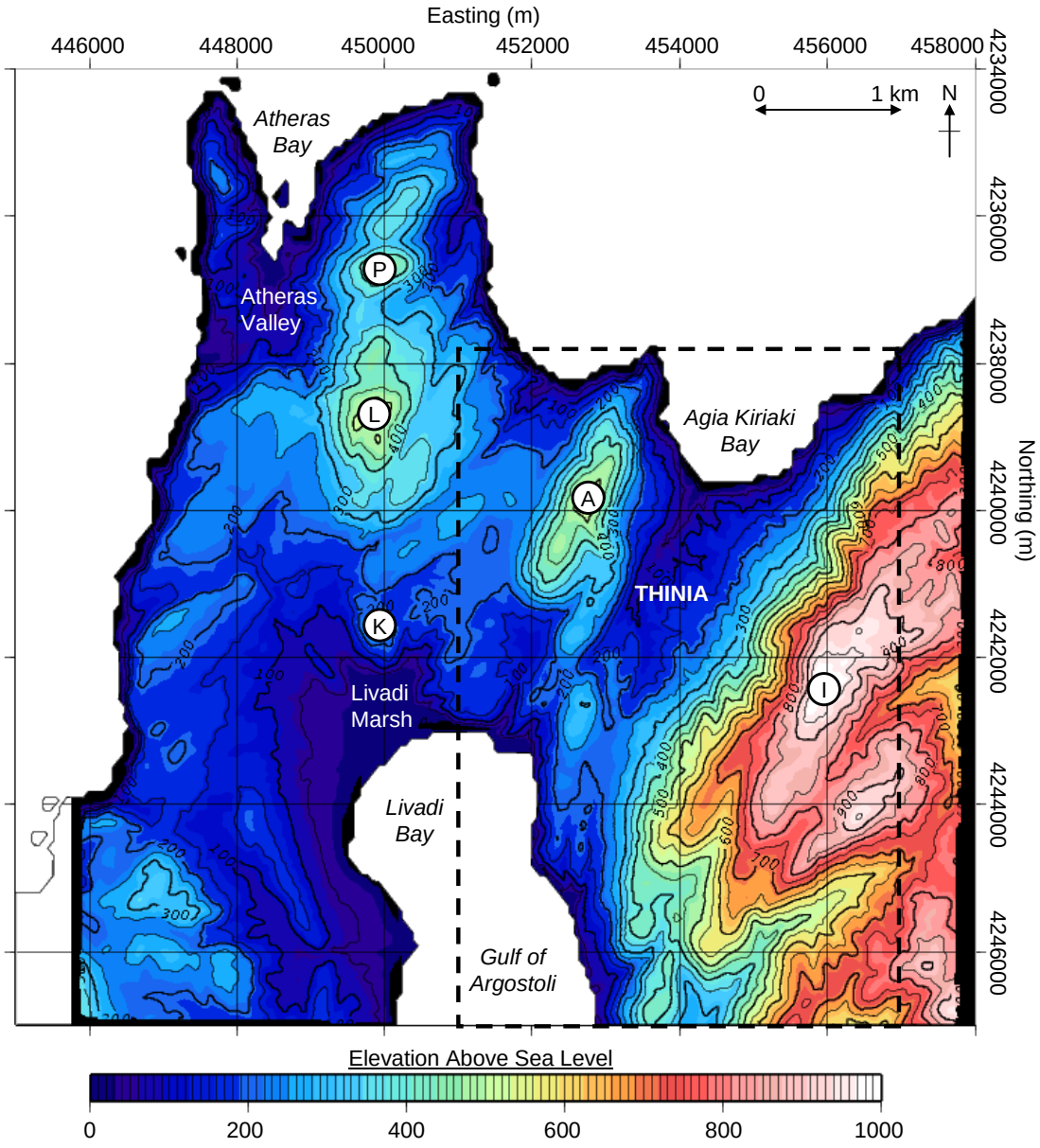

Figure 4.1 Topographic map of Northern Paliki created by plotting the high resolution digital elevation model (DEM) data provided by Fugro Airborne Surveys on Generic Mapping Tools (GMT). Resolution is 15 cm (horizontal) and 10 cm (vertical) to 2 sigma (95% confidence). Elevation is above average sea level (+22 m). L = Lachties, P = Polemi, K = Kastelli, A = Agrilias and I = Imerovigli. The location of Figure 1.31 is indicated by a black dashed line.

4.2 Northern Paliki: "Semi-regional" Airborne Overview

The helicopter-mounted electromagnetic survey was undertaken across the whole of Northern Paliki (Figure 4.1). In the following maps the topographic contours are labelled every 100 m. Areas of habitation were avoided by the survey to avoid the problem of interference from strongly conductive (metallic) surface objects (houses, cars, power lines, etc.) leaving small data coverage gaps (white areas on the maps). In these figures the "shallowest" (140 kHz), "middle" (8200 Hz) and "deepest" (400 Hz) resistivities are presented out of the five frequency maps acquired.

4.2.1 Magnetic Survey

The magnetic map was interpreted as a reflection on the distribution of *terra rossa* sediments with the most striking magnetic anomalies correlated with the thickest accumulations of this iron oxide-rich alluvium. What is immediately apparent from the reduced to pole (RTP) magnetic map is the strong contrast between the generally low (blue to green, -25 nT to ~0 nT) magnetic response of Northern Paliki and Eastern Kefalonia and the relatively higher magnetic (orange to red, ~10 nT to 40 nT) valley "fill" of Thinia (Figure 4.2). The magnetic response for Northern Paliki initially appeared complicated particularly around the Atheras region which was unexpected for a region of predominately homogenous (carbonate) geology. Closer inspection revealed that the magnetic signal could be resolved into an underlying low magnetic response cross-cut by numerous, strongly magnetic (up to 40 nT) NE-SW to NNE-SSW trending linear anomalies and several localised anomalies.

The low magnetic response could be tied to the limestone bedrock with the lowest signals generally coinciding with the highest elevations (350 m and above), particularly the mountains around Atheras Bay and Imerovigli on the eastern side of Thinia a response which correlated well with the zones of highest resistivity (Figure 4.3). The linear magnetic anomalies were very obvious and most numerous to the west of the Atheras Thrust, particularly along the north-western coast of Paliki where

they correlated with the NE-SW to NNE-SSW trending normal faults which cross-cut the northern part of the peninsula. This response seemed to reflect the thick deposits of *terra rossa* alluvium which had accumulated along the fault planes probably after being washed down from the mountains of the Atheras Thrust hangingwall.

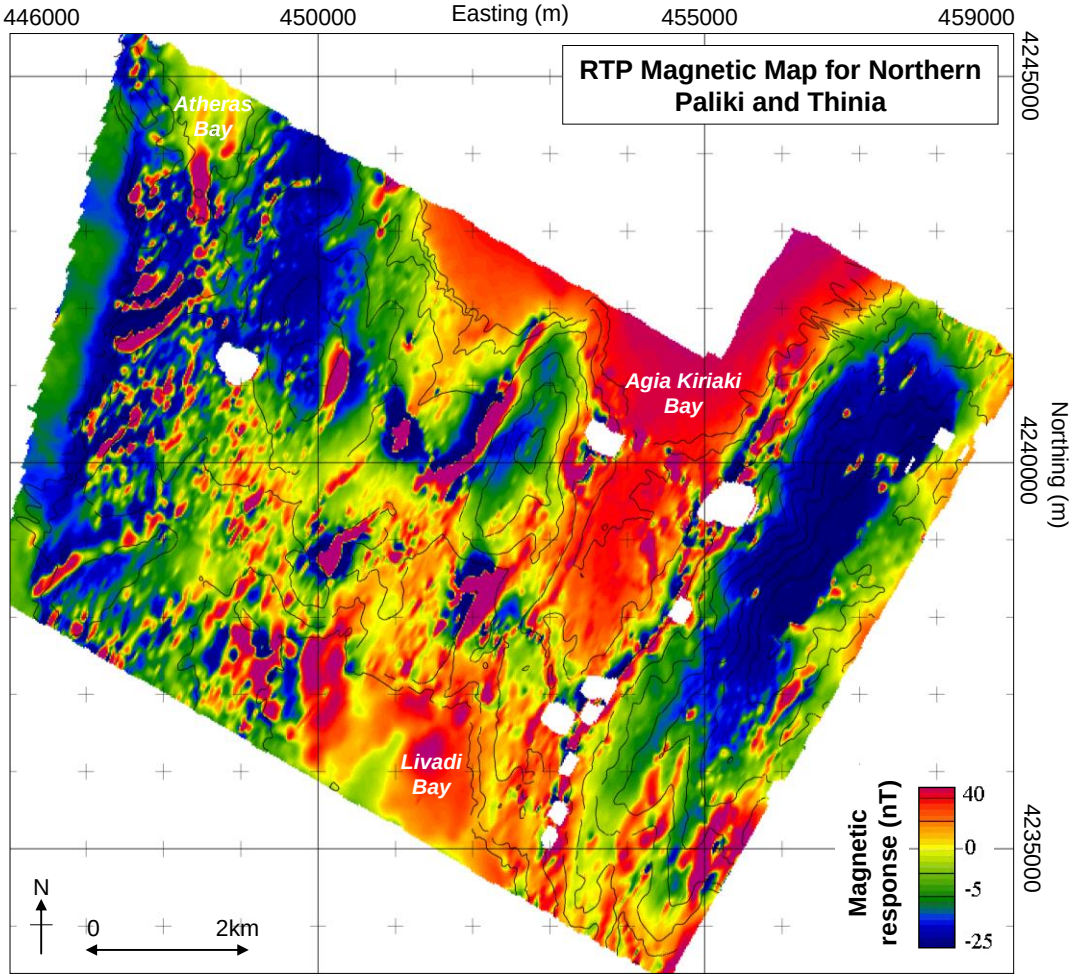

Figure 4.2 Reduced to pole (RTP) magnetic map for Northern Paliki and Thinia. The map shows a strong contrast between the strongly positive magnetised sediments of the Thinia valley "fill" and the negative response of the limestone geology of the rest of Northern Paliki. Data gaps occur over areas of habitation (white). Contours are every 100 m. Sea level (0m) is marked.

Equally strong magnetic anomalies also occurred within the low coastal areas of Atheras valley, Livadi Marsh and Agia Kiriaki Bay indicating these low-lying areas formed sediment catchment areas for alluvium washed down from the surrounding steep hills. Magnetic material could be seen extending from these areas into the

shallow water immediately offshore indicating transportation of this material out to sea. A similar affect also occurred where gullies drained directly into the sea on either side of the Thinia isthmus indicating a high terrigenous sediment input from the shore here.

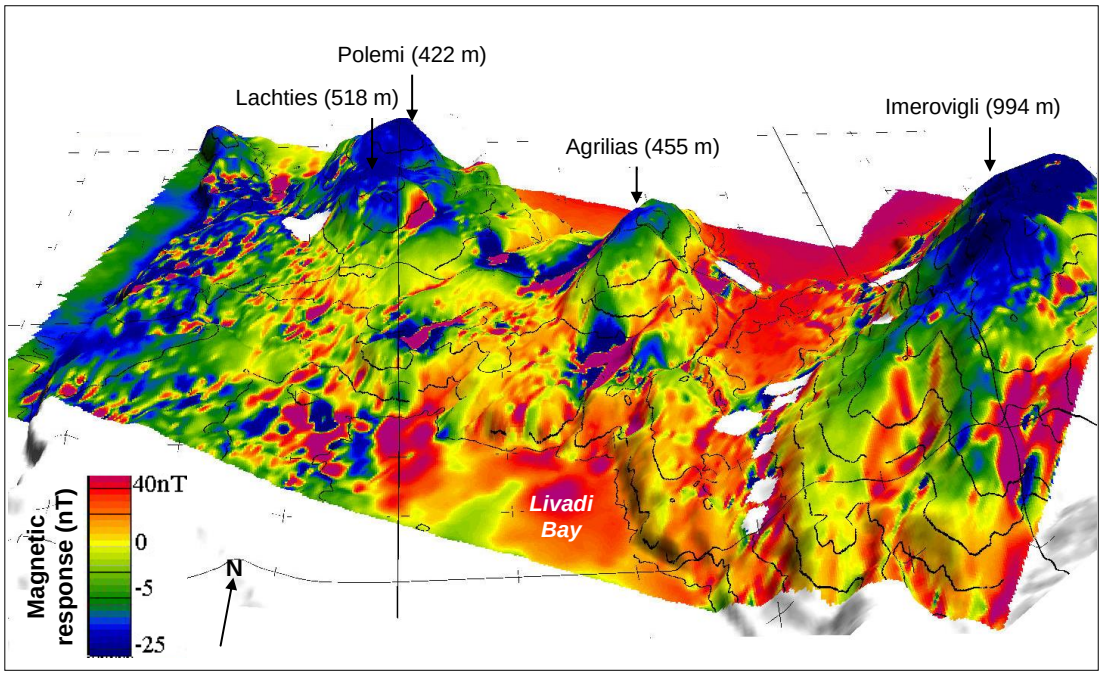

Figure 4.3 Reduced to pole (RTP) magnetic map for Northern Paliki and Thinia draped over 3D mesh. The map shows how the negative magnetic response generally correlates with the highest elevation mountains. Data gaps occur over areas of habitation (white). Contours are every 100 m. Sea level (0m) is marked. The crosses are 1 km apart.

While the magnetic response of the Atheras Thrust was very noisy and hard to define, the Ainos Thrust coincided with a strongly magnetic linear anomaly (>40 nT) running along the eastern valley side marking the contact between the magnetic valley fill and less magnetic limestone valley sides. The strength of this response was difficult to account for. This anomaly could not be attributed to roads, infrastructure or electricity pylons so was concluded to be entirely geological.

4.2.2 Apparent Resistivity Survey

In these maps “warm” colours correspond to low resistivity features while “cold” colours are associated with more resistive geology. Evident in all frequencies was the

strong contrast between the generally resistive (green to dark blue, ~1000 to 100 000 Ωm) response of Northern Paliki and Eastern Kefalonia and the conductive (orange-yellow to pale green, ~3 to 50 Ωm) valley fill of Thinia. This was most clearly shown in the shallowest frequency map (140 kHz) and indicated there was a major difference in the geology of the valley compared with the generally carbonate lithology of Northern Paliki and Eastern Kefalonia on either side of the land-bridge (Figure 4.4). As with the magnetic survey, the conductivity maps for Northern Paliki were interpreted as a reflection of the distribution of the fine-grained alluvium deposits in the area. There was also a clear correlation between resistivity and elevation with the highest resistivities correlating to the high elevation Cretaceous limestone-topped mountains and the lowest resistivities generally occurring within the low-lying, sediment-filled valley (Thinia, Atheras) and coastal areas (e.g. Livadi Marsh) (Figure 4.5).

The NE-SW orientated normal faults detected by the magnetic survey appeared as conductive (pale green to yellow, ~10 to 50 Ωm) linear anomalies overprinted on top of the overall high resistivity carbonate bedrock. The resistivity contrast of these features was not as striking as the magnetic response. Small, localised conductive anomalies corresponded to topographically flat pockets of *terra rossa* which occurred within closed-contour hollows in the limestone e.g. suspected dry lake beds, dolines etc. These features were still partially visible by the 8200 Hz map (Figure 4.6) indicating they were at least 20 to 40 m deep. This map clearly showed that the type of limestone has some effect on the resistive response with Paleogene limestone as well as the highest elevation limestone appearing more resistive (10 kΩm to 100 kΩm) than the Cretaceous (~1 kΩm) at a similar elevation.

By 400 Hz (Figure 4.7), only the contrast between resistive limestone and conductive marl could be seen. The position of the Atheras and Ainos Thrust could be identified in the 140 kHz map as the boundary between strongly the resistive (blue) limestone of the thrust hangingwalls and less resistive (green to yellow) sediment of the footwalls. The Atheras Thrust appears as a north-south orientated line separating the resistive (blue, 1 kΩm to 100 kΩm), high elevation limestone mountains of the thrust hangingwall to the west from the conductive (10 to 100 Ωm) fine-grained sediments

of the narrow Atheras valley. The Ainos Thrust was defined as the eastern limit of the conductive valley sediments.

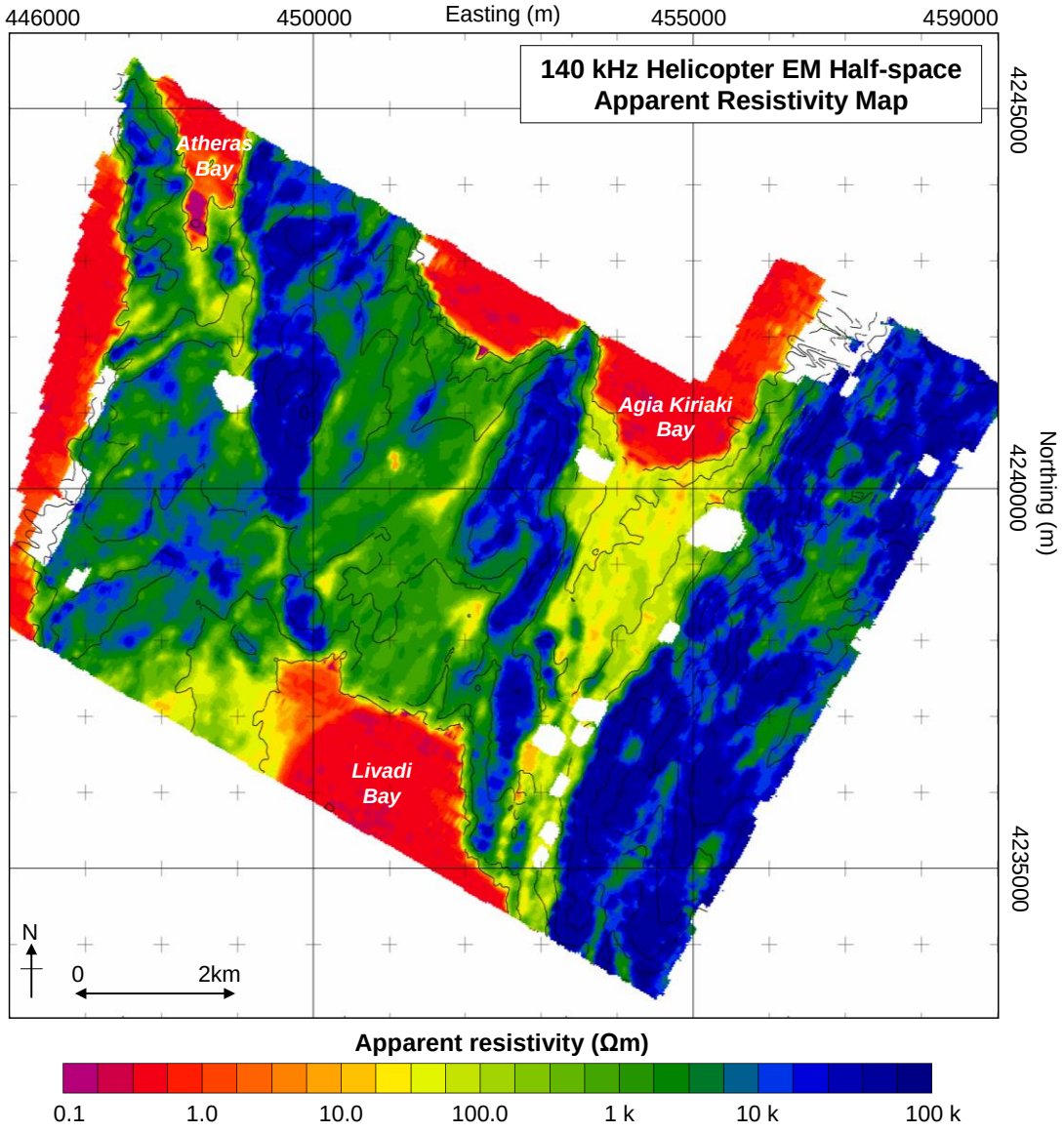

Figure 4.4 140 kHz helicopter EM half-space apparent resistivity map for Northern Paliki. "Warm" colours are low resistivity (conductive) and "cold" colours are high resistivity (less conductive). Resistivity scale is logarithmic. Contours are every 100 m. This map shows the contrast between the resistive limestone geology of Northern Paliki and the conductive valley "fill" sediments of Thinia indicating a major change in geology along the land-bridge compared with the rest of Northern Paliki and Eastern Kefalonia.

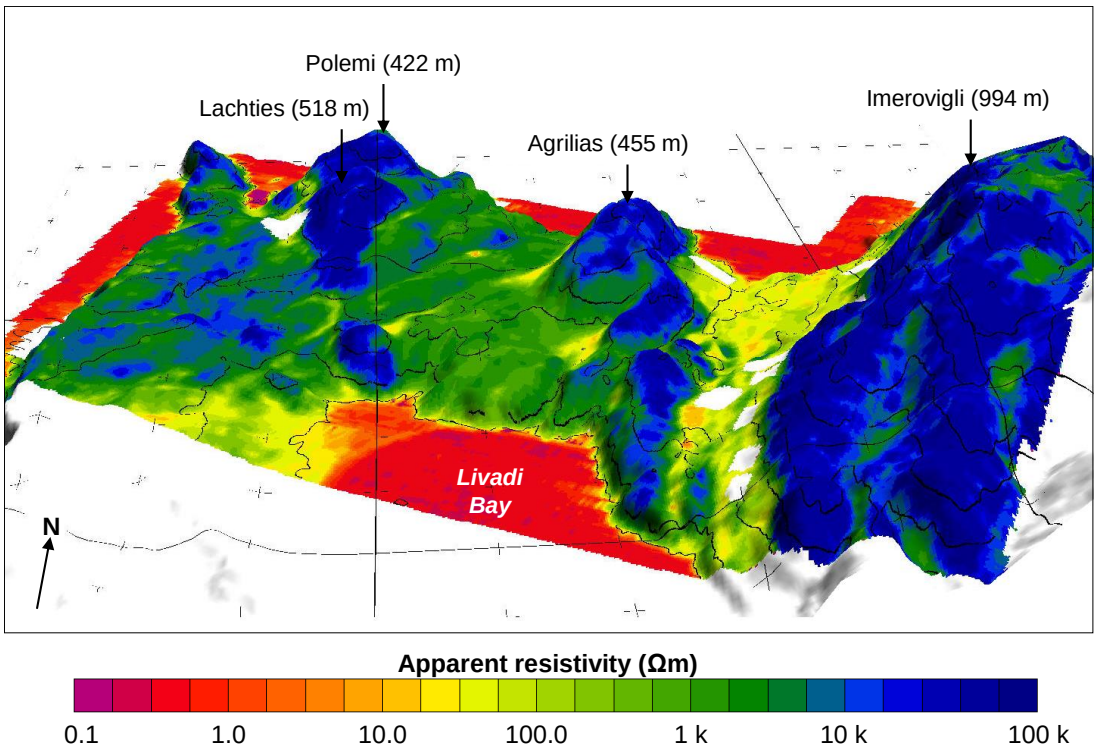

Figure 4.5 140 kHz helicopter EM half-space apparent resistivity map for Northern Paliki draped over a 3D mesh. "Warm" colours are low resistivity (conductive) and "cold" colours are high resistivity (less conductive). Contours are every 100 m. This map shows. The map shows a correlation between resistivity and elevation with the most resistive (blue) sediments occurring at the highest elevations and the Cretaceous limestone and the lowest resistivities equating to the low sediment-filled valleys. The crosses are 1 km apart.

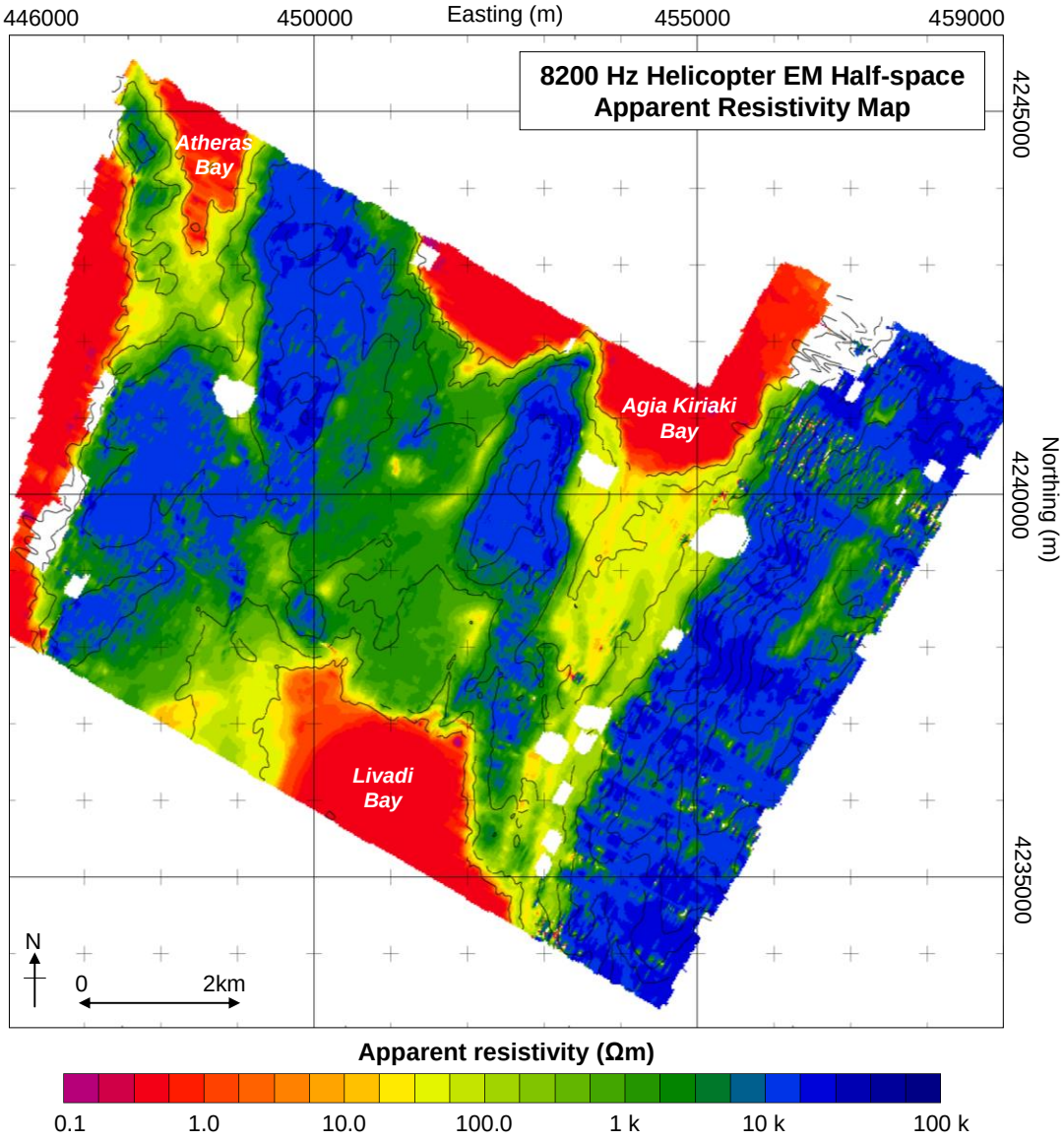

Figure 4.6 8200 Hz helicopter EM half-space apparent resistivity map for Northern Paliki. "Warm" colours are low resistivity (conductive) and "cold" colours are high resistivity (less conductive). Contours are every 100 m. With increasing depth, the contrast between lithologies becomes less pronounced however the contrast between Northern Paliki and Thinia is still striking.

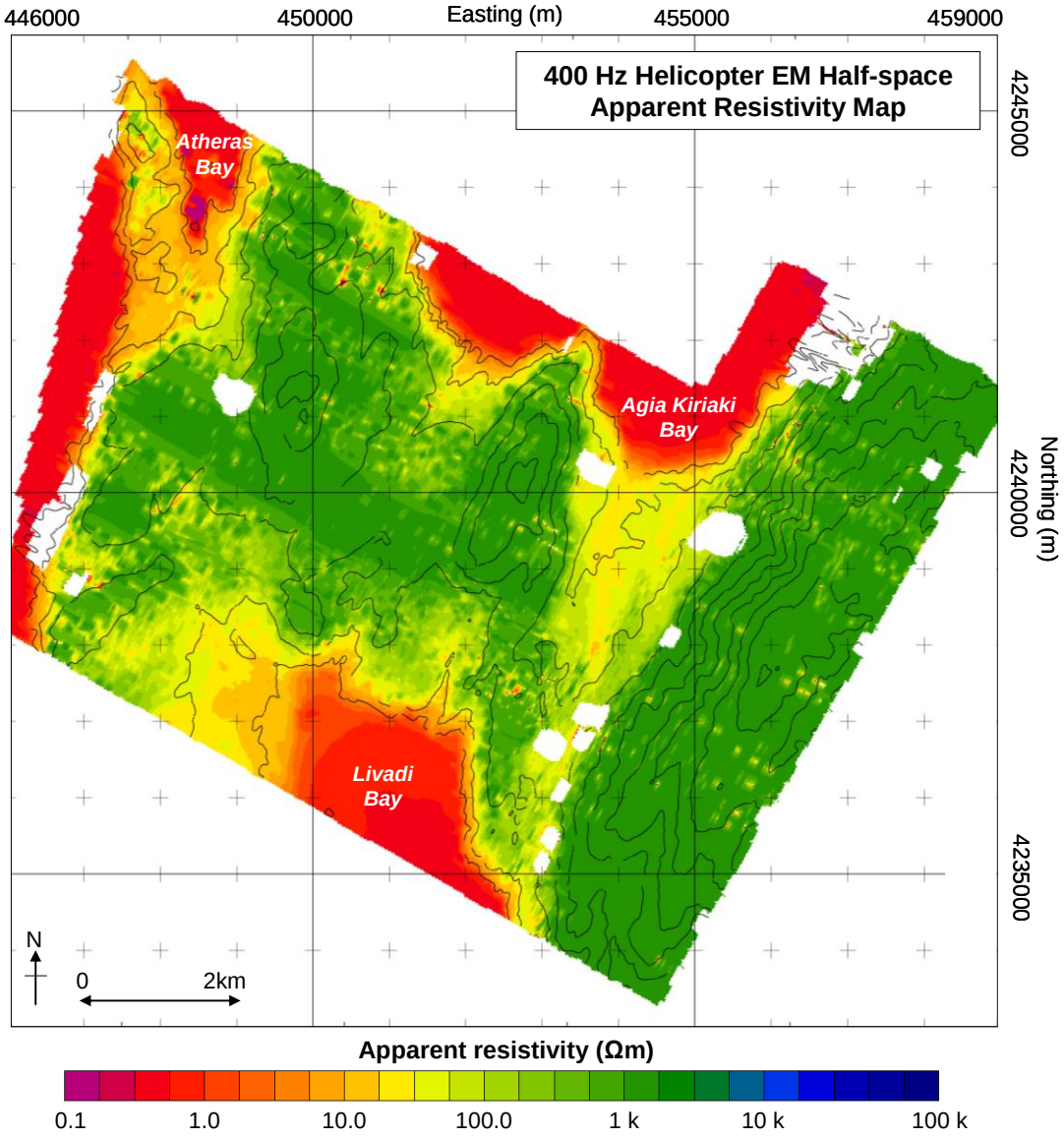

Figure 4.7 400 Hz helicopter EM half-space apparent resistivity map for Northern Paliki. "Warm" colours are low resistivity (conductive) and "cold" colours are high resistivity (less conductive). Contours are every 100 m. At the lowest frequency, the only resistivity contrast remaining is that of the limestone (green) of Northern Paliki and Eastern Kefalonia and the "yellow" values of the conductive valley fill of Thinia indicating this fill is at least 80 to 100 m deep.

4.3 Atheras Valley

4.3.1 Airborne Overview

The narrowness of this valley meant it was poorly resolved by the airborne surveys. Atheras valley appeared as a narrow north-south orientated zone of conductive (~10 to 50 Ωm) sediments at least 20 m thick with a predominately low magnetic response (blue, -25 nT) which was cross-cut by several NE-SW orientated strongly magnetic anomalies (Figure 4.8). The valley's conductive response appeared to be offset by these anomalies in a north-easterly direction. These NE-SW anomalies were attributed to the numerous normal faults of the same orientation which clearly continue below the valley sediment according to the airborne survey.

The mouth of the valley contained very strongly magnetic sediments indicating the presence of a thick accumulation of iron-rich *terra rossa* sediments and demonstrating that the valley acted as a catchment for sediment runoff from the steep surrounding limestone hills like in Livadi Marsh. This magnetic signature extended offshore indicating this material was being transported from the valley into the bay. Some evidence of bathymetry could be seen from the pattern this magnetic material formed. The small reef island visible within the bay formed part of a submarine ridge of low magnetic (green, ~0 to -5 nT) response which connected with a ridge of limestone onshore.

4.3.2 Resistivity

The E-W orientated Atheras valley profiles were composed of predominately low resistivity sediment (~1 to 12 Ωm) which onlapped resistive (~300 to 5000 Ωm) limestone surfaces which dipped into the basin reflecting the response of the HEM survey (Figure 4.9 to Figure 4.13, top). This very low resistivity signal suggested the sediments composing the valley were fine-grained and deep (at least 35 m thick) and water-saturated, possibly fed by springs emanating along the limestone-alluvial

contact defining the edges of the valley. ABL1 (Figure 4.9) to ABL4 (Figure 4.12) showed resistive surface material (~100 to 2000 Ωm) increasing from south to north. This might represent gravel deposits associated with relict beaches (they diminish southwards away from the current shoreline) created as sea levels dropped from this very low elevation, near-shore area in the last few thousand years. This may also represent colluvial debris derived from higher up the steep eastern slope. There was a clear thickening of more resistive surface material southwards in ABL5 (Figure 4.13). There was no sign of the subsurface continuation of the limestone on the eastern side of the valley. The 140 kHz apparent resistivity map had shown this limestone was completely enclosed with conductive material. The ground-based resistivity survey now demonstrated that this ridge might represent another easterly-dipping thrust fault lying to the west of the Atheras Thrust.

4.3.3 Seismic Refraction

The Atheras valley seismic refraction shot traces were of reasonable quality and while some lines were increasingly noisy with distance from the source, the first breaks could with picked with confidence. Lines ABL2 (Figure 4.10) and ABL3 (Figure 4.11) were problematic as the first break was very weak and difficult to distinguish from later strong reflections particularly at distance from the source. The RMSE for the tomographically-inverted profiles was reasonably low (between 2 and 3 msec) except for ABL3 where it was 5.64 msec. This large error was due to difficulty in picking the first breaks. The average RMSE for the time-term inversion was the largest of the five seismic refraction surveys (4.28 msec). The resulting tomographically-inverted profiles are presented in Figures 4.9 to Figure 4.13.

The E-W orientated profiles ABL2, ABL3 and ABL4 were composed of a low velocity zone (on average 1.23 km/s) contained within a higher velocity (2.50 km/s) basin. The long N-S line ABL5 showed a “stepped” structure at depth with a higher velocity than the surrounding sediment which aligned with one of the NE-SW trending northwest-dipping normal faults which cross-cut Atheras Bay.

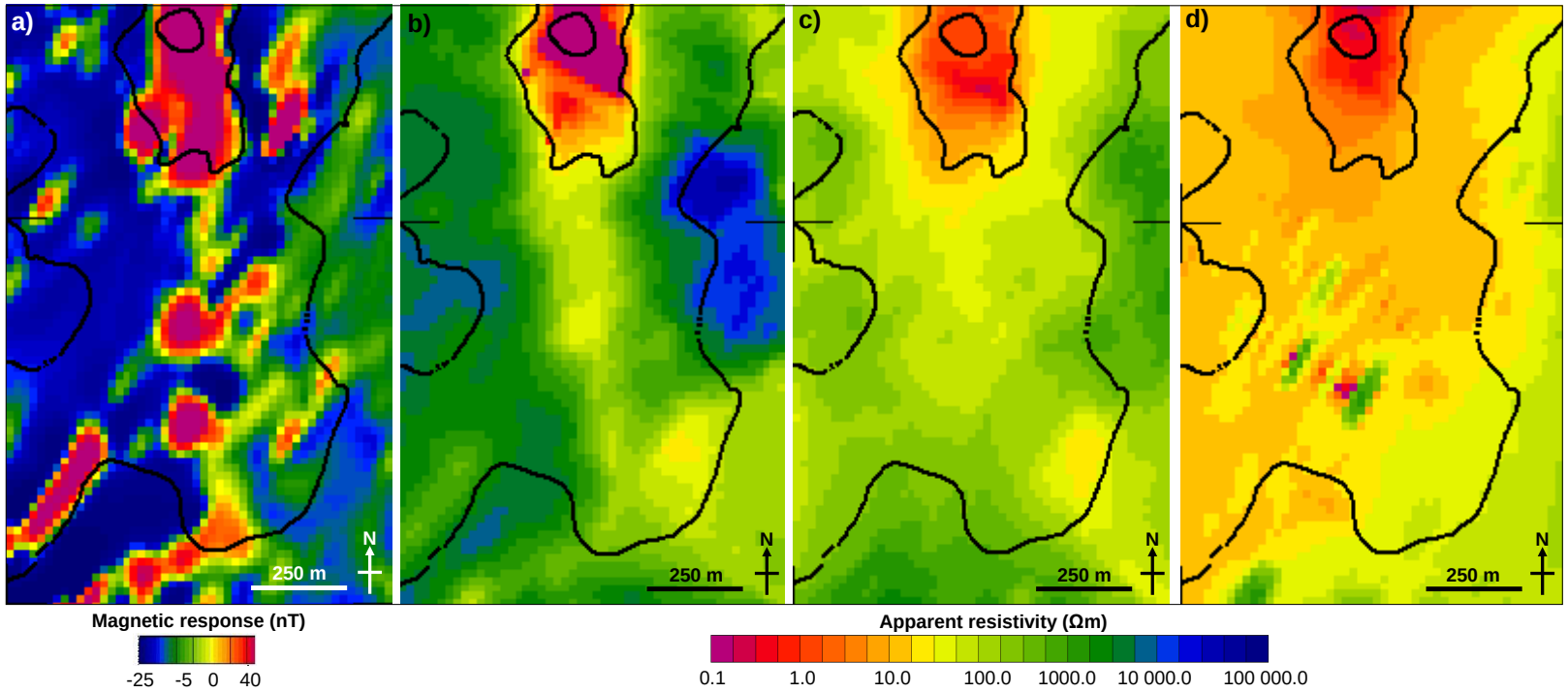

Figure 4.8 Results of the helicopter-mounted electromagnetic (HEM) survey for Atheras valley: a) Magnetic results; Apparent resistivity maps for 140 kHz (b), 8200 Hz (c) and 400 Hz (d). Contours at 100 m intervals.

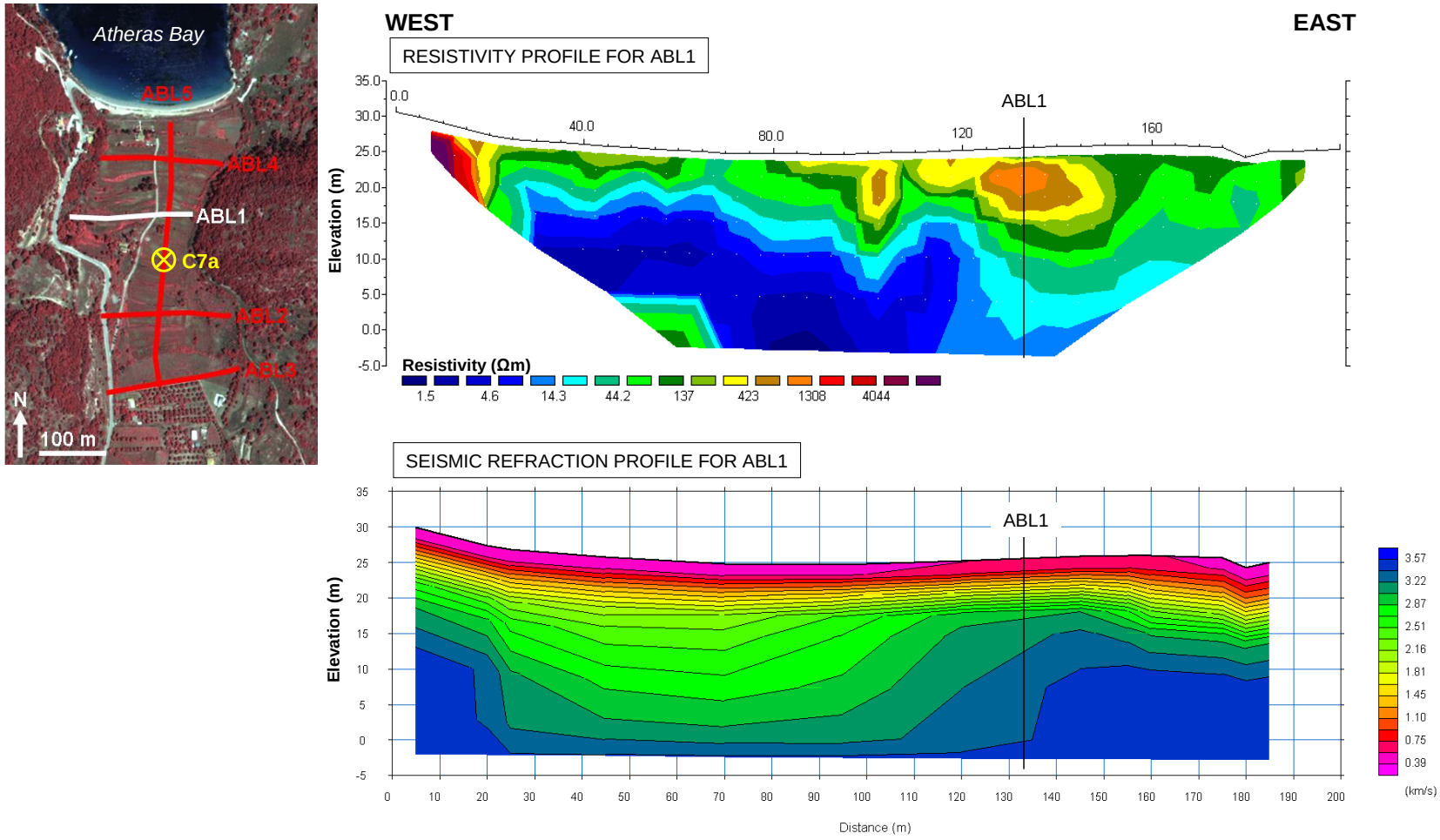

Figure 4.9 2D resistivity profile (top) and corresponding seismic refraction profile (bottom) for Atheras Bay profile, ABL1. Elevation/depth is in terms of elevation above mean sea level (where mean sea level is +22 m above present sea level). The location of this survey line is indicated in the map inset. Vertical exaggeration is V/H = 1.5. Vertical black lines indicate where the profile crosses another profile or borehole.

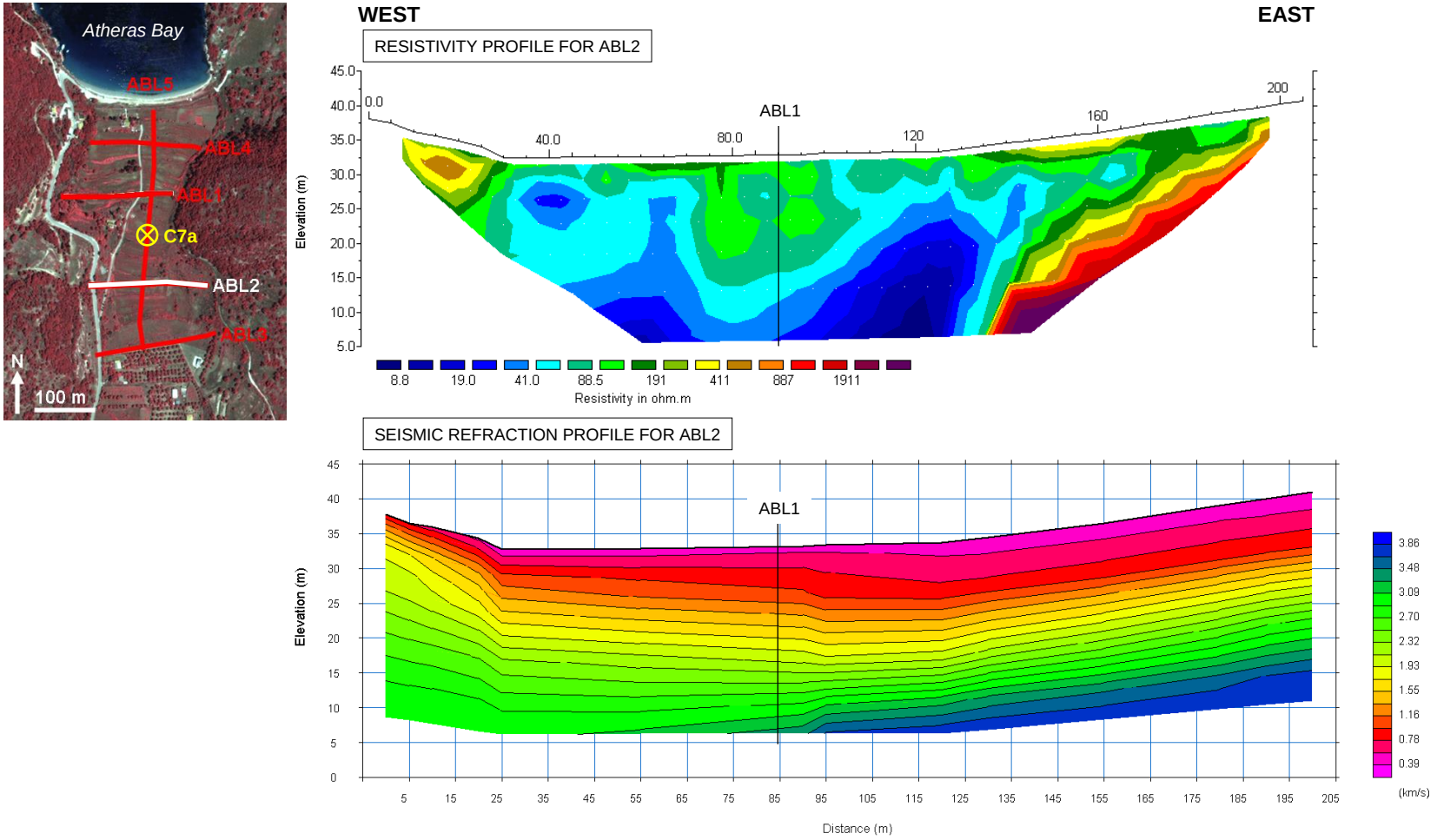

Figure 4.10 2D resistivity profile (top) and corresponding seismic refraction profile (bottom) for Atheras Bay profile, ABL2. Elevation/depth is in terms of elevation above mean sea level (where mean sea level is +22 m above present sea level). The location of this survey line is indicated in the map inset. Vertical exaggeration is V/H = 1.5. Vertical black lines indicate where the profile crosses another profile or borehole.

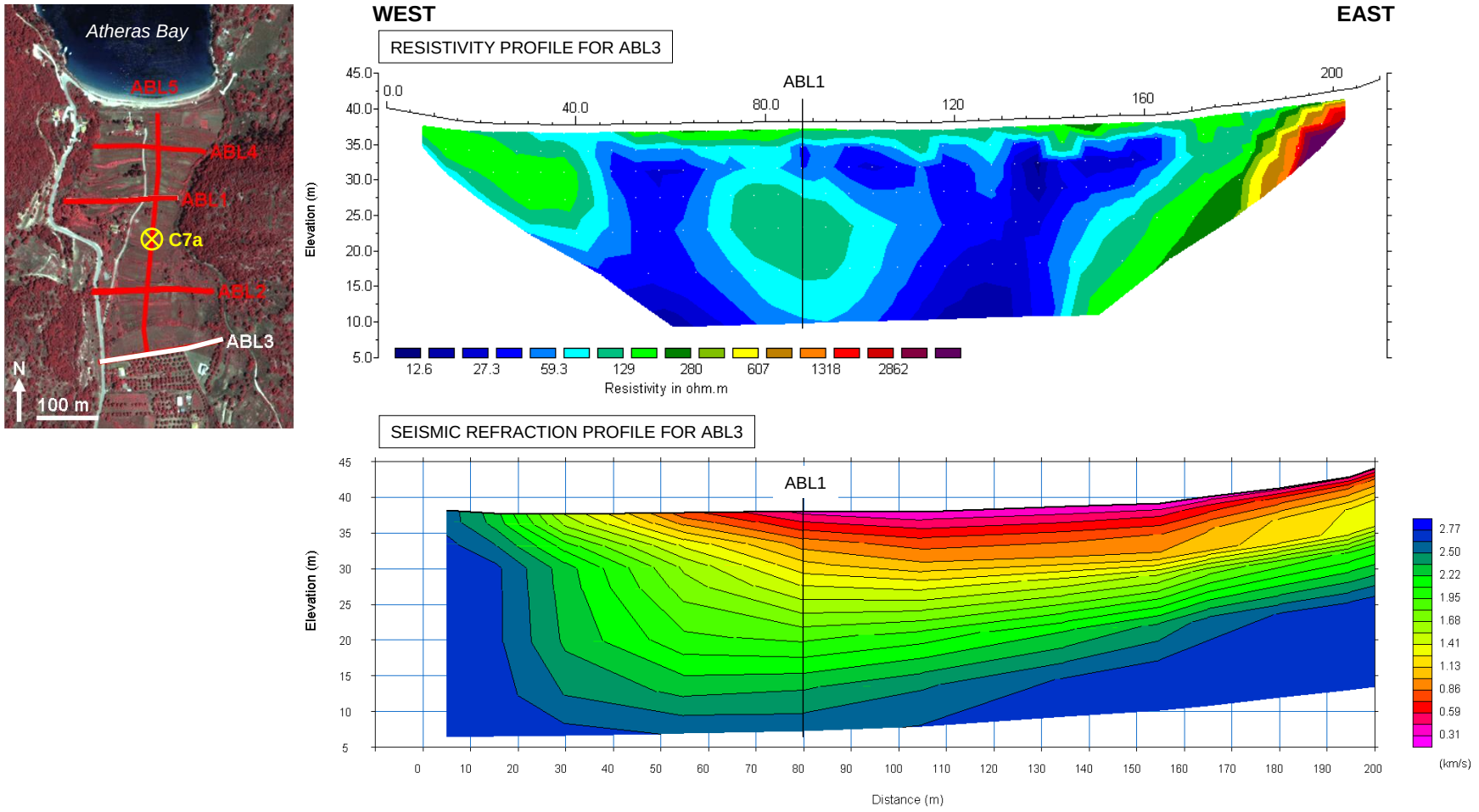

Figure 4.11 2D resistivity profile (top) and corresponding seismic refraction profile (bottom) for Atheras Bay profile, ABL3. Elevation/depth is in terms of elevation above mean sea level (where mean sea level is +22 m above present sea level). The location of this survey line is indicated in the map inset. Vertical exaggeration is V/H = 1.5. Vertical black lines indicate where the profile crosses another profile or borehole.

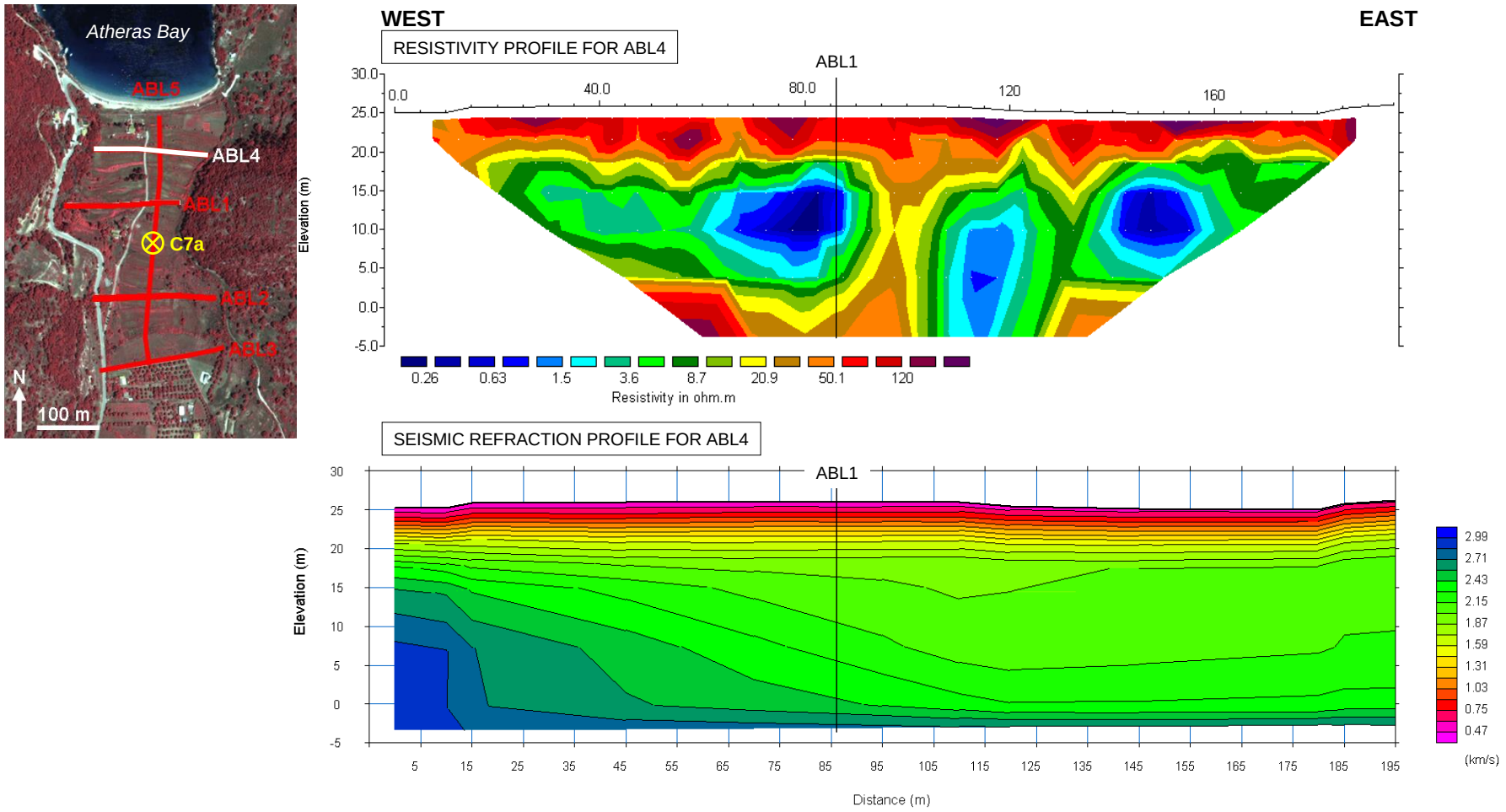

Figure 4.12 2D resistivity profile (top) and corresponding seismic refraction profile (bottom) for Atheras Bay profile, ABL4. Elevation/depth is in terms of elevation above mean sea level (where mean sea level is +22 m above present sea level). The location of this survey line is indicated in the map inset. Vertical exaggeration is V/H = 1.5. Vertical black lines indicate where the profile crosses another profile or borehole.

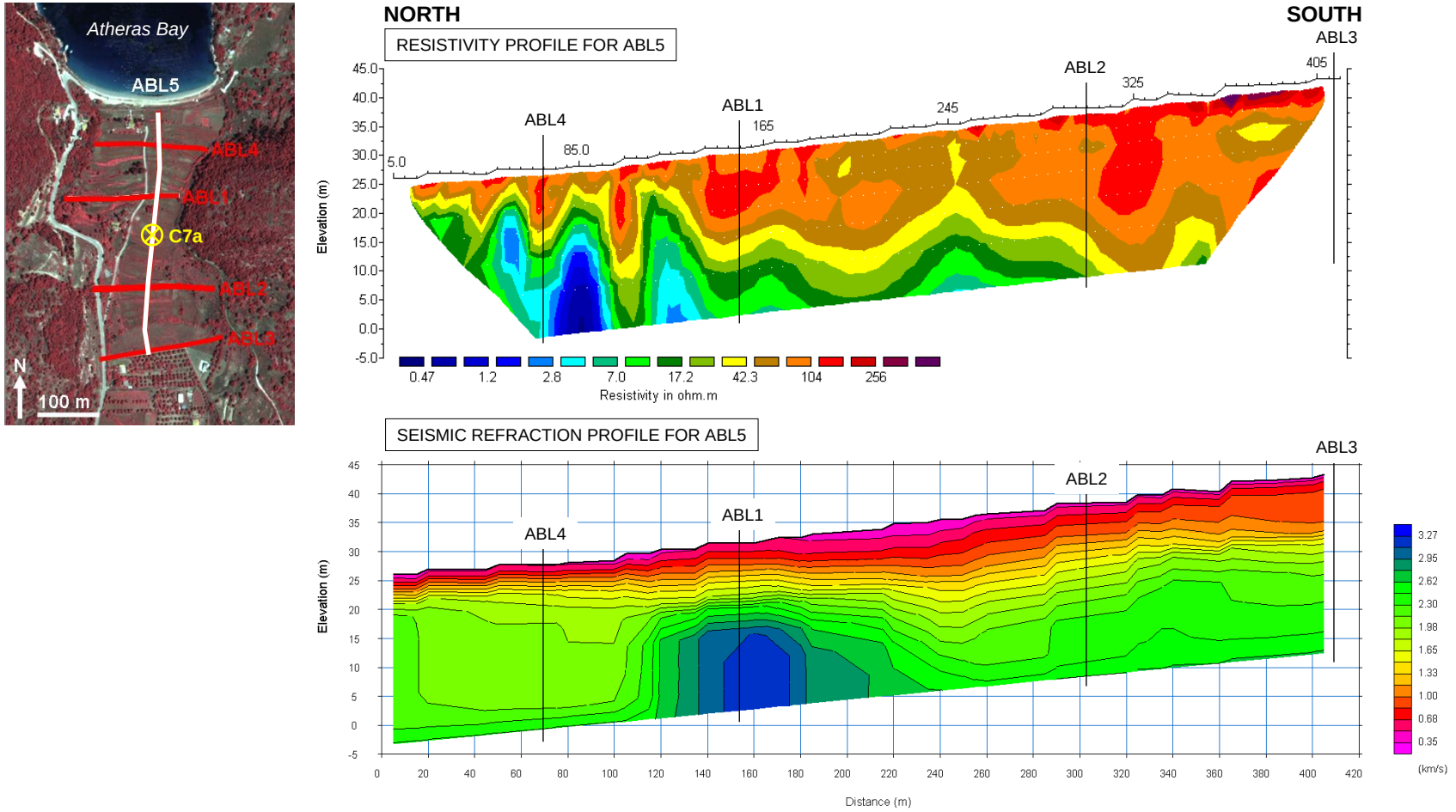

Figure 4.13 2D resistivity profile (top) and corresponding seismic refraction profile (bottom) for Atheras Bay profile, ABL5. Elevation/depth is in terms of elevation above mean sea level (where mean sea level is +22 m above present sea level). The location of this survey line is indicated in the map inset. Vertical exaggeration is V/H = 1.5. Vertical black lines indicate where the profile crosses another profile or borehole.

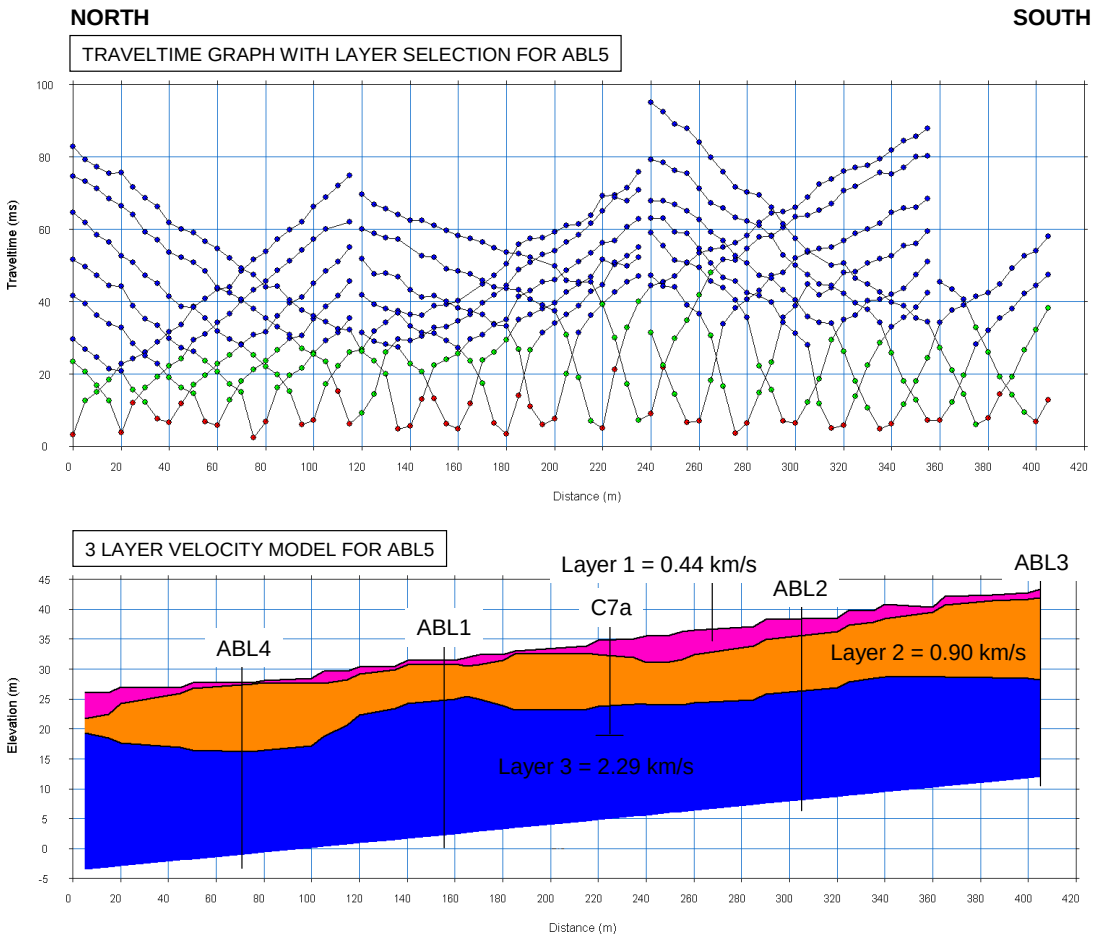

Layer assignment:

Layer 1 = Clay and gravel, recent soils.

Layer 2 = Unconsolidated clastic material, alluvium.

Layer 3 = Limestone or hard marls.

Figure 4.14 Time-term inverted profile for ABL5 (coloured section) with corresponding traveltime graphs (top) showing layer selection where red = layer 1, green = layer 2 and blue = layer 3. Layers are assigned possible lithologies based on P-wave velocities. The location of this line is given in Figure 4.13. Vertical exaggerated for the traveltime graphs is V/H = 1.5 and for the layered section is 2.5. Vertical black lines indicate where the profile crosses another profile or borehole.

The presence of a clear two-layer structure meant it was worth inverting these lines using the time-term inversion method as well as the tomographic method. The three-layered models produced contained, on average, the following layer assignment: Layer 1 = 0.43 km/s, Layer = 1.40 km/s and Layer 3 = 2.49 km/s. Time-term inversions for ABL5 (Figure 4.14) and ABL2 (Figure 4.15) are presented as because the traveltime graphs for these lines gave the clearest indication of a layered subsurface. Layer 2 was interpreted as representing the valley fill which had a very

low P-wave velocity suggesting the fill contained a large volume of clastic material. This layer sat on top of a high velocity layer suggesting this clastic material sat on top of denser bedrock such as limestone. The results indicated that the valley fill was on average c.13 m in thickness.

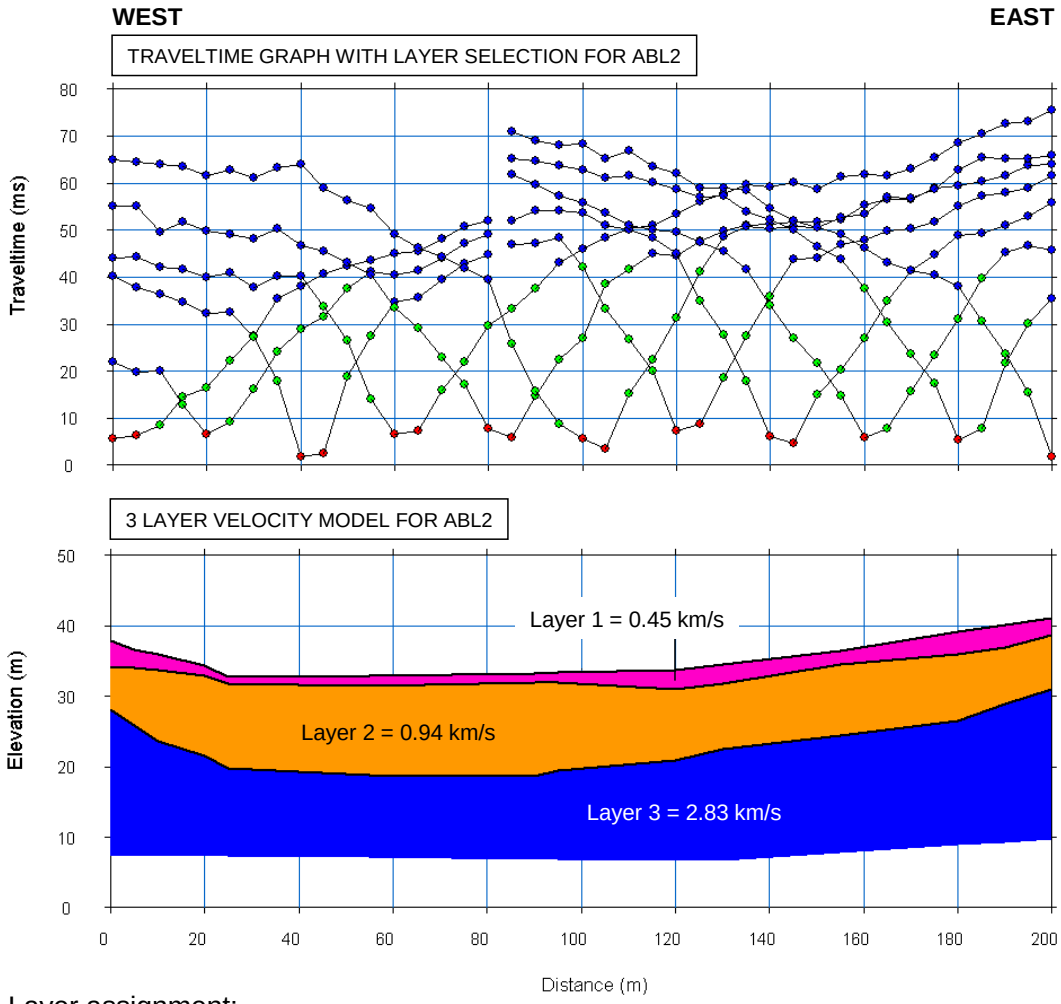

Layer assignment:

Layer 1 = Clay and gravel, recent soil.

Layer 2 = Unconsolidated clastic material, alluvium.

Layer 3 = Limestone or hard marls.

Figure 4.15 Time-term inverted profile for ABL2 (coloured section) with corresponding traveltime graphs (top) showing layer selection where red = layer 1, green = layer 2 and blue = layer 3. Layers are assigned possible lithologies based P-wave velocities. The location of this line is given in Figure 4.10. Vertical exaggerated for the traveltime graphs is V/H = 1 and for the layered section is 1.5. Vertical black lines indicate where the profile crosses another profile or borehole.

4.4 Livadi Marsh

4.4.1 Airborne Overview

Livadi Marsh appeared as a zone of strongly magnetised (≤40 nT), very conductive (red, 1.0 to 10 Ωm) sediments which form a striking contrast with the moderate to highly resistive (green to blue, 100 to 10 000 Ωm) high elevation limestone hills to the east of the marsh (Figure 4.16). These conductive sediments were at least 20 to 80 m in thickness and the thickest deposits were concentrated on the eastern side of the marsh immediately adjacent to the Atheras Thrust hangingwall. The western side of the marsh was shallower and dipped eastwards where the marsh fill onlapped the slightly more resistive (yellow), less magnetised (blue) buried part if the Livadi Quarry hill. The strong magnetic signature of these sediments suggested they iron oxide rich *terra rossa* alluvium. The source of this alluvium would be the steep limestone hills surrounding the marsh, particularly the deeply-incised gullies to the north-east of the marsh showing that this low elevation area formed a catchment for sediments transported through surface run-off. The magnetic map showed that this material extended offshore into Livadi Bay. The excessively low resistivity values were the lowest in the Northern Paliki survey and were due to the fine-grained nature of the "marsh fill" and the infiltration of saltwater into the sediment pores. Typical resistivity values for fresh, brackish and saline water are 40, 12 and 3 Ωm respectively (Van Dam and Meulenkamp, 1967).

The shoreline of the marsh formed a clear boundary between the marsh fill and the consistently very low resistivity (0.18 to 0.1 Ωm) seawater. The 140 kHz map showed that this shoreline was defined by a thin rim which had a slightly higher resistivity than the marsh fill (~3 Ωm) coincident with the path of the modern main road. This was probably a natural spit or baymouth bar used by the modern road protecting the marsh from further marine inundation. Determining the age of formation of the spit was therefore important in understanding the flooding history of the marsh.

4.4.2 Resistivity

Inversion of the survey data using RES2DINV produced 2D inverse resistivity profiles for LML2a, LML2b and LML3 to LML5 (Figure 4.18 to Figure 4.22, top). Due to data errors only part of LML1 was inverted producing a profile for the central part of the survey line (Figure 4.17, top). The four lines placed across the main part of the marsh (LML1, LML2a, LML2b and LML3) generally showed a low resistivity response (below 500 Ωm) which extended beyond the maximum imaging depth of the survey (at least 30 m in thickness), a response which agreed with the HEM survey. LML1 detected very low resistivity (less than 100 Ωm) along this line which reflects the saline infiltration of the sediments at this near-shore location.

LML2a, LML2b and LML3 showed a similar configuration to one another. Below a thin (2 to 6 m) resistive (~35 to 350 Ωm) surface layer these profiles were composed of a roughly 10 to 15 m thick low resistivity (0.13 to 20 Ωm) layer overlying a slightly more resistive (~35 to 200 Ωm) layer within an uneven surface which shallows northwards.

This resistive layer may represent a buried erosional surface created when sea levels were lower. The conductive material deposited on top represented an influx of fine-grained sediment which might have represented deposition of marine sediments and therefore a flooding event or increased deposition of sediment.

In terms of the narrow inlets at the edge of the marsh, LML4 imaged low resistivity sediment sitting between dipping resistive anomalies interpreted as a basin-like structure of limestone infilled with low resistivity fine-grained “marsh fill” to at least 30 m. This configuration is favourable for a sediment-filled inlet. LML5 on the other hand detected wedges of resistive material sitting at the surface above low resistivity material which tapered towards the centre of the profile and may represent influxes of the magnetic, conductive sediment washed in from the deeply-incised gullies in the slope above. There was no indication of underlying resistive limestone indicating the sediment fill across the mouth of this inlet was at least 30 m in thickness.

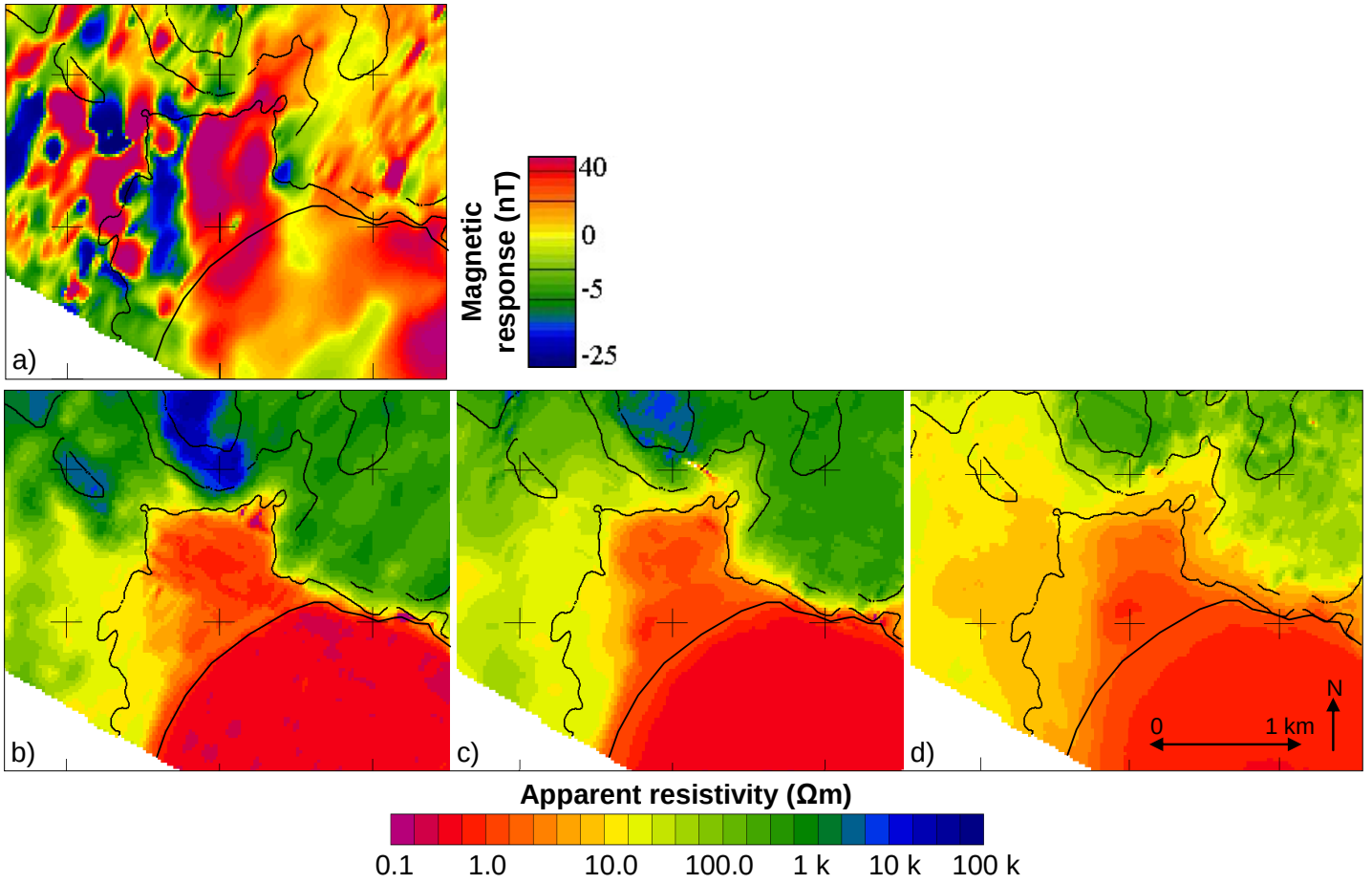

Figure 4.16 Results of the helicopter-mounted electromagnetic (HEM) survey for Livadi Marsh: Magnetic map (a); Apparent resistivity maps for 140 kHz (b), 8200 Hz (c) and 400 Hz (d). Shore line of Livadi Bay is indicated by a solid black line and contours are at 100 m intervals. The map indicates the thickest zone of magnetic, conductive marsh "fill" occurs adjacent to the Atheras Thrust hangingwall and is at least 20 to 80 m thick opening up the possibility this area was once a deep marine inlet. Kastelli Hill is the resistive (blue) hill at the top of the HEM figures.

4.4.3 Seismic Refraction

The seismic refraction data was of high quality and picking of the first breaks relatively easy as the data was fairly noise-free. The inconsistency from one shot record to the next suggested the noise was due to traffic passing along the main road or activity from the nearby quarry. In these cases the traces most badly affected were removed. LML2b could not be inverted as the data was very noisy and very few first breaks could be picked with confidence. The results are listed from Figure 4.18 to Figure 4.22 (bottom).

The RMSE of the tomographically-inverted profiles was consistently low (on average 1.59 msec) and the RMSE for the time-term inversion of these profiles was on average the lowest of the five surveys (2.78 msec). The tomographic profiles for LML1, LML2a and LML3 had a consistently low P-wave velocity (between 0.45 and 2.50 km/s) with little structure suggesting there was little variation in the sediment type with depth. There was no indication of the high velocity signature expected from an underlying limestone ridge associated with the Atheras Thrust hangingwall passing below the marsh or limestone rubble from a collapsed hangingwall suggesting the thrust skirted the eastern edge of the marsh.

The traveltime curves for LML4 and LML5 however showed that at least two reasonably-defined layers were present. LML4 showed a very clear multi-layered structure so this line was also inverted using the time-term inversion method which resolved this into a three-layered model with the following layer assignment: Layer 1 = 0.39 km/s, Layer 2 = 1.32 km/s and Layer 3= 2.87 km/s (Figure 4.23). The interface between Layers 2 and 3 showed a basin-like feature suggesting Layer 2 represented marsh fill sitting within a limestone basin. The traveltime curves for LML5 were less easy to interpret but could still be resolved into a 3-layered model: Layer 1 = 0.48 km/s, Layer 2 = 2.17 km/s and Layer 3 = 2.74 km/s (Figure 4.24). This line was positioned close to the Atheras Thrust and appeared to show the lower velocity marsh fill sediments onlapping the limestone hangingwall of the thrust.

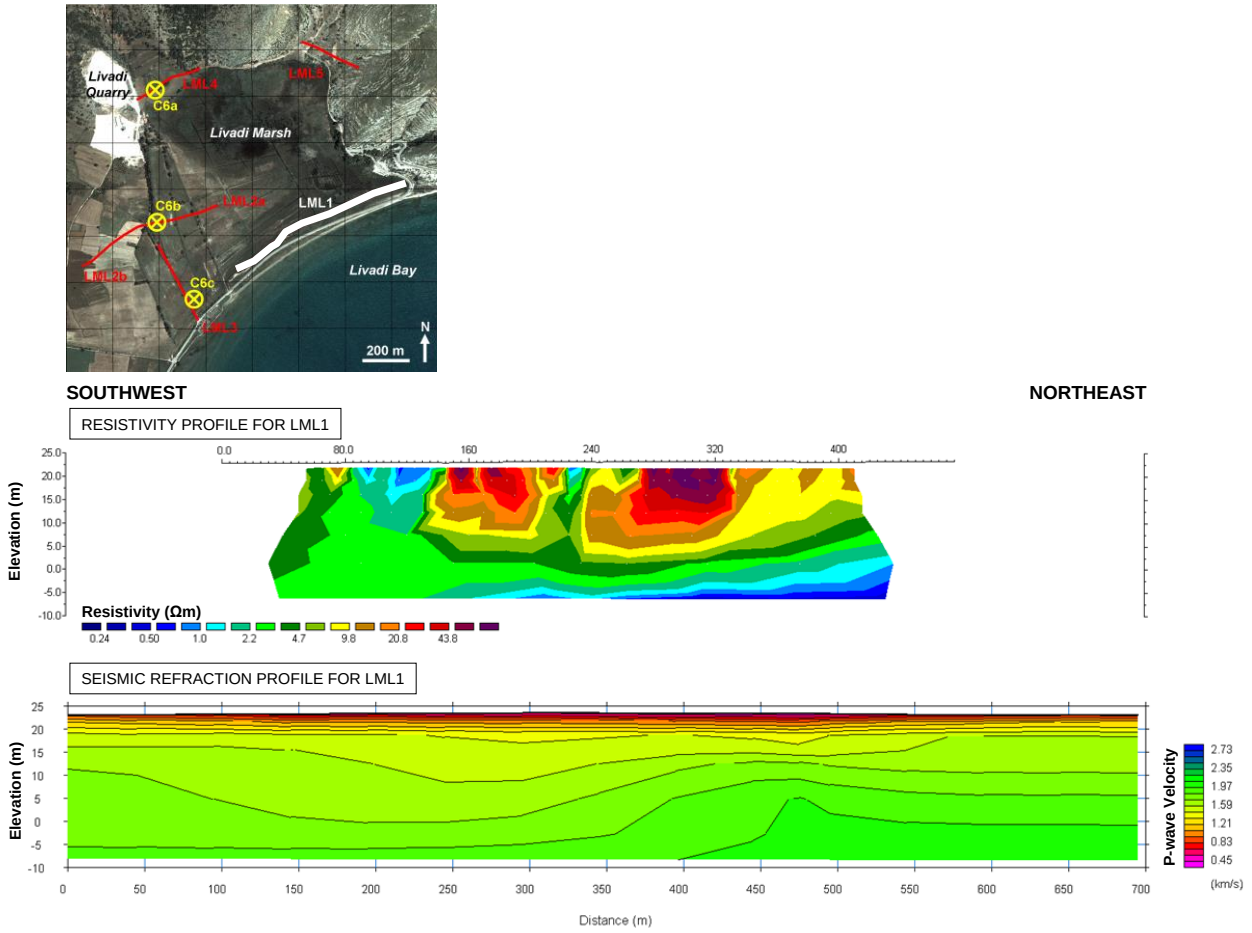

Figure 4.17 2D resistivity profile (top) and corresponding seismic refraction profile (bottom) for Livadi Marsh profile, LML1. Elevation/depth is in terms of elevation above mean sea level (where mean sea level is +22 m above present sea level). The location of this survey line is indicated in the map inset. Vertical exaggeration is V/H = 3.

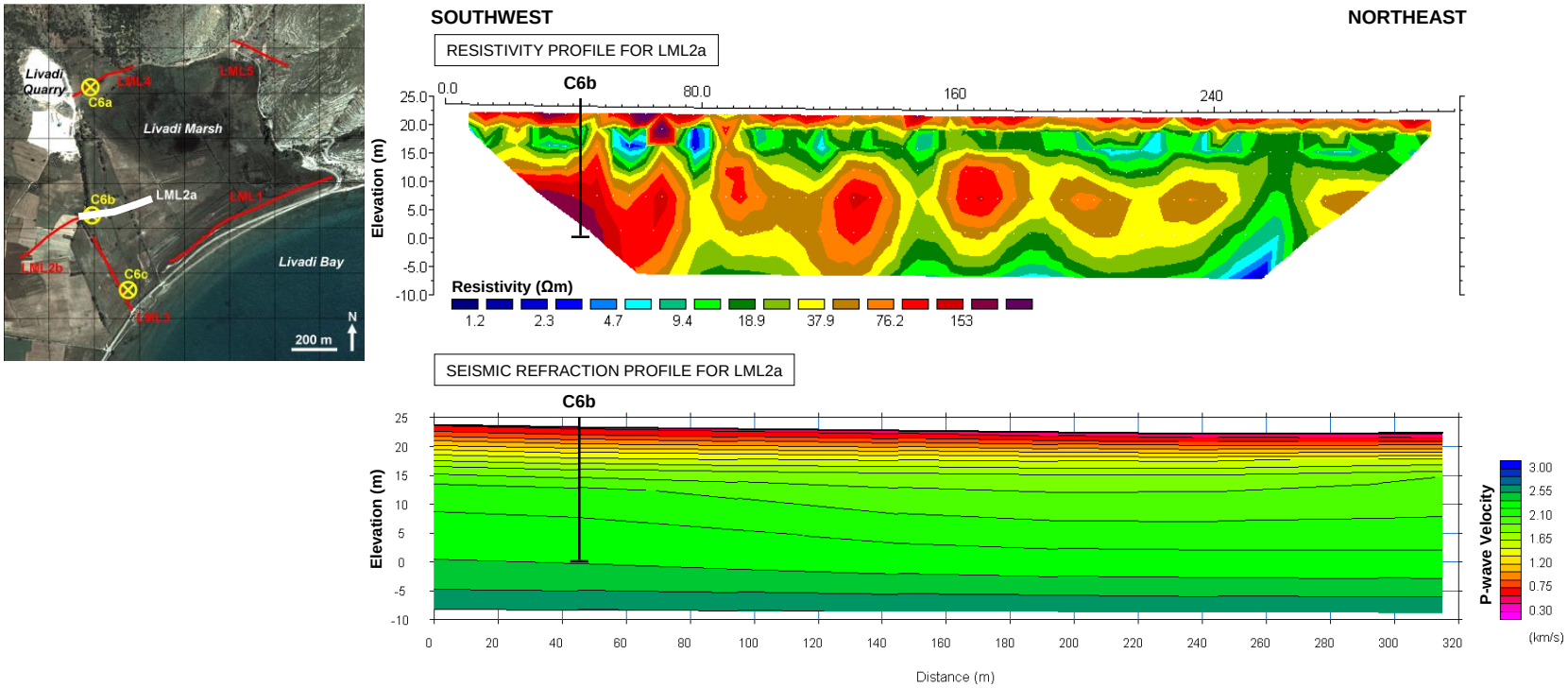

Figure 4.18 2D resistivity profile (top) and corresponding seismic refraction profile (bottom) for Livadi Marsh profile, LML2a. Elevation/depth is in terms of elevation above mean sea level (where mean sea level is +22 m above present sea level). The location of this survey line is indicated in the map inset. Vertical exaggeration is V/H = 1.80. Vertical black lines indicate where the profile crosses a borehole.

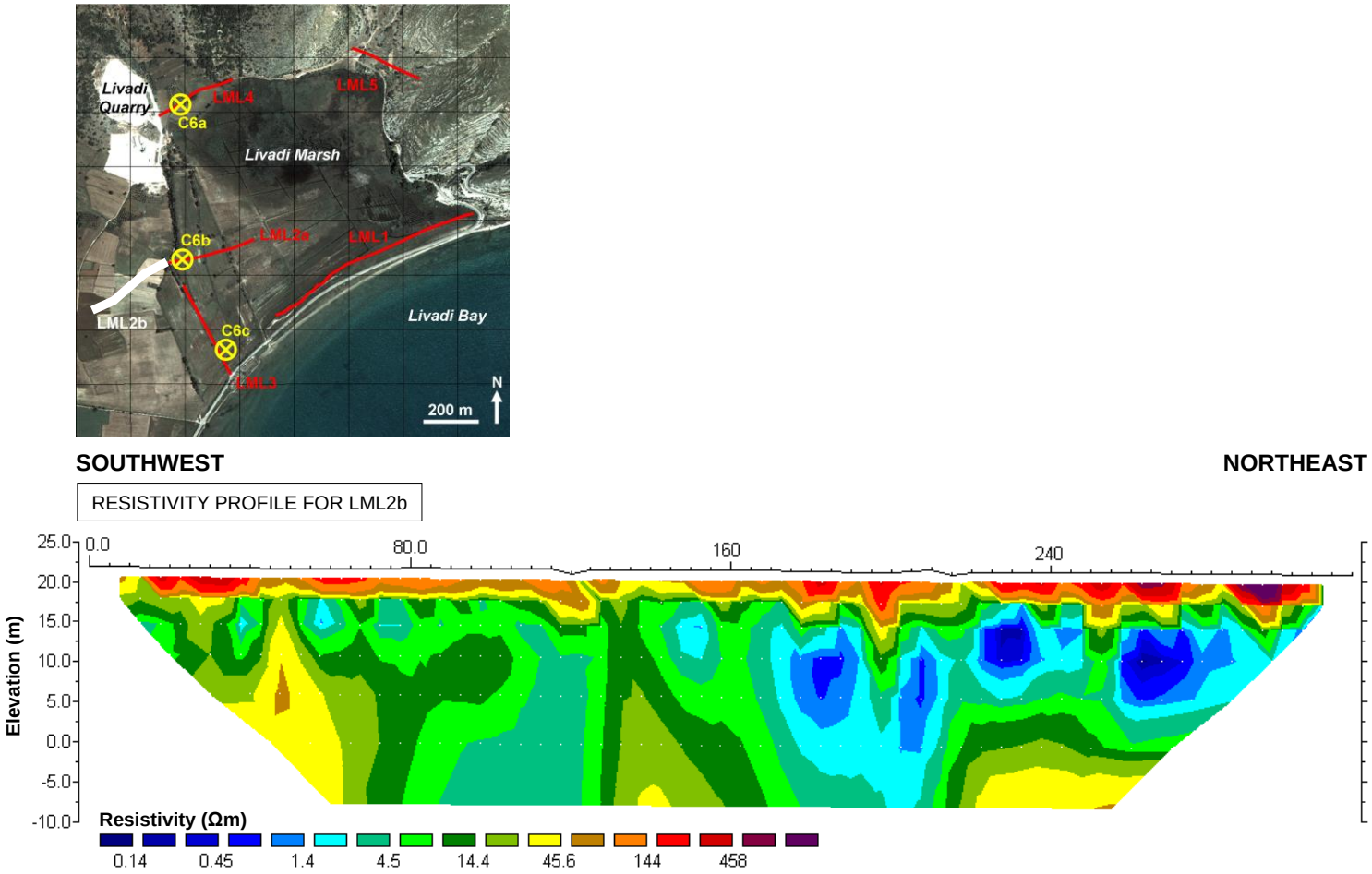

Figure 4.19 2D resistivity profile (top) and corresponding seismic refraction profile (bottom) for Livadi Marsh profile, LML2b. Elevation/depth is in terms of elevation above mean sea level (where mean sea level is +22 m above present sea level). The location of this survey line is indicated in the map inset. Vertical exaggeration is V/H = 2.

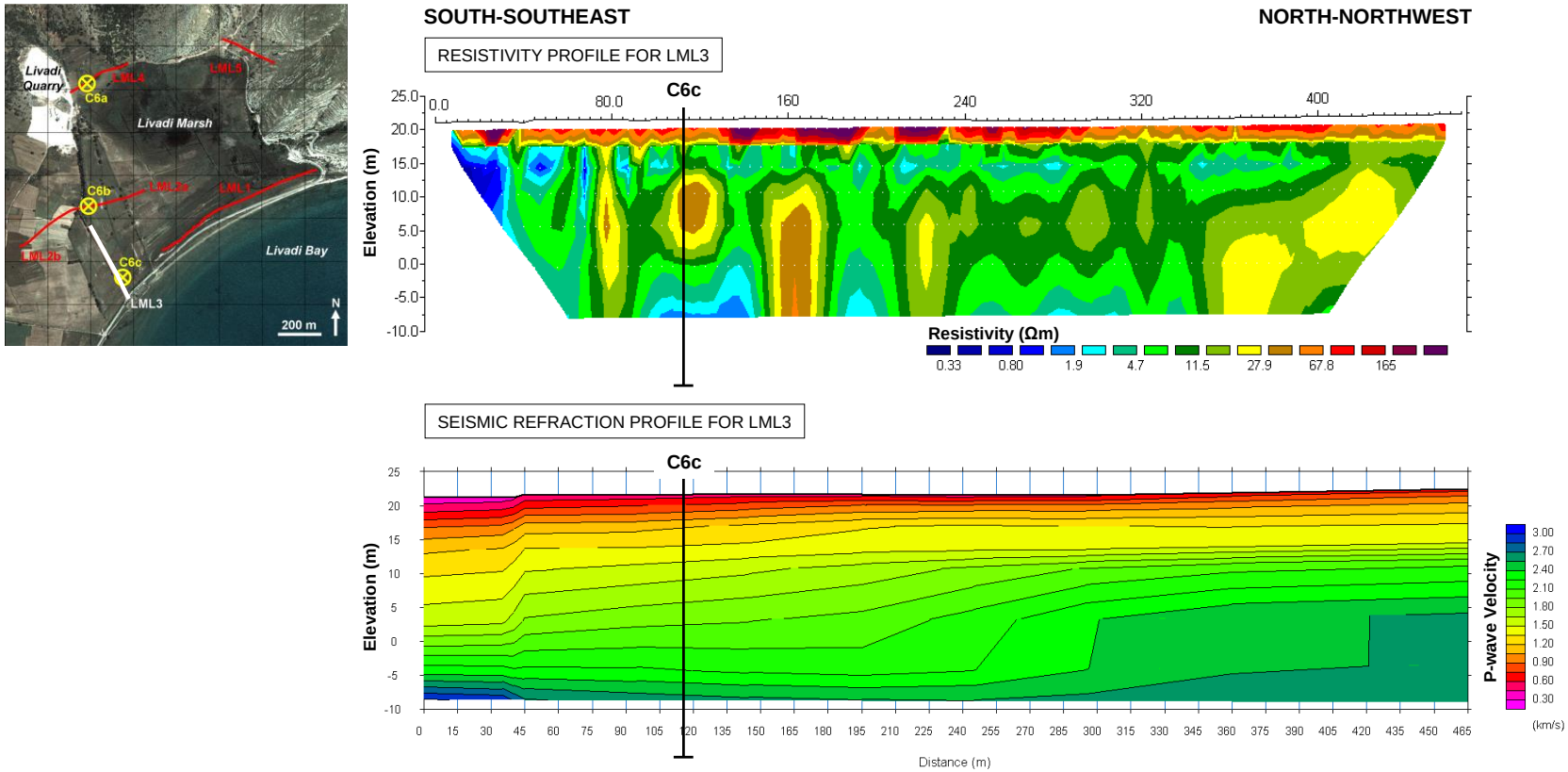

Figure 4.20 2D resistivity profile (top) and corresponding seismic refraction profile (bottom) for Livadi Marsh profile, LML3. Elevation/depth is in terms of elevation above mean sea level (where mean sea level is +22 m above present sea level). The location of this survey line is indicated in the map inset. Vertical exaggeration is V/H = 3. Vertical black lines indicate where the profile crosses a borehole.

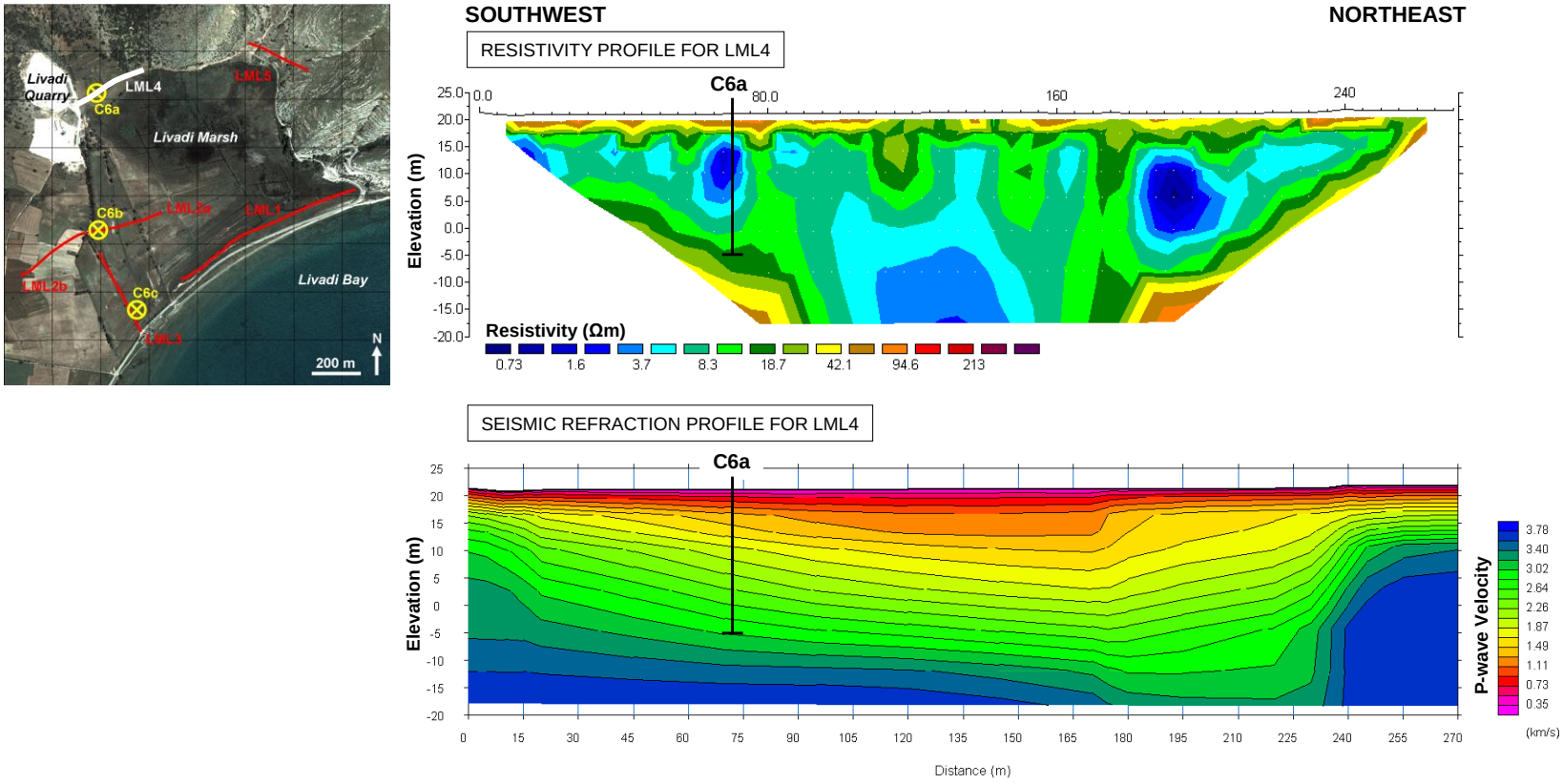

Figure 4.21 2D resistivity profile (top) and corresponding seismic refraction profile (bottom) for Livadi Marsh profile, LML4. Elevation/depth is in terms of elevation above mean sea level (where mean sea level is +22 m above present sea level). The location of this survey line is indicated in the map inset. Vertical exaggeration is V/H = 1.5. Vertical black lines indicate where the profile crosses a borehole.

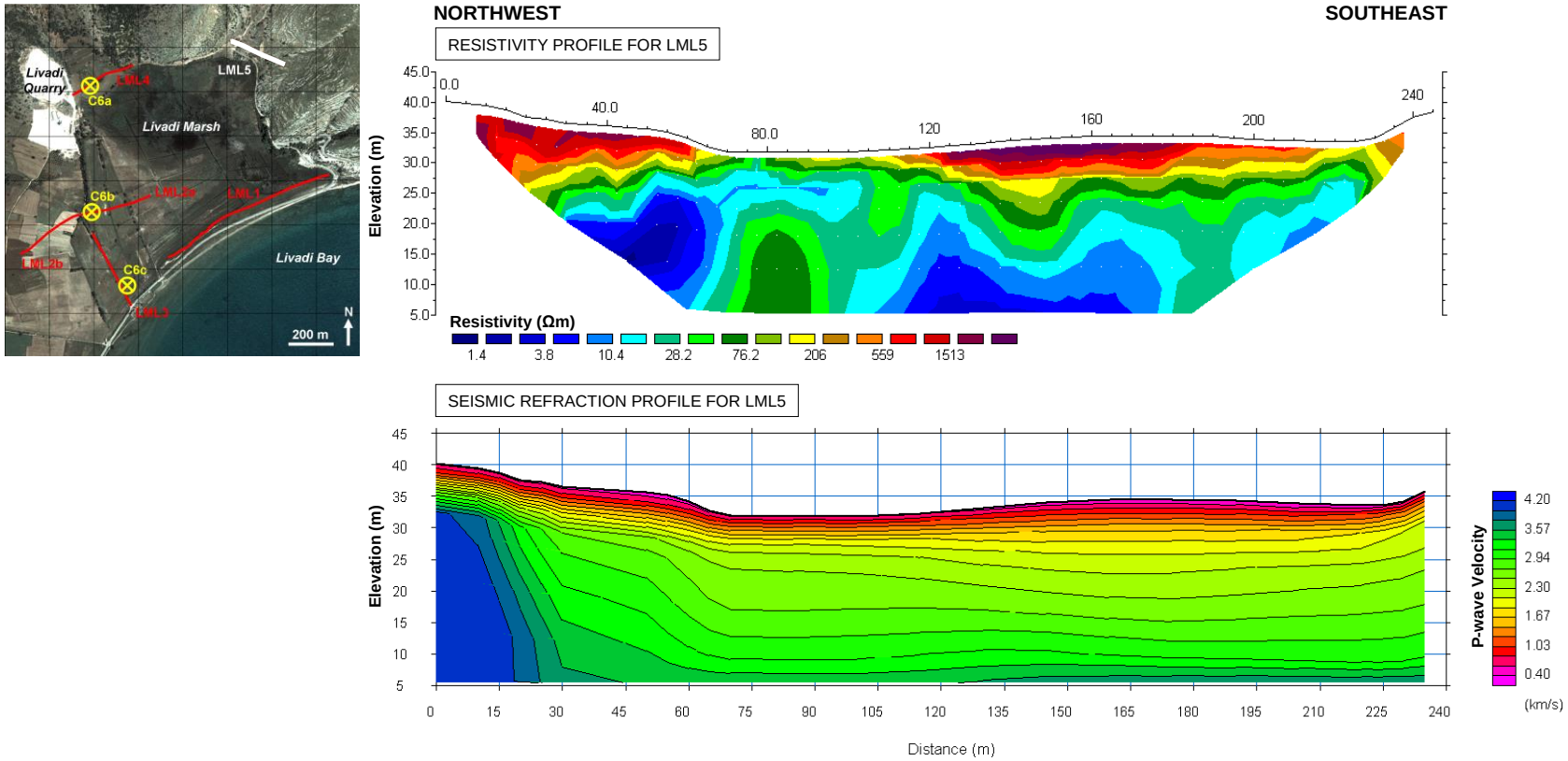

Figure 4.22 2D resistivity profile (top) and corresponding seismic refraction profile (bottom) for Livadi Marsh profile, LML5. Elevation/depth is in terms of elevation above mean sea level (where mean sea level is +22 m above present sea level). The location of this survey line is indicated in the map inset. Vertical exaggeration is V/H = 1.5.

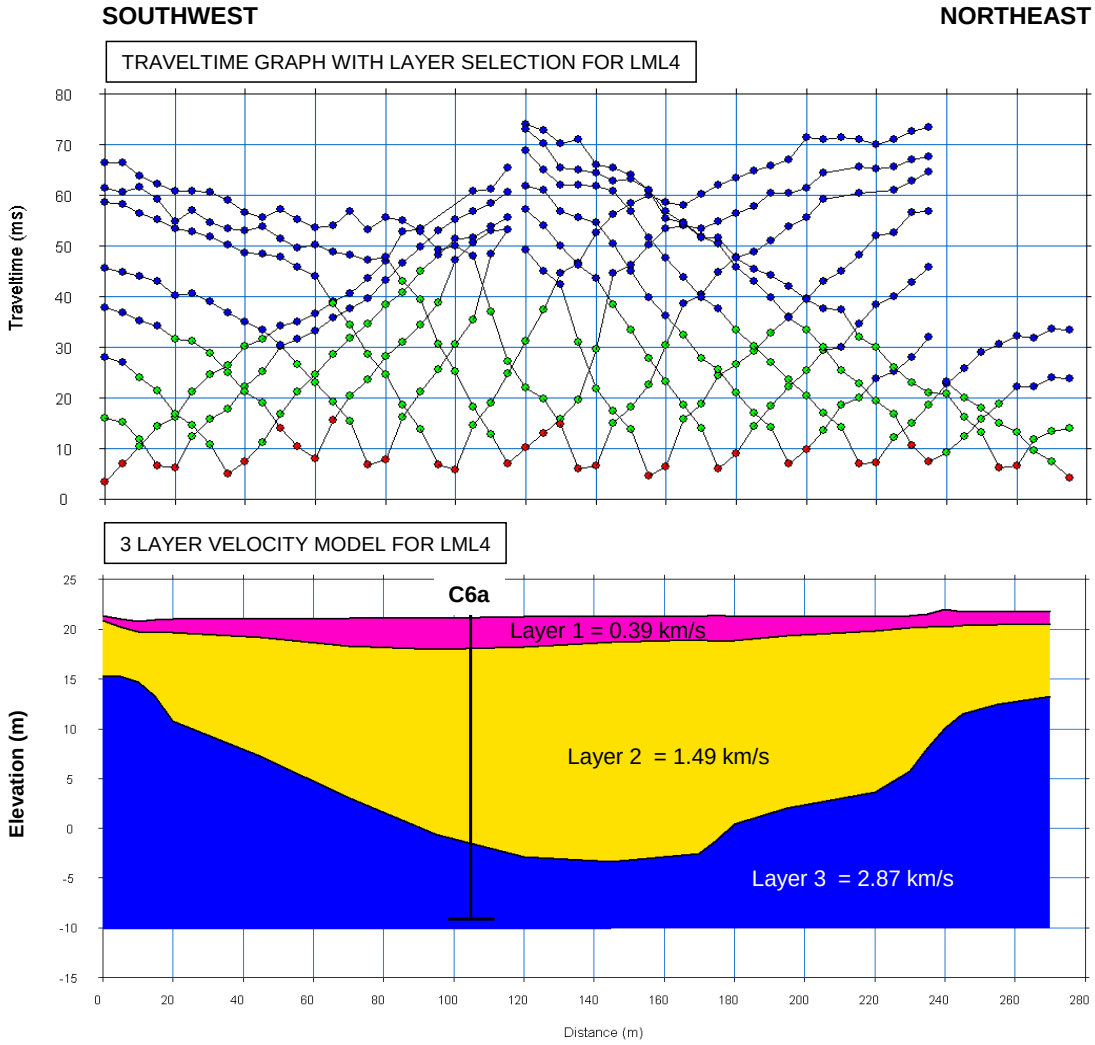

Layer assignment:

Layer 1 = Clays, recent soils.

Layer 2 = Clay, marls.

Layer 3 = Limestone

Figure 4.23 Time-term inverted profile for LML4 (coloured section) with corresponding traveltime graphs (top) showing layer selection where red = layer 1, green = layer 2 and blue = layer 3. Layers are assigned possible lithologies based on the corresponding P-wave velocities. The location of this line is given in Figure 4.21. Vertical black lines indicate where the profile crosses a borehole.

However, this model should be treated with caution since the configuration of the Atheras Thrust, emplacing limestone over the marsh clays which presumably have a much lower P-wave velocity, would result in the footwall sediments forming a "hidden" layer beneath the limestone and therefore would not be resolved by the

refraction method. Either limestone underlies this location and the layered refraction model is correct or there is a hidden marl layer beneath the limestone. The corresponding resistivity profile for LML5 detected low resistivity sediments underlying the surface layers which was interpreted as marsh fill clays suggesting the latter is true.

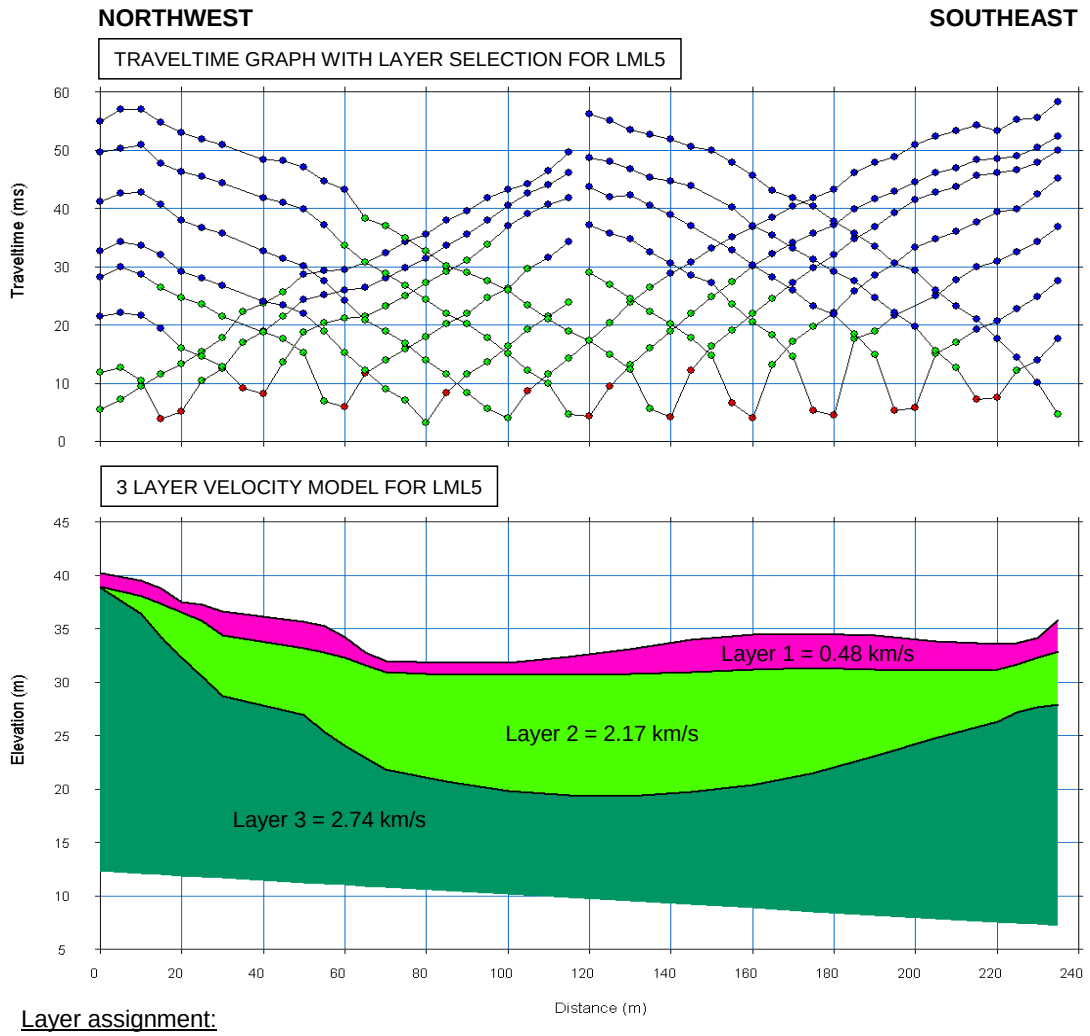

Layer assignment:

Layer 1 = Surface sediments.

Layer 2 = Clays, marls.

Layer 3 = Limestone

Figure 4.24 Time-term inverted profile for LML5 (coloured section) with corresponding traveltime graphs (top) showing layer selection where red = layer 1, green = layer 2 and blue = layer 3. Layers are assigned possible lithologies based on the P-wave velocities. The location of this line is given in Figure 4.22. Vertical black lines indicate where the profile crosses a borehole.

4.5 Thinia

4.5.1 Airborne Overview

A. Magnetic Survey

The magnetic valley "fill" of Thinia contrasted clearly with the less magnetic limestone valley sides (Figure 4.25). The greatest accumulation of magnetic sediment occurred within the northern part of the valley. The most magnetic sediment was focused along the incised gully which drained northwards from Lake Katachori and joined the asymmetric northern valley which appeared as a narrow linear anomaly. The consistence of this signal from its emanation point at the suspected paleo-lake also suggested this drainage route may serve as the primary surface outlet for Lake Katachori in times of flood. Several NW-SE trending discontinuous fan-like features emanated from the base of the steep eastern valley side and followed tributaries to the main stream. These coincided with accumulations of alluvium and clastic material washed down from the talus accumulations at Nifi and Angon. A similar feature occurred in the vicinity of the Zola talus fan.

In central and southern Thinia, the magnetic response was noisier due to interference from habitation and the numerous data gaps which made it less easy to interpret but still showed a raised magnetic response relative to the surrounding limestone. The magnetic sediment fill was sparser here, pinched out between less magnetic limestone ridges. The northern and southern areas of magnetic sediment fill were separated by a narrow "bridge" of lower magnetic material (-25 nT to ~0 nT) which corresponded to the limestone outcrops (e.g. Petrikata Quarry) at the highest point of the valley which clearly acted as the watershed for the magnetic sediment washing into these two drainage systems.

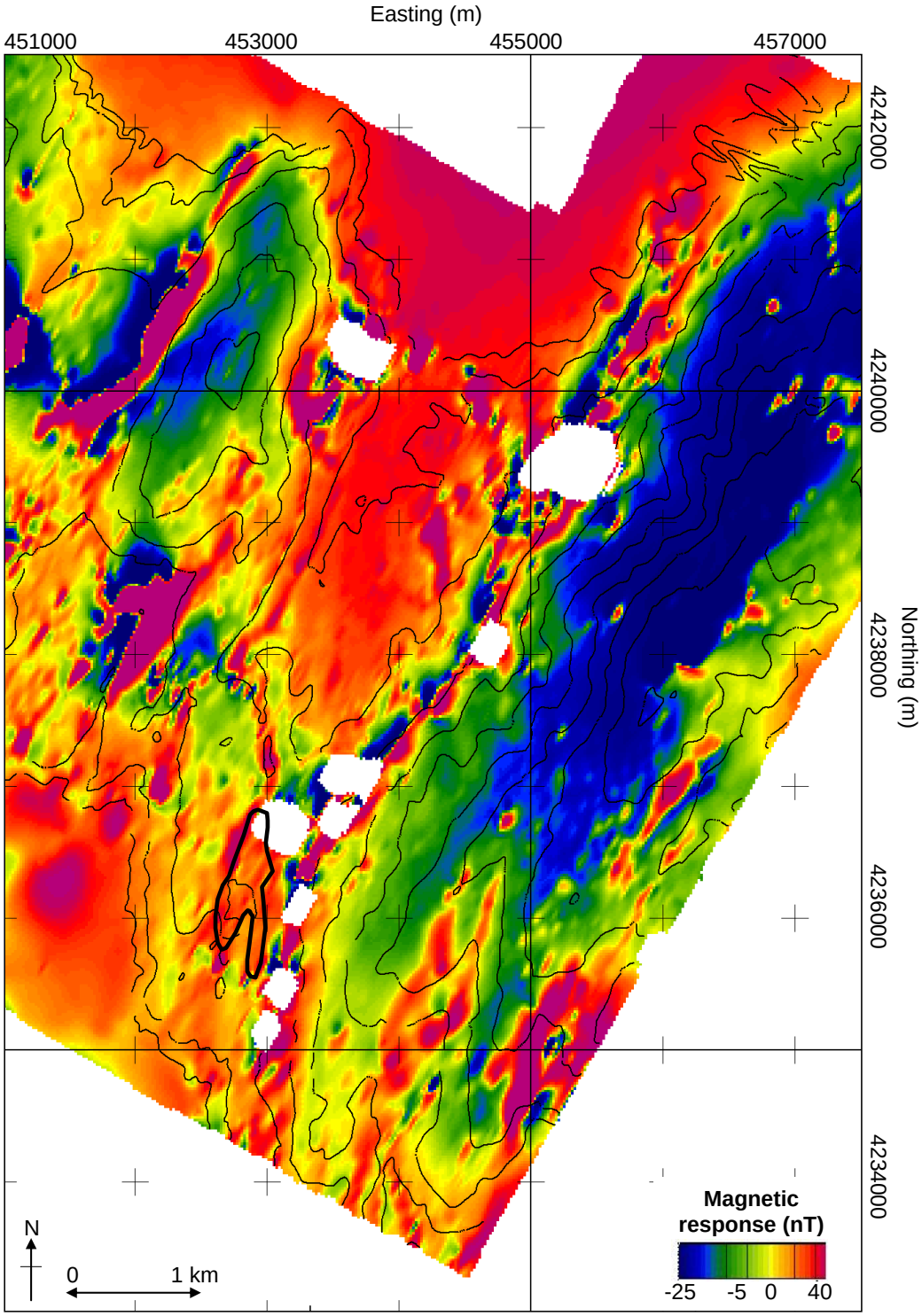

Figure 4.25 Reduced to pole (RTP) magnetic map for Northern Paliki and Thinia. The Thinia valley is outlined by a black box. Data gaps occur over areas of habitation (white). "Warm" colours are strongly magnetic while "cold" colours are less magnetic. Contours are every 100 m. Sea level (0m) is marked. Lake Katachori is outlined in black.

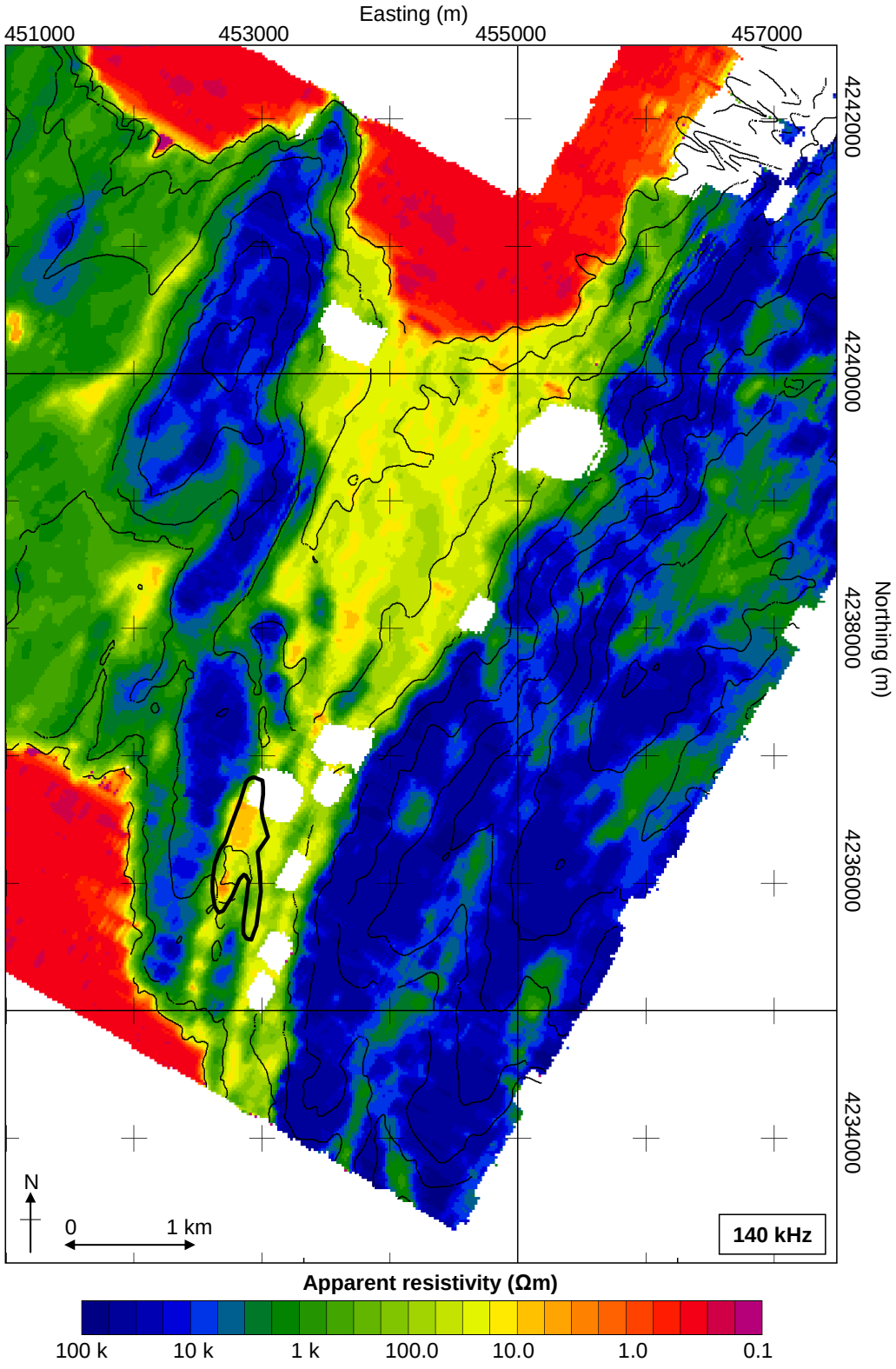

Figure 4.26 140 kHz apparent resistivity map for Northern Paliki. "Warm" colours are high conductivity (low resistivity) and "cold" colours are low conductivity (high resistivity). Contours are every 100 m. Lake Katachori is outlined in black.

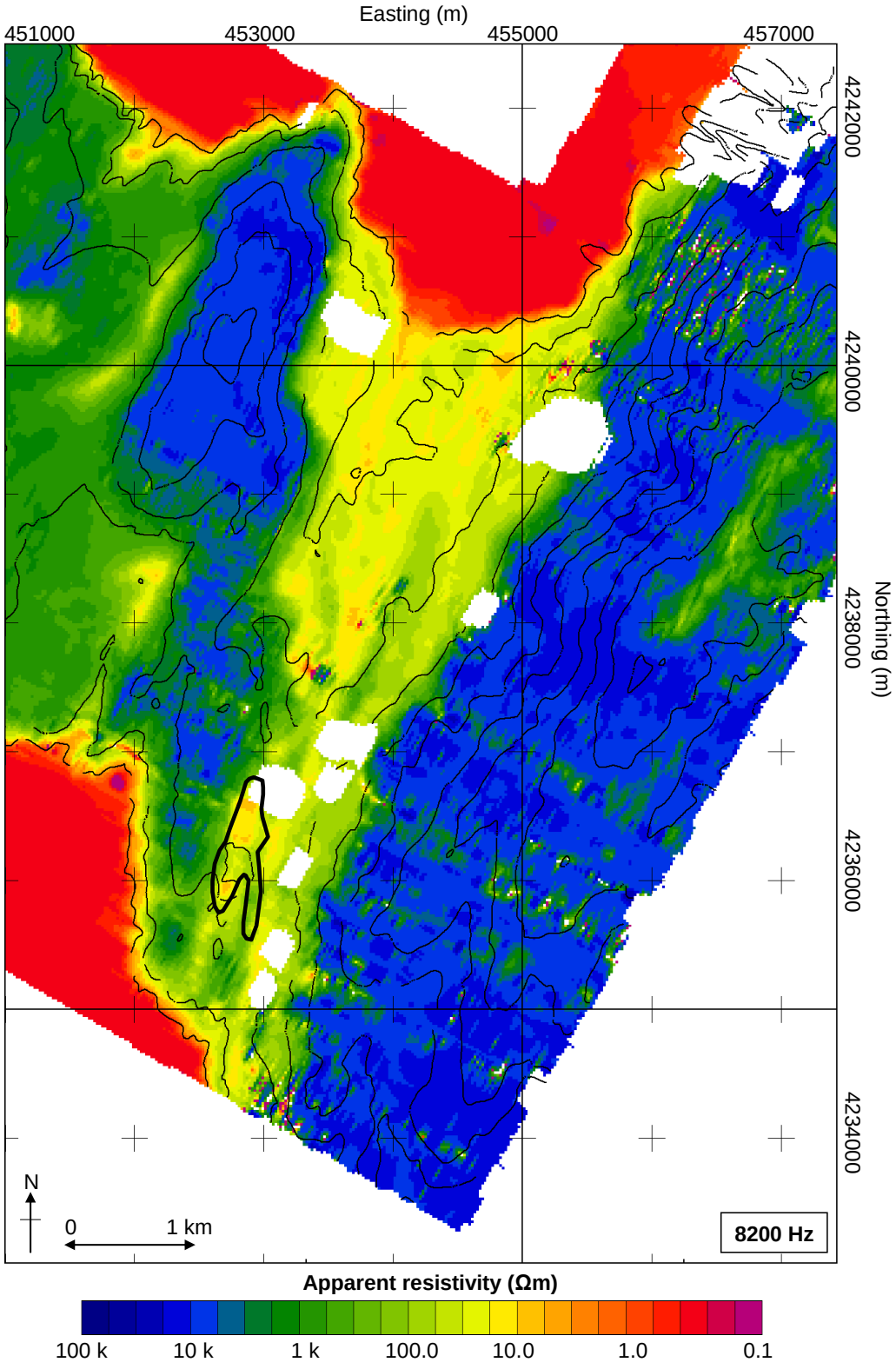

Figure 4.27 8200 Hz apparent resistivity map for Northern Paliki. "Warm" colours are high conductivity (low resistivity) and "cold" colours are low conductivity (high resistivity). Contours are every 100 m. Lake Katachori is outlined in black.

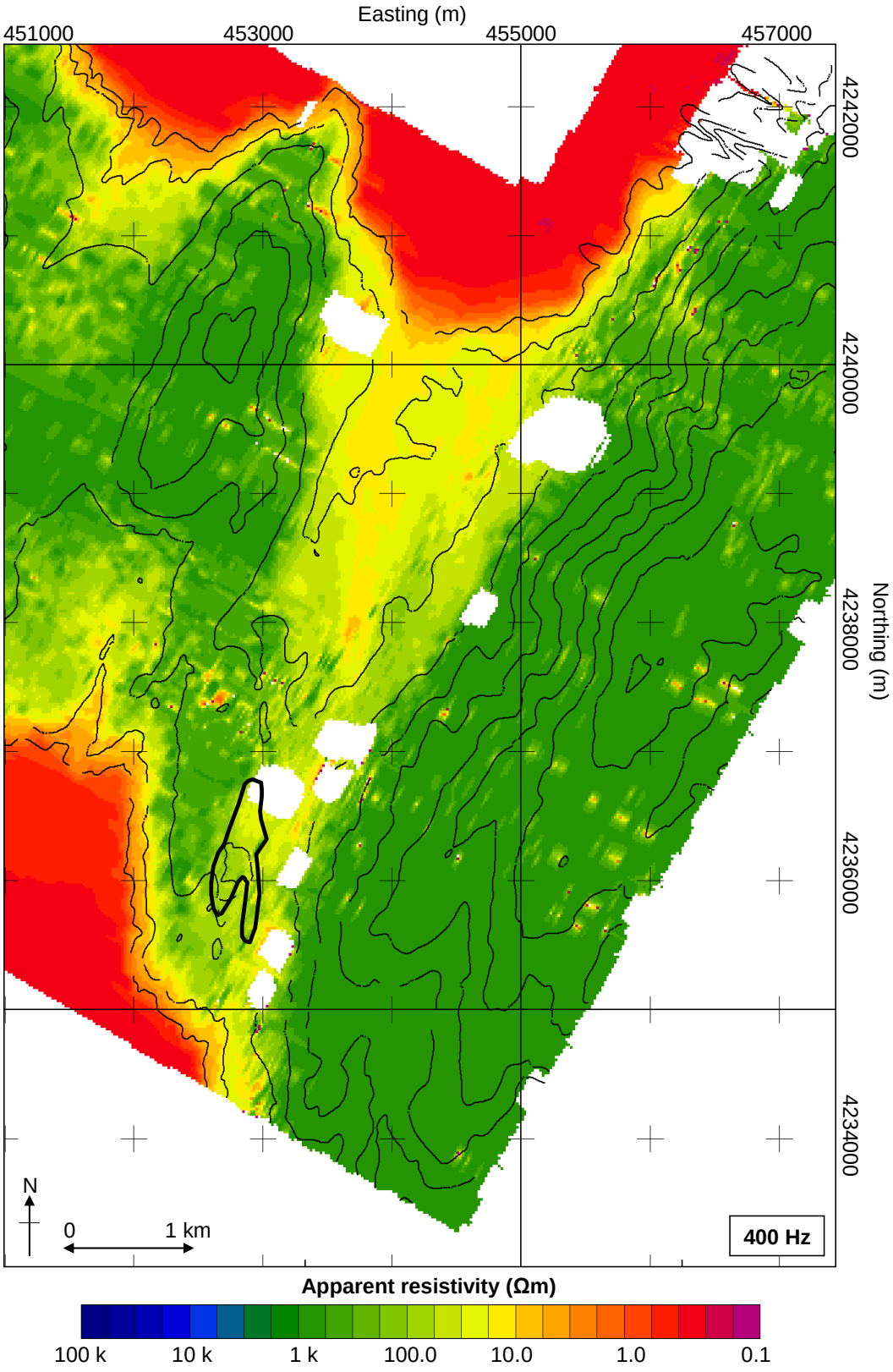

Figure 4.28 400 Hz apparent resistivity map for Northern Paliki. "Warm" colours are high conductivity (low resistivity) and "cold" colours are low conductivity (high resistivity). Contours are every 100 m. Lake Katachori is outlined in black.

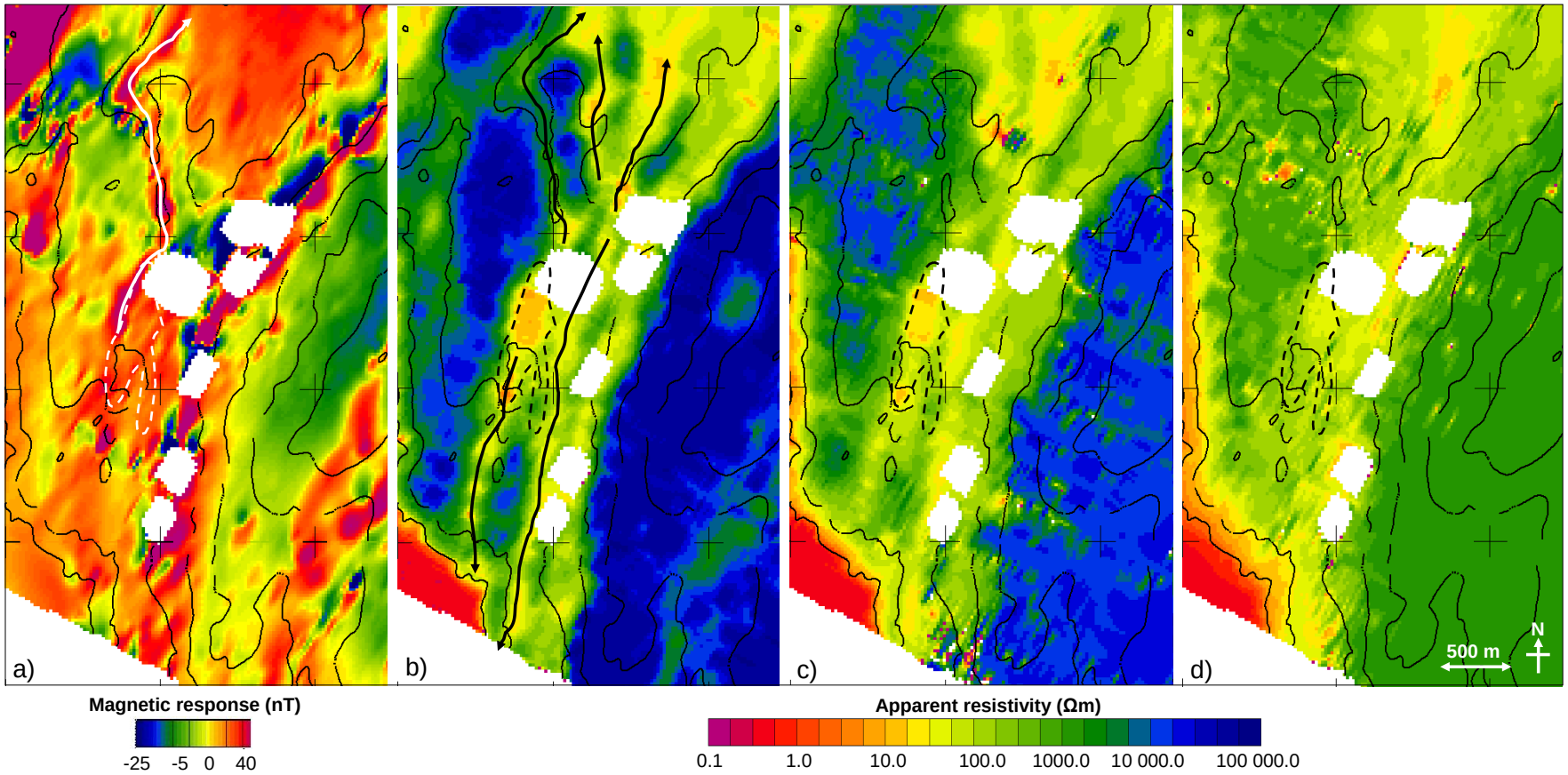

Figure 4.29 Results of the helicopter-mounted electromagnetic (HEM) survey for the saddle region and southern Thinia: a) Magnetic results; Apparent resistivity maps for 140 kHz (b), 8200 Hz (c) and 400 Hz (d). Lake Katachori is indicated by a black or white dashed line. Contours at 100 m intervals. Drainage gullies are indicated with black or white arrows

B. Apparent Resistivity Survey

The apparent resistivity map for Thinia showed a striking contrast between the low resistivity (orange-yellow to pale green, ~3 to 50 Ωm) low elevation valley "fill" and the highly resistivity (dark green to blue, ~300 to 10 000 Ωm) limestone bounding the high elevation valley sides with a strongly-defined contact between the sediments visible in all frequencies (Figure 4.26 to Figure 4.28). On the eastern side of the valley this contact represented the Ainos Thrust.

With decreasing frequency, the extent of this low resistivity fill did not diminish greatly and there was no sign of a significant increase in resistivity which might indicate the presence of underlying resistive bedrock (limestone). This meant this valley fill was at least 80 to 100 m thick. This material tied into the magnetic deposits detected by the previous survey. However, while the detection of a thick deposit of this conductive, magnetic sediment was a promising result since it meant the valley "fill" extended below sea level, the airborne surveys were not able to differentiate between "backfill" (alluvial sediments and landslide material) and underlying bedded marl and clays which turned out to be conductively identical.

In northern Thinia, the valley fill was composed of a series of narrow repeating conductive-resistive (~3 to 100 Ωm) linear anomalies resembling a "braided channel" like pattern contained between the high resistivity limestone valley sides. These "channels" were predominately orientated NNE-SSW indicating they tied into the underlying structural trend of the valley and visible in the low frequencies showing that they extended to at least 80 to 100 m. The most conductive of these tied into the proposed route of "Strabo's Channel" and a zone of pronounced slumping within the sea cliff at Agia Kiriaki Bay. This repeating pattern of high and low resistivities was interpreted as the conductive response of the asymmetric folded sediments observed during the field-mapping of northern Thinia.

In the central saddle region and southern Thinia, there was a similar repeating pattern of NNE-SSW orientated high and low resistivity linear anomalies best resolved by the highest frequency maps, however in this case the contrast between them was much more pronounced. The low resistivity valley "fill" was pinched out into three narrow "channels" separated by two resistive (100 to 10 000 Ωm) linear anomalies (Figure 4.29). This configuration could be discerned in all but the lowest frequency which meant the valley fill here extended around 80 m or more in depth. The resistive anomalies correlated to the marl enclosed limestone ridges of the thrust faults which disrupted the marl succession (e.g. Petrikata Thrust, Agia Sotira Thrust). The signal from these anomalies was strongest where these ridges broken through the sediments at the surface and the contrast between conductive valley fill and resistive limestone was strongest. The HEM maps also allowed these thrusts to be tracked below the sediment particularly where the Agia Sotira Thrust disappeared beneath Lake Katachori indicating this thrust acted as a divider between the lake drainage and proposed route of "Strabo's Channel" to the east of the thrust.

While the presence of data gaps in the saddle region made connecting the features seen in the northern part of the valley with those in the central and southern part difficult, the orientation of the repeating patterns of resistive-conductive linear anomalies in these regions suggested the thrusting in the central and southern part of Thinia were caused by the same deformation causing the folding of the marl sediments in the northern valley. It was hoped that the gravity survey which did not suffer from data gaps due to habitation would therefore be key in understanding the connection between the northern and southern drainage valleys.

The 140 kHz map detected the presence of low resistivity (green, ~1000 Ωm) "rafts" occurring on the high topographic plateau at the summit of Imerovigli to the east of Thinia. The largest of these measured roughly 2.12 x 1.06 km and were orientated in a similar direction to the strike of the Ainos Thrust. This material was connected to the Thinia valley via dendric "channels" which correlated to the incised drainage patterns within the scalloped embayments on the west-facing slope of the mountain and fed into the talus deposits at Nifi, Angon and Petrikata.

This material was still visible in the 8200 Hz map indicating the largest accumulation was around 20 m in thickness (volume ~ 4.5 x 10^7 m^3). There was some indication in the 140 kHz of this material forming "outfingers" along drainage gullies within the valley which agreed with the magnetic data indicting these talus deposits on the eastern valley side had undergone significant erosion by the incised streams draining from Imerovigli relative to the Zola talus.

4.5.2 Gravity

Figure 4.30 shows the distribution of gravity measurements with gravity stations displayed as black dots. The greatest density of data points occurred along the axis of the valley with fewer points taken along the valley sides and no measurements were collected upon the steepest elevations. This placed greater confidence upon the anomalies plotted by the GMT mapping software along the central part of the valley being related to actual physical changes in the subsurface. Less confidence was given to the anomalies where density of data points was less and therefore where the gridding algorithm used by GMT had more of an influence on the shape of those anomalies such as across the high elevation mountains bounding the valley. The extrapolation of the grid between data points was limited by the *–S* command which masked out the grid beyond a distance of 1 km from a data point.

The map resolved the gravity response of the Thinia valley into a series of NNE-SSW trending anomalies with a value range of -2.5 to +3 mGals. The lowest gravity values (-1 to -2.5 mGals) occurred on the eastern side of the valley along the base of Imerovigli particular across the talus fan at Angon and beneath the suspected rotational slump within the Ainos Thrust hangingwall above Petrikata. A gravity low (-1.2 mGals) also occurred in the vicinity of the Zola talus and Agrilias mountain.

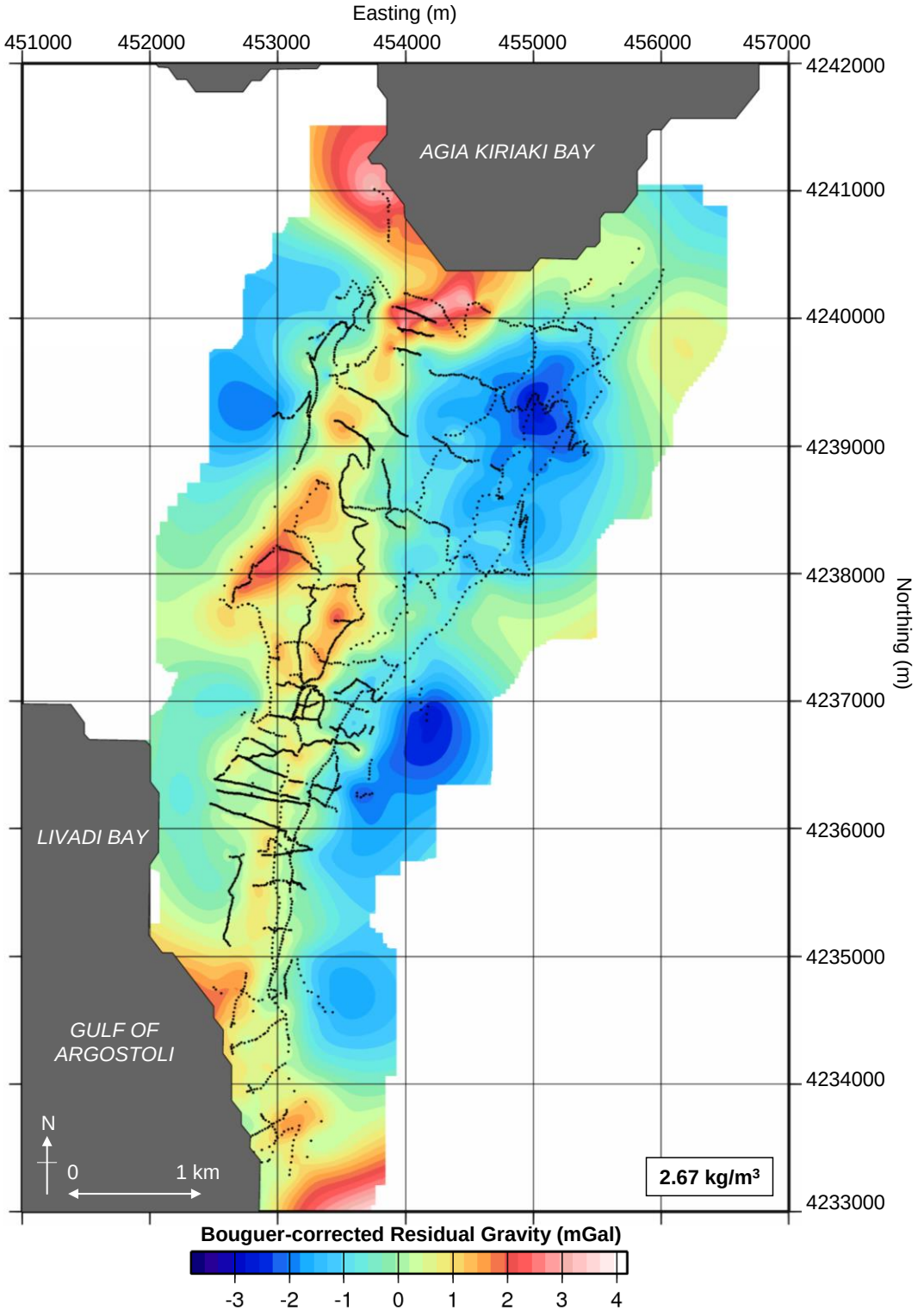

Figure 4.30 Bouguer-corrected residual gravity map in terms of mGals ($\rho = 2.67$ kg/m^3) showing data coverage of the gravity survey. Gravity stations are indicated as black dots. Low gravity anomalies dominate on the eastern side of the Thinia valley below the talus deposits of Petrikata, Nifi and Angon. The central part of the valley is defined by a narrow NNE-SSW striking positive linear anomaly which appears to correlate with the limestone ridges of the thrust faults disrupting the marl sediments.

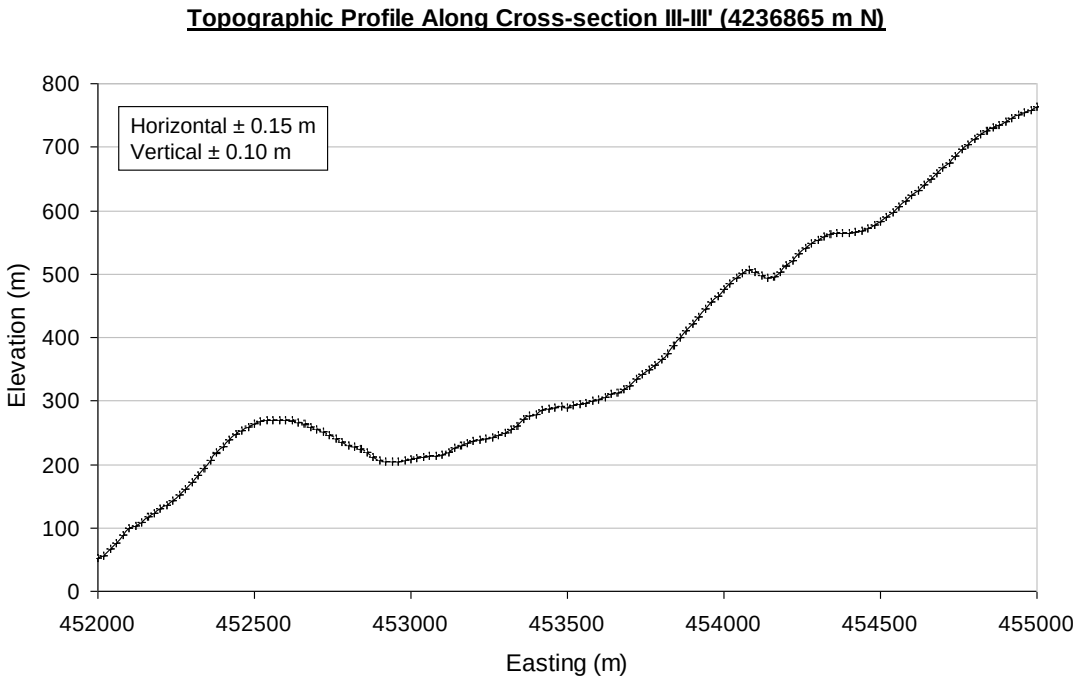

Figure 4.31 Topographic profile for cross-section III-III' which is positioned across the central sector of the valley, displaying error bars.

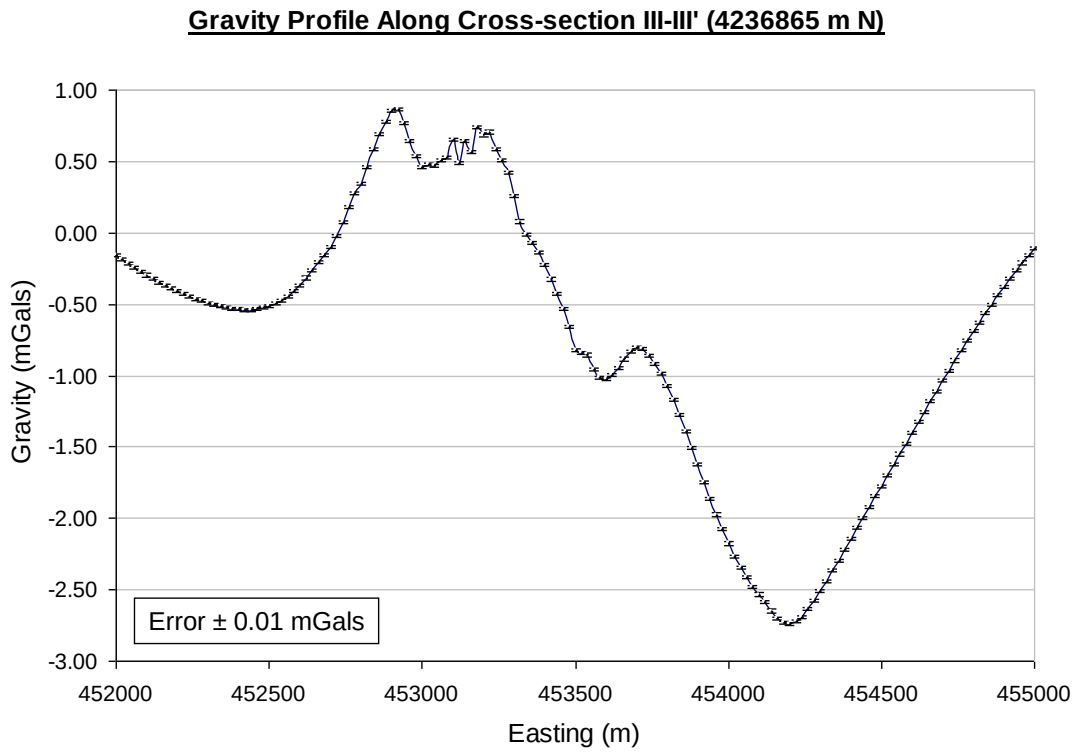

Figure 4.32 Gravity profile for cross-section III-III' showing vertical error on the gravity readings.

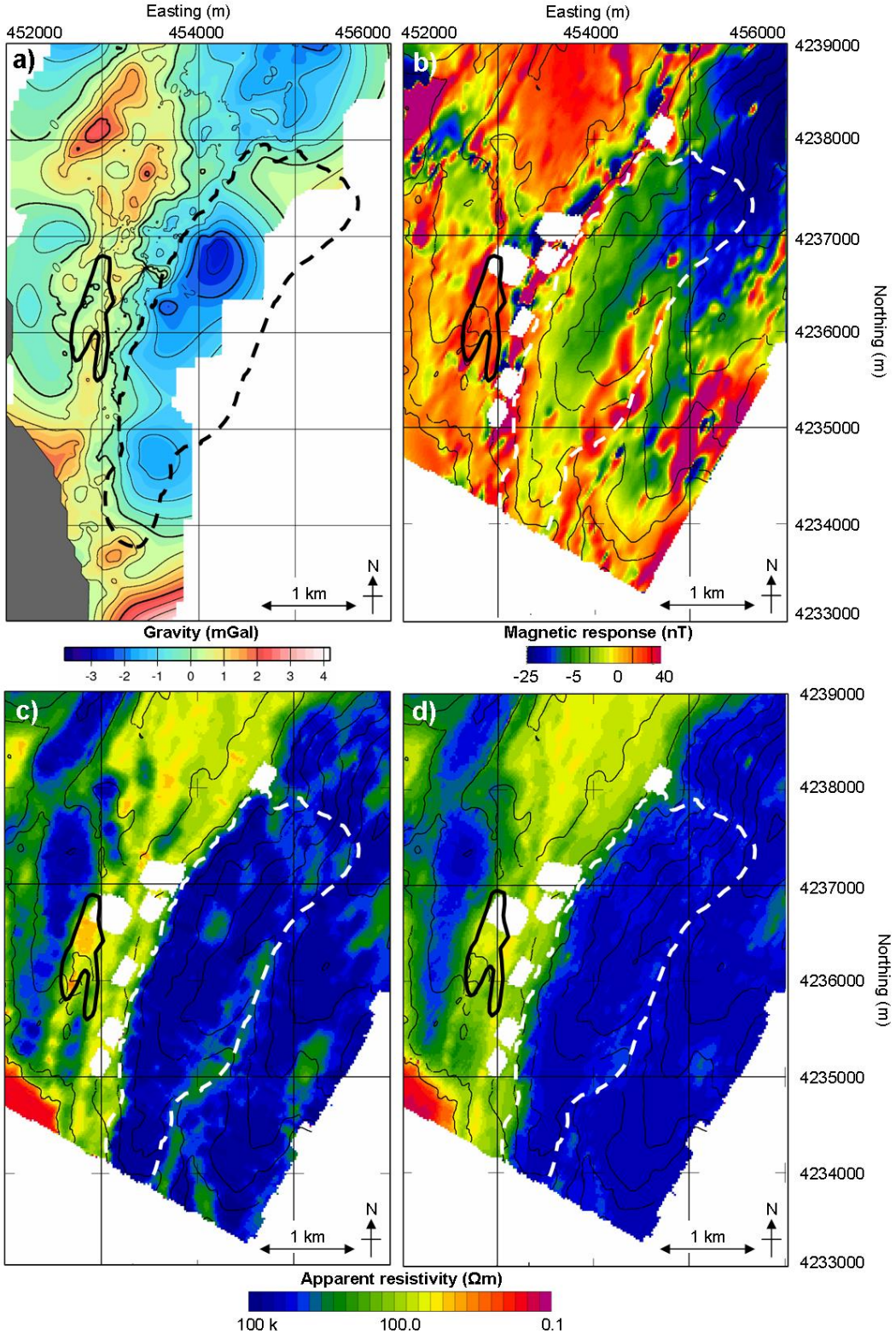

Figure 4.33 Series of maps showing the position of the suspected rotational slump within the Ainos Thrust hangingwall: a) Gravity; b) Magnetic response; c) 140 kHz; d) 40 kHz. Lake Katachori is outlined in black.

Although small, these anomalies were believed to relate to true geology rather than errors in the terrain correction. The error in the DEM was in the order of 15 cm (horizontal) and 10 cm (vertical) to 2 sigma (95% confidence). Figure 4.31 showed the topographic profile with error bars taken along cross-section III-III' (Figure 3.32, used later in this section). This resulted in errors of around 0.01 mGals (Figure 4.32) which confirmed that the gravity anomalies were not due to errors. Secondly, the NNE-SSW trend to the anomalies mirrored the dominant trend of the stratigraphy in Thinia. This and the good overall data point coverage of the valley meant that the anomalies observed on this map were believed to be a reliable reflection of the distribution of shallow sub-surface density contrasts.

The $\rho = 2.67$ kg/m^3 Bouguer-corrected residual gravity map was directly compared to the airborne apparent resistivity and magnetometry maps to aid the interpretation. The negative anomaly below Zola may have been due to the accumulation of low density talus material relating to the collapsed fault plane below Agrilias. Similarly, the low beneath Angon may have been due to the talus fans beneath Imerovigli. However, the anomaly at Petrikata was less easy to explain. The lack of data points across this area placed uncertainty on the extent and shape of the anomaly compared with the Angon low which had a very good coverage of data points.

This low may have been the source of the low gravity anomaly detected during the June 2006 gravity survey (Section 2.2.2). The negative response over the limestone mountains may have been due to of the isostatic correction from the raw gravity data (the removal of the gravitational effect of masses in the deep crust or mantle which isostatically compensative for topographic loads at the surface (Nabighian et al., 2005) i.e. application of an Airy model, Airy (1855)). The airborne survey resolved more details about this possible slump (Figure 4.33). The suspected slip plane ("Agia Ioanni Fault") identified in Section 3.3.4 which ran around the southern edge of the anomaly was clear in the magnetic survey as a strongly magnetic linear anomaly (~30 nT) (Figure 4.33, b), similar in appearance to the magnetic signatures of the normal faults along the western coast of Paliki (Figure 4.2). The 140 kHz map showed that this fault plane sediment was also conductive showing a marked decrease in resistivity (~1000 Ωm) relative to the surrounding limestone (10 000 to

100 000 Ωm) (Figure 4.33, c). The signature of this conductive, magnetic material was greatly reduced by 40 kHz suggesting it formed a thin (~10 to 20 m) veneer.

The negative anomalies were separated by a series of positive (~0.3 to +3 mGals) NNE-SSW trending linear anomalies which ran along the axis of the valley (Figure 4.33, black dotted lines). The proposed route of "Strabo's Channel" (in the case of an untranslated, buried channel presented in Figure 1.53) followed this positive anomaly. This positive response might reflect the presence of a high volume of limestone clastic material embedded within low density marls however, in the southern and central sector this anomaly tied into the limestone ridge of the Agia Sotira Thrust which suggested it was caused by the presence of the thrust faults running along the centre of the valley.

There was also evidence of the positive anomalies having been offset in a NW-SE orientation (roughly perpendicular to the dominant NE-SW to NNE-SSW stratigraphic trend of the valley) several times (black dashed lines, Figure 4.34). At least one these offsets tied into faulted structures visible at the surface (e.g. the Zola offset). Tying these offsets to the north-south topographic cross-section established for the valley axis and proposed route of "Strabo's Channel" (Figure 4.35) showed that they appeared as steps in the topography. To the north of Petrikata Quarry these steps dipped northwards and south of the quarry they dipped southwards. Several offsets occurred in the vicinity of the quarry which explains why this outcrop stands out from the surrounding topography.

Petrikata Quarry lay within this NNE-SSW trending anomaly. While the HEM survey showed some differentiation between the resistive (green, 1000 Ωm) limestone and conductive (10 Ωm) marl, the presence of data gaps and poor resolution at this scale were problematic for interpretation. The gravity map for the quarry resolved more detail (Figure 4.36). The active part of the quarry appeared as a lower density "hole" in the positive anomaly caused by a localised drop in gravity of this anomaly from around 0 mGals to -0.3 mGals. This drop was possibly caused by the excavation of limestone through quarrying to leave the underlying less dense marl sediment.

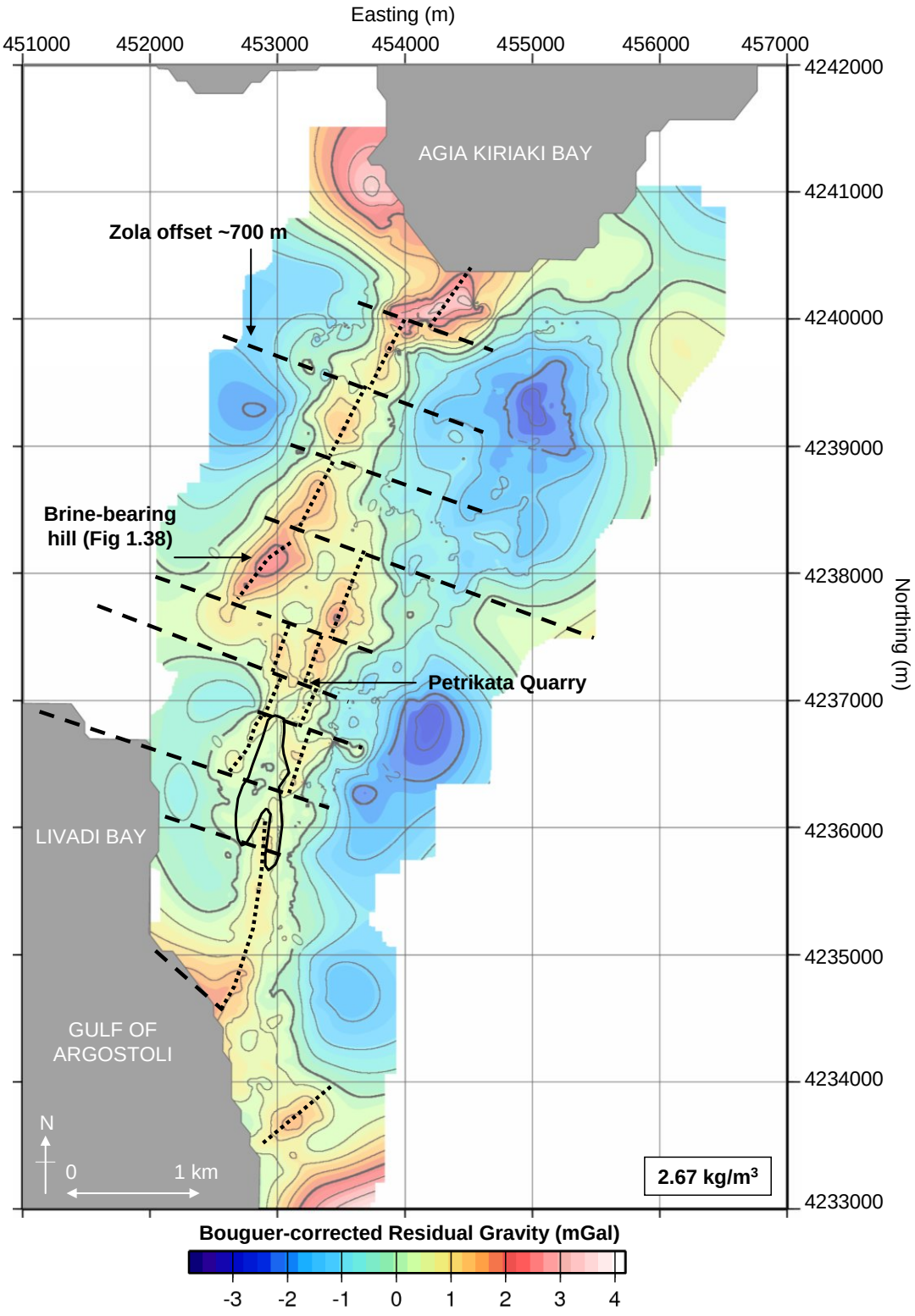

Figure 4.34 Interpretation of the Bouguer-correction residual gravity map for Thinia. The black dashed lines show the locations of possible faulted offsets while the black dotted lines indicate the position of the NNE-SSW trending positive anomalies running up the centre of the valley. At least one of these offsets (the Zola offset) corresponds to offsets observes within the geology of the valley. Petrikata Quarry's position amongst several closely-spaced offsets may explain why the outcrop stands out from the surrounding topography.

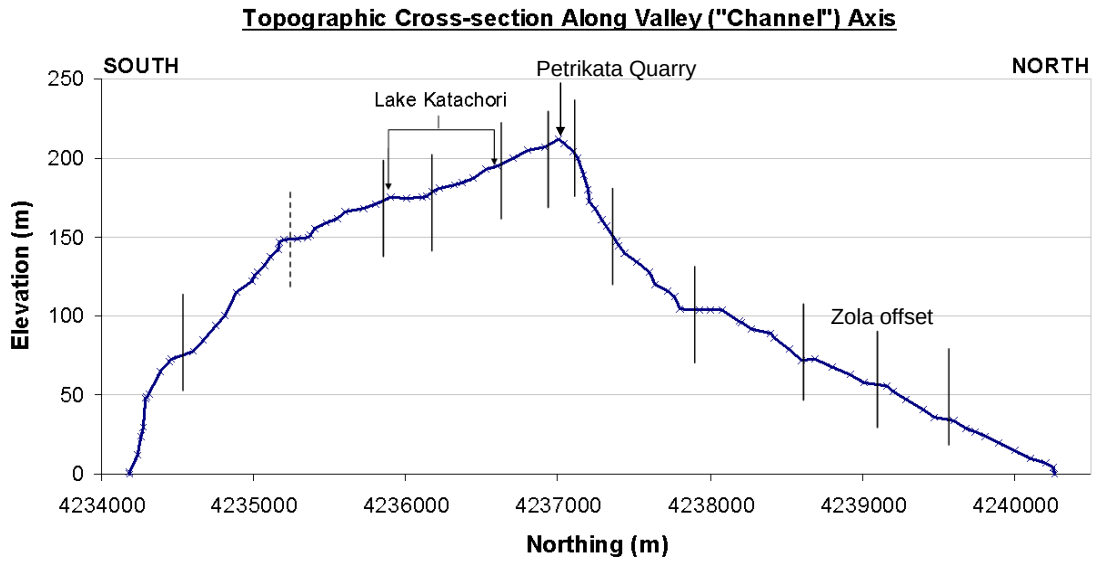

Figure 4.35 Vertically-exaggerated north-south topographic cross-section from Chapter 1 showing where the NW-SE offsets (vertical black lines) detected by the gravity survey cross-cut the proposed route of "Strabo's Channel" (the dotted line indicates a possible offset detected in the topography but was not clear in the gravity map). The offsets appear as a series of steps in the topography dipping northwards to the north of Petrikata Quarry and southwards south of the quarry.

The marl-limestone contact running around the main road could be seen as a sharp contrast between positive and negative values (black dotted line on Figure 4.36) while contouring to the east showed a more gradual change, indicative of an easterly-dipping carbonate slab. This suggested the quarry outcrop was caused by thrust-faulting therefore *in situ* bedrock rather than representing a large clast detached from the valley sides and embedded within marl sediment. The course of the Petrikata Thrust at the quarry was obscured by very large boulders which corresponded to a localised zone of low gravity (0 to -0.5 mGals).

One of the strongest positive anomalies (+2.5 mGals) was centred upon the limestone hill drilled by borehole G5 which contained the hypersaline brine (Figure 1.39). Because this hill occurred within the NE-SW striking positive anomaly it may also represent part of a thrust fault.

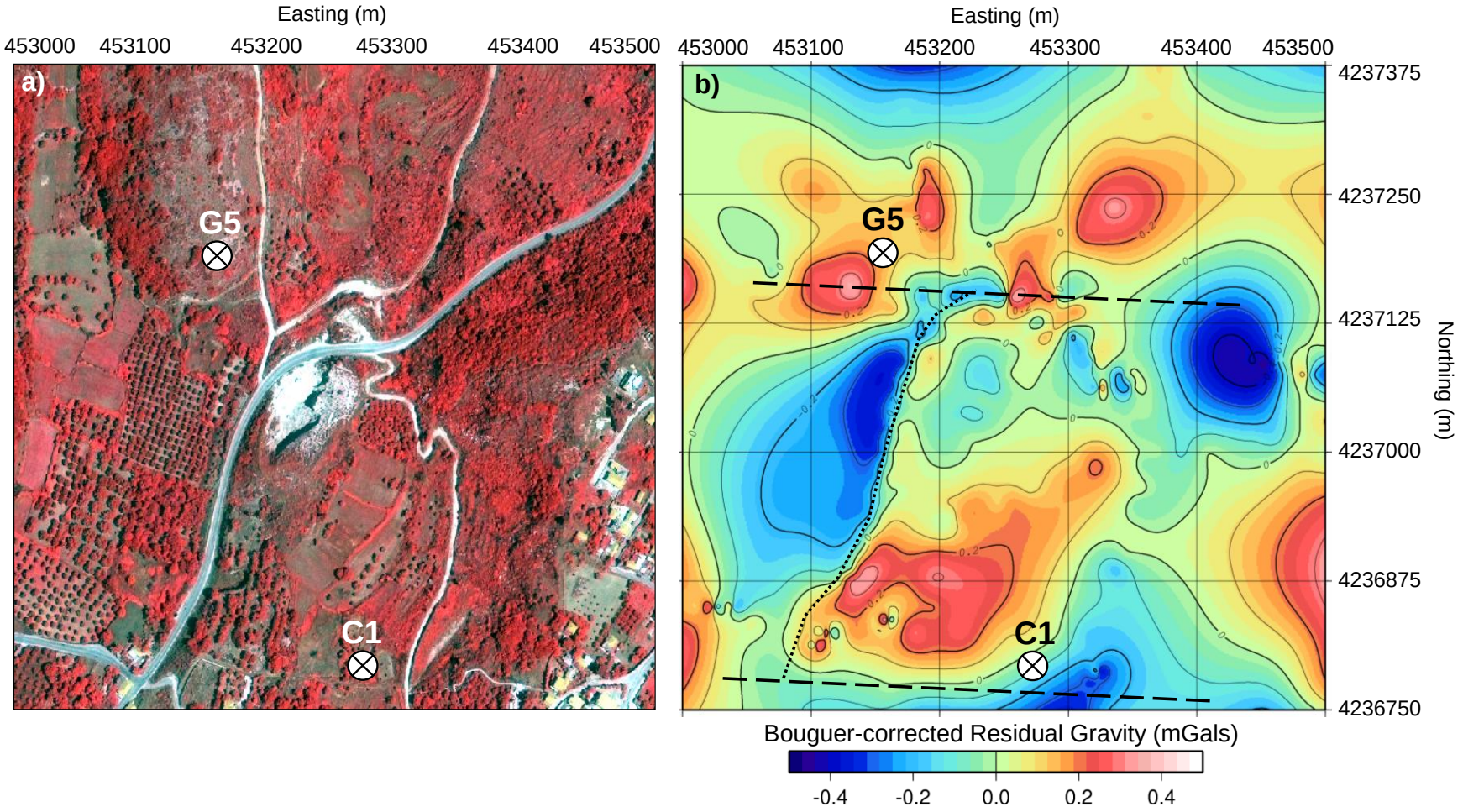

Figure 4.36 Bouguer-corrected residual gravity map for Petrikata Quarry showing the location of the C1 borehole and G5 borehole drilling into the brine-bearing hill (Figure 1.39).The thick dashed lines indicate possible offsets. The black dotted line indicates the (faulted) marl-limestone contact running along the side of the quarry.

A. Gravity Modelling

The gravity data was modelled along the five E-W cross-sections established from the surface geological map and presented in Section 3.5 (Figures 3.30 to 3.34). The locations of these are indicated in Figure 4.37. Five gravity models (Figure 4.40 to 4.44) were produced with an additional gravity model orientated north-south (VI-VI', Figure 4.45) constructed to investigate the gravity low beneath the village of Angon. Data points for the Gravmag profiles were chosen to be 20 m apart to ensure a good sampling rate. Data non-uniqueness means there are likely to be many differing configurations of polygonal layers which will lead to the same gravity response. Because these models were created to fit the geological cross-sections from Chapter 3 in order to control the size, orientation and density of the polygonal layers, the resulting profiles might not reflect the true subsurface.

The densities assigned to the polygons were based on the typical densities for the lithologies found during field-mapping. The geology of Thinia is mostly composed of limestones which typically have a density range of 2.5 to 2.8 kg/m^3 and marls which have a range of 1.7 to 2.6 kg/m^3 which varies according to whether they are clay-rich or sandy. These values are considered an average as the lithologies would have further variation within them particularly if they were water-saturated (water = 1000 kg/m^3) or air-rich (air ~1.2 kg/m^3). Since these densities are approximations, the resulting models should be considered likely but not unique solutions and may be improved with further surveys and sampling. Deep sampling (boreholes) of the subsurface is crucial to adequately determine stratigraphic surfaces and rock types.

Sharp anomalies in the gravity relating to similarly sharp changes in topography (e.g. small-scale (tens of metres) incised gullies or ridges) indicated that the terrain correction had not eliminated all the topography-related variations. These were resolved as well as possible while reducing the affect this had on the gravity model. Less confidence was placed on interpretation on parts of the models near the edge of the survey where data points were sparser since the gravity data used to construct the gravity profiles was extracted from the gravity map constructed by the GMT

software. The anomalies may have been due to GMT gridding algorithm attempting to resolve the sparse data points at this location and may not reflect a true low anomaly.

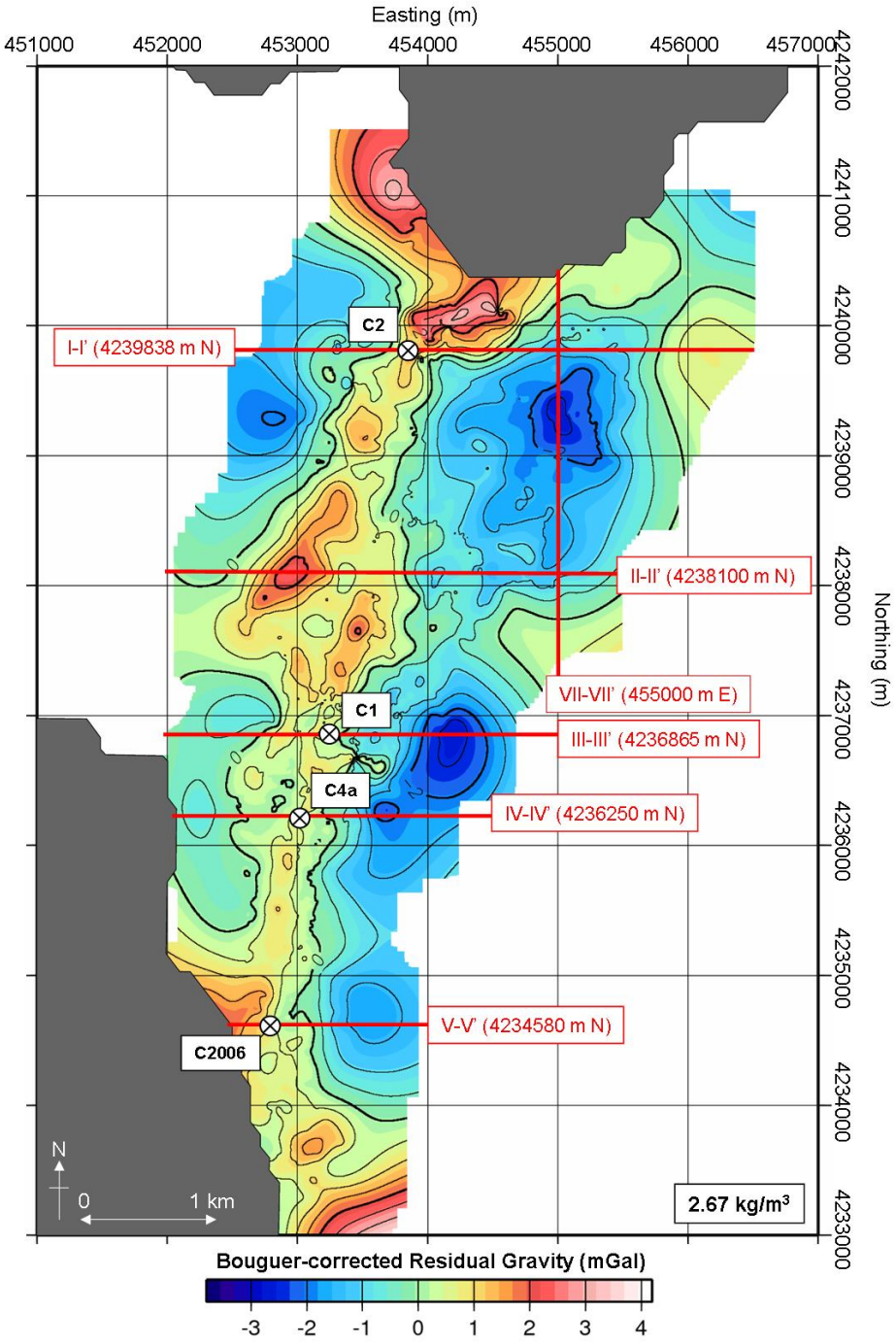

Figure 4.37 Bouguer-corrected residual gravity map for 2.67 kg/m^3 showing the locations of the six gravity profiles modelled with the Gravmag software and boreholes they cross. The profiles are named according to their northing or easting position. The positions of these cross-sections are given on the geological map in Chapter 3.

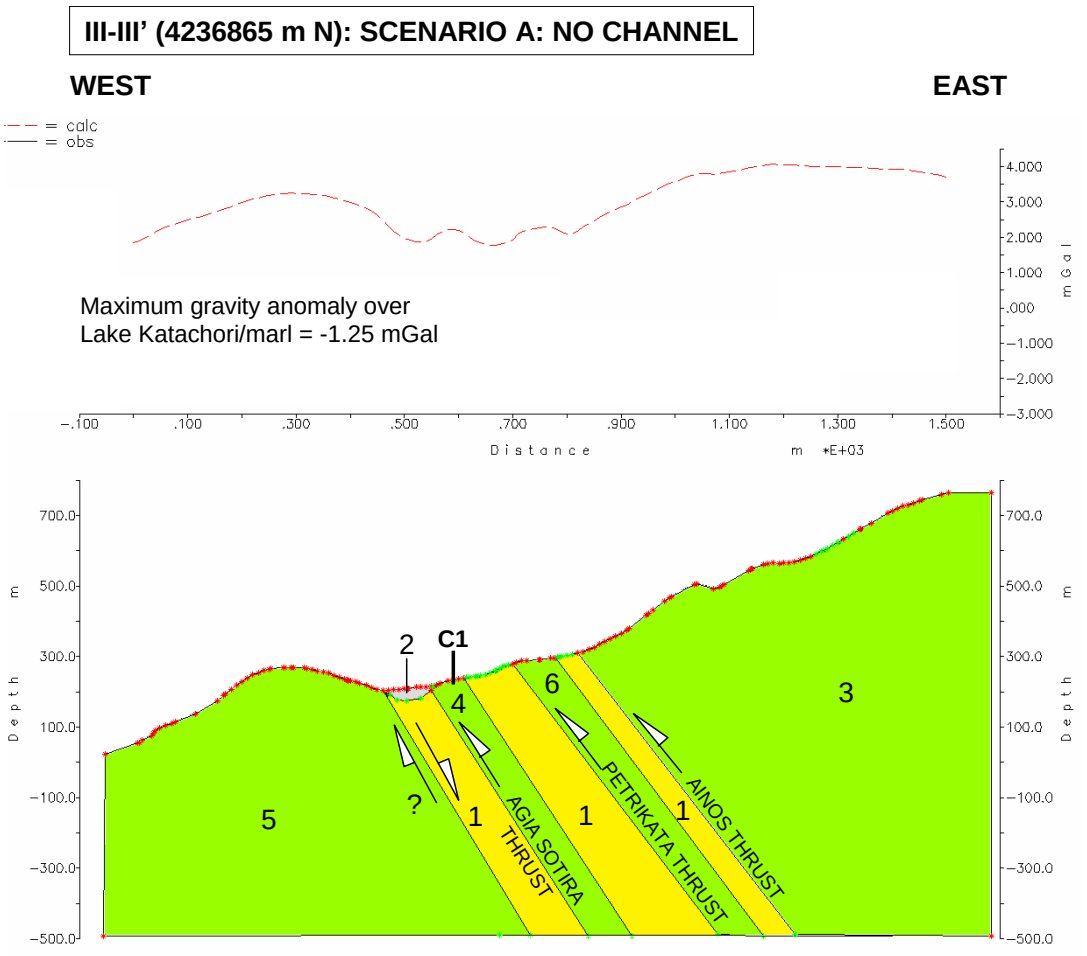

SCENARIO A: NO CHANNEL

Polygon No.	Colour	Density (kg/m^3)	Lithology
BACKG		2.320	
1		2.200	Marl
2		2.000	Lacustrine sediments (Lake Katachori)
3		2.600	Limestone (Ainos Thrust hangingwall)
4		2.500	Limestone (Agia Sotira Thrust)
5		2.500	Limestone
6		2.300	Limestone/limestone conglomerate (Petrikata Thrust)

Figure 4.38 Hypothetical gravity profile created for geological cross-section III-III' in the case that no landslide-filled buried channel occurs.

Hypothetical models were initially constructed to show the expected gravity response from the following scenarios – (1) there was not a landslide-filled marine-level channel present within the subsurface (Figure 4.38) and (2) there was a marine channel incised into the bedrock (Figure 4.39). The cross-section chosen to model these possible configurations was III-III' (4236865 m N) as it cross-cut the valley where the proposed route of "Strabo's Channel" set out in Figure 1.53 was most geologically constrained.

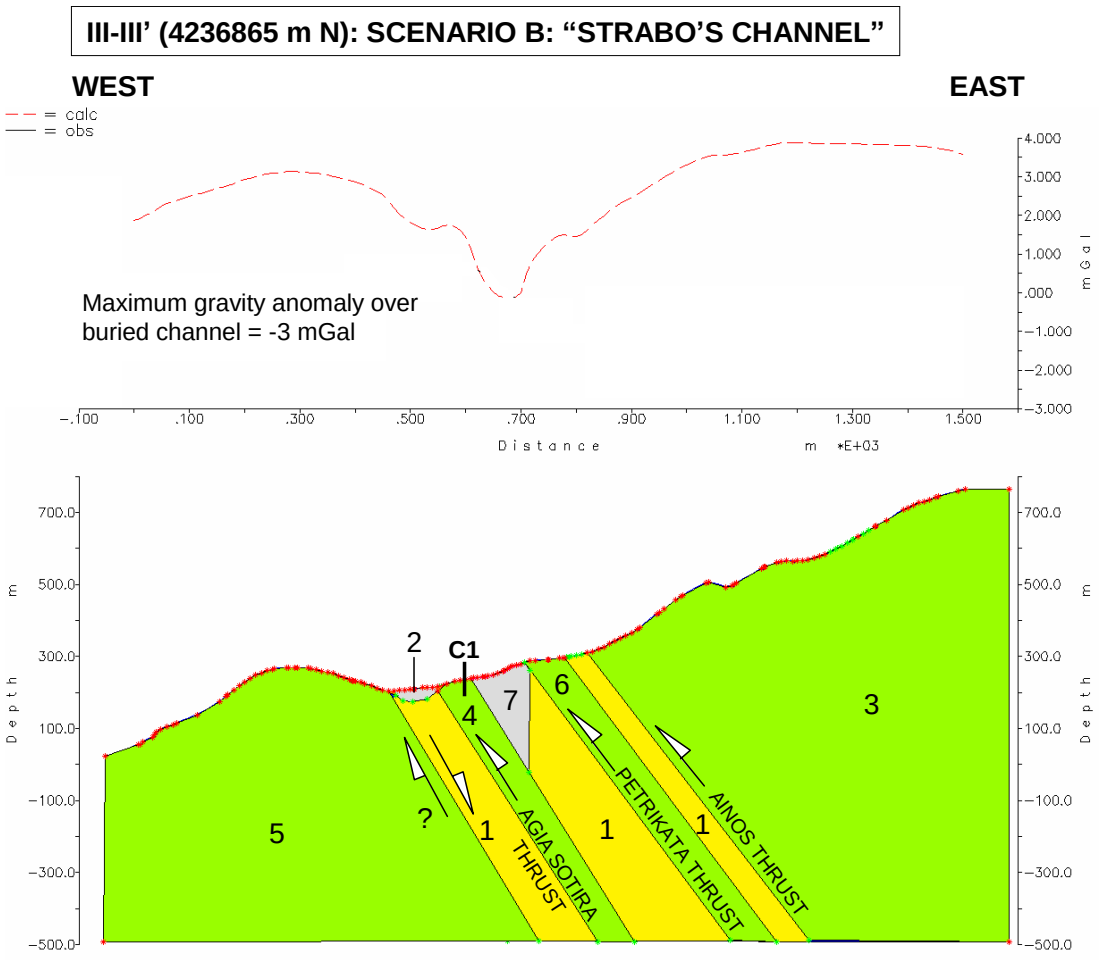

SCENARIO B: "STRABO'S CHANNEL"

Polygon No.	Colour	Density (kg/m^3)	Lithology
BACKG		2.320	
1		2.200	Marl
2		2.000	Lacustrine sediments (Lake Katachori)
3		2.600	Limestone (Ainos Thrust hangingwall)
4		2.500	Limestone (Agia Sotira Thrust)
5		2.500	Limestone
6		2.300	Limestone/limestone conglomerate (Petrikata Thrust)
7		1.500	Buried (landslide-filled) channel

Figure 4.39 Hypothetical gravity profile created for geological cross-section III-III' in the case that a landslide-filled buried channel occurs within the marl bedrock.

Both hypothetical gravity profiles showed a positive response with raised gravity over the limestone valley sides and lowered gravity response over the marl-filled valley. In Scenario A, the drop in gravity associated with the marl was around 1.25 mGals. There was a small double peak in the centre of the valley associated with the two thrust faults (Agia Sotira Thrust and Petrikata Thrust). In Scenario B, the landslide-filled channel wedge formed a distinct drop in gravity of around 3 mGals.

I-I' (Figure 4.40): This profile resolved the valley "fill" into two section: an easterly-dipping unit of density 2.480 kg/m^3 which onlapped the steeply-dipping normal fault defining the western valley side and a unit of less dense (2.180 kg/m^3) easterly-dipping sediments which were overthrust by the Ainos Thrust. The units were separated by an easterly-dipping limestone block (2.550 kg/m^3) associated with the suspected thrust fault in Agia Kiriaki Bay cliff (Figure 3.7). The increase in marl density in the footwall of this thrust was probably due to the presence of repeating hard strata (limestone, hard marl layers) observed within the marl sediments (Figure 3.1, and 3.4). The low gravity anomalies were associated with the low density talus material at Angon (2.060 kg/m^3) and Zola (2.040 kg/m^3). While the Zola talus was around 100 m in thickness and appeared to reach sea level, the Angon talus deposits were thinner and did not.

II-II' (Figure 4.41): This profile was placed to investigate the large limestone hill drilled by the brine-bearing borehole (G5) (Koumantakis and Mimides, 1989). The model produced showed this block and the Agia Sotira Thrust formed a large easterly-dipping limestone block. The presence of lower density marls on the western side of this block led to the conclusive this limestone hill was a thrust fault rather than a large clast.

III-III' (Figure 4.42): The modelled gravity profile for III-III' was quite different from both hypothetical models (Figure 4.38 and 4.39). There was a very striking drop in gravity of around 3.55 mGals however this was not centred on the route of "Strabo's Channel" but the suspected rotated slump within the Ainos Thrust hangingwall. The drop in gravity associated with a buried channel was absent and the resulting polygon configuration left no space for a channel to exist.

The gravity highs expected from the limestone on either side of the valley were less apparent due to the Ainos Thrust possibly having a shallower angle rather than the originally assumed steep (~60°) dip and the thrust plane itself being markedly less dense (due to fracturing along the thrust plane?). This suggested that while the bedding plane dip within the hangingwall is very steep (45 to 60°) the thrust plane

has a similar "ramp-and-flat" geometry (Figure 1.24) exhibited by the Ionian and Atheras Thrusts. The model also suggested that the Petrikata Thrust had a shallower angle of dip here and was connected to the Ainos Thrust (representing a toe-thrust) rather than existing as a separate steep-angled (~60°) thrust fault as imaged in II-II'.

The steepness of the contact between polygons 8 and 2 suggested the limestone ridge defining the western side of the saddle region formed a steep easterly-dipping normal fault similar to the fault at Zola. The response for the limestone on the western side of the valley may have been affected by the large-scale scalloped embayments and low density landslide material within them which occur on the seaward side (Figure 1.56, A) This affect may also suggest that the Atheras Thrust runs this way and low gravity response maybe caused by the limestone overthrusting lower density sediments.

IV-IV' (Figure 4.43): This profile showed a very similar response to III-III' and again demonstrated that the densely-packed easterly-dipping thrust faulting in the central sector resulted in no space to accommodate a buried marine-level channel.

V-V' (Figure 4.44): The low gravity anomaly tied into a ~250 m thick low density unit (2.080 kg/m^3) which sat above Ainos Thrust. This was an unexpected response as this ridge was composed of dense, resistive limestone. This response may have been caused by the limestone being very air-rich which might come about from heavy fracturing of the limestone. This result tentatively lends itself to the possibility that this part of the Ainos Thrust hangingwall might represent a rotational slump.

VI-VI' (Figure 4.45): This profile was positioned north-south through the low gravity anomaly observed in the 2.67 kg/m^3 gravity map in the north-eastern part of Thinia to resolve the north-south dimensions of this anomaly. The majority of the low gravity response came from a thick ~600 m layer of low density sediment (2.230 kg/m^3). This material corresponded to the thick (at least 80 to 100 m) deposit of conductive (~3 to 50 Ωm), magnetic (~10nT to 40 nT) material imaged by the HEM survey and was interpreted to represent fine-grained marls and clays underlying

alluvial deposits of a higher density compared to the marl. The Ainos Thrust could be seen as a roughly horizontal contact (because the cross-section cuts the thrust plane obliquely) between the marl and more dense (2.700 kg/m^3) limestone. This line provided a cross-section through the talus deposits of Nifi and Agon (outlined by black). These appeared in the modelled section as a draping layer between 10 to 180 m thick. The lowest density talus deposits (1.900 kg/m^3) occurred at the edge of the fan and probably related to "outfingers" of fine alluvium. These deposits equated to very conductive, magnetic sediments on the HEM survey. Within the main talus shield itself, densities reduced with elevation with the highest density material (2.500 kg/m^3) relating to the cemented edge of the talus and the lowest density (2.200 kg/m^3) relating to fine-grained alluvial deposits within the embayment above Nifi.

The configuration of the six density models constructed for the gravity data on Gravmag were based on their equivalent sketch geological cross-sections. The models reflected the easterly-dipping trend of the valley stratigraphy onlapping the steep normal fault defining the western valley side and overthrust by the Ainos Thrust.

All models agree that the Ainos Thrust plane is much shallower than previously proposed. The models also suggested that south of Petrikata Quarry the Petrikata Thrust may represent a shallow-angle toe-thrust to the Ainos Thrust.

However, the models clearly did not detect a buried channel. The dense NNE-SSW zone running along the centre of the valley along the proposed route of "Strabo's Channel" was due to the presence of steeply-dipping limestone thrust faults (e.g. Agia Sotira Thrust, the brine-bearing hill drilled by Koumantakis and Mimides (1989), Petrikata Quarry) and not due to densely-packed limestone boulders within a buried channel. The low gravity response on the eastern side of the valley was caused by low density (on average 2 kg/m^3) talus material which formed a surface veneer, on average around 100 m thick, which overlay easterly-bedded geology.

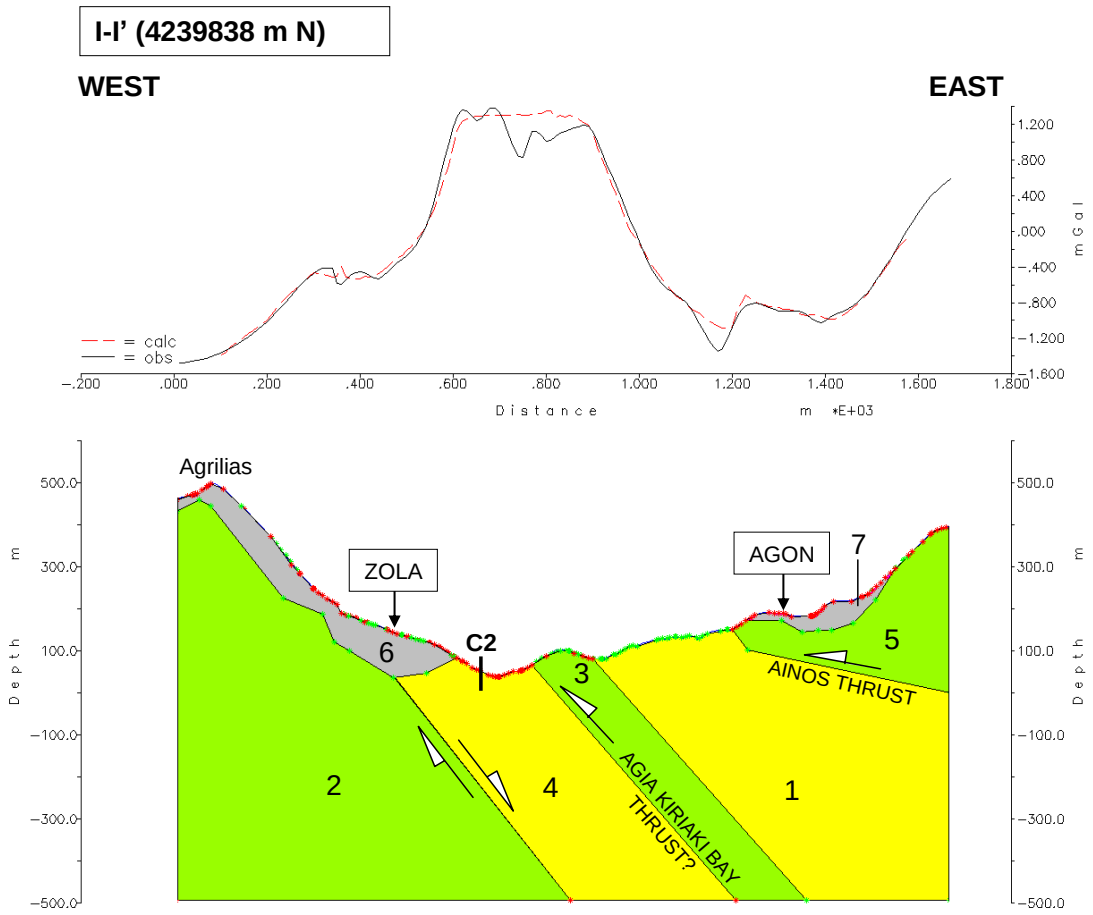

POLYGON DENSITIES AND GEOLOGICAL INTERPRETATION FOR I-I'

Polygon No.	Colour	Density (kg/m^3)	Lithology
BACKG		2.350	
1		2.180	Marl, clays
2		2.340	Limestone
3		2.550	Limestone (Agia Kiriaki Bay Thrust?)
4		2.480	Clay-rich marl interspersed with harder marl or limestone layers?
5		2.500	Limestone (Ainos Thrust)
6		1.700	Low density colluvium (Zola talus fan)
7		1.800	Low density colluvium (Angon talus fan)

Figure 4.40 Density profile produced by the Gravmag software for cross-section I-I' (4239838 m N): Bouguer-corrected residual gravity results for the cross-section (black) with modelled gravity line (red dashed line) resulting from polygon-constructed density profile (below). Details of the densities assigned to each polygon and interpretation of the model based on observations of surface geology and the results of the HEM survey are listed in the table. The location of this cross-section is given in Figure 4.37. The location of Borehole C2 is indicated in bold.

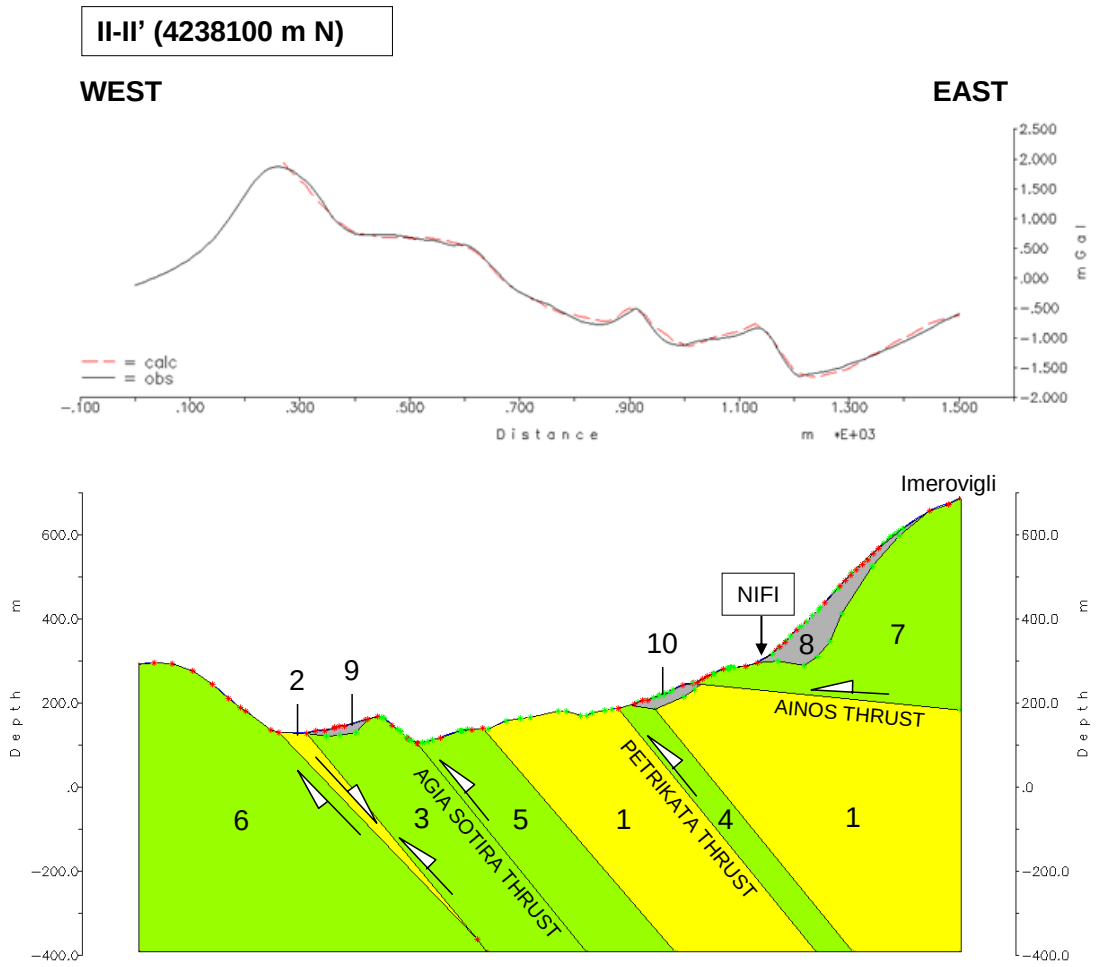

POLYGON DENSITIES AND GEOLOGICAL INTERPRETATION FOR II-II'

Polygon No.	Colour	Density (kg/m^3)	Lithology
BACKG		2.350	
1		2.210	Marl, clays
2		2.220	Marl, clays
3		2.260	Limestone
4		2.450	Limestone (Petrikata Thrust)
5		2.410	Limestone (Agia Sotira Thrust)
6		2.610	Limestone
7		2.360	Limestone (Ainos Thrust)
8		1.770	Low density colluvium
9		2.000	Low density colluvium
10		2.180	Low density colluvium

Figure 4.41 Density profile produced by the Gravmag software for cross-section II-II' (4238100 m N): Bouguer-corrected residual gravity results for the cross-section (black) with modelled gravity line (red dashed line) resulting from polygon-constructed density profile (below). Details of the densities assigned to each polygon and interpretation of the model based on observations of surface geology and the results of the HEM survey are listed in the table. The location of this cross-section is given in Figure 4.37.

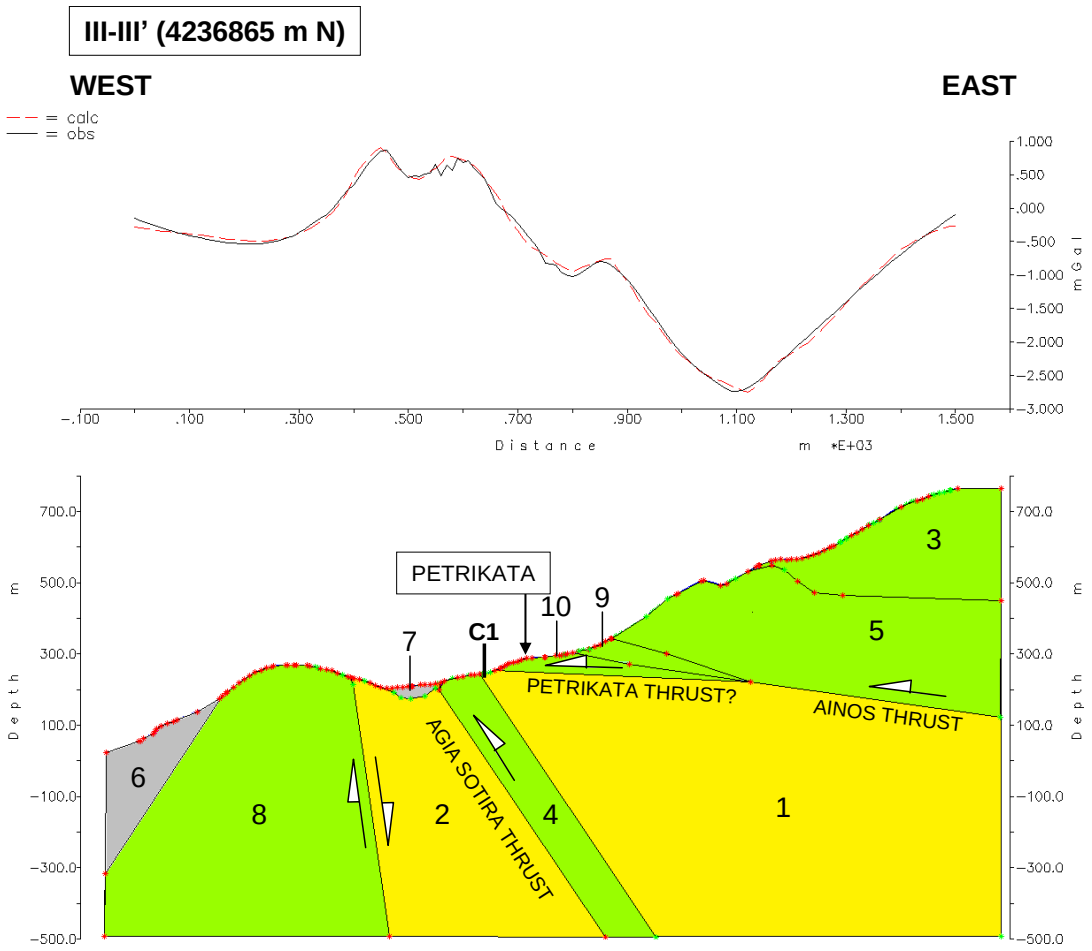

POLYGON DENSITIES AND GEOLOGICAL INTERPRETATION FOR III-III'

Polygon No.	Colour	Density (kg/m^3)	Lithology
BACKG		2.320	
1		2.220	Marl
2		2.545	Hard Marl?
3		2.500	Limestone
4		2.445	Limestone (Agia Sotira Thrust)
5		2.100	Limestone (less dense due to fracturing along Ainos Thrust plane?)
6		2.300	Low density colluvium within scalloped embayments along coast
7		1.650	Lacustrine sediments (Lake Katachori)
8		2.229	Limestone (less dense due to adundance of reefal material?)
9		2.415	Conglomerate/Limestone
10		2.050	Fractured limestone? Conglomerate? (Petrikata Thrust)

Figure 4.42 Density profile produced by the Gravmag software for cross-section III-III' (4236865 m N): Bouguer-corrected residual gravity results for the cross-section (black) with modelled gravity line (red dashed line) resulting from polygon-constructed density profile (below). Details of the densities assigned to each polygon and interpretation of the model based on observations of surface geology and the results of the HEM survey are listed in the table. The location of this cross-section is given in Figure 4.37. The location of Borehole C1 is indicated in bold.

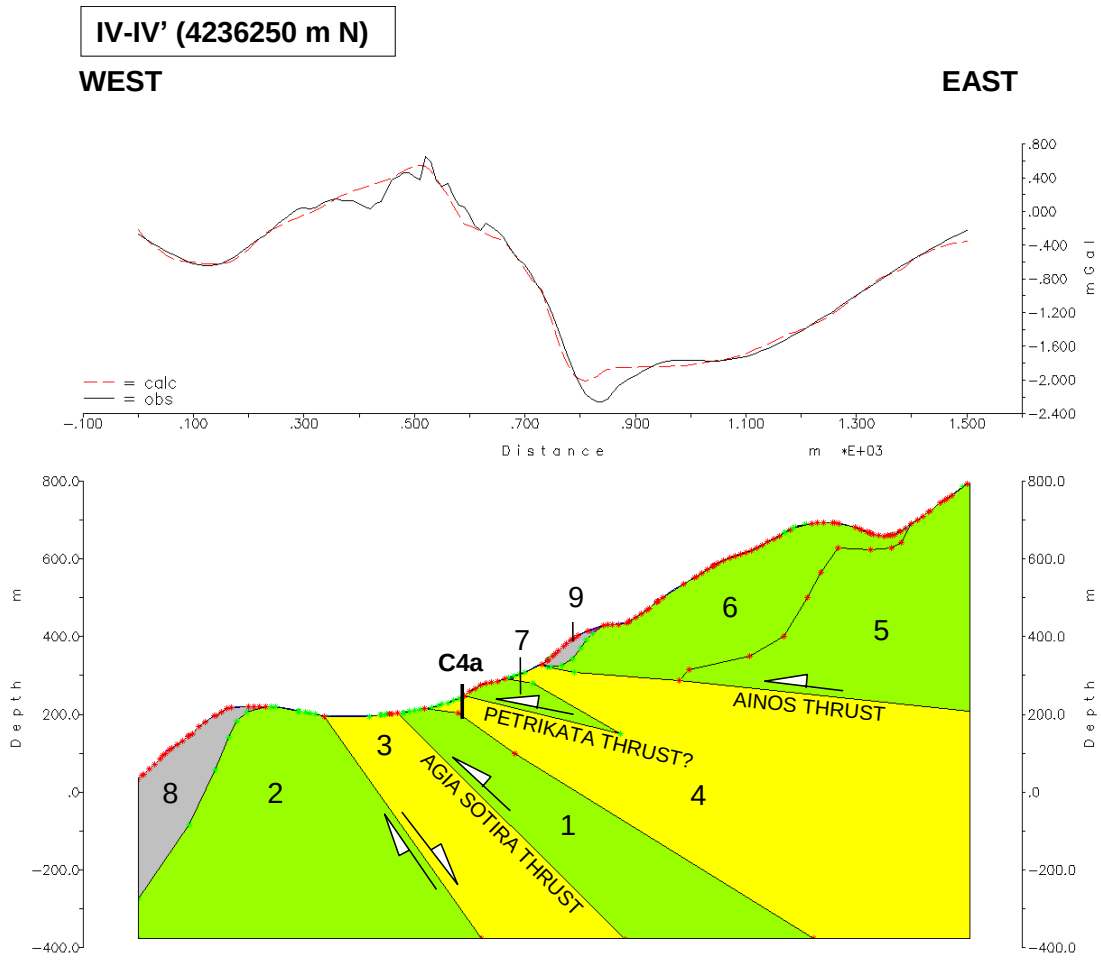

POLYGON DENSITIES AND GEOLOGICAL INTERPRETATION FOR IV-IV'

Polygon No.	Colour	Density (kg/m^3)	Lithology
BACKG		2.200	
1		2.050	Limestone (Agia Sotira Thrust)
2		2.200	Limestone
3		2.260	Marl
4		2.000	Marl
5		2.300	Limestone (Ainos Thrust)
6		2.090	Limestone (rotational slump?)
7		2.230	Limestone (Petrikata Thrust?)
8		2.000	Low density colluvium
9		1.590	Low density colluvium

Figure 4.43 Density profile produced by the Gravmag software for cross-section IV-IV' (4236250 m N): Bouguer-corrected residual gravity results for the cross-section (black) with modelled gravity line (red dashed line) resulting from polygon-constructed density profile (below). Details of the densities assigned to each polygon and interpretation of the model based on observations of surface geology and the results of the HEM survey are listed in the table. The location of this cross-section is given in Figure 4.37. The location of Borehole C4a is indicated in bold.

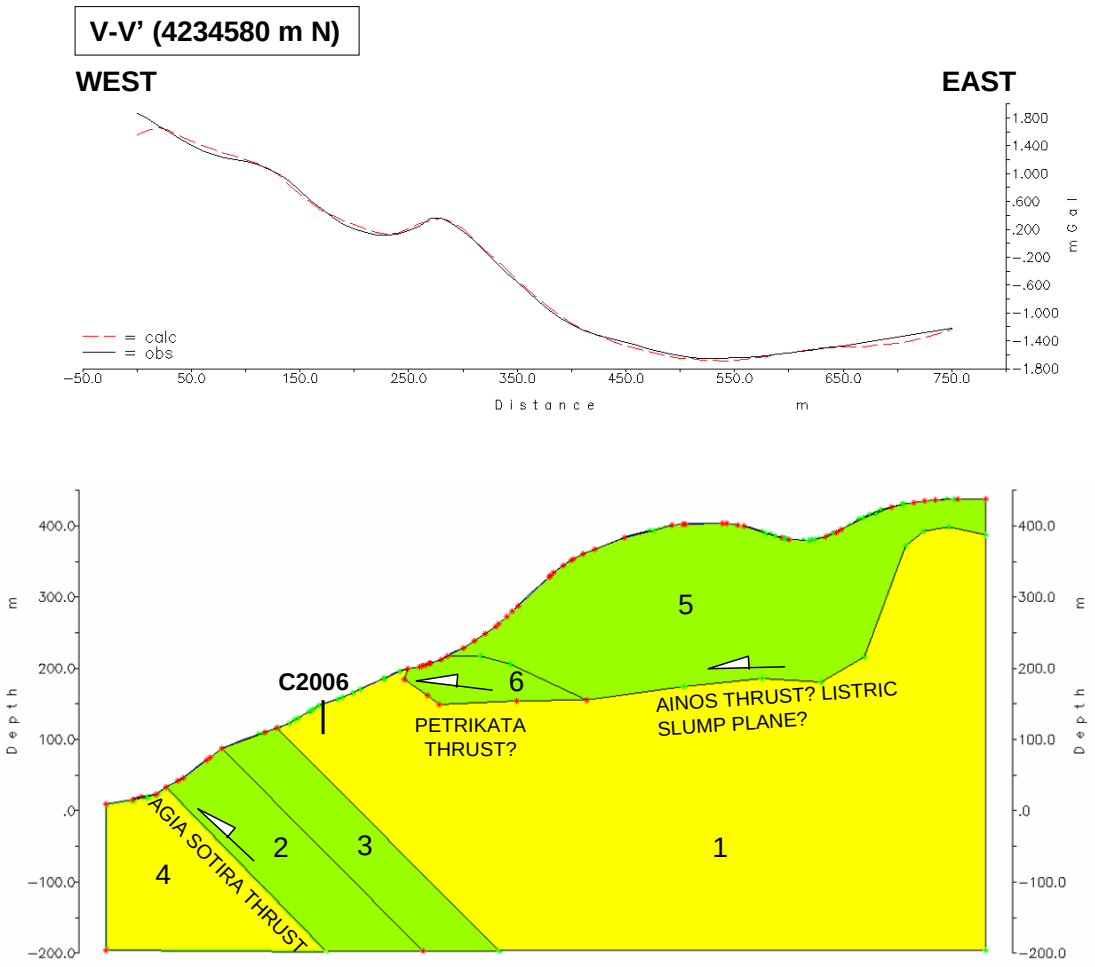

POLYGON DENSITIES AND GEOLOGICAL INTERPRETATION FOR V-V'

Polygon No.	Colour	Density (kg/m^3)	Lithology
BACKG		2.300	
1		2.200	Marl
2		2.450	Limestone
3		2.410	Limestone
4		2.680	Limestone
5		2.080	Limestone (Rotational slump?)
6		2.480	Conglomerate/limestone

Figure 4.44 Density profile produced by the Gravmag software for cross-section V-V' (4234580 m N): Bouguer-corrected residual gravity results for the cross-section (black) with modelled gravity line (red dashed line) resulting from polygon-constructed density profile (below). Details of the densities assigned to each polygon and interpretation of the model based on observations of surface geology and the results of the HEM survey are listed in the table. The location of this cross-section is given in Figure 4.37. The location of Borehole C2006 is indicated in bold.

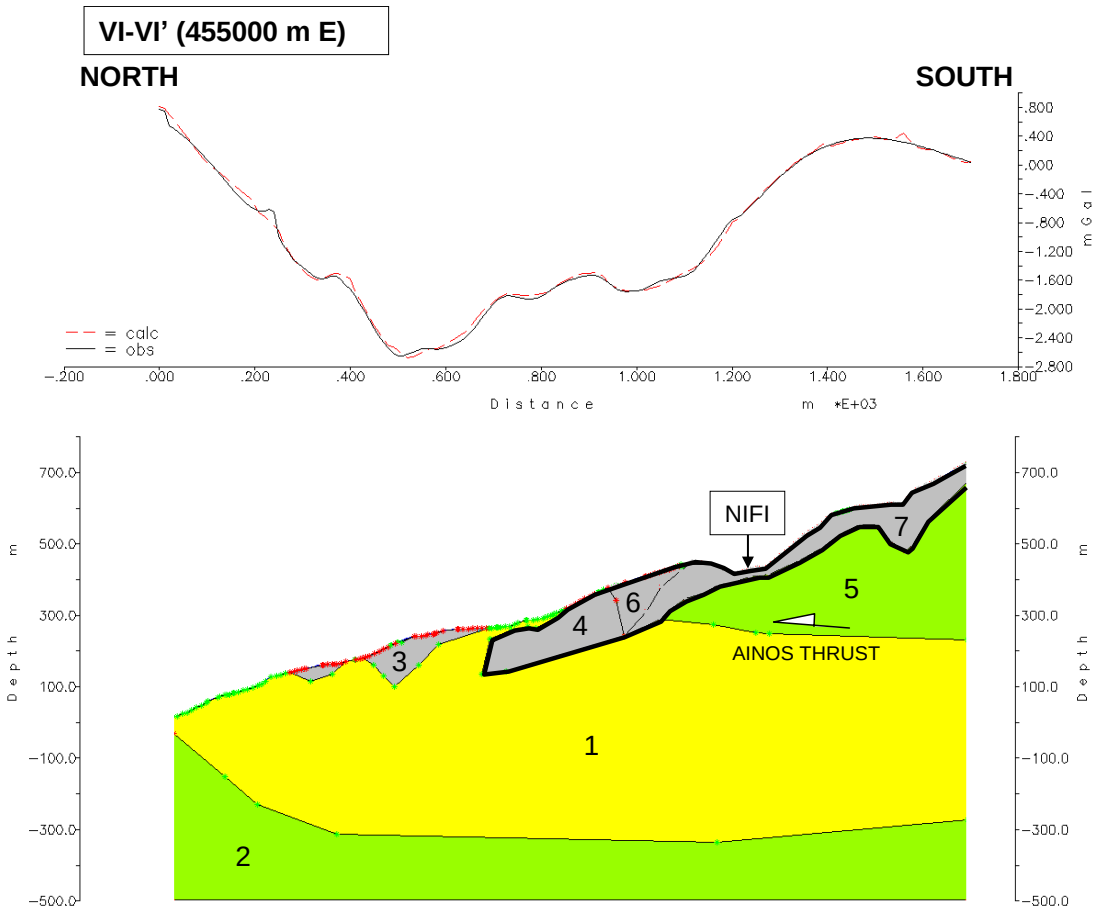

POLYGON DENSITIES AND GEOLOGICAL INTERPRETATION FOR VI-VI'

Polygon No.	Colour	Density (kg/m^3)	Lithology
BACKG		2.360	
1		2.160	Marls
2		2.690	Hard marls or limestone
3		1.900	Alluvium
4		2.500	Lithified edge of talus
5		2.700	Limestone (Ainos Thrust)
6		2.335	Talus material (finer-grained)
7		2.200	Alluvium/colluvium

Figure 4.45 Density profile produced by the Gravmag software for cross-section VII-VII' (455000 m N): Bouguer-corrected residual gravity results for the cross-section (black) with modelled gravity line (red dashed line) resulting from polygon-constructed density profile (below). Details of the densities assigned to each polygon and interpretation of the model based on observations of surface geology and the results of the HEM survey are listed in the table. The location of this cross-section is given in Figure 4.37.

4.5.3 Northern Thinia

A. Resistivity

The results of the Northern Thinia resistivity survey are presenting in Figures 4.46 to Figure 4.52 (top). Figure 4.46 illustrates a typical NW-SE dip line (NTL0). NTL0 was the northerly-most of the survey lines, positioned closest to the flattish near-shore part of the existing valley, and clearly shows the V-shaped topography displayed by all six dip lines. Figure 4.47 presents the NE-SW orientated strike line NTL1 which runs up the axis of the valley and was placed to connect the six dip lines. The topography of NTL1 ascends gradually from 18 m above sea level towards the raised central part of the valley reaching a maximum elevation of around 57 m and is incised by small V-shaped gullies where the survey line repeatedly cross-cut the modern stream gully.

The inverted resistivity profiles for the northern exit typically consisted of a thin (5 to 6 m) resistive (~100 Ωm to 1440 Ωm) surface layer which overlay predominantly low resistivity material (typically between 0.98 Ωm and 70 Ωm) which extended at least as far as the maximum imaging depth of the profiles (~35 m).

The resistive surface layer observed in all profiles was believed to represent landslide materials gathered at the base of the valley. This layer displayed a mottled appearance with the highest resistivities concentrated in a series of discrete, small (10 m or less) flattish ellipses a few metres in thickness. Some of these ellipses could be linked to the numerous 2 to 3 m high stone-build agricultural terraces or *pezoules* which are built into the steep sides of the modern stream valley. These terraces are very prevalent across western Kefalonia with many are associated with Venetians occupation (16^{th} and 17^{th} century) and some dating back as far as the Bronze Age (Souyoudzoglou-Haywood, 2000). This layer was generally thickest below the modern stream cut where it formed a resistivity wedge up to 12 m in depth. The uneven base of the resistive surface layer was defined by very closely-spaced contours and appeared to incise into the lower resistivity material beneath suggesting

this interface represented an eroded surface. At NTL0, this interface was around 3 below sea level. Moving southwards, the interface increased in elevation occurring at 24 m above sea level at the southerly-most line, NTL6.

The low resistivity material below this interface mirrored the HEM results which showed that the northern exit surveys cross-cut one of the NNE-SSW trending conductive, magnetic linear anomalies running along the axis of the northern valley. This response was probably tied into the alluvium deposits accumulated along the stream gullies or clay. Clay is one of the most electrically conductive sediments due to the electro-static charge of its fine-grained particles and typically exhibits resistivity values in the order of 1 to 100 Ωm.

Excessively low resistivity values (<5 Ωm) occurred directly below the modern stream and were probably related to the raised water table along the axis of the valley since as resistivity is a function of pore fluid, water-saturated sediments have a higher conductivity than their "dry" equivalent (Vickery, 2000). Some variation of the values occurred NTL3, NTL4 and NTL6 detected a slightly more resistive (~120 Ωm) anomaly at depth (around 20 m) on the eastern side of the profile overlain by the lower resistivity material. This might represent a more resistive stratigraphy such as harder marls or the northern progression of the Agia Sotira Thrust. It might also represent the base of the low resistivity "fill" suggesting the low response was due to a thick (~35 m) deposit of alluvium however not enough of this resistivity contrast was imaged to be sure.

The landslide-bedrock interface was interpreted as the tightly contoured zone between the resistive and underlying low resistivity "bedrock" as the strong contrast between these zones represented a clear break in the stratigraphy which may have been a depositional surface. The high, mottled resistivity signature of the surface veneer was the expected response from the non-invasive surveys for loosely-consolidated brecciated rubble. This is the only clear interface visible within the survey. However, this surface layer was very thin (5 to 6 m) suggesting the landslide material only formed a thin veneer. While this interface reached below sea level

along NTL0, moving southwards it increased in elevated to around 24 m above sea level. This is too high above sea level to fulfil the crucial requirement of "Strabo's Channel" colluvial deposits reaching Mycenaean sea level (-3.75 to 0 m). Even if 6 m of positive Late Holocene coseismic uplift has occurred since the time of Odysseus as speculated by Bittlestone et al. (2005) sea levels would still not be high enough to reach this interface and it therefore cannot be considered to represent the base of a buried marine Channel.

The lack of resistive landslide deposits at depth and the shallowness of this interface raised questions about how much of this stratigraphy was bedrock and how much was backfill. Another possibility was that the Channel was infilled with fine-grained, conductive alluvium rather than landslide debris having silted up rather than being buried at this location. The actual alluvium-bedrock interface may occur beyond the survey limits. However due to the similar physical properties of the marl bedrock in Thinia and the more recent alluvium it was not possible to distinguish between the two using the non-invasive surveys alone and this interface may have been higher but invisible in the surveys.

B. Seismic Refraction

The shot records for the northern exit seismic refraction survey were relatively free from noise and of good quality so the head wave arrivals could be picked with accuracy. The resulting tomographic inversions were considered to be a good representation of the subsurface with repeated inversions producing an RMSE of around 2 msec or less, consistently the lowest on average of the five surveys (Figures 4.46 to Figure 4.52, bottom). The highest RMSE (2.06 msec) was produced by the inversion of NTL1. This was partly due to the long length of this profile relative to the rest of the survey lines (1.1 km) and also due to an anomalous set of travel time curves near the centre of the line which may have been due to a large buried boulder near the surface or a steeply-dipping fault plane causing scattering of the seismic energy. The worst affected lines were removed from the shot record.

While the resistivity survey of the northern exit showed little variation in the resistivities of the subsurface beneath the surface layer, the seismic refraction survey showed structures within the subsurface in terms of P-wave velocity, in particular an increase in velocity from north to south demonstrating that while these strata had similar conductive properties, they had differing velocities.

The tomographically-inverted profiles showed that the first 5 to 15 m of the profile consisted of a low velocity zone (~0.30 to 1.80 km/s on average) under which was a relatively moderate velocity (~1.80 to 2.88 km/s) zone overlying a topographically-dramatic higher velocity zone (~2.95 to 3.20 km/s). Closer spacing of contours around the ridges formed by the higher velocity layer suggested a geological boundary. NTL6 detected the subsurface continuation of the easterly dipping limestone of the western valley side imaging this as a zone of higher velocity relative to the reasonably low velocities of the rest of the survey.

The RMSE for the time-term inversion method was generally higher and this was a reflection on how clear the layers were. The time-term inversion of NTL3 in the centre of the survey (Figure 4.53) resolved the profile into 3-layers: Layer 1 = 0.32 km/s, Layer 2 = 1.76 km/s and Layer 3 = 2.16 km/s. Layer 1 was interpreted to represent the ~2 m thick resistive layer detected in the equivalent resistivity survey composed of colluvium-rich surface soils and gravel-rich clays. Similarly to the resistivity profiles the base of this layer followed the surface topography and was defined by very closely-spaced contours. The shallowness of this layer meant that the refraction profiles were not above to resolve this layer in the same degree of detail as the equivalent resistivity profiles. Layer 2 was interpreted as (unconsolidated) marls and clays. Layer 3 was interpreted as bedded marls.

NTL1 was resolved into a similar configuration (Figure 4.54). Layer 1 was thicker on the northern half of this profile reflecting the thicker accumulation of alluvial clays southwards. This step up suggested the presence of a faulted structure. This step coincided with the NW-SE striking, structural feature causing NW-offset of the suspected NE-SW striking normal fault at Zola.

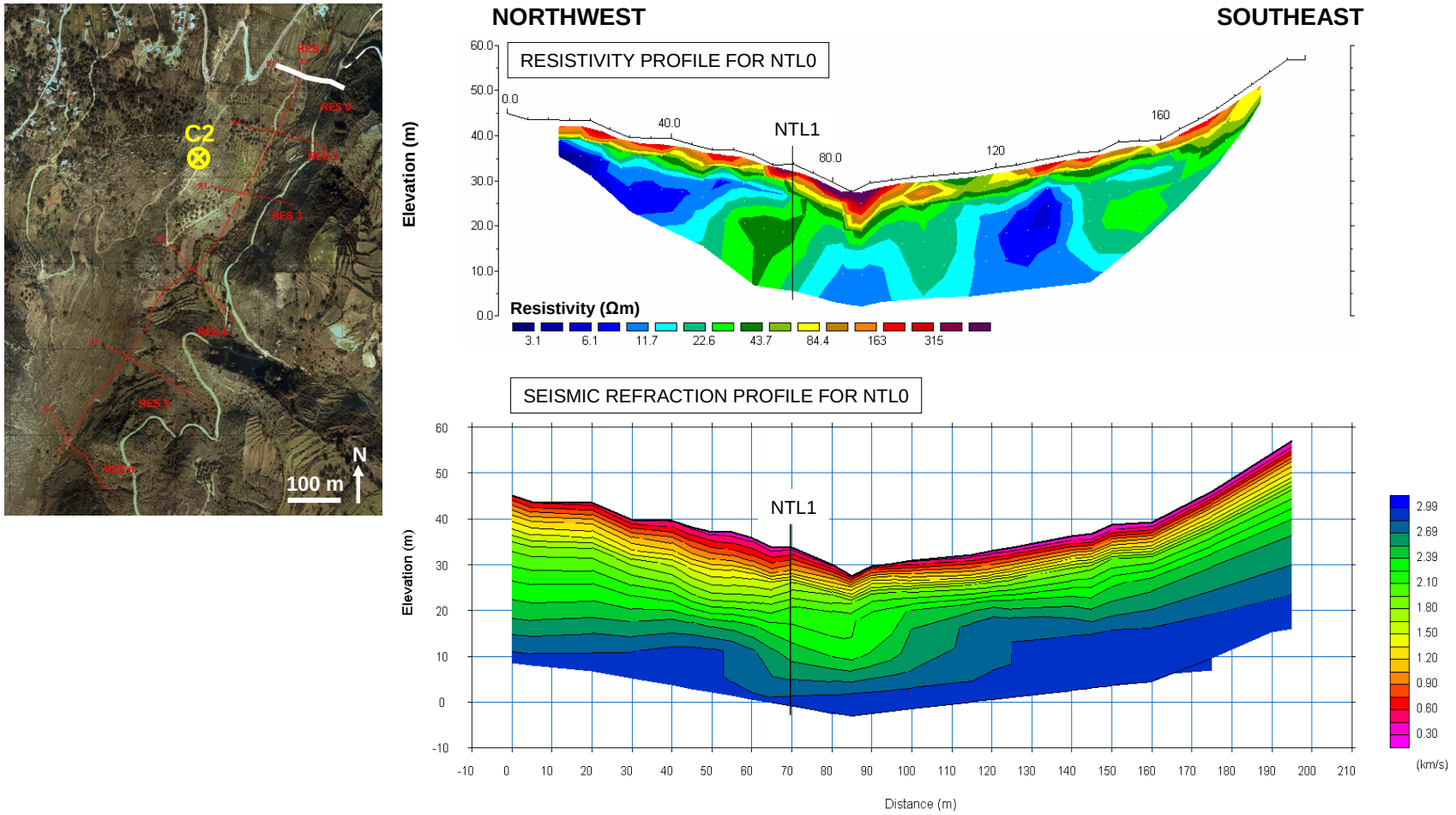

Figure 4.46 2D resistivity profile (top) and corresponding seismic refraction profile (bottom) for Northern Exit profile, NTL0. Elevation/depth is in terms of elevation above mean sea level (where mean sea level is +22 m above present sea level). The location of this survey line is indicated in the map inset. Vertical exaggeration is V/H = 1. Vertical black lines indicate where the profile crosses another profile.

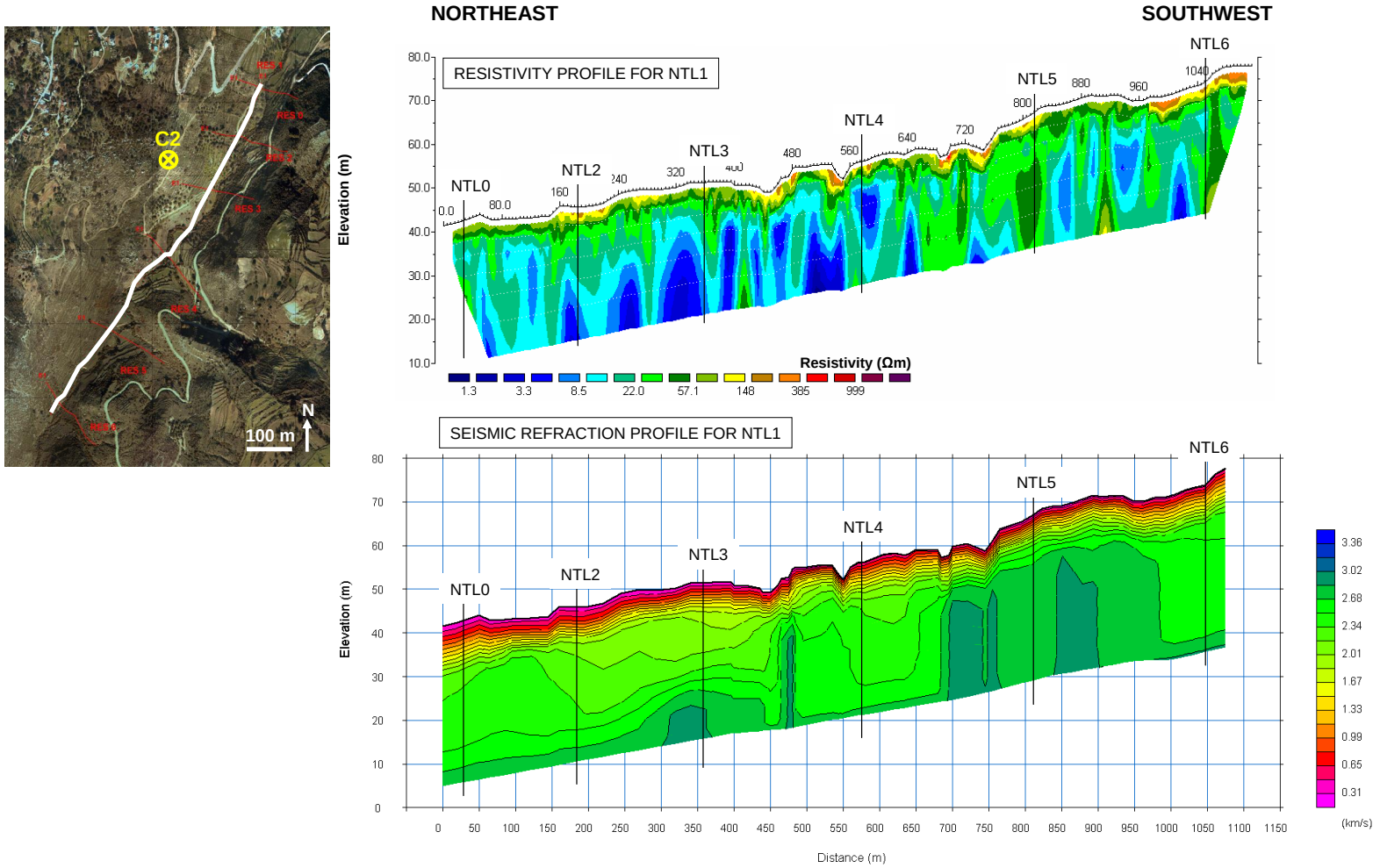

Figure 4.47 2D resistivity profile (top) and corresponding seismic refraction profile (bottom) for Northern Exit profile, NTL1. Elevation/depth is in terms of elevation above mean sea level (where mean sea level is +22 m above present sea level). The location of this survey line is indicated in the map inset. Vertical exaggeration is V/H = 6. Vertical black lines indicate where the profile crosses another profile.

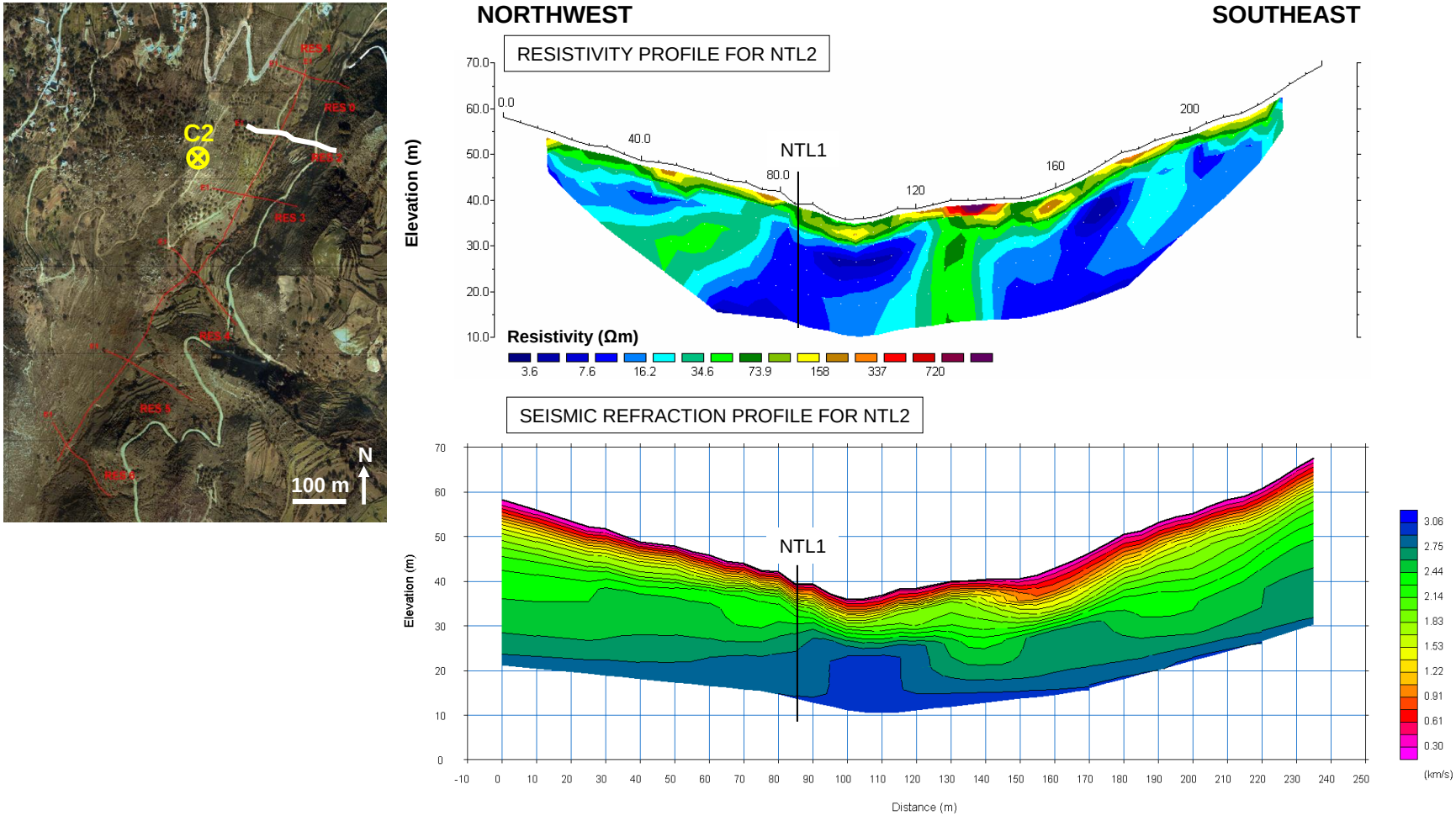

Figure 4.48 2D resistivity profile (top) and corresponding seismic refraction profile (bottom) for Northern Exit profile, NTL2. Elevation/depth is in terms of elevation above mean sea level (where mean sea level is +22 m above present sea level). The location of this survey line is indicated in the map inset. Vertical exaggeration is V/H = 1.2. Vertical black lines indicate where the profile crosses another profile.

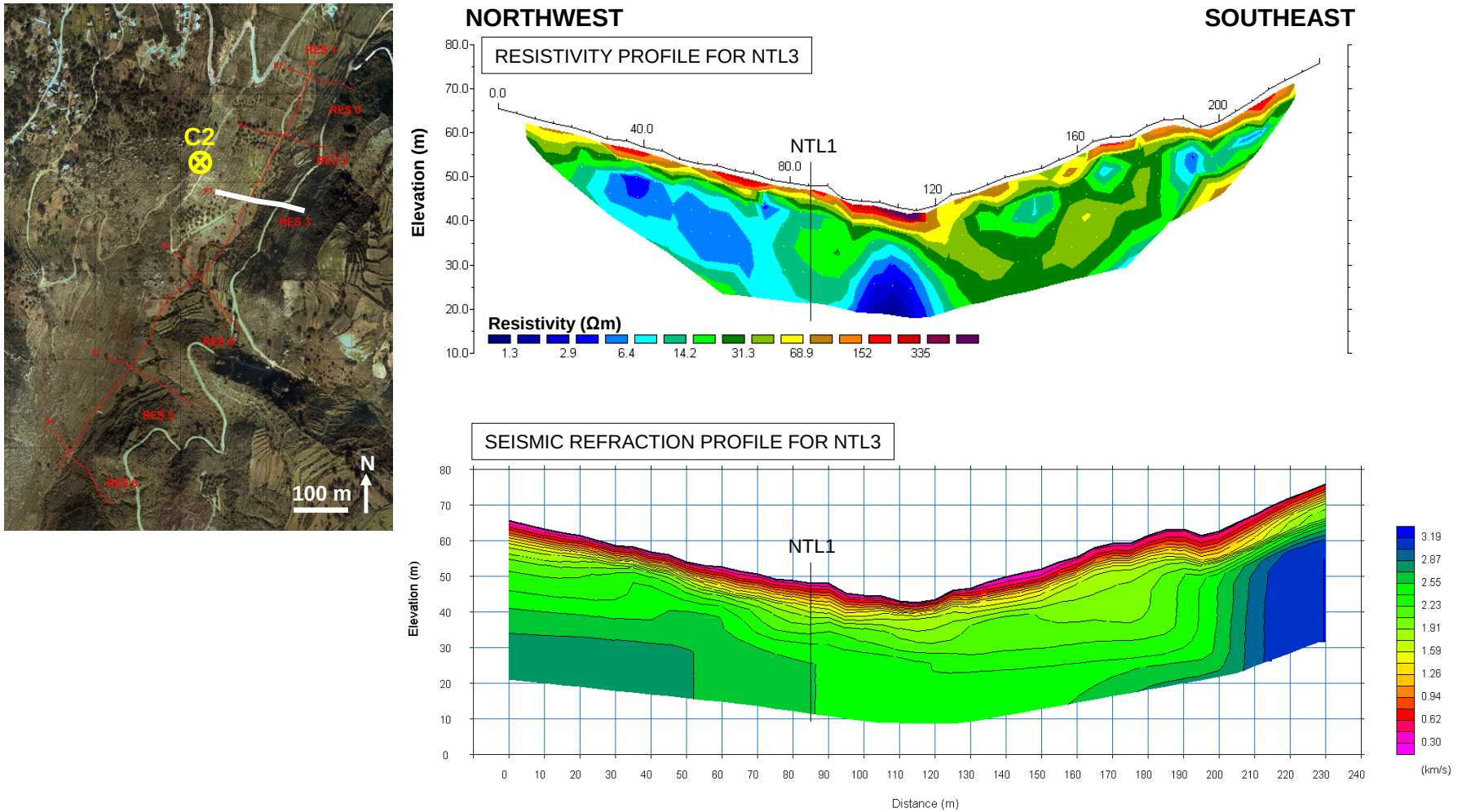

Figure 4.49 2D resistivity profile (top) and corresponding seismic refraction profile (bottom) for Northern Exit profile, NTL3. Elevation/depth is in terms of elevation above mean sea level (where mean sea level is +22 m above present sea level). The location of this survey line is indicated in the map inset. Vertical exaggeration is V/H = 1.2. Vertical black lines indicate where the profile crosses another profile.

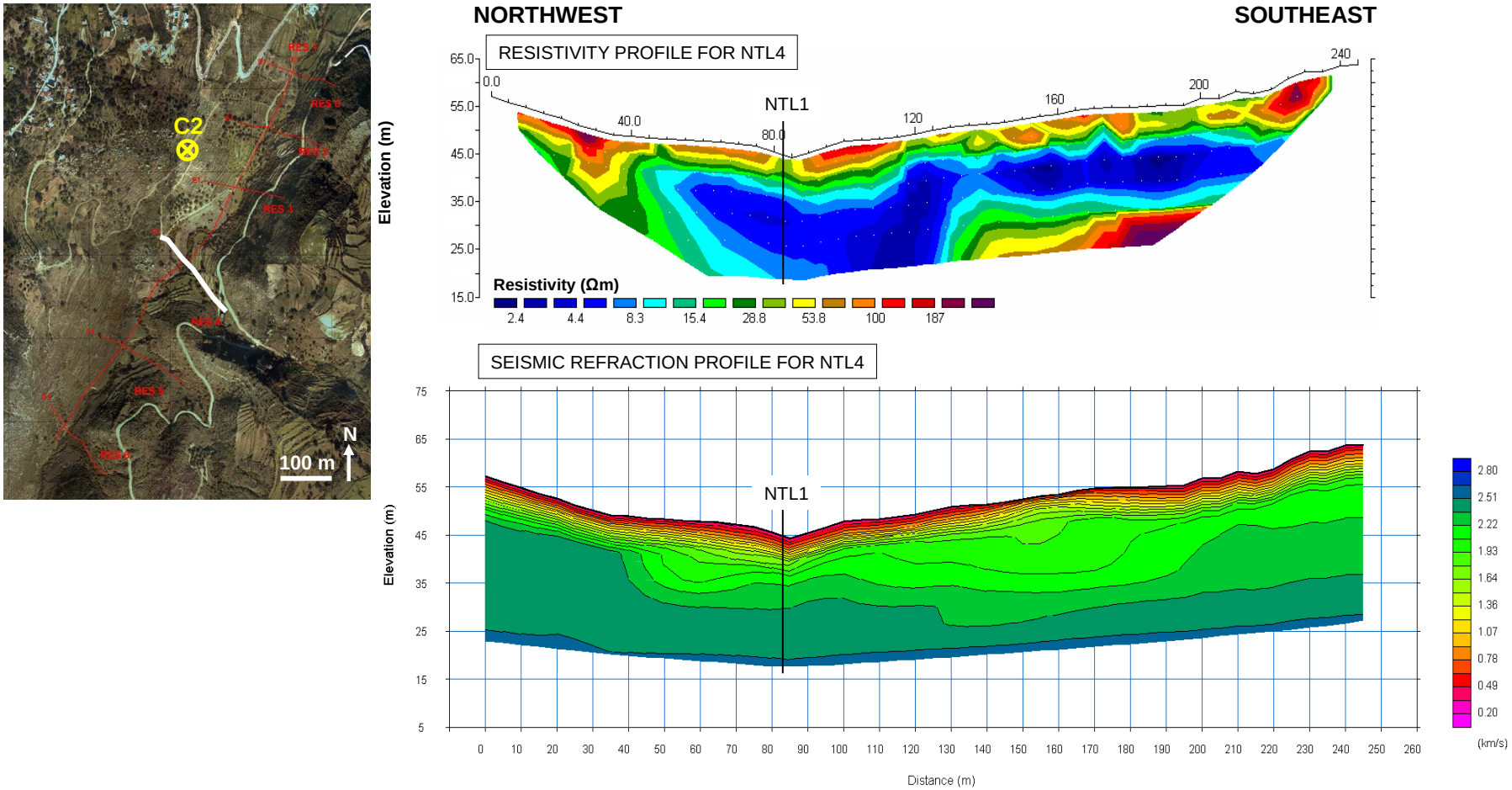

Figure 4.50 2D resistivity profile (top) and corresponding seismic refraction profile (bottom) for Northern Exit profile, NTL4. Elevation/depth is in terms of elevation above mean sea level (where mean sea level is +22 m above present sea level). The location of this survey line is indicated in the map inset. Vertical exaggeration is V/H = 1.2. Vertical black lines indicate where the profile crosses another profile.

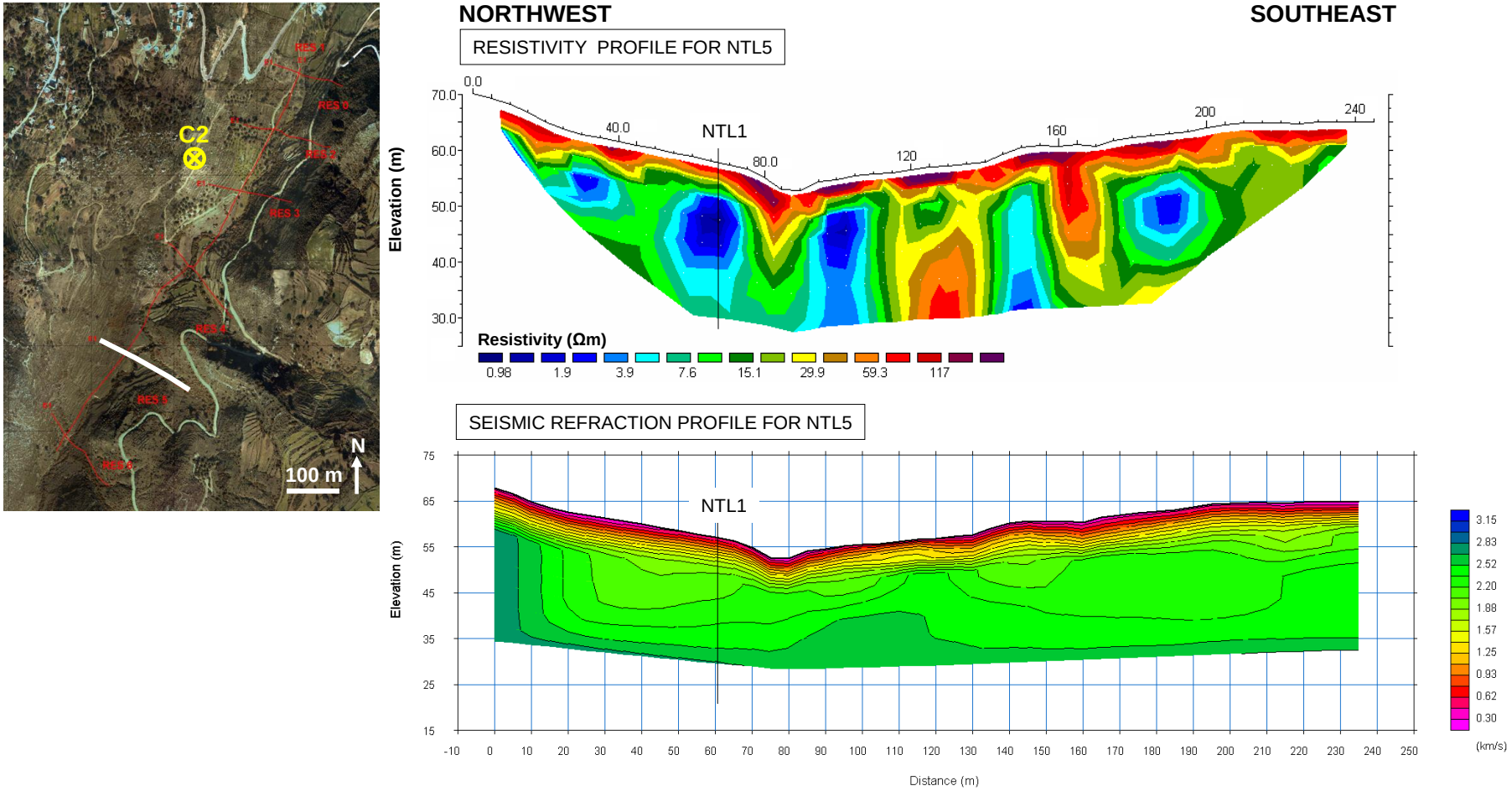

Figure 4.51 2D resistivity profile (top) and corresponding seismic refraction profile (bottom) for Northern Exit profile, NTL5. Elevation/depth is in terms of elevation above mean sea level (where mean sea level is +22 m above present sea level). The location of this survey line is indicated in the map inset. Vertical exaggeration is V/H = 1.5. Vertical black lines indicate where the profile crosses another profile.

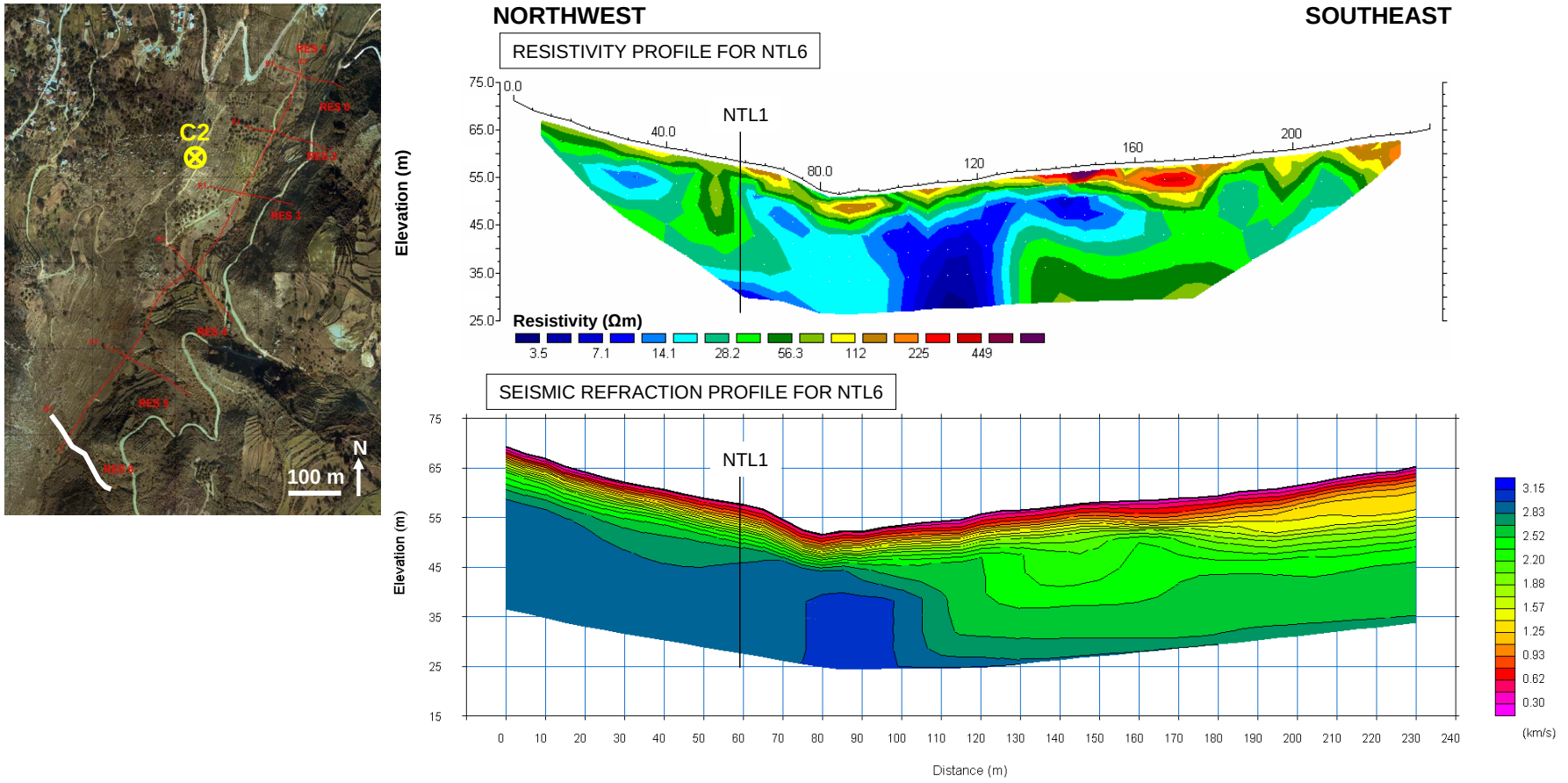

Figure 4.52 2D resistivity profile (top) and corresponding seismic refraction profile (bottom) for Northern Exit profile, NTL6. Elevation/depth is in terms of elevation above mean sea level (where mean sea level is +22 m above present sea level). The location of this survey line is indicated in the map inset. Vertical exaggeration is V/H = 1.2. Vertical black lines indicate where the profile crosses another profile.

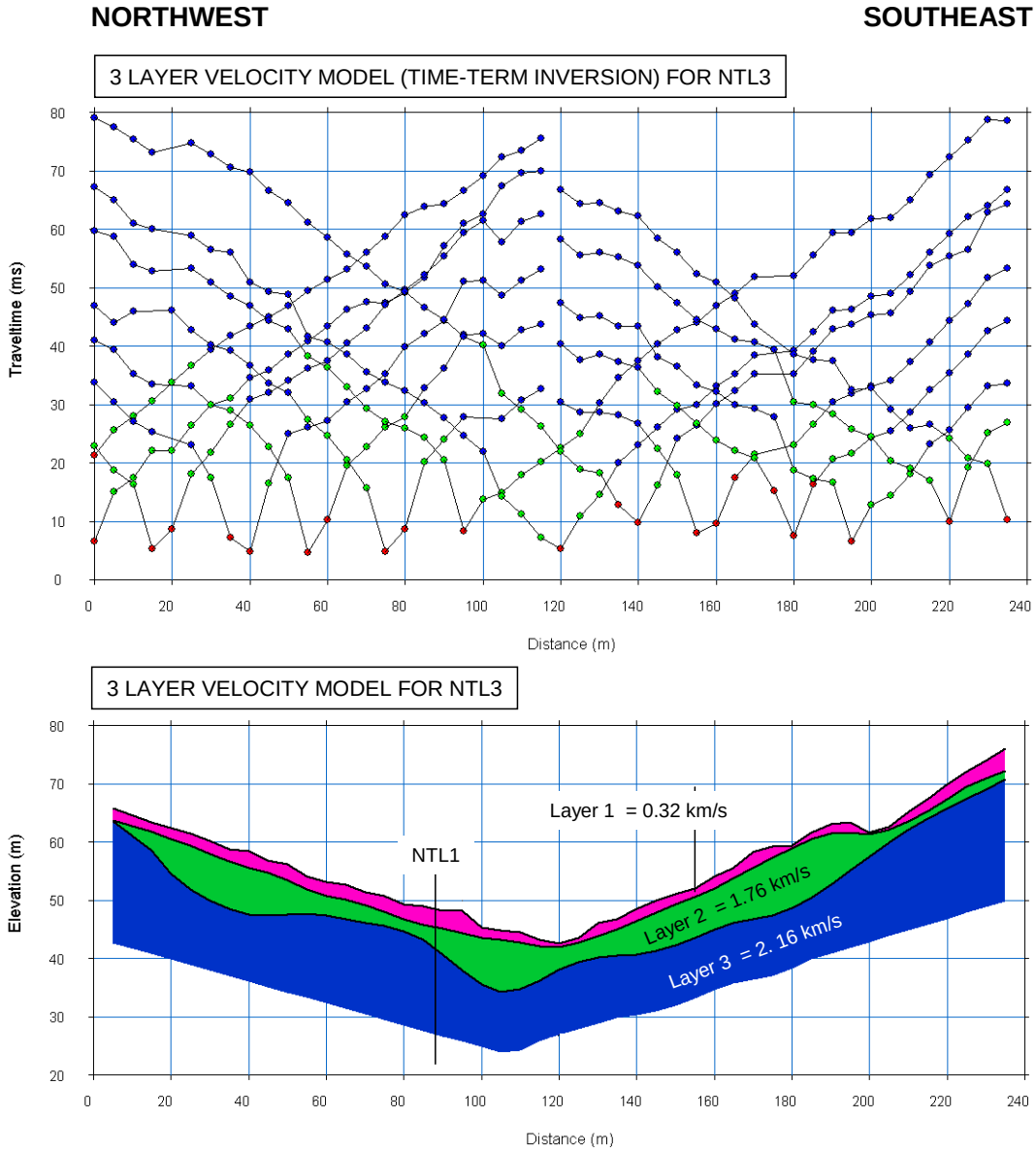

Layer assignment:

Layer 1 = Soils, colluvium.

Layer 2 = Marl, clays, poorly consolidated material, some limestone clasts.

Layer 3 = Bedded hard marls?

Figure 4.53 Time-term inverted profile for NTL3 (coloured section) with corresponding traveltime graphs (top) showing layer selection where red = layer 1, green = layer 2 and blue = layer 3. Layers are tentatively assigned possible lithologies based on the P-wave velocities for each layer. The location of this line is given in Figure 4.49. Vertical black lines indicate where the profile crosses another profile.

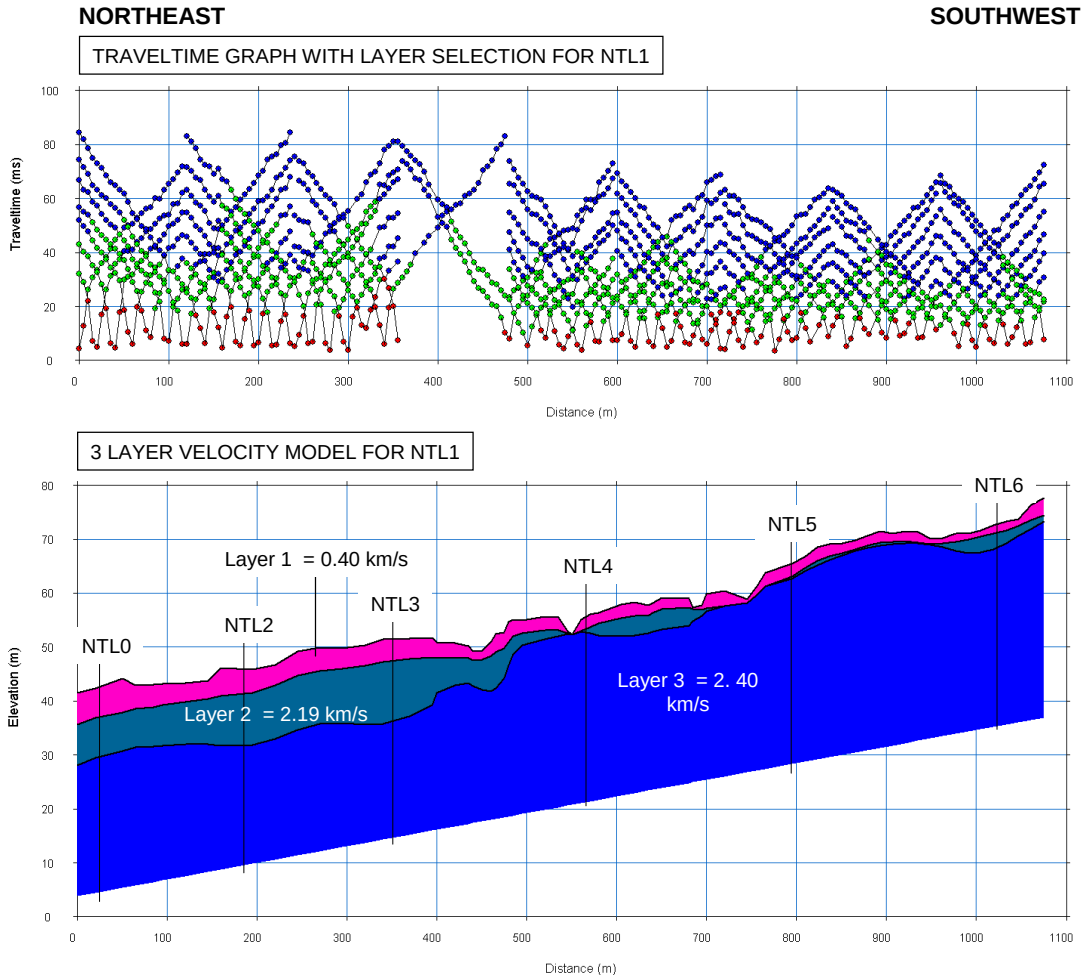

Layer assignment:

Layer 1 = Soils, colluvium.

Layer 2 = Marl, clays, poorly consolidated material, some limestone clasts.

Layer 3 = Hard marls? Limestone?

Figure 4.54 Time-term inverted profile for NTL1 (coloured section) with corresponding traveltime graphs (top) showing layer selection where red = layer 1, green = layer 2 and blue = layer 3. Layers are tentatively assigned possible lithologies based on the P-wave velocities for each layer. The location of this line is given in Figure 4.47. Vertical black lines indicate where the profile crosses another profile.

C. Gravity

These survey lines cross-cut the NE-SW trending positive anomaly which follows the course of the modern outwash stream along the axis of the northern valley which was associated thrusting (Figure 4.55). Two NE-SW orientated negative anomalies

(0 to -1.5 mGals) occur – one below the Zola talus fan which exits at Zola harbour and the other running beneath the low marl hills to the east of the stream (Figure 4.56). This suggests that the low gravity anomaly on the western side of the survey relates to a shallower low density feature than the eastern negative anomaly, possibly relating to the low density material of the Zola talus fan.

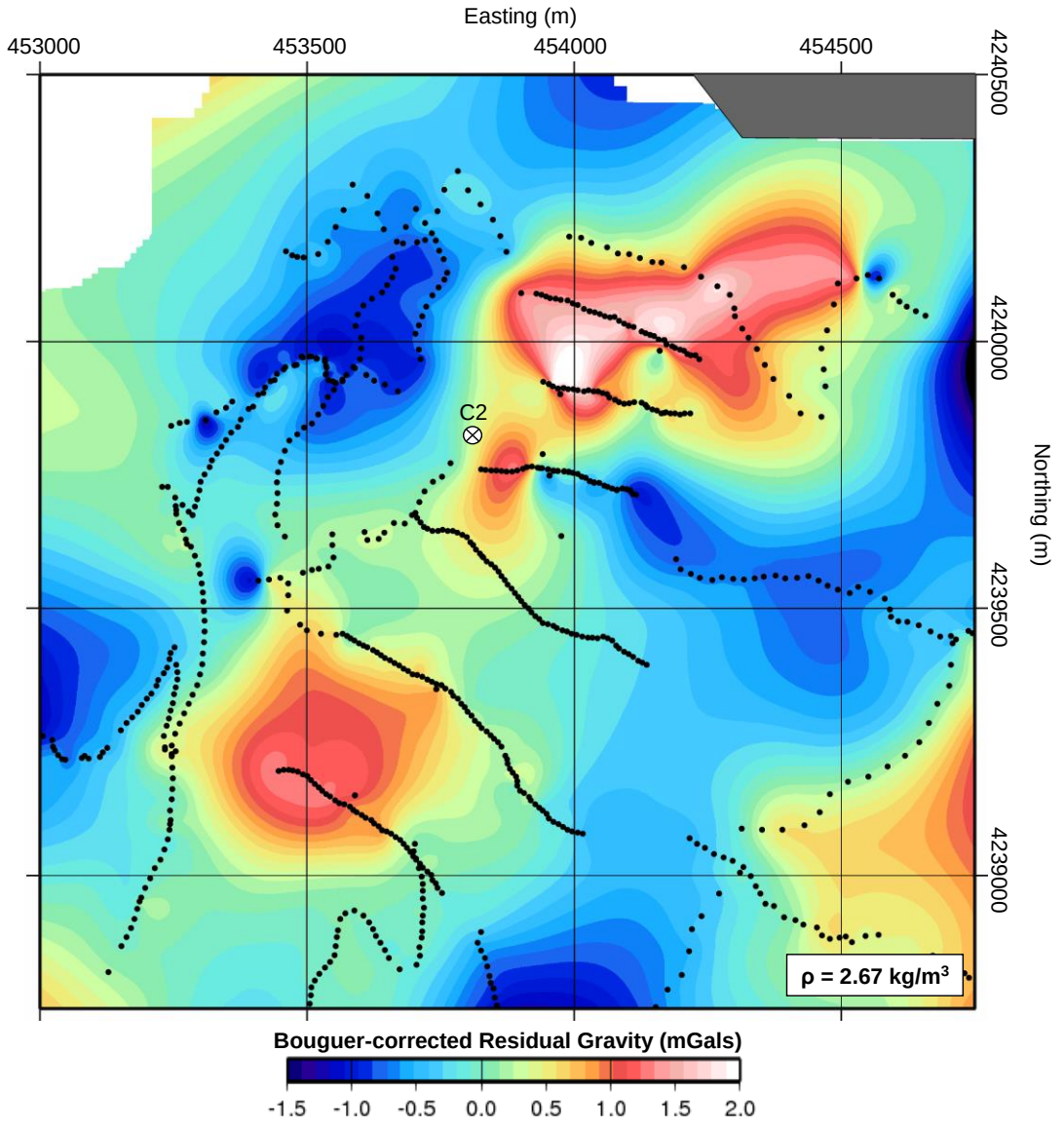

Figure 4.55 Bouguer-corrected residual gravity map in terms of mGals ($\rho = 2.67$ kg/m^3) showing data coverage of the gravity survey at the proposed Northern Exit. Gravity stations are indicated as black dots. The location of borehole C2 is shown.

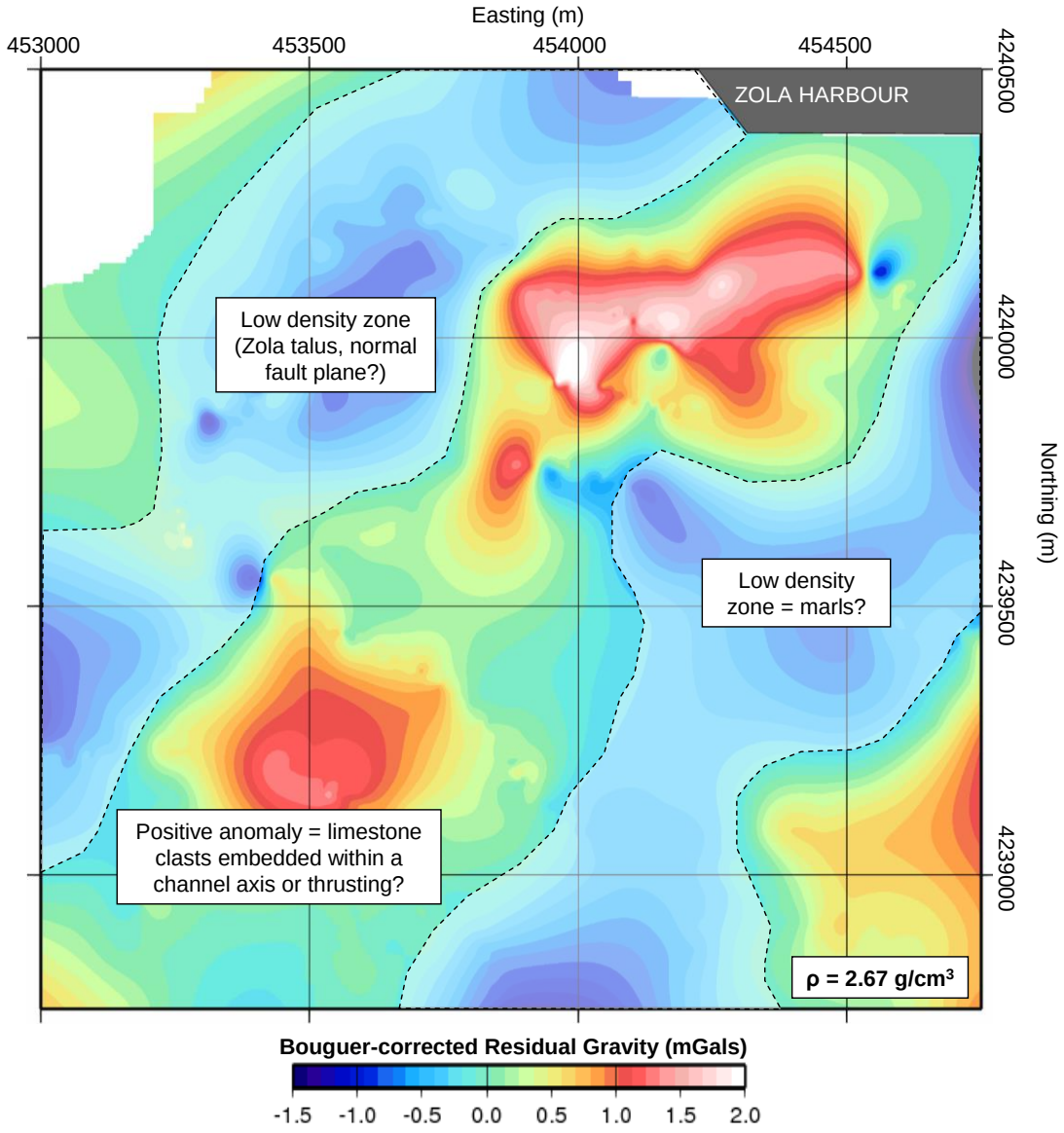

Figure 4.56 Interpreted version of the Northern Exit gravity response. The positive response may be a reflection of dense clastic material within a channel axis.

4.5.4 Lake Katachori

A. Airborne Overview

The response of the lake was partially missing due to the data gap corresponding to the village of Kardakata. The course resolution of the HEM maps at this small scale could not resolve the lake in detail. The response from the magnetic survey (Figure 4.57, a) was difficult to interpret due to interference caused by nearby habitation and

because the magnetic signal of subtler features was swamped by the strong magnetic response of the saddle region. The lake sat within a zone of strongly magnetic (red, ~20 nT) sediment which tied into the thick accumulation of *terra rossa* present within the saddle region which was dissected by a tenuous less magnetic linear anomaly which ran roughly parallel to the long axis of the lake which may have tied into the Agia Sotira Thrust. The most striking feature was a strongly magnetic (40 nT) linear anomaly which exited from the northern tip of the lake and followed the deeply-incised drainage gully to the north. This response was due to an accumulation of *terra rossa* sediments along this gully derived from the lake and was interpreted as a possible surface outflow for the lake area during times of heavy rainfall.

The apparent resistivity values associated with Lake Katachori were some of the lowest in the Northern Paliki survey (Figure 4.57, b to d). In the 140 kHz map the "lake fill" appeared as a NE-SW orientated lens of very low resistivity (red-orange to yellow, ~1 to 10 Ωm) bounded by moderate to highly resistive bedrock (green to blue, 100 to 100 000 Ωm). The very low resistivity signal suggested the lake fill was predominately composed of fine-grained clay or silt. This low resistivity response could be seen in all frequencies indicating that these conductive sediments were at least 80 to 100 m in thickness. With decreasing frequency the lateral extent of this conductive material diminished and moved eastwards suggesting a more resistive easterly-dipping surface ran beneath the lake. The absence of a strong resistive contrast at the lowest frequencies suggested this material may have extended even deeper.

Two narrow conductive (yellow, 10 to 30 Ωm) linear anomalies (marked by black arrows in Figure 4.28) could be seen in the highest frequency maps emanating from the north and south of the lake. These corresponded to the alluvium-filled drainage gullies exiting from the northern tip of the lake and to the west of the Agia Sotira Thrust respectively. The conductive anomaly draining southwards formed a series of conductive "bright spots" which may have related to disruption of the fine-grained sediments such as colluvial deposits within this gully.

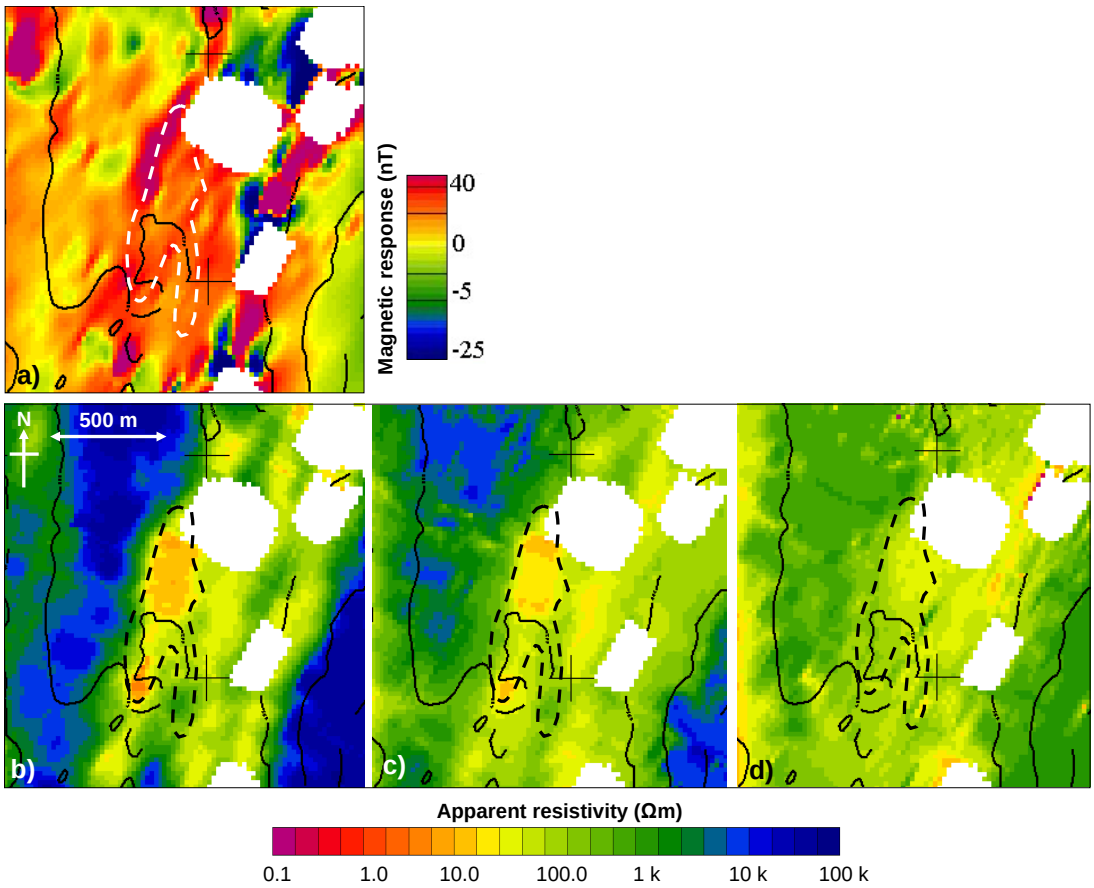

Figure 4.57 Results of the helicopter-mounted electromagnetic (HEM) survey for Lake Katachori: a) Magnetic results; Apparent resistivity maps for 140 kHz (b), 8200 Hz (c) and 400 Hz (d). Lake Katachori is indicated by a black dashed line. Contours at 100 m intervals.

The western shore of the lake was particularly well defined in the highest frequency maps as a striking curvi-linear contact between the conductive lake fill and highly resistive limestone, a contact which could be seen at the surface. The eastern limit of the conductive lake fill was less well-defined and coincided with a moderately resistive linear anomaly which ran along the eastern side of the lake. This anomaly tied into the resistive ridge formed by the Agia Sotira Thrust and the terraces on the eastern side of the lake and was therefore interpreted to represented the portion of the thrust buried by lake sediment. To the east of the thrust was another "channel" of conductive sediment at least 80 to 100 m in depth which appeared to be separate from the lake sediments. This may suggest Lake Katachori was contained to the west of the Agia Sotira Thrust allowing the lake and "Strabo's Channel" to co-exist on either side of this thrust.

B. Resistivity

The resistivity profiles for Lake Katachori are presented in Figures 4.58 to 4.64 (top). Softer top soils (due to intensity of agricultural activity) ensured good infiltration of the electrodes however dryness of the soil at times led to some instances of poor electrode contact. This caused localised spots of anomalously high resistivity (1000+ Ωm) at the surface at particular electrode positions which were detected during testing of how well the electrodes made ground contact before running of the survey. This was minimised by dampening the soil around the electrode. Metal fencing surrounding the small land-holdings presented obstruction to the positioning of lines and possible electrical signal noise.

There was a greater variation of resistivity values detected by the Lake Katachori survey compared with the resistivities detected by the northern exit survey indicating significant changes in the geology beneath the surface of this site. The seven resistivity profiles generally comprised of a thin (2 to 3 m) resistive (~70 Ωm and greater) surface layer attributed to the loose, heavily farmed top soils which overlay very low resistivity material (dark blue to pale blue, ~1 to 25 Ωm) contained between resistive (yellow to purple, ~40 to 16 000 Ωm) anomalies.

This low resistivity material underlying this layer was initially interpreted as the conductive "lake fill" and the resistive anomalies were interpreted as the sides of the lake. Of the E-W orientated lines placed to cross-cut the lake fill, LKL4 and LKL3 detected the deepest deposit of this sediment which extended at least 30 m in depth. Because these lines could not image deep enough to resolve the base of this material, presumed initially to be the lake bed, lines LKL6 and LKL7 were deployed. These lines were positioned parallel to the lake's long axis and located according to where the thickest lake fill was detected. This was determined using a rough on-site inversion of the resistivity data using the RES2DINV software's basic least squares inversion with no altering of the default software parameters. The longer length of these lines increased the imaging depth of these profiles up to 40 m however they were still unable to resolve the base of the low resistivity lake fill. Moving

southwards, the lake fill became separated into isolated, narrow vertiginous lobes by resistive anomalies.

One of these anomalies corresponded to the buried limestone ridge of the Agia Sotira Thrust hangingwall. This feature was best imaged by LKL1 and LKL2 and appeared on the eastern side of the E-W profiles as a very resistive (yellow to purple, ~100 to 16 000 Ωm) ~100 m wide, vertiginous-sided block extending from near the surface to beyond the maximum imaging depth of the profiles (~30 m). Moving northwards, the anomaly diminished in width and strength. This anomaly coincided with the easterly of the resistive (100 to 10000 Ωm) NNE-SSW orientated linear anomalies detected by the HEM apparent resistivity maps. The very high resistive values recorded were most likely a reflection of the strongly brecciated nature of the limestone within the hangingwall near a characteristic observed in the exposed parts of this ridge. This survey confirmed that the substantial terraces defining the eastern side of the lake were probably caused by this thrust.

To the east of this thrust block was another low resistivity (~1 to 20 Ωm) zone partially disconnected from the majority of the lake fill which coincided with the NNE-SSW striking conductive linear anomaly imaged by the HEM which ran along the eastern side of the thrust.

The subsurface continuation of the contact between the conductive lake fill and limestone defining the western shore could be clearly seen in the E-W resistivity profiles as an easterly-dipping resistive (~100 to 16 000 Ωm) anomaly underlying the low resistivity sediment. The uneven contact suggested the weathered surface observed at the surface continued below the lake fill. This contact ran from the surface to beyond the maximum imaging depth of the E-W profiles. It was imaged by LKL7 around 10 m below ground-surface, where it formed a roughly horizontal layer, and partially in LKL6. The marked change in steepness of the subsurface continuation of this contact (~45° in LKL1) relative to the visible surface of this ridge (~ 20°) suggested that the lake fill sediments either onlapped the slope break of

an easterly-dipping normal fault scarp with a similar orientation to the Agia Sotira Thrust or that it represented a particularly eroded part of the ridge.

LKL1 and LKL2 revealed a further high resistivity (100 to 240 Ωm) anomaly present within the low resistivity sediments on the western side of the profile which was not recorded by the HEM survey. This anomaly might represent another easterly-dipping thrust fault, a deposit of colluvial debris or a facies change within the lake sediments from fine to coarser-grained sediment.

C. Seismic Refraction

The seismic refraction profiles for Lake Katachori are presented in Figure 4.58 to Figure 4.64 (bottom). The proximity of the main road and habitation caused some interference of the signal as the lake bed sediments were affected by the vibrations of passing traffic however the shot records were generally free of noise and first breaks could be picked with reasonable accuracy. There was some scattering of the seismic signal in the vicinity of the Agia Sotira Thrust (LKL4) and the worst affected travel times were deleted. This site consistently produced the highest RMSE values during tomographic inversion with the highest (3.91 msec) produced by the inversion of LKL1. As the resulting velocity models correlated well with the corresponding inverted resistivity profiles this suggested that the higher RMSE produced by the Lake Katachori lines was due to the faulted geology beneath the lake which the refraction technique struggled to resolve such as the Agia Sotira Thrust which emplaced limestone with its relatively high P-wave velocity over “slower” marls.

The E-W orientated seismic refraction profiles revealed a zone of low velocity sediment (0.30 to 2.50 km/s) which sat within an asymmetric higher velocity basin-like structure. The eastern side of the profiles was defined by a vertiginous high velocity anomaly which correlated to the resistive anomaly detected by the resistivity survey and associated with the subsurface continuation of the Agia Sotira Thrust. The western side of this basin was defined by an easterly-dipping layer higher

velocity layer onto which the low velocity sediment onlapped which correlated to the limestone-marl contact defining the western lake shore.

In the expectation that a simple three-layer model (consisting of lake fill, marl, limestone) would resolve the subsurface of the lake, the data was also inverted using the time-term method. Like the tomographic method, the time-term inversion also had difficulty resolving the faulted structures beneath the lake. However, the presence of a layer within the low velocity sediment prevented further layers from being resolved. The traveltime curve for LKL1 in particular revealed the presence of a deeper fourth layer which may have related to the underlying limestone. The time-term method resolved the subsurface of the lake into three layers: Layer 1 = 0.30 km/s, Layer 2 = 1.76 km/s and Layer 3 = 2.04 km/s which was a very similar range of average velocities found at the northern exit survey. The low resistivity "lake fill" sediments roughly correlated to layers 1 and 2. The average velocity for layer 1 and 2 were very similar suggesting they were composed of the same lithology.

The time-term inversions of LKL4 (Figure 4.65) and LKL6 (Figure 4.66) are presented as these lines cross-cut the "deepest" part of the lake. The underlying layer for LKL6 was of a lower P-wave velocity suggesting this might have been harder marls. It is not certain if the limestone continues below the lake from the HEM and ground-based resistivity results and this interface might only be caused by the limitations of the refraction model in resolving the Agia Sotira Thrust which is known to be present beneath the lake.

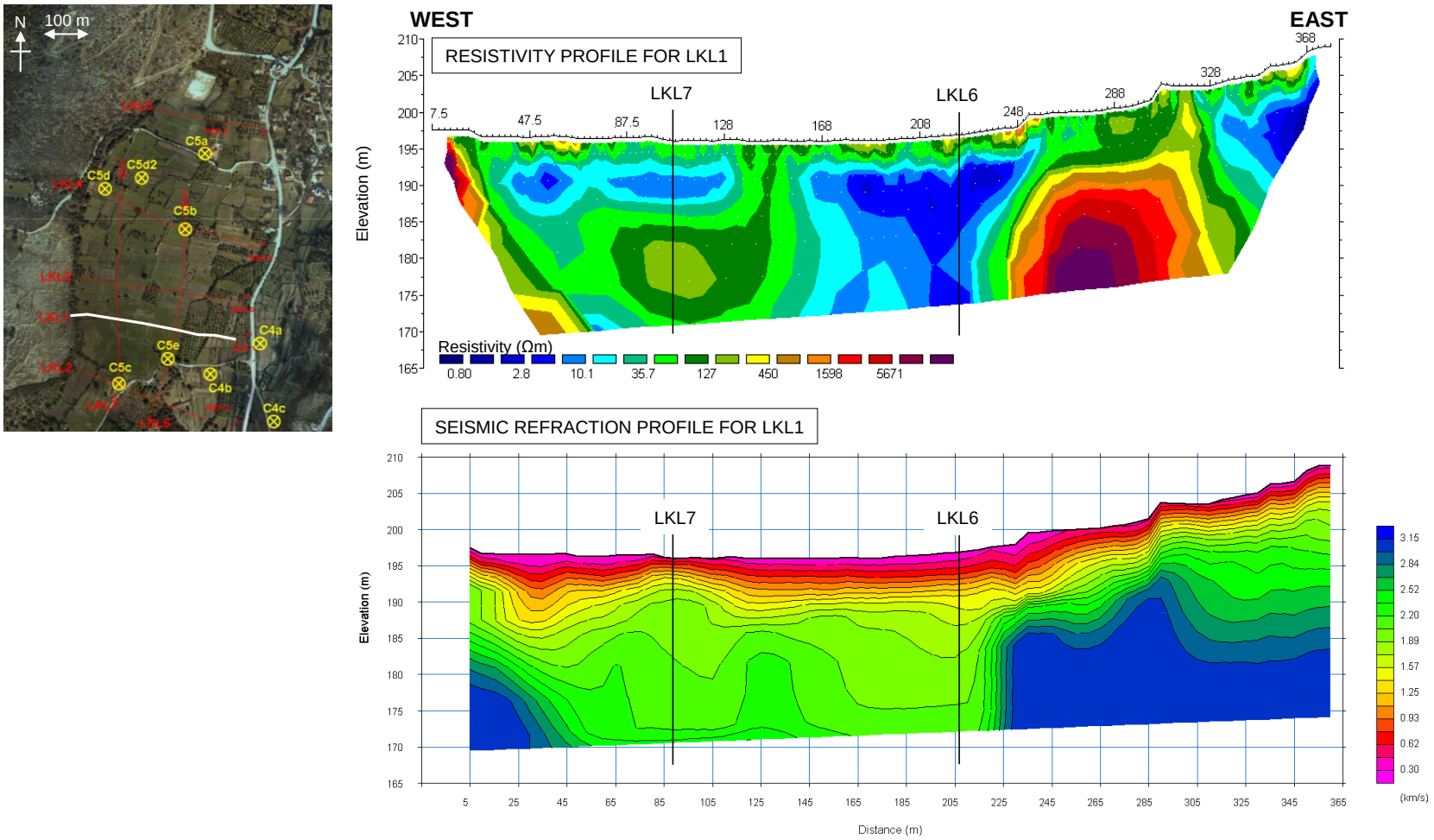

Figure 4.58 2D resistivity profile (top) and corresponding seismic refraction profile (bottom) for Lake Katachori profile, LKL1. Elevation/depth is in terms of elevation above mean sea level (where mean sea level is +22 m above present sea level). The location of this survey line is indicated in the map inset. Vertical exaggeration is V/H = 2.5. Vertical black lines indicate where the profile crosses another profile or borehole.

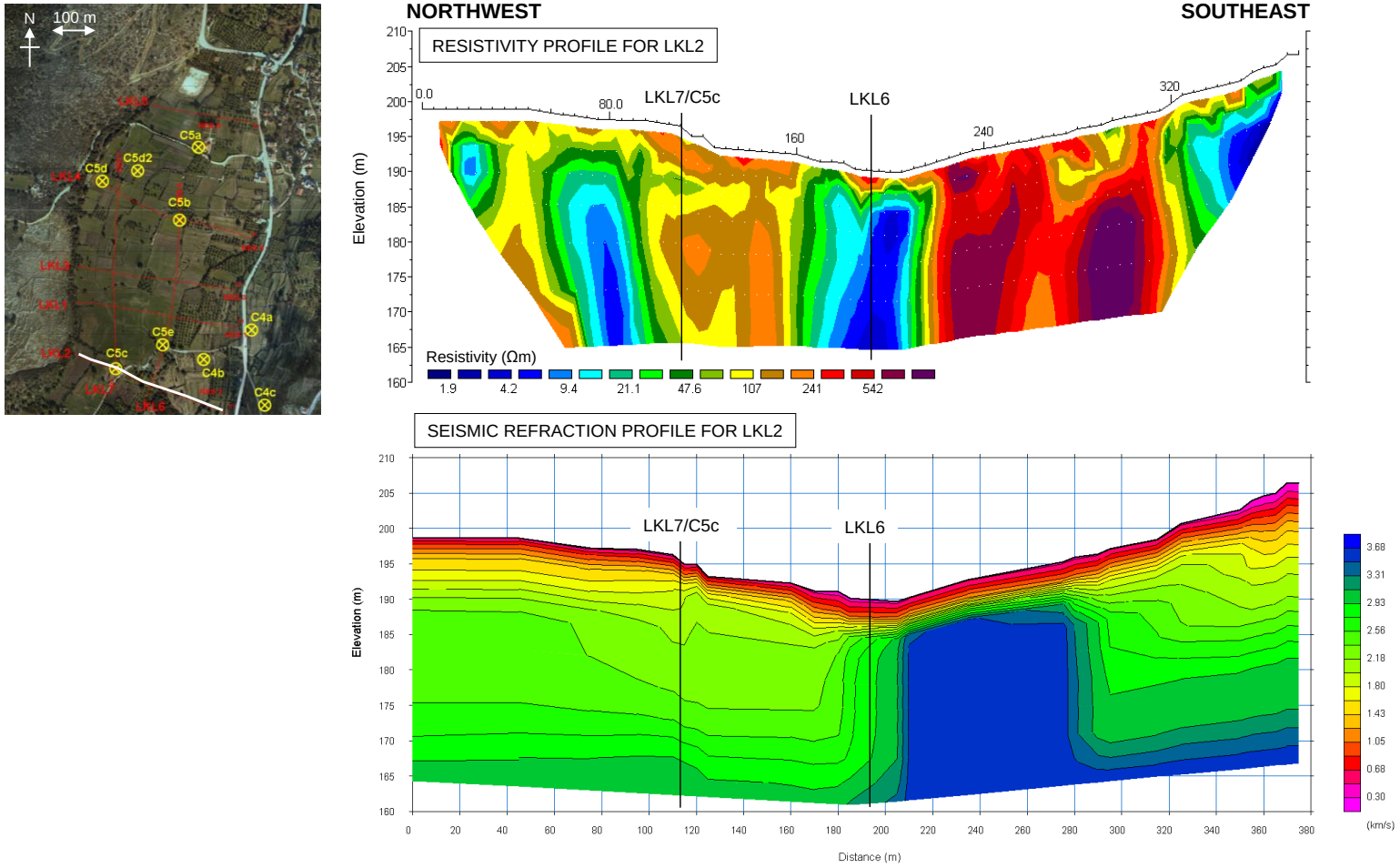

Figure 4.59 2D resistivity profile (top) and corresponding seismic refraction profile (bottom) for Lake Katachori profile, LKL2. Elevation/depth is in terms of elevation above mean sea level (where mean sea level is +22 m above present sea level). The location of this survey line is indicated in the map inset. Vertical exaggeration is V/H = 2.5. Vertical black lines indicate where the profile crosses another profile or borehole.

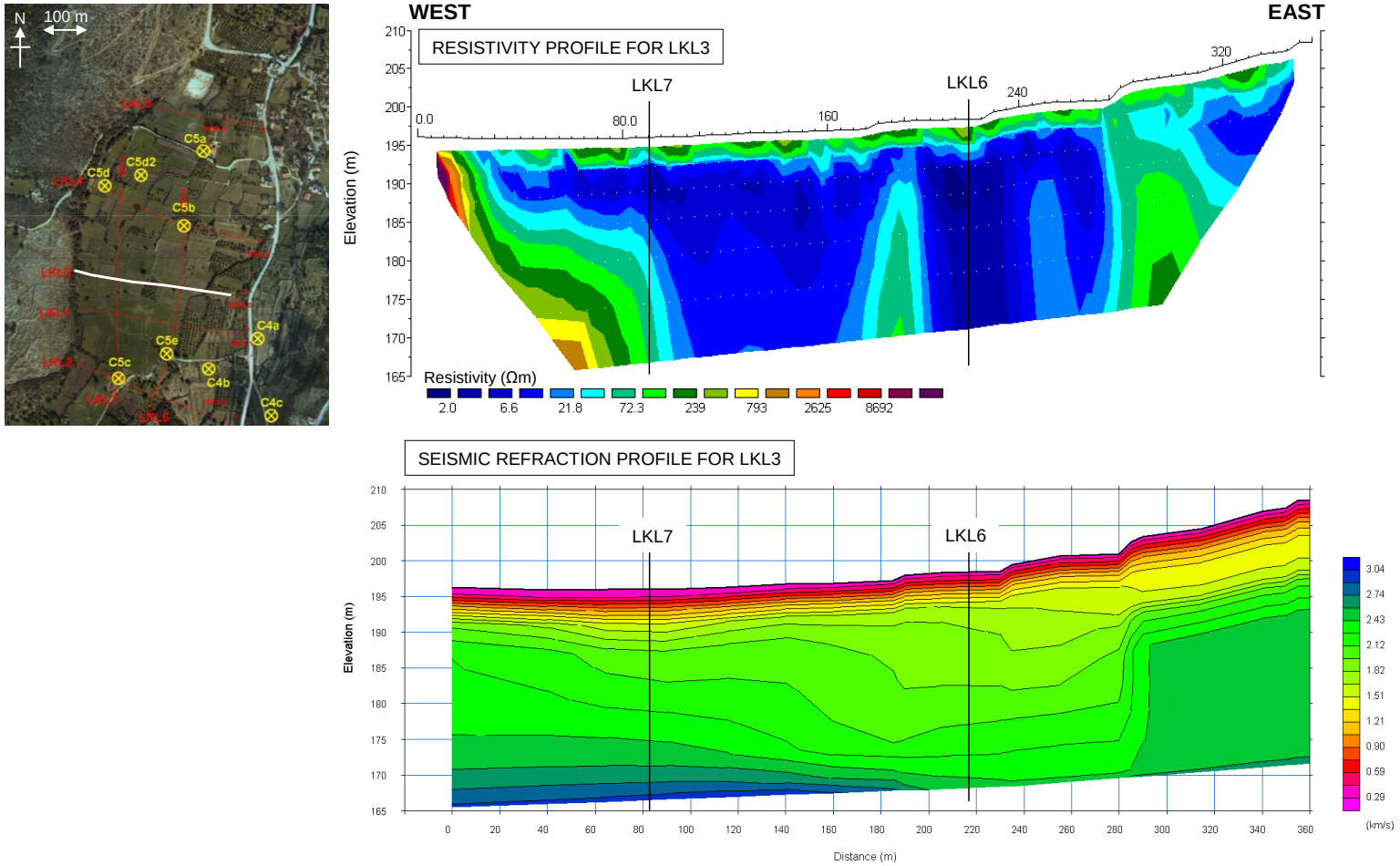

Figure 4.60 2D resistivity profile (top) and corresponding seismic refraction profile (bottom) for Lake Katachori profile, LKL3. Elevation/depth is in terms of elevation above mean sea level (where mean sea level is +22 m above present sea level). The location of this survey line is indicated in the map inset. Vertical exaggeration is V/H = 2.5. Vertical black lines indicate where the profile crosses another profile or borehole.

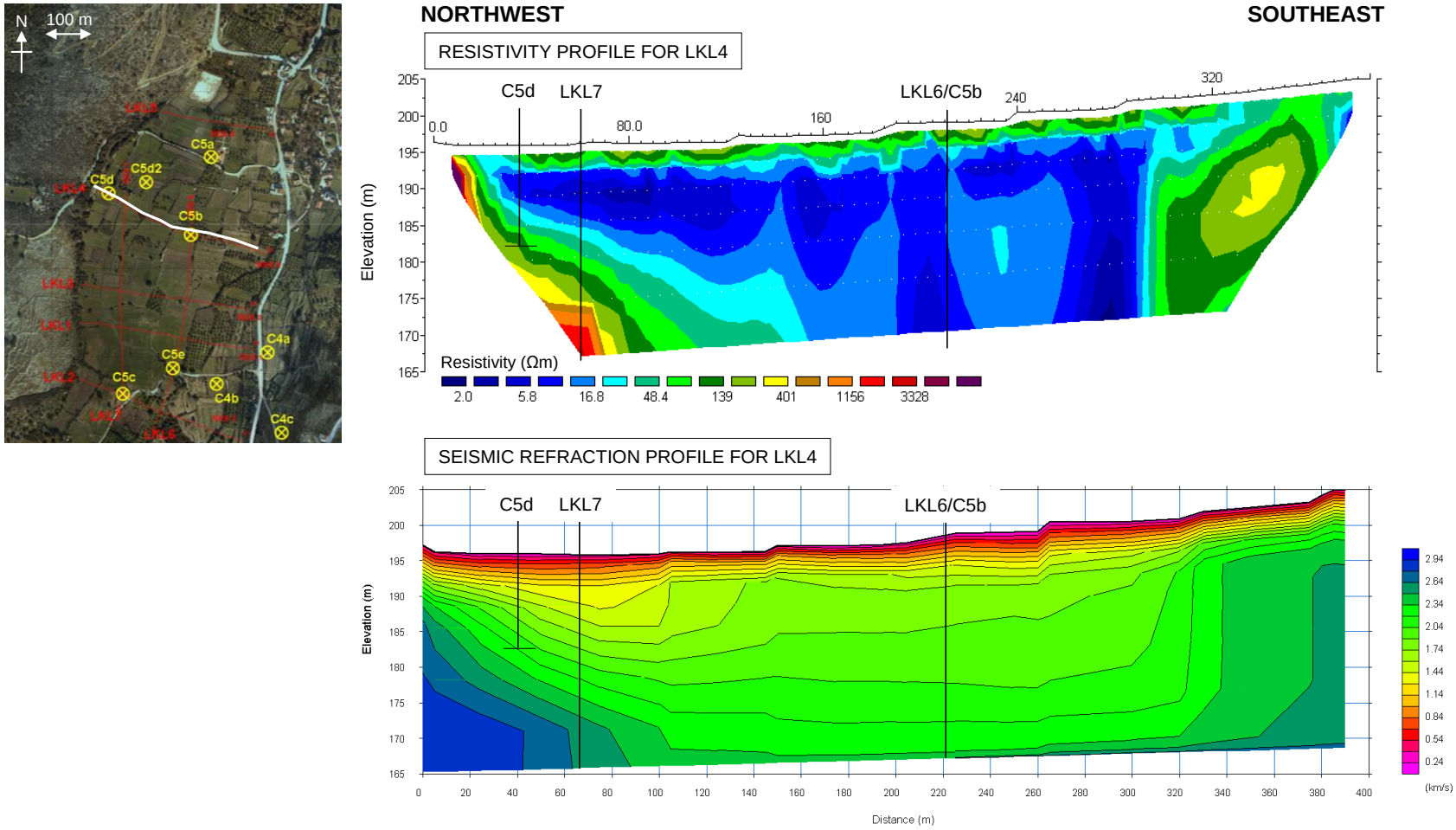

Figure 4.61 2D resistivity profile (top) and corresponding seismic refraction profile (bottom) for Lake Katachori profile, LKL4. Elevation/depth is in terms of elevation above mean sea level (where mean sea level is +22 m above present sea level). The location of this survey line is indicated in the map inset. Vertical exaggeration is V/H = 2.5. Vertical black lines indicate where the profile crosses another profile or borehole.

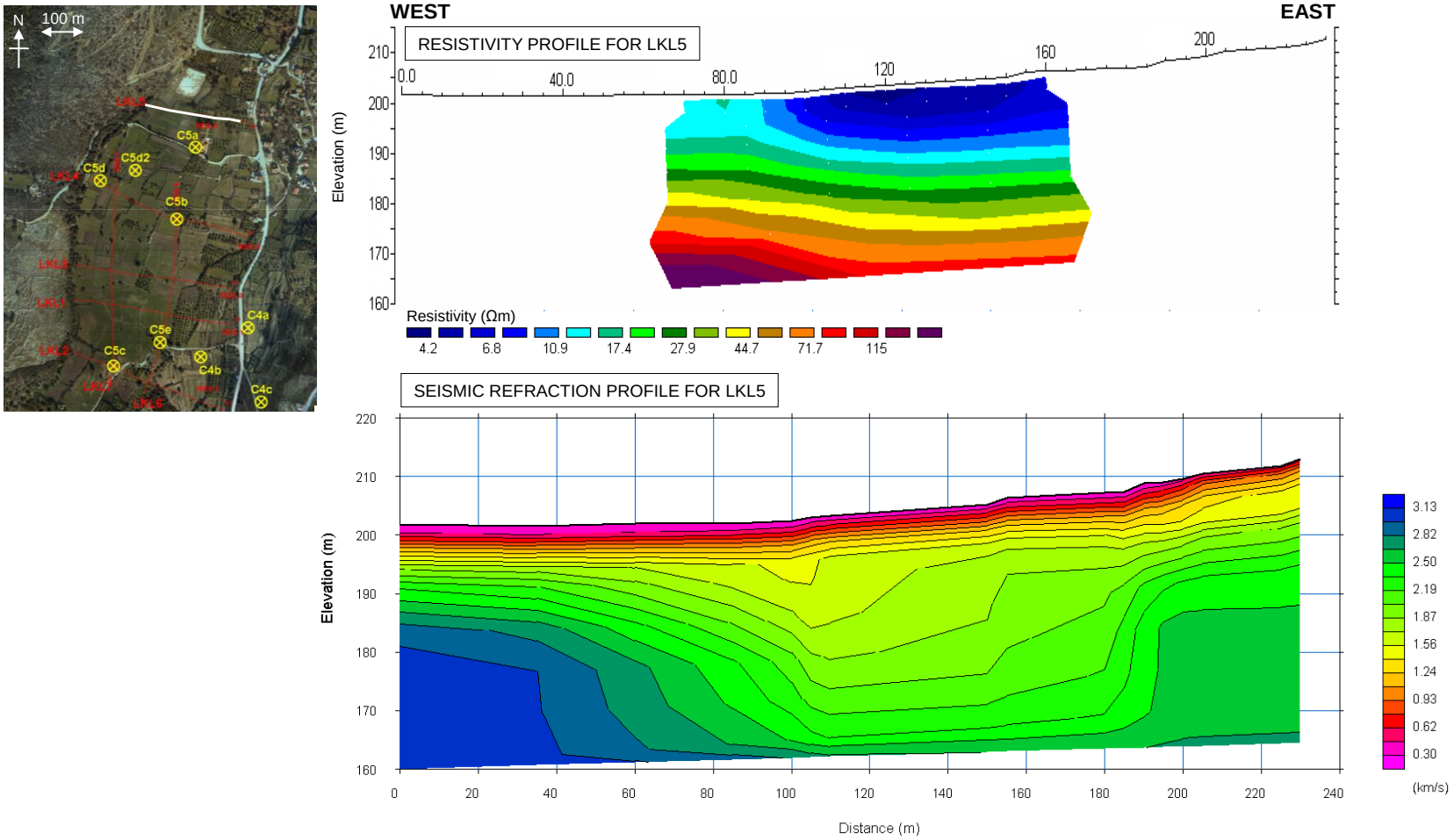

Figure 4.62 2D resistivity profile (top) and corresponding seismic refraction profile (bottom) for Lake Katachori profile, LKL5. Elevation/depth is in terms of elevation above mean sea level (where mean sea level is +22 m above present sea level). The location of this survey line is indicated in the map inset. Vertical exaggeration is V/H = 2.5. Vertical black lines indicate where the profile crosses another profile or borehole.

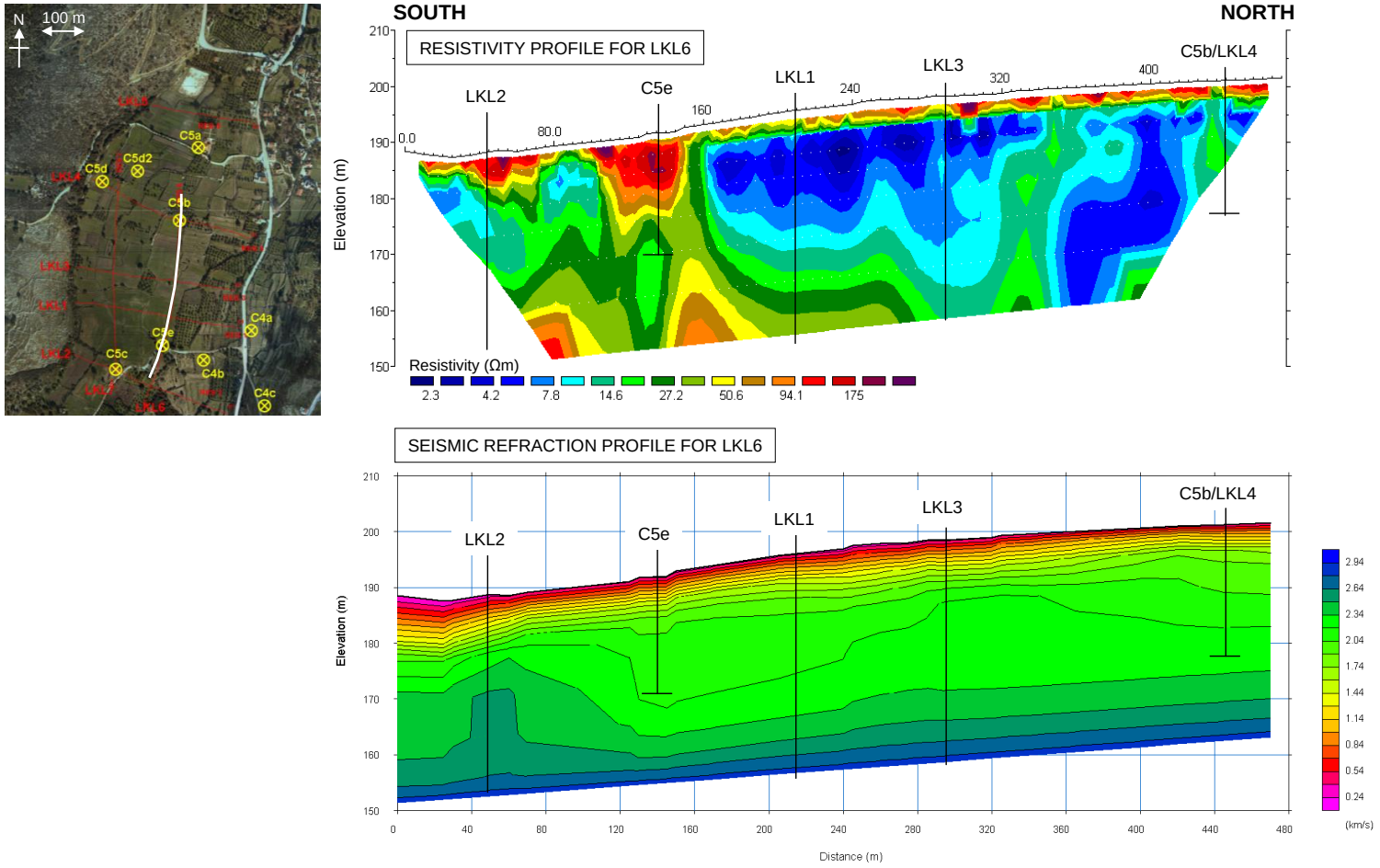

Figure 4.63 2D resistivity profile (top) and corresponding seismic refraction profile (bottom) for Lake Katachori profile, LKL6. Elevation/depth is in terms of elevation above mean sea level (where mean sea level is +22 m above present sea level). The location of this survey line is indicated in the map inset. Vertical exaggeration is V/H = 2.5. Vertical black lines indicate where the profile crosses another profile or borehole.

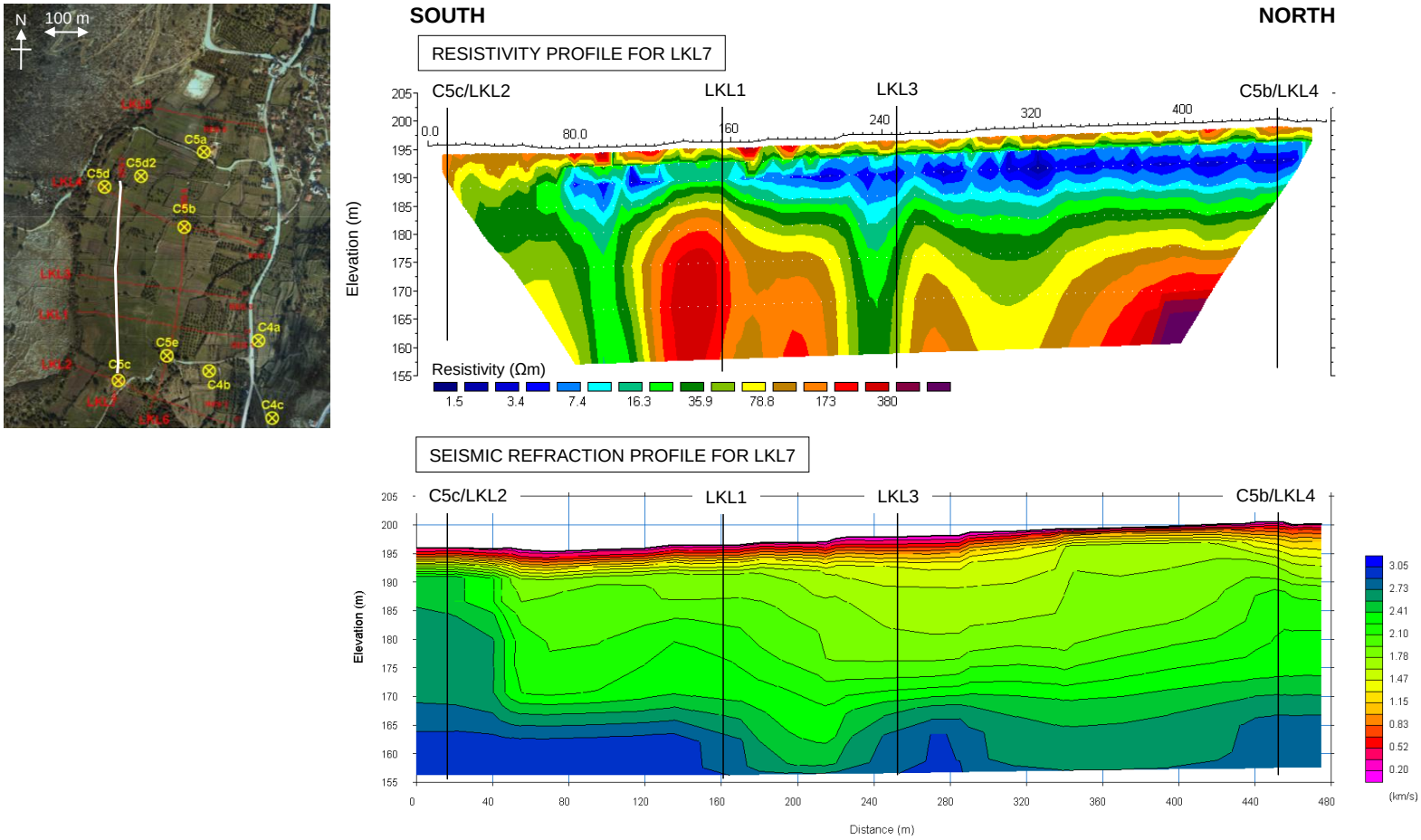

Figure 4.64 2D resistivity profile (top) and corresponding seismic refraction profile (bottom) for Lake Katachori profile, LKL7. Elevation/depth is in terms of elevation above mean sea level (where mean sea level is +22 m above present sea level). The location of this survey line is indicated in the map inset. Vertical exaggeration is V/H = 2.5. Vertical black lines indicate where the profile crosses another profile or borehole.

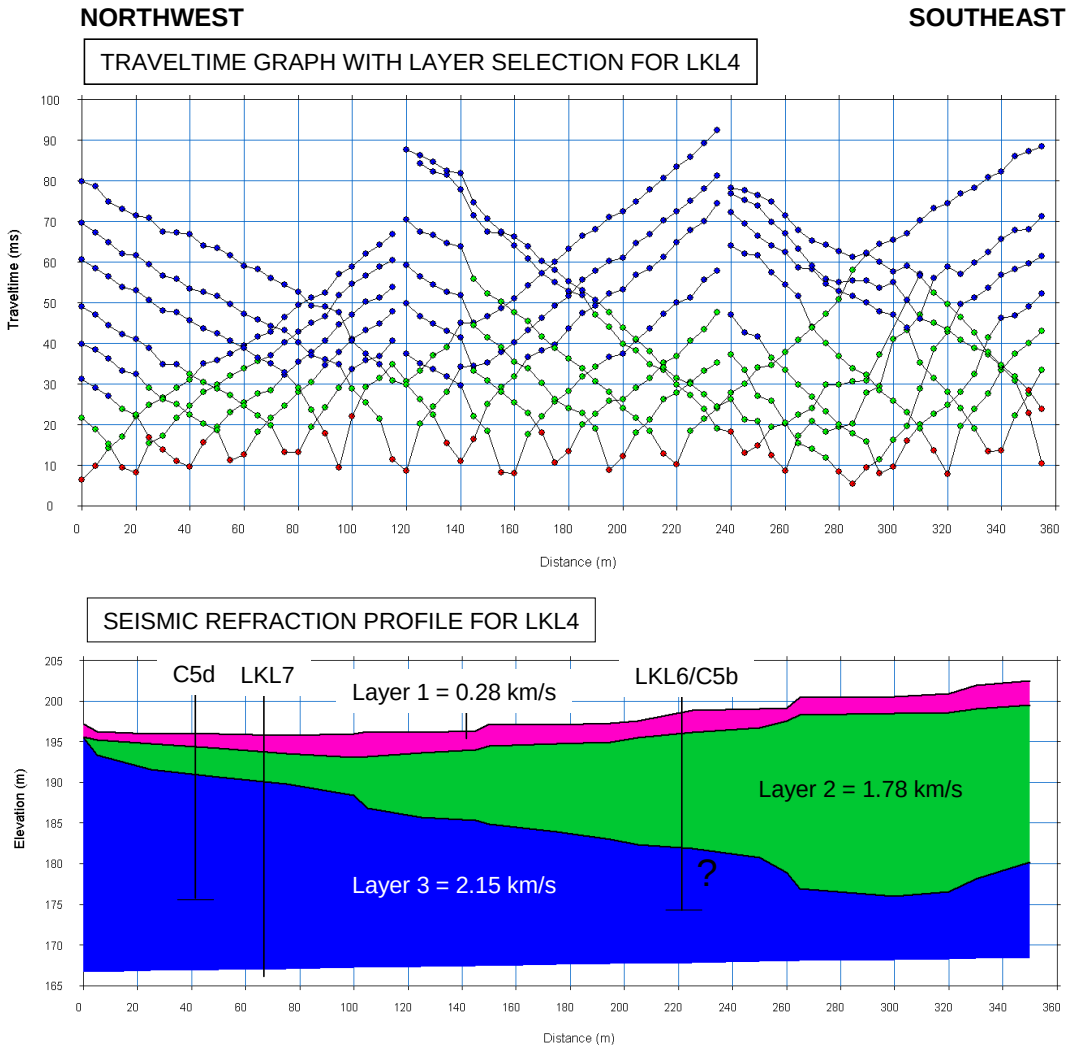

Layer assignment :

Layer 1 = Surface (lacustrine) sediments, clays, clastic material.

Layer 2 = Clays, marls.

Layer 3 = Limestone? Marl?

Figure 4.65 Time-term inverted profile for LKL4 (coloured section) with corresponding traveltime graphs (top) showing layer selection where red = layer 1, green = layer 2 and blue = layer 3. Layers are tentatively assigned possible lithologies based on the P-wave velocities for each layer. The question mark indicates where the model is less confident. This is probably due to the presence of faulting which the refraction method has difficulties resolving and has affected all the Lake Katachori seismic refraction inversions. The location of this line is given in Figure 4.61. Vertical black lines indicate where the profile crosses another profile or borehole.

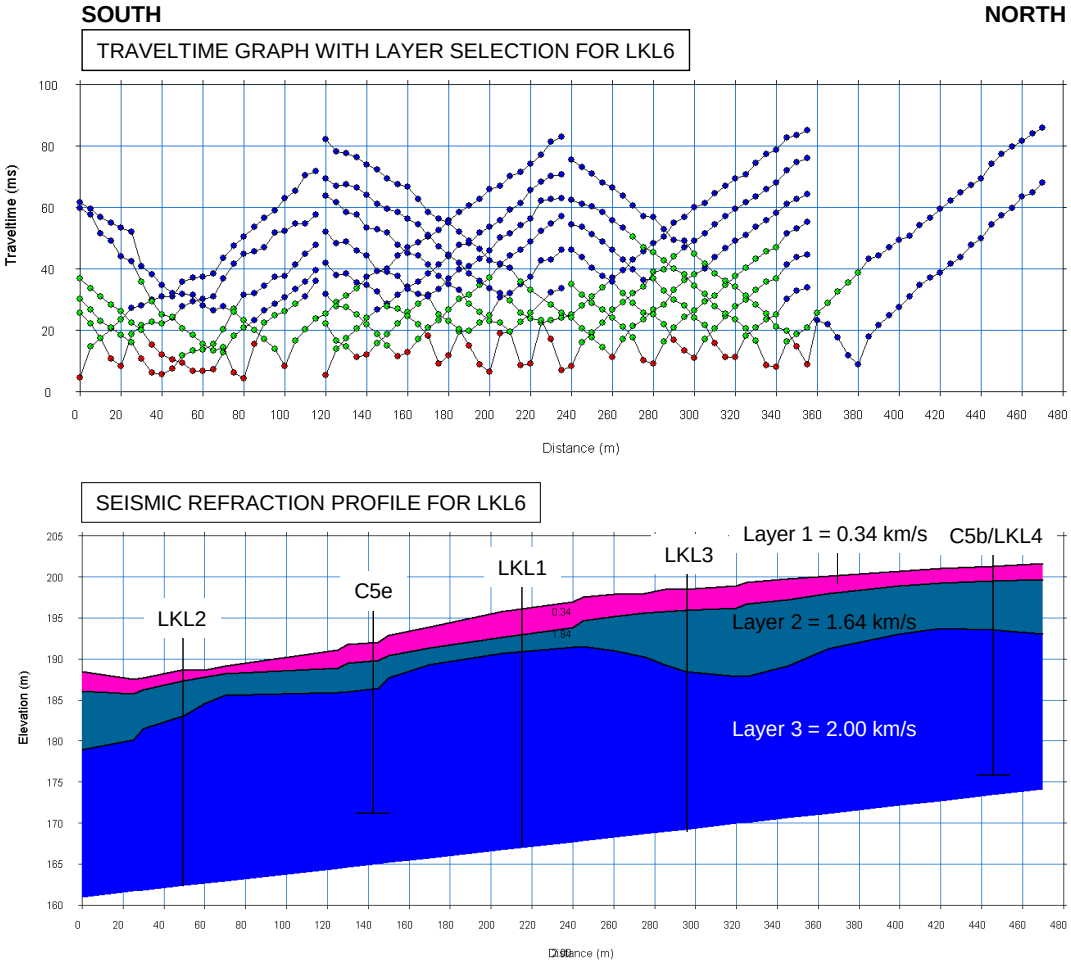

Layer assignment:

Layer 1 = Surface (lacustrine) sediments, clays, clastic material.

Layer 2 = Clays, marls.

Layer 3 = Marl, clastics.

Figure 4.66 Time-term inverted profile for LML6 (coloured section) with corresponding traveltime graphs (top) showing layer selection where red = layer 1, green = layer 2 and blue = layer 3. Layers are tentatively assigned possible lithologies based on the P-wave velocities for each layer. The location of this line is given in Figure 4.63. Vertical exaggerate is V/H = 4.5. Vertical black lines indicate where the profile crosses another profile or borehole.

D. Gravity

The ρ = 2.67 kg/m^3 Bouguer-corrected residual gravity map showed that Lake Katachori formed a NE-SW orientated ellipse-shaped low gravity anomaly (between 0 and -0.65 mGals) indicating Lake Katachori contained lower density sediments relative to the surrounding bedrock (Figures 4.67 and 4.68). The lowest gravity values corresponded to where the HEM survey had detected the thickest accumulation of low resistivity sediment. The raised topography to the north and south of the lake formed "bridges" of higher gravity (0 to 0.2 mGals). In particular, the suspected tongue of talus defining the south-western shore of the lake (Figure 3.9) sat within a clear positive anomaly (0.2 to 0.8 mGals) indicating the presence of particularly dense material. A clear NW-SE trending linear drop of gravity (around 0.4 mGals) cross-cut the central part of the lake and the bedrock on either side which not correlate to a change in stratigraphy but corresponded to a break in the topography. This feature tied into one of the linear structural offsets mapped in Figure 4.34.

The gravity response to the east of the lake was harder to interpret. The mottling of high and low gravity signals may have tied to the presence of pulses of low density colluvial material sitting on top of denser bedrock but was impossible to quantify the extent of this material. The eastern lake shore was defined by a generally positive NE-SW orientated anomaly interpreted as the sediment buried Agia Sotira Thrust. The contrast between the low and high anomalies was slightly sharper along the eastern lake shore than on the west supporting the idea that this feature represented a thrust fault.

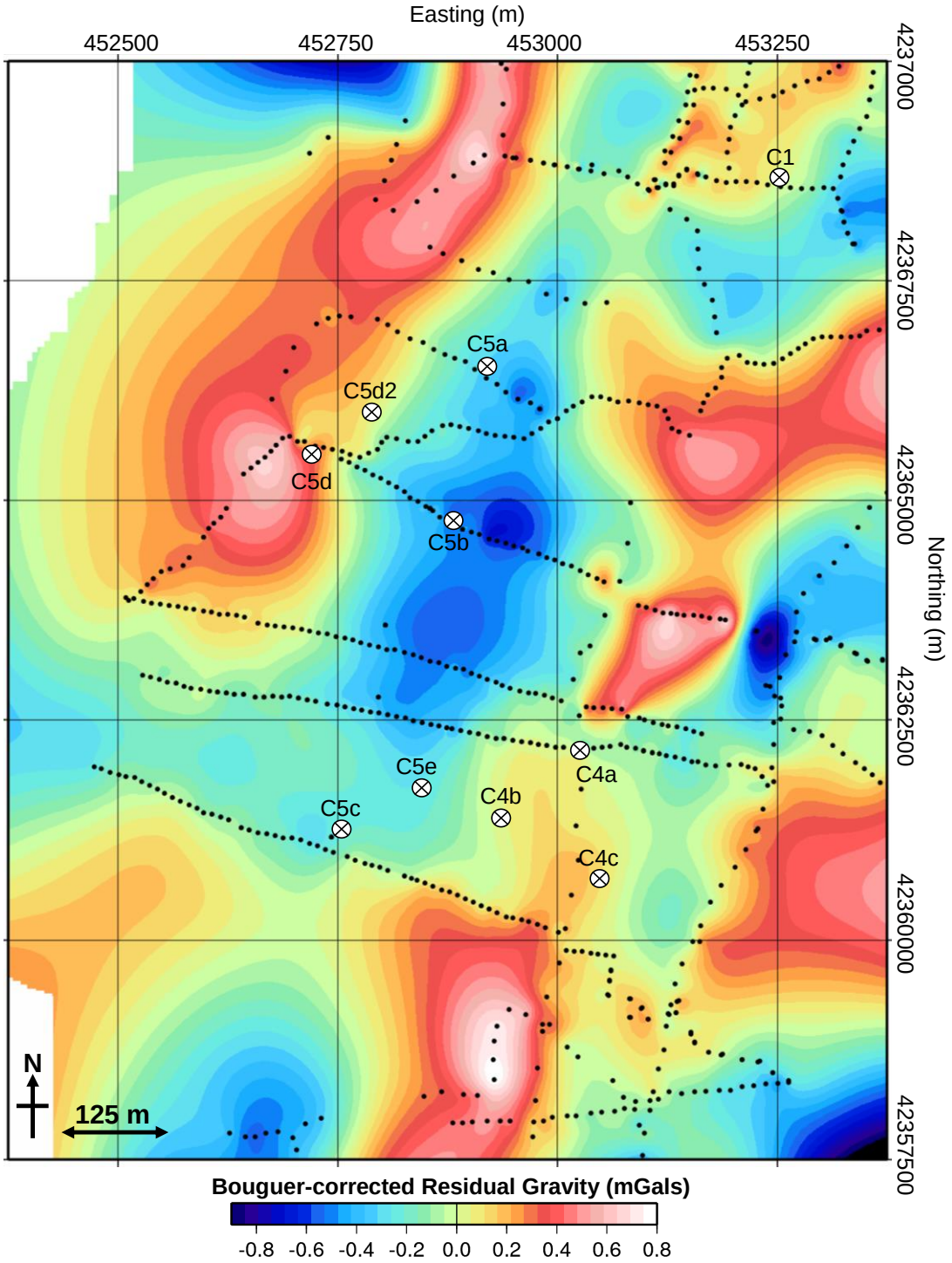

Figure 4.67 Bouguer-corrected residual gravity map in terms of mGals (ρ = 2.67 kg/m^3) showing data coverage of the gravity survey at Lake Katachori. Gravity stations are indicated as black dots. The locations of the Lake Katachori boreholes are shown.

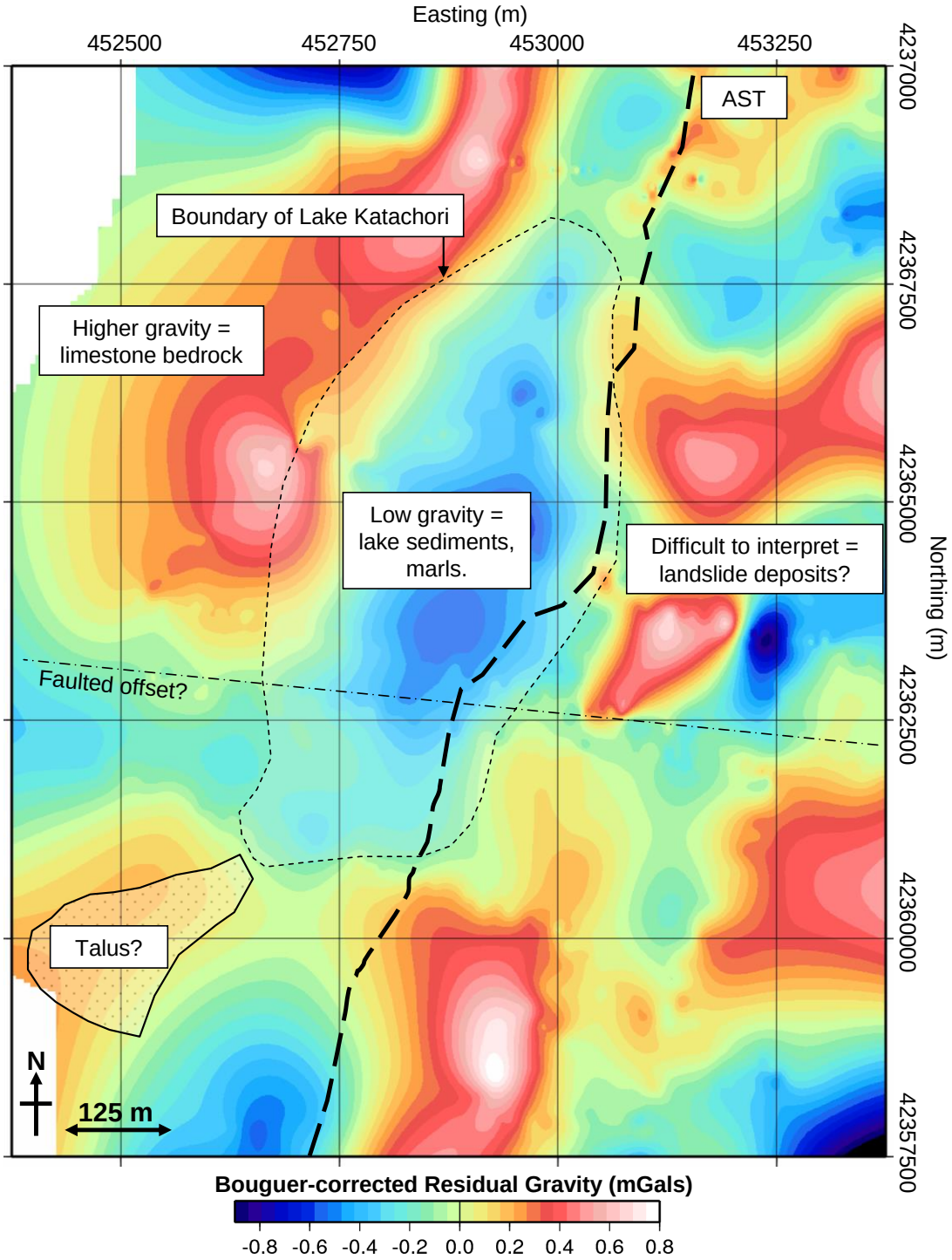

Figure 4.68 Interpreted version of the Lake Katachori gravity map showing the low gravity lens of the paleo-lake.

4.5.5 Southern Thinia

A. Resistivity

The resistivity profiles for the proposed southern exit of "Strabo's Channel" are given in Figure 4.69 to Figure 4.72 (top). The surface survey site consisted of a thin (1 to 5 m) veneer of resistive material (between 40 Ωm to 100 Ωm) which contained discrete resistive (~200 Ωm to 4000 Ωm) lens-shaped anomalies up to 20 m across (particularly at ~240 m along STL1 and ~40 m in STL3) which may represent large partially buried limestone clasts similar to those distributed across the surface.

The three profiles which cross-cut the proposed Channel route (STL1, STL3 and STL4) imaged the Channel "fill" as a deep (at least 35 m), 100 to 125 m wide zone of very low resistivity (0.4 Ωm to ~15 Ωm) which contrasted strongly with the bedrock on either side. This low resistivity zone formed part of the narrow NNE-SSW trending conductive linear anomaly imaged by the HEM survey which ran between the Ainos and Agia Sotira Thrusts. This response suggested the Channel fill was composed of fine-grained sediments such as clays or alluvium. The ground-based resistivity survey was unable to resolve the depth of this zone as it extended to beyond the maximum imaging depth of the profiles (around 35 m below the ground surface. In the case of the lowest elevation profile (STL4), this meant this material reached at least within 60 m of sea level and may have been deeper. Rounded anomalies of slightly higher resistivity were detected within the "fill" which may have represented changes of the sediment (e.g. reduction of pore fluid content) or the presence of clasts of higher resistivity material embedded within the lower resistivity sediment.

STL1 and STL4 cross-cut the contact between the limestone of the Agia Sotira Thrust ridge and hard, steeply-bedded marl which onlapped this limestone, a contact which could be traced from the surface. This lithological boundary appeared as an easterly- to south easterly-dipping (45°) contact between high resistivity (~300 Ωm to 9853 Ωm) limestone and onlapping ~20 Ωm to 100 Ωm resistivity material. In

STL3 only the marl was imaged and the profile did not extend far enough to the northwest to cross-cut the limestone-marl contact. In STL1, the contact between Channel "fill" and marl was very steeply-dipping which indicated an abrupt change in the nature of the sediments within the Channel route or the presence of a fault plane. In STL4, the low resistivity zone was onlapped by a south easterly-dipping wedge of 200 Ωm to 4921.4 Ωm material. This wedge corresponded to the limestone conglomerate cliff defining the eastern side of the Channel route. This feature either represented the lithified edge of a talus apron similar to those observed in the northern part of the valley or a thrust fault. If it represented a thrust fault, it may have been the southern continuation of the "Petrikata" thrust.

STL2, which was taken outside of the Channel route to test the second possible Channel exit point, revealed the subsurface continuation of this resistive wedge and showed it formed a south-easterly-dipping layer imaged by STL4. This line revealed a jumble of low and high resistivity material at least 35 m thick. This material onlapped the resistive wedge imaged by STL4 and was composed of discrete highly resistive anomalies (~300 Ωm to 11 057 Ωm) sitting within lower resistivity (~11.6 Ωm to 100 Ωm) material. This configuration was the expected response to a colluvium-filled channel wedge where the resistive anomalies represented a jumble of fallen limestone clasts embedded within finer-grained sediment. The possibility of a colluvial unit at least 35 m thick in this area opened the possibility that the Channel exit may have been located further south.

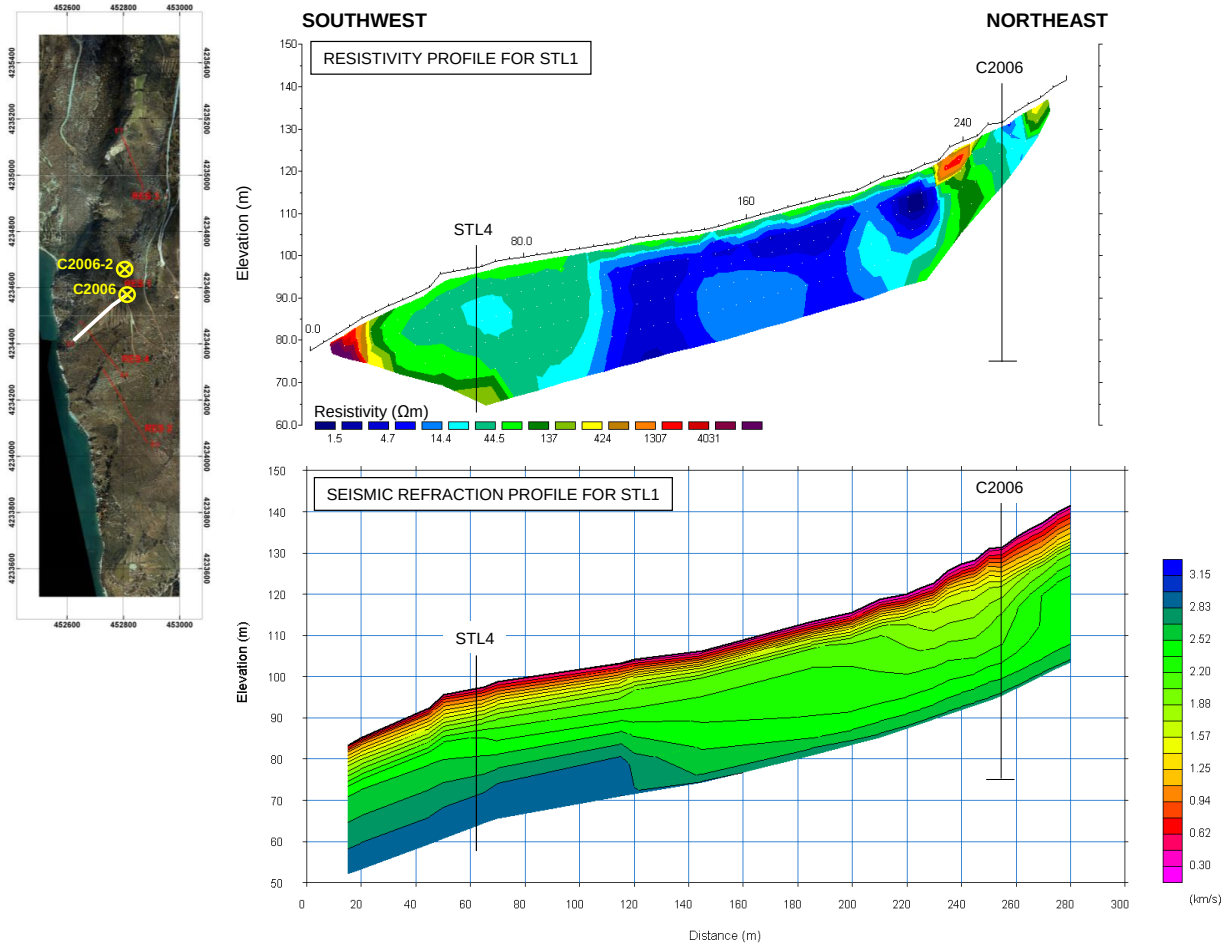

Figure 4.69 2D resistivity profile (top) and corresponding seismic refraction profile (bottom) for Southern Exit profile, STL1. Elevation/depth is in terms of elevation above mean sea level (where mean sea level is +22 m above present sea level). The location of this survey line is indicated in the map inset. Vertical exaggeration is V/H = 2.5. Vertical black lines indicate where the profile crosses another profile or borehole.

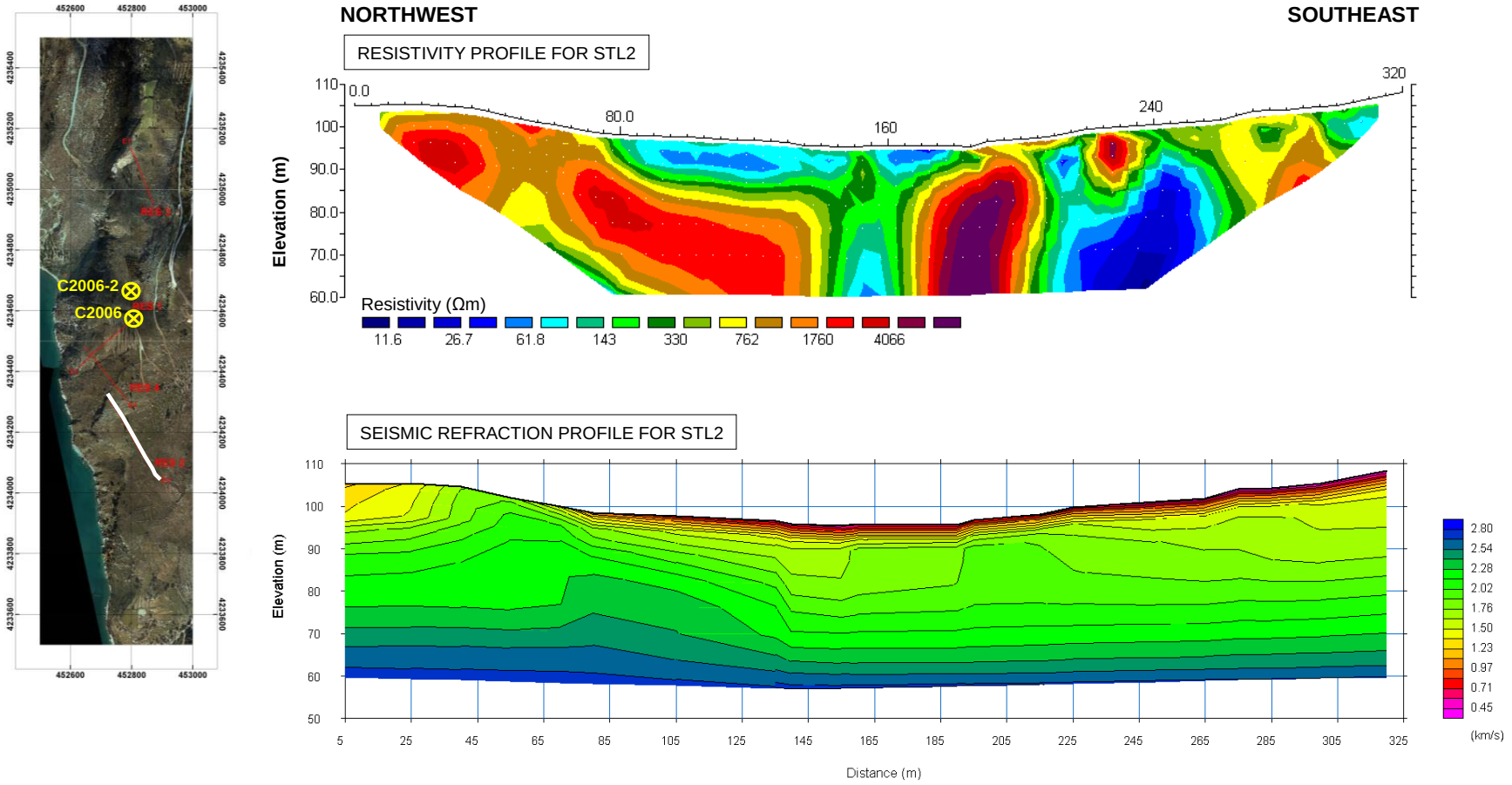

Figure 4.70 2D resistivity profile (top) and corresponding seismic refraction profile (bottom) for Southern Exit profile, STL2. Elevation/depth is in terms of elevation above mean sea level (where mean sea level is +22 m above present sea level). The location of this survey line is indicated in the map inset. Vertical exaggeration is V/H = 2.5.

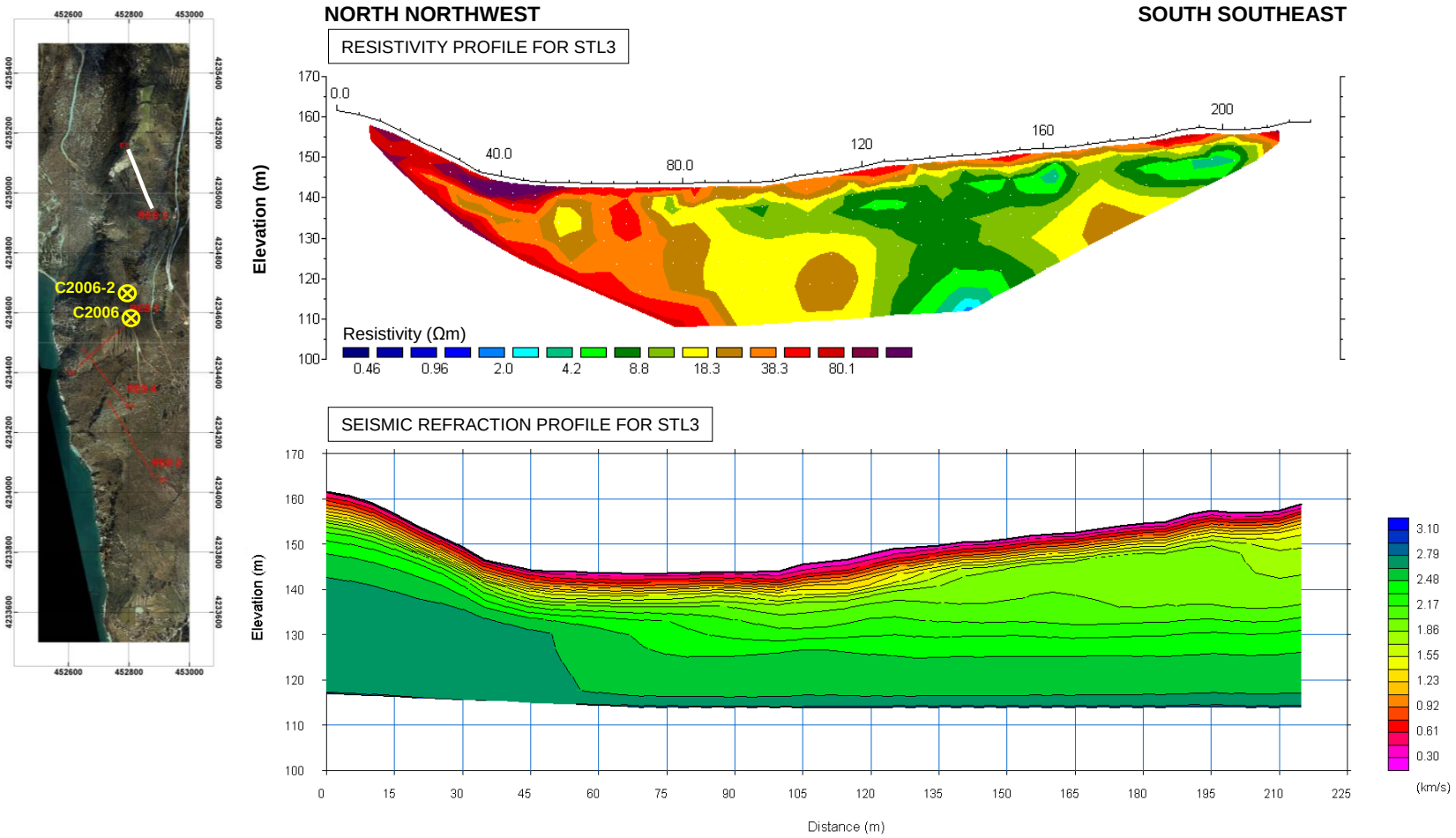

Figure 4.71 2D resistivity profile (top) and corresponding seismic refraction profile (bottom) for Southern Exit profile, STL3. Elevation/depth is in terms of elevation above mean sea level (where mean sea level is +22 m above present sea level). The location of this survey line is indicated in the map inset. Vertical exaggeration is V/H = 2.5.

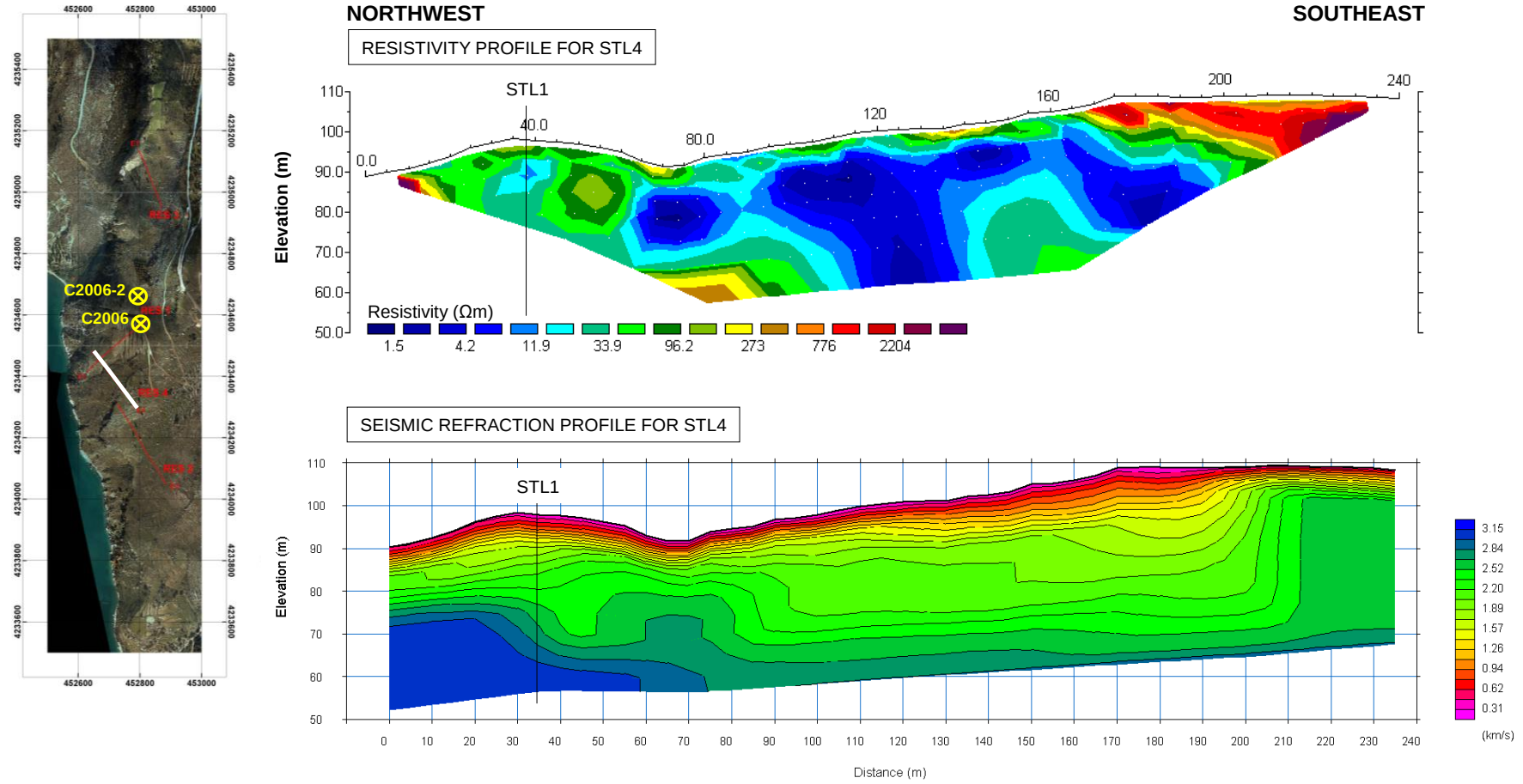

Figure 4.72 2D resistivity profile (top) and corresponding seismic refraction profile (bottom) for Southern Exit profile, STL4. Elevation/depth is in terms of elevation above mean sea level (where mean sea level is +22 m above present sea level). The location of this survey line is indicated in the map inset. Vertical exaggeration is V/H = 2.5. Vertical black lines indicate where the profile crosses another profile.

B. Seismic Refraction

The seismic refraction results for Southern Thinia are presented in Figure 4.69 to 4.72 (bottom). The shot records were reasonably good quality but became noisier with distance from the source making first breaks further from the source more difficult to pick. This was a particular problem at STL4 where reflectivity may have been due to the repeating, steep-dipping geology. While the first break picks for STL4 were considered the least confident of the southern exit survey, the highest RMSE was produced by the tomographic inversion of STL2 (3.55 msec). The results of equivalent resistivity line showed resistive, dense conglomerate emplaced on soft marl which suggested the high RMSE of STL2 was due to the presence of a low velocity layer (marl) underlying the conglomerate and the failure of the refraction method to adequately resolve such a configuration. The structure was instead imaged as a vertiginous block. STL4 also failed to adequately resolve this structure.

Other than this, the tomographic models were considered to be a good representation of the subsurface of southern Thinia as the velocity structures correlated very well with the structures imaged in the corresponding resistivity profiles particularly in the case of STL1. These survey lines imaged a zone of low velocity (around 2 to 2.60 km/s) Channel "fill" bounded on either side by relatively higher velocity (2.60 to 2.80 km/s) material. This low velocity zone corresponded to the low resistivity sediment imaged by the electrical survey.

Time-term inversion resolved STL1 (Figure 4.73) into three layers: Layer 1 = 0.40 km/s, Layer 2 = 1.61 km/s and Layer 3 = 2.35 km/s. Layer 1 was attributed to the layer of dry surface soils and colluvium which appeared to only be very thin. Layer 2 could be correlated with the low resistivity Channel "fill" detected by the ground-based resistivity survey. Layer 3 was attributed to bedrock which was the easterly-dipping limestone of the Agia Sotira Thrust and hard onlapping marl. While the resistivity survey was unable to resolve the base of the low resistivity "fill" the time-term method suggested this unit was only an average 9 m in thickness on however

this may be due to the refraction method falsely resolving thrust faults and this low velocity material may in fact be thicker. The three layer model for STL4 (Figure 4.74) revealed a similar configuration (Layer 1 = 0.40 km/s, Layer 2 = 1.87 km/s and Layer 3 = 2.04 km/s). The low velocity (Layer 2) fill reached a maximum of 14.3 m in thickness onlapping the southerly-dipping Agia Sotira Thrust (Layer 3).

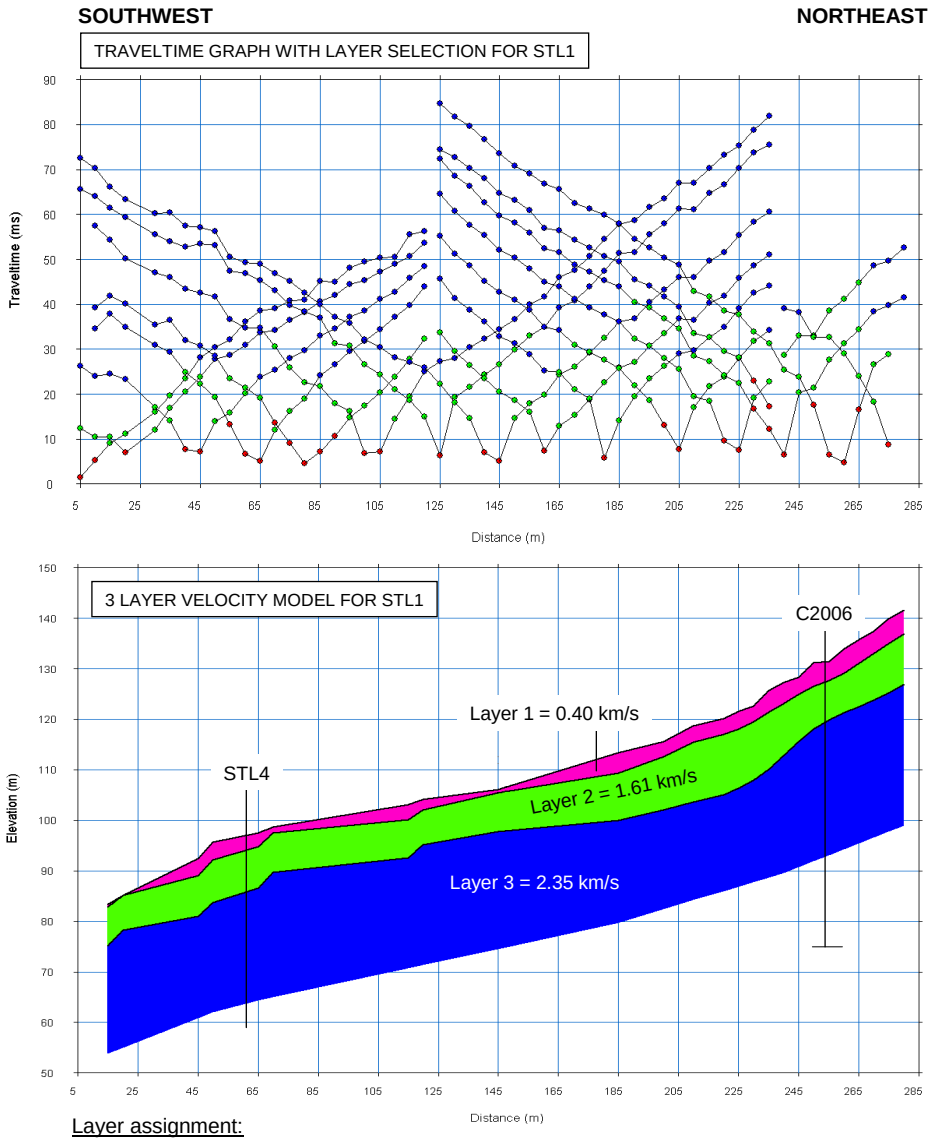

Layer assignment:

Layer 1 = Surface soils, colluvium.

Layer 2 = Clays, reworked sediment.

Layer 3 = Limestone? Marls?

Figure 4.73 Time-term inverted profile for STL1 (coloured section) with corresponding traveltime graphs (top) showing layer selection where red = layer 1, green = layer 2 and blue = layer 3. The location of this line is given in Figure 4.69. Vertical exaggerate is V/H = 2.5. Vertical black lines indicate where the profile crosses another profile or borehole.

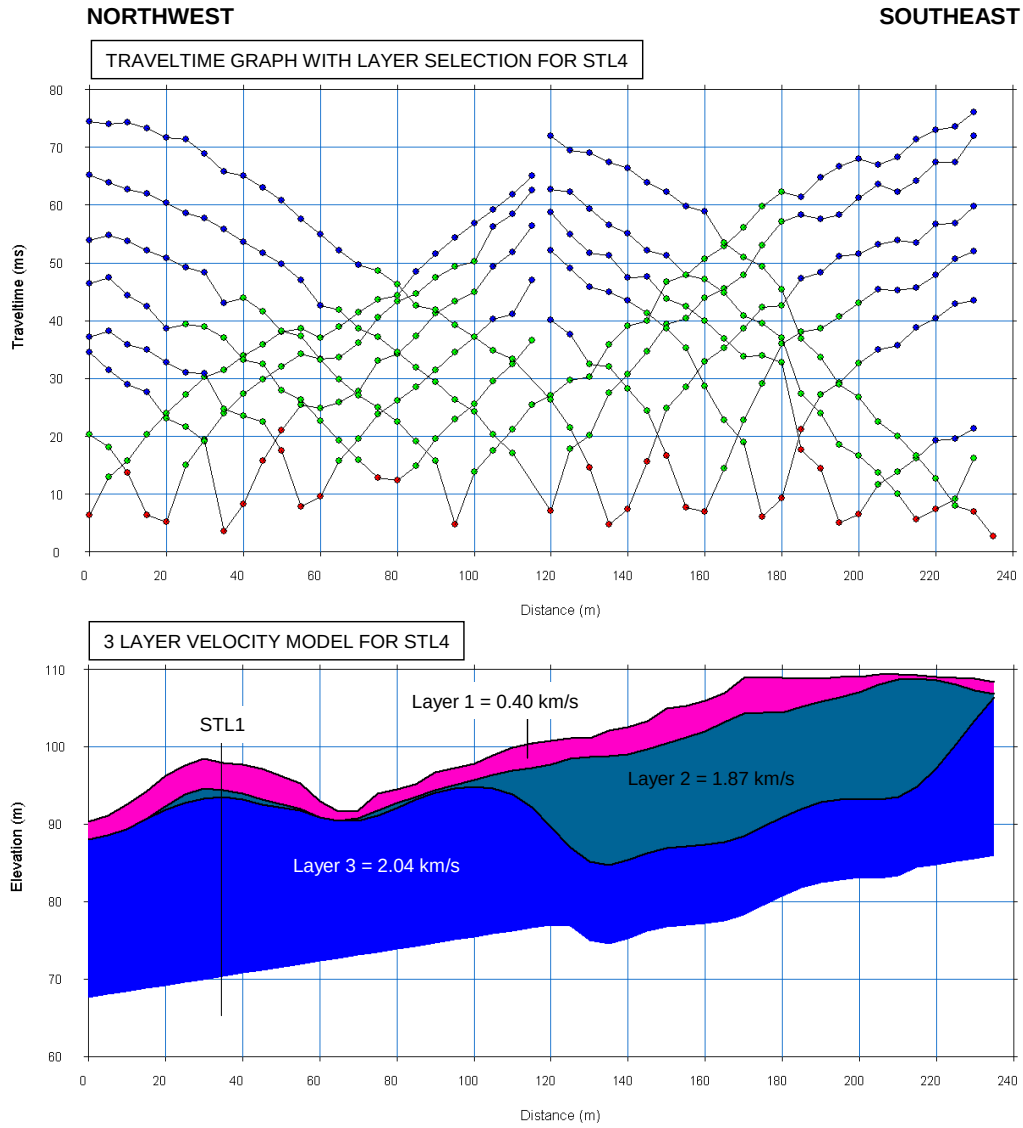

Layer assignment :

Layer 1 = Surface soils, colluvium.

Layer 2 = Clays, reworked sediment.

Layer 3 = Limestone? Marls?

Figure 4.74 Time-term inverted profile for STL4 (coloured section) with corresponding traveltime graphs (top) showing layer selection where red = layer 1, green = layer 2 and blue = layer 3. The location of this line is given in Figure 4.72. Vertical exaggerate is V/H = 2.5. Vertical black lines indicate where the profile crosses another profile.

C. Gravity

The Bouguer anomaly map for the southern exit was a complicated pattern of high and low (Figure 4.75). Some of this effect may have been due to inadequate terrain correction but it is most likely a reflection of the complicated geology here.

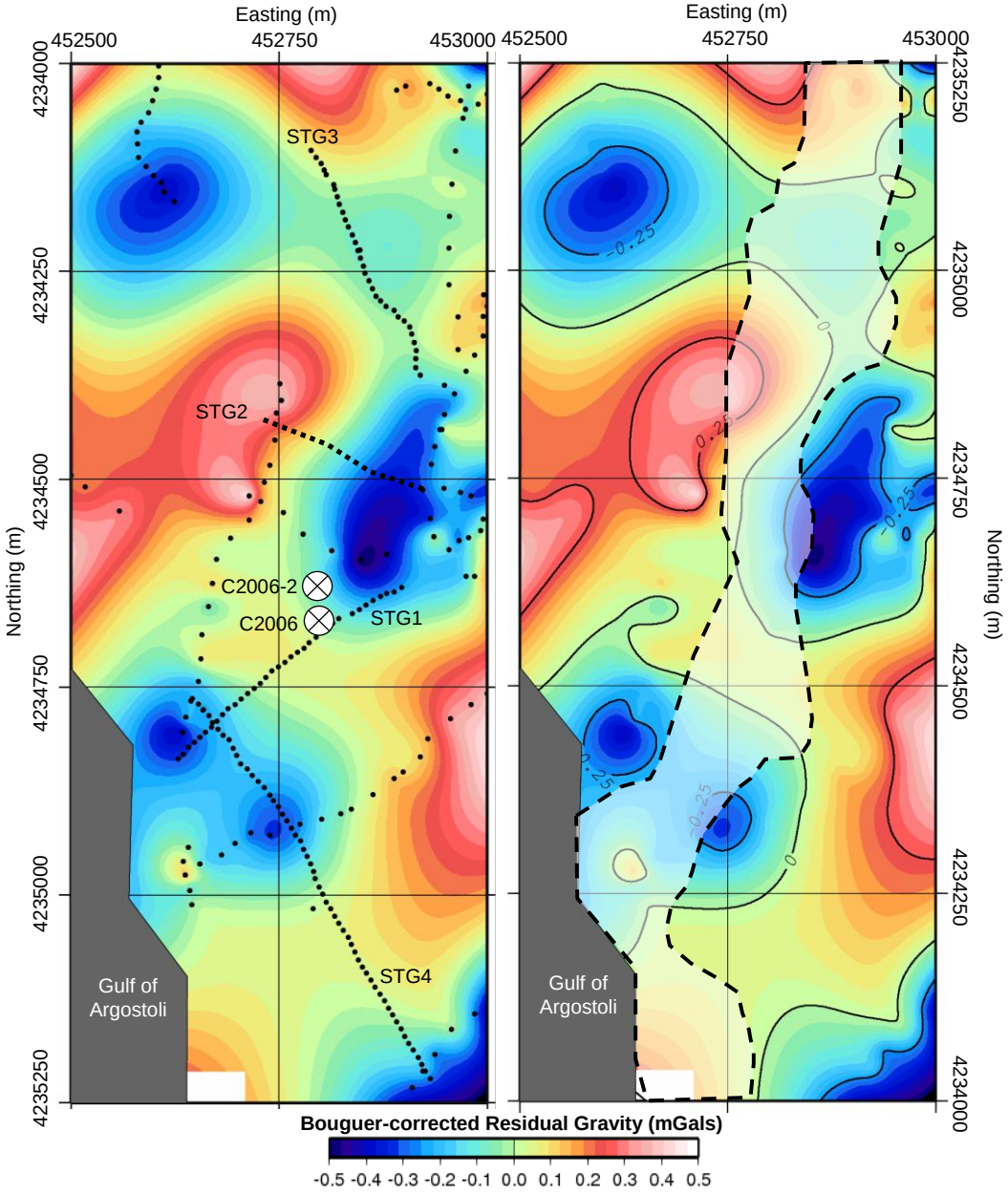

Figure 4.75 Bouguer-corrected residual gravity map in terms of mGals ($\rho = 2.67$ kg/m^3) showing data coverage of the gravity survey at the proposed Southern Exit (left). Gravity stations are indicated as black dots. The locations of C2006 and C2006-2 are shown. Interpreted version on the right with the proposed route of "Strabo's Channel" indicated by white shading.

4.6 Summary

The helicopter-mounted electromagnetic (HEM) survey indicated the striking contrast between the low conductivity, low magnetic limestone of Northern Paliki and the highly conductive, magnetised sediments of the low-lying areas of the Thinia valley and Livadi Marsh. The airborne conductivity survey was unable to detect the base of this conductive valley "fill" imaging to a depth of at least 80 to 100 m and did not detect an increase in resistivity beneath this material which would suggest limestone lay close to the surface. The ground-based surveys detected predominately low resistivity material bounded by highly resistivity limestone ridges reflecting the HEM results for the proposed northern and southern exits of "Strabo's Channel" and Lake Katachori.

The non-invasive surveys detected easterly-dipping and folded sediments within the valley but produced inconclusive results regarding the presence of Strabo's Channel in the case that the channel formed a landslide-filled gorge detecting neither the sides nor base of a buried gorge within the marl sediments. However, this may have been due to the physical similarities between the infilling colluvial material and surrounding marly-clay bedrock rendering a channel invisible to the non-invasive surveys.

CHAPTER 5: Onshore Subsurface Calibration

5.1 Introduction

This chapter presents the results of the boreholes and the core-ties and cross-sections constructed. The acquisition of the geophysical surveys was followed by a phase of shallow sedimentary coring which ran from Sept 2010 to Feb 2011. The aims of the coring survey were to test the subsurface and provide crucial calibration of the non-invasive geophysical surveys which would aid geophysical models, particular the gravity models, towards a more satisfactory solution. Core-ties and cross-sections using the borehole results were produced to help visualise the complicated structural geology of the area.

The 85-day drilling campaign was carried out by Fugro's French affiliate Géotechnique using a 6 ton Ecofore CE-603 rig with sample steel barrels which measured 1.6 m long with a 100 mm diameter (Figure 5.1 and 5.2). The drilling was undertaken with the permission of the Greek Institute of Geological and Mineralogical Exploration (IGME), local municipality support from the mayors of Argostoli and Lixouri, landowners and the Archaeological Ephorate of Prehistoric and Classical Antiquities. A total of 17 continuous shallow sedimentary cores (denoted by the letter "C") were drilled with almost 700 m of core collected in total. The elevation and depths of the boreholes were measured in terms of absolute sea level (0 m). The locations and depths of these boreholes are summarised in Table 5.1. The deepest core was 102.2 m (C5c).

The boreholes were initially placed according to where the thickest deposits of Late Holocene sediment was expected to be. The first three cores were drilled in Livadi Marsh. As the results came in, particularly in the case of the Lake Katachori boreholes, the locations of the originally proposed boreholes were adjusted and new sites were visited. For example, C4b was drilled deeper than originally proposed in order to reach the end of the limestone to investigation whether this was a large clast

or a thrust fault. In the absence of substantial Holocene deposits at the other Thinia borehole sites, the site of the October 2006 borehole where Holocene deposits (*Emiliania huxleyi*) had been detected to a depth of 26 m [core] was revisited. C2006-2 was located according to where the Channel axis was proposed based on the original October 2006 results as this was where the thickest Holocene material should be found.

Figure 5.1 The Fugro Géotechnique Ecofore CE-603 rig in the process of drilling C5b, Lake Katachori.

Figure 5.2 Retrieval of the C5b core by Fugro Géotechnique team (A). Example of core after it has been laid out in 1 m boxes (B) showing the first 0 to 6.5 m of C5b.

After drilling, the cores were dispatched to Fugro Robertson Limited in North Wales for sedimentological logging, sampling and analysis for information on depositional paleo-environment of these sediments. Biostratigraphic age-dates for the cores were

acquired using the following analysis types: micropalaeontology (processed residue, M, and thin section, T), nannopalaeontology (calcareous nannofossils, N) and palynology (P). Detailed stratigraphic logs (core description charts) were prepared for each borehole by O. Davis using WellCAD 4.1 software providing information on the age, grain size, sedimentary structures, reworked zones, mud log, level of bioturbation, lithology and core description (each core log is presented in Appendix C). QEMSCAN (Q) age-dating of representative samples was also undertaken (results are presented in Appendix E).

Calibration of the microfossils was primarily achieved via reference to TimeScale Creator (TSC, 2012) and publications. These reports used the standard zonal nomenclature of Martini (1971) (Nannoplankton Neogene or "NN" zones) as a basis in the above references which were further refined and supplemented with events specific to the Mediterranean region (denoted by the prefix "M"). For sediments of Paleogene age the Martini prefix of "NP" (Nannoplankton Paleogene) for global planktonic and nannoplankton zonations has been used. Occasionally Shallow Benthonic Zonation (SBZ) has been used. The level of reworked microfossils and long-ranging planktonic foraminifera and nannoplankton incorporated within the cores made the determination of *in situ* microfossils difficult and age-dates were sometimes assigned with low confidence. Zonations are also assigning using the following: Fornaciari and Rio, 1996; Fornaciari et al., 1996; Raffi et al., 2003; Rio et al., 1990).

The results of this analysis were prepared by J.P.G. Fenton and presented in Appendix D. The radiocarbon dates for the Livadi Marsh borehole C6c were provided by Christopher Ramsey of Fugro Robertson. All core photographs presented in this chapter are provided by J. Crawshaw. The cores are currently stored in Fugro Robertson's facility in North Wales. Sea levels quoted are in terms of relative sea level in metres. A full summary of the drilling programme is presented in Appendix B.

BOREHOLE INFORMATION

Location	Borehole	Coordinates (WGS 84 - Zone 34S)			Length of core (metres)	Depth below surface (metres above/below sea level)	Dates Drilled
		Easting (X)	Northing (Y)	Elevation (Z)			
Petrikata quarry anomaly	**C1**	453255	4236865	212	19.7	192.3	14 Jan 2011 to 15 Jan 2011
Agia Kiriaki area	**C2**	453851	4239838	56	67.9	-11.9	07 Oct 2010 to 15 Oct 2010
Agia Sotira	**C4a**	453030	4236211	179	72.9	106.1	02 Dec 2010 to 15 Dec 2010
	C4b	452938	4236135	166	90.5	75.5	20 Oct 2010 to 02 Nov 2010
	C4c	453053	4236064	192	42.7	149.3	10 Jan 2011 to 13 Jan 2011
Lake Katachori	**C5a**	452924	4236652	178	30.0	148.0	17 Dec 2010 to 20 Dec 2010
	C5b	452886	4236474	174	23.7	150.3	16 Oct 2010 to 19 Oct 2010
	C5c	452752	4236125	164	102.2	61.8	03 Nov 2010 to 01 Dec 2010
	C5d	452724	4236552	172	14.5	157.5	15 Dec 2010 to 17 Dec 2010
	C5d2	452791	4236597	171	24.0	147.0	20 Dec 2010 to 22 Dec 2010
	C5e	452847	4236168	160	22.2	137.8	27 Jan 2011 to 28 Jan 2011
Livadi marsh	**C6a**	449569	4237613	2	26.4	-24.4	27 Sept 2010 to 30 Sept 2010
	C6b	449583	4237086	1	24.7	-23.7	01 Oct 2010 to 04 Oct 2010
	C6c	449729	4236722	0	39.0	-39.0	05 Oct 2010 to 07 Oct 2010
Atheras	**C7a**	448471	4243008	2	15.0	-13.0	29 Jan 2011 to 31 Jan 2011
2006 borehole calibration	**C2006**	452797	4234580	101	58.5	42.5	17 Jan 2011 to 24 Jan 2011
	C2006-2	452795	4234620	99	21.4	77.6	25 Jan 2011 to 26 Jan 2011

Table 5.1 Summary of the shallow sedimentary borehole programme.

5.2 Boreholes

Northern Paliki was split into seven areas on the basis of the designations used by the report KEFALONIA: ONSHORE SHALLOW DRILLING PROGRAMME (Appendix D) authored by J.P.G. Fenton of Fugro Robertson Limited compiled to present the results of the programme.

5.2.1 AREA 1: Atheras

A single 15 m deep core (C7a) was drilled into the Atheras valley (Figure 2.5) to determine the depth of the recent bay-fill and whether this narrow sediment-filled valley could have been submerged during the Late Holocene. Dating of these sediments, if possible, may determine whether coseismic uplift caused the numerous terraces cross-cutting the bay.

5.2.2 AREA 2: Livadi Marsh

Three continuous cores of depth c. 30 m depth were drilled into Livadi Marsh (C6a, C6b and C6c) (Figure 2.7) to sample estuarine bay-fill sediments and investigate the postglacial (Holocene) flooding history of Ithaca's possible "deep harbour" and whether any Late Holocene coseismic activity has affected this part of Northern Paliki in order to calibrate this with the Atheras core. Radiometric dating of flooding surfaces at depths 5 m, 6.3 m and 7.2 m was undertaken using downhole samples from the C6c borehole where the recent fill was found to be thickest. If marine cores are subsequently drilled into the Gulf of Argostoli, the Livadi Marsh cores will provide an important onshore reference for the marine sediments. These boreholes also calibrated the following resistivity/seismic lines: C6a (LML4), C6b (LML2a and C6c (LML3).

5.2.3 AREA 3: Agia Kiriaki

A single core (C2) was located to penetrate the edge of the Zola talus fan (Figure 3.24) and proposed northern exit of "Strabo's Channel" (Figure 2.8). The results of the field-mapping suggested that this location near Zola was the most likely route that a marine channel could have taken. As previously discussed in Section 3.4, previous studies suggest the Zola talus is very young (thousands to hundreds of years old) (Gaki-Papanastassiou et al., 2011) and this opened the possibility that the Zola landslide might have covered "Strabo's Channel". The aim of the core was to sample this talus material, to determine its depth and volume and whether young (Late Holocene) marine sediments existed below this landslide.

5.2.4 AREA 4: Agia Sofira – Nifi

A single core (C1) was drilled within the positive anomaly detected by the gravity survey near Petrikata Quarry (Figure 2.9). This borehole was aimed at investigating whether this outcrop was a large clast detached from the west-facing slope of Imerovigli and embedded within the valley axis or if it formed part of a thrust fault and therefore *in situ* bedrock at c. 200 m above sea level. If this outcrop was *in situ* bedrock, then the borehole was aimed at determining bedding plane dip and whether a channel could still reach sea level at this location after projection of this dip to sea level. It also looked for evidence of recent marine sediments onlapping this block which is located at the furthest and highest point from present sea level in Thinia.

5.2.5 AREA 5: Kondogourata – Petrikata Lakebed – north

Six cores were located within Lake Katachori: C5a, C5b, C5c, C5d, C5d2 and C5e (Figure 2.9). These cores were located on the basis of where the conductive "lake fill" sediments were at their thickest based on inversion of the 2007 ground-based resistivity survey. In order to determine an age-date for the earliest lake deposits the

cores were required to precisely identify the lake bed (i.e. the interface between the "lake fill" and bedrock) as this was not clearly defined in the geophysical surveys due to these two sediment types having very similar physical properties, at the deepest part of the lake. The first lacustrine sediment laid upon the bedrock at this location represented with the first lake sediments to be laid down and therefore the oldest lake fill (assuming minimal post-depositional reworking or disturbance of sediments from their original deposition position). These cores were also looking for evidence of landslide material within and below the lake to help diagnose how the lake was formed. C5e was positioned to penetrate the deepest lake-related sediments and youngest sediments to be overthrust by the Agia Sotira Thrust. The dating of the uppermost sediments of C5e was therefore crucial as these would age-date the formation of the Agia Sotira Thrust.

5.2.6 AREA 6: Kondogourata – Petrikata Lakebed – south

"Area 6" covers the boreholes drilled in the southern part of the lake (C5c and C5e) and those within the proposed route of "Strabo's Channel" to the east of the Agia Sotira Thrust (C4a, C4b and C4c) (Figure 2.9). The "C4" cores were drilled to investigate the channel cut directly and to detect whether the subsurface continuation of the easterly-dipping limestone of the Agia Sotira Thrust extended cross-cut the proposed Channel route preventing such a channel from reaching Mycenaean sea level. C4b was drilled to determine the eastern side of the lake and found thick limestone. This borehole was made deeper than its original 10 to 20 m in order to determine whether this limestone represented a very large clast or the continuation of the Agia Sotira thrust fault and to gauge the steepness of the limestone bedding plane dip. This borehole continued to be drilled for 90.5 m and still did not find the base of the limestone however, towards the bottom of the core the limestone was heavily brecciated suggesting the core was close to penetrating the fractured base of the "clast" or thrust plane of the Agia Sotira Thrust. C4a was also an important core as, in the case of an untranslated buried Channel, it would penetrate the Channel axis.

5.2.7 AREA 7: Par Sofia – Kouroukata - Farsa

In the absence of Late Quaternary to Holocene deposits elsewhere in Thinia, the Oct 2006 borehole site was revisited to re-sample the sediments here. C2006 was located to re-drill the original Oct 2006 borehole with the aim of re-sampling and definitively age-dating the suspected Quaternary sediments (*Ehux*) detected by the Oct 2006. A further borehole (C2006-2) was drilled into what would be the axis of the buried channel deduced from the Oct 2006 results (Figure 2.10).

5.3 Core Ties and Cross-sections

Five dip-orientated core-ties and three core-penetrated cross-sections (in the case of where only a single borehole was drilled in the case of C1, C2 and C7a) have been constructed by the author using the core ties and analysis produced by Fugro Robertson Ltd (Figure 5.8 to Figure 5.20). The purposed of these core-ties and cross-sections was to while providing clarity of the complex sub-surface structural geology of the survey areas. The locations and lengths of these core ties are summarised in Table 5.2. These core-ties followed the area conventions laid out by Fugro Robertson Ltd except for G-G' which provided a N-S core-tie between Area 5 and Area 6.

Two versions of the core-ties are presented. The first presents the core-ties with a vertical = horizontal scale and was constructed to show the configuration of the basic stratigraphic units and their angle of apparent dip. This was combined with cross-sections constructed using projection of the dip of visible surface bedrock taken during field-mapping. Angle of bedding projected from surface measurements where no borehole data available. The second version had an exaggerated vertical scale to show detail within the units themselves including fine veneer of recent sediment and any clastic influxes. An easterly apparent bedding plane dip is assumed due to field observations. Direction of apparent dip is extrapolated from surface measurements of dip. The cores were tied according to their lithology logs. The core-ties are accompanied by maps showing their location. Heights are in terms of elevation above mean sea level (MSL).

Location	Core-tie	Cores	Orientation (approximate)	Length (m)
AREA 1: Atheras	A-A'	C7a	W-E	536
AREA 2: Livadi Marsh	B-B'	C6a - C6b - C6c	N-S	1348
AREA 3: Agia Kiriaki	C-C'	C2	W-E	1043
AREA 4: Agia Sofira - Nifi	D-D'	C1	W-E	366
AREA 5: Kondogourata - Petrikata Lakebed - north	E-E'	C5c - C5e - C4b - C4a - C4c	W-E	906
AREA 6: Kondogourata - Petrikata Lakebed - south	F-F'	C5c - C5b - C5a	NE-SW	904
AREA 5 to AREA 6: Petrikata Lakebed - north to south	G-G	C5d - C5d2 - C5a - C5b	W-E	727
AREA 7: Par Sofia - Kouroukata - Farsa	H-H'	C2006 - C2006-2	W-E	290

Figure 5.2 Summary of core-tie and cross-section information.

5.3.1 AREA 1: Atheras (C7a) = A-A’

The A-A’ cross-section (536 m long) was placed to cross-cut the narrow valley fill of Atheras Bay and tie this into the limestone on either side of the valley (Figure 5.8). The geophysical surveys for this location (Section 4.3) showed that the valley contained a thick (at least 20 m) deposit of conductive (~1 to 20 Ωm), magnetic sediments suspected to be alluvial in origin and resulting from marine inundation sometime in the recent past.

While C7a confirmed the presence of marine clays to a depth of 11.5 m, the sediments were difficult to date due to the amount of unconsolidated clastic and reworked debris they contained. The clays were tentatively assigned a ?Pleistocene-Aquitanian age and these onlapped ?Paleogene limestone. The presence of clastic deposits suggested close proximity to a fault. ABL5 suggested that the borehole may have entered the south-easterly dipping limestone ridge of one of the NW-dipping, NE-SW orientated normal faults which cross-cut the valley buried here by sediment. In which case, the ?Pleistocene-Aquitanian unit detected by this core may be thicker elsewhere.

Figure 5.21 Limestone and conglomeritic clastic material from the lower part of C7a between 9.1 and 15 m [core].

The abundance of reworked clastic material made identification and dating of marine assemblages inconclusive and it wasn't possible to tell if any coseismic uplift had affected the valley (Figure 5.21). However, possible *Gephyrocapsa carribeanica* at 3.5 m [core] suggested the upper clay unit are marine in origin and Middle Pleistocene (Ionian) in age (0.79 Ma to 0.126 Ma) which would suggest that sea levels once filled this narrow inlet at least as far inland as this borehole at that time. It was not possible to tell if the area had been inundated by sea more recently (within the last 10 000 years).

The well-rounded igneous or basement clasts scattered throughout the 4.0 and 7.9 m [core] unconsolidated conglomerate unit may represent volcaniclastics transported into the valley from elsewhere.

5.3.2 AREA 2: Livadi Marsh (C6a-C6b-C6c) = B-B'

The Livadi Marsh core-tie was orientated roughly north to south, running from the top of the marsh to the shoreline and spanned 1348 m (Figure 5.9 and 5.10). The geophysical surveys at Livadi Marsh (Section 4.4) detected a thick (at least 20 to 80 m) deposit of conductive (1.0 to 10 Ωm), magnetic (≤40 nT) sediments interpreted as being marine in origin. The key outcome of the coring here was to determine the age of these sediments.

The core-tie was composed of a thick (at least 31.5 m) deposit of Early Pliocene to Middle Pleistocene (Ionian) aged sediments which became younger southwards which were overlain by a thin layer (0.75 to 7.5 m) of recent sediments. The Early Pliocene-Middle Pleistocene sediments were deposited in a shallow estuarine marine (less than 50 m) to a marginal marine (beach)/lagoonal setting with intermittent disconnection from marine influences. The oldest marine sediments and beach deposits (Early Pliocene) occurred all the way to the base of Kastelli Hill demonstrating that the marsh area could have formed a deep natural "harbour" between the Pliocene and Middle Pleistocene. *Zygnema* type algae was detected

within the recent unit and just below the recent stratigraphic break (within boreholes C6a (1.25 m [core]) and C6b (0.25 m [core])). *Zygnema* is a genus of common free-floating filamentous algae which occurs in a strictly freshwater setting (Guiry and Guiry, 2012) and confirmed the current freshwater lagoonal environment.

Figure 5.22 Close-up of limestone beach pebbles (top) between 16.5 m and 20.5 m [core] in C6b and conglomerate at 13.30 m [core] (bottom). Image credits: JRU.

These sediments were of a comparable age to those sampled in Thinia however they were at sea level while the Thinia sediments stood up to 210 m (C1) above sea level indicating the sediments in the saddle region had undergone significant uplift relative

to the Livadi Marsh sediments. As the marsh sediments lay within the footwall of the Atheras Thrust, some of this uplift (~150 m) is presumably due to emplacement of this thrust. If the Ionian sediments are the youngest to be overthrust by the Atheras Thrust, this would date this thrust to 125 ka or younger.

The marsh sediments onlapped the buried, weathered Late Paleocene limestone (C6a, 22.5 m [core]) of the Livadi Quarry limestone ridge. The abundant layers of conglomerate and limestone beach pebbles in C6b (Figure 5.22) suggested tectonic activity at this location and implied this ridge was another thrust fault located ahead of the Atheras Thrust.

The core-tie also showed that the marsh had experienced changes in relative sea level leading to possible brief subaerial events signified by increased influxes of terrigenous material (e.g. C6a at 1.35 m [core], C6b at 11.5 m [core] and C6c at 17.75 m [core]), increase in input of freshwater input in the Late Gelasian (e.g. C6a between 1.5 m [core] and 6.0 m [core]) and C6c between 10.25 m [core] and 11.5 m [core]) or establishment of rootlet horizons (C6a, 13.5 m [core]) or *Glomus* sp. (e.g. C6c, 10.25 m [core]).

Some of these events represented changes in global sea levels. At 7.5 m [core] in C6c was a significant unconformity in which the Late Pleistocene (Tyrrhenian and Tarantian) was missing. This was interpreted as the erosive event associated with the sea level lowstand leading up to and during the Last Glacial Maximum (LGM) (~21 500 BP) lowstand erosional surface in which this area would have been subaerially exposed for around 120 ka. There was at least one possible intra-Pleistocene coseismic uplift event at in C6a marked by a rootletted horizon. This uplift event may have produced the 6 m high beach terrace which encircles the marsh.

A record of the more recent Late Holocene flooding history (since ~5000 BP) came from the radiocarbon dated samples taken from C6c. C6c was chosen for radiocarbon sampling because it contained the thickest recent sediment deposit of the three marsh boreholes (7.5 m). The deposition of thick recent sediment in C6c indicates the

marsh area was partially flooded since the LGM. The calibrated radiocarbon samples yielded the following results calculated in term of years before present (BP):

5.0 m [core]: 3362 ± 34 calBP
6.3 m [core]: 4471 ± 31 calBP
7.2 m [core]: 5206 ± 67 calBP

In the absence of a relative sea level curve for Western Kefalonia, the Fairbanks eustatic sea level curve was used to determine equivalent ancient sea level for each of these flooding surfaces. The Fairbanks curve assumes postglacial sea level continued to rise until present day and ignores any land movement independent of the eustatic mean generated by tectonism. The equivalent eustatic sea levels for these age-dates are as follows:

5.0 m [core]: 3362 ± 34 calBP = -3.8 m
6.3 m [core]: 4471 ± 31 calBP = -5.6 m
7.2 m [core]: 5206 ± 67 calBP = -7.5 m

C6c sits at 0 m. The samples therefore lie at the following depths in terms of ancient relative sea level:

5.0 m [core]: 3362 ± 34 calBP = -1.2 m
6.3 m [core]: 4471 ± 31 calBP = -0.7 m
7.2 m [core]: 5206 ± 67 calBP = +0.3 m

Sample 7.2 m stood close to the 5206 BP sea level suggesting that the shoreline was roughly in the same position as it is now in terms of how far inland it stood and represented postglacial sea levels as they rose high even to reach the marsh. The samples taken at 6.3 m [core] and 5.0 m [core] showed that postglacial sea levels then continued to rise by 3.7 m flooding the C6c site. The key radiocarbon sample taken from C6c is 5.0 m as this flooding surface is close to the time of Odysseus and showed that the 3362 BP shoreline extended inland along the core-tie at least 75 m

where it onlaps the Ionian unit. It is probable at this time that the marsh area would also have been flooded but only to around 1.2 m which can hardly be considered a "deep" harbour. Further drilling and sampling of sediments in the central part of the marsh would be required to further investigate this.

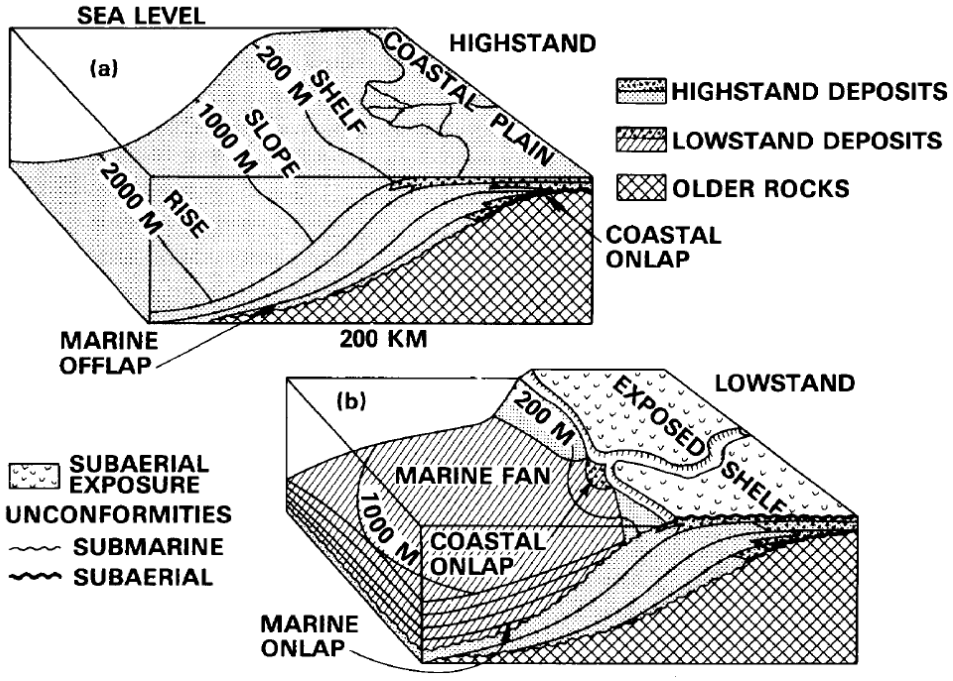

Figure 5.23 Block diagrams illustrating depositional patterns during highstand (a) and lowstand (b) of sea level (from Vail et al., 1977).

Above 5.0 m [core] a low diversity of marine microfossils were detected at 2.5 m [core] with algae on the sea bed (but not sea grasses). With no rootlets reported until 0.25 m [core] which can be tied to the most recent exposure of the marsh, the plant/lignitic material present below this came from the shore suggesting a marginal marine (lagoonal) setting. A 1.5 m thick unit of sand suggested the marsh was exposed (highstand systems tract, HST) above 1.5 m [core] with a maximum flooding surface (MFS) around 1.5 m [core] (Figure 5.23)

The radiocarbon samples showed that the flooding surfaces since the Bronze Age corresponded well to the equivalent ancient sea level with no need for coseismic uplift. The subsequent "drying-out" of the marsh was due to Late Holocene

coseismic uplift of the shoreline as previously believed and could instead be explained in terms of progradation and aggradation of the marsh sediments where sedimentation input from the land overtook sea level rise. Establishment of the land spit across the mouth of the marsh (Figure 2.6) would have occurred since 3362 BP preventing further marine inundation.

5.3.3 AREA 3: Agia Kiriaki (C2) = C-C'

This cross-section ran through the Zola talus and was placed to tie this borehole into the observed bedrock formations to the east of the talus fan (Figure 5.11). The core from C2 represented a tectonically-disturbed succession of Late to Early Pliocene (Zanclean to Piacenzian) marls and clays (1.0 m [core] to 55.9 m [core] in depth) alternating with Late Miocene (Tortonian) limestones and marls. Below 15.5 m [core] of reworked clays and siltstones are hard marls which show bedding, an interface marked by a large (50 cm) limestone boulder. It was hard to interpret the findings of core without a further borehole nearby with which to tie the observed strata in C2.

C2 was aimed at penetrating the edge of the Zola talus fan. However, the core missed the lithified edge of the fan and instead penetrated the boulder field around 30 m to the east of the edge. The first 20.4 m of the core penetrated Early to Late Pliocene marls and clays which had no clear bedding which suggested these upper sediments were deposited after the deformation episode which tilted the Neogene sediments elsewhere in the valley. Gravelly horizons occurred throughout, particularly within the top 12 m of the core, indicating regular small clastic influxes and a possible limestone clast (50 cm in diameter) occurred at 15 m [core]. Notably absent were the large-scale, chaotic clast-rich deposits expected if the borehole had penetrated a thick deposit of talus material but these were probably further to the west of this location within the lithified part of the fan.

The sediments from 20.4 m [core] were tilted to 60° which matched the dip detected elsewhere in the valley and suggested they were *in situ* bedrock. The repeating elements and large block of ?Miocene sandy limestone penetrated between 38.45 m [core] and 55.9 m [core] were most likely to be part of tectonically-emplaced block similar to that observed in the Agia Kiriaki Bay sea cliff rather than a slump of the steep limestone scarp above Zola. Evidence in favour of this was where the core appeared to penetrate a loop-like structure between 38.25 m [core] to 41.2 m [core] marked by a flattening of dip from 60°.

Pliocene beach deposits occurred at c. 62 m (core) beneath a thrusted contact. These had initially been classed as Quaternary in age which suggested the Zola talus fan covered a Quaternary beach and therefore supported the idea that this was a very young landslide (hundreds to thousands of years) however the revised findings of this borehole suggested the Zola talus didn't extend this far east.

5.3.4 AREA 4: Agia Sofira - Nifi (C1) = D-D'

This cross-section was 366 in length and orientated E-W to cross-cut the limestone outcrop at Petrikata Quarry from east to west (Figure 5.12). C1 penetrated 2.6 m metres of gravelly clay (?Plio-Pleistocene) before entering heavily fractured Late to ?Middle Paleocene (Thanetian to ?Selandian)? limestone for the remainder of the core. The quantity of limestone clasts within these uppermost clays suggested this material was reworked. There are several rubbled sections within the limestone with possible dissolution cavities infilled with dark, gravelly clays and at least one open hole (between 6.3 and 6.7 m [core]) (Figure 5.24). The presence of this limestone accounts for the strong positive response in the gravity survey (Figure 4.36).

The fractured nature of this limestone supported the idea that this outcrop was a large clast which had been generated during catastrophic slope collapse of the valley side and deposited in the soft sediment of the valley axis. However, the limestone also exhibited a 60° to sub-vertical bedding plane and increased in age with depth which

tied it to the *in situ* bedrock sampled by the other cores within the valley and suggested the outcrop was another thrust fault. Projecting a bedding plane dip of 60° to sea level, the presence of this thrust fault makes fitting a marine-level channel at this location impossible.

Figure 5.24 Sections from C1 core (6 to 13.1 m) showing the heavily-fractured nature of the limestone containing dark gravelly clay-filled dissolution cavities and open holes.

5.3.5 AREA 5: Kondogourata – Petrikata Lakebed – north (C5d – C5d2 – C5a – C5b) = E-E'

B-B' formed a core-tie through the proposed deepest part of the lake running (from west to east) from the limestone defining the western shore of Lake Katachori, across the northern part of the lake and to the Agia Sotira Thrust on the eastern side of the lake (Figure 5.13 and 5.14).

The lake "fill" sediment in C5d and C5d2 were composed of bright chestnut-red oxidised clays (Figure 5.25). These clays had sub-horizontal to planar bedding planes and contained localised horizons of limestone gravel, lignite and charcoal concretions as well as degrading rootlet horizons. C5b had the thickest deposit of recent sediment which was mixed in with clastic material (Figure 5.26). These clays accounted for the low resistivity, low gravity signature detected by the non-invasive surveys across the lake (Section 4.5.4).

The limestone-lake "fill" contact was detected by C5d and C5d2. Cargenuele deposits – a non-dolomitic veined or brecciated carbonate rock described as being yellow-brown in colour and associated with Triassic dolomite, gypsum and anhydrite (Warrak, 1974; Grandjacquet and Haccard, 1975) - were found in C5d and C5d2 at the unconformable surface between the "lake" sediments and limestone. This rock type is usually closely associated with evaporates and often associated with the soles of thrust planes (Vearncombe, 1982).

Figure 5.25 Section from C5d (4 to 10 m [core]) showing the characteristic chestnut-red oxidised soils of Lake Katachori.

Figure 5.26 The first 6 m of C5b showing the clastic material mixed into the recent unit.

Plio-?Pleistocene was detected in C5a to the west of the thrust however it was not clear if this was overthrust. If this stratigraphy was overthrust then the age of movement along the Agia Sotira Thrust could be dated to 1.81 Ma or younger. Unfortunately precise dating of the lake sediments was not possible. The radio-carbon dating of lignite samples was not successful due to them being contaminated with debris from the 1953 Ionian Earthquake.

5.3.6 AREA 6: Kondogourata – Petrikata Lakebed – south (C5c – C5e – C4b – C4a – C4c) = F-F'

A-A' formed a cross-section across the southern part of Lake Katachori perpendicular to the lake's long axis and tied the lake boreholes C5c and C5e with C4b, C4a and C4c (Figure 5.15 and Figure 5.16). This core-tie was intended determine whether the "lake" sediments overlapped the proposed Channel route and whether there was a marked different between these sediments and those to the east

of the Agia Sotira Thrust. The sediments formed repeating Quaternary-Neogene stratigraphically conformable units which aged eastwards and dipped 40 to 60° separated by the Agia Sotira Thrust. The presence of interbedded thick and thin layers of marl suggested a similar configuration of bedded marl to that observed in the northern part of the valley (described in Section 3.2.1). There was some evidence of small-scale (centimetres) bedding deformation within this section but no evidence of major dislocation of the sediments. The core-tie could be split into 3 sections (from west to east):

1. "Sub-lakebed" sediments (C5c and C5e): Early to Late Pliocene succession of clastic material and conglomerates composing the footwall of the Agia Sotira Thrust. Bedding plane dip is difficult to determine due to the unconsolidated nature of much of the core including the entire lower portion of C5c (28.7 m to 102.2 m). C5c was composed of Pliocene clays interbedded with limestone clastic material with a limestone debris matrix which were interpreted as tectonically-controlled submarine debris flows originating from submarine fault scarps. C5c is important because it penetrates the suspected landslide, the tongue of which can be seen onlapping the western valley side. The repetition of sedimentary packages may reflect repeated debris flows or faulting of the succession.

Despite reaching a maximum depth of 102.2 m below the surface, and being situated around 200 m from the edge of the lake shore C5c did not detect the subsurface continuation of the easterly-dipping limestone ridge defining the western "lake shore". A projection of the surface dip of this ridge would mean the limestone surface was expected at ~2.5 m [core] depth. This suggested that the ridge dipped too steeply to be detected by the borehole (60° or more) possibly due to dramatic topography of the limestone surface or indicated the presence of a fault, either the northern continuation of the westerly-dipping backthrust observed above Agia Sotira bay or an easterly-dipping normal fault.

Borehole C5e was placed to collect dating evidence of these sediments. C5e was composed of very poorly consolidated limestone debris with limestone and limestone

breccia clasts (Figure 5.27). In the first 2.5 m of the core, these clasts date to the basal Paleocene (Danian) and below this they are Upper Cretaceous (?Santorian-Campanian) (sampled from 1.75 m [core] and 2.0 m [core]). The Danian is missing from other limestone exposures pointing towards an erosive event. The unconsolidated nature of the limestone in this core may suggest that C5e penetrated the fault gouge within the fault plane. The presence of clastic material indicated the proximity of this material to an active tectonic feature (extensional faulting, formation of the Ainos Thrust or Agia Sotira Thrust). There was also evidence of beach deposits (sandstone, polymict pebbles).

While *Zygnema* algae was detected in C5e confirming a freshwater depositional environment to the west of the Agia Sotira Thrust, the Recent unit only formed a thin veneer (less than a metre) and the algae was actually found within the Pliocene unit at 2.5 m [core] indicating a possible much older freshwater phase.

Figure 5.27 The top 2 to 8 m of C5e which was composed of very poorly consolidated limestone debris with limestone and limestone breccia clasts.

2. Agia Sotira Thrust (C4b): C4b penetrated the Agia Sotira Thrust hangingwall but did not encounter the thrust plane itself. The thin layer of sediment above the limestone was very similar in appearance (pale and poorly-consolidated) to the equivalent-aged material in C5e suggested these units could be correlated. The limestone penetrated by C4b had a very steep (60°) angle of dip which mirrored the dominate angle of dip detected by the Thinia boreholes.

The Early Eocene – Late Paleocene (Ypresian – Thanetian) unit showed evidence of being deposited in a distal outer ramp neritic setting (keeled planktonic foraminifera) indicating an increase in accommodation space relative to the underlying Cretaceous and classing these sediments as post-rift. The Cretaceous was rich in rudist reefal material and was indicative of a shallow neritic to lagoonal setting. The unconformity between the two sedimentary units represents the boundary between syn-rift and post-rift carbonate sediments.

3. Stratigraphically conformable Middle-Late Miocene to Early Pleistocene succession (C4a and C4c): The Agia Sotira Thrust brought an Early Pleistocene (Gelasian) - Middle (Burgadalian) to Late Miocene (Tortonian) stratigraphically conformable succession over the Late to Early Pliocene sediment of the lake area. Neither C4a nor C4c encountered the expected subsurface continuation of the easterly-dipping limestone associated with the thrust hangingwall despite being located only ~100 m and 150 m respectively from C4b implying the angle of dip of this thrust was at least 45°.

The uppermost 0.75 m [core] to 8.0 m [core] of C4c consisted of Early Pleistocene aged sediments dating emplacement of the Petrikata thrust to the east of this location to no later than 1.80 Ma. This unit contained rich reworking of *Orbulina* spp. and *Globigerina regina* interpreted to be derived from Late to Middle Miocene (Tortonian – Serravallian) sediments. This suggested that the Miocene-Pleistocene had been emplaced again to the east by the Petrikata Thrust.

Most significantly, despite being located within the proposed axis of "Strabo's Channel" C4a and C4c showed no sign of the thick deposits of landslide debris expected from a buried Channel wedge and were interpreted to contain *in situ* bedrock.

5.3.7 AREA 5 TO AREA 6: Petrikata Lakebed – north to south (C5c-C5b-C5a) = G-G'

Core-tie G-G' was established to provide a link between A-A' and B-B' and trended roughly NE-SW and placed along the deepest part of the lake (Figure 5.17 and 5.18). The age of stratigraphy within C5c correlates with the stratigraphy within the boreholes in the north of the lake without much change in depth of the stratigraphic layers. Little thickening of the layers was observed which agreed with the idea that the sediments thickened eastwards in NE-SW striking blocks.

5.3.8 AREA 7: Par Sofia – Kouroukata – Farsa (C2006-C2006-2) = H-H'

Core-tie H-H' tied the two boreholes drilled at the southern exit (Figure 5.19 and Figure 5.20). The Oct 2006 borehole (Section 2.2.3) had detected possible traces of *Ehux* Quaternary nannofossils up to 47 m in depth below the surface suggesting reworked Quaternary material occurred here and the borehole had penetrated the edge of an infilled channel wedge. However, no trace of *Ehux* could be found by C2006 or C2006-2. This is very significant since it meant no sediment younger than Gelasian was sampled in the valley. It is possible that the Quaternary material was contamination from higher up the stratigraphy perhaps from windblown deposits at the surface. A similar-looking Neogene species *Orbulina universa* was identified throughout C2006 (e.g. 3.25 m [core], 24.5 m [core], 37.5 m [core]) so the original identification may have been incorrect.

The upper 3 to 4 m of H-H' was interpreted as valley "fill" (rockfall) material due to the lack of internal structure and abundance of reworked material predominately from the Middle to Early Miocene (MNN4 – MNN5). The large (c. 12 m) ?Oligocene – basal Miocene (Aquitanian) boulder sampled at 31 m [core] (Oct 2006) and 43 m [core] (C2006) serves as a marker bed. The Oct 2006 results suggested that the first *in situ* Late Miocene (Tortonian?) occurred below this boulder at 44 m (core). However the presence of bedding plane dip below this level similar to equivalent sediments elsewhere in the saddle region suggested that, although these sediments contained a lot of re-working, these sediments were bedrock. As no dip information was contained within the Oct 2006 results it was not possible to tell whether a similar change in dip regime (from sub-horizontal to 60°) could be detected at 5.75 m. It is likely therefore that the limestone boulder was incorporated into the Pliocene sediments are they were being deposited.

The bedding plane dip generally shallows with depth (60° to 20°). The changing of dip angle suggested the presence of shear thrusts within the sediments. Possible correlative faulted zones were found between 12.75 to 14.0 m [core] in C2006-2 and 39.75 to 44.0 m [core] in C2006. A significant horizon which did occur within C2006 and in no other borehole was a layer of igneous or basement clasts at 5.5 m ranging from 5 cm to +10 cm in diameter (Figure 5.28). These clasts were suspended within a clay matrix beneath the reworked possible rockfall unit. No equivalent volcani-clastic horizon was detected in C2006-2. A lot of the strata in this core-tie are inferred from observations of the stratigraphy from further up the valley, outcrop samples.

Figure 5.28 Section of C2006 showing the horizon of suspected igneous clasts at c. 5.5 m [core] (outlined in yellow box).

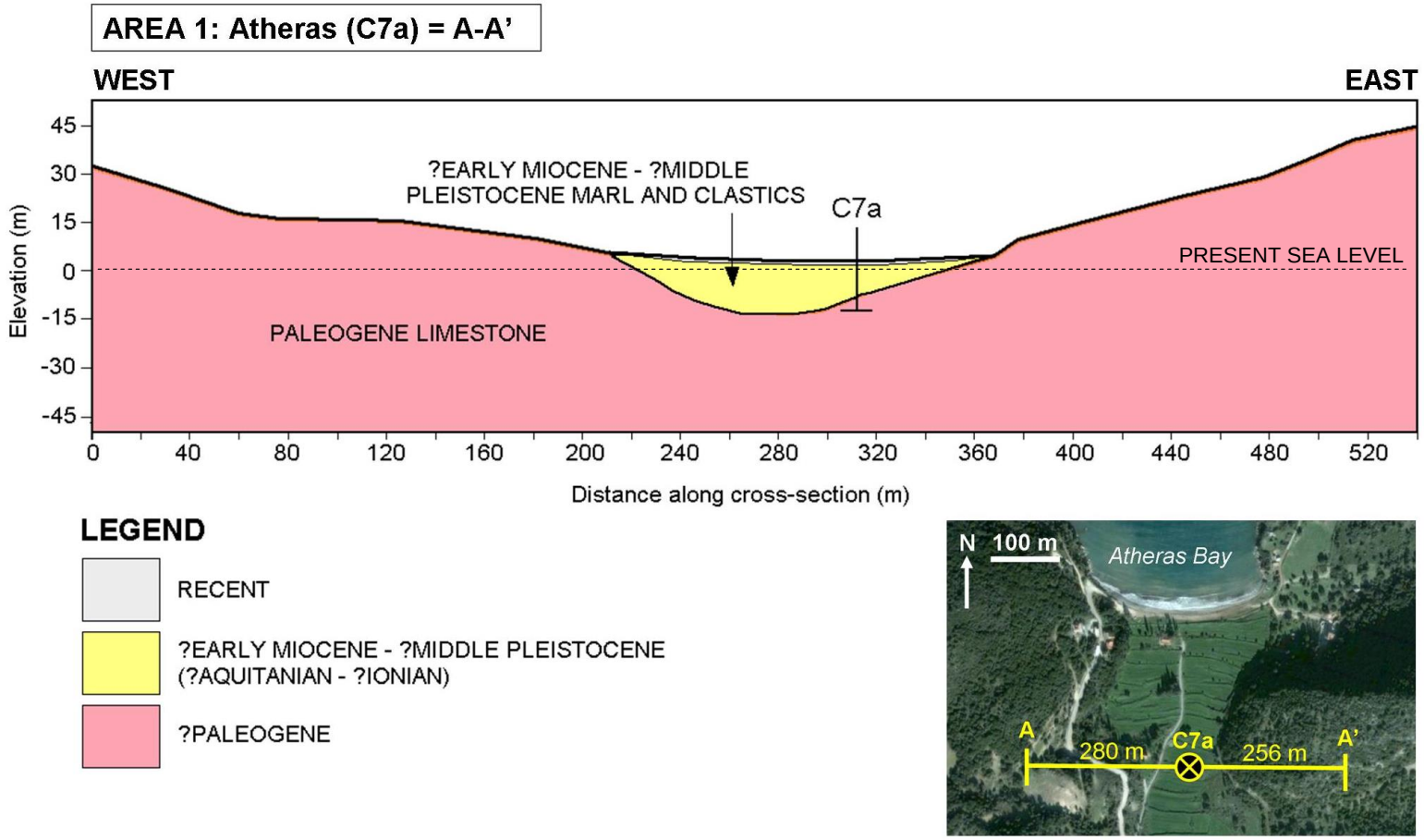

Figure 5.8 AREA 1: Vertical=horizontal scale cross-section A-A' incorporating the Atheras borehole (C7a).

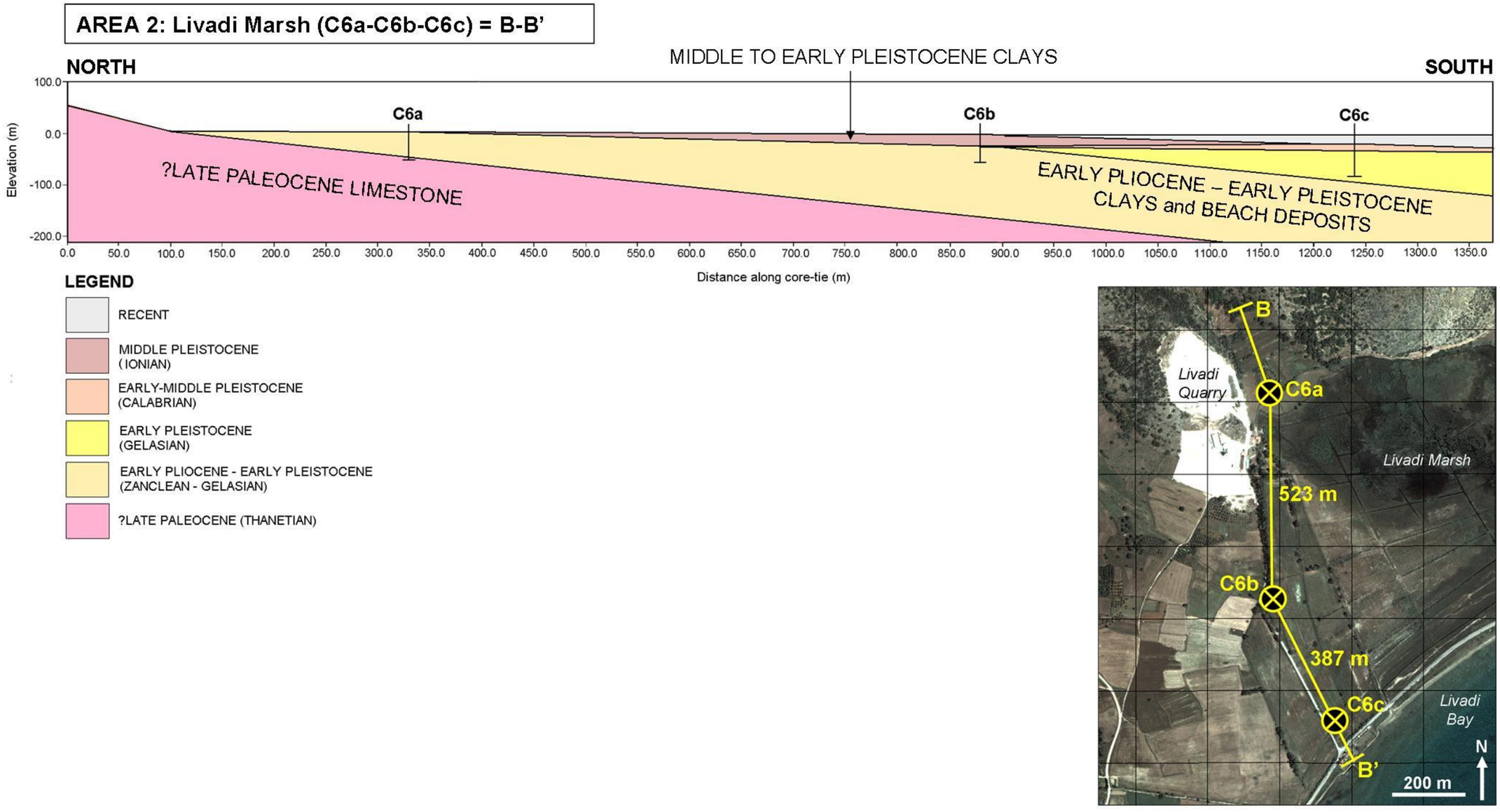

Figure 5.9 AREA 2: Vertical=horizontal scale version of Core-tie B-B' incorporating the Livadi Marsh boreholes (C6a, C6b and C6c).

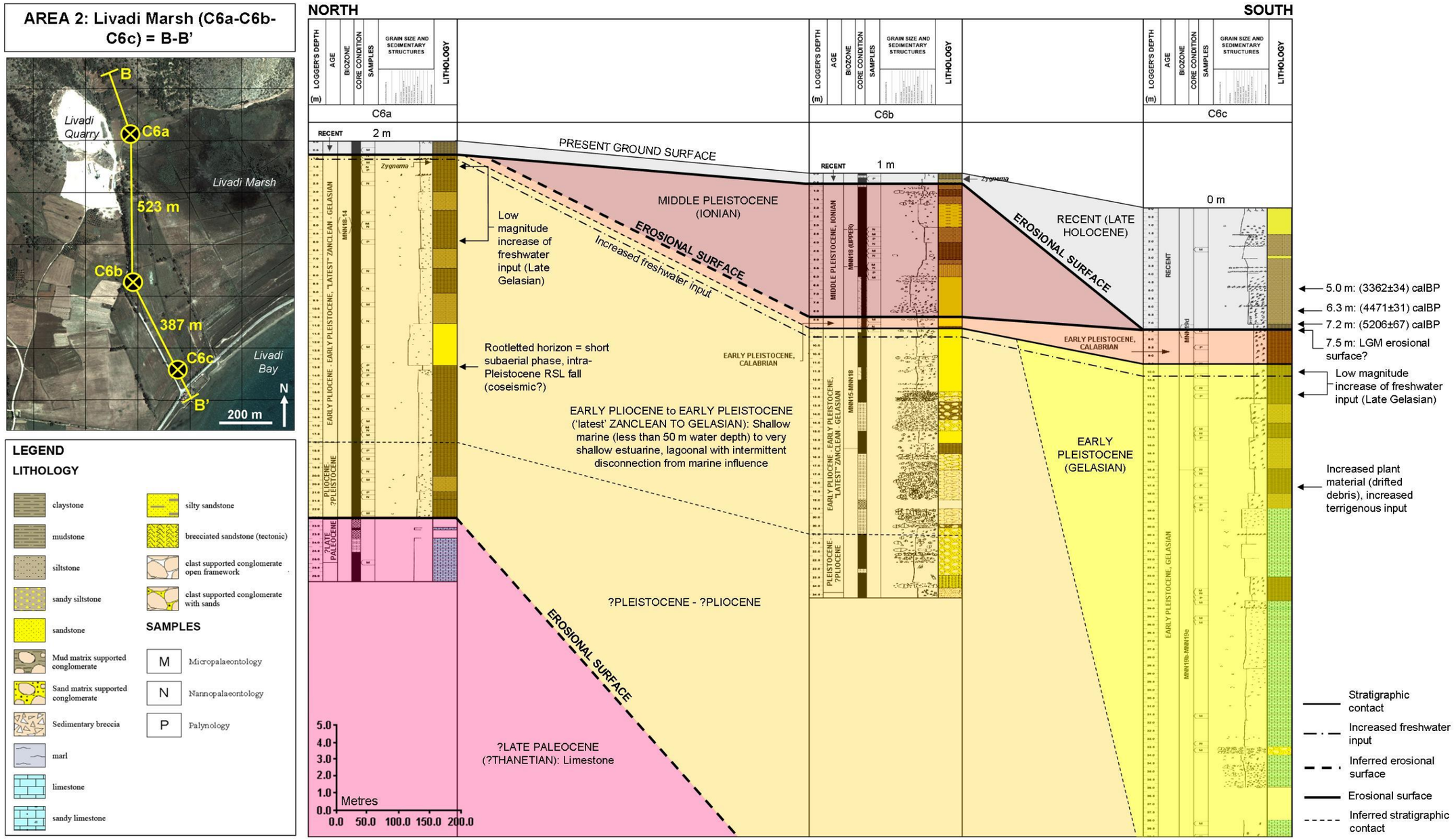

Figure 5.10 AREA 2: Vertically-exaggerated version of Core-tie B-B' incorporating the Livadi Marsh boreholes (C6a, C6b and C6c).

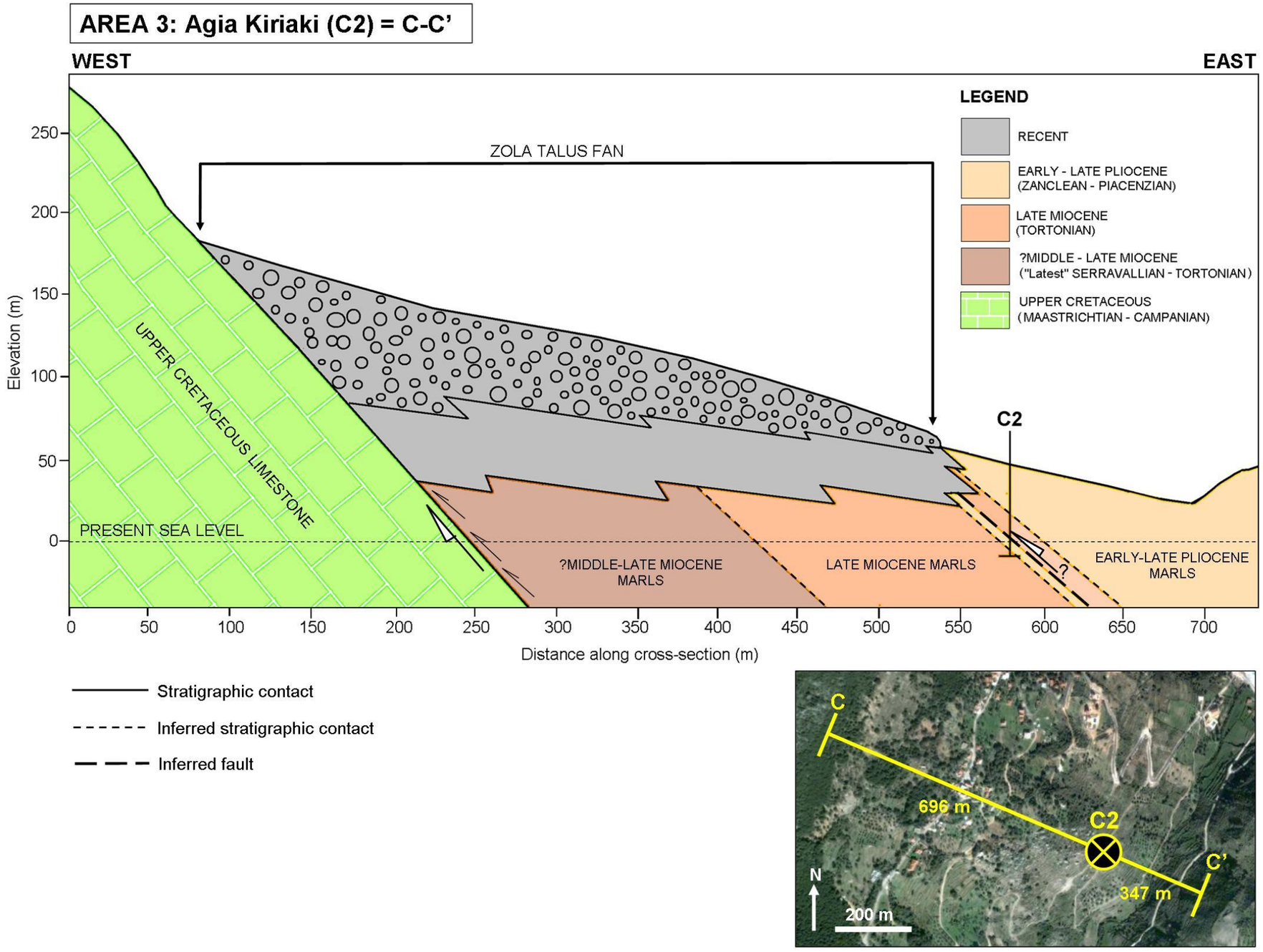

Figure 5.11 AREA 3: Vertical=horizontal scale cross-section C-C' incorporating the Zola borehole (C2).

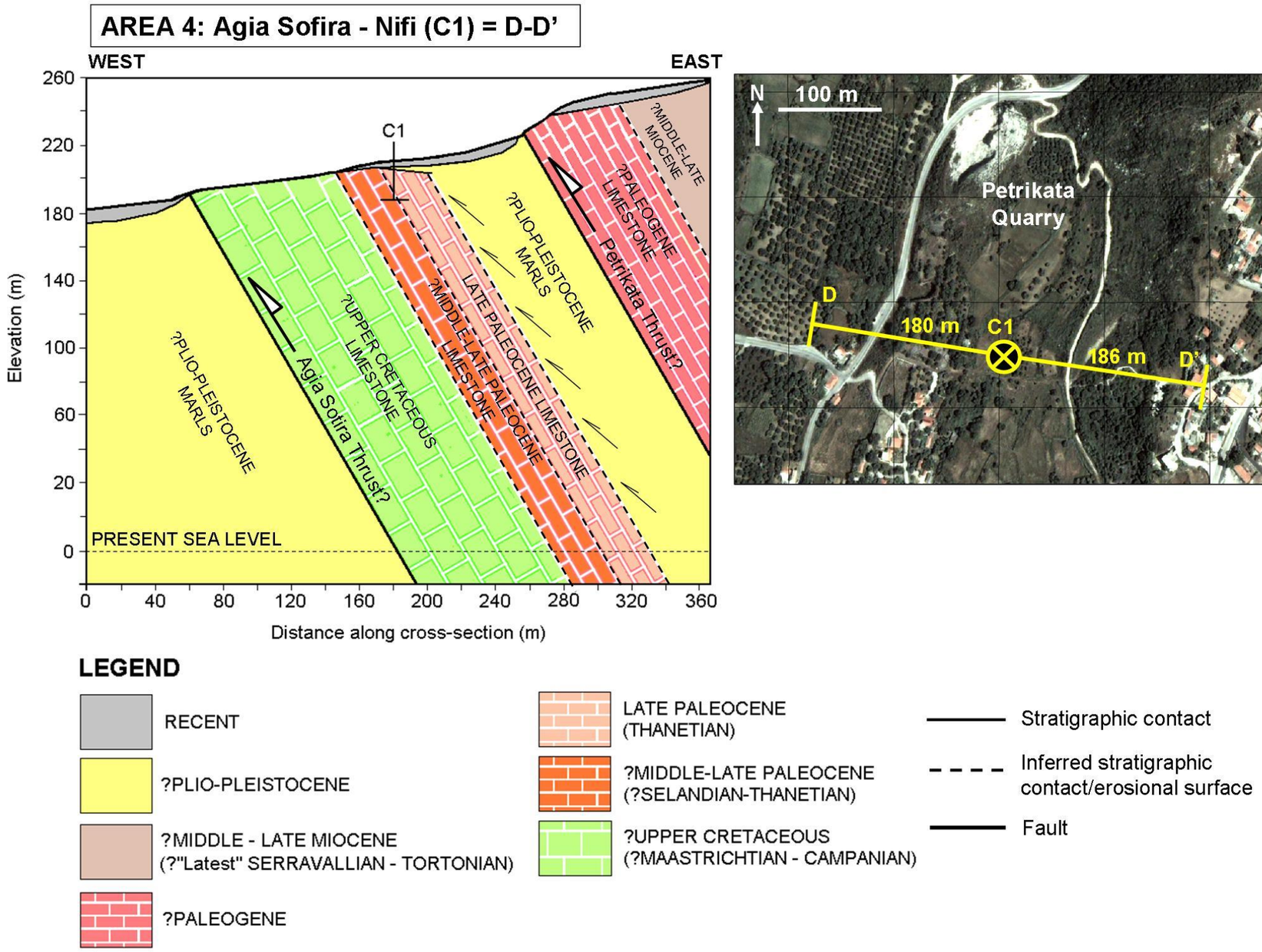

Figure 5.12 AREA 4: Vertical=horizontal scale cross-section D-D' incorporating the Petrikata Quarry borehole (C1).

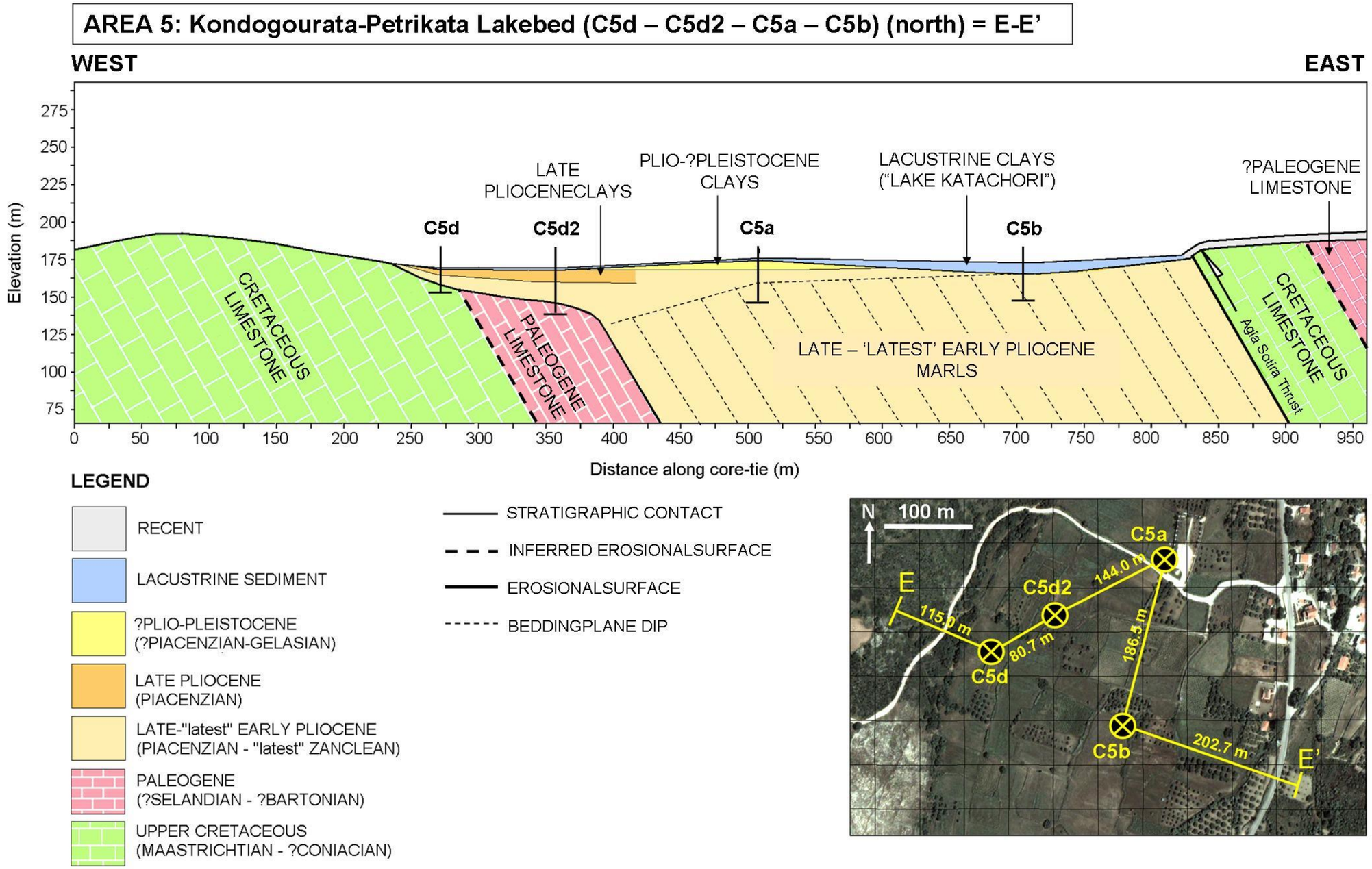

Figure 5.13 AREA 5: Vertical=horizontal scale cross-section E-E' incorporating the northern Lake Katachori boreholes (C5d, C5d2, C5a and C5b).

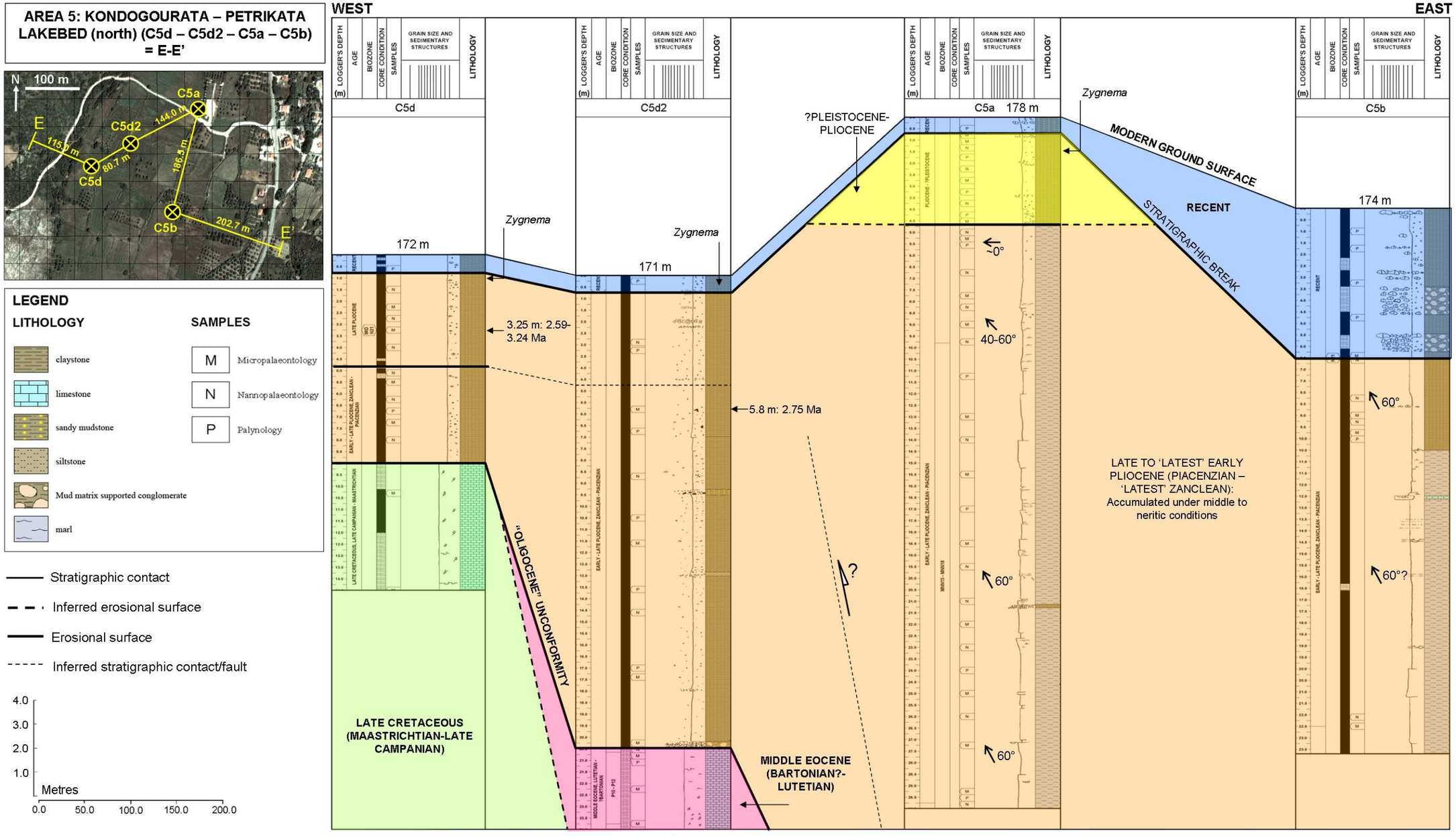

Figure 5.14 AREA 5: Vertically-exaggerated version of Core-tie E-E' incorporating the northern Lake Katachori boreholes (C5d, C5d2, C5a and C5b).

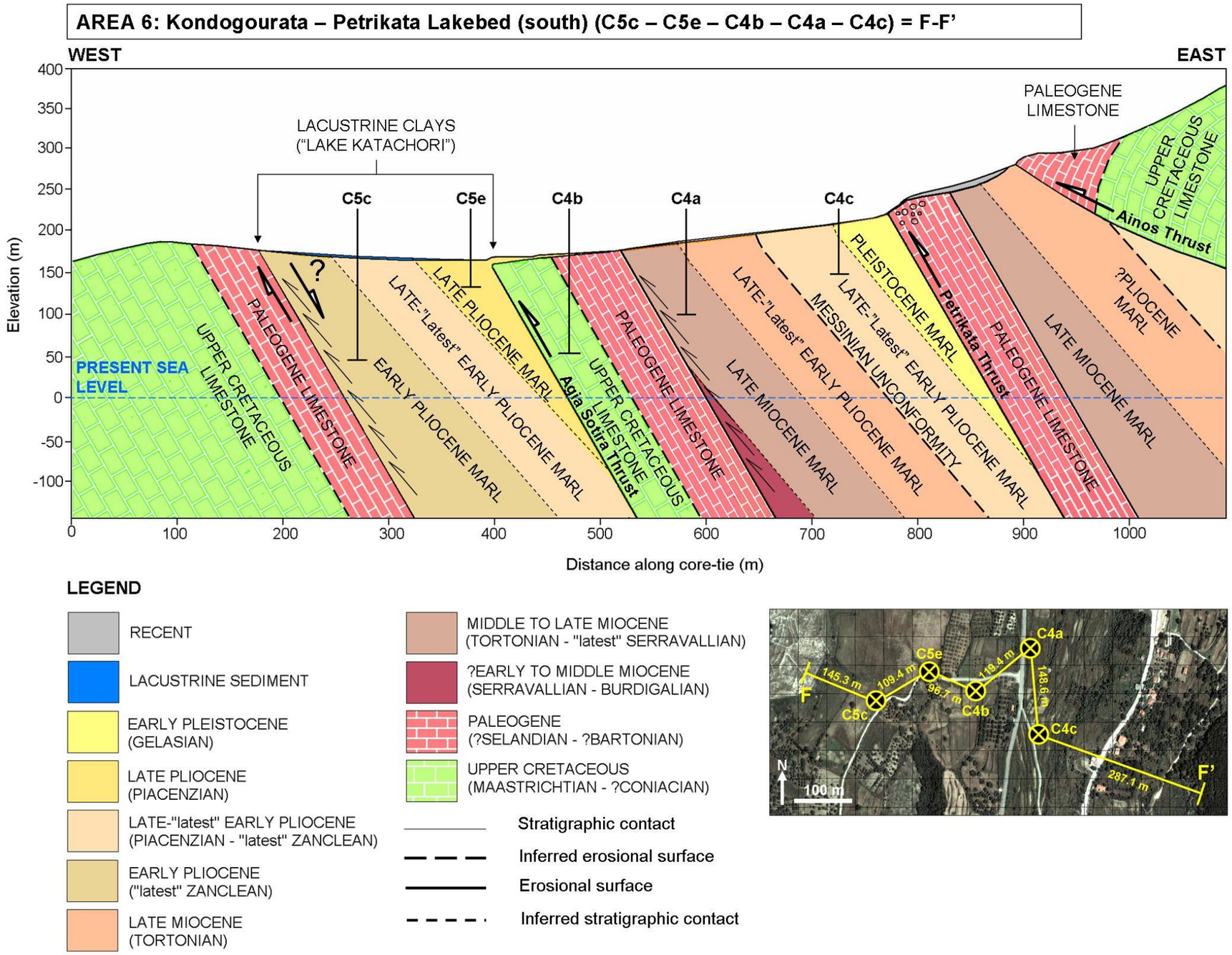

Figure 5.15 AREA 6: Vertical=horizontal scale cross-section F-F' incorporating the southern Lake Katachori boreholes (C5c, C5e, C4b, C4a and C4c).

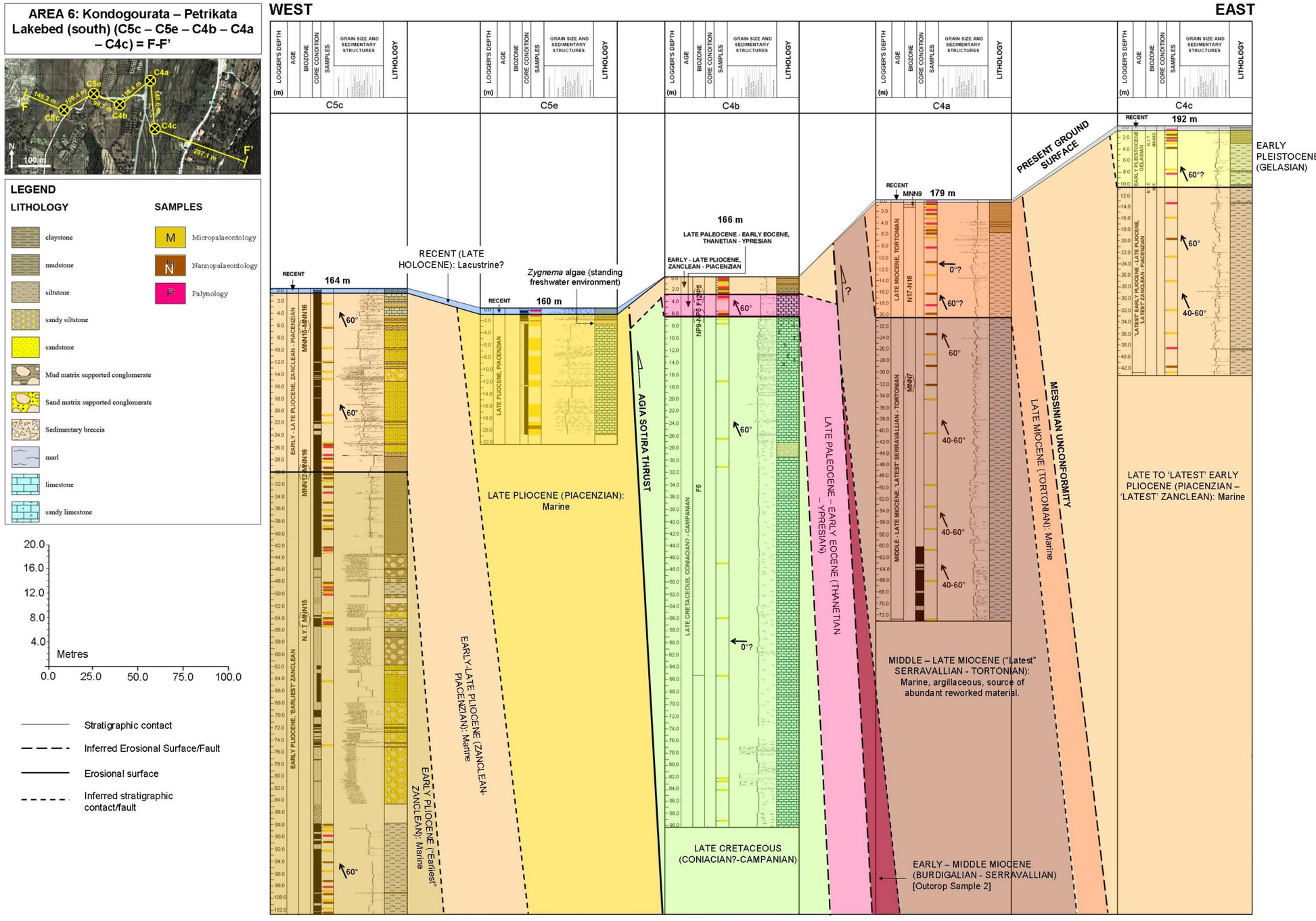

Figure 5.16 AREA 6: Vertically-exaggerated cross-section F-F' incorporating the southern Lake Katachori boreholes (C5c, C5e, C4b, C4a and C4c).

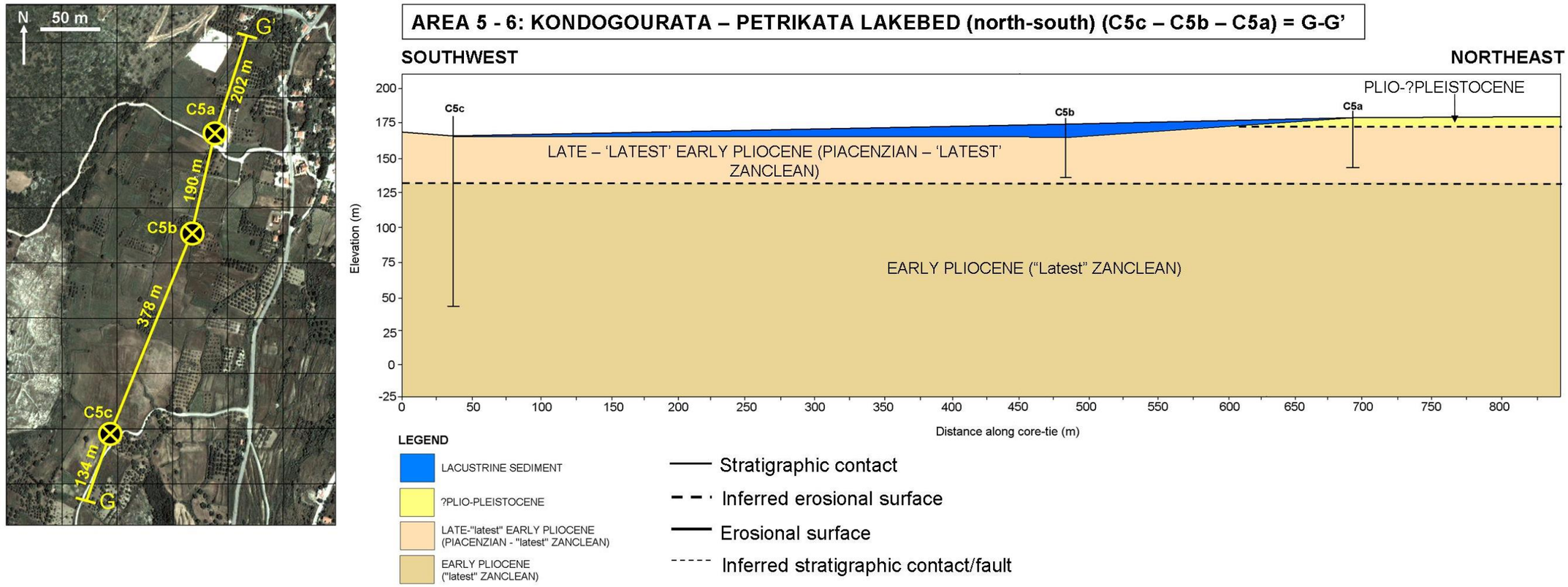

Figure 5.17 AREA 5-6: Vertical=horizontal scale cross-section G-G' incorporating the Lake Katachori boreholes (C5c, C5b and C5a).

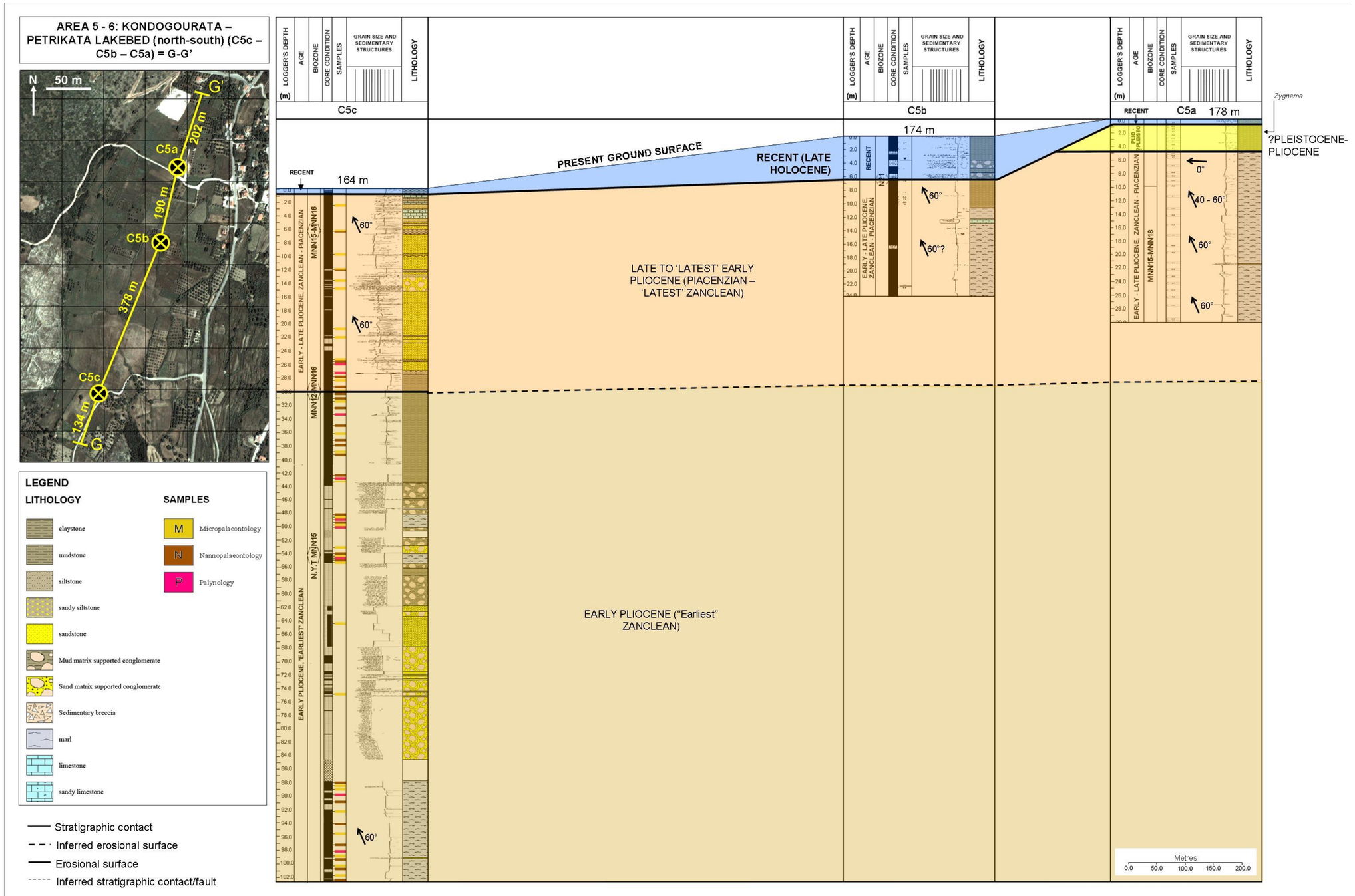

Figure 5.18 AREA 5-6: Vertically-exaggerated cross-section G-G' incorporating the Lake Katachori boreholes (C5c, C5b and C5a).

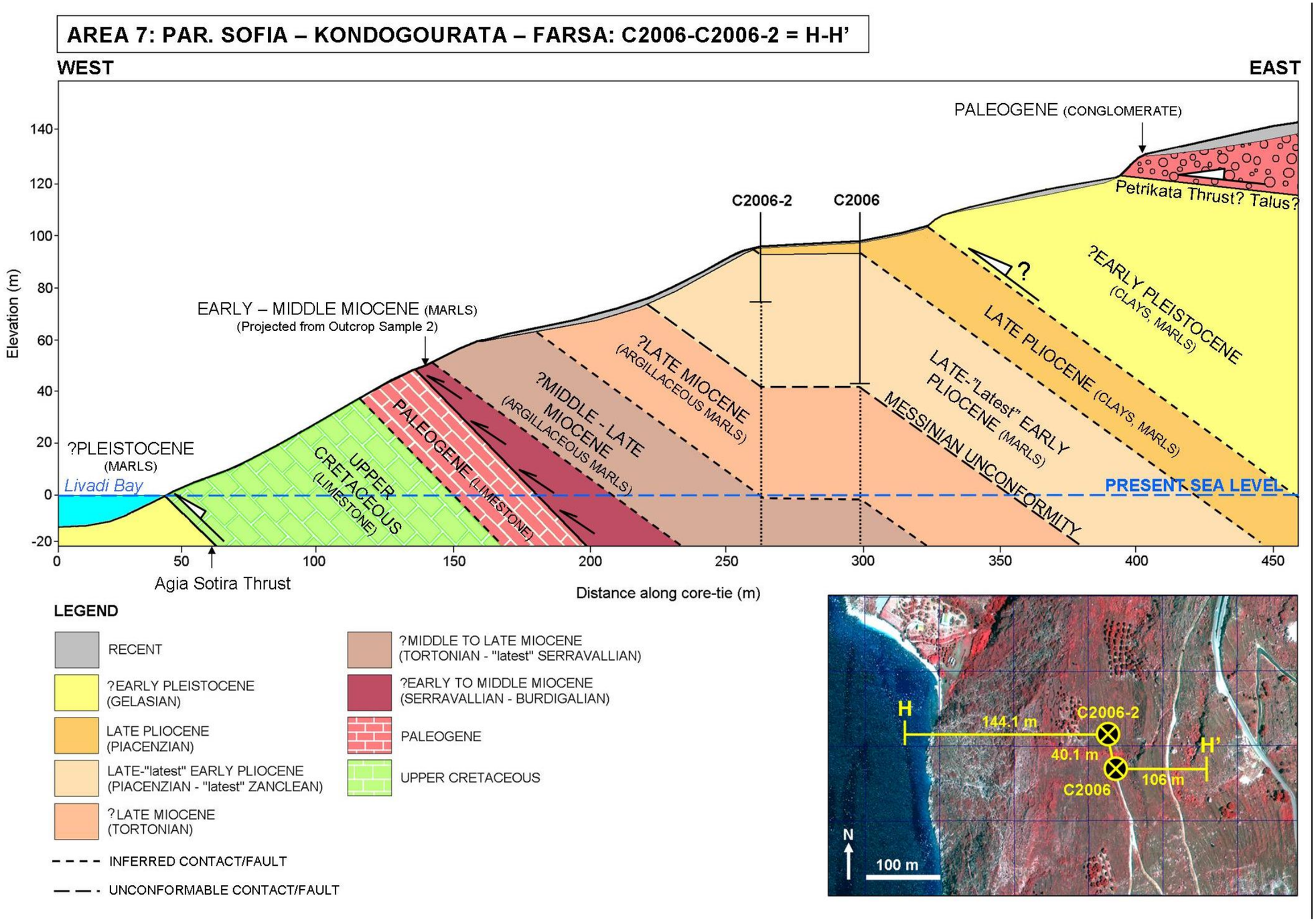

Figure 5.19 AREA 7: Vertical=horizontal scale cross-section H-H' incorporating the southern exit boreholes (C2006 and C2006-2).

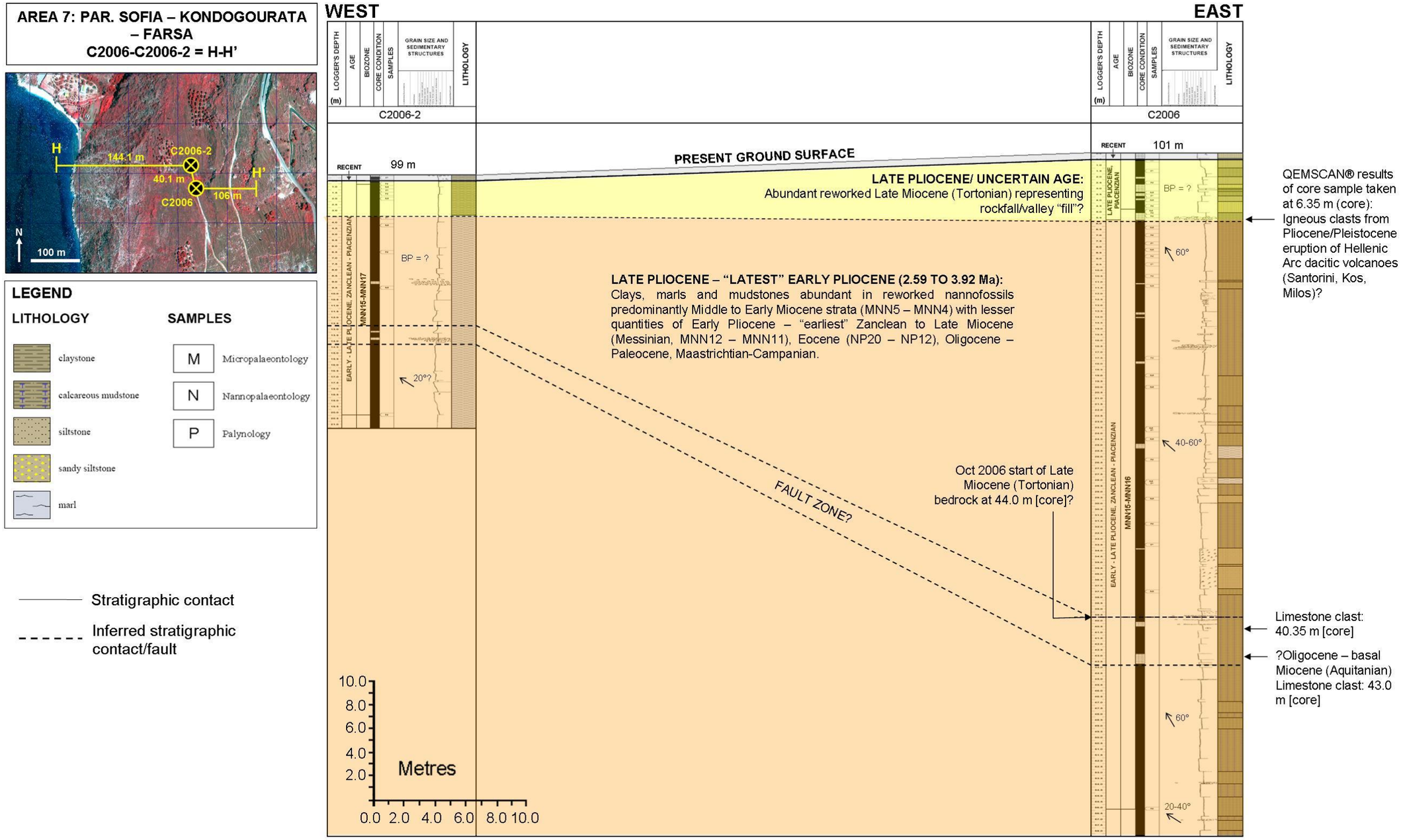

Figure 5.20 AREA 7: Vertically-exaggerated scale cross-section H-H' incorporating the southern exit boreholes (C2006 and C2006-2).

5.4 Stratigraphy

5.4.1 Thinia

Based on the findings of the boreholes and the surface samples, the stratigraphy of Thinia can be resolved into five sequences (Figure 5.29):

1. **Recent:** Lacustrine sediments, landslide material, alluvium (*terra rossa*).

2. **Early Pleistocene (Gelasian) - Pliocene (Piacenzian to Zanclean):** Marls and clays deposited in middle to outer neritic, open marine conditions.

3. **Late Miocene (Tortonian) to Early-Middle Miocene (Serravallian to Burdigalian):** Argillaceous marls deposited in neritic, open marine conditions.

4. **Late to ?Middle Paleocene (Thanetian to ?Selandian) - Middle Eocene (?Bartonian to Lutetian):** The single sample taken from the Ainos Thrust (7_Oct11) yielded an age-date of Lower-Middle Eocene and represented a fining upwards debris flow with shallow marine elements transported into a deeper, open marine setting. This confirmed that the limestones of the Ainos Thrust hangingwall were deposited in a deep water setting while the limestones within the footwall of the thrust were shallow water in origin. This also confirmed that this thrust represented a major reactivated normal fault and that reactivation occurred sometime after the Lower-Middle Eocene.

5. **Upper Cretaceous (Maastrichtian to late Campanian):** The presence of *Thaumatoporella* algae and rudist splinters within the limestones sampled by the coring survey indicated were all deposited in shallow marine conditions.

These were separated by four key unconformities or stratigraphic break (sequence boundaries) listed below. The boreholes where the unconformity was found or inferred is indicated in brackets:

1. **Middle-Early Pleistocene [all Thinia boreholes]**

2. **Messinian Salinity Crisis Unconformity [inferred between C4a and C4c, C1]:** Representing the unconformity caused during the Messinian Salinity Crisis and the removal of Upper Miocene (Messinian) and Early Pliocene ("earliest" Zanclean) sediments at these locations. Messinian-aged sediments only occur to the west of Ainos Thrust in a thin wedge at Cape Liakka at the south-western tip of the Argostoli Peninsula (Underhill, 1989).

3. **Oligocene-basal Miocene Unconformity [C5d, C5d2, C1)]:** Associated with the removal of the Upper Eocene (Priabonian), entire Oligocene and early Miocene (Aquitanian) during the erosive event caused by uplift of the Thinia area by the peripheral bulge associated with the formation of the Ionian basin? *In situ* Oligocene and basal (Aquitanian) Miocene was absent in the boreholes which penetrated the Neogene-limestone contact (C1, C4b, C5d, C5d2 and C6a). Reworked Oligocene assemblages were found in C4c, C5b, C5c, C2006, C2006-2 and C6c and reworked Aquitanian assemblages were detected in C4c. Possible *in situ* Oligocene limestone was found in 4a_Oct11 within the Agia Kiriaki sea cliff thrust. In C4c and C2006, large clasts (c. 50 cm) of Oligocene to Eocene limestone occurred within the Upper – Uppermost Pliocene (Piacenzian – Uppermost Zanclean).

4. **Unconformity between Cretaceous and Paleogene sediments [C4b]:** Representing the boundary between syn-rift carbonates (Cretaceous – Early Selandian) and post-rift (ramp) carbonates (Late Selandian – Bartonian)?

Reworked material from these "missing" sections is found abundantly within the upper sediments of Thinia. There was also evidence of further erosive events which

may tie into a phase of increased tectonism. Reworked Early to Middle Miocene (Upper Burdigalian to Langhian, MNN5-MNN4) was the most abundantly reworked stratigraphic unit but was not detected *in situ* which may relate to a period of compression affecting the area to the east which began around this time (Cushing, 1985). There were lesser quantities of Early Pliocene – "earliest" Zanclean to Late Miocene (Messinian, MNN12 – MNN11), Eocene (NP20 – NP12), Oligocene – Paleocene and Maastrichtian-Campanian specimens. A large (c. 12 m) ?Oligocene – basal Miocene (Aquitanian) boulder was sampled at 31 m [core] in C2006 within the Upper Pliocene section.

There were numerous examples of small-scale (metres) disturbance of bedding within the Thinia cores which took the form of a brief flattening of dip (e.g. C2, 38.25 m to 41.2 m [core], C2006) or evidence of faulting or thrusting (e.g. C2, c. 62 m [core]; C4b, 29.5 m to 31.25 m [core]; C2006, 39.75 m to 44.0 m [core]. This was interpreted as evidence of tectonic disturbance experienced by the subsurface sediments of Thinia and thus further evidence of the strong tectonic forces affecting the sediments. The recurring dip angle of 40 to 60° within marl and clay sediments was very steep, mirroring that of the bedding within the penetrated thrust faults (e.g. C1, C4b, C2) suggesting post-depositional deformation.

"Basement" or igneous clasts were detected within three of the boreholes: C2005 (5.5 m [core], C7a (between 4.0 and 7.9 m [core]) and C6b (14.4 to 15.0 m [core]). These clasts occurred in strongly reworked or rubbled sections of these cores and within the Early Pleistocene to Pliocene sediments. Given the presence of ash deposits from a previous Mt Etna eruption (2002, Kelepertsis et al., 2003) across the Ionian Islands it was initially thought that these sediments were derived from Mt Etna. However, the age of the stratigraphy in which they are deposited (Gelasian-Zanclean) disputes this and they may instead have been derived from Hellenic Arc volcanoes (e.g. Santorini, Kos, Milos and Nisyros with Milos the closest at 376 km) which were known to have been intensely active in the late Neogene and Quaternary (Francalanci et al., 2002).

5.4.2 Livadi Marsh

The stratigraphy of the marsh could be split into four possible sequences separated by unconformities (Figure 5.30). The sequences are as follows:

1. **Recent:** Lagoonal, marginal marine with terrigenous influence and surface soils containing rootlets.

2. **Middle Pleistocene (Ionian):** Open marine associated with transgressive flooding phase with increased terrigenous input upwards.

3. **Early to Middle Pleistocene (Calabrian) to Late to "latest" Early Pliocene (Piacenzian to "latest" Zanclean):** Shallow marine (less than 50 m water depth) to very shallow estuarine lagoon with marine influence.

4. **?Late Paleocene (Thanetian):** Protected shallow, subtidal environment.

These were separated by the three unconformities or stratigraphic breaks (sequence boundaries) listed below. The boreholes where the unconformity was found or inferred is indicated in brackets:

1. **Late Pleistocene (Tyrrhenian):** Associated with transgression of sea into marsh area during Last Interglacial?

2. **Upper Early-Middle Pleistocene (upper Calabrian):** Intra-Pleistocene sea level fall and subaerial exposure of marsh?

3. **Oligocene-basal Miocene Unconformity [C6a]:** Representing the boundary between syn-rift carbonates (Cretaceous – Early Selandian) and post-rift (ramp) carbonates (Late Selandian – Bartonian)?

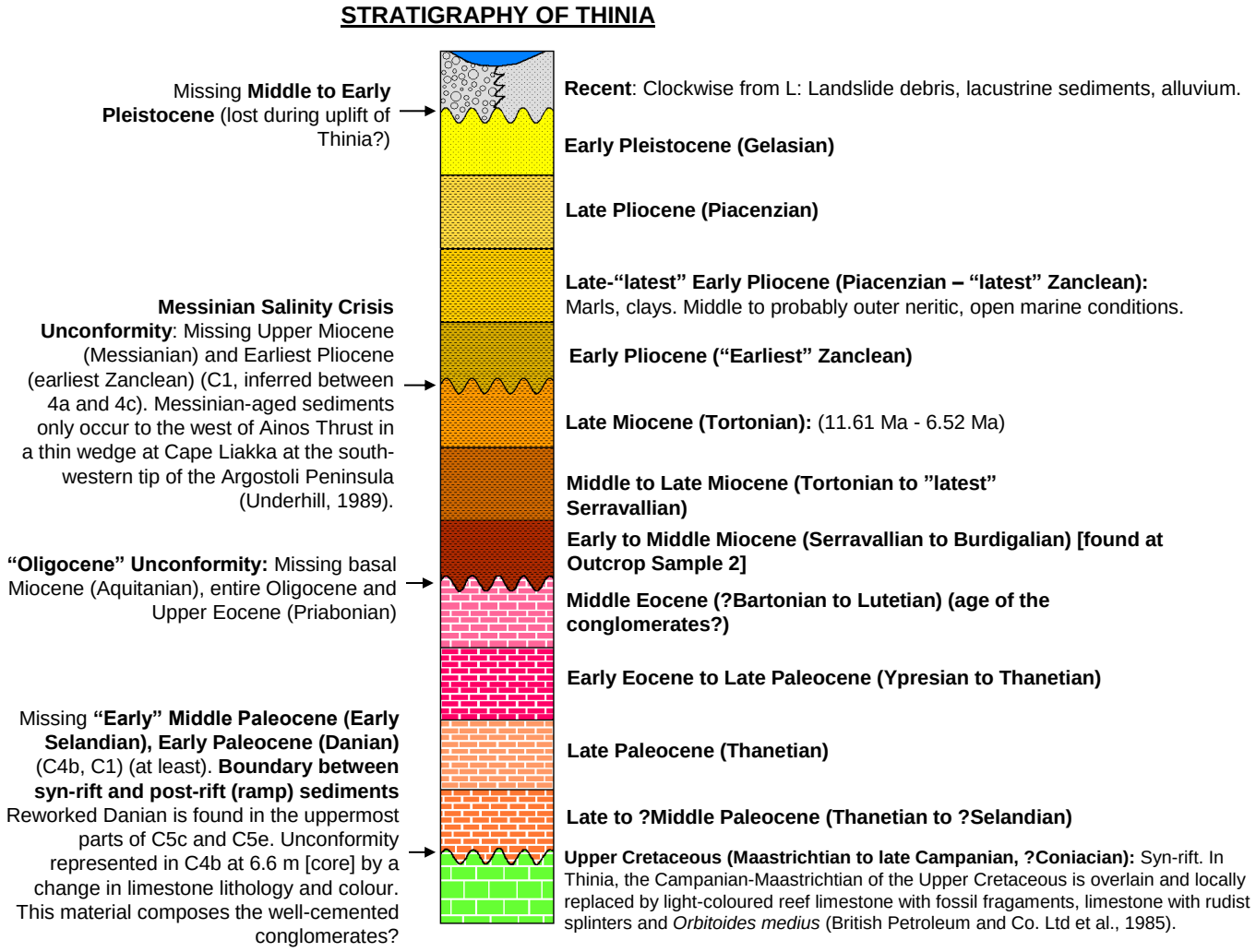

Figure 5.29 Stratigraphic column for Thinia deduced from the borehole and surface sample data.

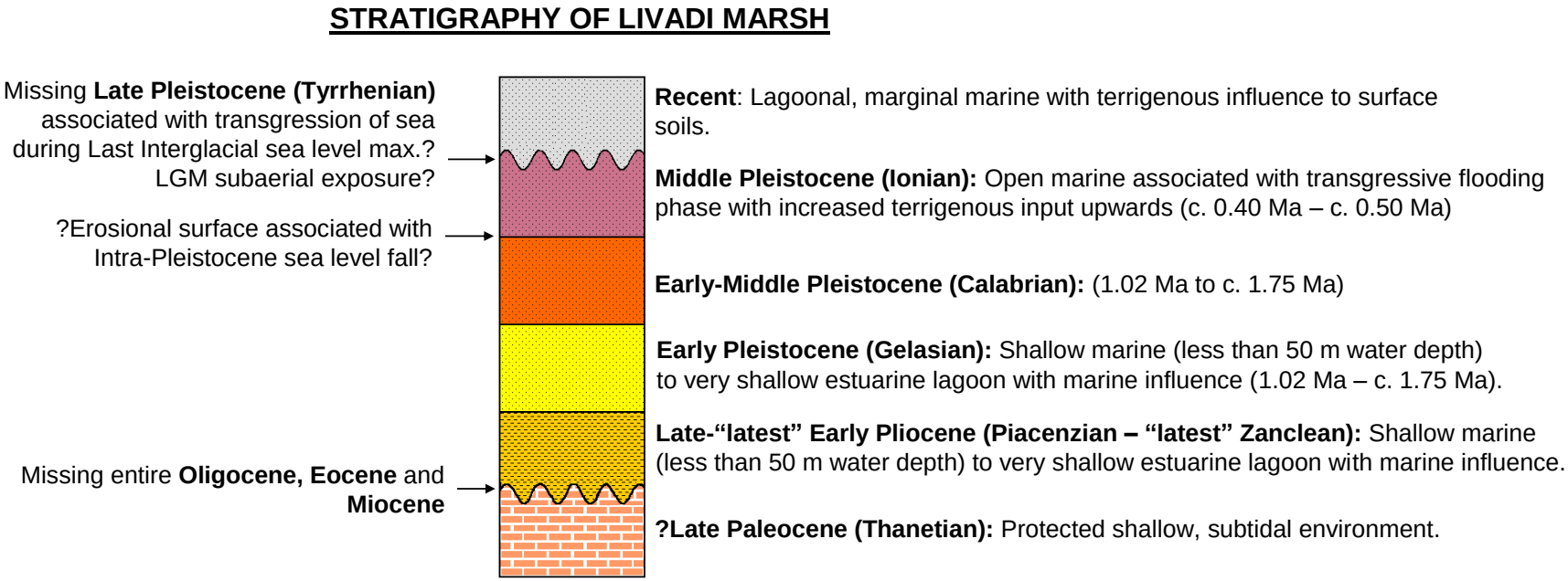

Figure 5.30 Stratigraphic column for Livadi Marsh deduced from the borehole and surface sample data.

5.5 Summary

The shallow sedimentary coring survey for Thinia showed the valley sediments were composed of a thick deposit of south-easterly-dipping (40 and 60°) Early to Middle Miocene (Serravalian to Burdigalian) – Early Pleistocene (Gelasian) sediments deposited in a marginal to open marine, neritic (less than 50 m water depth) setting. These sediments occurred in stratigraphically conformable units emplaced onto one another by thrust faults and post-depositional deformation had fractured and tilted these sediments steeply (40 and 60°). While this confirmed that a seaway existed where Thinia now stands during the Neogene to Early Pleistocene, no sediments younger than the Gelasian (1.81 Ma) were sampled. This was a very significant finding. The core C2006 was placed to re-drill the original Oct 2006 borehole (Section 2.2.3) and confirm the presence of *Emiliania huxleyi* sampled by this borehole which would point towards a much younger marine environment. However, *Ehux* was not detected in this borehole or in any other Thinia borehole.

Borehole C1 suggested that the Petrikata Quarry limestone outcrop formed part of an easterly-dipping thrust fault and ruled out the possibility of a buried channel running through the central part of the valley.

Borehole C2 was drilled into the edge of the Zola talus however did not detect significant landslide debris indicating the talus was thinner than expected and sat on top of bedded sediment.

While confirming a freshwater environment, the six cores acquired for Lake Katachori (C5a, C5b, C5c, C5d, C5d2 and C5e) detected only a thin veneer (0.65 to 6.40 m) of lake fill suggesting this was a very shallow feature. These deposits were sited on steep, easterly-dipping Plio-Pleistocene sediments uplifted to ~170 m above sea level. The occurrence of freshwater algae with uppermost Pleistocene (Gelasian) sediments suggested departure from a marine depositional setting occurred in Thinia sometime after Early Pleistocene times (1.80 Ma).

While being placed within the proposed route of “Strabo’s Channel” in the central part of the valley, C4a and C4c did not detect any evidence of a buried channel.

The Livadi Marsh cores (C6a, C6b and C6c) detected a similar set of sequences. C6b contained the youngest marine sediments to be sampled by this survey (Ionian) and several possible instances of subaerial exposure and flooding events linked with changes in relative sea level. Radiocarbon dating of three flooding surfaces within the recent fill of C6c suggested that no significant coseismic uplift was believed to have occurred since 5206 BP and the current “drying out” of Livadi Marsh was due to coastal out-building and creation of a land spit along the entrance to the marsh.

The core at Atheras Bay (C7a) confirmed the presence of marine clays but was too disturbed through rubble to make confident inferences on the age of the sediments.

CHAPTER 6: Offshore Geophysics

6.1 Introduction

This chapter will present the interpreted results from the shallow marine seismic reflection surveys taken in the Gulf of Argostoli (volumes A1, A2 and B), Atheras Bay (C) and Agia Kiriaki Bay (D). The key aims of the interpretation of the offshore surveys were:

1. To investigate sea floor morphology in terms of finding evidence for "Strabo's Channel" in the Gulf of Argostoli and Agia Kiriaki Bay.

2. To interpret and contour prominent horizons in two-way travel time (TWTT) in order to investigate the seismic megasequences.

3. To investigate evidence for (and against) Neotectonic (co-seismic) activity on offshore "Alpine" (Hellenide) structures and determine the relationship between these and similar geological structures mapped onshore (Section 6.6.2).

4. To determine postglacial flooding histories of these shallow coastal areas (Section 6.6.3).

The seismic sections and maps are generated on Kingdom seismic interpretation software unless otherwise stated or referenced. Where seismic sections are presented, the uninterpreted section is illustrated at the top and the interpreted version is below. The locations of these seismic lines are presented in the following base maps: Gulf of Argostoli (Figure 6.3), Atheras Bay (Figure 6.30) and Agia Kiriaki Bay (Figure 6.36). The designation "SBP" refers to lines taken by the side-bottom profiling survey.

6.2 Interpretation of Shallow Marine Seismic Reflection Data and Nomenclature

Interpretation of the seismic data was conducted using the Kingdom 8.3 (32-bit) 2d/3dPAK-EarthPAK software mounted on the University of Edinburgh's in-house Seismic Interpretation Laboratory. This allowed the digital tracking and mapping of individual key horizons.

Due to the wide spacing of the seismic lines (100-150 m), mapping of key horizons could not be satisfactorily done by interpreting the lines alone. Maps were instead created using a function of the software called "gridding". This technique extrapolated the data points for the horizon to be gridded along each line into the space between them (using the gridding parameter of inverse distance to a power [TKS 8.0]). There were some minor drawbacks to this technique. While producing overall satisfactory results this method created an issue with "line-biasing" where the extrapolation became less reliable with distance from the data point creating a "scalloped" pattern. One way to mitigate this problem was to increase the size of the grid increment thus smoothing the grid however this resulted in a trade off with resolution. The Kingdom software also did not recognise the coastline of the culture map which resulted in erroneous extrapolation of the grid and contouring across the land surface. This was mitigating to some extent by creating a "zero" contour separately along the coastline and integrating this during the gridding and contouring process, but not entirely solved since some contours still overlapped with the coastline. The contours and extrapolation produced near the coast therefore should be considered approximations with possible errors of several metres.

The sequence stratigraphic nomenclature adopted for interpretations of the seismic reflection data is after Mitchum et al. (1977) and Vail et al. (1977) (Figure 6.1). The subsurface was divided in terms of seismic facies units, which are defined as mappable, 3-dimensional seismic units composed of reflections whose configuration differs from those of adjacent facies units (Figure 6.2, Mitchum et al., 1977).

6.2.1 Depth Conversion

Depths to sea bed were determined using the separate bathymetric data collected by the seismic vessel's sonar and onboard GPS (accurate to within 3 m) during acquisition of the seismic data. The seismic sections, grids and isochrons are in presented terms of two-way travel time (TWTT) in seconds. Where depths are quoted, they are the result of a "rough and ready" depth conversion of the time-dependent grid or individual TWTT.

The P-wave velocity used during this depth conversion was derived from the results of an earlier, independent investigation into the composition of the near-surface sediments in the Gulf of Argostoli by Braune (1973). Sediments were sampled up to 256 m in depth and were composed predominately of Quaternary-aged terrigenous material (marl and sand) mixed with recent near-shore organisms. The velocity of sandy-marl typically ranges between 1000 and 2500 m/s (Boyd, 1999[3]) so an average of 1500 m/s was considered a reasonable assumption for the P-wave velocity of the upper sediments and was used in the calculations. This value was also very helpful for depth converting sub-seabed reflector grids as the P-wave velocity of saltwater used was 1500 m/s.

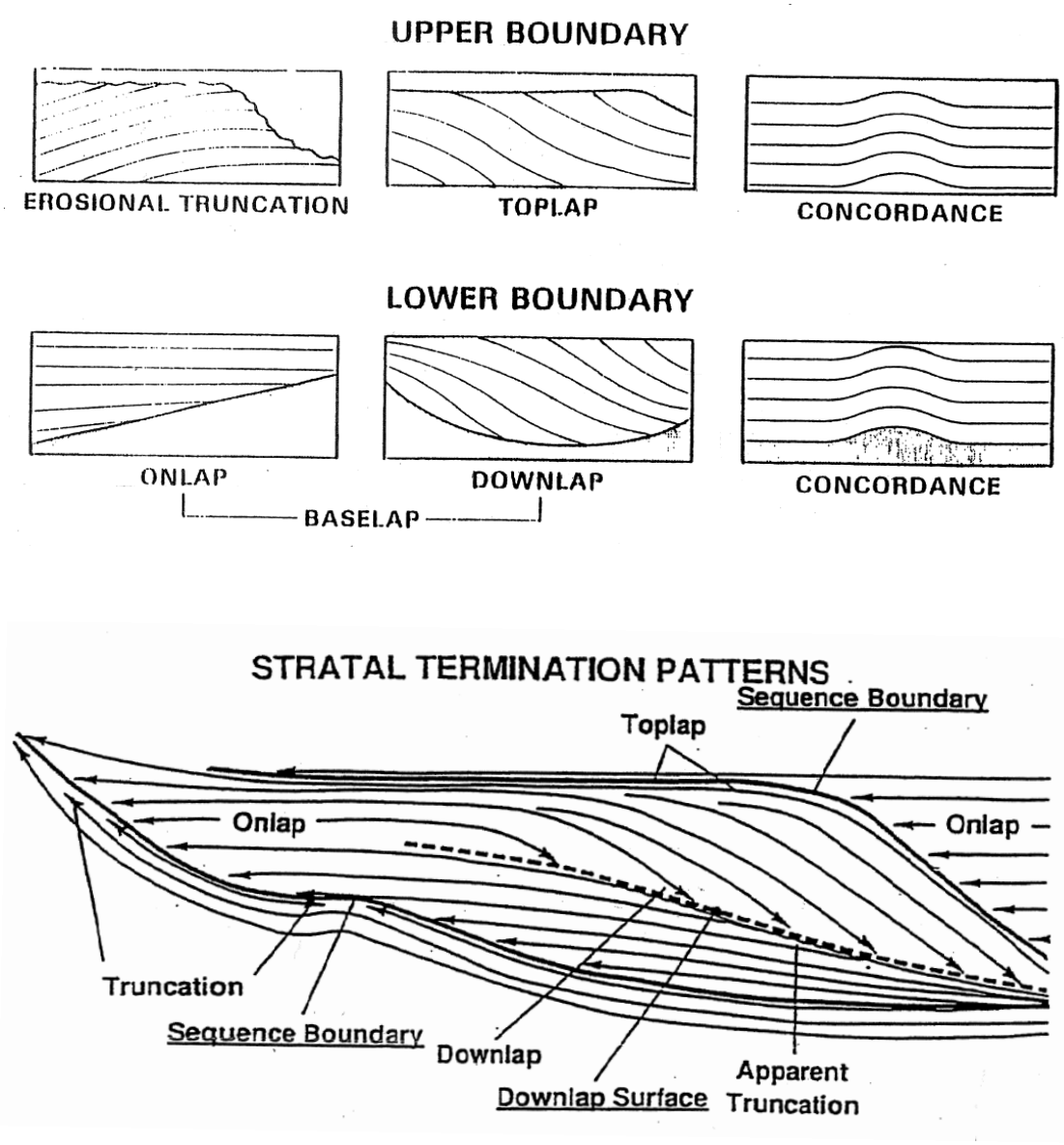

Figure 6.1 The sequence stratigraphic nomenclature adopted for seismic interpretations. After Mitchum et al. (1977) and Vail et al. (1977).

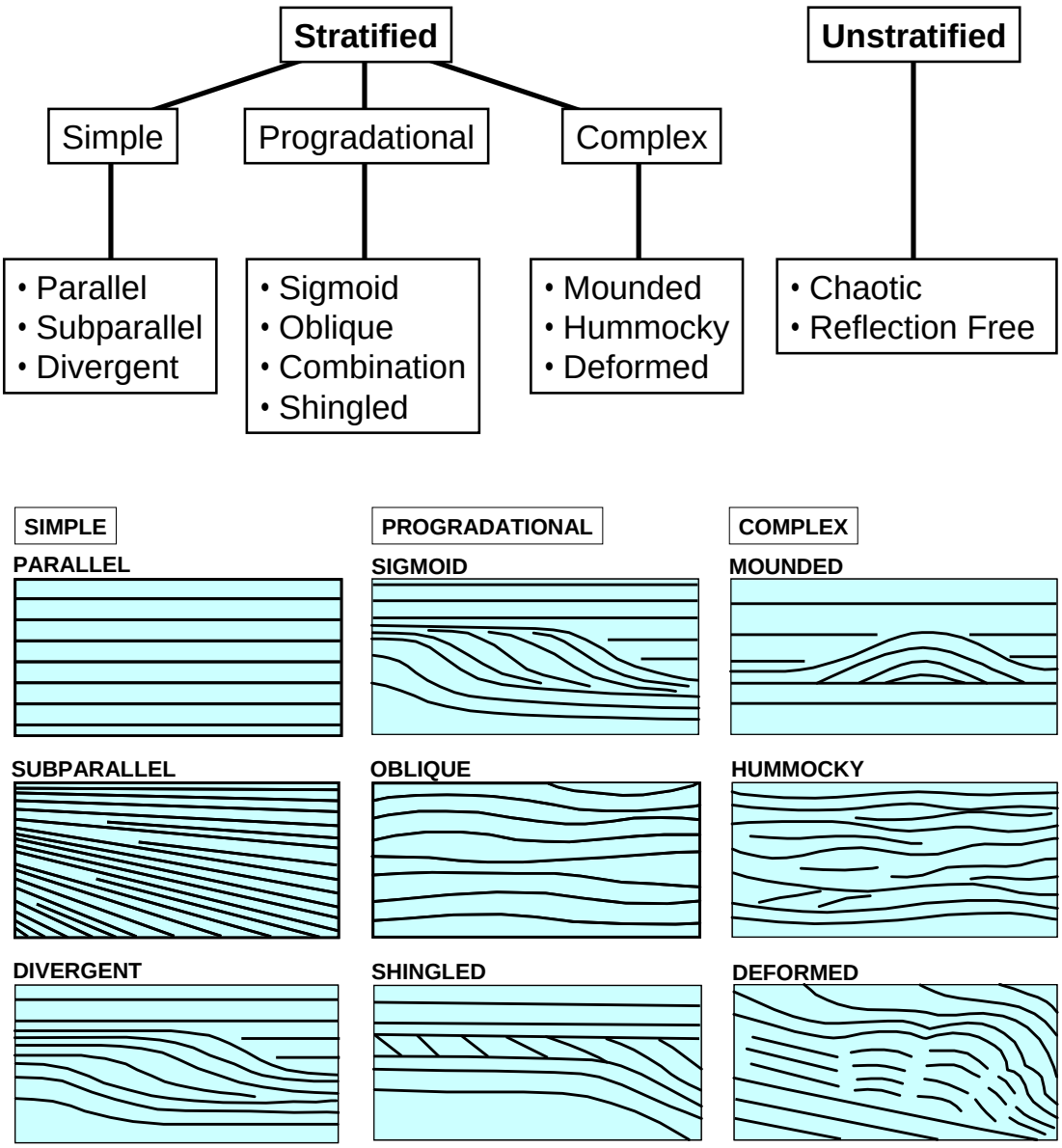

Figure 6.2 Seismic facies analysis (after Mitchum et al., 1977): Flowchart showing the recognised configurations of internal reflection patterns (top) and illustrations of the typical configurations of these patterns (bottom).

6.3 Gulf of Argostoli (A1, A2 and B)

Best penetration of the seismic energy in the Gulf of Argostoli occurred within volume B and the southern and western part of A1. This was most likely due to the presence of a soft substrate at the sea bed reducing reflectivity and scattering of the seismic pulse. Reliable interpretation was possible in the clearest lines to a maximum depth of approximately 0.15 s (225 m). A2 and the north-eastern part of A1 suffered significantly diminished quality of image due to shallower (< 5 m) operational depth and the presence of acoustic turbidity which caused significant attenuation of the seismic signal. The affected profiles showed little to no reflector definition with strong sea bed multiples which prevented mapping with accuracy, although some very deep features could be seen below the zones of acoustic impedance (0.08 sec in TWTT). The seismic could be resolved into the following configuration of seismic megasequences and key reflectors:

1. **Sea bed** (Section 6.3.1).

2. An **upper seismic megasequence** (Section 6.3.2) (shaded yellow in Figure 6.4) composed of planar, dark and transparent reflectors. In A2 and the north-eastern part of A1 this megasequence contained an opaque unit which caused severe degradation of the seismic where it occurred.

3. A **high amplitude reflector** (Section 6.3.3) interpreted as a major erosional surface as it truncated the tilted reflectors of the underlying stratigraphy and was onlapped by reflectors within the upper seismic megasequence.

4. **Lower seismic megasequence** (Section 6.3.4) (shaded pink in Figure 6.4) which appeared very different from the upper seismic megasequence, consisting of strongly deformed (locally folded and faulted) reflectors which were truncated by the erosional surface.

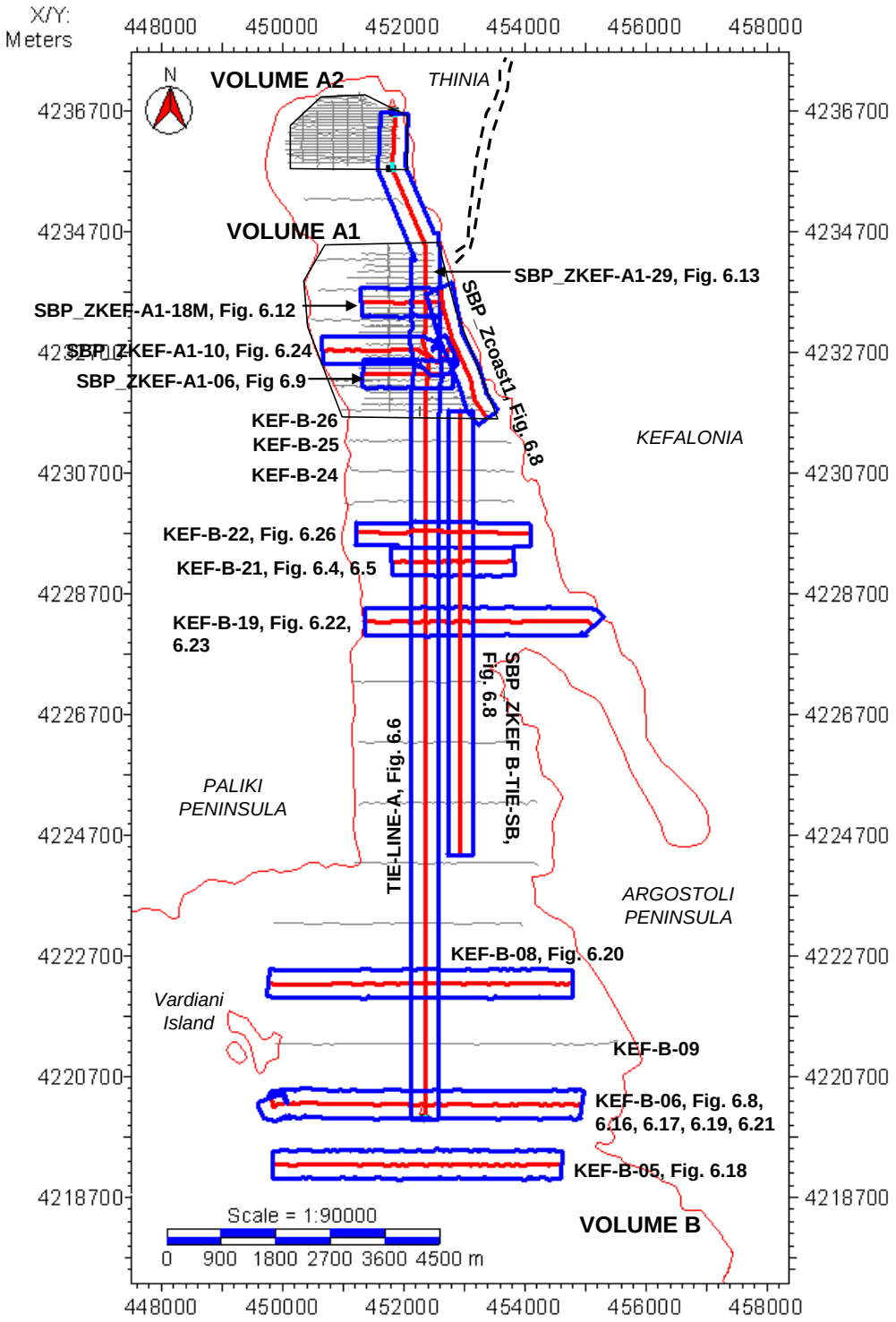

Figure 6.3 Kingdom base map showing the location of the Gulf of Argostoli shallow marine seismic reflection survey (Volumes A1, A2 and B), Western Kefalonia. The survey lines illustrated in the text are highlighted in blue and red. The proposed route of "Strabo's Channel" is indicated by a dashed black line. Due to rough resolution of the culture map, the coastline (in red) overlaps the survey lines in some places.

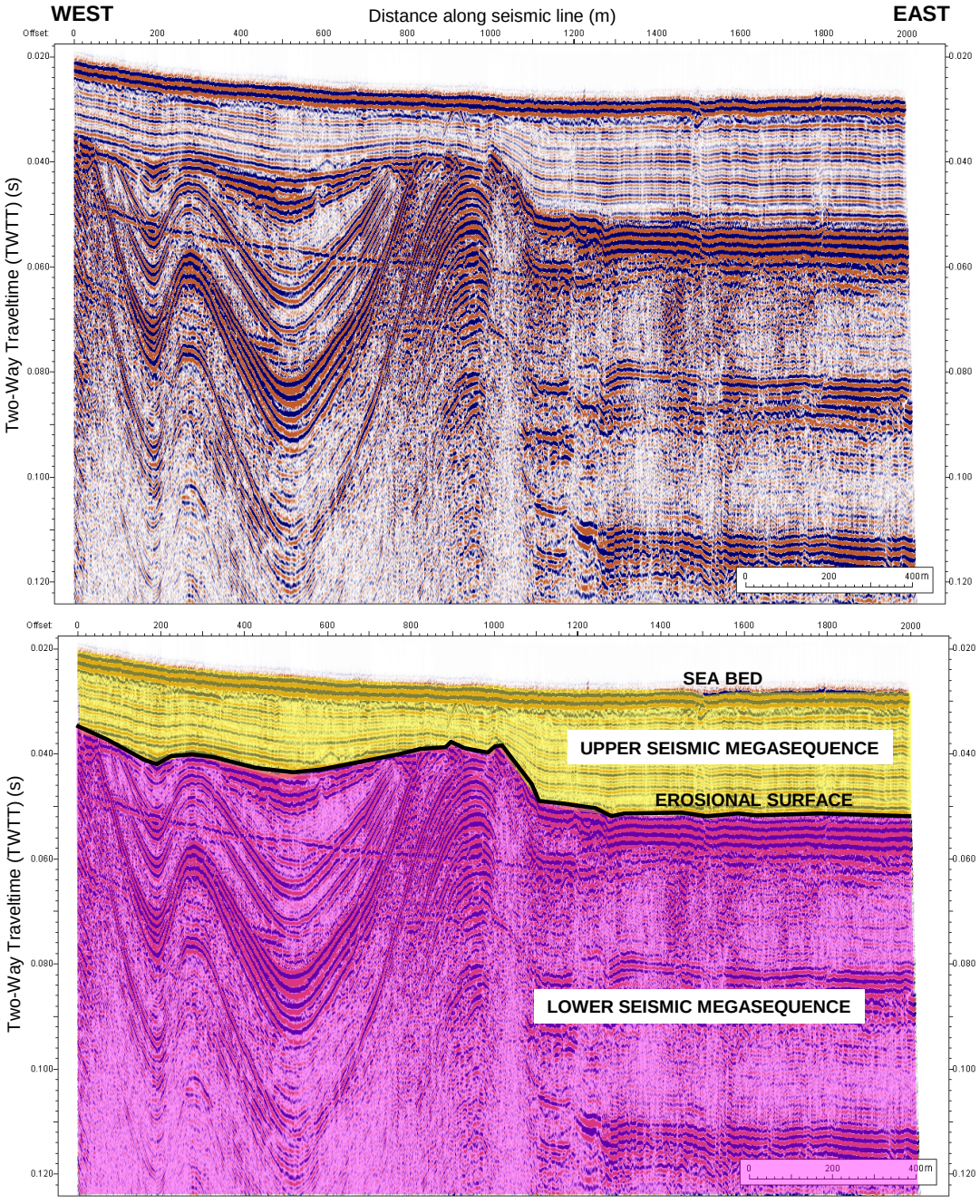

SEISMIC MEGASEQUENCE	TOP OF UNIT	BASE OF UNIT
Upper Seismic Megasequence	Sea Bed	Erosional Surface
Lower Seismic Megasequence	Erosional Surface	

Figure 6.4 Typical E-W "dip" line (KEF-B-21) illustrating the main sedimentary units and key reflectors detected by the Gulf of Argostoli shallow marine seismic reflection survey with a table summarising these units. The upper seismic megasequence (Section 6.3.2) is shaded in yellow while the lower seismic megasequence (Section 6.3.4) is shaded in pink. The location of this line is given in Figure 6.3.

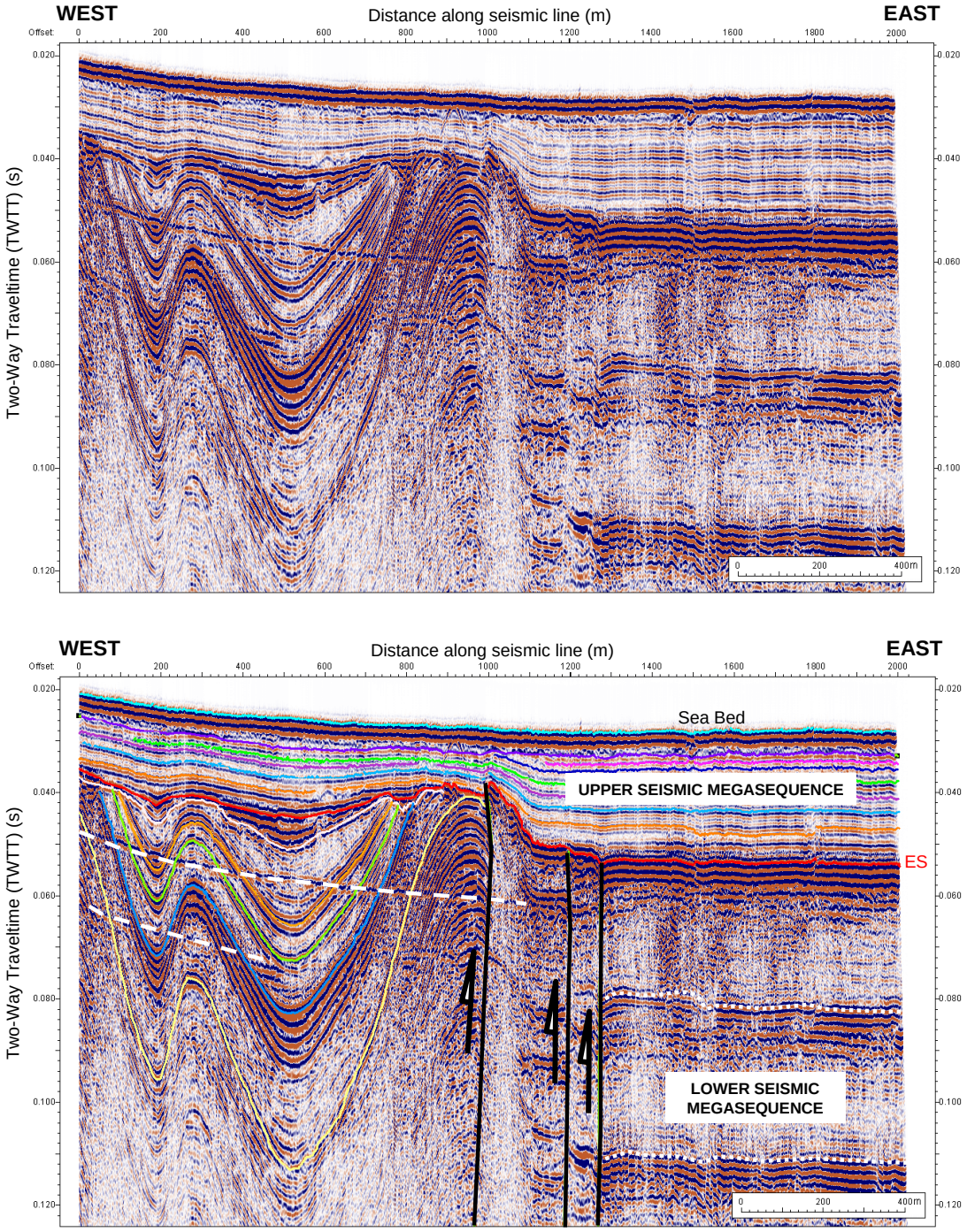

Figure 6.5 Fully interpreted version of Figure 6.4 (KEF-B-21) where ES (red) = Erosional Surface. Upper Seismic Megasequence horizons (top to bottom): purple = Sed5, pink = Sed6, dark blue = Sed10, light green = Sed13, lilac = Sed19, blue = Sed22 and orange = Sed26. Lower Seismic Megasequence horizons (top to bottom): white = PreHol1, orange = PreHol3, green = PreHol4, blue = PreHol5 and yellow = PreHol6. White dotted line = erosional surface multiple, white dashed line = sea bed multiple. Location of line shown on Figure 6.3.

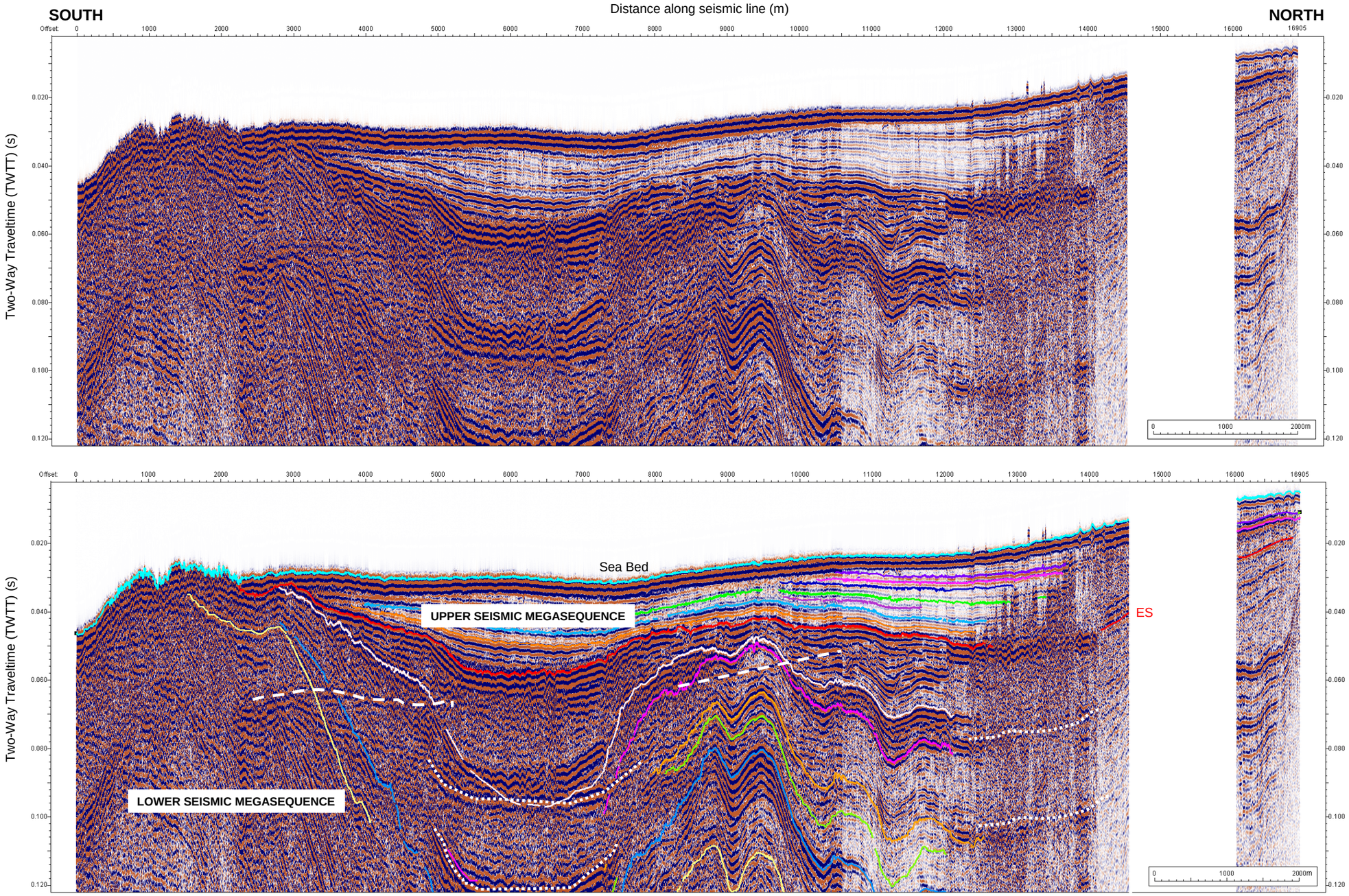

Figure 6.6 Typical N-S "strike" line for the Gulf of Argostoli, TIE LINE A (composed of KEF-B-29, KEF-A1-29, KEF-A2-16). The gap in the seismic section corresponds to the gap between seismic volumes A1 and A2. Annotations as for Figure 6.5. Location of line shown on Figure 6.3.

This configuration is illustrated by Figure 6.4 using typical "dip" line KEF-B-21 (interpreted fully in Figure 6.5). Figure 6.6 shows a "strike" line (Tie Line A) constructed by linking lines KEF-B-29, KEF-A1-29 and KEF-A2-16 so that it extends from the northerly to southerly-most limit of the Gulf of Argostoli survey. The SBP survey was unable to image much deeper than the prominent reflector. This attenuation may also have been caused due to the upper seismic megasequence being fine-grained in nature (Anderson et al., 1998) or due to scattering of the seismic energy due to the reflectivity of the erosional surface.

6.3.1 Sea Bed Morphology

Mapping the sea bed and roughly depth-converting the resulting TWTT grid showed that the Gulf formed a shallow basin (with a maximum water depth of around 26 m) (Figure 6.7). Towards the southerly limit of the survey, the sea bed deepened rapidly marking the edge of the coastal shelf on which the Gulf sat. While the parts of the sea bed where the erosional surface was exposed showed dramatic topography, there was no evidence that a channel had been eroded into the sea bed around the vicinity of the proposed southern exit.

Figure 6.8 shows the morphology of the sea bed in a selection of seismic cross-sections taken through the Gulf. The sea bed was smooth except at locations where the dramatic topography of the erosional surface broke through the upper seismic megasequence to form bathymetric ridges devoid of sediment cover or where the upper megasequence was sparse or pinched out particularly towards the edges of the seismic survey.

Figure 6.8 (a) ran parallel to the coast close to the proposed southern exit of "Strabo's Channel" and shows the smooth morphology of the upper seismic megasequence draped over a rough and incised topography suggesting eroded structures existed below the sediment cover. Figure 6.8 (b) shows the offshore continuation of the raised land forming the Argostoli Peninsula. Figure 6.8 (c) takes a

cross-section across the offshore continuation of the Paliki peninsula to the west and the bathymetric escarpment observed running along the eastern coast of the Gulf.

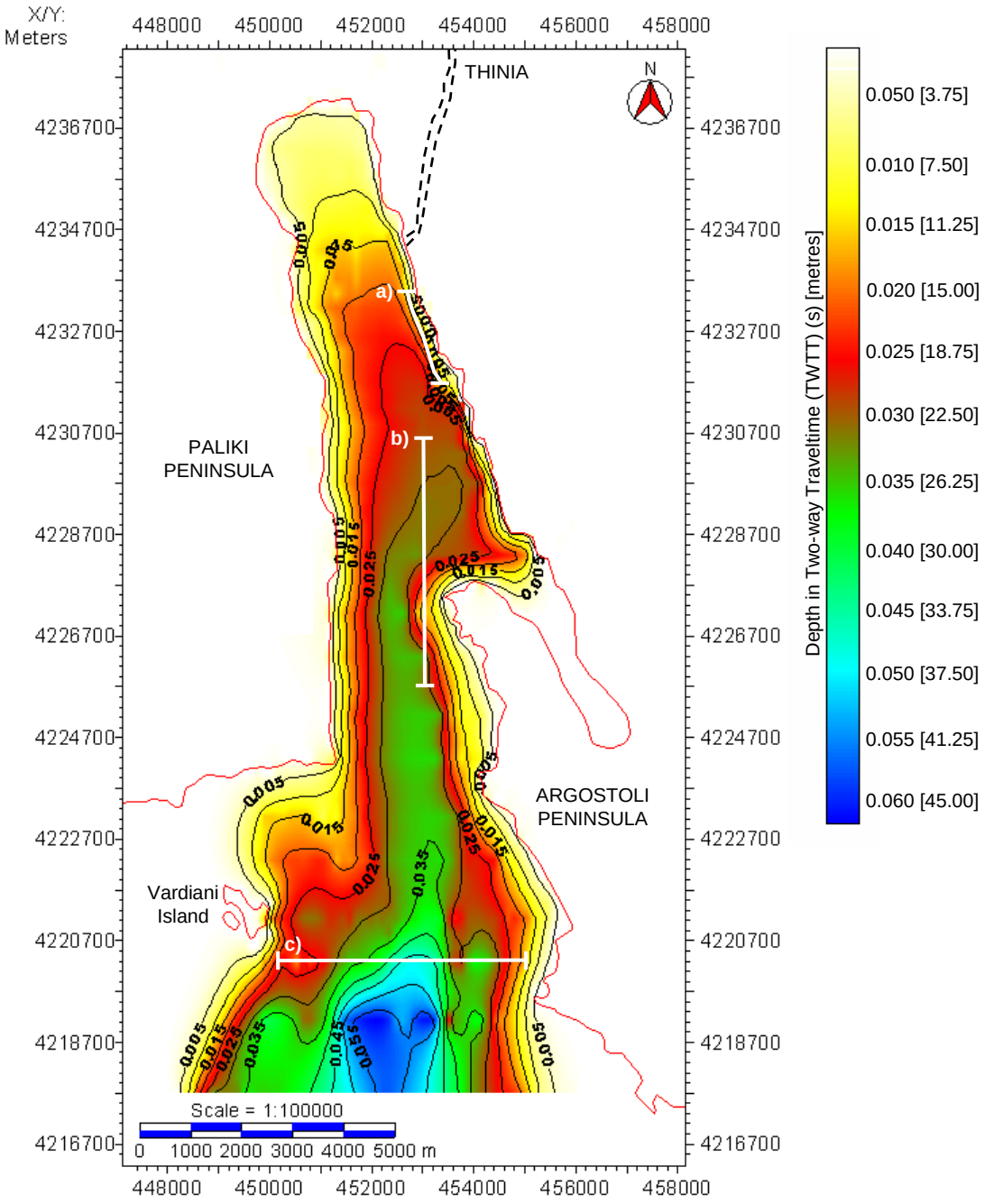

Figure 6.7 Two-way traveltime (TWTT) (in seconds) sea bed map for the Gulf of Argostoli showing the shallow, mostly smooth bathymetry. Rough depth conversion of this map was carried out (indicated in square brackets on the scale bar) using a P-wave velocity for sea water of 1500 m/s. The proposed route of "Strabo's Channel" is indicated by a black dashed line. The seismic lines highlighted in white are presented in Figure 6.8.

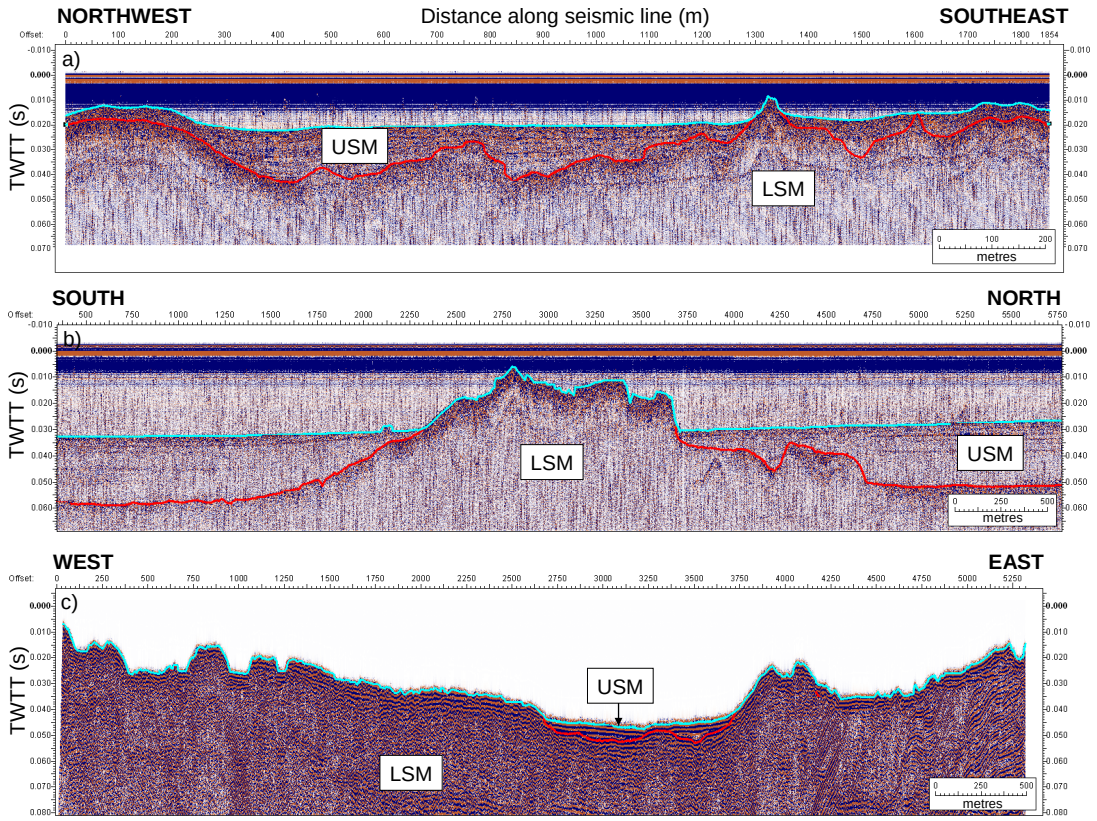

Figure 6.8 Selection of seismic lines illustrating the morphology of the sea bed (location of lines indicated in Figure 6.3 and 6.7): a) SBP_Zcoast1; b) SBP_ZKEF-B-TIE-SB; c) KEF-B-06. USM = Upper Seismic Megasequence, LGM = Lower Seismic Megasequence, red = erosional surface, pale blue = sea bed.

6.3.2 Upper Seismic Megasequence

The upper seismic megasequence formed a series of sub-horizontal to horizontal reflectors which onlapped the dramatic topography of the erosional surface (Figure 6.9). SBP survey imaged this unit most clearly revealing the as a series of opaque reflectors separated by thicker transparent layers. The sparker survey detected the layering of reflectors within this unit but the shallowest reflectors were lost due to reflections from the sea bed. No faulting or folding of the bedding was observed despite the heavily disturbed nature of the sediments underlying the major erosional surface.

The reflectors detected by the SBP survey were strongest and thickest towards the top of the megasequence (e.g. Sed5 (purple) and Sed13 (light green) on Figure 6.9). One reflector in particular (Sed5) was very strong and continuous throughout the Gulf lying on average around 2 to 5 m below the sea bed. The consistent brightness of this reflector suggested it was formed by particularly reflective sediments. Mapping Sed5 (Figure 6.10) showed that this reflector had a similar gentle morphology to the sea bed and was entirely confined to the inner shelf of the Gulf suggesting it had a terrigenous rather than marine source composed of particles washed in from the land. This reflector also appeared to have been onlapped by further dark reflectors e.g. Sed4 (dark green, Figure 6.9). This raised questions as to how much of the upper seismic megasequence sediment was sourced from the land (e.g. alluvial) and which onlaps were "true" marine.

An isochron (thickness in two-way travel time) was constructed for the upper seismic megasequence to determine the distribution and thickness of this unit across the Gulf of Argostoli (Figure 6.11). This isochron showed that this unit was not uniformly distributed across the Gulf but was concentrated within two NNE-SSW striking, lozenge-shaped regions. Outside of these regions upper seismic megasequence coverage was minimal, pinching out completely around the southern coast of Paliki, the western coast of Argostoli Peninsula and the raised bathymetric ridge defining the edge of the coastal shelf. The northerly lozenge measured around 2.7 by 9.5 km and ran from Livadi Bay to the tip of Argostoli Peninsula. The southerly accumulation was smaller measuring around 1.8 by 7.2 km and was displaced 2 km to the west of the northerly basin, running between the Paliki and Argostoli Peninsulas almost as far as the coastal shelf. The thickest deposits of sediment formed fan-shaped features which appeared to emanate from an onshore source. These features were most prevalent in the northern lozenge. The thickest of these fans (indicated by hatched black lines in Figures 6.11) reached up to 24 m in thickness and were concentrated in the central part of the northern and south lozenges. In the case of the northern lozenge this accumulation appeared to emanate from the proposed southern exit of "Strabo's Channel".

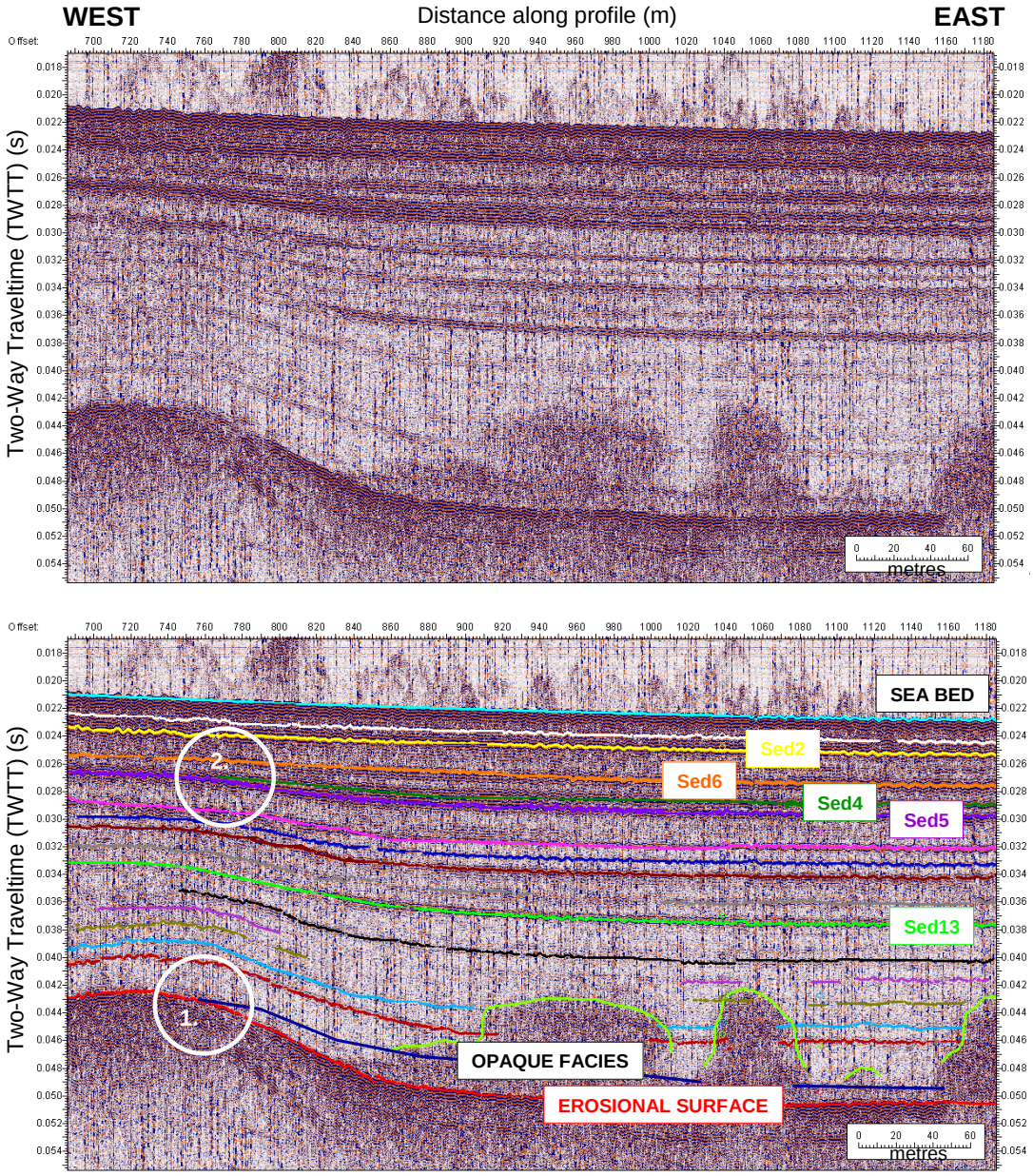

Figure 6.9 Close-up of dark reflectors within the upper seismic megasequence (SBP_ZKEF-A1-06) with possible onlaps circled in white. Onlap onto the erosional surface (1) and a possible internal onlap (2) within this unit of Sed4 (dark green) onto Sed5 (purple). Particularly prominent reflectors are indicated: Sed2 (yellow), Sed6 (orange), Sed5 (purple) and Sed13 (light green) are indicated. The opaque facies near the base of the unit is presence only within the upper seismic megasequence and is most prevalent in the north-eastern part of the Gulf of Argostoli survey. Annotations are for Figure 6.5. Location of this line is given in Figure 6.3.

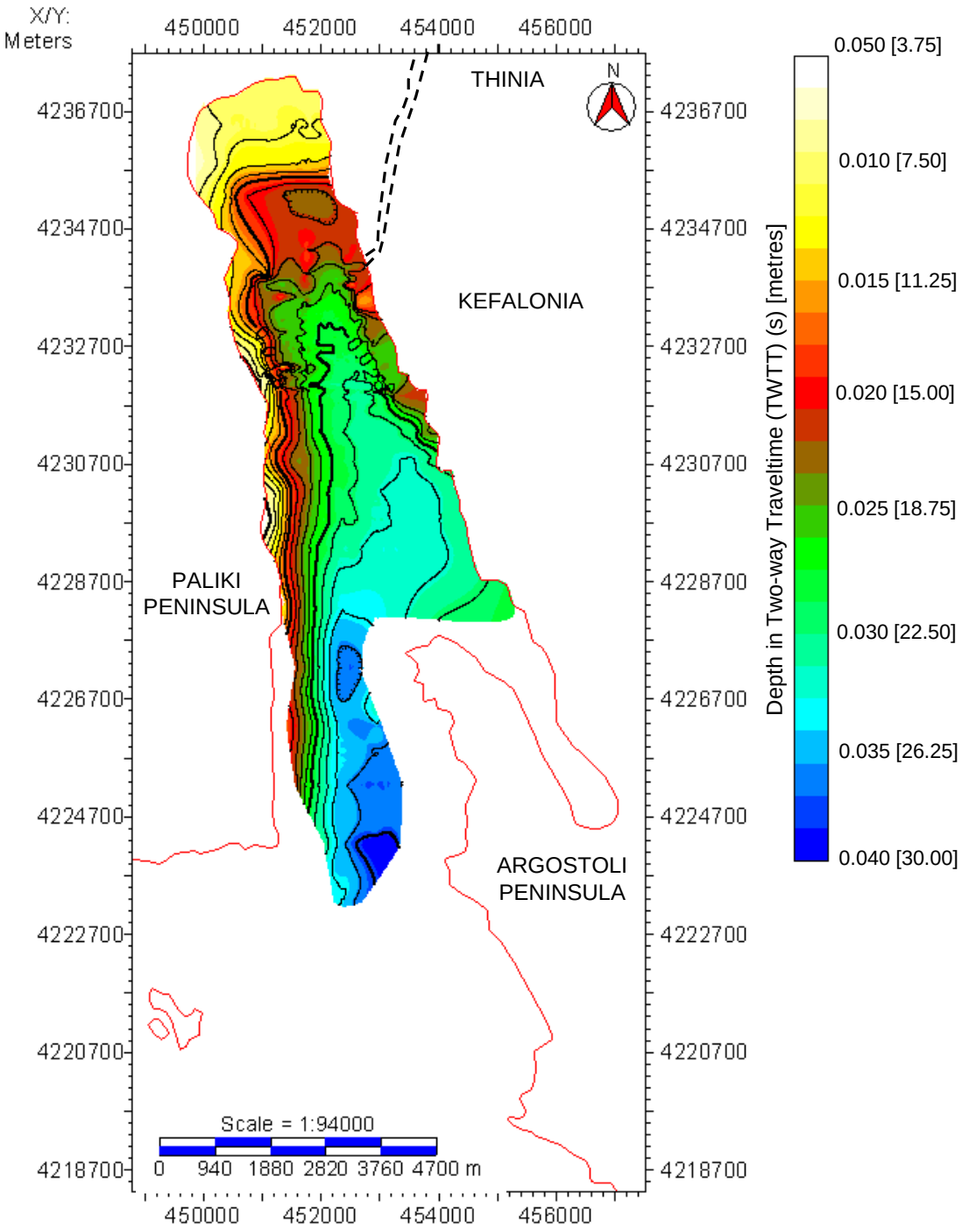

Figure 6.10 Two-way traveltime (TWTT) (in seconds) map of Sed5, the most prominent upper seismic megasequence reflector in the Gulf of Argostoli (shown in purple in Figure 6.9). Rough depth conversion of this map was carried out (indicated in square brackets on the scale bar) using fine-grained sediment P-wave velocity of 1500 m/s. The white areas correspond to areas where this reflector was not apparent. The map suggests the reflector is terrigenous in origin as it is entirely contained within the Gulf. The proposed route of "Strabo's Channel" is given by the black dashed lines.

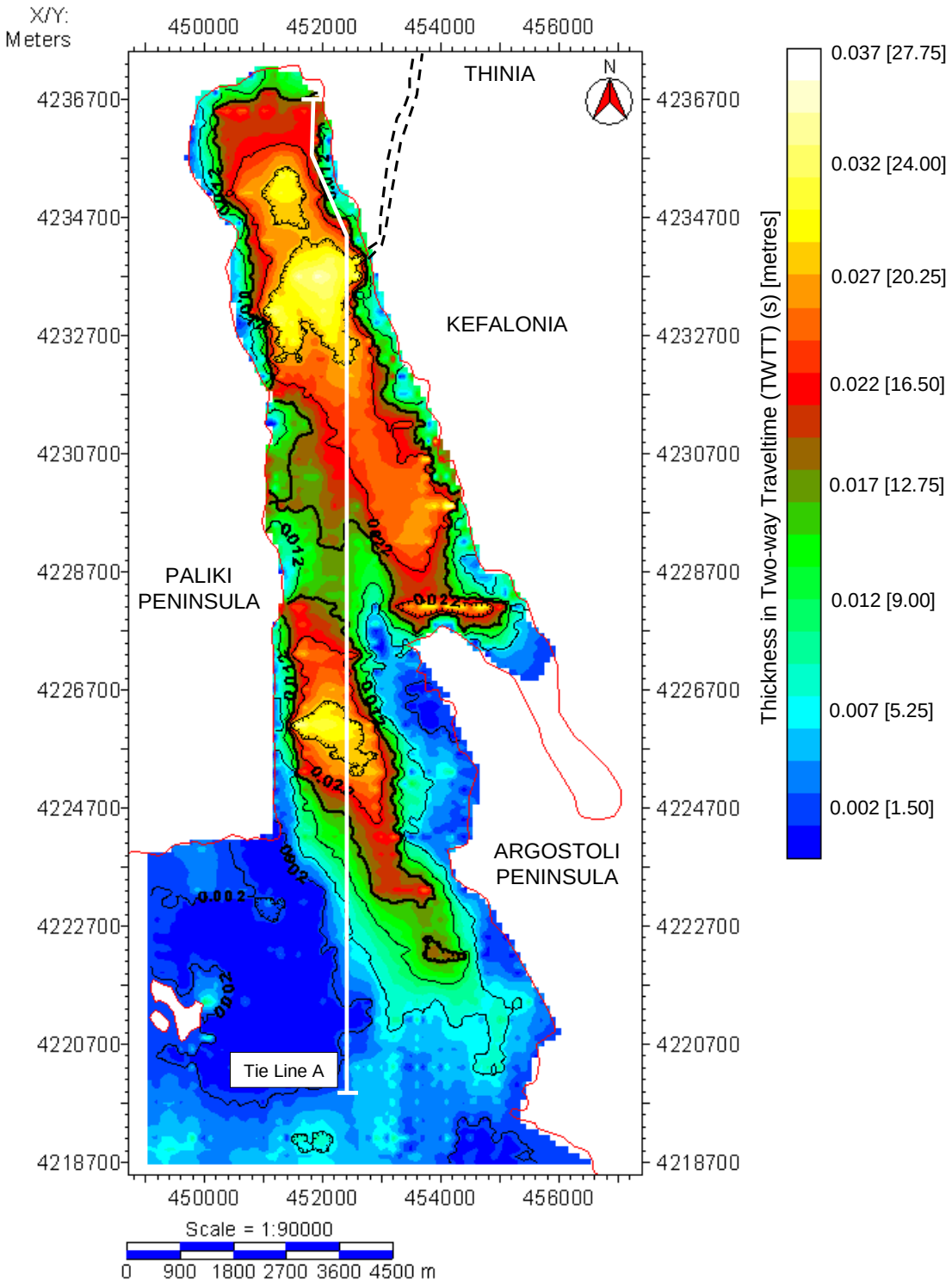

Figure 6.11 Isochron (thickness in two-way travel time (TWTT) (sec)) for the upper seismic megasequence of the Gulf of Argostoli. "Warm" colours indicate the thickest accumulation of sediment. The proposed route of "Strabo's Channel" is indicated by a black dashed line. The location of Tie Line A (Figure 6.6) is indicated.

Tie Line A (Figure 6.6) cross-cut these two basins and showed the thickening of the upper seismic megasequence. In the northern basin the uppermost reflectors onlapped from north to south implying they were derived from the shore.

A. Opaque Unit

The SBP survey revealed the presence of an opaque unit within the upper seismic megasequence which showed a completely different character to the surrounding reflector sequences. The sparker survey was not able to resolve this unit well as it formed localised zones of diffuse and chaotic acoustic turbidity which caused deterioration of the seismic data.

Figure 6.12 and 6.13 illustrate east-west and north-south lines respectively through this unit. This unit typically took the form of an opaque, curtain-like structure contrasting sharply with the transparent horizontally-stratified structure of the upper megasequence, cutting across the planar reflectors of this sequence. The vertiginous edges diminished in a series of steps which terminated at the dark planar reflectors within the upper seismic megasequence (particularly Sed5) to create a "ziggurat" like structure or dissipated into a series of very narrow, vertiginous plumes. This unit measured from only a few metres high above the erosional surface to encompassing the entire upper sequence (~25 m) such as in Livadi Bay and the north-eastern part of the Gulf where it was continuous to the sea bed. The base of this unit was obscured by an acoustically-impeding "shadow" which masked out the seismic making interpretation below occurrences of this formation almost impossible. However, the strong reflectors of the upper seismic megasequence (Sed5, Sed13) could sometimes be observed passing unhindered through the unit and some appeared markedly amplified (by 2 or 3 times).

An isochron of this unit was constructed (Figure 6.14). The Kingdom software struggled to resolve the vertical sides of this unit and so the stepped nature of the thicker occurrences and lateral distribution is less sharp in the map than in reality. The resulting map showed that the facies occurred exclusively within the near-shore sediments of Livadi Bay (A2) and north-eastern A1.

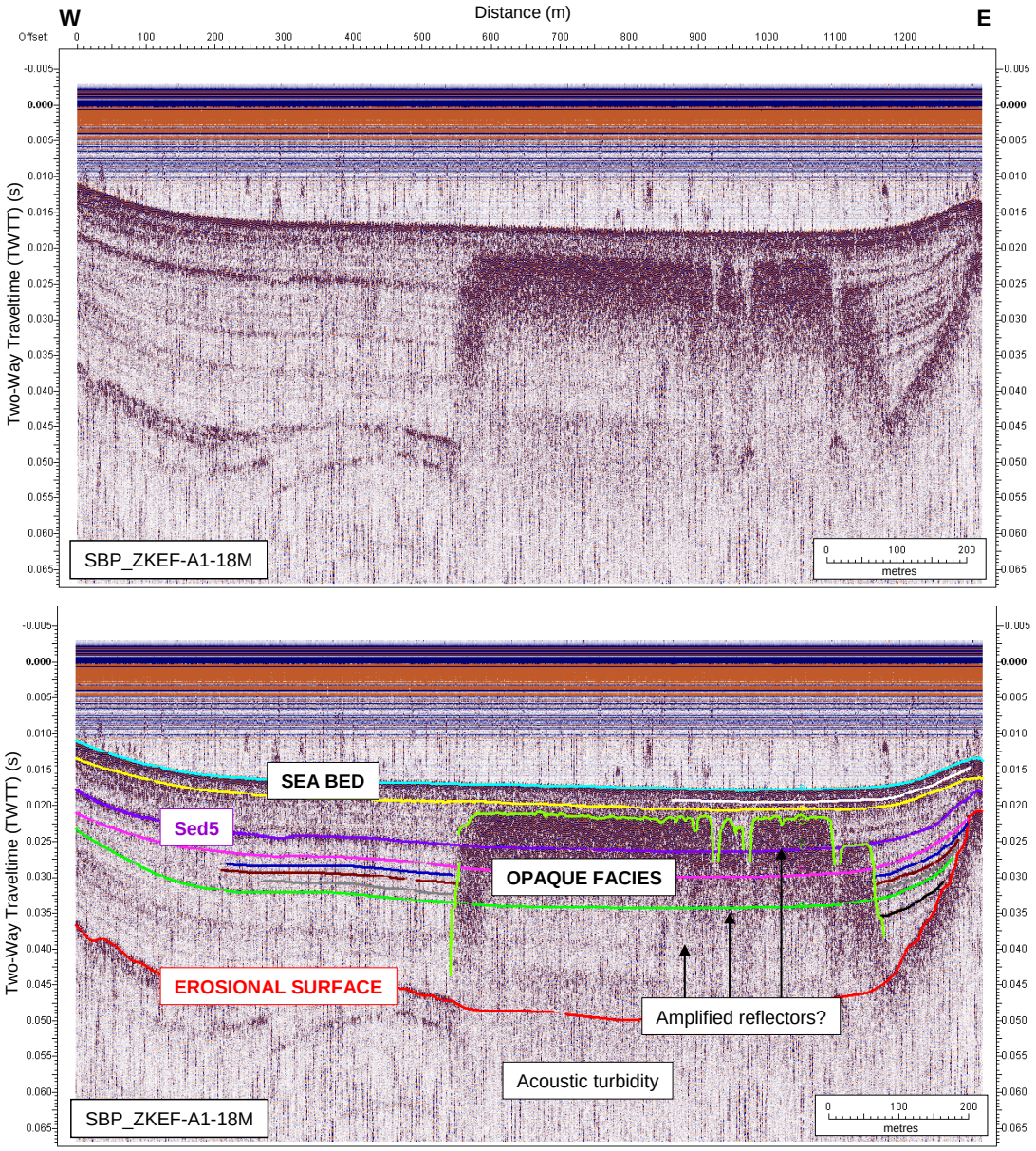

Figure 6.12 Line SBP_ZKEF-A1-18M which cross-cuts the opaque facies, occurring within the upper seismic megasequence in the northern Gulf of Argostoli, in an E-W direction. The vertiginous, dark facies contrasts strikingly with the surrounding horizontally-stratified sediments. Annotations as for Figure 6.5. Location of line is shown in Figure 6.3.

Interestingly, the thickest part of the facies also correlated to the thickest accumulations of the upper seismic megasequence (Figure 6.11) in the northern part of the Gulf as depicted in Figure 6.14. There were two possible causes of this turbidity: 1) The acoustic contrast caused by an abrupt change of grain size resulting from the deposition of coarse material e.g. clastic deposits or gravel or sand beds within predominately fine-grained sediment (Missiaen et al., 2002) or (2) the

presence of shallow gas within the upper sediments. While a change of grain size is a possibility given the prevalence of scallop-shaped slumps along the vertiginous eastern shore introducing sudden influxes of terrigenous sediment into the fine-grained "recent" sediment, the opaque facies was almost certainly caused by accumulations of biogenic shallow gas within the upper seismic megasequence as shown by the typical forms shallow gas takes in seismic as depicted in Figure 6.15.

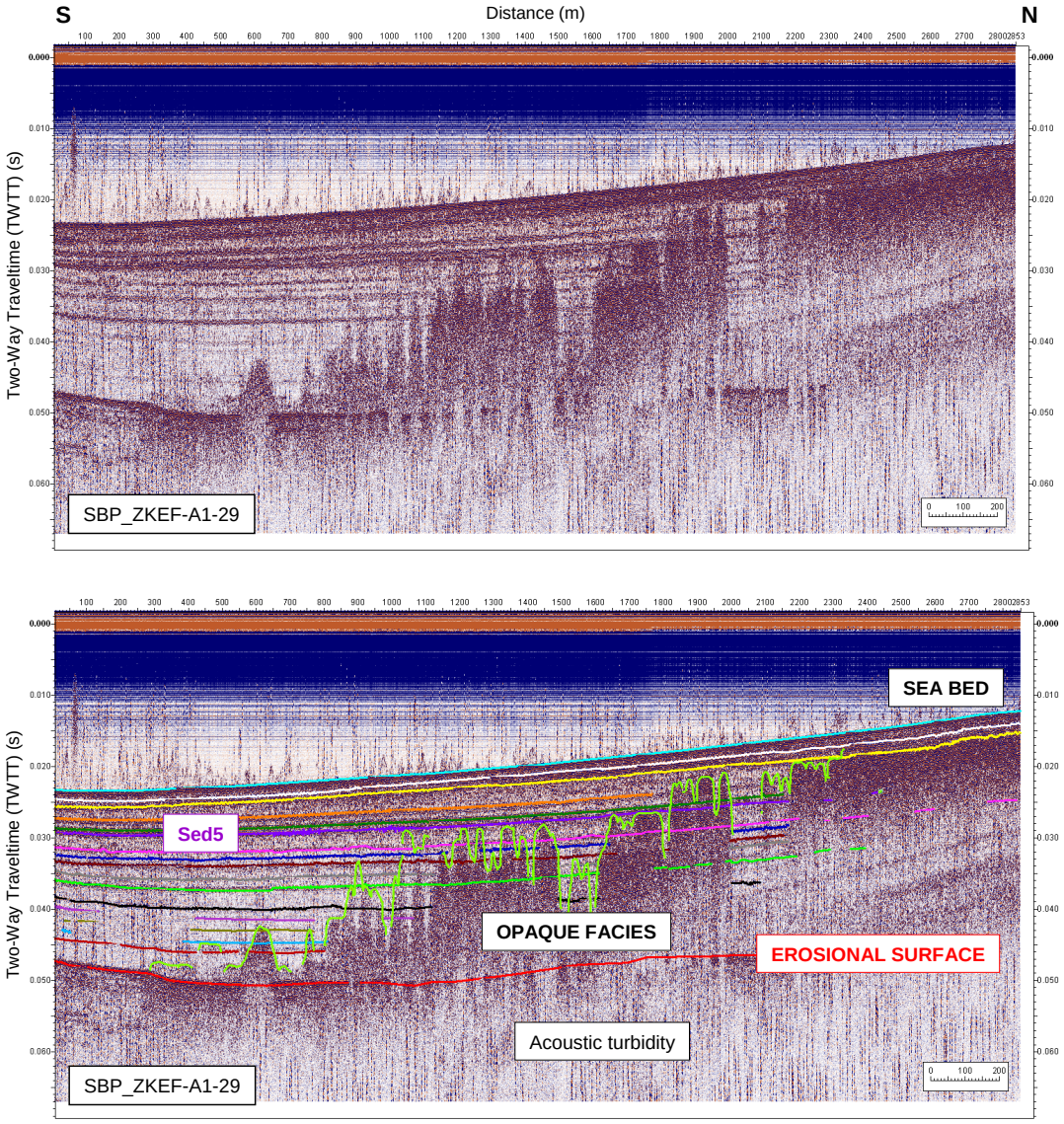

Figure 6.13 Line SBP_ZKEF-A1-29 which cross-cuts the opaque facies, occurring within the upper seismic megasequence in the northern Gulf of Argostoli, in a N-S direction. The vertiginous, dark facies contrasts strikingly with the surrounding horizontally-stratified sediments. Annotations as for Figure 6.5. Location of line is shown in Figure 6.3.

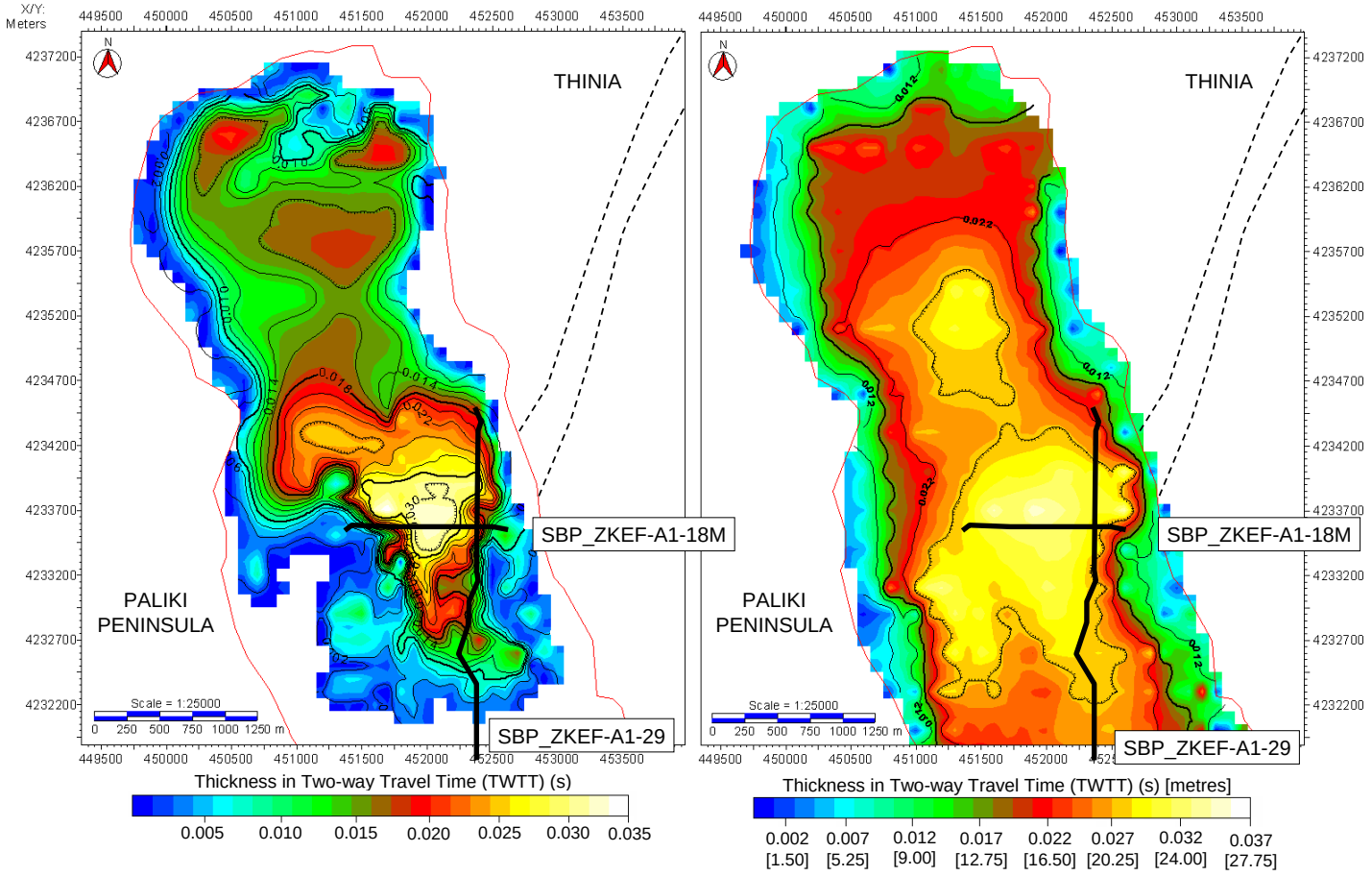

Figure 6.14 Isochrons of the opaque facies (left) and upper seismic megasequence (right) in the northern Gulf of Argostoli illustrating how the thickest accumulation of the opaque facies occurs within the thickest zone of the upper seismic megasequence. The locations of Figures 6.12 (SBP_ZKEF-A1-18M) and 6.13 (SBP_ZKEF-A1-29) are indicated. The proposed route of "Strabo's Channel" is indicated by a black dashed line.

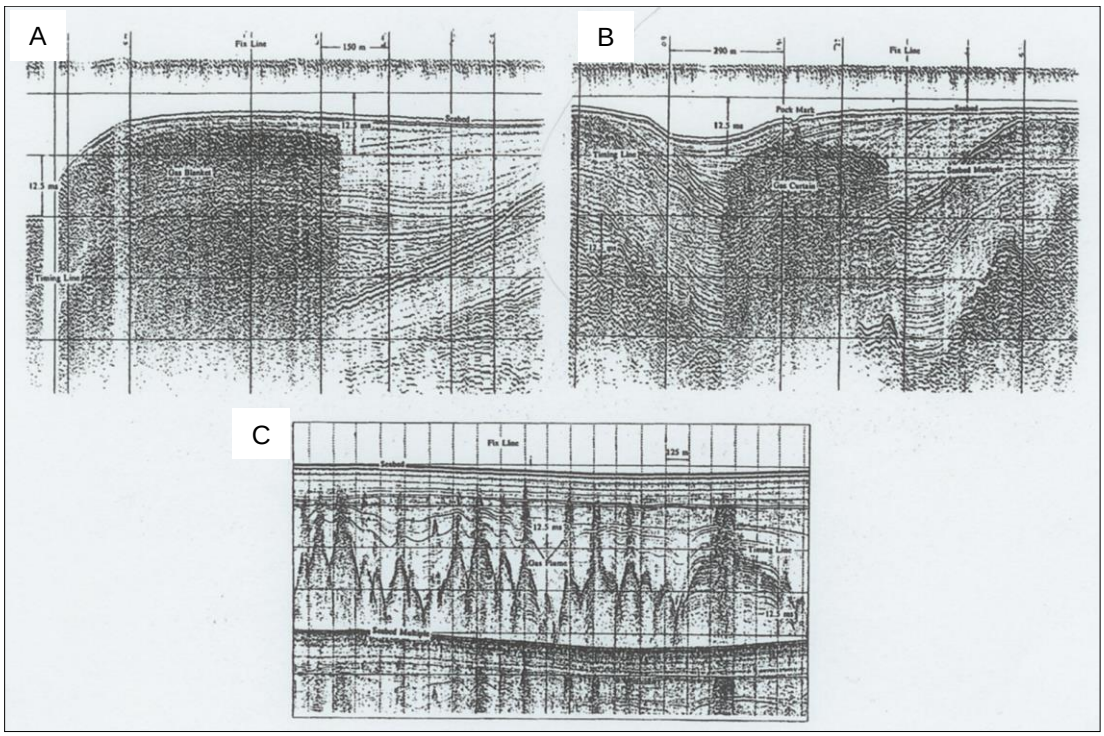

Figure 6.15 Examples of the three recognised forms of shallow gas accumulation: A) Gas blanket, the largest type of accumulation, typically extending for more than 1 km in length; B) Gas curtains, the most common sort of accumulation extending around 100 m to 500 m (Firth of Forth); C) Gas plumes which are typically less than 50 m and often have a clear vertical connection to their source (NE Irish Sea) (after Taylor, 1992).

6.3.3 Lower Seismic Megasequence

A. Lower Gulf

The survey data imaged the seismic reflectors beneath the erosional surface very well in some areas (where the upper seismic megasequence was thin). However, the presence of strong sea bed and erosional surface multiples masked areas of the seismic. These multiples were believed to have been caused by a particular reflective substrate which occurred along the erosional surface and sea bed in some areas. The reflectors of the lower seismic megasequence were very different from those above the erosional surface as they showed a high degree of deformation. Where the upper seismic megasequence was most thickly deposited, the internal structures within the lower seismic unit were almost entirely obscured by very strong erosional surface and sea bed multiples.

The E-W “dip” lines showed that between the Paliki Peninsula and Argostoli Peninsula, the Gulf of Argostoli formed a major asymmetric syncline (Gulf of Argostoli Syncline) with a steep eastern side composed of westerly-dipping sediments and a more gently easterly-dipping western side in which the sediments onlapped the offshore continuation of the Paliki peninsula. The key seismic line for showing this structure was KEF-B-06 (Figure 6.16 and Figure 6.17). The upper seismic megasequence was entirely contained within the basin of this syncline which the sides were relatively free from draping sediment.

The eastern side of the syncline formed a very steep to near vertiginous scarp (clearly seen in the most southerly line, KEF-B-05 (Figure 6.18). This scarp was interpreted as an easterly-dipping thrust fault running along the western coast of Argostoli Peninsula. The lack of erosion suggested it was active recently. This scarp raised the level of the sea bed by around 15 m to form a shallow bathymetric shelf (30 m water depth or less) which extended along the length of the Argostoli Peninsula’s western coast and formed a pronounced peak above the sea bed.

The reflectors defining the raised shelf were most clearly imaged in KEF-B-06 (Figure 6.19). Within the scarp, they were tightly-packed, parallel to sub-parallel and exhibited a very steep to near vertical westerly-dip indicating the sediments had undergone dramatic tilting since deposition. A possible unconformable boundary between the parallel-bedded reflectors of the scarp (blue in Figure 6.19) and more convoluted bedding further to the east (red-orange in Figure 6.19). This might have been caused by a very steep, westerly-dipping backthrust within the raised shelf exploiting the steeply-dipping sediment beds similar to those observed within the west-facing sea cliff of Argostoli Peninsula (Section 1.2.3, Figure 1.28). The tilted reflectors of this raised shelf were truncated and draped by a discontinuous sequence (base of unit in yellow in Figure 6.18) of horizontally-bedded, planar reflectors. The dip of the reflectors suggested it was part of the upper seismic megasequence which had been uplifted to this position through possible tectonic dislocation which would support the idea that this scarp represented a normal fault. This may also be evidence of drowned beach deposits in a similar configuration to the raised Paleomilazzien

beach (labelled as 3 in Figure 1.28) which form a sub-horizontal stratigraphy draped over the eroded top of the tilted Plio-Quaternary sediments making up the sea cliff of Argostoli Peninsula.

In KEF-B-08 (Figure 6.20) and KEF-B-09 there was evidence of oblique prograding clinoforms which would indicate formation of a delta emanating from the shelf running along the western coast of Argostoli Peninsula. The top of this possible delta was eroded suggesting it had been partially subaerially exposed. This structure may also be evidence of significant bedding plane slip down the steeply-dipping bedding of the raised shelf.

The reflectors on the western side of the syncline dipped more gently and towards the east (Figure 6.21). These reflectors were moderately strong in amplitude, parallel-bedded and steepened as they onlapped the raised bathymetric high which represented the offshore continuation of the Paliki Peninsula Anticline. The surface of the resulting bathymetric ridge was devoid of sediment cover and the surface was heavily eroded with a series of micro-channels in a similar fashion to the top of the shallow shelf defining the western coast of the Argostoli Peninsula which clearly truncated these dipping reflectors. The reflectors defining the synclinal basin itself were not easily to define as they were almost entirely masked by powerful repeating multiples.

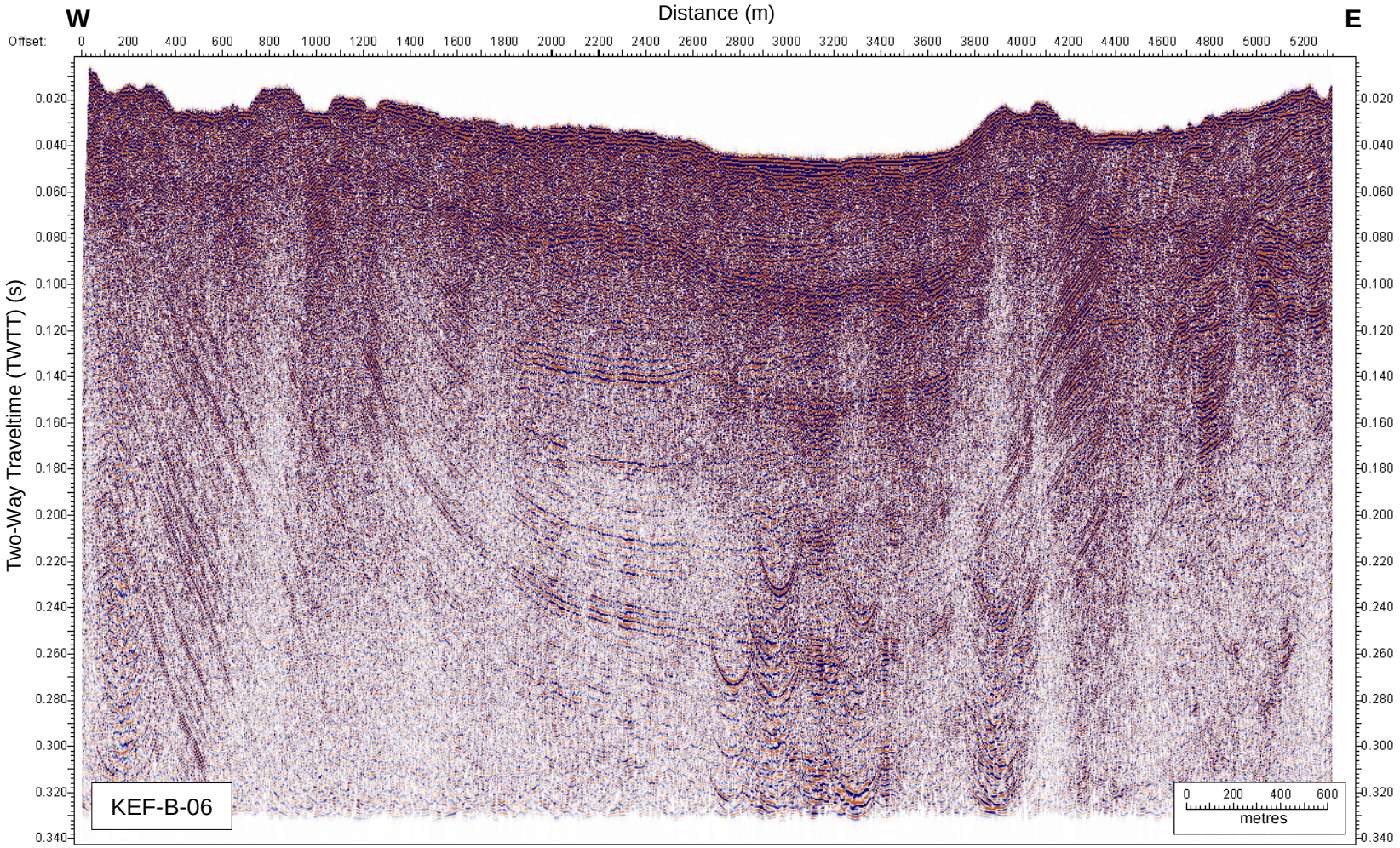

Figure 6.16 Uninterpreted version of seismic line KEF-B-06 which is orientated E-W and cross-cuts the lower Gulf of Argostoli. Location of line shown in Figure 6.3.

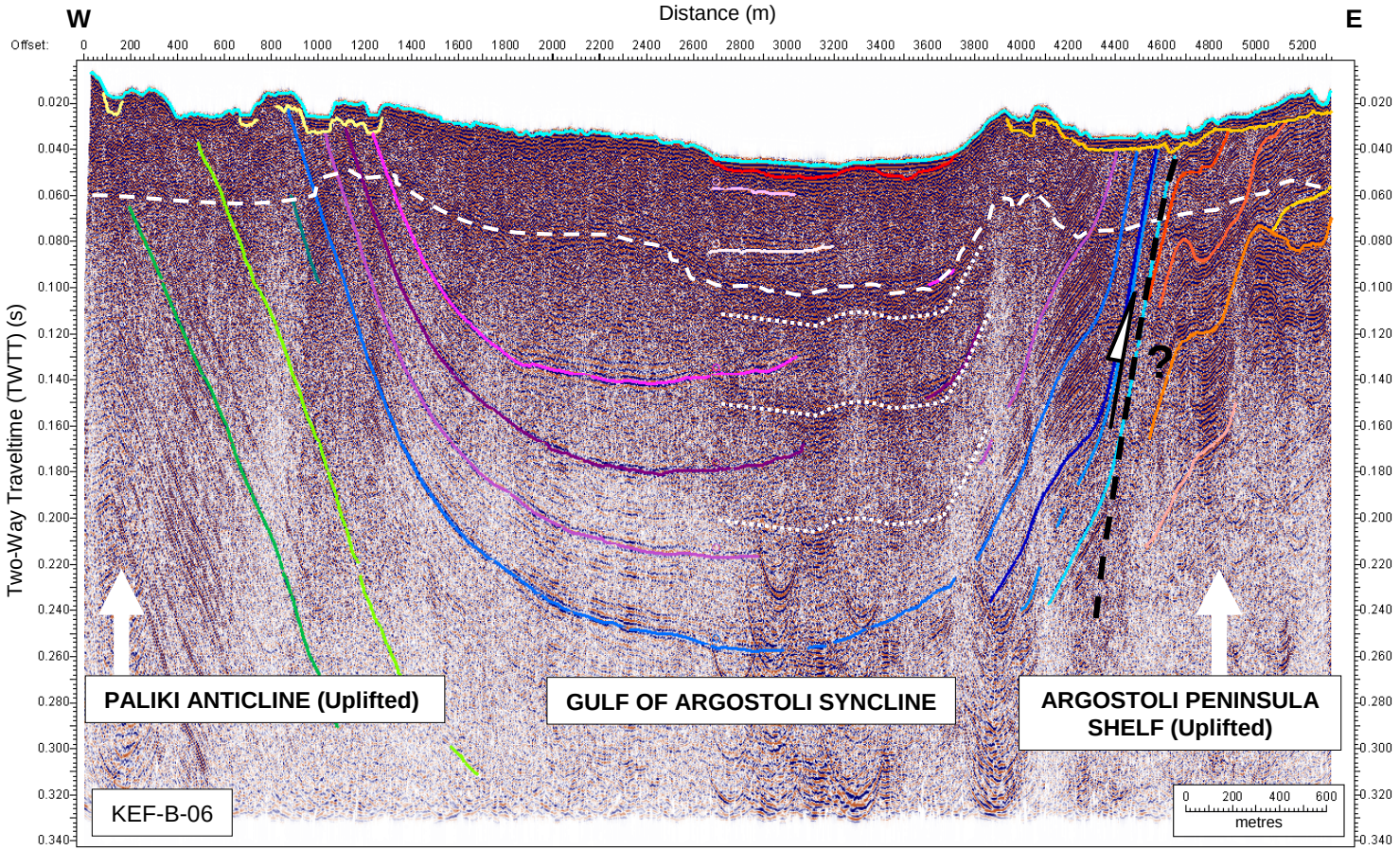

Figure 6.17 Interpreted version of Figure 6.16. Pale blue = sea bed, red = erosional surface, white dashed lines = sea bed multiples, white dotted lines = erosional surface multiples, yellow = possible drowned beach deposits. The green-coloured reflectors are associated with the Paliki Anticline, the "cold" coloured reflectors compose the Gulf of Argostoli syncline and "warm" coloured reflectors indicate the convoluted reflectors within the raised shelf running along the western coast of the Argostoli Peninsula. A possible westerly-dipping backthrust, like those observed along the Argostoli Peninsula west coast (Section 1.2.3, Figure 1.28), is marked by a black dashed line.

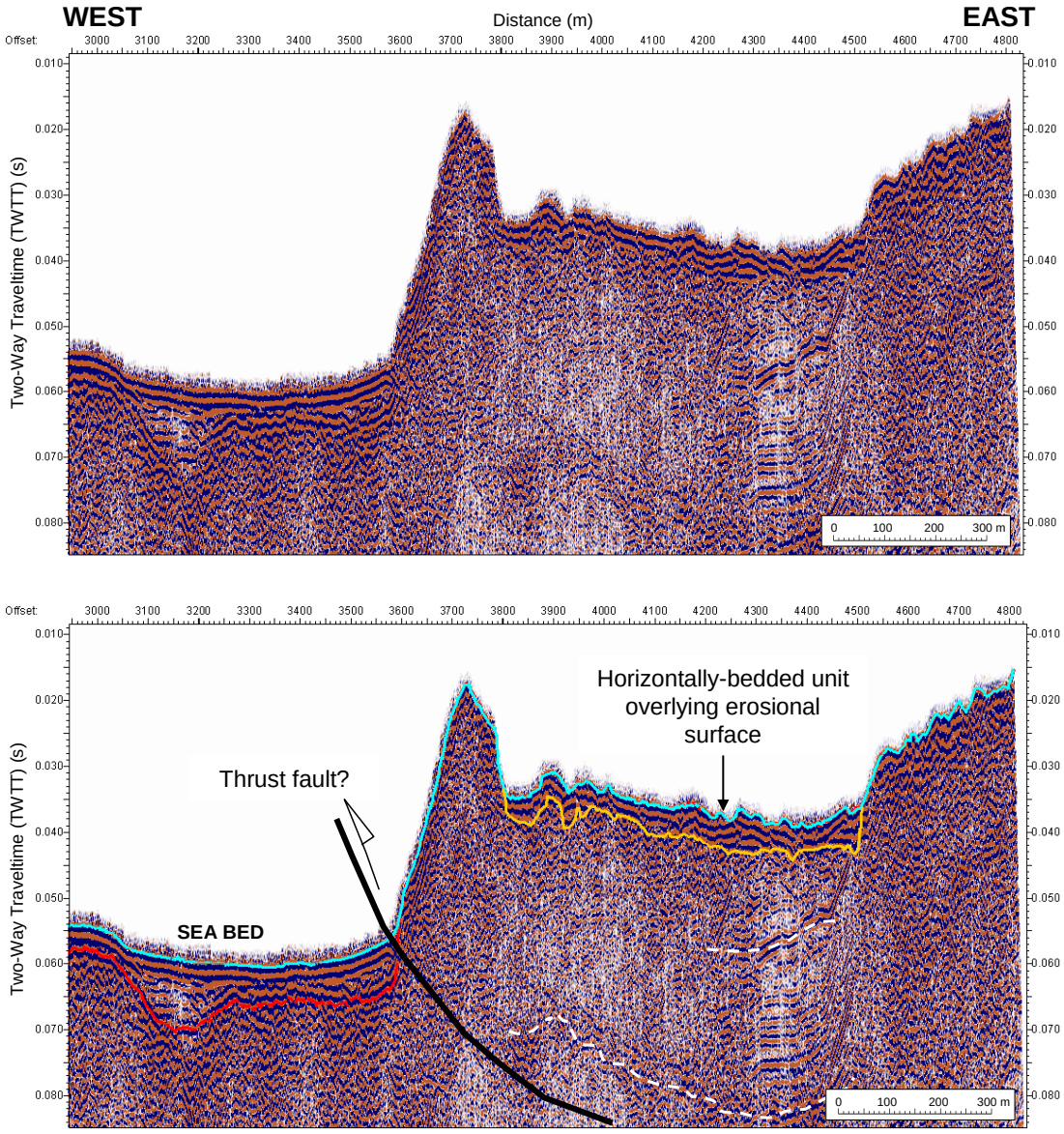

Figure 6.18 Seismic line KEF-B-05 depicting the scarp running along the western coast of Argostoli Peninsula. Pale blue = sea bed, red = erosional surface, yellow = drowned beach?, white dashed lines = sea bed multiples, black line = possible thrust fault. Location of line in Figure 6.3.

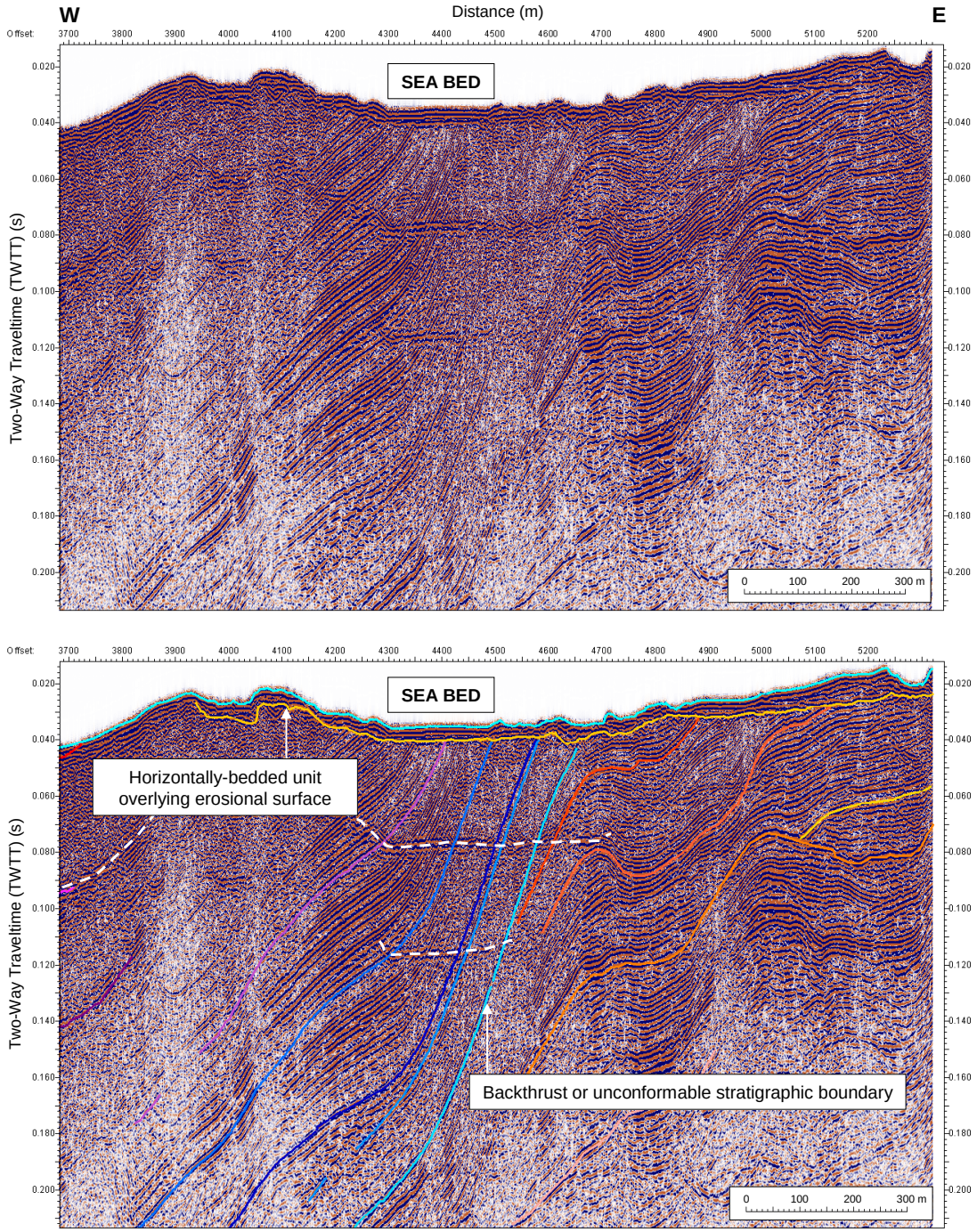

Figure 6.19 Seismic line KEF-B-06 showing details of the reflectors within the raised shelf running along the western coast of Argostoli Peninsula. "Warm" colours correspond to convoluted beds while the "cold" colours are associated with a possible westerly-dipping backthrust. Pale blue = sea bed, red = erosional surface, yellow = possible drowned beach and white dashed lines = sea bed multiples. Location of line is shown in Figure 6.3.

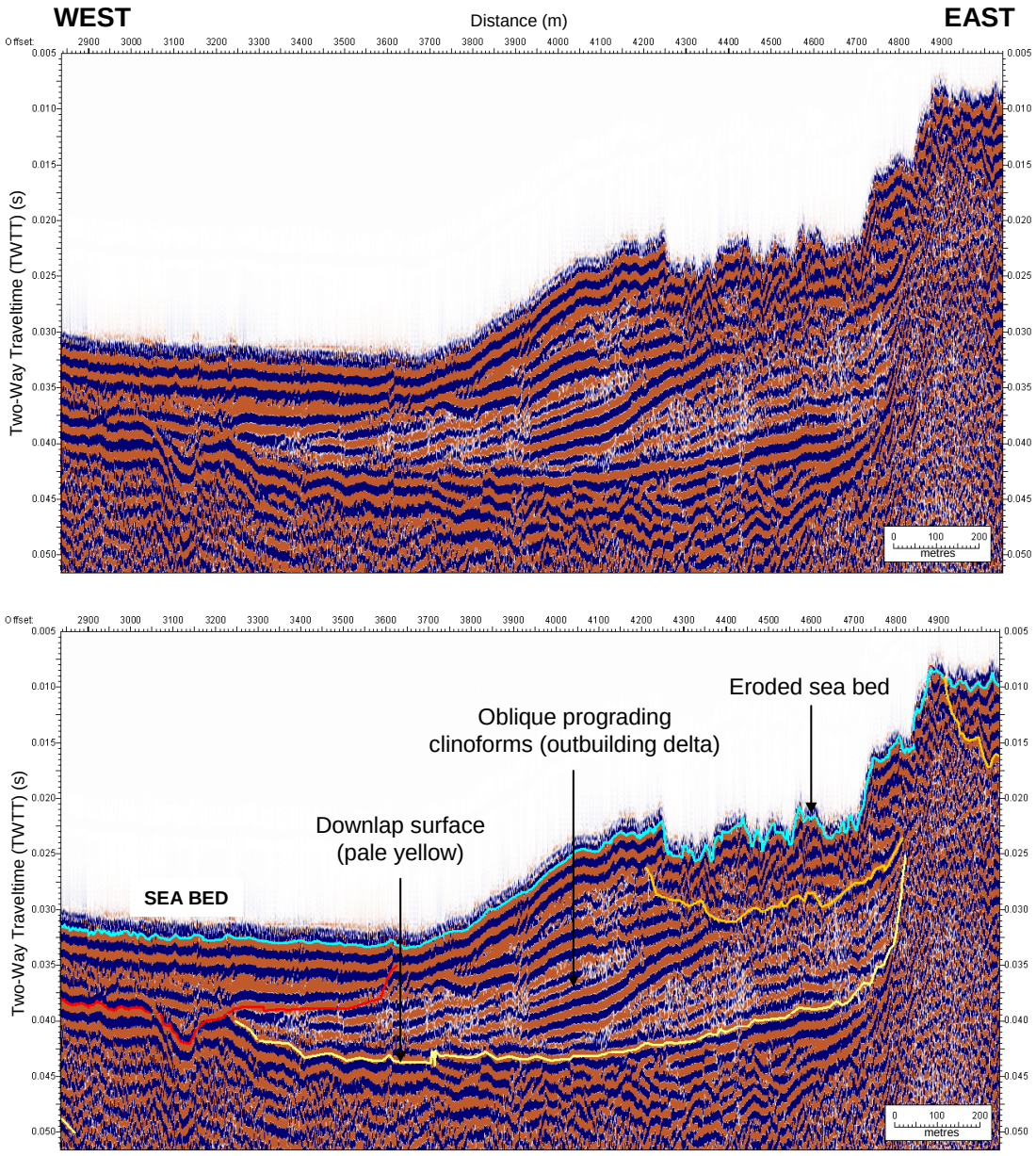

Figure 6.20 Evidence of a possible oblique prograding Clinoforms at the western tip of KEF-B-08 caused by deltaic sediments outbuilding from the western shore of Argostoli Peninsula. The downlap surface is indicated in pale yellow. Pale blue = sea bed (the top of the delta is heavily eroded), red = erosional surface, yellow = possible drowned beach. Location of line is shown in Figure 6.3.

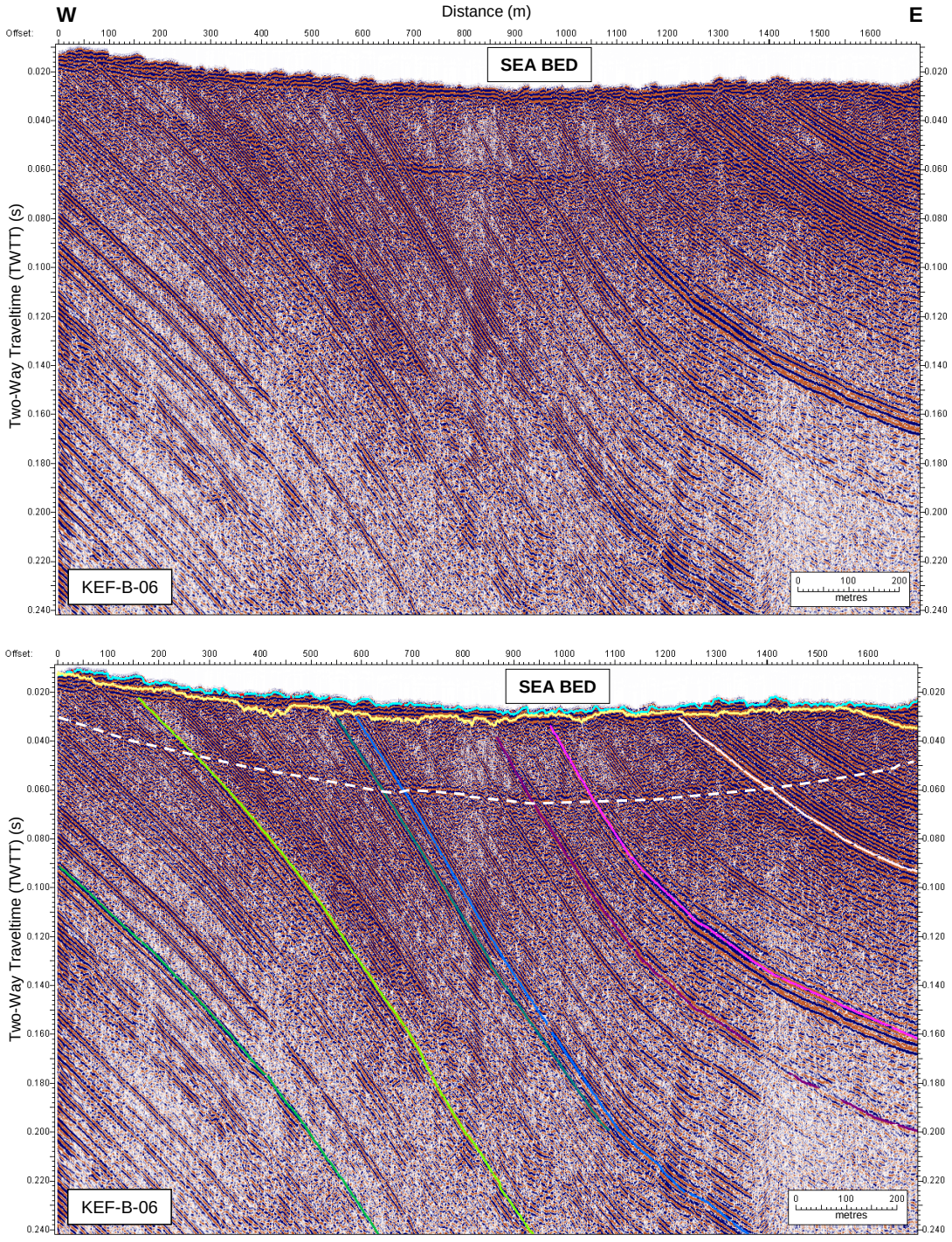

Figure 6.21 Line KEF-B-06 showing detail of the parallel-bedded, dipping reflectors (green, blue, pink and white) onlapping the Paliki Peninsula Anticline. Pale blue = sea bed, yellow = drowned beach?, white dashed line = sea bed multiple. Location of line shown in Figure 6.3.

B. Middle to Upper Gulf

To the north of the Argostoli Peninsula, the lower seismic megasequence formed a distinct "W"-shaped pattern of deformation composed of steeply-dipping folds (Figure 6.22 (uninterpreted), 6.23) which died out northwards. To the east of the deformation zone the lower seismic unit reflectors were largely obscured by erosional surface and sea bed multiples and degradation from shallow gas northwards

In KEF-B-19 and KEF-B-21 this deformation was most sharply-defined. The eastern "arm" of the "W" was defined by a very steep westerly-dipping backthrust. The reflectors within the hangingwall of this backthrust were very closely-spaced and parallel-bedded. The very steep dip of this backthrust (~45°) suggested that, like other thrust structures observed within Thinia (e.g. Agia Sotira Thrust in Section 3.3.1), this thrust had extensional origins and may represent a re-activated normal fault. Moving northwards, the backthrust died away to a shallow west-verging anticline and the eastern "arm" of the "W" became an easterly-dipping thrust fault (KEF-B-22 to B-24). By A1, the folds of the deformation belt became progressively deeper and less defined dying away into a series of gentle undulations. The shifting active front of this deformation zone and acute nature of the folds suggested the deformation was being restricted to the west forming a "crumple zone" as westwards-migrating compression was obstructed.

The eastern shore of Paliki was defined by an easterly-dipping normal fault scarp was apparent at the far western end of the survey (SBP_ZKEF-A1-10, Figure 6.24) although it wasn't clear if this was the cause of the "crumple zone" further to the east. This scarp could clearly be seen in aerial view as a NNE-SWW-striking coastal shelf running up the Paliki coastline to Livadi Marsh (Figure 6.25) however degradation of the seismic prevented it from being defined north of volume A1. Instances of westwards thickening of the lower seismic megasequence occurred along the western side of the Gulf (Figure 6.26) which may have related to this extensional feature or may be evidence of an underlying easterly-dipping extensional structure.

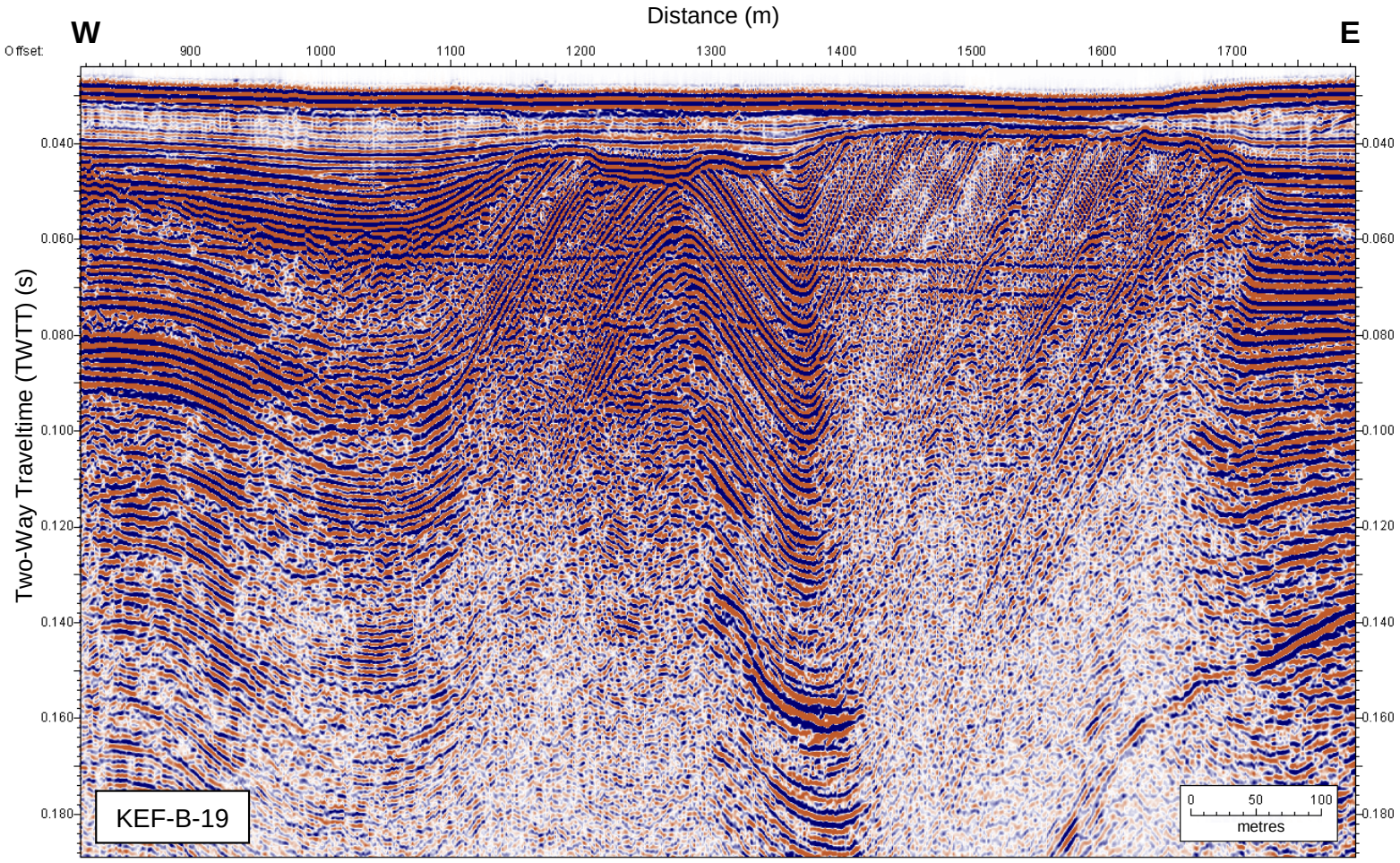

Figure 6.22 Uninterpreted version of KEF-B-19 illustrating the strong folding which occurs within the middle Gulf of Argostoli, north of the Argostoli Peninsula. Location of line is shown on Figure 6.3.

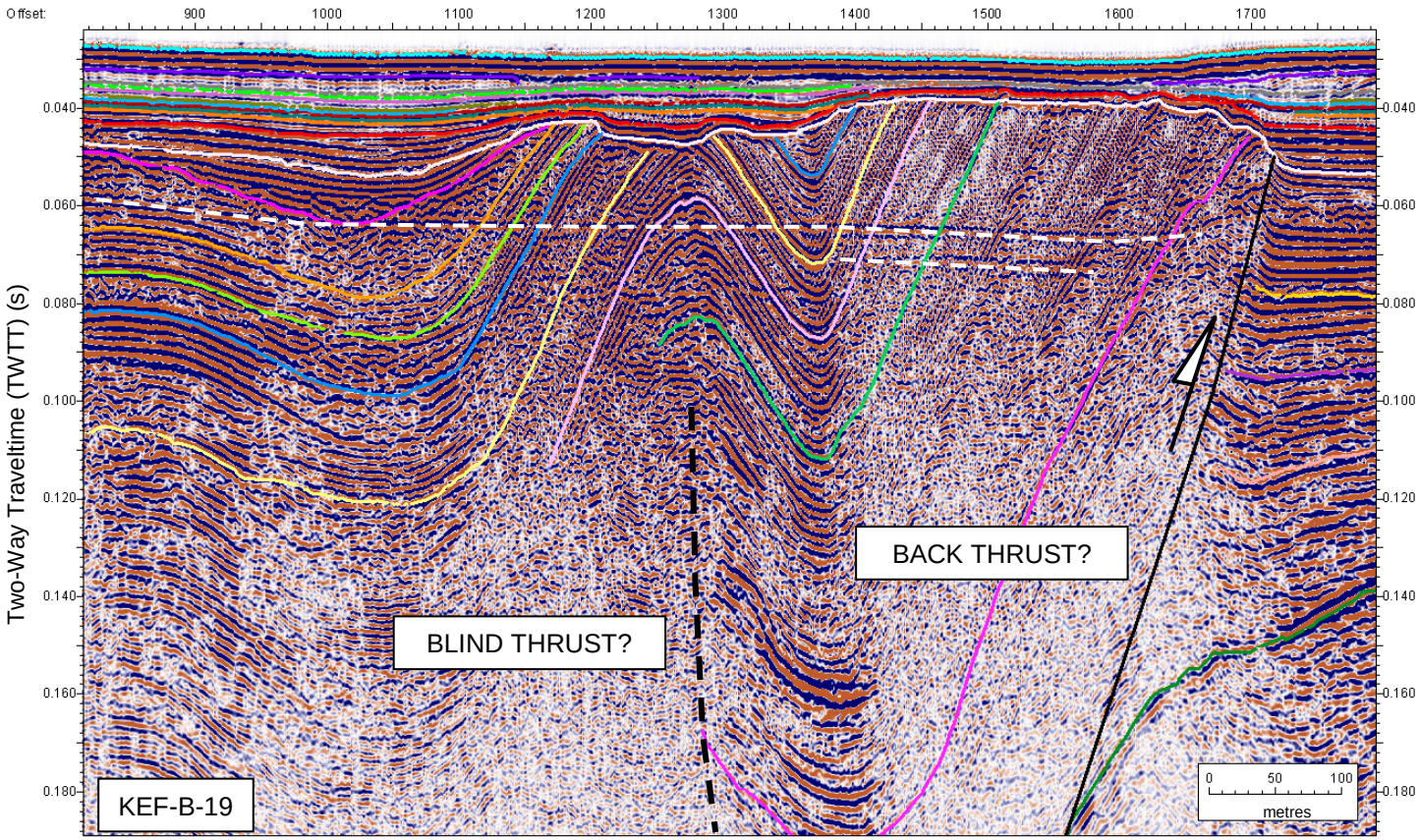

Figure 6.23 Interpreted version of Figure 6.24 (KEF-B-19) showing truncation of the dramatically-folded reflectors of the lower seismic megasequence by the erosional surface which is in turn onlapped by the horizontal reflectors of the upper seismic megasequence. The reflectors below the erosional surface have been faulted by a westerly-dipping backthrust (solid black line) and the sharp anticline to the east suggests the presence of an easterly-dipping blind thrust (black dashed line). The erosional surface has eroded further into the crest of the anticline facilitated by fracturing caused by the fold. Annotations as for Figure 6.5. Location of line shown on Figure 6.3.

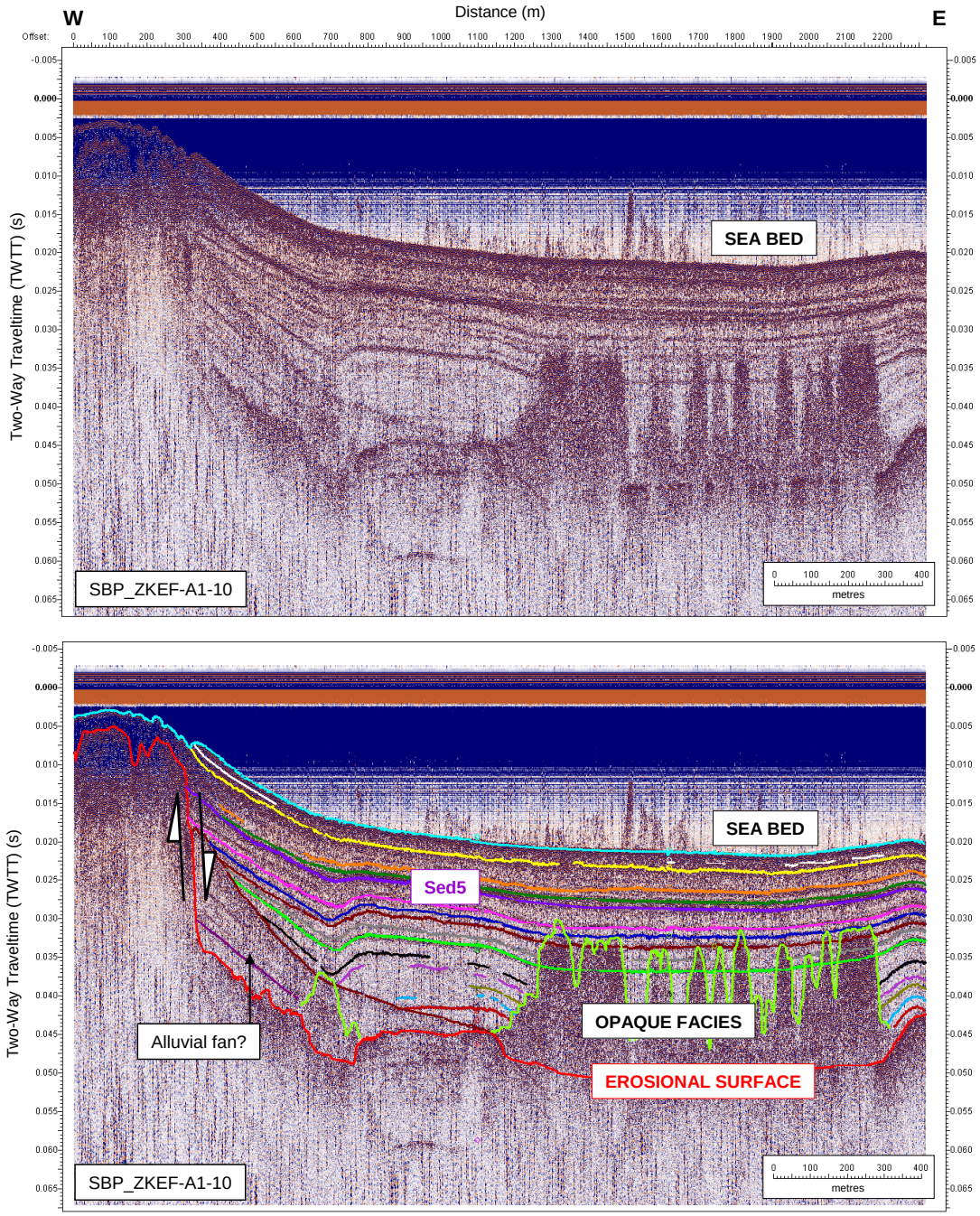

Figure 6.24 Line SBP_ZKEF-A1-10 illustrating the easterly-dipping normal fault scarp which runs along the west coast of the Gulf of Argostoli. Location of line in Figure 6.3. Annotations as for Figure 6.5.

A structural map of the entire Gulf was created by mapping the approximate positions of the folds and faults at the erosional surface (Figure 6.27). Mapping the deformation within the Gulf revealed a NNW-SSE striking belt of compressional deformation which ran along the western coast of the Argostoli Peninsula and along

the eastern coast of Paliki. The folded sediments in the middle and upper Gulf were interpreted as being linked to the Argostoli Peninsula faults (White Rocks and Argostoli Fault) and therefore were part of the same Hellenide fold-and-thrust system observed onshore (Section 1.2.3, A).

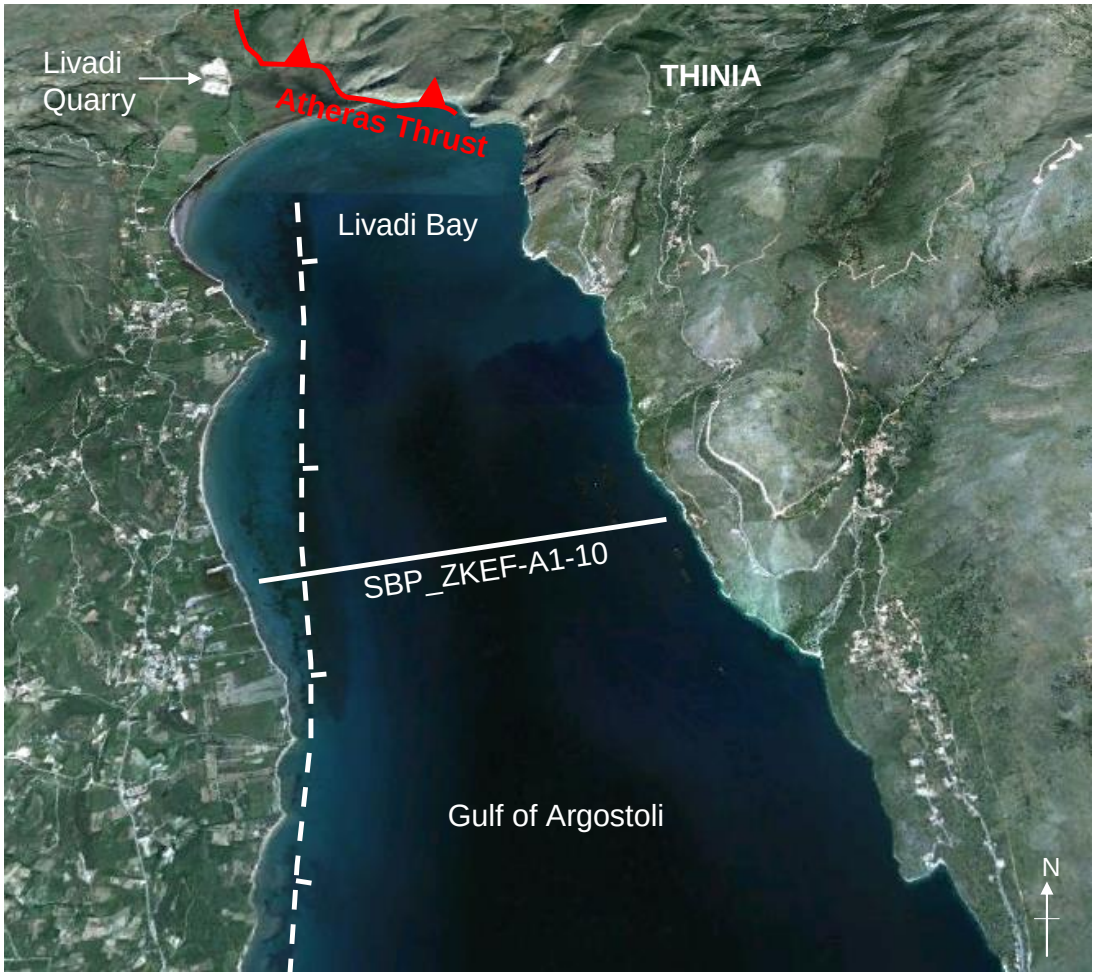

Figure 6.25 Satellite image from Google Earth depicting the normal fault scarp (white dashed line), cross-cut by line SBP_ZKEF-A1-10 (marked by a white line and depicted in Figure 6.24) running along the west-coast of the Gulf into Livadi Marsh.

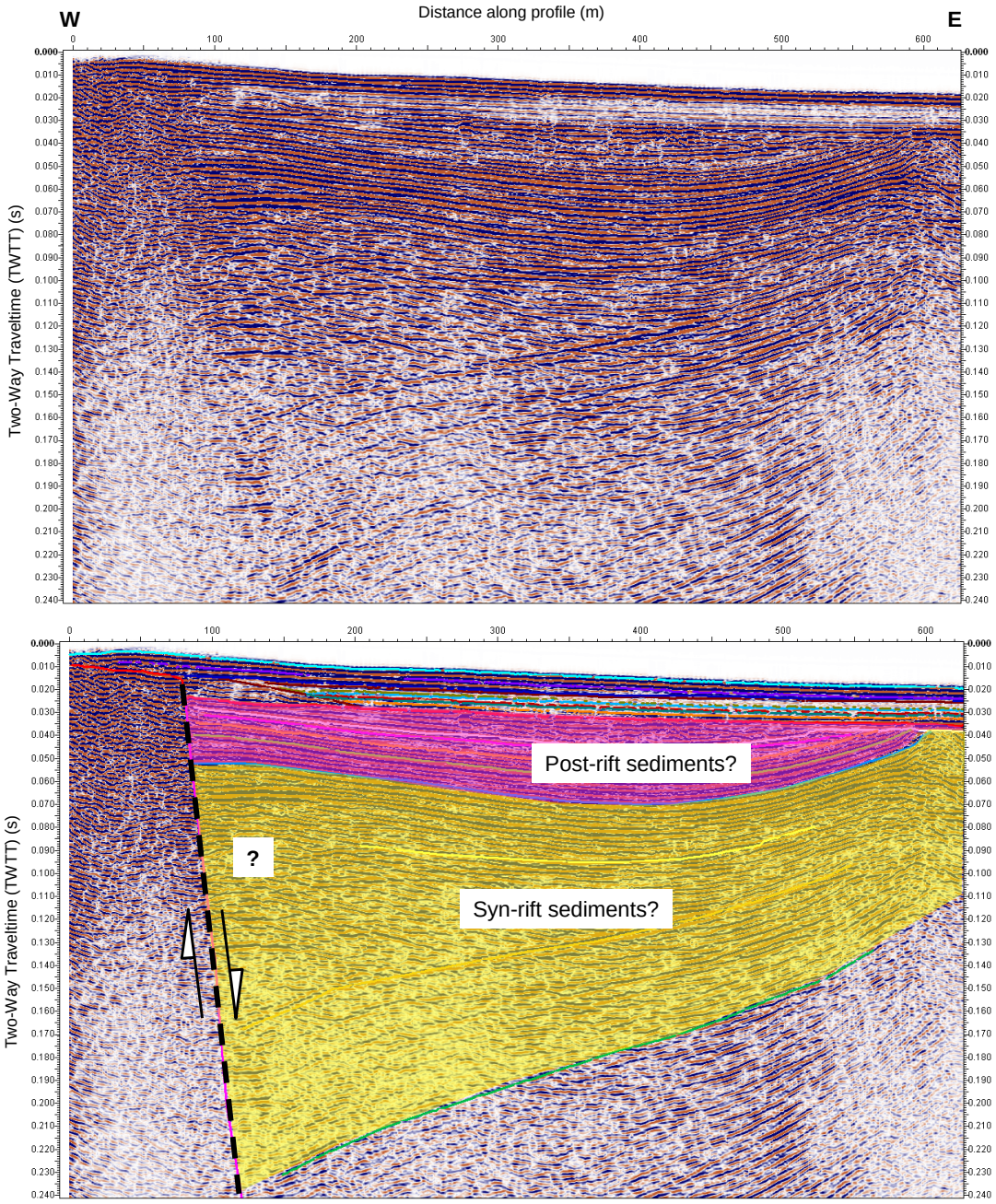

Figure 6.26 Seismic line KEF-B-22 showing possible westwards thickening of sediments beneath the erosional surface in response to a large easterly-dipping extensional feature. This thickening may relate to the normal fault scarp imaged in Figure 6.24.

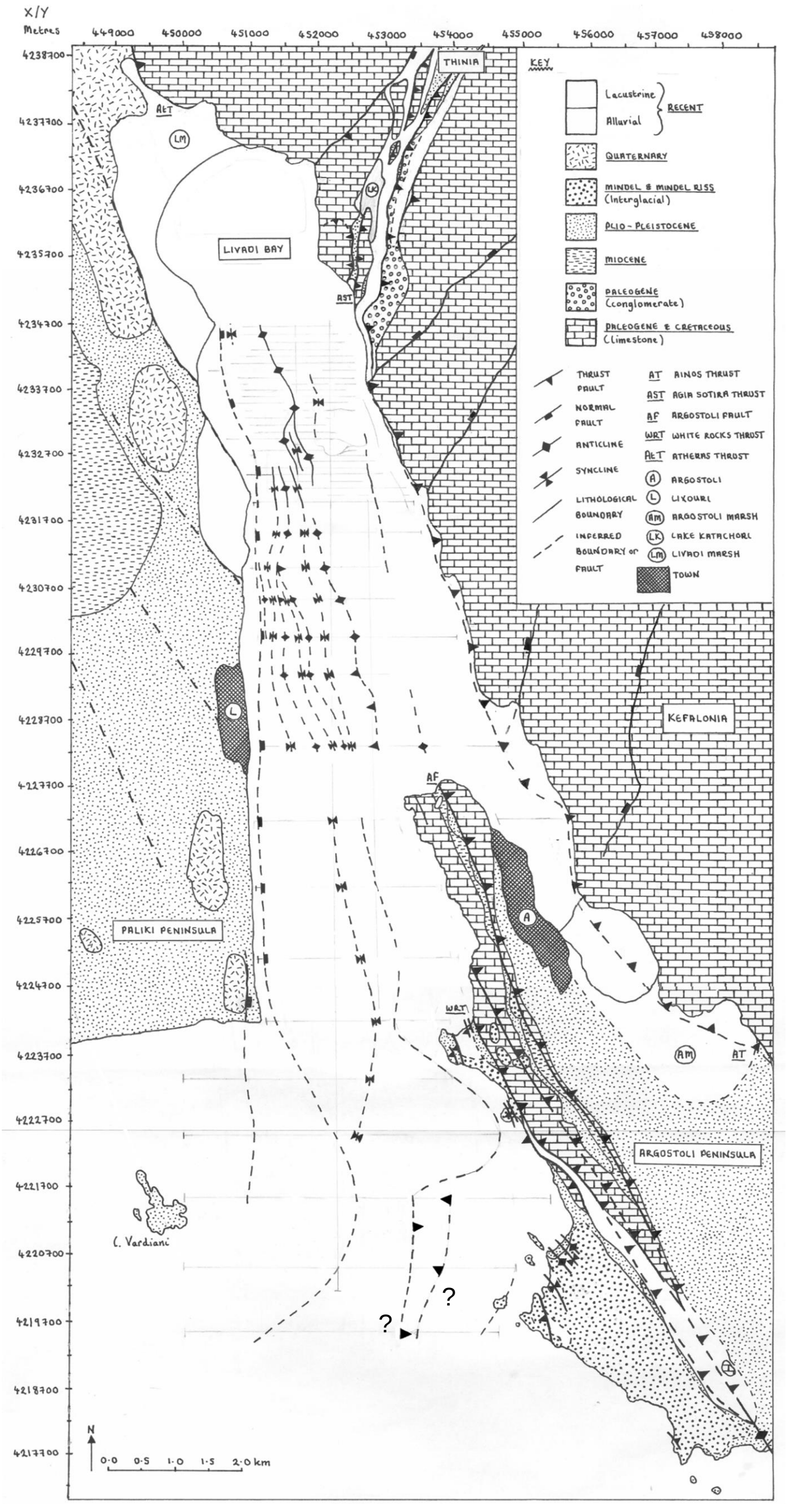

Figure 6.27 Sketch map showing the configuration of faulting within the Gulf of Argostoli using the faulting and folded structures observed within the lower seismic megasequence close to the depth where they are truncated by the erosional surface.

6.3.4 Buried (Quaternary-Holocene?) Transgressional Surface

The major erosional surface underlying the upper seismic megasequence and truncating the folded lower megasequence could be identified consistently throughout all three volumes except where the masking effect of the shallow gas caused most interference of the seismic in Volume A2 and north-east of A1. The amplitude of the erosional surface was most powerful where the erosional surface was deepest suggesting a particular hard or reflective substrate was present on the surface. This reflectivity resulted in the strong multiples which almost completely obscured any internal structure of the underlying sediments. The presence of such a widespread erosional surface suggested that the Gulf had been subaerially exposed at some points in its geological history when relative sea levels dropped below the edge of the shallow coastal shelf resulting in erosion of the sediments making up the shelf.

Gridding the erosional surface revealed the existence of a deeply-incised valley between 10 and 44 m deep, buried beneath the upper seismic megasequence (Figure 6.28). This valley was composed of three NNE-SSW striking, flat-bottomed lens- or canoe-shaped basins set in an en-enchelon configuration and offset to the NE-SW of one another (Figure 6.29). It was not clear if these offsets had any vertical displacement however, the southerly-most offset coincided with the edge of the shelf defining the Gulf (scarp with a SW-dip).

The depth of these basins was around 40 to 44 m metres below current sea bed and they were linked to one another by a much shallower narrow “creek”. These basins acted as depocentres for the sediment of the upper seismic megasequence as shown by the isochron in Figure 6.11 with the thickest accumulations of this unit contained within the northerly two basins. The shape of the basins was primarily controlled by the underlying Hellenide faulted structures of the lower seismic megasequence (Figure 6.27). The offsets were harder to date since it wasn’t clear whether the course the river took simply exploited the weakening of rocks along the fault planes or if the valley was dissected up by this faulting after formation. The complete lack of

faulting within the upper seismic megasequence suggested that all faulted occurred after deposition of this unit and, therefore, before transgression of sea back into the Gulf.

The northerly-most basin measured c. 7 km by 2 km and ran from southern Thinia to Argostoli Bay. While the primary source appeared to be southern Thinia, the basin was also fed by several other streams along the steep eastern side of the Gulf via sharply incised stream channels still visible onshore. The western side of this basin was defined by the NNE-SWW striking zone of deformation. The southerly basin was more rounded and measured around 6 km by 2 km and lay within the Gulf of Argostoli syncline between the Paliki peninsula and scarp running along the west-coast of Argostoli Peninsula. A third possible basin occurred to the south of Vardiani Island and the SW tip of Argostoli Peninsula.

The deep, flat-bottomed morphology of these basins and the lack of weathering on the erosional surface within them compared to the edges suggested they formed lakes during subaerial exposure of the Gulf (shaded white in Figure 6.29). The greater reflectivity of the erosional surface within these basins suggested the presence of possible buried organic matter associated with these lakes and a possible source for the shallow gas observed in the northern basin. The lack of sediment cover and heavily eroded surface of the raised bathymetric ridges outside of the basins (e.g. south of Paliki Peninsula, the west coast of Argostoli Peninsula) suggested these areas formed islands and coastal extensions during subaerial exposure, up to 4.5 km further south in the case of Paliki and ~2 km westwards in the case of Argostoli Peninsula.

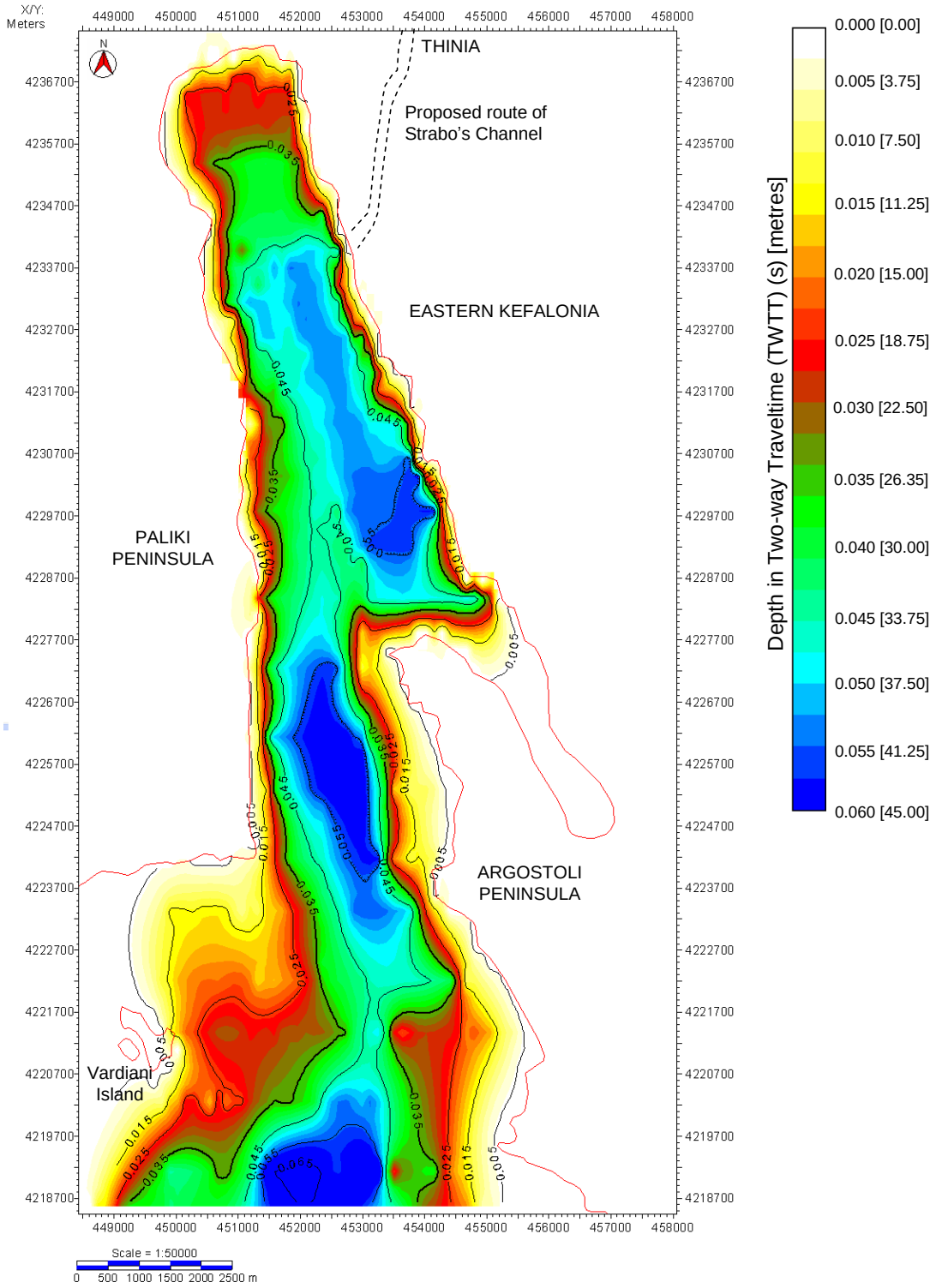

Figure 6.28 Two-way traveltime (TWTT, in seconds) grid (with depth conversion in square brackets) of the erosional surface revealing a buried drainage valley incised into the deformed sediments of the lower seismic megasequence. The flat-bottomed areas (dark blue) may correspond to ancient, sediment-infilled lakes.

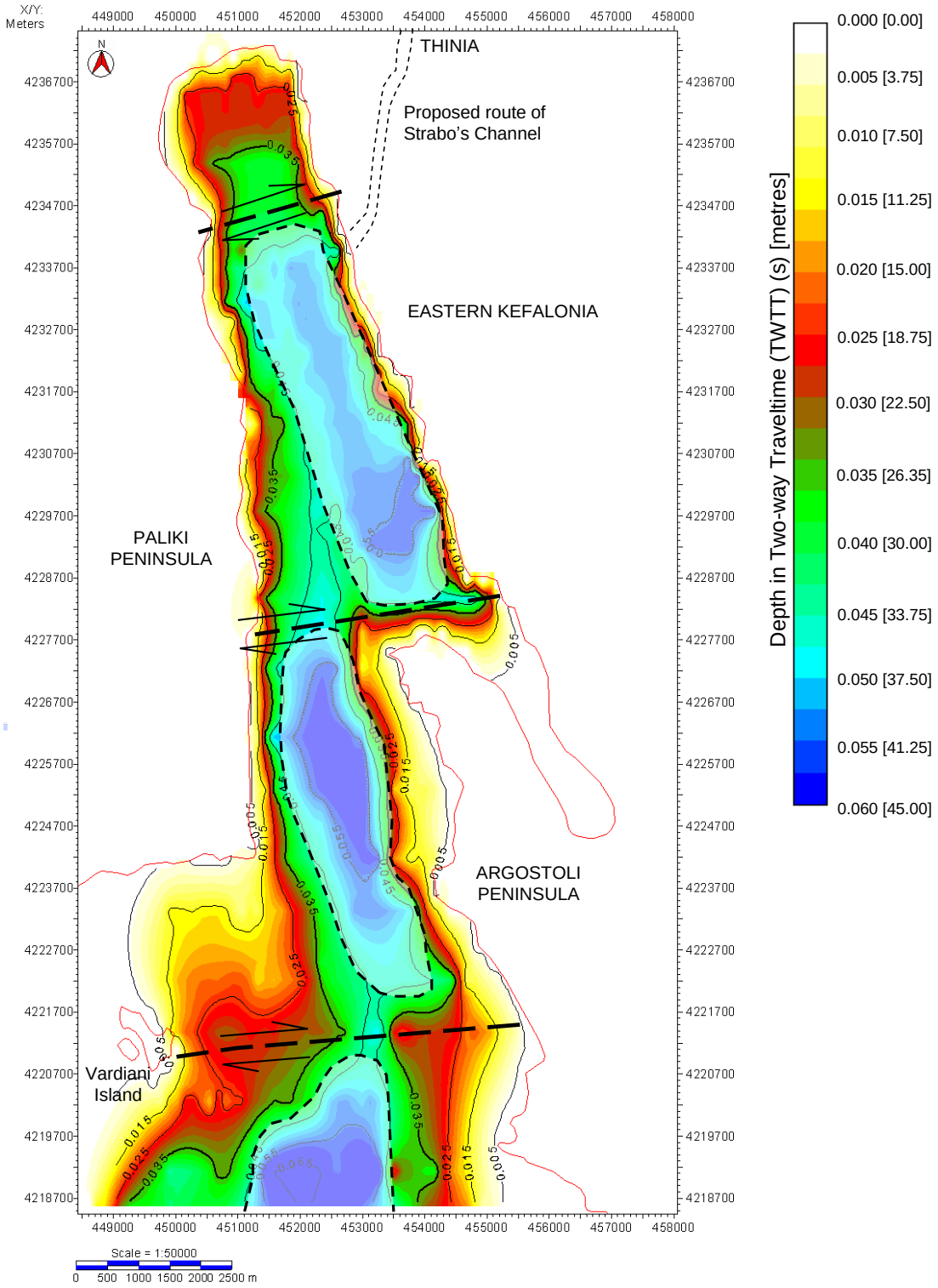

Figure 6.29 Erosional surface map from Figure 6.28 with interpretation of the three lens-shaped depocentres (shaded) and NE-SW striking offsets (black dashed lines).

6.4 Atheras Bay (Volume C)

The sub-seabed configuration of Atheras Bay was difficult to determine. The quality of the seismic here was far less than that of the Gulf of Argostoli survey. The sparker survey suffered from interference due to the presence of a hard or reflective substrate at the sea bed so very little in the way of reflectors could be seen. The SBP survey produced the clearest results and revealed a similar configuration to the Gulf with a topographically dramatic erosional surface onlapped by (where it occurred) a stratified upper seismic megasequence. The close proximity to the shore of the survey grid meant that the approximate culture map assigned by the Kingdom software overlapped some near-shore seismic lines. For this reason the culture was eliminated when presenting grids.

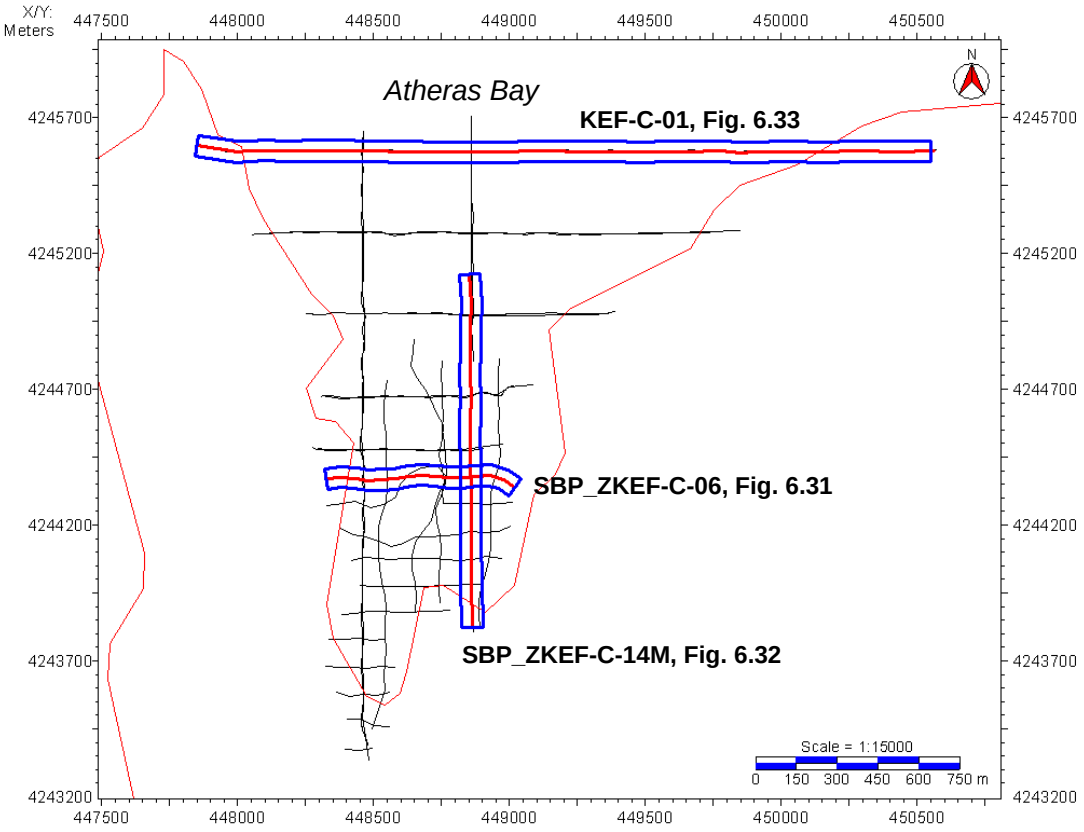

Figure 6.30 Kingdom base map showing the location of the Atheras Bay shallow marine seismic reflection survey (Volume C), Western Kefalonia. The survey lines illustrated in the text are highlighted in blue and red. Due to approximation of the culture map, the coastline (in red) overlaps the survey lines.

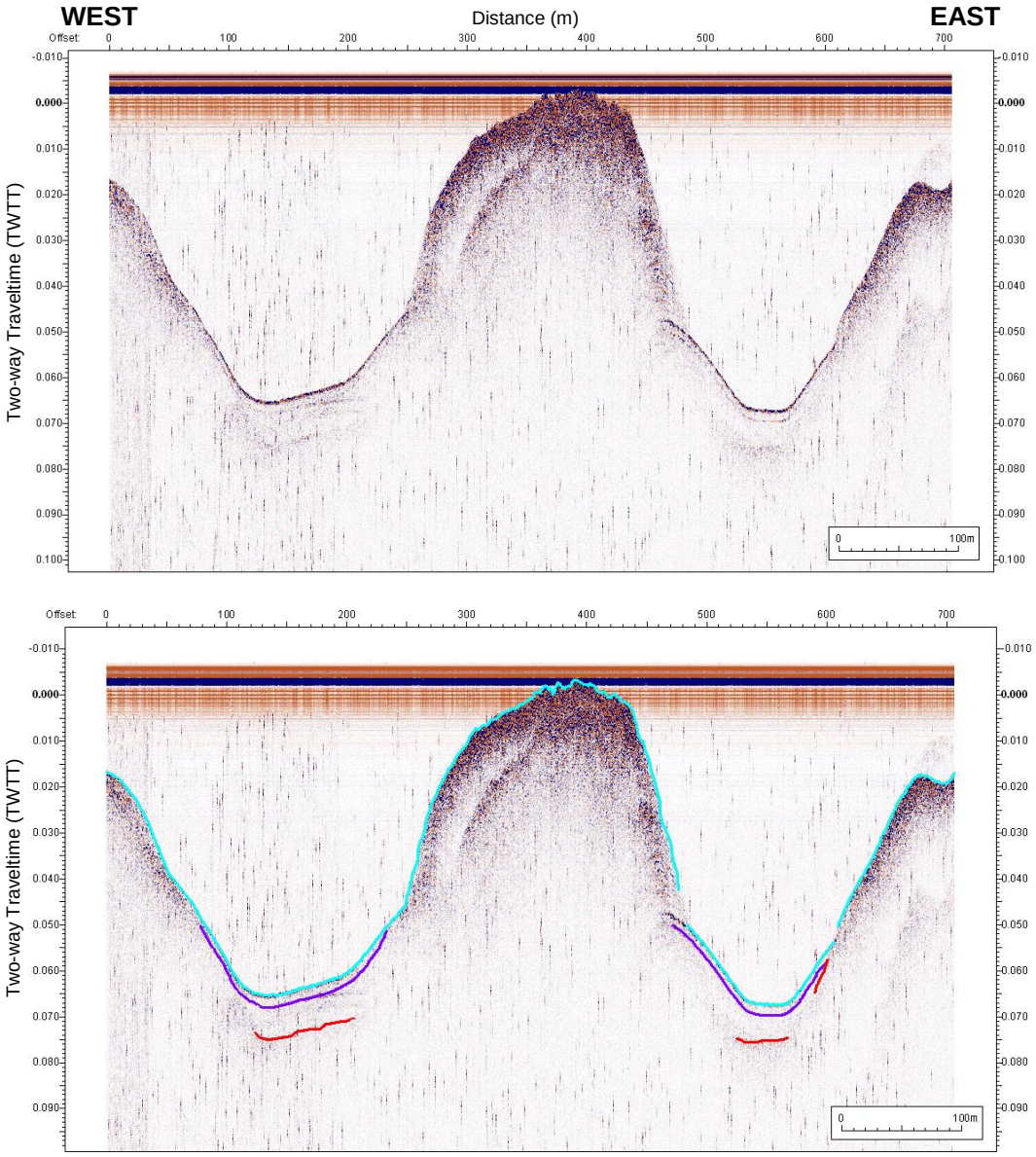

Figure 6.31 Typical E-W "dip" line (SBP_ZKEF-C-06) taken across Atheras Bay indicating the dramatic bathymetry of the inner bay. Pale blue = sea bed, purple = prominent postglacial unit reflector (Sed5?), red = erosional surface. The location of this line is shown in Figure 6.30.

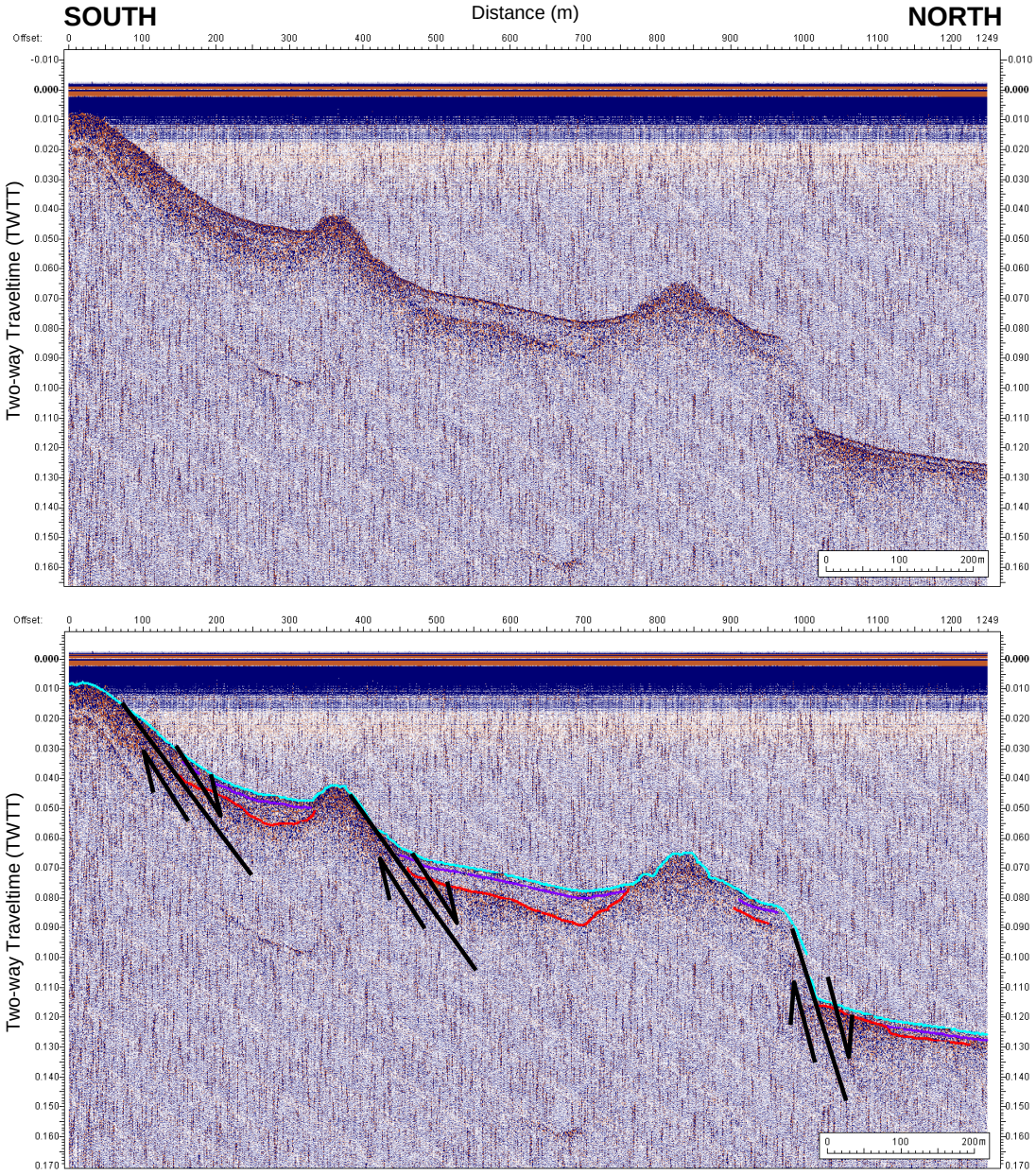

Figure 6.32 Typical N-S "strike" line (SBP_ZKEF-C-14M) taken across Atheras Bay indicating the numerous normal faults (indicated in black) which cross-cut the bay in a NE-SW to E-W orientation. Annotations as for Figure 6.31. The location of this line is shown in Figure 6.30.

6.4.1 Sea Bed Morphology

The inner bay of Atheras Bay was dominated by a bathymetrically dramatic ridge running up the centre of the survey, deeply-incised on either side by V-shaped channels (Figure 6.31) and cross-cut and offset by the numerous NE-SW trending normal faults observed on either side of the bay (described in Section 1.2.3, B, Figure 1.30). The small island near the shore appeared to be caused by a section of this ridge being uplifted by a southeast-dipping fault to the south and a northwest-dipping fault to the north to create a tiny "horst block" type feature.

As the bay widens, the sea bed bathymetry drops down in a series of 10 to 20 m high steps caused by the normal faulting illustrated most clearly by the north-south line SBP_ZKEF-C-14M (Figure 6.32). The sides of the outer bay are defined by two striking N-S orientated scarps (KEF-C-01, Figure 6.33). The eastern scarp has a throw of around 48 m and lack of erosion suggests it was active recently (tens to hundreds of years). The sea bed map for Atheras Bay (Figure 6.34) reflects the abrupt drop in bathymetry to the north of the island. The paucity of the upper seismic megasequence means that the sea bed map is roughly equivalent to the erosional surface map.

6.4.2 Upper Seismic Megasequence

The upper seismic megasequence was almost entirely absent from the Atheras Bay seismic occurring only within the sharply-eroded valleys below the ridge close to shore. The unit was too sparse and discontinuous to achieve a reasonable isochron. Several faint, draping reflectors could be determined. The strongest occurred near the top of the sequence suggesting it could be related to the strong reflector visible in the Gulf of Argostoli (Sed5, Figure 6.9 and 6.10). The proximity to the shore of these deposits and their position at the base of steep slopes suggest they are most likely terrigenous in origin (e.g. alluvial fans).

6.4.3 Lower Seismic Megasequence

Little could be defined of the structures within the lower seismic megasequence due to interference from the hard sea floor and multiples. Only in the seismic lines towards the outer bay of Atheras Bay (KEF-C-01, Figure 6.33) was there some definition of internal reflectors, in this case possible synsedimentary structures. These occur relative to the steep scarp on the western side of the bay suggesting this too is a faulted structure, in this case an easterly-dipping normal fault.

The structure of the westerly-dipping scarp in KEF-C-01 very similar to the westerly-dipping scarp observed along the western coast of Argostoli Peninsula (Figure 6.18) associated with the White Rocks/Argostoli Thrust system and was interpreted as the offshore extension of the Atheras Thrust. Wide spacing of the lines in the outer bay made it difficult to tell whether this thrust had been offset by the NE-SW striking normal faults.

Atheras Bay is clearly a complicated area structurally with at least three fault trends (Figure 6.35): at least nine NE-SW striking normal faults which dip either NW or SE, a major north-south striking normal fault defining the western side of the outer bay and the Atheras Thrust ascribing a roughly north-south route along the eastern side of the bay.

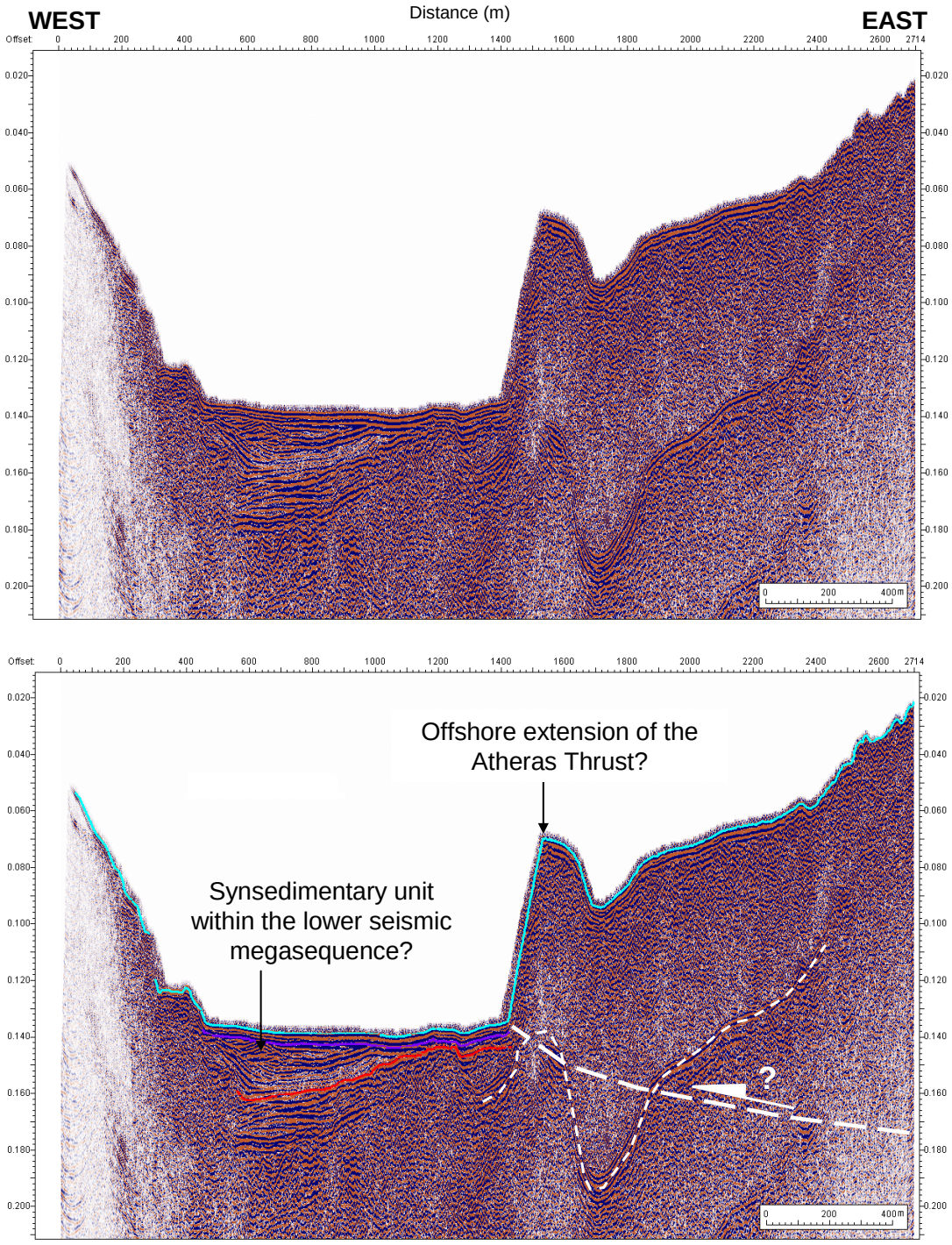

Figure 6.33 E-W line KEF-C-01 showing striking scarps defining the edges of the outer bay. The westerly-dipping scarp is a very similar structure to that observed off the coast of Argostoli Peninsula in Figure 6.18. White dashed line = sea bed multiple. Other annotations as for Figure 6.31. Thick white dashed line = proposed position of Atheras Thrust. The location of this line is shown in Figure 6.30.

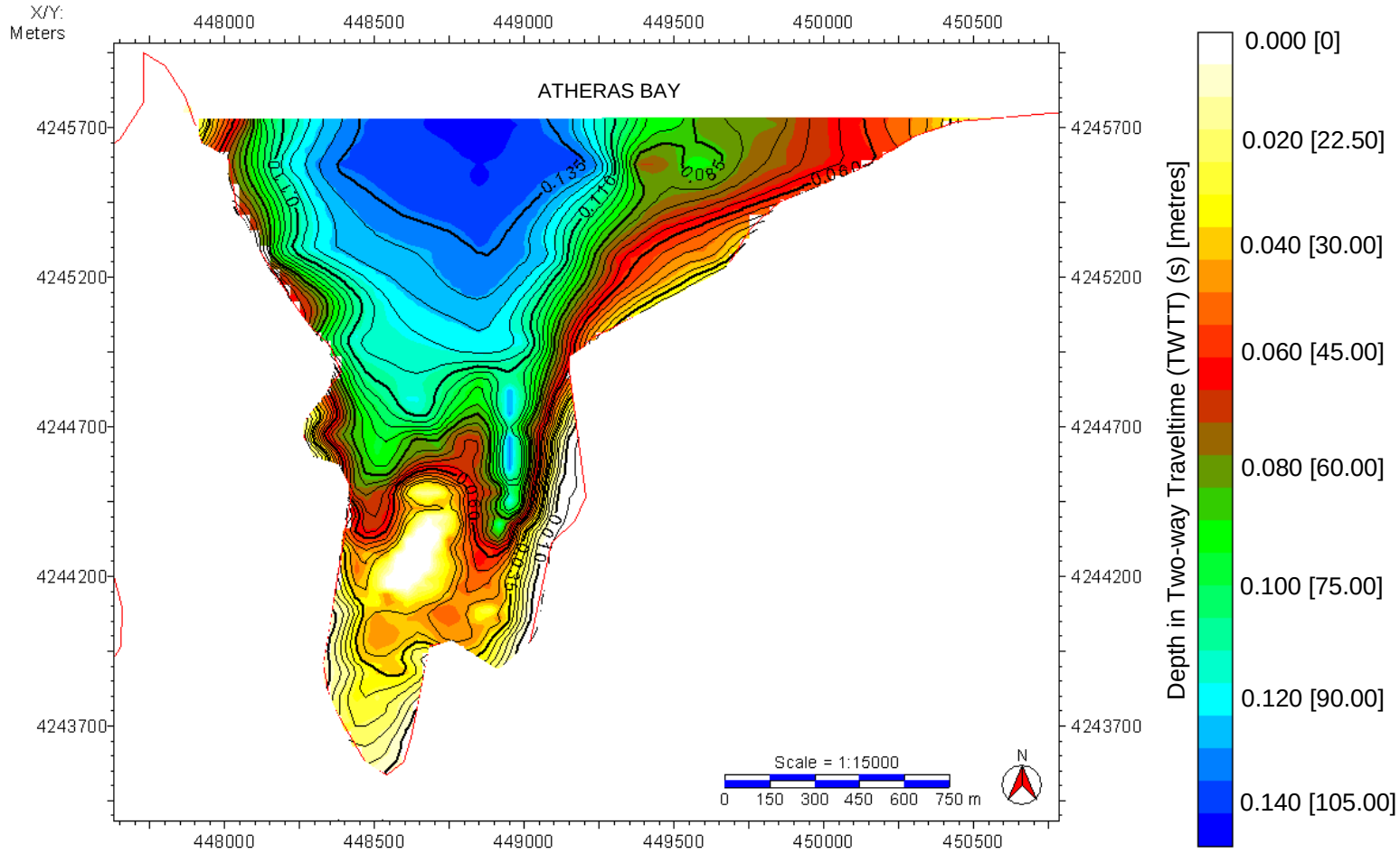

Figure 6.34 Two-way traveltime (TWTT) (in seconds) sea bed map for Atheras Bay showing the dramatic bathymetry. Rough depth conversion of this map was carried out (indicated in square brackets on the scale bar) using a P-wave velocity for sea water of 1500 m/s. The white elliptical area close to the shore equates to the location of the small island.

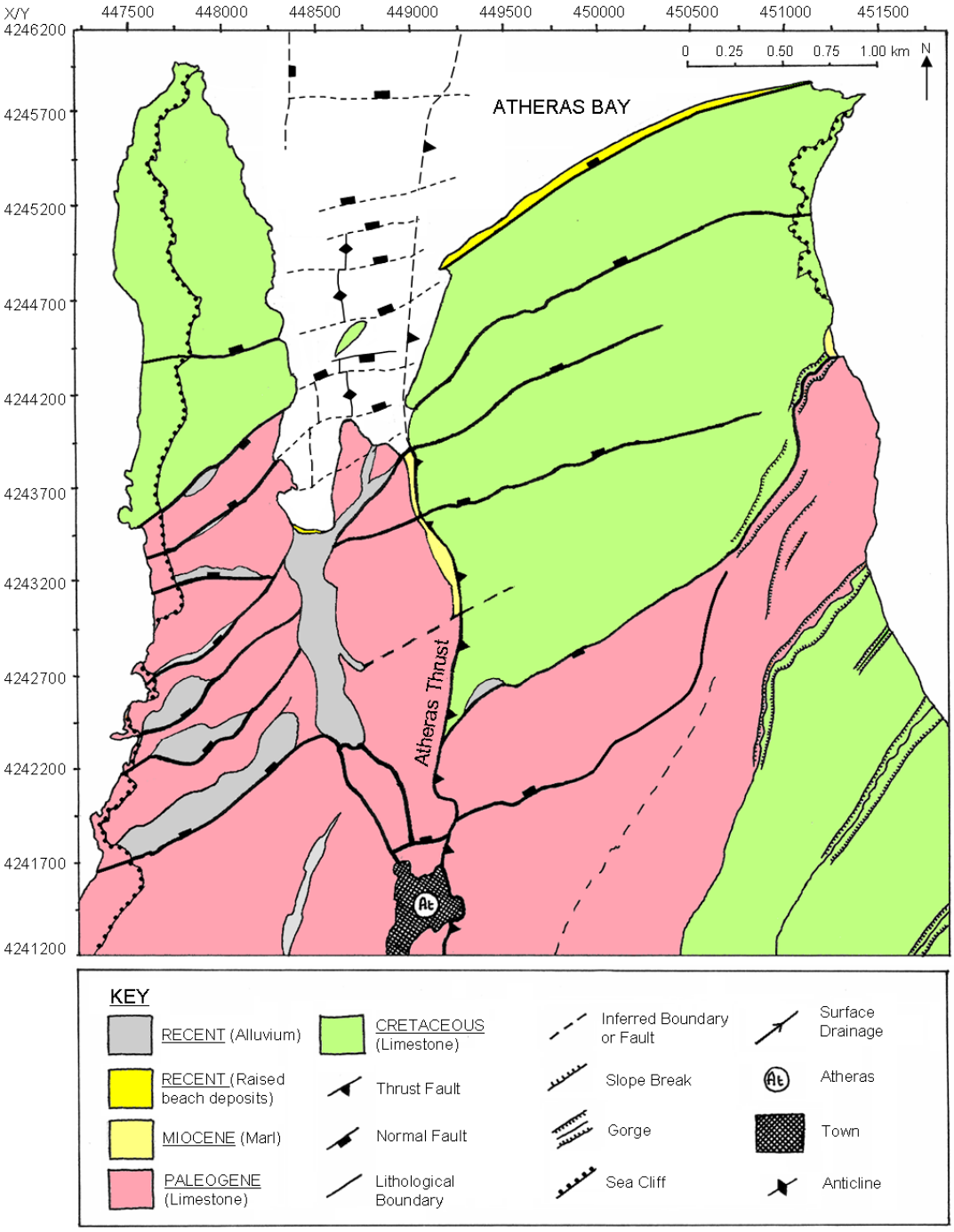

Figure 6.35 Geological sketch map from Chapter 1 (Figure 1.30) showing the deformation within Atheras Bay detected within the lower seismic megasequence tied with the onshore geology (based on map by British Petroleum Co. Ltd et al. (1985) and the Institute of Geological and Mineral Exploration (IGME), Figure 1.25).

6.5 Agia Kiriaki Bay (Volume D)

The sub-seabed configuration of Agia Kiriaki Bay was very similar to that of the Gulf of Argostoli. The seismic response could be divided into a stratified upper seismic megasequence consisting of thin dark reflectors and transparent layers which onlapped a prominent erosional surface (Figure 6.37 and Figure 6.38). As with Atheras Bay, the sparker survey was badly affected by interference most likely caused by a hard or very reflective substrate at the sea bed due to prevailing currents having winnowed and eroded its sediment cover.

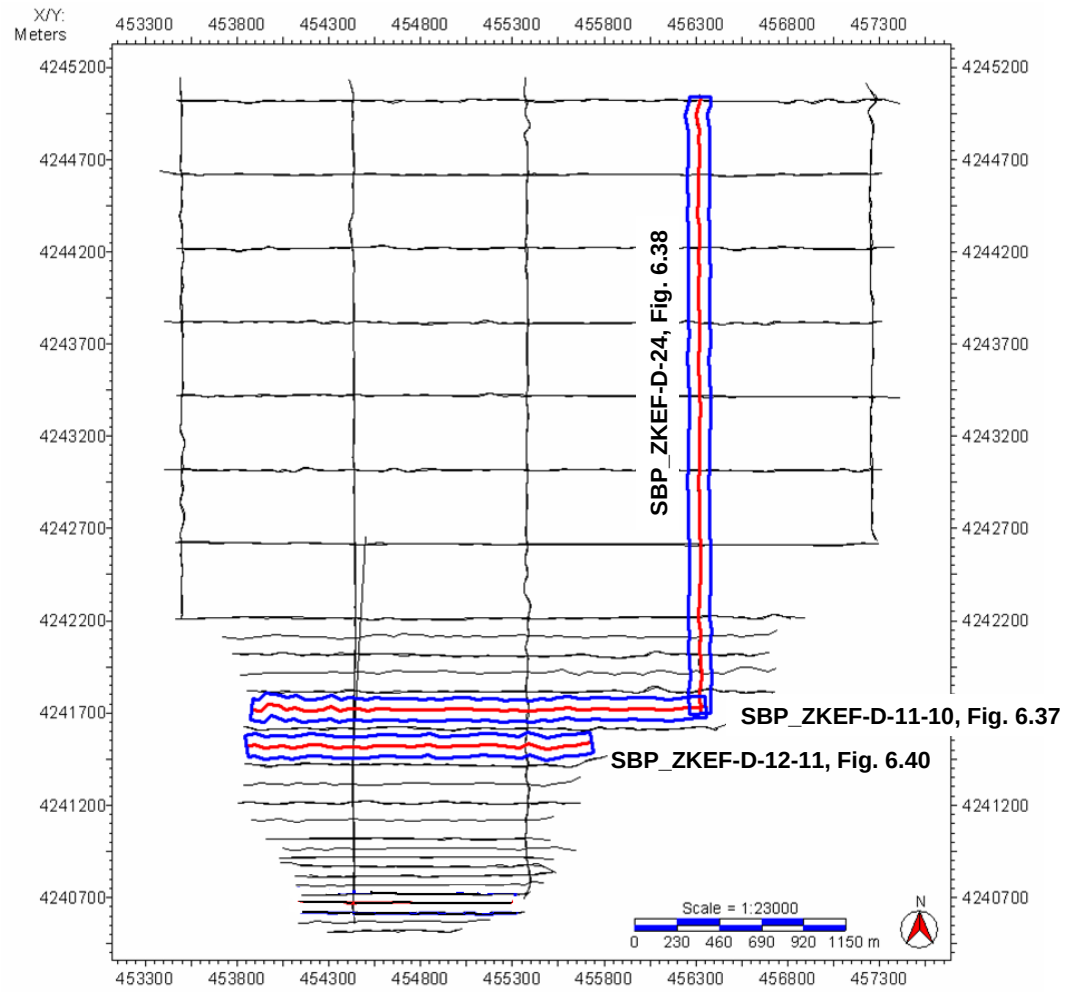

Figure 6.36 Kingdom base map showing the location of the Agia Kiriaki Bay shallow marine seismic reflection survey (Volume D), Western Kefalonia. The survey lines illustrated in the text are highlighted in blue and red. The proposed route of "Strabo's Channel" is indicated by a dashed black line. Due to rough resolution of the culture map, the coastline (in red) overlaps the survey lines in some places.

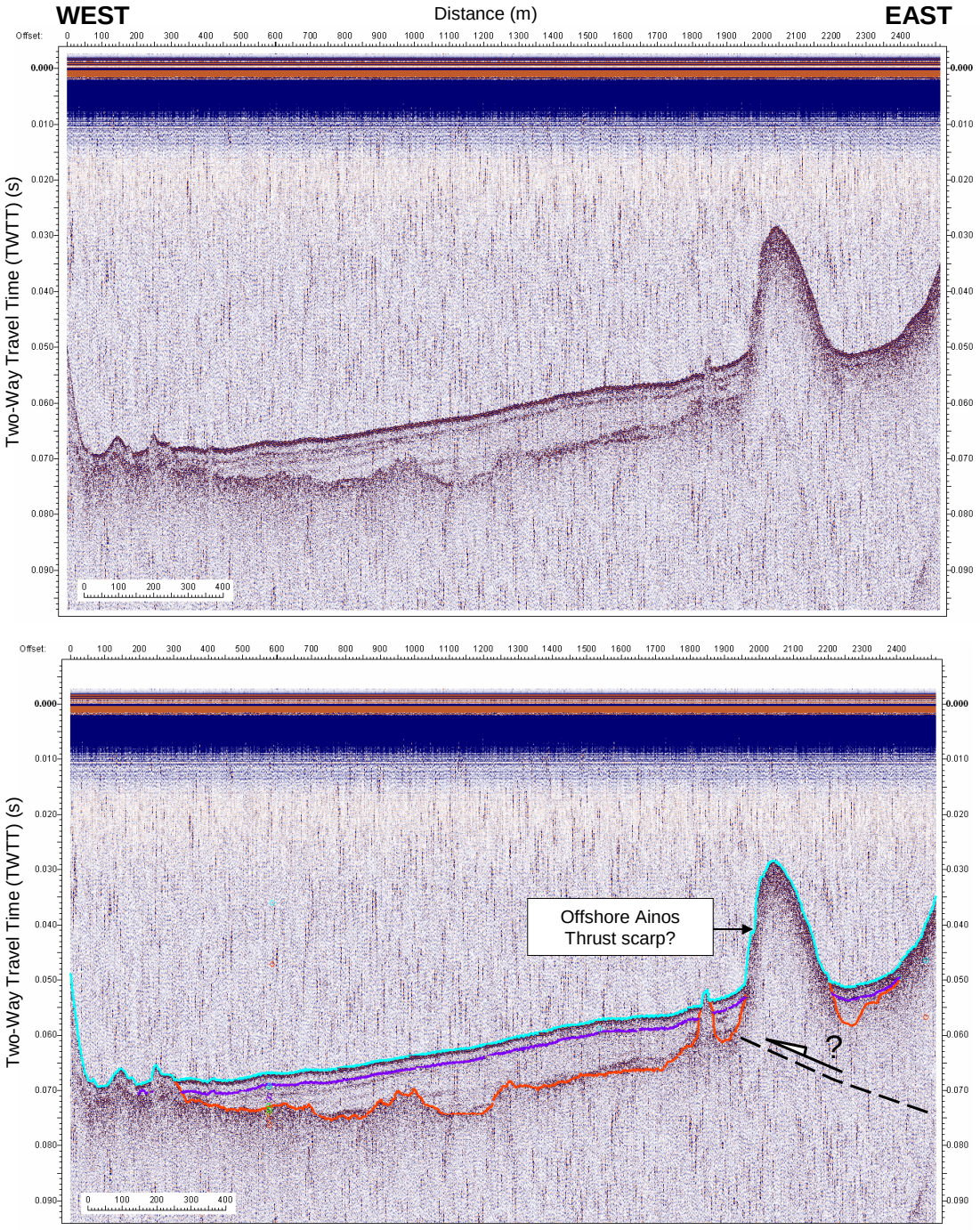

Figure 6.37 Typical E-W "dip" line (SBP_ZKEF-D-11-10) for Agia Kiriaki Bay. Pale blue = sea bed, purple = prominent postglacial unit reflector (Sed5?), red = erosional surface. A similar fault scarp to those observed in Gulf of Argostoli (Figure 6.18) and Atheras Bay (Figure 6.33) is indicated and may be associated with the offshore continuation of the Ainos Thrust. Location of this line is shown in Figure 6.36.

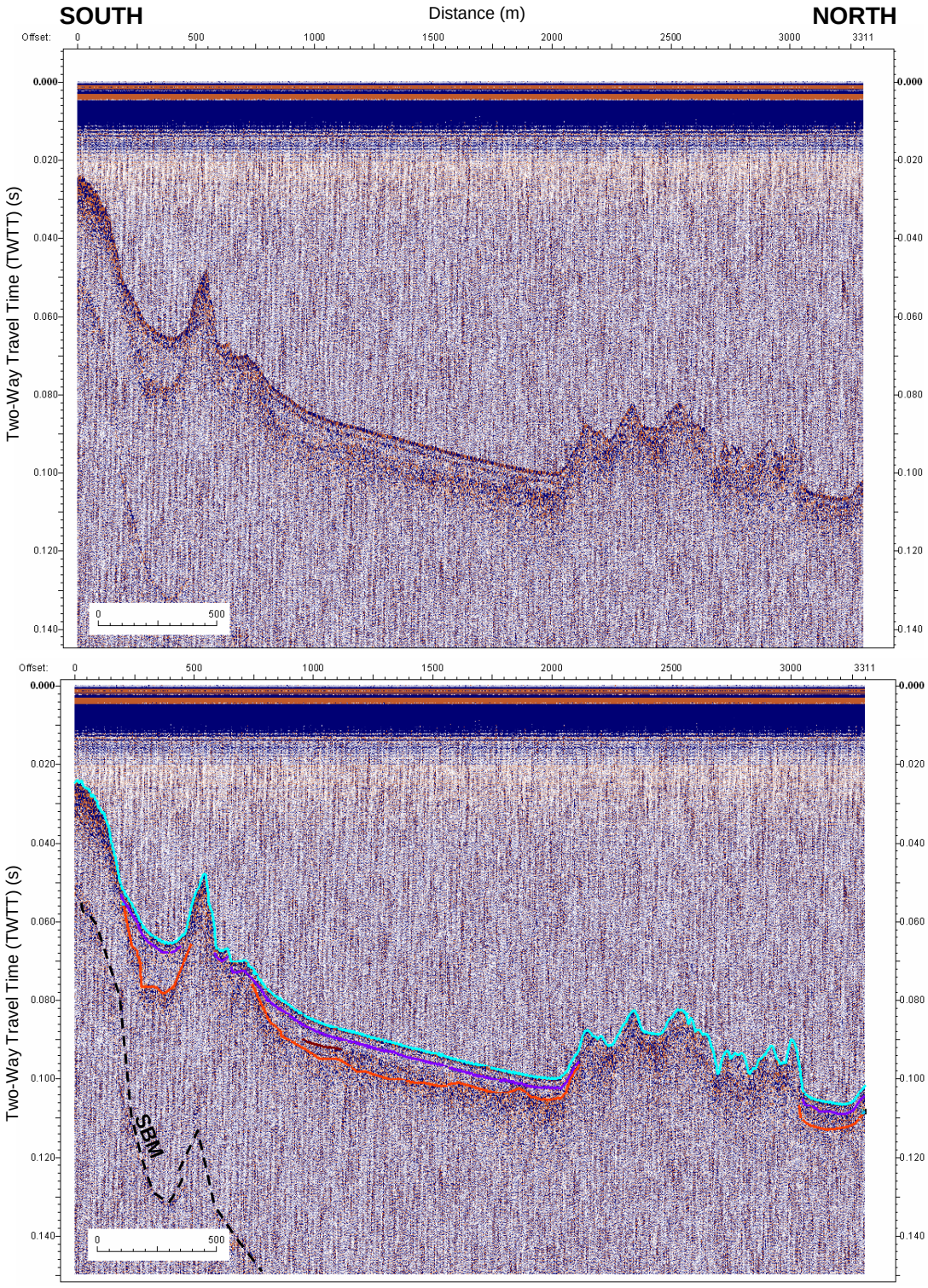

Figure 6.38 Typical N-S "strike" line (SBP_ZKEF-D-24) for Agia Kiriaki Bay. SBM = sea bed multiple. Other annotations as for Figure 6.37. Location of this line is shown in Figure 6.36.

Almost nothing of the structures within the lower seismic megasequence could be determined. The inner bay seismic lines were almost entirely obscured by strong

interference from repeating sea bed multiples. This reduction of quality meant that little structure other than the sea bed topography could be determined with reflections obscuring much of the detail below the erosional surface. However, because the upper seismic megasequence was thicker than in Atheras Bay, the sub-bottom profiling survey imaged this unit in better detail.

6.5.1 Sea Bed Morphology

The sea bed of Agia Kiriaki Bay had a smooth, shallow bathymetry contained to the west and east by steeply-dipping topography and broken by sharp hills and deepened towards the north-west (Figure 6.39). There was no evidence of a recent channel incised into the near-shore sea bed. In the inner bay, the sea bed was affected by a dramatic westerly-dipping slope (~15 m higher than the sea floor on the western side of the bay). The sea bed of the eastern side of the bay was defined by a sharp, westerly-dipping scarp (Figure 6.37) similar to those observed along the Argostoli Peninsula coast (Figure 6.18) and Atheras Bay (Figure 6.33). The sharpness of this ridge suggested differential erosion had occurred (the ridge lithology is harder than the surrounding sediment) or indicative of recent tectonic activity.

6.5.2 Upper Seismic Megasequence

This unit was much thinner than the equivalent deposits in the Gulf of Argostoli (up to a maximum of 8.25 m) and was discontinuous, occurring in isolated lens within hollows formed by the topography of the erosional surface which offered some shelter from strong offshore currents in this more open, exposed bay. Unlike in the Gulf of Argostoli and Atheras Bay, in the inner bay the reflectors of the upper seismic megasequence were not sub-horizontal but tilted westwards at the same steep angle as the sea bed suggesting they had been disturbed after deposition (Figure 6.40).

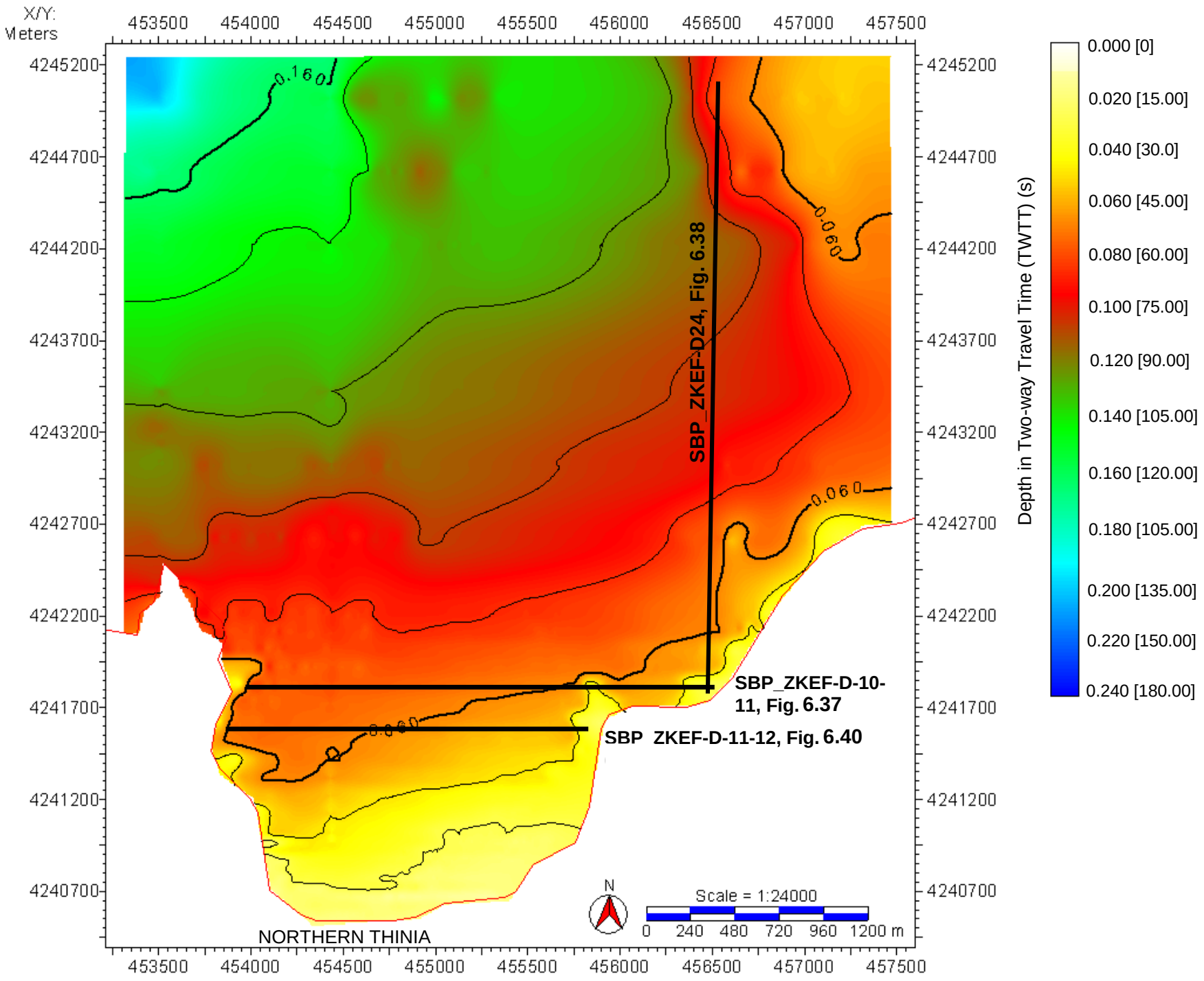

Figure 6.39 Two-way traveltime (TWTT) (in seconds) sea bed map for Agia Kiriaki Bay showing the smooth sea floor bathymetry. Rough depth conversion of this map was carried out (indicated in square brackets on the scale bar) using a P-wave velocity for sea water of 1500 m/s. The locations of line SBP-ZKEF-D-11-12 (Figure 6.40) and SBP-ZKEF-D-10-11 (Figure 6.37) are indicated by black lines. There is no evidence of a channel ("Strabo's Channel") incised into the sea bed, emanating from Northern Thinia.

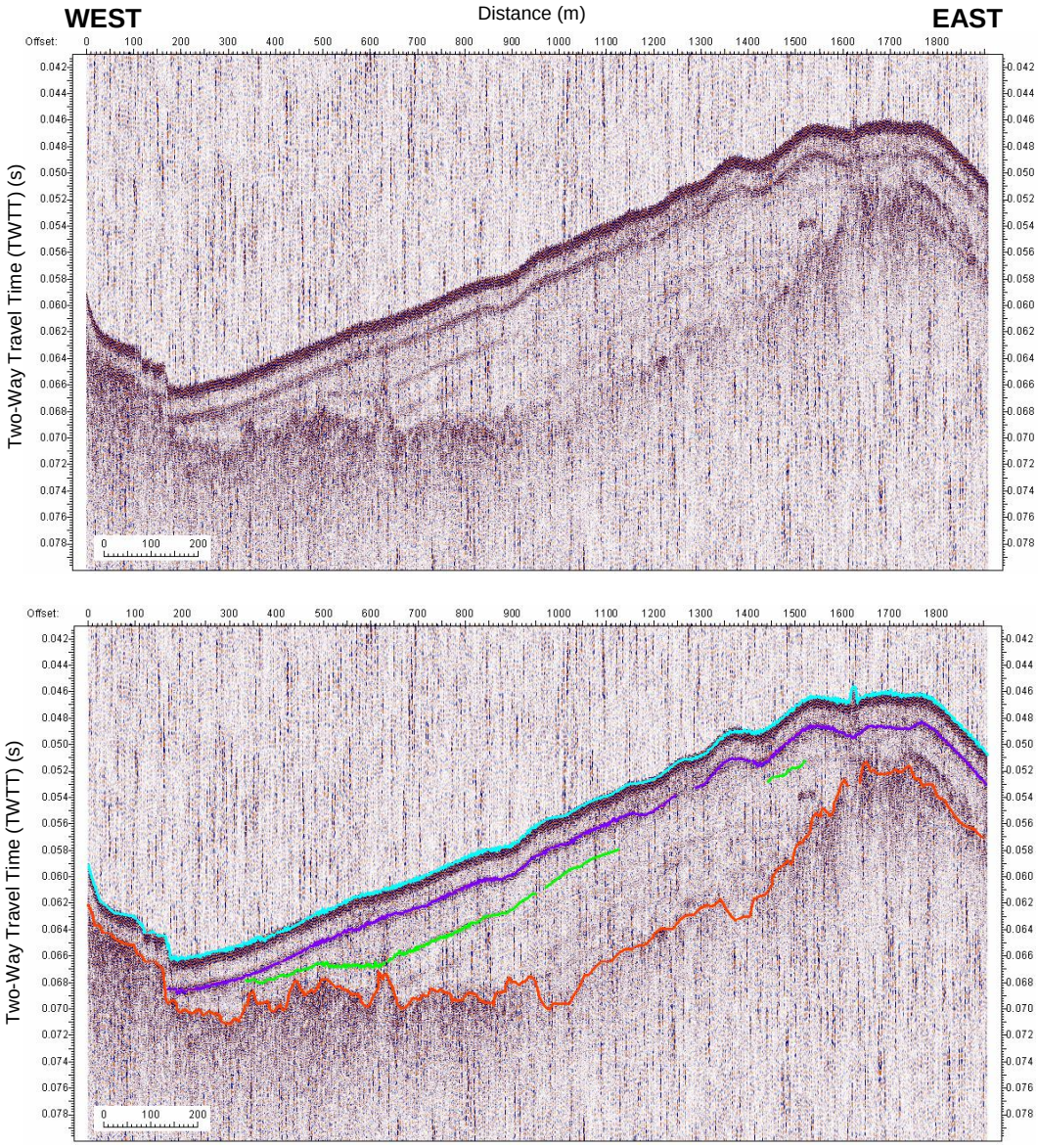

Figure 6.40 Seismic line SBP_ZKEF-D-12-11 showing tilted sea bed in inner Agia Kiriaki Bay**.** Green = strong upper seismic megasequence reflector (Sed13?). Other annotations as for Figure 6.37. Location of this line is shown in Figure 6.36.

The isochron constructed for this unit showed that the thickest deposits of this unit occurred nearest to the shore where the sediments had been given some degree of protection by the headlands of the bay (Figure 6.41). Elsewhere it was pinched out to less than a metre. This thicker deposit of upper sediment correlated to the accumulation of magnetic material imaged by the airborne survey (Section 4.2.1, Figure 4.1) suggesting much of this material was terrigenous (magnetic *terra rossa*) in source, transported by the northern valley drainage system. Further out into the

bay the pattern of sediment accumulation resembled a meandering drainage system however it wasn't as thick (~10 m maximum) as the deposits in the Gulf of Argostoli.

6.5.3 Buried (Quaternary-Holocene) Erosional Surface

The erosional surface map for Agia Kiriaki Bay (Figure 6.42) did not contain a deeply-incised drainage system like the one observed in the Gulf of Argostoli. The map produced is very similar to the sea bed map suggesting the dendric pattern created by the upper seismic megasequence isochron was did not represent a meandering drainage channel but was created by sediment drift shaped by marine currents.

6.5.4 Lower seismic megasequence

Figure 6.43 presents the interpretation of faulted features at the erosional surface. The ridge running along the eastern side of the inner bay in Figure 6.37 was interpreted as the offshore continuation of the Ainos Thrust. Due to the poor quality near-shore seismic, there was no sign of the offshore continuation of the possible subsidiary thrust observed within the Agia Kiriaki Bay sea cliff (Section 3.2.1., A, Figure 3.7). Additionally, possible offshore continuation of the Kalon Thrust to the northeast of Thinia valley can be seen to the northeast of Agia Kiriaki Bay as a zone of raised bathymetry. Despite entering the Gulf of Mirtos close together, it appeared that these two thrusts did not join together once offshore.

The progression of the easterly-dipping normal fault bounding the western side of northern Thinia can be seen as a very steep easterly-dipping scarp on the far west of the seismic profiles. The sea bed at the base of the scarp had a raised, uneven surface suggesting it represented an accumulation of clastic debris derived from this scarp in a similar fashion to the Zola talus.

.

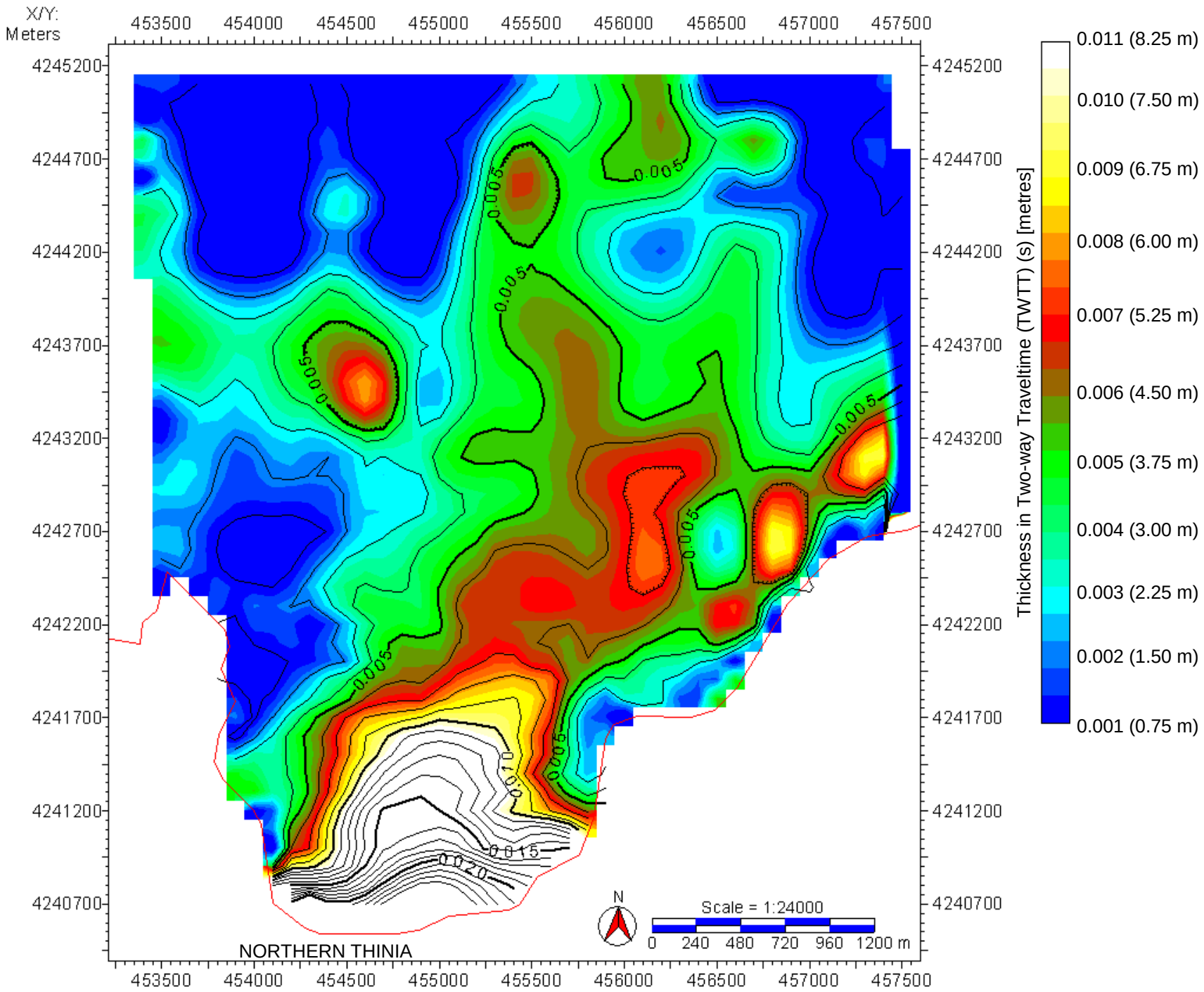

Figure 6.41 Isochron (thickness in two-way traveltime in seconds) for the upper seismic megasequence for Agia Kiriaki Bay. The isochron revealed a dendric pattern of sediment which may represent a drainage system similar to that in the Gulf of Argostoli emanating from the shoreline and carrying sediment out to sea. Rough depth conversion of this map was carried out (indicated in square brackets on the scale bar) using a P-wave velocity for sea water of 1500 m/s.

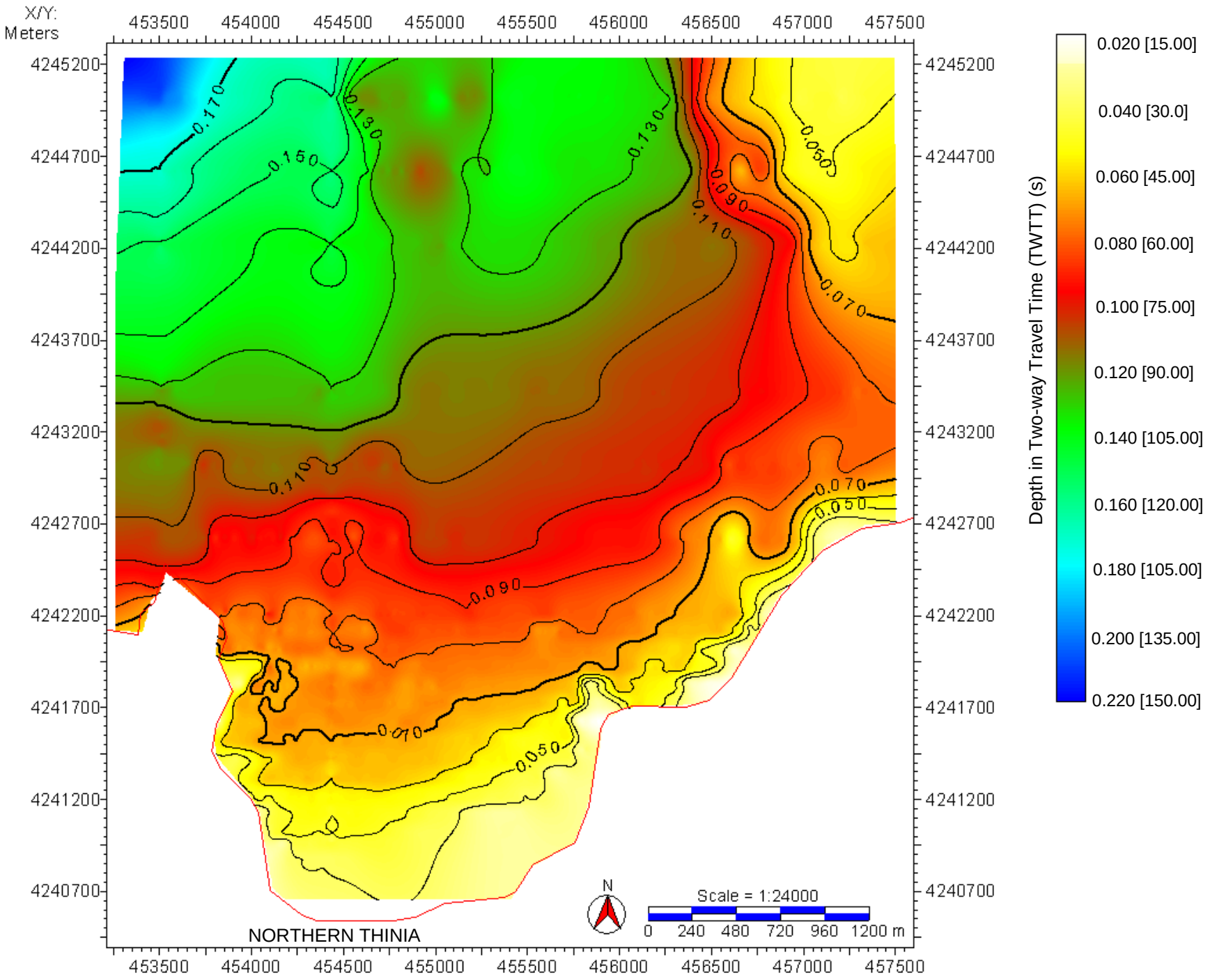

Figure 6.42 Two-way traveltime (TWTT) (in seconds) erosional surface map for Agia Kiriaki Bay. Rough depth conversion of this map was carried out (indicated in square brackets on the scale bar) using a P-wave velocity for sea water of 1500 m/s. There is no sign of a similar deeply-incised drainage system to that mapped in the Gulf of Argostoli to the south of Thinia.

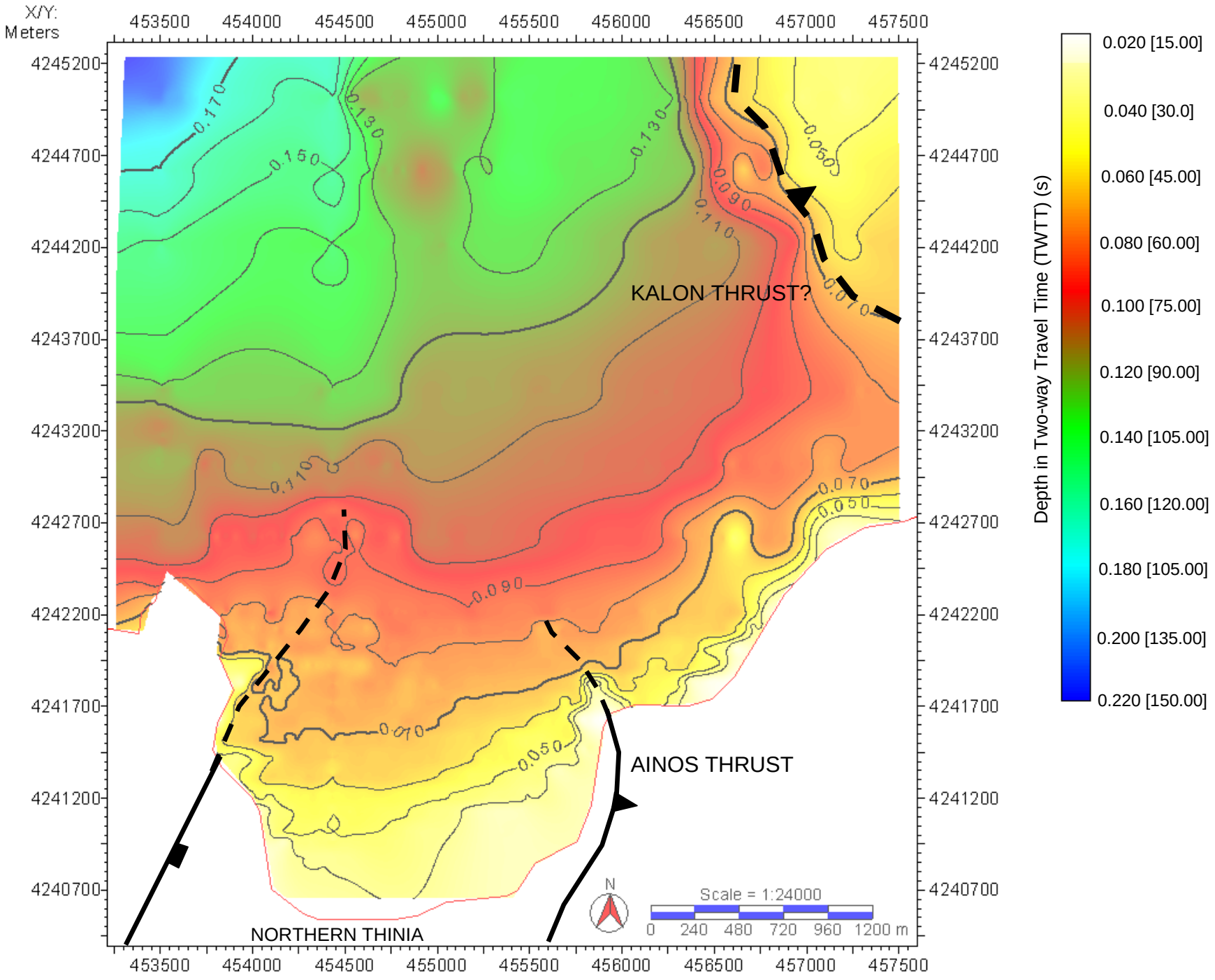

Figure 6.43 Two-way traveltime (TWTT) (in seconds) erosional surface map for Agia Kiriaki Bay showing possible offshore continuation of major faults (black dashed lines) observed onshore based on the seismic interpretation. The three key faults visible offshore are the Ainos Thrust, the dramatic NE-SW striking easterly-dipping normal fault defining the western side of Northern Thinia and possible evidence of the Kalon Thrust to the northeast of the survey.

6.6 Discussion

In the absence of direct sampling, the following interpretations are tentative and based purely on likelihood using the eustatic sea level curves (Fairbanks, 1989; Mix et al., 2001; Lambeck et al., 2003; Lambeck and Chappell, 2001) (Figure 1.40) and work by Perissoratis and Conispoliatis (2003) ignoring local tectonic affects. These assumptions should only be taken as preliminary until the marine seismic can be properly "ground-truthed" by intrusive sampling of the sub-seabed, a test which will post-date this thesis. Such future calibration of the marine seismic may revise this interpretation.

6.6.1 Age of the Seismic Megasequences

The results of the shallow marine seismic reflection survey showed that the subsurface of all three coastal locations could be resolved into one or both of two key sedimentary units: a stratified horizontal upper seismic megasequence overlying a strongly-deformed lower megasequence separated by a topographically dramatic widespread erosional surface. This configuration was best preserved in the Gulf of Argostoli which had the thickest upper seismic megasequence of all three areas believed to be a reflection of the low mechanical disturbance (wave-action, transportation) of sediment within the Gulf. The low energy environment of the Gulf comes about from its narrow, land-enclosed shape which has sheltered its softer sediments from the strong offshore currents which have winnowed away much of the same sediments of Atheras and Agia Kiriaki Bay.

Immediately clear was the lack evidence of a channel incised into the sea bed near the proposed exits of "Strabo's Channel" in the northern Gulf of Argostoli or Agia Kiriaki Bay. In this case of Agia Kiriaki Bay, the channel remains may have been winnowed away by marine currents however, this is unlikely to have happened in the Gulf suggesting no major outwash feature had emptied from Thinia in the recent past (last few thousand years).

However, the striking topography of the erosional surface marking the boundary between the upper and lower seismic megasequences indicated strongly erosive processes had occurred before deposition of the upper seismic megasequence. The presence of this erosional surface in all three areas demonstrated that a major subaerial exposure event had affected the shallow coastal shelves of Northern Paliki and the dating of this surface was key in understanding the flooding history of the area.

Mapping of the erosional surface in the Gulf of Argostoli produced dramatic evidence of a deeply-incised channel apparently emanating from southern Thinia and extended throughout the entire Gulf, thus providing clear evidence that a major fluvial system had drained from southern Thinia in the deeper geological record (millions of years). A similar deeply-incised set of channels occurred in inner Atheras Bay (Figure 6.31) and a more subtle drainage system occurred in Agia Kiriaki Bay.

Subaerial exposure of these shallow coastal areas would have last occurred during the sea level lowstand of the Last Glacial Maximum (LGM) (~21 500 BP) where sea levels dropped to around 120 m below present day levels, well below the level of the shallower (<75 m depth) coastal shelves. This would mean that the strongly deformed sediments truncated by the erosional surface were the original "pre-Holocene" sediments which composed the coastal shelves prior to the LGM lowstand. The upper seismic megasequence therefore represents the transgressional "Holocene" sediments which were deposited over these eroded shelf sediments during the postglacial sea level rise of ~120 m which followed the glacial lowstand.

This seismic sequence configuration resulting from the LGM lowstand and following postglacial sea level rise is recognisable in the coastal shelves of the Ionian Sea (Perissoratis and Conispoliatis, 2003) as well as across the globe. Typically the outer shelf zone is characterised by having a relatively thin veneer of recent Holocene sediment (less than a few metres in thickness) deposited over the harder bedrock, thickening where old river channels occur and pinching off towards the shelf break

(Perissoratis and Conispoliatis, 2003). Erosion of the shelf occurred as rivers draining off the land incised deeply into the shelf sediments towards the sea. Further erosion was caused by the formation of lakes within the inner coastal shelves (Perissoratis and Mitropoulos, 1989; Perissoratis et al., 2001; Perissoratis and Van Andel, 1991; Lykousis and Anagnostou, 1992) which certainly appeared to be the case in the Gulf of Argostoli (Figure 6.28 and 6.29). The ridges of pre-Holocene which break through the postglacial unit would have formed islands or coastal extensions during initial sea level rise. As postglacial sea level drew close to present day levels, small rivers draining off steep, near-shore Neogene-Quaternary hills rapidly deposited large mid-Holocene alluvial sedimentary prisms within the eroded channels of the inner coastal shelf which dramatically altered the coastal configuration (Angelopoulos et al., 1991). This accumulating of sediment was clearly observed in the upper seismic megasequence isochron for the Gulf of Argostoli (Figure 6.11).

While the presence of shallow gas in the northern part of the Gulf of Argostoli obscured reflector detail within the seismic, its high concentration within the thickest fan of postglacial (Figure 6.14) which emanated from the south of Thinia suggested a change of sediment quality in these areas. This may suggest a very recent (within the last few 1000 years) influx of material from southern Thinia into the Gulf and raises questions as to whether this could be through normal erosion of the saddle region or an increase of outwash due to a change in climate. This prioritises future age-dating of the postglacial to determine the most recent deposition into this fan.

The strength of some of the reflectors within the postglacial unit (Sed5, Section 6.3.2) suggested they were formed from particularly reflective particles. The pattern of alternative transparent and dark layering seen in the postglacial unit resembled those imaged in the high resolution seismic survey taken by Sacchi et al. (2009) off the Amalfi coast in the eastern Tyrrhenian Sea. In the Tyrrhenian Sea case, the layering was caused by deposition of loose volcaniclastics, such as ash or tephra derived from eruptions of Vesuvius, washed into the delta during climatic oscillations.

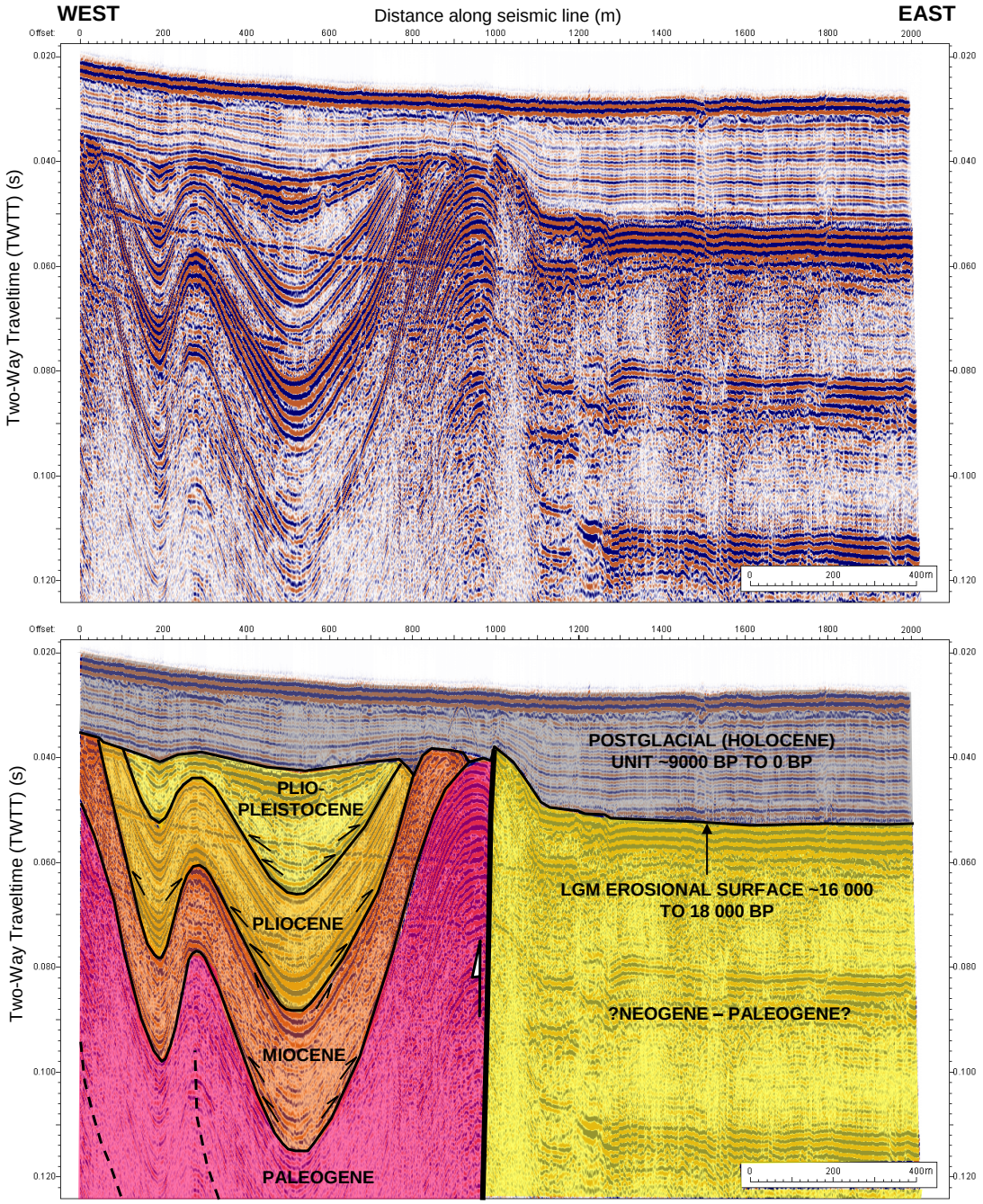

Figure 6.44 KEF-B-19 with possible stratigraphic ages assigned based on extrapolation of Livadi Marsh boreholes and onshore stratigraphic columns constructed for the borehole data and the Fairbanks eustatic sea level curve. Line located on Figure 6.3.

The detection of volcaniclastics within the Thinia boreholes, particularly C2006, C7a and C6b (Section 5.4.1) and the documented presence of ash deposits across Kefalonia (Kelepertsis et al., 2002) suggests the particular dark postglacial reflections, such as Sed5, were also derived from tephra. The presence of tephra would potentially create clear date markers within the unit.

Extrapolating the results of the Livadi Marsh core-tie B-B' (Figure 5.9 and 5.10), and corresponding stratigraphic column derived in Section 5.4.2 (Figure 5.30), stratigraphic ages were tentatively assigned to the sedimentary units within the pre-Holocene based on the positions of unconformities. This assignment is presented for dip line KEF-B-21 in the Gulf of Argostoli which showed the pre-Holocene strata most clearly (Figure 6.44). The key erosional surfaces (labelled using the convention listed in Figure 6.5) were dated as follows: PreHol3 (orange) = Plio-Pleistocene – Pliocene, PreHol5 (blue) = Messinian Unconformity and PreHol6 (yellow) = Oligocene Unconformity.

6.6.2 Evidence for (and against) Neotectonic (co-seismic) activity on offshore "Alpine" (Hellenide) structures

A. Gulf of Argostoli

The pre-Holocene of the Gulf of Argostoli showed a very complicated faulting history. The sediments clearly showed deformation relating to the Hellenide fold-and-thrust system with easterly-dipping thrust-faulting and westerly-dipping backthrusts, the continuation of features mapped onshore. Mapping these structures (Figure 6.27) showed that they formed a NNE-SSW striking band of deformation rather than a single thrust fault. This will have caused the seismic discontinuity mapped by Stiros et al. (1994) in Figure 1.48 affecting which parts of the island experience coseismic movement relative to others.

There was evidence of extensional features in the form of westwards-thickening (syn-sedimentary) pre-Holocene sediments (Figure 6.26). These sediments appeared to be overprinted by the easterly-dipping thrusts mapped in Figure 6.27 indicating the extension which caused this thickening features pre-dated the arrival of the Hellenide fold-and-thrust system. The westwards-thickening pre-Holocene sediments in Figure 6.26 may have been related to the N-S striking, easterly-dipping extensional fault (Figure 6.24 and 6.25) which defined the western side of the Gulf. Both these sets of deformation appeared to be offset in turn by three NE-SW trending offsets

interpreted in Figure 6.29, which showed a similar strike to the normal faulting observed around Atheras Bay (Figure 1.30). These offsets were the youngest features overprinting the extensional-compressional regime.

Despite the strong deformation within the pre-Holocene there was no indication of recent breakage of the postglacial unit other than slight deformation due to compaction of the postglacial sediments over sharp topography in the erosional surface. This indicates activity on these faults pre-dates deposition of the postglacial i.e. there has been no coseismic activity since ~16 000 to 18 000 BP.

B. Atheras Bay

The NE-SW striking faults which cross-cut Atheras Bay onshore were clearly apparent (Figure 6.32). However, the wide-spacing of the survey lines particularly towards the outer bay made it impossible to tell if these NE-SW faults offset the underlying compressional features. The lack of erosion on the N-S striking fault (e.g. KEF-C-01, Figure 6.33) suggested recent activity however, the paucity of the postglacial in this bay made it impossible to tell whether this unit had been affected by this activity. A further, more thorough seismic investigation would be required to fully investigate these structures and any offset.

C. Agia Kiriaki Bay

There could be several reasons for the tilting of the sea bed and upper seismic megasequence as shown in Figure 6.40. This sequence may represent a westwards prograding alluvial fan emanating from the eastern shore of the inner bay, like the prograding clinoforms imaged to the west of the Argostoli Peninsula (Figure 6.20).

Another possibility is that the sea bed on the eastern side of the bay has been uplifted since deposition of the most recent sediment. If so, this uplift would be around 15 m and very young (tens to hundreds of years) and may tie into the 6 m high raised

beach platform observed by Underhill (2009) (Section 1.3.2., Figure 1.50, B). The freshness of the scarp imaged in Figure 6.37 suggested very recent activity along the Ainos Thrust, possibly due to the 1953 Great Ionian Earthquake, the last major earthquake to affect this area which was known to cause coseismic movement on many parts of Kefalonia's coastline (Section 1.3.2, Figure 1.47).

However, such a large amount of recent (tens to thousands of years) coseismic uplift is unlikely given that no more than 2.1 m of historic uplift has been observed around Kefalonia (Papazachos and Papazachou, 1989; Pirazzoli et al., 1994). It is more likely that the cause of the tilted sediments is sediment drift which occurs when strong marine currents enter and circulate around an open bay causing the reworking and building-up of sediments up against existing bedrock. The open nature of Agia Kiriaki Bay makes this a strong possibility.

6.6.3 The postglacial flooding history of the coastal areas of Thinia and Northern Paliki

Postglacial flooding maps for the Gulf of Argostoli (Figure 6.45), Atheras Bay (Figure 6.46) and Agia Kiriaki Bay (Figure 6.47) were constructed to understand how these coastal areas evolved in the Holocene. These were constructed assigning ages in terms of BP (years before present) to the depth contours of the erosional surface maps (sea bed in the case of Atheras Bay) – Gulf of Argostoli (Figure 6.28), Atheras Bay (Figure 6.34) and Agia Kiriaki Bay (Figure 6.42) – using sea level curves in Figure 1.40. These maps should be considered tentative as they assumed negligible coseismic uplift and only accounted for sea level change below present day sea levels (0 m).

A. Gulf of Argostoli

Sea level reached the raised bathymetric ridge defining the edge of the Gulf of Argostoli coastal shelf around 9220 BP (Figure 6.45). Initial flooding of the river

valley corresponds with the 33.75 m depth contour. This contour was the first to breach both the lower basin and northern basin. The contour immediately preceding the breach of the first basin was assigned an age of 8958 BP suggesting the flooding event occurred very rapidly (tens to hundreds of years) infiltrating both depocentres in quick succession. The steep-sided nature of the valley meant that while postglacial sea level continued to rise, the coastal position, particularly in the inner Gulf, stayed at a similar position. This agrees with the study by Braune (1973) who detected a significant drowned coastal terrace about -24 to -28 m depth in the Gulf of Argostoli indicating a relatively constant sea level corresponding to around 8200 BP.

Given the narrow morphology of the river valley mapped in Figure 6.28, it is likely that the Gulf forms a "ria" created as rising sea levels flooded the valley. A ria is a coastal inlet formed through the partial or complete submergence of a river valley. The shape of a ria is typically dendritic, reflecting the branching tributaries of the original river valley. A coastline containing numerous "drowned" river valleys appears extremely irregular and indented. Langston and Portsmouth Harbours are good present examples of drowned valleys which formed when postglacial sea level flooded the tributaries of the Solent River (where the Solent which separating the mainland from the Isle of Wight now exists) flowing down from Portsdown Hill (Tweed, 2000). The possible lakes interpreted in Figure 6.29, would have quickly overflowed into one another with the marine influx.

While the postglacial maps in this section only account for sea level below zero, the radiocarbon dating of core samples in the Livadi Marsh borehole C6c (Section 5.3.2) showed that the marsh was flooded during the Bronze Age. At 5206 ± 67 calBP, the marsh stood at sea level (around 7.5 m below present day levels). Between 4471 ± 31 calBP and 3362 ± 34 calBP it was flooded to a maximum depth of around 1.2 m while sea levels were still below zero.

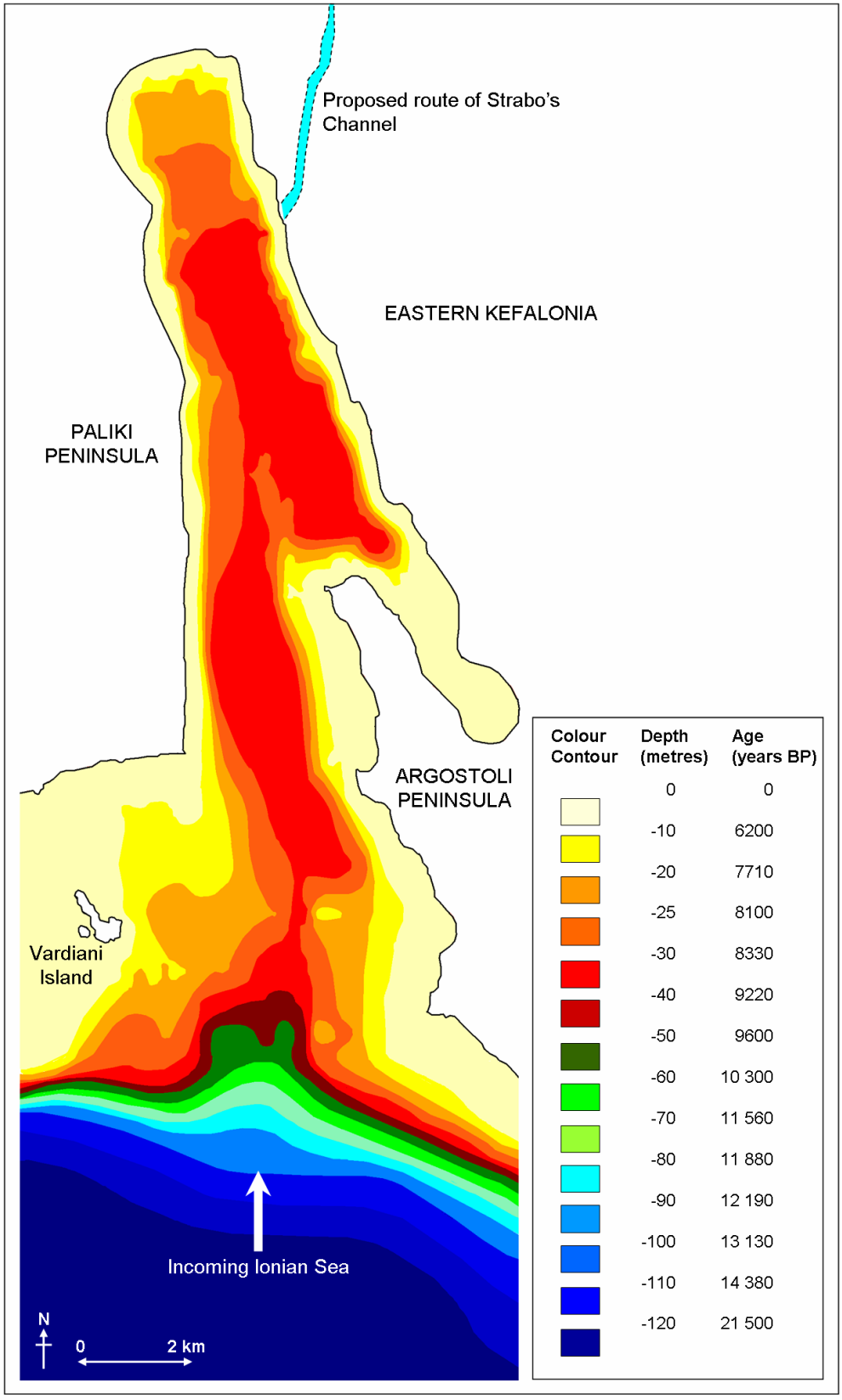

Figure 6.45 Postglacial flooding history map for Gulf of Argostoli constructed by equating the depth contours of the Last Glacial Maximum (LGM) erosional surface with the Fairbanks (1989) global sea level curve. Ignores the effects of tectonic uplift.

B. Atheras Bay

The postglacial flooding map for Atheras Bay (Figure 6.46) showed that flooding occurred in a series of steps as rising sea levels breached the various ~E-W trending fault scarps visible as tightening of contours, particularly north of the small island (between 11 560 and 9220 BP). The V-shaped incised channels within the sea bed (Figure 6.31) were possibly caused through drainage of the bay as sea levels dropped during the Last Glacial Maximum (LGM) lowstand. Isolated closed contours occurred near the shore and might have represented small lakes which accumulated within hollows in the near-shore topography and were subsequently flooded by marine waters during sea level rise. Sea level infiltrated the inner bay from the eastern side of the small island initially (~8330 BP). At this time the small island was linked to the shore. Between 8330 and 6200 BP the sea infiltrated from the western side and met marine waters flooding from the east ascribing a pincer-movement.

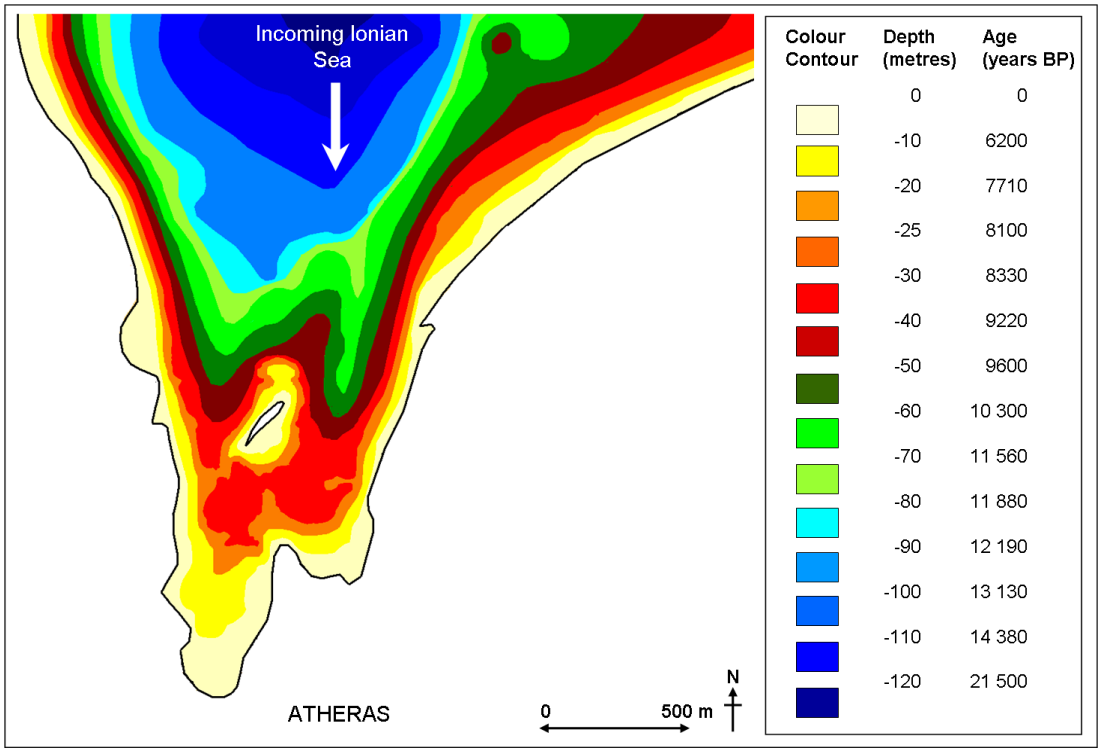

Figure 6.46 Postglacial flooding history map for Atheras Bay constructed by equating the depth contours of the Last Glacial Maximum (LGM) erosional surface with the Fairbanks (1989) global sea level curve. Ignores the effects of tectonic uplift.

C. Agia Kiriaki Bay

The postglacial flooding map for Agia Kiriaki Bay showed that sea level encroached into Agia Kiriaki Bay from the north-west (Figure 6.47). Around 11 880 BP the Bay formed a crescent-shaped inlet with the offshore raised ridge associated with the Ainos Thrust which formed the eastern side of the bay.

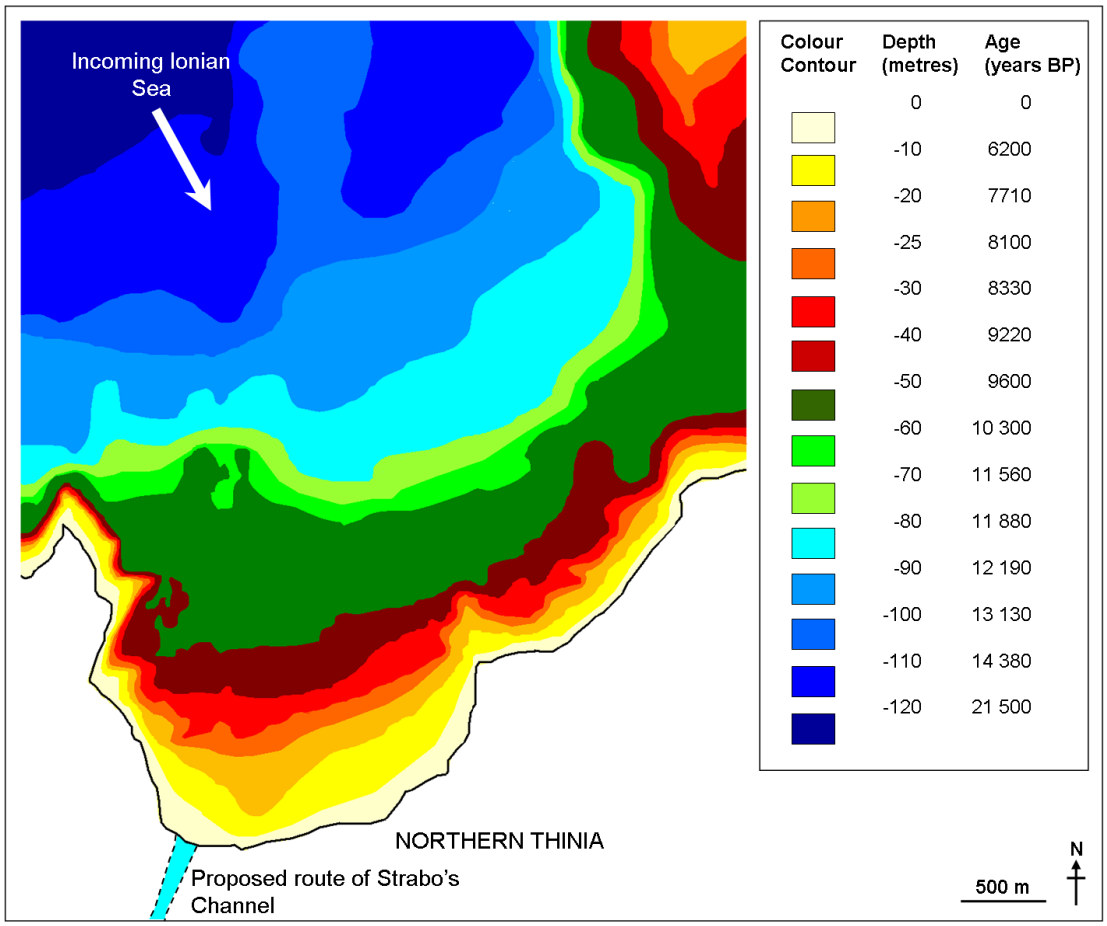

Figure 6.47 Postglacial flooding history map for Agia Kiriaki Bay constructed by equating the depth contours of the Last Glacial Maximum (LGM) erosional surface with the Fairbanks (1989) global sea level curve. Ignores the effects of tectonic uplift.

6.7 Summary

The shallow marine seismic reflection surveys taken across the Gulf of Argostoli, Atheras Bay and Agia Kiriaki Bay resolved the sub-seabed of these coastal areas into two main sedimentary units separated by a prominent erosional surface. The erosional surface was believed to be associated with the subaerial exposure of the shallow coastal areas during the Last Glacial Maximum (around 21 500 BP) when sea levels were low enough (-120 m) to drop below the edge of the shallow coastal shelf surrounding Paliki. The tectonically-disturbed sediments below this surface represent the pre-existing "pre-Holocene" shelf sediments while the upper seismic megasequence represented the postglacial sediments deposited as sea level rose present day levels.

While no evidence of a recent "Strabo's Channel" could be found in incised into the sea beds of the Gulf of Argostoli or Agia Kiriaki Bay (although the acoustic interference caused by gas in northern Gulf of Argostoli and winnowing of the postglacial sediments in Agia Kiriaki Bay made interpreting the most coastal seismic lines difficult) evidence of a channel-like structure in the deep geological record of the Gulf. Mapping the erosional surface revealed the presence of a significant drainage system caused where a glacial river had eroded into the pre-Holocene during the sea level lowstand. When postglacial sea level rise occurred, this valley flooded to form a ria.

The seismic survey revealed the pre-Holocene shelf sediments had a complicated deformation history. This was most clearly revealed in the Gulf of Argostoli which showed an existing easterly-dipping extensional system which had been overthrust by Hellenide fold-and-thrust deformation. This extensional-compression regime was overprinted by NE-SW striking offsets. In Atheras Bay, this was overprinted by the same NE-SW striking normal faults observed onshore.

CHAPTER 7: Discussion and Conclusions

7.1 Introduction

The "Strabo's Channel" hypothesis offered a feasible solution to how the Paliki peninsula could have been an island during the time of Odysseus in the Late Bronze Age thus providing a viable solution for the relocation of Homer's Ancient Ithaca. However, from the onset of the investigation, it became clear that the outcome to this study would be far more complicated than a simple "yes or no" test due to the complicated geology and tectonic setting of the area.

The investigation of "Strabo's Channel" inevitably draws on parallels with the investigation of Xerxe's Canal by Jones et al. (2000), described in Section 1.1.2, which used a similar series of complementary non-invasive geophysical and coring techniques. This provides plausibility to theory being tested given the similarity in age and time period. Like in Thinia, the Canal was situated on an isthmus (around 2 km in length), the proposed route was very narrow (25 to 35 m) and little surface expression of the Canal still remains. The life of the Canal was short. The lack of marine organisms within the central sector of the isthmus suggested that once maintenance of the navigable seaway ceased, the vertiginous sides soon began to collapse. However, a note of caution should be voiced since this Canal was far less deep (14 to 15 m below the surface) than the proposed gorge of "Strabo's Channel" (over 200 m). It was even possible, given the lack of definition at the southern end, that Xerxe's Canal was not continuous across the entire isthmus but may only have been connected with the sea at one end with the other acting as a short slipway.

While the surface geological and geomorphological mapping of Thinia, presented in Chapter 3, helped to constrain the extent of recent colluvial (landslide) deposition, the most likely mechanism which led to the destruction of "Strabo's Channel", the non-invasive geophysical surveys (Chapter 4) allowed detailed investigation of the subsurface of the valley. Of the four non-invasive survey techniques used onshore,

the resistivity surveys (airborne apparent resistivity and ground-based resistivity) produced the most striking results. This was due to the strong conductivity contrast between the two predominate lithologies which composed the area: resistive limestone and very low resistivity marls and clays. The airborne surveys allowed confident tracking of thrust faults within Thinia particularly where they were not visible at the surface due to sediment cover. The helicopter-mounted electromagnetic survey allowed data collection over areas of very steep terrain where ground-based surveying was not possible. However, the presence of numerous data gaps due to habitation made linking anomalies seen in the northern half of the valley with those in the south difficult.

Although intended as the primary survey type, the gravity survey (Section 4.5.2) did not resolve details of the subsurface as clearly as hoped. This was due primarily to the level of complexity in the structural geology of the valley in a relatively small area rather than the simple low density wedge expected from a buried marine channel as previously anticipated but also is a natural consequence of the technique's non-unique interpretations. In addition, the affects of sharp topography could not be entirely removed despite terrain correction with the high resolution digital elevation model (DEM).

While it was hoped that the land-based seismic refraction survey would provide information on layering within the subsurface of Thinia, this survey technique struggled to resolve bedding due to their steep dips and transaction by thrust faulting which resulted in a "hidden" lower velocity (marl) sediment layer beneath a high velocity (limestone) layer. This was a particular problem in the Lake Katachori area where the Agia Sotira Thrust passed through the eastern side of the survey and in southern Thinia (particularly line STL2) generally resulting in a higher root mean squared error (RMSE) for those models affected. A certain degree of caution was applied when making inferences where faults were believed to be present. Also, the refraction method assumed an increase of velocity with depth which led to increase of velocity in the models with depth and a false base to the low velocity sediments in the valley. These problems were mitigated by interpreting the seismic refraction

results with the equivalent resistivity profile, a survey which produced clear and useful results and could be tied to the airborne apparent resistivity survey and the combined data sets were much more useful, allowing direct comparison between the two survey types.

The key limitation of the onshore non-invasive surveys was the lack of differentiation between recent (Late Holocene) sediment deposits (landslide "backfill", alluvium and lacustrine sediments) and underlying marl and clay bedrock due to the physical similarities, particularly electrical conductivities, between these lithologies. "Ground-truthing" of this non-invasive data with the shallow sedimentary coring proved absolutely crucial. Only the shallow boreholes were able to provide a true measure of how much recent fill occurred within specific sites with all the consequent impact for the theory being tested.

Offshore, the shallow marine seismic reflection survey also produced very striking results. This was in part due to the specialised seismic interpretation software (Kingdom) used to interpret this data. Limitations in the interpretation came from unsatisfactory extrapolation of grids between widely-spaced data points which is a natural consequence of any spaced 2D interpretation, and problems with contouring in small (~2 km across) bays due to the software not recognising the coastline as the "zero metre" contour. These results could be further improved with an offshore shallow core drilling programme similar to that carried out onshore.

Despite data limitations and complexity of the problem, the results of this investigation have provided meaningful insights into the geological history of the area and confident interpretations of the data can now be presented. This chapter will be divided into the following three sections:

1. **Discussion (Section 7.2)**
2. **Suggestions for Future Work (Section 7.3)**
3. **Conclusions (Section 7.4)**

7.2 Discussion

The discussions section will be divided into four parts. Section 7.2.1 will concern the structural evolution of Thinia in terms of explaining the current geology and geomorphology. Section 7.2.2 will discuss the results for Lake Katachori and explore the possible causes for its formation. Section 7.2.3 presents a series of paleo-geographic reconstructions illustrating the evolution of the Thinia coastline since the Last Glacial Maximum by combining the results of the onshore and offshore surveys. Section 7.2.4 discusses the implications for "Strabo's Channel".

7.2.1 Structural evolution of Thinia

The results of the fieldmapping carried out across Thinia and the shallow marine seismic reflection survey carried out in the Gulf of Argostoli and Atheras Bay showed that the structural geology of the Thinia area was far more complicated than initially believed. Instead of exclusively a compressional or extensional system, both extensional and compressional structures were evident with an underlying easterly- to southeasterly-dipping extensional structure overthrust and reactivated by migration of the Hellenide deformation front into the Pre-Apulian zone. This was overprinted by further neotectonic deformation relating to continued late stage Hellenide deformation (out-of-sequence thrust reactivation) and formation of the Kefalonia Transform Fault (KTF) with the establishment of bookshelf faulting resulting from dextral strike-slip movement along this fault (e.g. Atheras Bay, Figure 1.30). It was difficult to differentiate between these two sources of deformation. The resulting steep slopes created by this neotectonic deformation are inherently unstable lending themselves to collapse – geomorphic failure due to structural feedback. The structural evolution of Thinia and Northern Paliki occurred in the following stages:

A. **Extension and rifting of the Upper Cretaceous to Paleogene carbonates.**
B. **Late Paleogene (intra-Oligocene) uplift and erosion.**

C. **Deposition of Oligocene to Late Miocene (post-rift ramp geometry). Uplift of area (formation of the Oligocene to Early Miocene Unconformity).**
D. **Base level fall and the formation of the Messinian Salinity Crisis Unconformity.**
E. **Renewed (Plio-Pleistocene) deposition.**
F. **Westwards migration of Hellenide compressional front into Pre-Apulian Zone and reactivation of Cretaceous-Paleogene extensional structures.**
G. **Outer-arc neotectonic deformational overprinting.**
H. **Late Holocene-Recent slope failure, reactivation of release faults.**

A. Extension and rifting of the Upper Cretaceous to Paleogene carbonates

As described in Section 1.2.1, during the Upper Cretaceous to Middle Paleogene, NNE-SSW and NW-SE striking, south-easterly-dipping extensional faults were active within the Pre-Apulian Zone (Sorel, 1976; Mercier et al., 1976, 1979). These faults are believed to have formed to accommodate the extension associated with downwarping of the distal margin of the foreland (Ionian) basin (Underhill, 1988) ahead of the Pindos Thrust (Underhill, 1989) caused by lithospheric flexure due to thrust load (Allen et al., 1986; Homewood et al., 1986; Ricci Lucchi, 1986). Some of these normal faults would be reactivated as thrust faults when the area later went into compression (e.g. Argostoli Fault, Ainos Thrust) (Underhill, 1989).

Such faults can be traced throughout the Southern Adriatic in South Italy and are important both in the offshore domain and onshore at Gargano (e.g. Graziano, 2000; Borgomano, 2000). Figure 7.1 shows a regional map of the Adriatic and Apulian area where extension prevails. The Apulia platform represents the unshortened foreland which is cross-cut by Cretaceous-Paleogene normal faults and onlapped by the "feather-end" of the Mio-Pliocene and Quaternary foreland basin sediment.

Meanwhile to the south-west of the Kefalonia Transform Fault the crust experiences compression and the same extensional faults have been overridden by compressional Hellenide deformation.

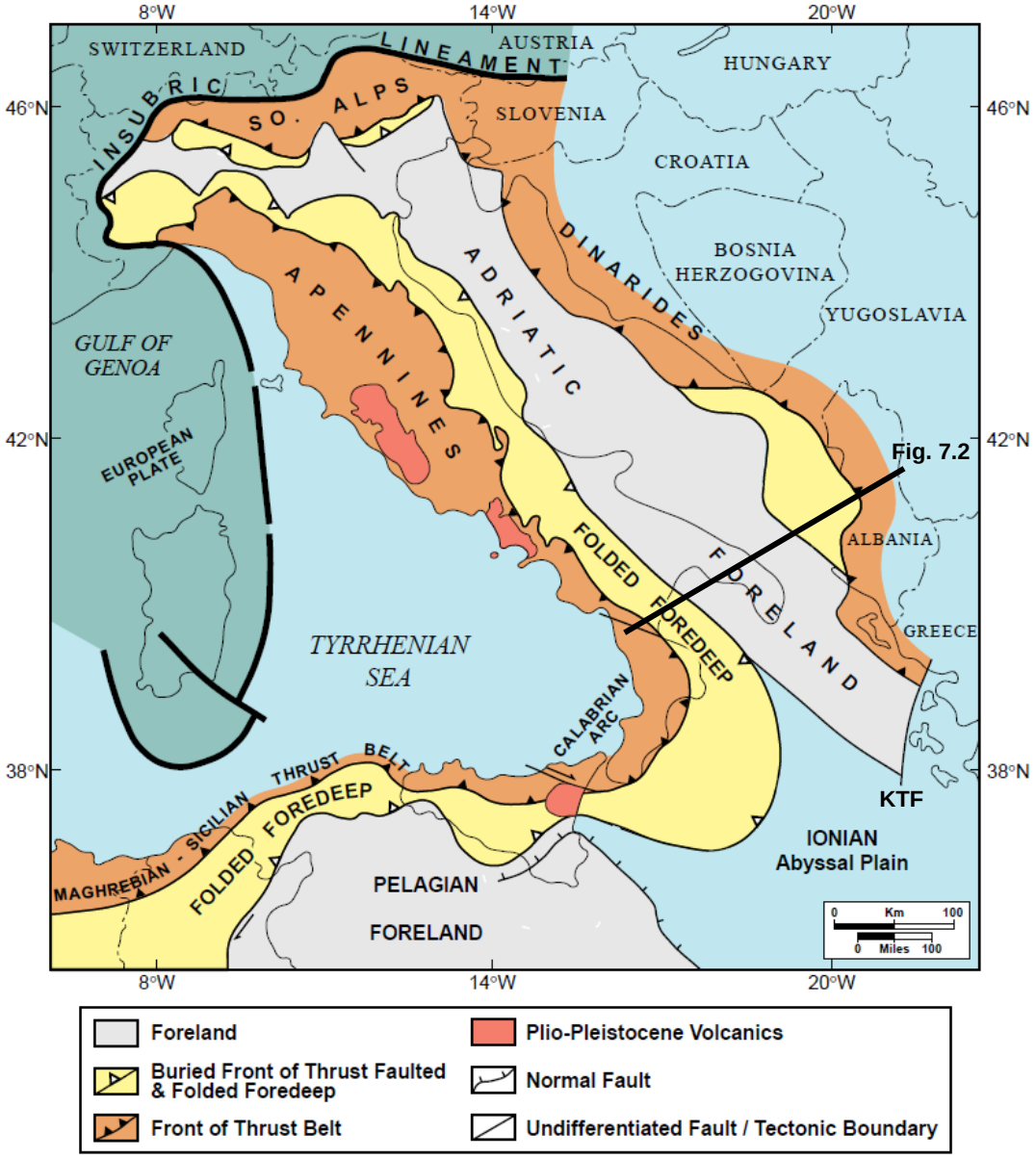

Figure 7.1 Regional view of the Adriatic and Apulian area. Across the Adriatic Foreland (grey area east of Italy), extension prevails while to the south-west of the Kefalonia Transform Fault (marked as KTF), the crust experiences compression (modified from Zappaterra, 1994).

The interpreted marine seismic reflection line (from Peace et al., 2012) depicted in Figure 7.2 provides a regional cross-section through these two regimes extending

from the dome of the Apulian Platform in the extensional foreland setting of the Adriatic Sea to the thrusted regime of Albania and Western Greece. The Mio-Pliocene and Quaternary sediments (orange and yellow on Figure 7.2) onlap the rifted Mesozoic sediments (blue and green) of the Apulian Platform from either side (Peace et al., 2012).

Evidence of this Upper Cretaceous to Middle Paleogene rifting could be found both on shore and offshore. The Ainos Thrust (Figure 1.38) was known to be a major NNE-SSW striking normal fault reactivated as a thrust fault as the region went into compression (Underhill, 1989). The analysis of outcrop sample 7_Oct11 (described in Section 5.4.1) taken from the Ainos Thrust hangingwall confirmed this. This sample was composed of a fining upwards debris flow, with shallow marine elements transported into a deeper, open marine setting through gravity of Lower-Middle Eocene age and suggested that the Ainos fault formed an easterly-dipping normal fault that was still active during the Middle Paleogene.

The NNE-SSW striking Agia Sotira Thrust (as described in Section 3.3.1) had an unusually high-angle bedding plane dip (45 to 60°) and a very smooth, steep east-facing slope with evidence of slicken-sides. This suggested this thrust also represented a Cretaceous-Paleogene easterly-dipping normal fault which was re-activated as thrust faults as the area went into compression. The geological map produced in Figure 3.29 showed that several extensional features still remained in the form of at least one large NNE-SSW striking normal fault of south-southeast dip.

Extensional features were also discovered offshore in the Gulf of Argostoli in particular in the form of a large, NNE-SSW striking, easterly-dipping normal fault running along the western side of the Gulf (Figures 6.24 and 6.25). There was also evidence of westwards-thickening of the pre-Holocene sediments (Figure 6.26) which may have been associated with this fault.

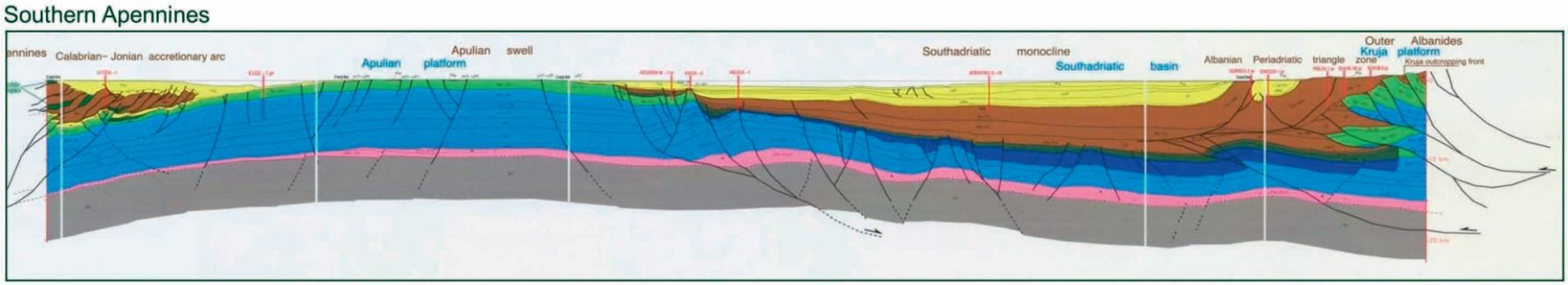

Figure 7.2 Interpreted seismic line representing a cross-section through the Adriatic Foreland (location indicated in Figure 7.1) extending from the dome of the Apulian Platform in the extensional foreland setting of the Adriatic Sea to the thrusted regime of Albania. The Mio-Pliocene and Quaternary sediments (orange and yellow) onlap the rifted Mesozoic sediments (blue and green) of the Apulian Platform from either side (Peace et al., 2012).

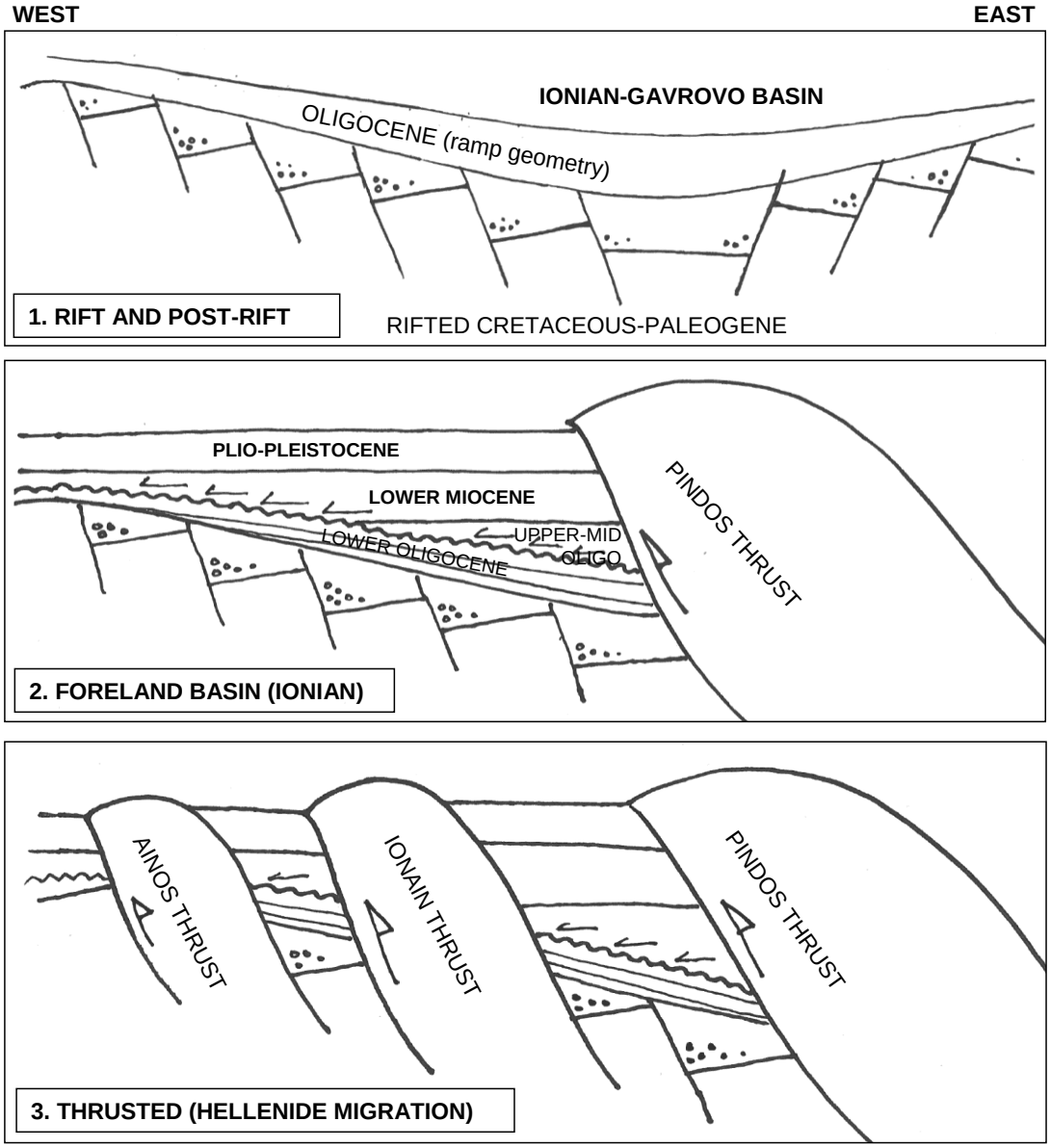

Figure 7.3 Series of schematic sketches showing evolution of Western Greece: 1) Rifting of Mesozoic sediments due to downwarping of the crustal ahead of the westwards migrating Hellenides; 2) Deposition of Neogene sediments into the foreland basin and emplacement of the Pindos Thrust; 3) Migration of Hellenide deformation into the foreland basin and inversion of extensional faults.

Extension and rifting of the Upper Cretaceous and Paleogene carbonates and formation of Paleogene conglomerates (intra-Oligocene uplift and erosion)

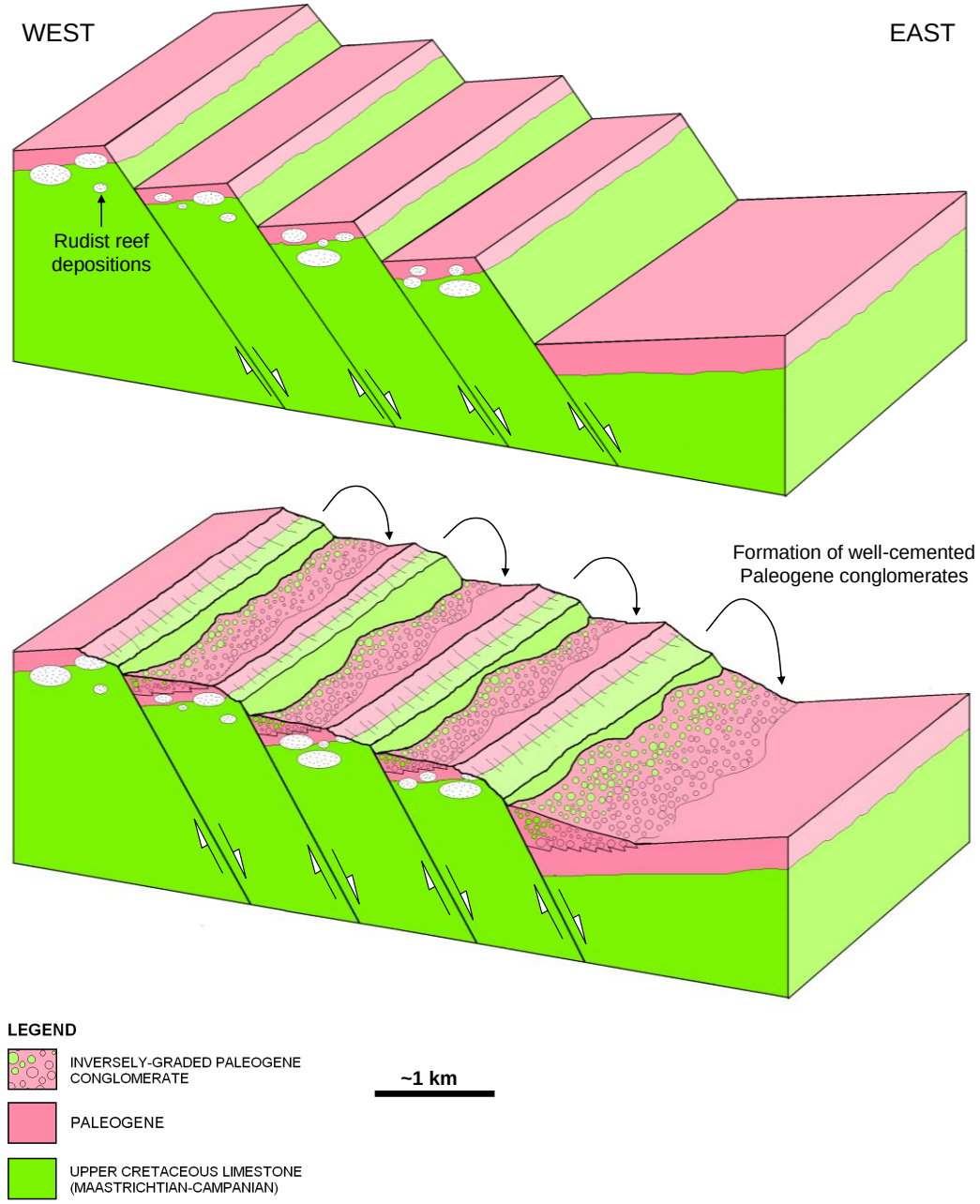

Figure 7.4 Vertically-exaggerated block diagram showing the rifting of the Upper Cretaceous to Middle Paleogene by south-easterly dipping normal faults established by opening of the foreland basin ahead of the Pindos Thrust (top). Formation of the well-cemented conglomerates observed along the Ainos Thrust plane during Late Paleogene (intra-Oligocene uplift and erosion) (bottom).

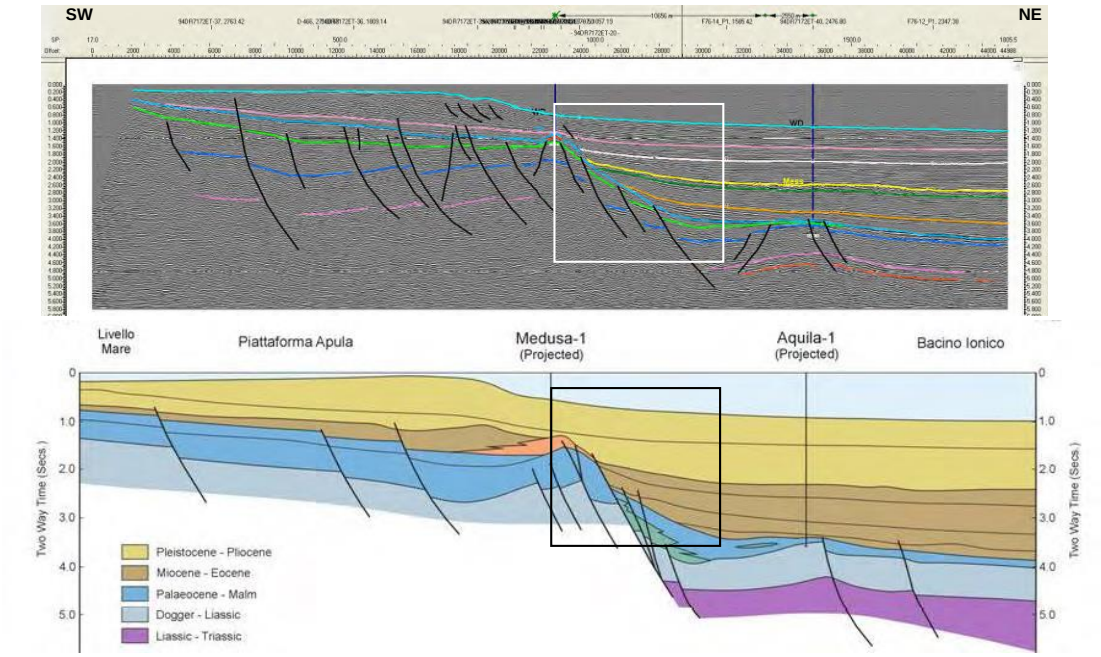

Figure 7.5 The box indicates the analogous location of the pre-shortened Thinia valley with the easterly-dipping Mesozoic extensional faults onlapped by the "feather-end" of the Miocene and Pleistocene-Pliocene onlapping unit, Aquilia-1 area (Modified from Southern Adriatic – Play Types, Northern Petroleum).

Figure 7.4 (top) shows the Thinia valley during this Cretaceous-Paleogene rifting in the form of a block diagram. An analogous location to the Thinia valley prior to reactivation through compression of the normal faults before the External Hellenide deformation reached the Pre-Apulian Zone is the Aquila-1 area in the Southern Adriatic (Figure 7.5) which shows a similar configuration of easterly-dipping normal faults onlapped by the basinal Mio-Pliocene units.

At this time, the well-cemented Paleogene-aged limestone conglomerates visible on the eastern side of the valley (e.g. Kondogourata road turn-off, Figure 3.14, B) were created as clasts from the footwall of these faults were transported down the fault scarps as submarine gravity flows (Figure 7.4, bottom).

B. Late Paleogene (intra-Oligocene) uplift and erosion

Early Oligocene sediments formed a drape over the rifted and post-rifted sediments (Middle Eocene and younger) (Figure 7.3, 1). Uplift and doming of the area in the mid-Oligocene due to formation of the peripheral bulge ahead of the Ionian basin caused erosion of the Middle Oligocene. This unconformity was onlapped by the Late Oligocene. The Early Oligocene and younger sediment represent the "feather-end" of the foreland basin sediments onlapping the rifted sediments (infilling the basin created by downwarping).

C. Deposition of Oligocene to Late Miocene (post-rift ramp geometry). Uplift of area (formation of the Oligocene to Early Miocene Unconformity)

Oligocene and Early Miocene clastics derived from Pindos Mountains were deposited into the Ionian foreland basin in a post-rift ramp geometry (Figure 7.6, top) (Clews, 1989). The entire Oligocene and basal Miocene were removed through erosion as the area was uplifted through formation of a peripheral bulge ahead of the Ionian Thrust due to the weight of the thrust sheet ("diver on a diving board" effect). This occurred towards the end of the Early Miocene as continued westward migration of the Hellenide deformation initiated the Ionian Thrust and caused steepening of the easterly-dipping Paleogene-Cretaceous faults and subsequent erosion of the Oligocene and basal Miocene (Figure 7.6, bottom). This unconformity was detected by the Northern Paliki boreholes by the almost complete absence of *in situ* Oligocene to Early Miocene stratigraphy (detected in boreholes C6a, C5d, C5d2 and C1) and abundance of reworked assemblages of this age (Section 5.4.1, Figure 5.29). The Oligocene Unconformity is visible as the eroded limestone surfaces observed around Thinia e.g. the western shore of Lake Katachori.

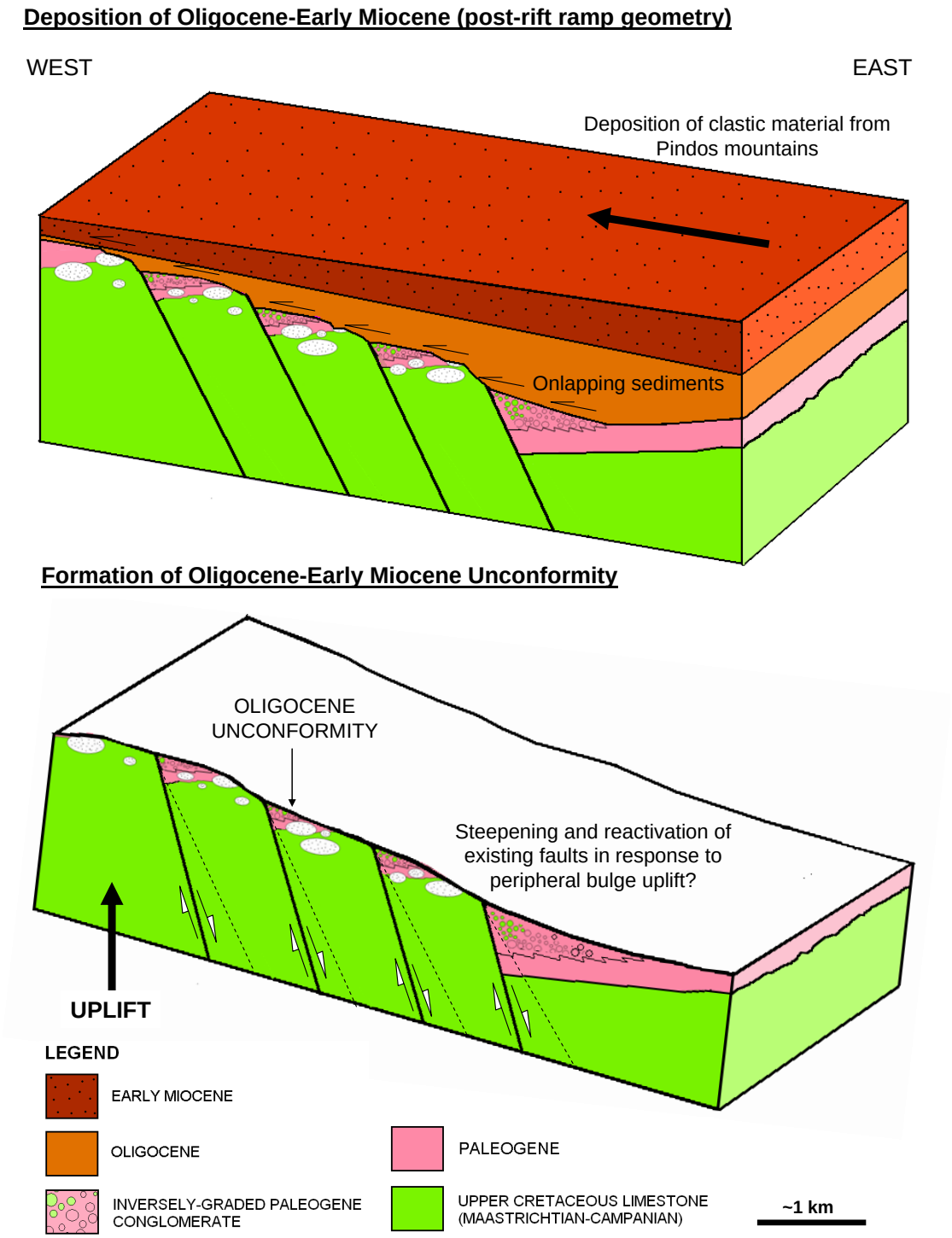

Figure 7.6 Vertically-exaggerated block diagram showing the deposition of Lower-Mid Oligocene clastic sediments derived from the Pindos Mountains in post-rift ramp geometry (top) and subsequent formation of the Oligocene Unconformity through Early Miocene uplift of Thinia due to development of the peripheral bulge ahead of the Ionian Basin.

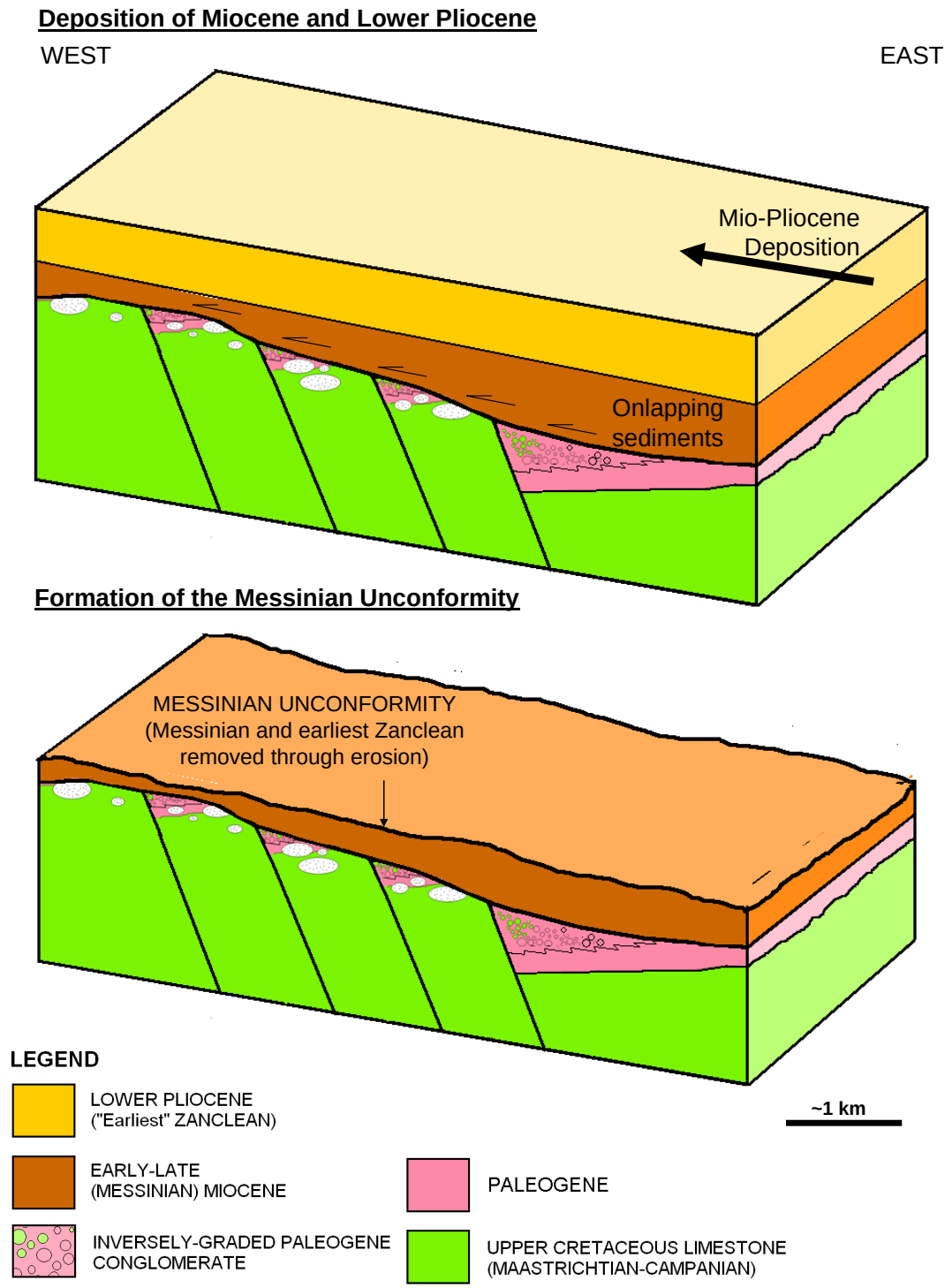

Figure 7.8 Onlapping of the Miocene and Lower Pliocene onto the Oligocene Unconformity (top) and subsequent formation of the Messinian Unconformity as falling sea levels removed the lowermost Pliocene and Messinian (bottom).

D. Base level fall and the formation of the Messinian Salinity Crisis Unconformity

The Oligocene Unconformity was onlapped by Mio-Lower Pliocene sediments (Figure 7.8, top). The dramatic c. 1500 m sea level drop which accompanied the tectonic disconnection and desiccation of the Mediterranean Sea created a layer of evaporites at lower elevations and an unconformity at higher elevations. In Thinia, this event formed an unconformity detected in borehole C1 and inferred in C4a, C4c (Section 5.4.1, Figure 5.29). The Messinian Unconformity resulted in the loss of the Late Miocene (Messinian) to "Earliest" Lower Pliocene ("earliest" Zanclean) in the Northern Paliki boreholes (Figure 7.8, bottom).

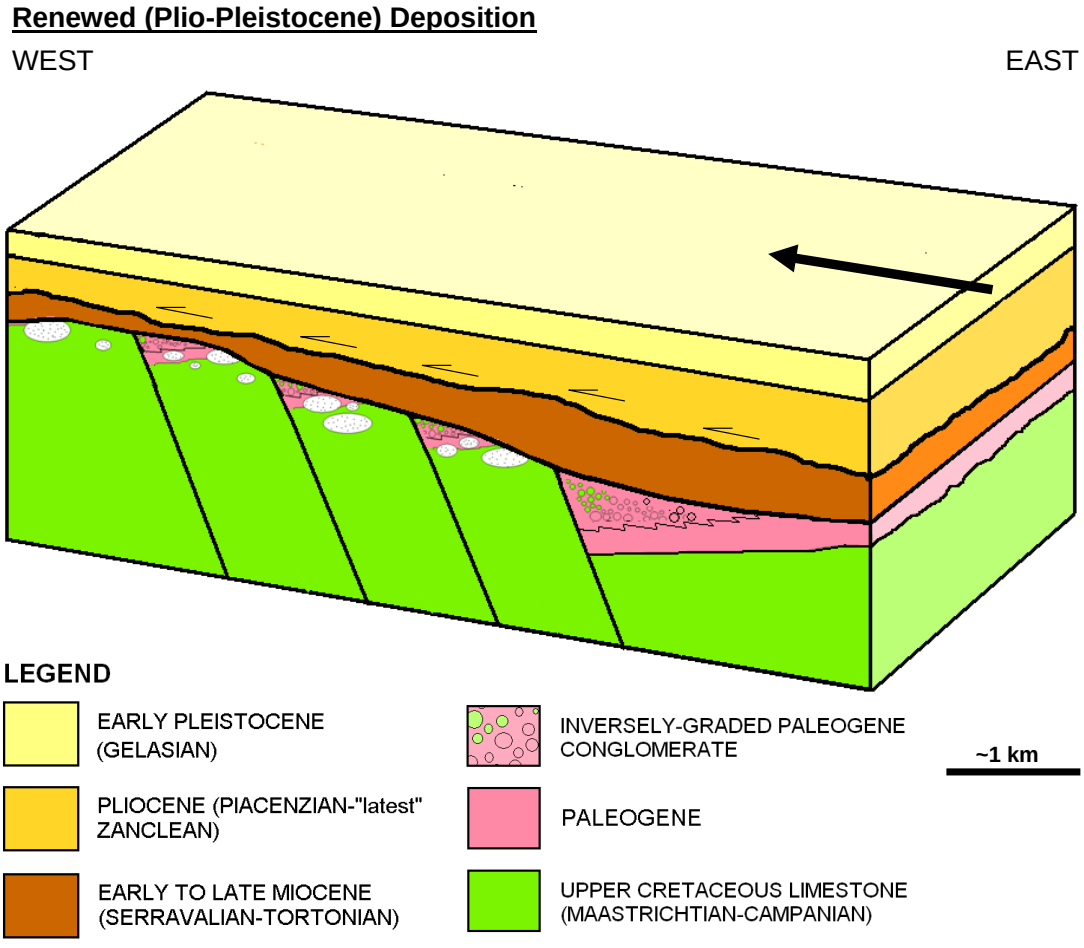

Figure 7.9 Renewed (Plio-Pleistocene) deposition.

E. Renewed (Plio-Pleistocene) deposition

The Messinian Unconformity was onlapped by Uppermost Lower Pliocene to Quaternary sediments during sea level rise of the Zanclean which followed the Messinian Salinity Crisis (Figure 7.9).

F. Westwards migration of Hellenide compressional front into Pre-Apulian Zone and reactivation of Cretaceous-Paleogene extensional structures

During the Early Miocene, the locus of Hellenide compressional deformation migrated westwards from the Ionian Thrust to the Pre-Apulian Zone (Underhill, 1989). The migration of the deformation front into the Pre-Apulian Zone led to the initiation of thrust faults, folding and reactivation of large, easterly-dipping normal faults as thrust faults and formation of folding. Some of the Cretaceous-Paleogene normal faults of Thinia were reactivated as easterly-dipping thrust faults under compression (e.g. Ainos Thrust, Agia Sotira Thrust) (Figure 7.10).

G. Outer-arc neotectonic deformational overprinting

This westwards migration of the compressional deformation front caused deformation of the Plio-Quaternary sediment of the Pre-Apulian Zone. However, it is difficult to distinguish between late stage Hellenide deformation and outer-arc neotectonic deformation relating to the formation of the Kefalonia Transform Fault (KTF). The KTF, a dextral strike-slip fault, formed to accommodate the rotational motion caused by the roll-back of the Hellenic Arc subduction zone (Underhill, 1989).

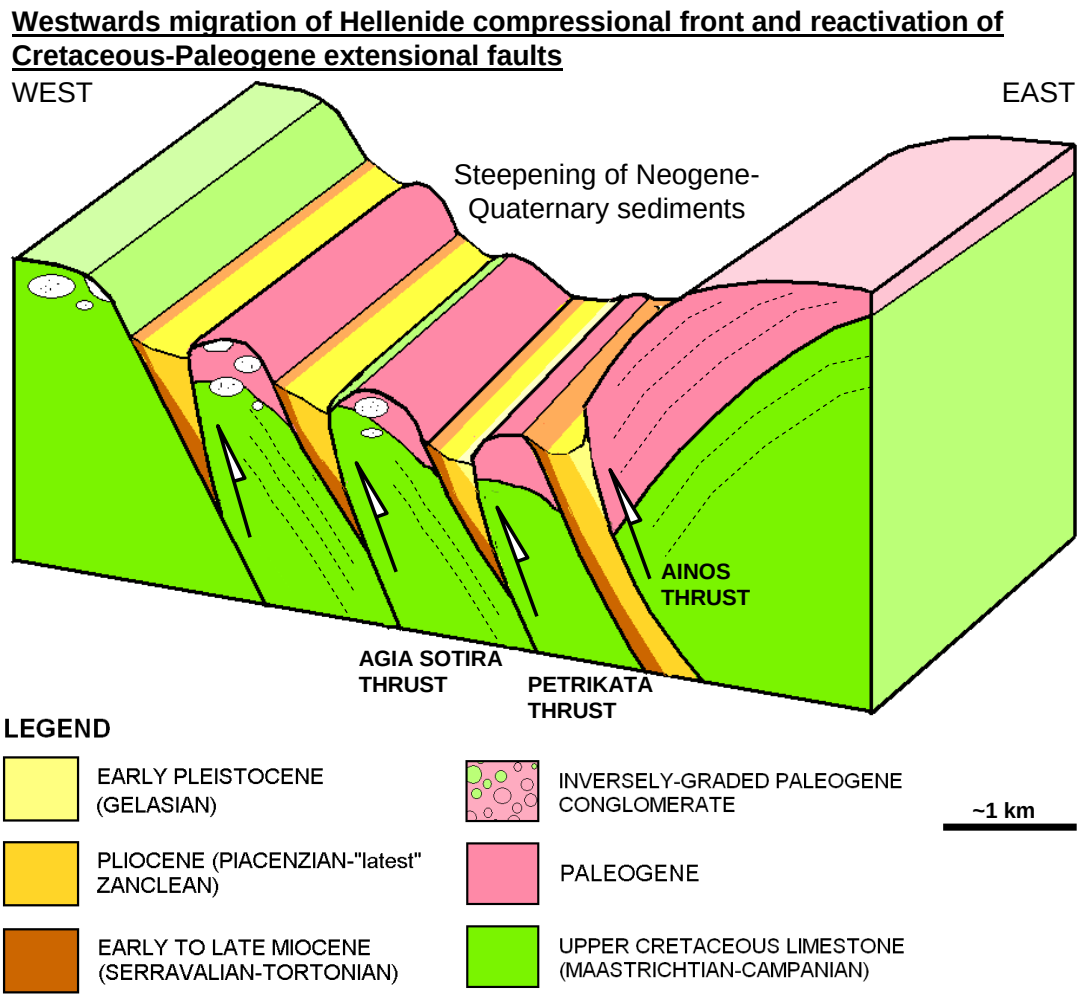

Figure 7.10 Westwards migration of Hellenide compressional front into Pre-Apulian Zone and reactivation of Cretaceous-Paleogene extensional structures.

Figure 7.11 depicts the characteristic pattern of oblique folds and secondary faults associated with a dextral strike-slip transform fault aligned parallel to the KTF. This strain ellipse is based on the Harding (1974) model, compiled through clay model experiments (e.g. Cloos, 1955; Tchalenko, 1970; Wilcox et al., 1973). Antithetic strike-slip faults are minor faults which dip in an opposite direction to the dip of the beds displaced with a displacement sense opposite to that of the main strike-slip fault (Wilcox et al., 1973). Synthetic faults dip in the same direction as the bedding plane dip and have the same displacement sense as the main strike-slip fault (Gibbs, 1984).

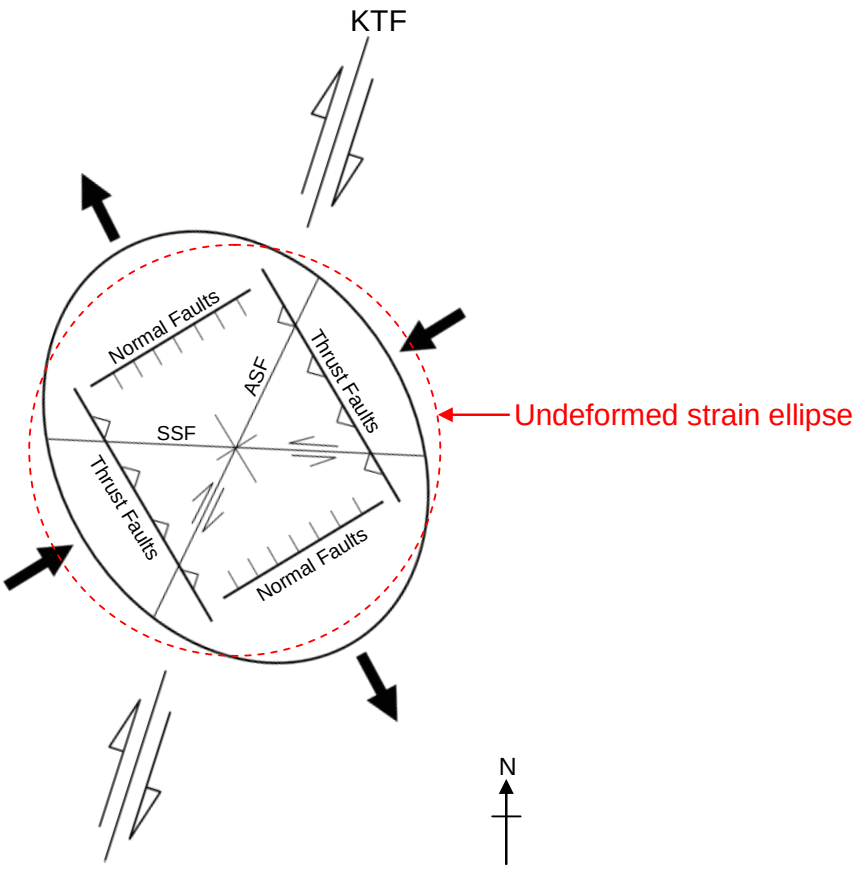

Figure 7.11 Strain ellipse for the Kefalonia Transform Fault (KTF) depicting the characteristic pattern of drag folds and secondary faults associated with a strike-slip fault zone. SSF = Synthetic Strike-slip Fault. ASF = Antithetic Strike-slip Fault. Inward arrows indicate compression while outwards pointing arrows indicate extension (After Harding, 1974; in Reading, 1980). The undeformed strain ellipse is superimposed with a red dashed line (after Wilcox et al., 1973).

In a pure strike-slip regime, *en echelon* folds form at an oblique angle to the strike-slip fault while if transpression is present i.e. where the Earth's crust experiences strike-slip and a component of thrusting, the folds are rotated to an also parallel to the strike-slip fault (Harland, 1971). Figure 7.11 shows that this strike-slip configuration results in the formation of NE-SW striking, NW- and SE-dipping normal "bookshelf" faults. Bookshelf faults are defined as a system of sub-parallel faults which involve the progressive rotation of beds and faults as displacement occurs typically causing a steepening of beds and decrease in the dip of the faults (Mandl, 1987) and the "bookshelf mechanism" is the accommodation of extension through rotation of the parallel faults (Mandl, 1984) (Figure 7.12).

This pattern of deformation was visible onshore in the form of NNE-SSW to NE-SW striking faults visible along the west coast of Paliki (Figure 1.25) and Atheras Bay (Figure 1.30) which dipped both NW and SE. These faults be identified in the HEM maps as linear anomalies of magnetic, conductive material reflecting the predominance of fine-grained *terra rossa* sediments accumulated along these fault planes (Figure 4.2 and 4.4).

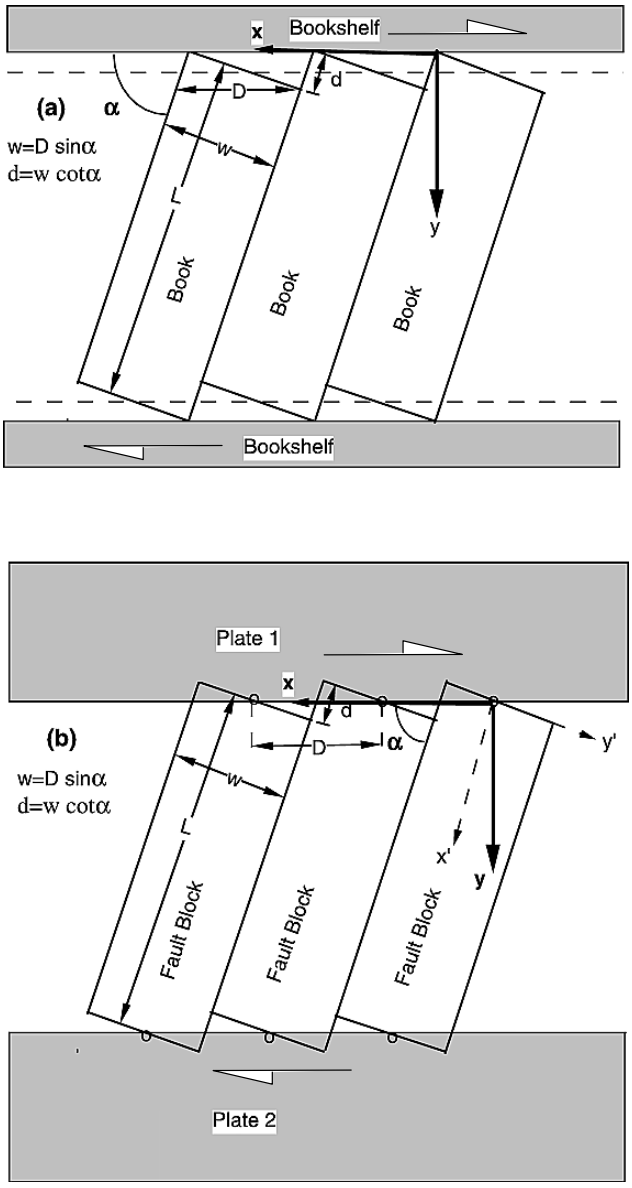

Figure 7.12 Bookshelf model where slip between the "books" of dimension L x w is accommodated by rotation of the books (a), applied to fault blocks (b). Distance between blocks (D) is constant. Modified from Savage et al. (2004).

Figure 7.13 Neotectonic overprinting of Paliki due to movement along the Kefalonia Transform Fault (KTF). The fault scarps of the bookshelf faulting are shaded.

Displacement along these faults (shaded grey on Figure 7.13) was at a maximum along the coast, dying out eastwards before reaching the Thinia valley. These bookshelf faults offset the Atheras Thrust demonstrating that they post-dated the Hellenide deformation. Since the Atheras Thrust was active during the Upper Quaternary (Sorel, 1967) the formation of these faults could be date to 800 000 years

or less. Similarly striking striking-slip faults were detected within the Gulf of Argostoli where they offset the three depocentres in a NE-SW direction (Figure 6.29) suggesting that these structures, too, were related to activity along the KTF rather than late-stage Hellenide activity.

H. Late Holocene-Recent slope failure, reactivation of release faults

The NE-SW trending "offsets" observed within Thinia sediments detected during field-mapping (Figure 3.29) and by the gravity survey (Figure 4.34) were hard to explain. These faults are not the same as the bookshelf faults running along the western coast of Paliki. According to the strike-slip strain ellipse established for the KTF, they are wrongly-orientated to those faults resulting from movement along this transform fault. Faults of this orientation occur nowhere else in Northern Paliki, perpendicular to the normal faults defining the western valley side.

These offsets may have been release faults (Figure 7.14). Release faults are classed as faults which occur within the hangingwall of a listric normal fault and are usually orientated perpendicular to the trend of the parent fault dying out with distance from the fault plane (Destro, 1993). They form in order to accommodate differential vertical displacements and growth of length along strike as the normal fault grows laterally, dying out away from the hangingwall. The Thinia offsets may have formed during Cretaceous-Paleogene rifting of the area. While release faults typically do not exhibit strike-slip movement unless there are other forces acting upon them (Destro, 1993), the Thinia faults are downthrown on the NE side to the north of Petrikata Quarry and to the SW to the south of the quarry (Figure 4.35) and exhibit a sinstral strike-slip motion. This strike-slip behaviour was therefore interpreted as reactivation of these release faults overprinting the extensional-compressional structures of the valley. As these faults caused offsetting of the Agia Sotira Thrust they must be younger than the Early Pleistocene (Gelasian) (1.81 Ma). It is thought that the release faults may have been reactivated as effective lateral ramps to subsequent contractional deformation and more recent slope failure during formation of the talus fans e.g. Zola and Nifi.

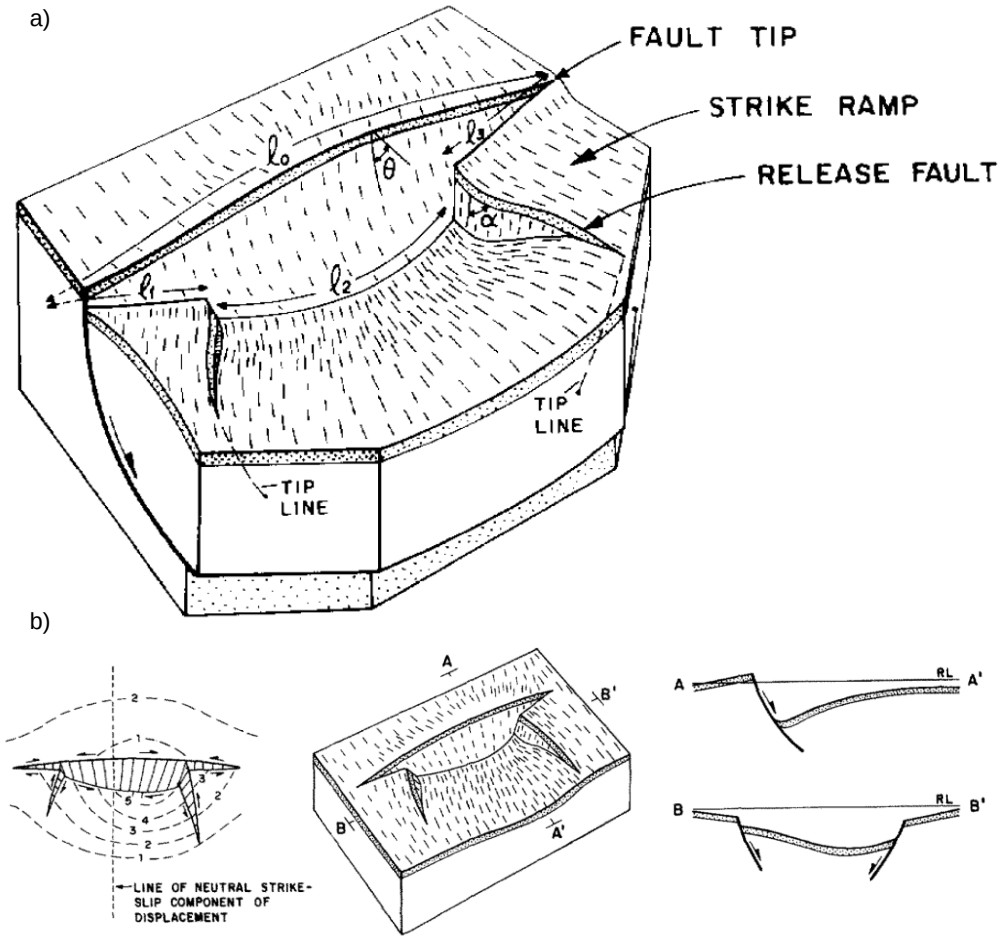

Figure 7.14 Block diagram showing displacements variation along the strike of a normal fault with release faults forming (a). (b) Left to right: Idealised structural contour map, block diagram and cross-section of basic release fault structure (bottom). Arrows indicated the apparent lateral movements exhibited by the release fault. From Destro, 1993.

7.2.2 Lake Katachori

One of the key focuses of investigation was the site of the suspected paleo-lake Lake Katachori. This was due to the location of the lake relative to the proposed route of "Strabo's Channel" (Figure 1.53) in the case of a buried, untranslated channel. Questions were raised as to why a lake existed here at all due to the shape of the topography. While the DEM for the paleo-lake (presented in Figure 1.35) showed that the lake sat within a flattish area within the topography, there was a sharply-

incised gully draining south-eastwards (marked by a dashed white line) which surely would have drained the lake before it had a chance to form.

The geophysical surveys revealed that Lake Katachori formed a lens of low density, low gravity (-0.65 mGals), magnetic, very low resistivity (0.5 to 15 Ωm) sediments which were at least 80 to 100 m thick and onlapped the heavily-weathered resistive, easterly-dipping limestone defining the western shore. However, the apparent thickness of these "lake fill" deposits raised questions about how much of this response could be attributed to lacustrine deposits and how much related to underlying colluvium or bedded clays and marls which had very similar physical properties to the clays observed at the surface of the lake. The time-term inversion of the seismic refraction data was more promising and resolved the lake subsurface into a layered structure composed of a low velocity (0.30 km/s) surface layer around 3 m thick which overlay a unit of higher velocity sediments (1.76 km/s) around 8 m in thickness. The inversion resolved the interface between the second and third layers (2.04 km/s) at around 10 m, however, the presence of the Agia Sotira Thrust at the eastern side of the survey reduced the confidence of this layer boundary's position as the denser limestone overthrusting marl produced a stratigraphic configuration which the refraction method is unable to resolve.

The non-invasive geophysical results gave rise to two possible scenarios: 1) Lake Katachori was either a very deep (at least 80 to 100 m) and narrow lake or (2) it was shallower and sat within a basin of physically similar bedrock or landslide material and the contact between these deposits was invisible or not confidently resolved in the non-invasive tests.

The six boreholes drilled within the lake (C5a, C5b, C5c, C5d, C5d2 and C5e), however, were able directly sample the lake's subsurface. The boreholes detected only a thin veneer (0.65 to 6.40 m) of gravel-rich Late Holocene-Recent clays with the thickest deposit (6.40 m) occurring in C5b in the central part of the lake. These upper sediments contained some Neogene marine deposits (*Orbulina*) but these were

considered to be reworked into the clastic deposits, particularly in the case of C5b which contained a thick deposit of clastic material in the upper 6 m.

The base of recent unit was defined by a stratigraphic break. Below this break was a Plio-?Pleistocene succession (up to 101 m thick in C5c). The uppermost few metres of these sediments generally consisted of chestnut-red oxidised clays with ferruginous traces overlying steeply-bedded (40 to 60°) marls. These sediments were generally believed to have been deposited in middle to outer neritic, open marine conditions with the exception of C5d2 which showed evidence of a rapid phase of intra-Pliocene uplift (rootletted horizon at 9.1 m [core]) and subaerial plant colonisation prior to rapid renewal of sedimentation under neritic conditions. The steep angle of dip and age of these bedded sediments was identical to what was found in the other Thinia boreholes suggesting that the sediment below the stratigraphic break represented steeply-dipping *in situ* Neogene-Quaternary bedrock rather than a jumble of clastic debris which may have built the lake up from sea level. However, the presence of smooth shear planes within the marl in cores C5a, C5b and C5c indicated these sediments had experienced strong post-depositional deformation.

The key observation was the presence of the *Zygnema* type freshwater algae within the uppermost few metres of some of the Lake Katachori boreholes. Spores were found within the Recent unit of C5d (0.70 m [core]), C5d2 (0.25 m [core]) and C5e (0.5 m [core]) and in the very uppermost part of the Plio-?Pleistocene unit of C5a (1.75 m [core]) and C5e (2.5 m [core]) (Figure 7.15).

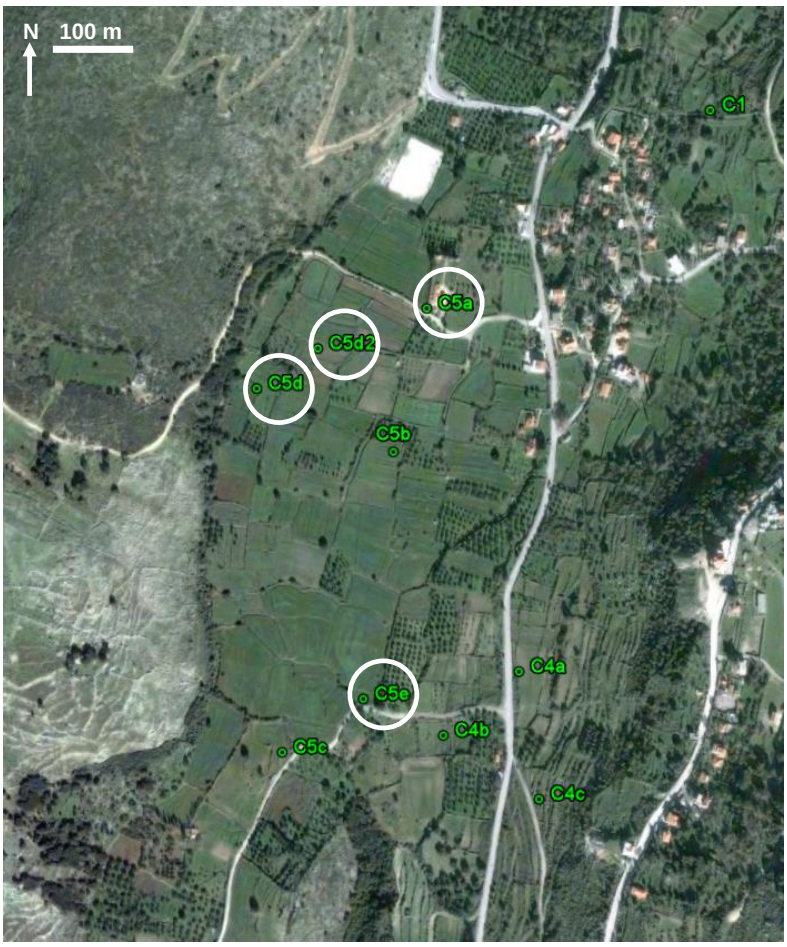

Figure 7.15 Distribution of *Zygnema* algae in Lake Katachori confirming a freshwater environment existed within the bounds of the lake area. The algae was notable absent in C5b, the borehole sunk into the deepest part of the lake however this was due to the presence of clastic material diluting the palynofauna. Satellite image source: Google Earth.

The only other site sampled by the coring survey where *Zygnema* also occurred was Livadi Marsh where a freshwater lagoon still exists (Section 5.3.2). This confirmed that a lacustrine depositional environment had existed within Lake Katachori. The lack of *Zygnema* algae in C5b, the borehole located at the deepest part of the lake could be explained by the presence of clastic debris detected within the upper 6 m of this borehole as this rapid influx of debris may have diluted the palynofauna. The core evidence showed it was a very shallow lake (a maximum of 6.4 m in thickness).

Unfortunately, despite several attempts to do so, precise dating of the lake sediments was not possible. The radio-carbon dating of lignite samples was not successful due to them being contaminated with debris from the 1953 Ionian Earthquake. The

presence of *Zygnema* algae within the very uppermost Plio-?Pleistocene unit implied the departure from the open marine conditions of the earlier Neogene to a freshwater setting occurred during the Early Quaternary however because these spores occurred very close to the Quaternary-recent stratigraphic break it is highly likely these are reworked sediments and the lake is a very young (Late Holocene) feature.

In terms of lake formation, the boreholes detected numerous pulses of angular limestone gravel and reworked material from higher up the stratigraphy a few centimetres to metres in thickness (over 6 m in C5b and the upper c. 10 m of C5c). This indicated that the lake had experienced frequent influxes of colluvium from the valley sides. The key observation is the tongue of talus on the south-western shore described in Section 3.2.2, A (Figure 3.9). This deposit was clearly very recent as it onlapped a ruined settlement (only tens to thousands of years old) and it had the power and volume to travel from west-facing slope of Imerovigli, across the valley and pile up against the opposite valley side. It was likely, given the seismicity in this region, that these colluvial influxes were earthquake-driven.

It is possible this landslide or one like it created a natural dam blocking the south-eastwards draining outlet identified in Figure 1.35 causing concentration of surface runoff from the surrounding hills in this clay-filled basin and a build-up of standing water. Eventually this dam was breached, re-opening this outlet and draining the lake. Lake Katachori may therefore represent a shallow landslide-dammed or "earthquake" lake. Earthquake lakes occur in mountainous areas which experience a high degree of seismic activity where earthquake-triggered landslides cause the blocking of rivers and subsequent flooding of the river valley (Costa and Schuster 1988; Shang et al. 2003; Chai et al.2000a, b; Kallen et al. 2006; Dai et al. 2005).

The most famous earthquake lake is "Quake Lake", a large, very deep lake created during the 1959 Yellowstone or Hebgen Lake Earthquake in Montana (Figure 7.16). This magnitude 7.1 earthquake caused a rock slide of volume 28 to 33 x 10^6 m^3 to fall 400 m into the Madison River Canyon (Figure 7.17, A) (Adams, 1981; Carl et al., 1993).

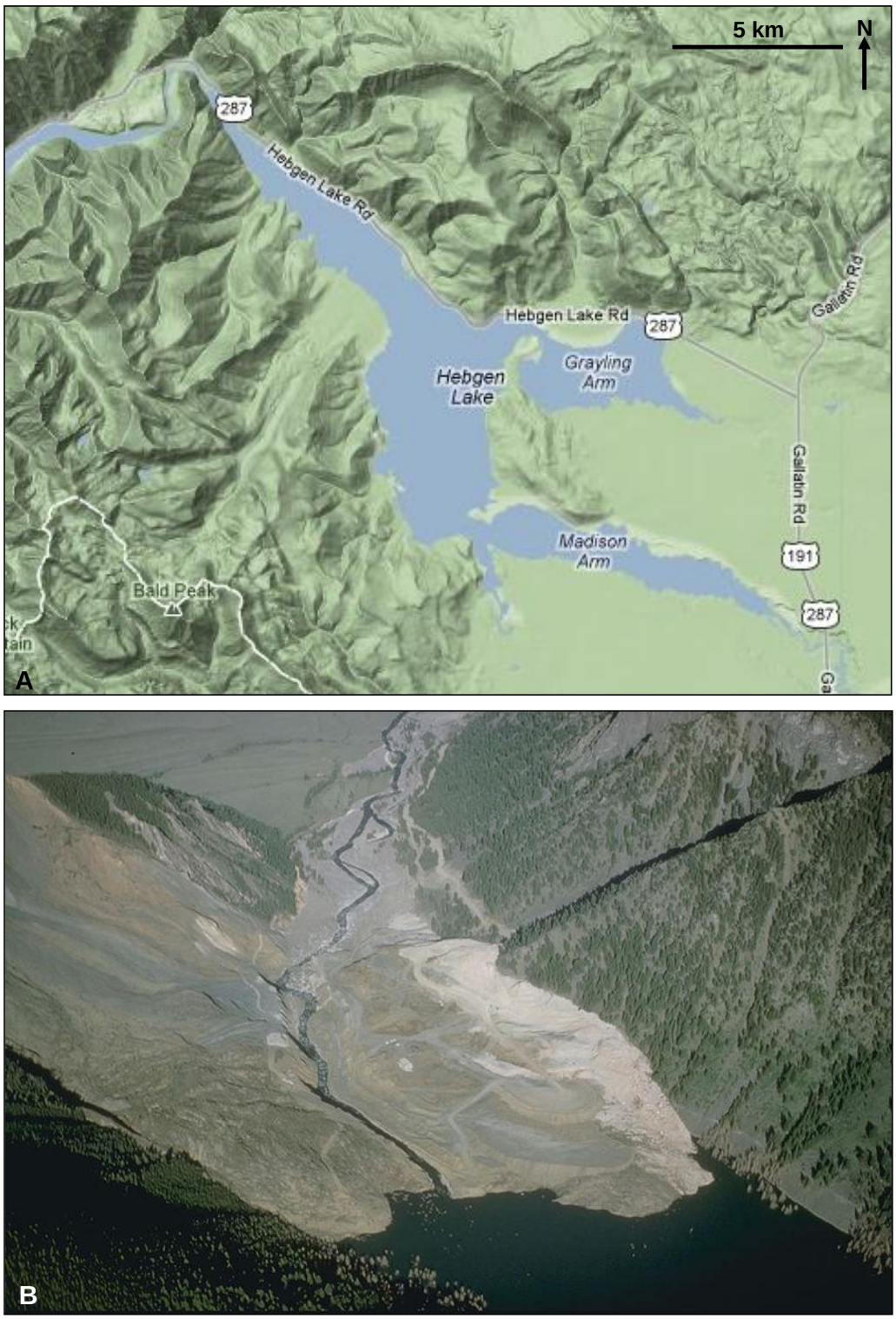

Figure 7.16 Hebgen "Quake" Lake: A. Topographic map showing the location of Hebgen Lake ("Quake Lake") and the steep, deeply-incised mountains surrounding the lake. Map source: Google Maps. B. The Madison River down-cutting into the landslide material can be seen feeding the lake. Image source: US Geological Survey.

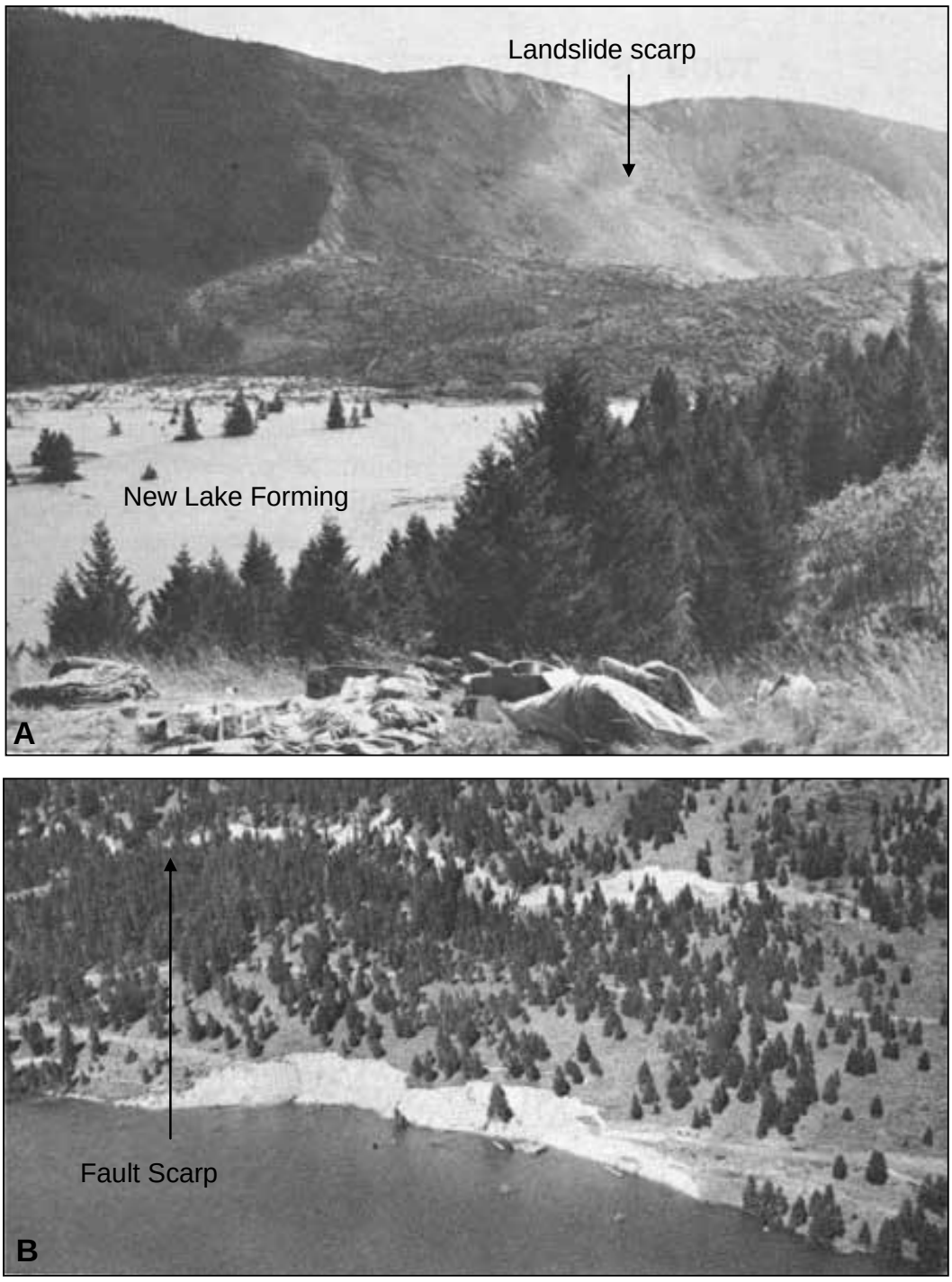

Figure 7.17 Photographs taken in the aftermath of the Hebgen Lake landslide: A. The landslide damming the Madison River with the newly forming "Quake Lake" in foreground of photo. The massive scarp in the south canyon wall is visible (Image source: W. G. Hall, 21 Aug 1959). B. New fault scarp (Hebgen Fault) on the north shore of Hebgen Lake which showed vertical displacement of up to 20 feet (image source: U.S. Forest Service Photo).

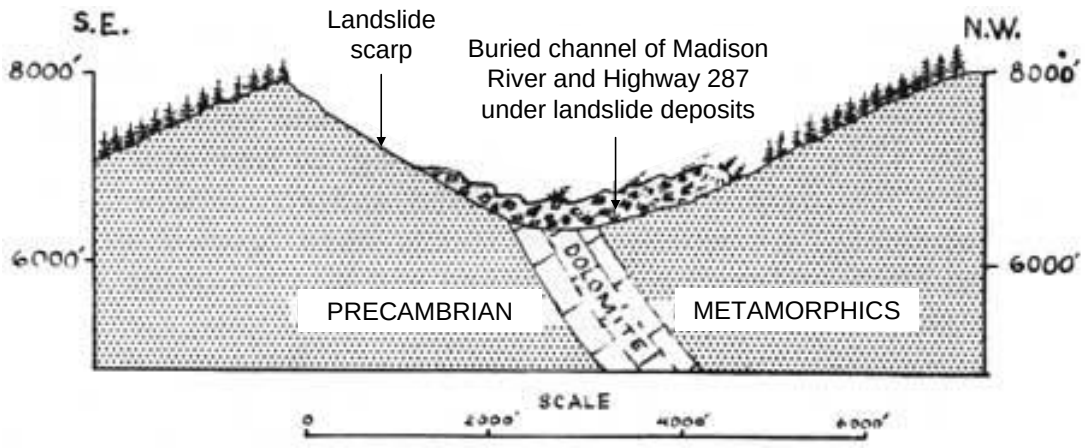

Figure 7.18 Sketch geological cross-section through the Madison Canyon Landslide. The landslide occurred within the weathered, brittle metamorphic rocks of the south wall of the canyon. The Modified from Witkind (1959).

Two-thirds of this material crossed the river and some was pushed up around 130 m on the opposite bank to form a natural dam to the river (Figure 7.18) (Adams, 1981). This dam material consisted of large clasts measuring 1 to 10 m long bound in a fine-grained matrix (produced through transport abrasion) of sand, silt and clay. The fine-grained material forms a low-permeability barrier and harder boulders prevent erosion of the dam. Over the course of three weeks the "Earthquake Lake" measuring 9.5 km long and 60 m deep was formed upstream of the landslide dam as trapped river waters built up behind this dam. This earthquake also produced new fault scarps up to 6 m high with the largest of these occurring along pre-existing normal faults northeast of the lake (Figure 7.17, B) (Carl et al., 1993).

Other well-known examples include Lake Sarez in Tajikistan which formed in 1911 when the earthquake-triggered Usoi rockslide, which measured around 2 km^3 in volume, formed a 600 m high dam, the highest dam ever recorded, blocking the Murgab River (Schuster and Alford, 2004). Recent examples include the 2008 magnitude 8.0 Wenchuaen Earthquake which struck Sichuan Province, China, which formed 257 earthquake lakes from rivers draining off the Tibetan Plateau (Cui et al., 2009). There are numerous earthquake-dammed lakes in New Zealand with at least 11 having created as a result of the 1929 Buller earthquake, a magnitude 7.6 earthquake centred in the northwestern part of South Island (Adams, 1981).

Typically, earthquake-dammed lakes are formed rapidly (weeks to years) and can last from days to thousands of years depending on the stability of the landslide dam which formed them (Evans et al., 2011) and the rate of continuing erosion of the instable mountain sides which formed them in the first place (Adams, 1980a). These lakes can be very deep, having typically formed within a steep river gorge, and vary in volume from <1 Mm^3 to >10 Gm^3 (Evans et al., 2011). Quake lakes typically have a primary outlet which becomes active during high water levels otherwise drainage usually occurs through springs which permeate through the landslide material and regroup in the valley below. The material composing the dam typically forms a jumble of large blocks and open crevices in its upper levels bound in fine-grained cement formed through pulverisation of clasts during transportation (Adams, 1981). Breaching of the dam can result in a sudden "outburst" flooding event which can devastate the valley floors below them which makes them a geohazard (Evans et al., 2011). The drained lake appears in the topography as a low-gradient sandy bed surrounded by steep, boulder-strewn slopes (Adams, 1981).

The presence of incised streams running to the north and south of the saddle region implied a large volume of water drained from the central region. As determined in Section 3.4, around 70 m of marl erosion had occurred along the northern stream (Figure 3.27) and above Agia Sotira inlet. However, it was impossible that this was caused by Lake Katachori breaching and flooding the valley due to the lake's shallowness and low water volume. They were most glacial streams established as sea levels dropped towards the last glacial lowstand (-120 m, ~21 500 BP).

7.2.3 Paleo-geographic evolution of Thinia since the Last Glacial Maximum

The postglacial flooding history maps from Section 6.6.3 (Figures 6.46, 6.47 and 6.48) and onshore results were combined to produce three paleo-reconstructions of the Late Quaternary-Holocene coastline of Thinia and Northern Paliki to demonstrate the dramatic evolution of the coastline in the last 21 500 years:

A. **Last glacial sea level lowstand, 21 500 BP to ~16 000 BP (-120 m).**

B. **Transgression of sea into the Gulf of Argostoli (formation of the Gulf of Argostoli ria), ~8400 BP (-34 m).**

C. **Mycenaean Era (Late Bronze Age), 3240 BP (0 to-3.75 m).**

A. Last Glacial Sea Level Lowstand, 21 500 BP to ~16 000 BP (-120 m)

During the Last Glacial Maximum, the coastline of western Kefalonia extended between 0.5 and 8 km further out to sea as Late Quaternary sea levels dropped to a lowstand of -120 m exposing the shallow coastal areas of Paliki (Figure 7.19). The northern coastline of Thinia extended around 5 m further north while the southern coast was around 18 km further south as Paliki became completely joined to the rest of Kefalonia.

During this time two major drainage valleys were active in Thinia which can still be seen in the topography of the valley (Figure 1.31), one draining to the north and one draining southwards as glacial streams draining from the watershed in the Petrikata Quarry area incised down towards sea level. These eroded into the soft Plio-Miocene sediment of the valley leaving the more resistive limestone to form sharp ridges in the topography. The southwards draining stream split into two, one draining into Agia Sotira inlet, the other exiting along the proposed southern exit of "Strabo's Channel".

After leaving Thinia, the south-draining stream developed into a major, Late Quaternary-Holocene deeply-incised river valley where the Gulf of Argostoli now exists which was mapped by the shallow marine seismic reflection survey and presented in Section 6.3.4 (Figure 6.28).

Figure 7.19 Paleo-shoreline of Western Kefalonia during the Last Glacial Maximum (LGM) sea level lowstand (21 500 BP to ~16 000 BP) (ignoring tectonic affects) when sea level was 120 m below present day levels. The -120 m contour is indicated by a dashed line. Black dotted lines indicate the proposed key drainage patterns from Thinia. The locations of suspected lakes (dark blue) within the subaerially exposed Gulf of Argostoli are marked by numbers 1 to 3. The question mark indicates the possible drainage pattern detected by the postglacial isochron for Agia Kiriaki Bay (Figure 6.41).

This river valley was formed as the stream eroded into the tectonised pre-Holocene sediments making up the shelf between Paliki peninsula and the rest of Kefalonia. The course of this river valley was controlled by faulting, initially running along the footwall of the Ainos Thrust before breaking through the NNW-SSE trending zone of Hellenide deformation running up the centre of the Gulf to follow the footwall of the Argostoli Peninsula thrusts. Three deep, flat-bottomed areas were identified (labelled as 1 to 3 on Figure 7.19) which were interpreted as freshwater lakes which existed prior to marine inundation. The upper two formed depocentres (marked on Figure 6.29) during deposition of postglacial sediments as shown by the postglacial sediment isochron created in Section 6.3.2 (Figure 6.11).

B. Transgression of Sea into the Gulf of Argostoli (formation of the Gulf of Argostoli ria), ~8400 BP (-34 m)

After the glacial lowstand, postglacial sea levels rose (Figure 1.40, C) eventually flooding the deeply-incised river valley incised into the Gulf of Argostoli to form a "ria" as discussed in Section 6.6.3, Part A (Figure 7.20). The postglacial flooding map for the Gulf (Figure 6.45) suggested that flooding of the river valley was a relatively rapid event (tens to hundreds of years). The steep-sided nature of the valley meant that while postglacial sea level continued to rise, the position of the coast, particularly in the inner Gulf, stayed at a similar position. The flooding of the possible lakes within the inner Gulf led to swamping of organic matter and generation of the shallow biogenic gas imaged by the seismic survey described in Section 6.3.2, Part A and mapped in Figure 6.14.

While the southern part of Paliki and the Argostoli Peninsula still extended some 5 km further south than they do presently, the coastline of Northern Paliki during this time looked similar to present day.

Figure 7.20 Paleo-shoreline of Western Kefalonia during initial transgression of sea into the Gulf of Argostoli flooding the deeply-incised river valley to form a ria, following the last glacial lowstand (~8400 BP) (ignoring tectonic affects). The -34 m contour is indicated by a dashed line. Black dotted lines indicate the proposed key drainage patterns from Thinia.

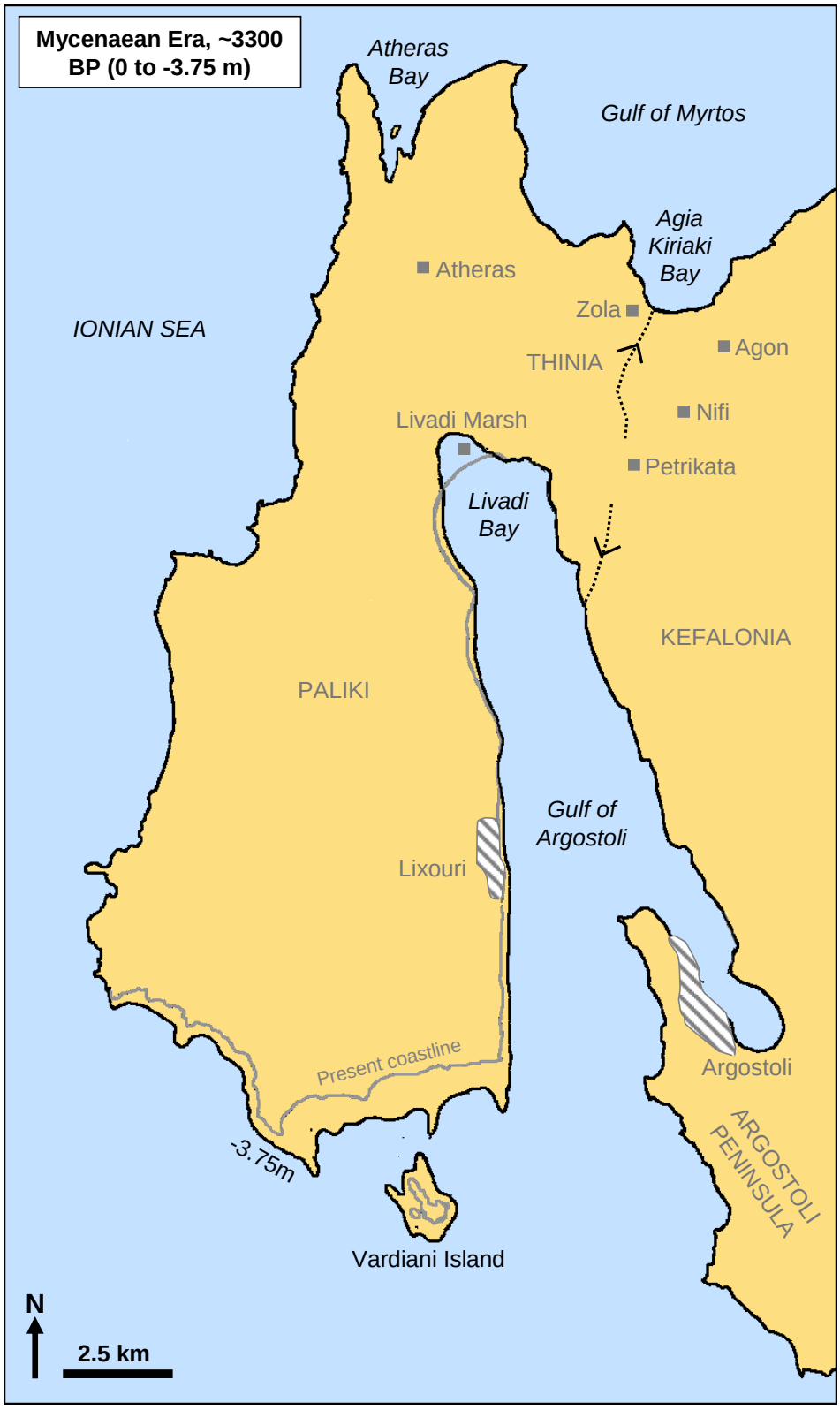

Figure 7.21 Paleo-shoreline of Western Kefalonia during Mycenaean times (~3300 BP) when sea level was around 0 to 3.75 m below present day levels (ignoring tectonic affects). Black dotted lines indicate the proposed key drainage patterns from Thinia. At this time, Livadi Marsh was flooded to a depth of around 1.2 m.

C. Mycenaean Era (Late Bronze Age), ~3300 BP (0 to -3.75 m)

The coastal configuration for the Mycenaean Era was very similar to the present day coastline (Figure 7.21). The shallow reefal islands of Vardinoi and in Atheras Bay may have been larger but unlikely to have been connected to the shore at this point. During this time the low-lying Livadi Marsh at the head of the Gulf of Argostoli was flooded to a depth of around 1.2 m as demonstrated by the radiocarbon dating of core C6c in Section 5.3.2. Assuming similar sedimentation rates to the marsh, the flat-bottom, low-lying valley in Northern Thinia may also have been flooded but this wouldn't have extended much further inland than the village of Zola.

The difference between the coastline during the Last Glacial Maximum and Mycenaean Era demonstrated the rapid (~20 000 years) and dramatic change in coastal configuration caused by postglacial sea level rise after the glacial sea level lowstand. From around 8000 BP to present day there was less of a change in the coastal configuration. Changes in the coastline were mainly caused by sedimentation as rising sea levels slowed to reach 0 m. The most notable changes are the "drying out" of Livadi Marsh due to accumulation sediments and formation of a land spit across the marsh entrance preventing further inundation.

7.2.4 Implications for "Strabo's Channel"

The "Strabo's Channel" theory proposed by Bittlestone et al. (2005) stated that during the Late Bronze Age the Paliki peninsula was entirely separated from the rest of Kefalonia by a seaway located where the Thinia isthmus now stands extending from Agia Kiriaki Bay in the north to the Gulf of Argostoli in the south. This channel subsequently disappeared since the time of Odysseus to leave a land-bridge (the Thinia valley) connecting Paliki peninsula to Kefalonia. The geological sketch map produced by J. Underhill for Bittlestone et al. (2005) (Figure 1.37) detected *in situ* bedrock at the surface of the valley. Ruling out a major fall in global sea level (around 210 m in 2000 years) which would have left a marine channel "high and dry" and significant coseismic uplift which might have uplifted the valley from

Mycenaean sea level (0 to -3.75 m) to its present elevation, "Strabo's Channel" could only have taken the form of a narrow (70 to 200 m wide) gorge incised into the marl bedrock. The resulting channel route proposed by Bittlestone et al. (2005) followed the valley axis (indicated in Figure 1.53 as a dark blue area).

Bittlestone et al. (2005) suggested that down-cutting of the two glacial streams within Thinia leading up to and during the sea level lowstand of the Last Glacial Maximum (LGM) could have led to the formation of "Strabo's Channel". If these were allowed to incise into the marl bedrock enough to reach 0 to -3.75 m the resulting deep gorges could then be inundated by marine waters when postglacial sea level reached its maximum. "Strabo's Channel" was then subsequently infilled through collapse of its vertiginous sides (particularly in the central and southern sector of the valley) and deposition of (Late Holocene) sturzstrom landslide deposits into the seaway through repeated large-scale sloughing of the valley sides, a process which took place over less than 3300 years. The volume of landslide material required to fill this channel would be in the region of 4×10^4 km^3.

Straight away the high topography (Figure 1.32) and geology of Thinia (Figure 3.29) presented problems for the theory. While fitting such a channel in the northern part of the valley would be relatively easy (Figure 1.33), in the high elevation central and southern sectors the channel would have to take the form of a vertiginous, deep (up to 210 m deep) gorge in order to reach sea level. A similar modern structure to this would be the Corinth Canal (Figure 7.22). The Corinth Canal is 6.3 km long and reaches a maximum height of 75 m above sea level and 10 metres below sea level and excavation of it was started in the 1880s (Anagnostopoulos et al., 1991). The Canal is built within marls which show remarkable stability given the vertiginous-sides of the canal and the degree of seismic activity experienced by the area which was believed to be due to cementation of the marl grains due to shear stress (Anagnostopoulos et al., 1991).

Initial observations of Thinia valley (Figure 1.37) suggested the geomorphology and geology was favourable for the presence of a landslide buried channel gorge. The

lower slopes of the valley consisted of easily-eroded soft marls leading to severe undercutting of the denser limestone and conglomerate emplaced on top of the marl and slope collapse. Slumping of the marl and clay was particularly prevalent along the Agia Kiriaki Bay shoreline where the soft, steeply-dipping (40 to 60º) sediments had been undercut by wave action along the shoreline and also down the V-shaped stream gullies draining from Imerovigli. Collapse of the limestone valley sides was actively occurring along the entire length of the valley, particularly in southern Thinia (Figure 1.36) generating large boulders.

Figure 7.22 In the central and southern sector of Thinia, "Strabo's Channel" would have to assume the form of a vertiginous gorge to reach sea level or close to sea level. An analogous structure in the modern world is Corinth Canal, Greece. Image source: Wikipedia (left) and Google Maps (right).

However, the results of this study were not favourable for a buried channel. The new surface geology map (Figure 3.29) constrained the surface extent of colluvial depositions within the valley as well as carefully mapping the location of *in situ* bedrock. This map showed that colluvial deposits (shaded grey in Figure 7.23) were not as widespread as previously believed. The revised route of "Strabo Channel" (dark blue in Figure 7.23) was restricted even further by *in situ* bedrock. In

particular, the discovery of a previously unmapped thrust fault (the "Petrikata Thrust") as described in Section 3.3.2 restricted the route at Petrikata Quarry to less than 50 m across. Borehole C1, as described in Section 5.3.4 penetrated the hangingwall of an easterly-dipping thrust fault (Figure 5.12) demonstrating that the high elevation Petrikata Quarry limestone outcrop was also part of a thrust. The presence of these thrusts meant that even a vertiginous channel at this central location would still encounter limestone bedrock long before reaching sea level (c. 140 m above sea level). This would mean "Strabo's Channel" could not have been continuous from north to south. While a narrower, discontinuous gorge reduced the amount of infilling landslide material required for infill, it pushed the boundaries as to what was physically possible. While the easily-eroded nature of the Thinia marls could feasibly have allowed formation of such a channel, it is unlikely such a structure could become established as a navigable seaway particularly in the central and southern sector of "Strabo's Channel" due to the high instability of these sediments as the marine waters of the channel continually undercut the vertiginous gorge sides. Also, the amount of observed down-cutting by the glacial streams into the marl bedrock (around 60 to 70 m, Figure 3.27) falls far short of the 200 m+ required to allow these streams to reach sea level to allow the formation of "Strabo's Channel" in the high elevation central and southern parts of the valley.

The geophysical surveys showed that the Thinia valley was composed of conductive, magnetic, low density sediments to a depth of up to 500 m overthrust by resistive, dense limestone ridges. However, these surveys were unable to differentiate between the physically very similar recent colluvial fill and bedded marls nor could they detect the sides or bottom of a possible buried channel. The shallow sedimentary coring of the valley fill provided the most conclusive results. The key boreholes which penetrated the proposed channel route were (from north to south) C2, C1, C4a, C4c, C2006-2 and C2006 (indicated on Figure 7.23 in red). While there was extensive surface evidence of colluvial and alluvial material across the proposed route of "Strabo's Channel" there was a significant lack of Late Holocene clastic deposits within these cores.

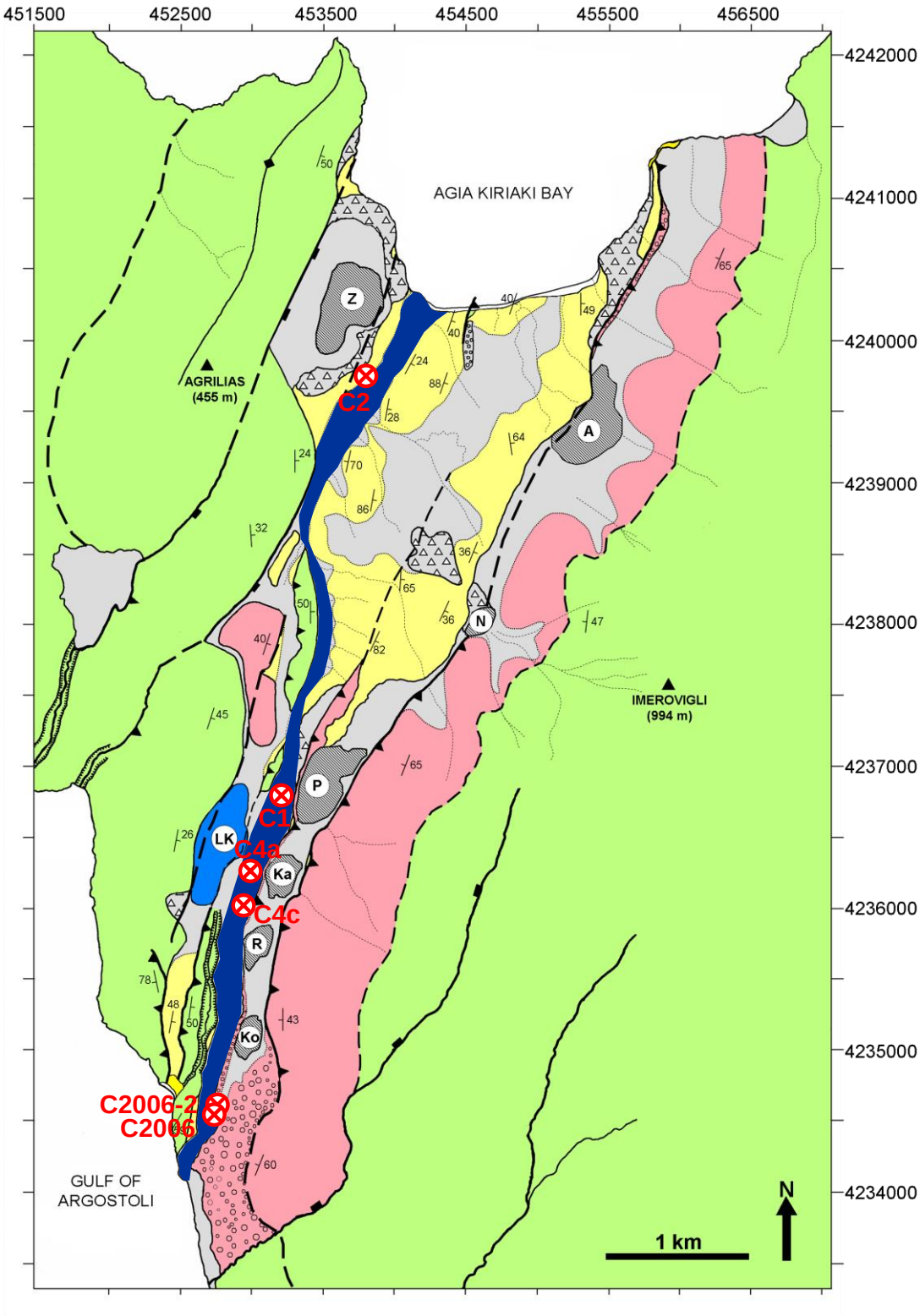

Figure 7.23 The revised route of "Strabo's Channel" in the case of a buried, untranslated channel deduced from the surface geology map created from field-mapping undertaken as part of this thesis. The locations of boreholes which penetrate the proposed Channel route (C2, C1, C4a, C4c, C2006-2 and C2006) are marked in red.

Instead, coring revealed that the sediments were composed of a thick deposit of south-easterly-dipping (40 and 60°) Early to Middle Miocene (Serravalian to Burdigalian) – Early Pleistocene (Gelasian) sediments deposited in an open marine, neritic (less than 50 m water depth) setting. The presence of these marine sediments confirmed that a substantial seaway (around 1 to 4 km across) which extended from "sea to sea" did exist here during the early Neogene to at least the Early Pleistocene (Gelasian) (1.81 Ma).

However, despite the initially promising results of the original October 2006 borehole (described in Section 2.2.3) which detected Late Quaternary material (*Emiliania huxleyi*) to a depth of 26 m [core], no new independent sediment younger than Early Pleistocene (Gelasian) was retrieved from any of the Thinia boreholes. The re-drilling of the October 2006 borehole (C2006) did not produce any samples of *Ehux* which raised questions as to whether the original *Ehux* deposits were correctly identified and this issue remains unexplained. The *Ehux* samples in the Oct 2006 were questionably small and may have been misidentified. Contamination by modern seawater during the 2006 drilling operations is one possibility although it had been thought the drilling only sourced freshwater. The samples may also have been modern windblown species which became mixed into the underlying samples as the top soils were reworked during extraction.

Figure 7.24 shows the north-south topographic cross-section established for the revised route of Strabo's Channel (dark blue line) with the proposed position of the underlying bedrock (in pink) derived from the borehole results. This shows the recent sediments only form a thin veneer, draping underlying bedrock. The recent sediment is thinnest (~ cms) at the highest part of Thinia (C1) and thickens north and southwards, particularly within the northern valley.

Ultimately, the results of the fieldmapping, non-invasive geophysical tests and coring undertaken during this PhD have definitively shown that the Thinia valley could not have contained a landslide-buried marine-level channel incised into the bedrock during the Bronze Age.

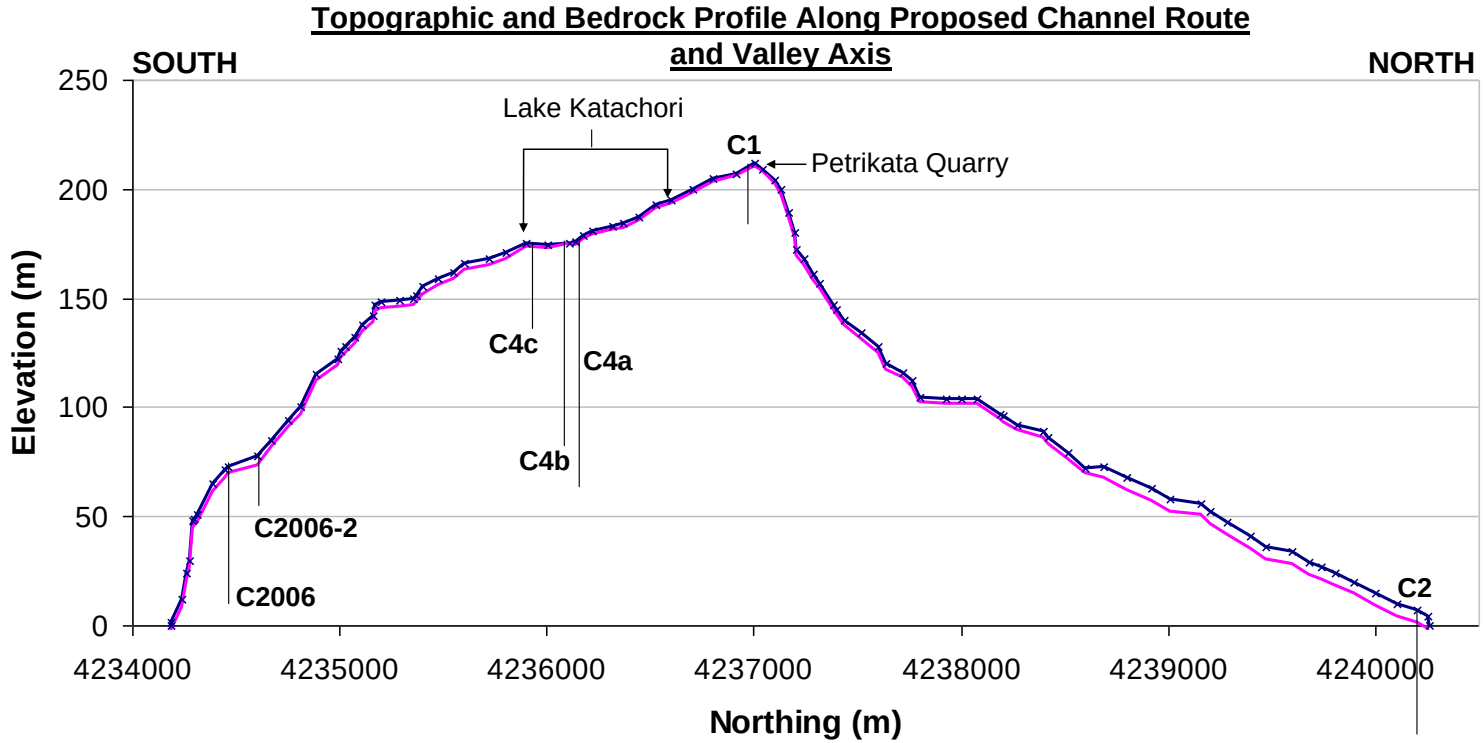

Figure 7.24 Surface topography (blue) and proposed bedrock topography (pink) (based on the findings of the boreholes) cross-section taken along the axis of the Thinia valley and most probable route of "Strabo's Channel" with the positions of boreholes which penetrated this route (from north to south): C2, C1, C4a, C4c, C2006-2 and C2006. The location of Lake Katachori is indicated.

A. Tectonically-driven Uplift and Westerly Translation

Given the degree of tectonic disturbance within Thinia and the difference in elevation of the Thinia sediments relative to the Livadi Marsh sediments which were comparable in age (around 210 m), a very tentative, alternative tectonically-driven mechanism was explored. The remains of "Strabo's Channel" may instead have been tectonically-dislocated from Mycenaean sea level and translated westwards. The folded and thrusted sediments observed in Thinia today may represent the sediments of a Late Holocene marine channel which have been compressed, folded then cross-cut and uplifted by thrust faults. However, this scenario is much harder to investigation since the softness of the valley sediments would mean evidence of the channel at the ground surface would have been eroded rapidly after formation.

A mechanism by which this could have occurred is through development of a contraction-extension linked gravity-driven spreading system (Figure 7.25 and 7.26). Contraction-extension linked gravity-driven spreading systems are usually characterised by a broad region of up-dip (headwall) extension which is linked to a region of down-dip contraction via weaker detachment layers such as shale, marls or salt (Morley and Guerin, 1996; Rowan et al., 2004). Such a system could have been formed if a large coherent rotational-translational slump from the valley side was introduced into the soft sediment of the valley, pushing up the sediments ahead in a "toe-thrust complex".

The key point of investigation in this scenario is therefore determining the timing of the uplift of the Thinia sediments and determining a source for this uplift. The approximately 150 m offset of the Ainos Thrust at Agia Ioanni may offer a source for this uplift. In Section 3.3.4, a 1 x 4 km "clast" was identified within the hangingwall of the Ainos Thrust. Tracing the "Agia Ioanni Fault", identified as a major extensional dislocation defining a pronounced valley, inland it forms a curvi-linear structure best seen from Livadi Bay (Figure 3.21 and 3.22). Crucially, this fault appears to have a listric plane which continues below the Gulf. Following the curve

around it would either décolle in the Miocene marl or connect with the Atheras Thrust. If this listric fault connected with the Atheras Thrust then the whole of the central and southern sector of the Thinia valley might represent a massive linked array of up-dip (headwall) extension (Agia Ioanni Fault) and down-dip contraction (Petrikata Thrust, Agia Sotira Thrust and Atheras Thrust) (Figure 7.27 and 7.28).

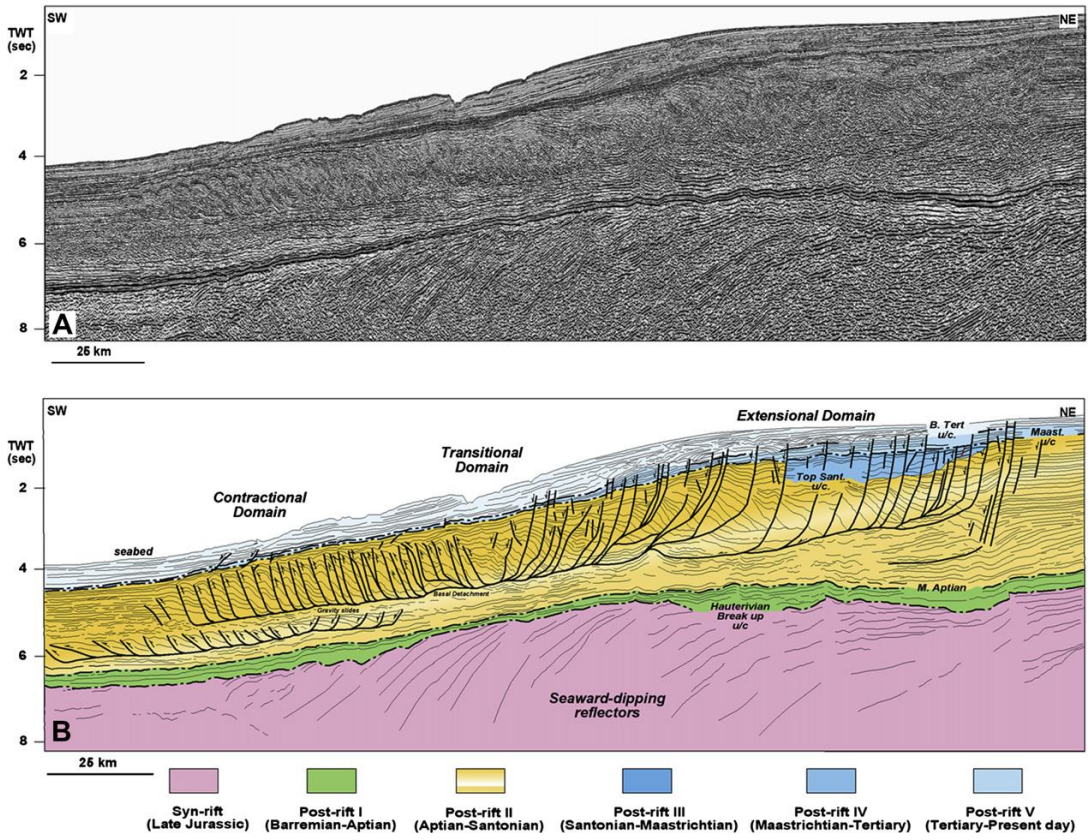

Figure 7.25 Marine seismic reflection line from depicting contraction-extension linked gravity spreading (from Vera et al., 2010).

In terms of timing, as the youngest sediment to be overthrust by the Ainos Thrust is Early Pleistocene (Gelasian) in age (sampled in C4c and C1), the formation of the Agia Ioanni Fault must be younger than 1.81 Ma. The focus of future investigation would therefore be determining slippage history of the suspected "Agia Ioanni fault" plane. An age and for this fault could be derived through ^{36}Cl cosmogenic dating of the slip plane, a method which uses in-situ cosmogenic nuclide isotopes to determine when a slip plane surface was exposed to cosmic rays. Also, if the Atheras Thrust represented the basal sole of this rotational fault this placed importance on dating the

youngest Livadi Marsh sediments to be overthrust, dating activation of the entire rotational system.

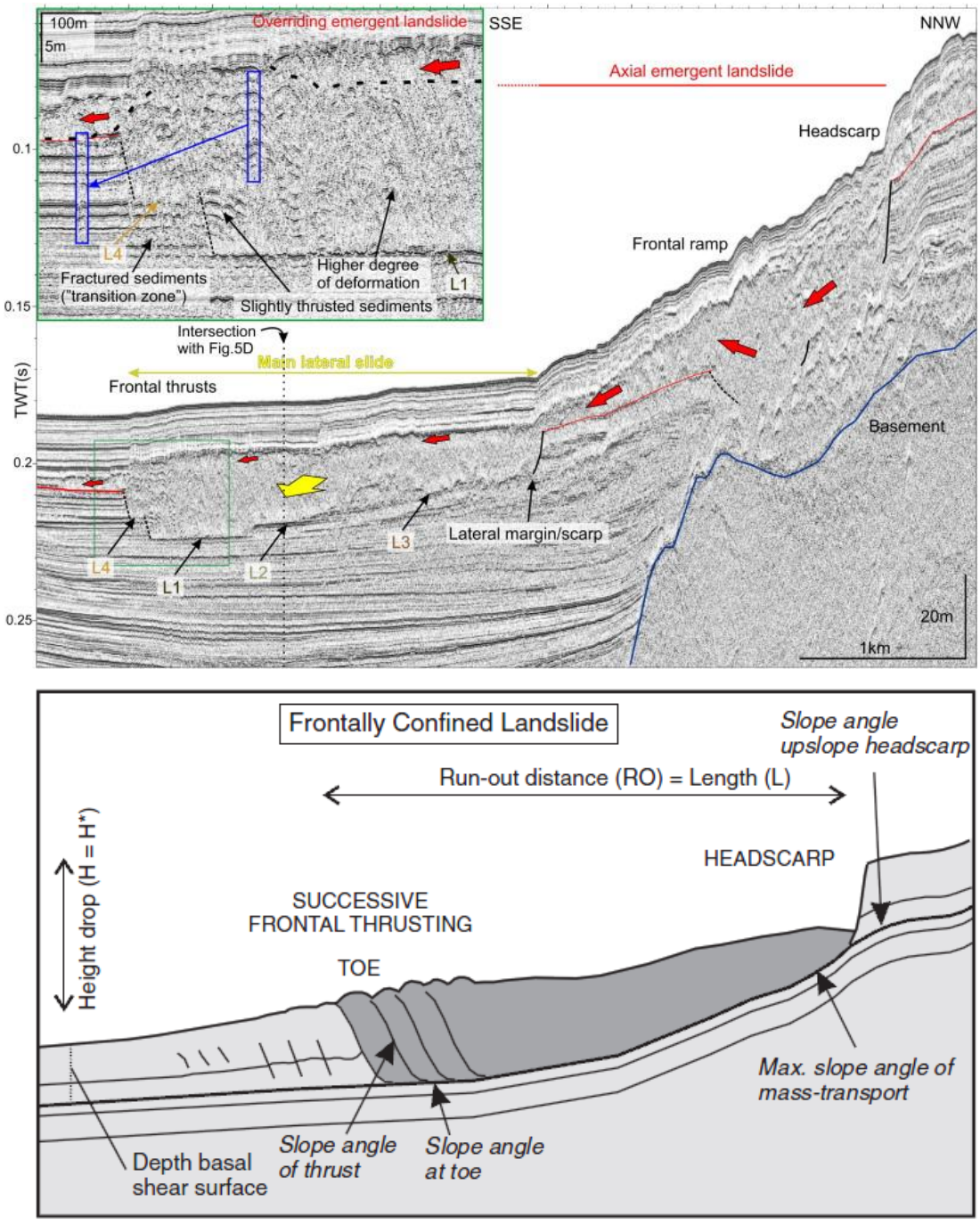

Figure 7.26 Interpreted reflection seismic line illustrating compressional-extensional structure resulting from a landslide in Lake Le Bourget emerging from the paleo-Rhône fan delta slope (top). Schematic diagram (below) of frontally confined landslide showing formation of toe-thrusts at compressional head and extensional scarp at top of landslide (Moernaut and De Baptist, 2011).

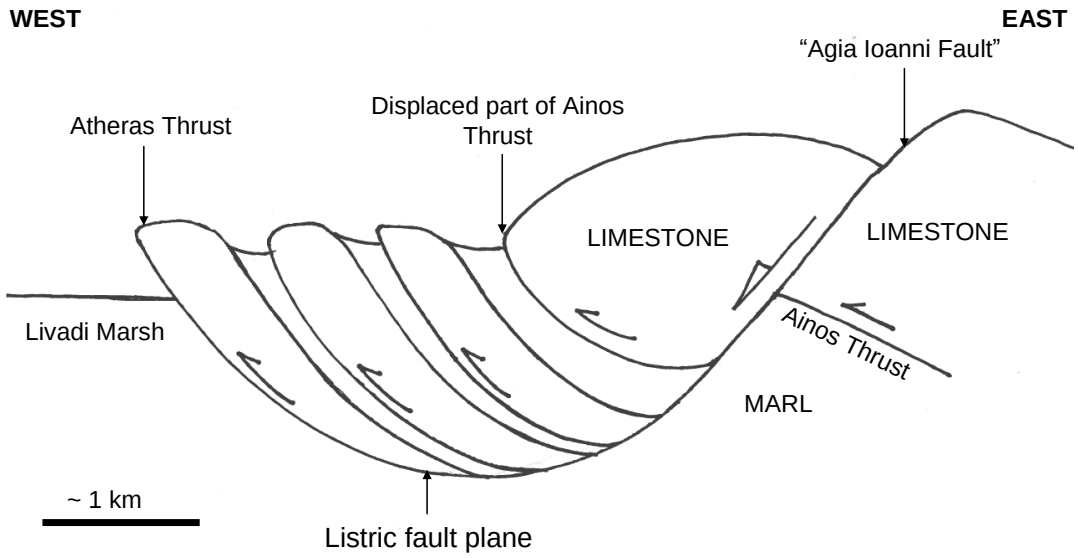

Figure 7.27 Cartoon sketch of possible rotational block configuration in Thinia.

This tectonic model may explain some of the unusual features observed within Thinia such as the ~150 m offset of the Ainos Thrust observed at Agia Ioanni Bay and reactivation of the Cretaceous-Paleogene release faults affecting the sediments (Section 7.2.1, Part H) and imaged as lateral offsets in the gravity survey. These release faults may have been reactivated to accommodate movement of this large rotational block and could therefore be explained in terms of lateral ramps linking sections of uplift and westwards translation of the Thinia sediments.

However, the unavoidable issue with this alternative theory is the timing of initiation of the slump within the Ainos Thrust hangingwall. It is highly unlikely that such a slump and uplift would occur in only 3300 years. It also cannot explain the complete lack of recent, marine sediments within Thinia which would be expected to be found within the valley axis. Ultimately, it is very unlikely that so little evidence would remain from what would have been such a dramatic feature.

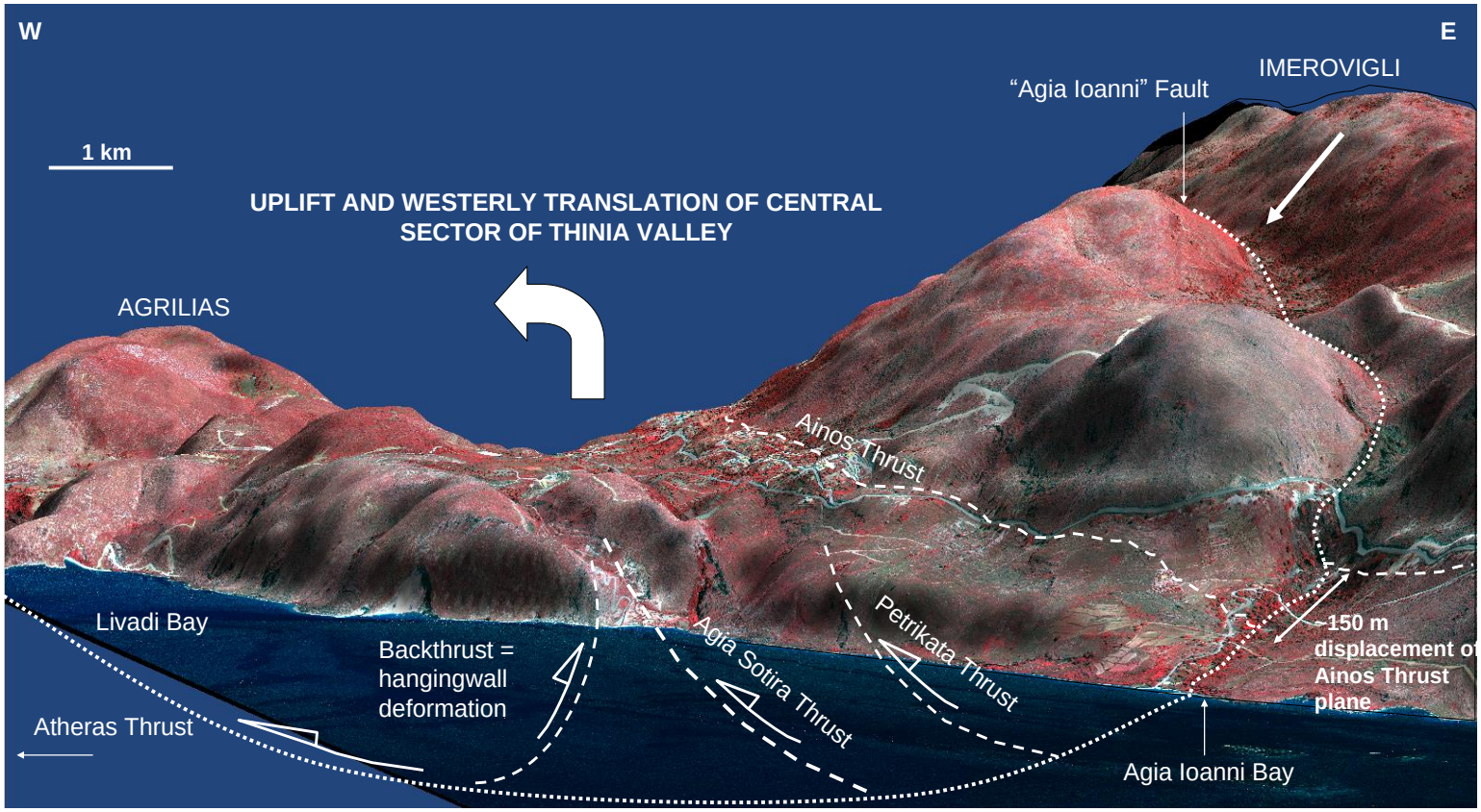

Figure 7.28 View of Thinia from Livadi Bay showing possible interpretation in relation to a linked array of up-dip (headwall) extension and down-dip contraction akin to rotational deformation. Produced on the OziExplorer3D mapping visualization software using the 100 pc false colour Quickbird satellite map draped over a 3-dimensional grid. Vertical exaggeration is 1.5.

7.3 Suggestions for Future Work

Given sufficient time and budget the following proposals for are put forward.

7.3.1 Offshore drilling and sampling

The absence of age-dating cores within the Gulf of Argostoli and Agia Kiriaki Bay has meant that decisive stratigraphic ages could not be determined for the offshore megasequences. Age-dating is crucial as it would greatly improve interpretation of these sequences and allow construction of a relative sea level curve for Paliki which will take into account tectonic affects on sea level and make inferences on the postglacial flooding and paleo-geographic reconstructions of the coastal areas of the isthmus more accurate. A proposal for marine boreholes based on the interpretations in Chapter 6 is presented in Appendix F.

7.3.2 Onshore drilling and sampling

Onshore drilling and sampling is lower priority with the exception of two areas:

1. Drilling on the eastern side of the Thinia valley where the youngest marine sediments were found: The coring survey undertaken for this thesis did not extend far enough to the east to determine the youngest sediments overthrust by the Ainos Thrust. This would require drilling down through the hangingwall of the thrust into the sediments of the footwall.

2. Drilling of the eastern side of Livadi Marsh: Drilling through the Atheras Thrust into the footwall sediments would determine the age of the youngest sediments to be overthrust by the Atheras Thrust and whether the Ionian sediments sampled on the western side of the marsh were overthrust or if they formed a more recent marine onlap onto the Atheras Thrust hangingwall.

7.3.3 Onshore fieldmapping and sampling

1. Southern slopes of southern Thinia: In the case that "Strabo's Channel" had been uplifted and translated by the possible rotational slump described in Section 7.2.4, A, this might explain the exclusive presence of *Ehux* deposits in the Oct 2006 borehole if it had been drilled into the remaining shallow wedge-tip of the uplifted channel (the rest of the channel being eroded through surface drainage). This makes the investigation of the near-shore of the proposed southern exit supplemented by auguring a high priority (Figure 7.29).

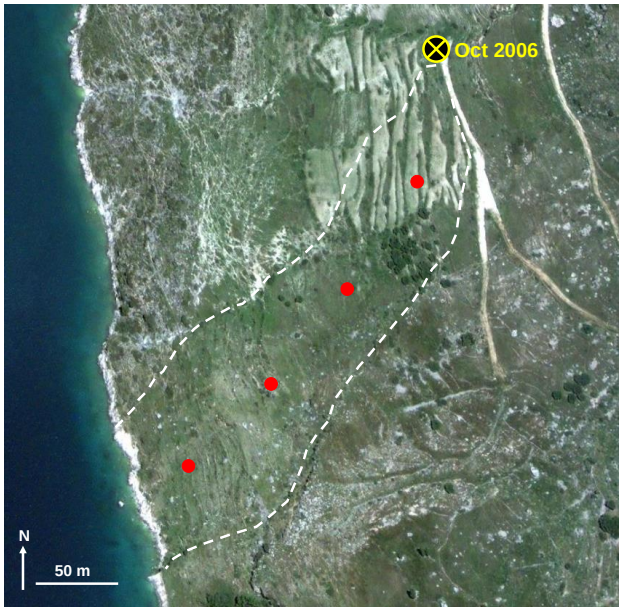

Figure 7.29 Proposed augur or borehole locations (red) to investigate whether the southern portion of Strabo's Channel (white dashed outline) has been uplifted due to the uplift and westwards translation of the Thinia (and channel sediments) due to the rotational slump.

2. Auguring of soil base of lithified flow: Dating of the base of the debris flow depicted in Figure 3.15 (as a dashed black line).

3. "Agia Ioanni Fault": Identification of sample locations along the suspected fault scarp for cosmogenic sampling in order to age-date the formation of this scarp.

7.4 Conclusions

Integration of geophysical, geological and geomorphic methods has provided a new-found basis by which to evaluate the hypothesis that Odysseus' homeland, Ancient Ithaca, was sited on the Paliki peninsula of Kefalonia rather than the Ionian Island bearing its name today. The following conclusions can be drawn from this study:

1. The geology and geomorphology of Thinia was far more complicated than originally believed with the bedrock geology recording the Cretaceous-Quaternary evolution of an extensional-compressional regime brought about through the foreland-migration of the Hellenide fold-and-thrust deformation in the Early Miocene which reactivated earlier south-easterly-dipping extensional faults. The peninsula was affected by further neotectonic deformation caused by the formation of the Kefalonia Transform Fault (KTF). The resulting steep slopes lend themselves to collapse and represent geomorphic failure due to structural feedback.

2. The shallow marine seismic reflection survey showed striking differentiation between the tectonised "pre-Holocene" and onlapping postglacial sediments separated by a prominent erosional surface associated with the Last Glacial Maximum (LGM) (~21 500 BP) sea level lowstand of -120 m. The survey detected a major drainage buried valley deeply-incised into the pre-Holocene of the Gulf of Argostoli indicating that during this lowstand a major glacial fluvial system drained from Thinia. During postglacial sea level rise this valley was infiltrated by marine waters to form a ria, flooding two large glacial lakes which acted as depocentres for postglacial sediments. This process may have led to the formation of "Strabo's Channel" and its subsequent infill resulting from lacustrine and marine onlap. A similar drainage system was not detected to the north (Agia Kiriaki Bay) due to erosion and winnowing from marine currents.

3. The onshore tests detected a thick deposit of steeply-dipping and tectonised marine sediments within the valley which coring dated to the Early Miocene to Early Pleistocene (Gelasian). This indicates marine waters existed along the valley until at least 1.80 million years ago, an order of magnitude younger than previously reported. However, the Quaternary and Holocene deposits (*Ehux*) detected by the original Oct 2006 borehole were found to be completely absence in the re-drilling of this borehole (C2006) and were also not found in the adjacent borehole (C2006-2) drilled into the proposed Channel axis deduced from the Oct 2006 data. As such, no new independent sediment younger than Early Pleistocene (Gelasian) was retrieved within Thinia.

4. While the prevalence of slope collapse of the steep valley sides favoured the idea that "Strabo's Channel" was infilled through repeated deposition of landslide debris into its narrow gorge, the geophysical surveys and cores failed to detect the sides or bottom of a channel or evidence of substantial clastic debris within the subsurface thus ruling out the possibility of a buried marine-level channel which extended from "sea-to-sea".

5. Radiocarbon dating of core samples from Livadi Marsh suggested that the marsh was flooded during the Bronze Age to a depth of 1.2 to 5 m making it a candidate for Ancient Ithaca's harbour. However, there was no evidence for significant coseismic uplift or structural reactivation since the Late Bronze Age ruling out a major change in relative sea level due to earthquake-driven tectonic uplift in the Thinia area. The current coastal location of the marsh was due to progradation and aggradation of marsh sediments and establishment of a land spit at the shoreline preventing further inundation from the sea with no more than 1.2m of coseismic uplift relating to more recent (within the last 1700 years) historic coseismic events.

6. The presence of freshwater algae within the upper few metres of the cores confirmed a lacustrine environment existed at the Lake Katachori site

however the geophysical and core evidence showed that the lake deposits were very shallow (no more than 6 m thick) and sited on steep, easterly-dipping Plio-Pleistocene sediments uplifted to ~170 m above sea level. The occurrence of this algae admixed with uppermost Plio-Pleistocene (Gelasian) sediments suggested departure from marine depositional setting occurred in Thinia sometime after Early Pleistocene times (1.80 Ma).

7. The lack of Holocene-Late Quaternary sediment relating to an uplifted marine channel and the presence of Lake Katachori may be explained through the uplift and westwards translation of the sediments of central Thinia through establishment of a contractional-extensional linked gravity driven rotational slip linking the listric "Agia Ioanni Fault" with the Atheras Thrust. In favour of this, the boreholes within the valley detected shear-thrusting and steep dips within the Miocene and Plio-Pleistocene marl sediments demonstrating that the area experienced strong tectonic dislocation which is in favour of this model however further tests are required to investigate this and the exact timing of this slump (through cosmogenic age-dating) which is younger than 1.80 Ma as it may have uplifted, deformed and eroded any evidence of a Late Holocene marine channel within the sediment record.

References

*Note on reference citation convention

The references section has been divided into two sections to accommodate the diversity of sources used during this investigation: 1) “Classic” style of scientific references, 2) Web references.

1. References

Accordi, G., Carbone, F., and Pignatti, J. (1998). Depositional history of a Paleogene carbonate ramp (western Cephalonia, Ionian Islands, Greece): Geologica Romana, Vol. 34, 131–205.

Adams, J. (1981). Earthquake-dammed lakes in New Zealand. Geology, Vol. 9, 215-219.

Adams, J. (1980a). Contemporary uplift and erosion of the Southern Alps, New Zealand. Geological Society of America Bulletin, Part II, Vol. 91, 1-114.

Airy, G. B. (1855). On the computation of the effect of the attraction of mountain-masses, as disturbing the apparent astronomical latitude of stations in geodetic surveys: Philosophical Transactions of the Royal Society of London, Vol. 145, 101–104.

Allen, P. A., Homewood, P. and Williams, D. (1986). Foreland basins: an introduction. In: Allen, P. A. and Homewood, P. (Eds.). Foreland Basins. Special Publication of the International Association of Sedimentologist, Vol. 8, 3-12.

Anagnostopoulos, A. G., Kalteziotis, N., Tsiambaos, G. K. and Kavvadas, M. (1991). Geotechnical properties of the Corinth Canal marls. Geotechnical and Geological Engineering, Vol. 9, Issue 1, 1-26.

Anderson, A. L., Abegg, F., Hawkins, J. A., Duncan, M. E. and Lyons, A. P. (1998). Bubble populations and acoustic interaction with the gassy sea floor of Eckernforde Bay. Continental Shelf Research, Vol. 18, No. 14, 1807‑1838.

Anderson, H. and Jackson, J. (1987). Active tectonics of the Adriatic region. Geophys. J. R. Astron. Soc., Vol. 91, 937-983.

Anzidei, M., Baldi, P., Casula, G., Crespi, M. and Riguzzi, F. (1996). Repeated GPS surveys across the Ionian Sea: evidence of crustal deformations, Geophys. J. Int., Vol. 127, 257-267.

Aubouin, J. (1959). Contribution à l'étude géologique de la Grèce septentrionale: les confines de L'Épire et de la Thessalie. Annls géol. Pays hell, Vol. 10, 1-525.

Aubouin, J. (1965). Geosynclines. New York (Elsevier).

Aubouin, J. and Dercourt, J. (1962). Zone Preapoulien, Zone Ionienne et Zone de Gravrovo en Pelloponnese occidentale. Bull. Soc. Geol. Fr., Vol. 4, 785-794.

Aubouin, J., Bonneau, M., Davidson, J., Leboulenger, P., Matesco, S. and Zambetakis, A. (1976). Esquisse structurale de l'arc Egéen externe: des Dinarides aux Taurides. Bulletin de Sociétè Gèologique de France, Vol. 7, No. 43, 327-336.

Babbage, C. (1847). Observations on the Temple of Serapis, at Pozzuoli, near Naples, with remarks on certain causes which may produce Geological Cycles of great extent. Quaternary Journal of the Geological Society, Vol. 3, 186 – 217.
DOI: 10.1144/GSL.JGS.1847.003.01-02.22

Bache, F., Olivet, J. L., Gorini, C., Rabinaeu, M., Baztan, J., Aslanian, D. and Suc, J.-P. (2009). Messinian erosional and salinity crises: View from the Provence Basin (Gulf of Lions, Western Mediterranean). Earth and Planetary Science Letters, Vol. 286, Issues 1-2, 139-157.

Badley, M. E. (1985). Practical seismic interpretation. International Human Resources Development Corporation (Boston).

Bard, E., Hamelin, B. and Fairbanks, R. G. (1990). IJ-Th age obtained by mass spectrometry in corals from Barbados: sea level during the past 130 000 years. Nature, Vol. 340, 456 - 458.

Bittlestone, R., Diggle, J. and Underhill, J. R. (2005). Odysseus Unbound: The Search for Homer's Ithaca. Cambridge, UK: Cambridge University Press.

Bizon, G. (1967). Contribution a la connaissance des Foraminfères planctoniques d'Épire et des iles ioniennes (Grèce occidentale) depius le Paléogène supérieur jusqu'au Pliocène [Ph.D. thèses]. Publications de L'Institut Français du Petrole.

Boggs Jr., S. (2006). Principles of Sedimentology and Stratigraphy. Pearson Prentice Hall: Upper Saddle River, New Jersey.

Borgomano, J. R. F. (2000). The Upper Cretaceous carbonates of the Gargano-Murge region, southern Italy: A model of platform-to-basin transition. AAPG Bulletin, Vol. 84, No. 10, 1561-1588.

Bousquet, B., Dufaure, J. J., Keraudren, B., Pechoux, P. Y., Philip, H. and Sauvage, J. (1976). Essai de corrélations stratigraphies entre les facies marins, lacustres et continentaux du Pléistocène de Grèce. Bulletin de la Société Géologique de la France, Vol. 18, 413-418.

Boyer, S. R. and Elliott, D. (1982). Thrust systems. American Association of Petroleum Geologists Bulletin, Vol. 66, 1196-1230.

Boyd, T. (1999)[1]. Gravity: Introduction to Geophysics Short Course Assignments (lecture notes).University of Melbourne.

Boyd, T. (1999)[2]. Resistivity: Introduction to Geophysics Short Course Assignments (lecture notes).University of Melbourne.

Boyd, T. (1999)[3]. Seismic Refraction: Introduction to Geophysics Short Course Assignments (lecture notes).University of Melbourne.

Braune, K. (1973). Die rezenten und pleistozaenen Sedimente des Sublitorals von Kephallinia (Ionische Inseln): Senckenbergiana Maritima, Vol. 5, 99–133.

British Petroleum Co. Ltd. (1966). Geological map of Kefallinia (1:100 000).

British Petroleum Co. Ltd. (1971). The geological results of petroleum exploration in western Greece: Athens, Greece. Institute for Geological and Subsurface Research, Report No. 10.

British Petroleum Co. Ltd., Bergmann, H., Braune, K., Dremel, G., Hatzopoulos, E., Hug, F., Uliczny, E. and Migiros, G. (1985). Geological Map of Greece, 1:50 000 scale, Cephalonia Island (Northern and Southern parts), Institute of Geology and Mineral Exploration.

Butler, R. H. W. (1982). The terminology of structures in thrust belts. Journal of Structural Geology, Vol. 4, 239-245.

Chai, H. J., Liu, H. C. and Zhang, Z. Y. (2000a). The temporal–spatial distribution of damming landslides in China. J Mt Sci. 18 (Supplement), 51–54 (in Chinese).

Chai, H. J., Liu, H. C., Zhang, Z. Y. and Wu, Z.W. (2000b). The distribution, causes and effects of damming landslides in China. J Chengdu Inst. Technol., Vol. 27, 1–19 (in Chinese).

Chamot-Rooke, N., Rabaute, A. and Kreemer, C. (2005). Western Mediterranean Ridge mud belt correlates with active shear strain at the prism-backstop geological contact. Geological Society of America, Vol. 33, No. 11, 861-864.

Clarke, P. J., Davies, R. R., England, P. C., Parsons, B., Billiris, H., Paradissis, D., Veis, G., Cross, P. A., Denys, P. H. Denys, Ashkenazi, V., Bingley, R., Kahle, H. –G., Muller, M. –V. and Briole, P. (1998). Crustal strain in central Greece from repeated GPS measurements in the interval 1989-1997. Geophys. J. Int., Vol. 135, 195-214.

Clews, J. E. (1989). Structural controls on basin evolution: Neogene to Quaternary of the Ionian zone, Western Greece. Journal of the Geological Society, London. Vol. 146, 447-457.

Cloos, E. (1955) Experimental analysis of fracture patterns Geol. Soc. Am. Bull., Vol. 66, 241-256.

Conispoliatis, N. (1984). Study of the sediments of Strymonicos Gulf. PhD. Thesis (in Greek). National Technical University of Athens, Greece.

Costa, J.E. and Schuster, R. L. (1988). The formation and failure of natural dams. Geol Soc Amer. Bull., Vol. 100, 1054–1068.

Cushing, E. M. (1985). Evolution structurale de la marge nord oust Hellénique dans l'Ile Levkas et ses environs (Grèce nord-occidentale). These du 3e cycle. Université de Paris-Sud, Centre d-Orsay.

Dai, F. C., Lee, C. F., Deng, J. H., Tham, L. G. (2005). The 1786 earthquake-triggered landslide dam and subsequent dam-break flood on the Dadu River, southwestern China. Geomorphology, Vol. 65, 205–221.

D'Anville, J. -B. B. (1768). Géographie Ancienne Abrégée. Merlin, Paris.

Dercourt, J. (1959). Sur la geologie du Peloponnese Occidental. Remarks sur le massif du Scolis (Achaia. Grece), Prakt. Akad. Athenon, Vol. 34, 96-100.

Destro, N., Szatmari, P., Alkmim, F. F. and Magnavita, L. P. (2003). Release faults, associated structures, and their control on petroleum trends in the Recôncavo rift, northeast Brazil. AAPG Bulletin, Vol. 87, No. 7, 1268-1279.
DOI: 10.1 306/02200300156.

Dewey, J. E., Pitman, W. C. and Ryan, W. B. F. (1973). Plate tectonics and the evolution of the Alpine System. Geological Society of America Bulletin, Vol. 84, 3137-3180.

Dewey, J. F. and Sengör, A. M. C. (1979). Aegean and surrounding regions: Complex multiplate and continuum tectonics in a convergent zone. Geological Society of America Bulletin, Vol. 90, 84-92.

Dikau, R., Brunsden, D., Schrott, L. and Ibsen, M.-L. (eds.) (1996). Landslide recognition, identification, movement and causes. Chichester, Wiley.

Edwards, L. S. (1977). A modified pseudosection for resistivity and induced-polarization. Geophysics, Vol. 42, 1020-1036.

EERI Special Earthquake Report (2003). Learning from Earthquakes: Preliminary Observations on the August 14, 2003, Lefkada Island (Western Greece) Earthquake.

Eisenstadt, G. and De Paor, D. G. (1987). Alternative model of thrust-fault propagation. Geological Society of America, Vol. 15, No. 7, 630 – 633.

Evans, S. G., Hermanns, R. L., Strom, A. and Scarascia-Mugnozza, G. (2011). Natural and Artificial Rockslide Dams.

Fairbanks, R. G. (1989). A 17 000 year glacioeustatic sea-level record: influence of glacial melting rates on the Younger Dryas event and deep ocean circulation. Nature, Vol. 342, 637-642.

Fairbanks, R. G. and Matthews, R. K. (1978). Quaternary Research, Vol. 10, 181-195.

Finetti, L. (1982). Structure, stratigraphy and evolution of the central Mediterranean Sea: Bollettino di Geofisica Teorica ed Applicata, Vol. 24, 247-312.

Flemming, N. C. (1978). Holocene eustatic changes and coastal tectonics in the northeast Mediterranean: implications for models of crustal consumption. Philos. Trans. R. Soc. London, Vol. 289, 405-458.

Flemming, N. C. and Webb, C. O. (1986). Tectonic and eustatic coastal changes during the last 10 000 years derived from archaeological data. J. Geom. N.F., Vol. 62, 1-29.

Fornaciari, E. and Rio, D. (1996). Latest Oligocene to early Middle Miocene quantitative calcareous nannofossil biostratigraphy in the Mediterranean region. Micropaleontology, Vol. 42. 1-37.

Fornaciari, E., Di Stefano, A., Rio, D. and Negri, A. (1996). Middle Miocene quantitative calcareous nannofossil biostratigraphy in the Mediterranean region. Micropaleontology, Vol. 42, 38-64.

Francalanci, L., Vougioukalakis, G. E., Perini, G. and Manetti, P. (2005). A West-East Traverse along the magnetism of the south Aegean volcanic arc in the light of volcanological, chemical land isotope data. Developments in Volcanology, Vol. 7, No. 7, 65-111

Fytikas, M., Giuliani, O., Innocenti, F., Marinelli, G. and Mazzouli, R. (1976). Geochronological data on Recent magmatism of the Aegean Sea. Tectonophysics, Vol. 31, 29-34.

Fykitas, M., Innocenti, F., Manetti, P., Mazzouli, R., Peccerillo, A. and Villari, L. (1984). Tertiary to Quaternary evolution of volcanism in the Aegean region, in Dixon, J. E. and Robertson, A. H. F. (Eds.). The geological evolution of the eastern Mediterranean. London, England, Geological Society Special Publication 17, 687-699.

Gaki-Papanastassiou, H. M., Karymbalis, E. and Papanastassiou, D. (2011). Geomorphological study and paleogeographic evolution of NW Kefalonia Island, Greece, concerning the hypothesis of a possible location of the Homeric Ithaca. In Brown A. G., Basell, L. S. and Butzer, K. W. (Eds.), Geoarchaeology, Climate Change, and Suspectibility: The Geological Society of America, Special Paper 476, 69-79.
DOI 10.1130/2011.2476(06).

Galanopoulos, A. G. (1955). Seismic geography of Greece. Ann. Géol. des pays Helléniques, Vol. 6, 83-121.

Ghilardi, M. and Desruelles, S. (2009). Geoarchaeology: where human, social and earth sciences meet with technology. S.A.P.I.E.N.S. (Surveys and Perspectives Integrating Environment and Society). Vol. 2. No. 2, special issue.

Ghilardi, M., Le Rhun, J., Courel M. –F., Chamard, P., Queyrel, F., Styllas, M. and Paraschou, T. (2007). Localisation de sites portuaires pour la cité antique de Methoni (Piérie—Grèce) via l'utilisation des Modèles Numériques de Terrain, Travaux archéologiques en Macédoine et en Thrace AEMTh, Vol. 19, 317-321.

Ghilardi, M., Kunesch, S., Styllas, M. and Fouache, E. (2008). Reconstruction of Mid-Holocene sedimentary environments in the central part of the Thessaloniki Plain (Greece), based on microfaunal identification, magnetic susceptibility and grain-size analyses, Geomorphology, Vol. 97, Issues 3-4, 617-630.
http://dx.doi.org/10.1016/j.geomorph.2007.09.007

Ghilardi, M., Fouache, E., Queyrel, F., Syrides, G., Vouvalidis, K., Kunesch, S., Styllas, M. and Stiros, S. (2008b). Human occupation and geomorphological evolution of the Thessaloniki Plain (Greece) since Mid Holocene, Journal of Archaeological Science, Vol. 35, Issue 1, 111-125.
http://dx.doi.org/10.2112/06-0786.1

Gibbs, A. D. (1984). Structural evolution of extensional basin margins. J. Geol. Soc. Lond., Vol. 141, 609-620.

Gordy, P. L., Frey, F. R. and Norris, D. K. (1977). Geological Guide for the CSPG 1977 Waterton-Glacier Park Field Conference. Canadian Society of Petroleum Geologists, Calgary.

Grandjacquet. A. and Haccard, D. (1975). Analyse des sediments polygeniques neogenes a facies cargneules associes a des gypses dans les Alpes du Sud. Extension de ces facies au pourtour de la Mediterranee occidentale. Bull. Soc. Geol. Fr., Vol. 17, 242-259.

Graziano, R. (2000). The Aptian-Albian of the Apulia Carbonate Platform (Gargano Promontory, southern Italy): evidence of palaeoceanographic and tectonic controls on the stratigraphic architecture of the platform margin. Cretaceous Research, Vol. 21, 107-126.

Griffiths, D. H. and Barker, R. D. (1993). Two-dimensional resistivity imaging and modelling in areas of complex geology. Journal of Applied Geophysics, Vol. 29, 211-226.

deGroot-Hedlin, C. and Constable, S. (1990). Occam's inversion to generate smooth, two-dimensional models from magnetotelluric data. Geophysics, Vol. 55, 1613-1624.

Guiry, M. D. and Guiry, G. M. (2012). "Zygnema". *AlgaeBase*. World-wide electronic publication, National University of Ireland, Galway.
http://www.algaebase.org (accessed on 07 July 2012)

Haq, U. B., Hardenbol, J. and Vail, P. R. (1987). Chronology of Fluctuating Sea Levels since the Triassic (250 million years ago to present). Science, Vol. 235, 1156-1167.

Harding, T. P. (1974). Petroleum traps associated with wrench faults. Bull. Am. Ass. Petrol. Geol. Vol. 58, 1290-1304.

Harland W. B. (1971). Tectonic transpression in Caledonian Spitsbergen. Geological Magazine, Vol. 108, Issue 1, 27-41.
DOI:10.1017/S0016756800050937

Hatzfeld, D., Pedotti, G., Hatzidimitriou, P. and Makropoulos, K. (1990). The strain pattern in the western Hellenic arc deduced from a microearthquake survey. Geophys. J. Int., Vol. 101, 181-202.

Hatzopoulos, M.V. (1990). Deux sites pour Méthone de Macédoine, Bulletin de Correspondance Hellénique, Vol. 114, No. 2, 639-668.

Hendron, A. J. and Patton, F. D. (1987). Vaiont Slide: a geotechnical analysis based on new geologic observations of the failure surface. Eng. Geol., Vol. 24, 475-491.

Hollenstein, Ch., Geiger, A., Kahle, H.-G. and Veis, G. (2006). CGPS timeseries and trajectories of crustal motion along the West Hellenic Arc. Geophys. J. Int., Vol. 164, 182–191.

Homewood, P., Allen, P. A. and Williams, G. D. (1986). Dynamics of the molasse Basin of Western Switzerland. In: Allen, P. A. and Homewood, P. (Eds.). Foreland Basins. Special Publication of the International Association of Sedimentologists, Vol. 8, 199-218.

Hsü, K., J. (1975). Catastrophic Debris Streams (Strurzstroms) Generated by Rockfalls. Geological Society of America Bulletin, Vol. 86, 129-140.
Hsü, K. (1983). The Mediterranean Was a Desert: Princeton, New Jersey, Princeton University Press, Princeton, 197 pages.
DOI:10.1002/gj.3350190212.

Hubert, M. K. (1948). A line-integral method of computing the gravimetric effects of two-dimensional masses. Geophysics, Vol. 13, 215-225.

Innocenti, F., Manetti, P., Peccarillo, A. and Poli, G. (1981). South Aegean volcanic arc. Geochemical variations and geotectonic implications. Bulletins of Volcanology, Vol. 44, 377-391.

Innocenti, F., Kolios, N., Manetti, P., Rita, F. and Villari, L. (1982). Acid and basic late Neogene volcanism in the central Aegean Sea: Its nature and geotectonic significance. Bulletin of Volcanology, Vol. 45, 87-97.

Institute Francais Du Petrole (IFP) (1966). Etude géologique de l'Epire (Grèce nord-occidentale). Paris (Edition Technipress).

Jackson, J. (1994). Active Tectonics of the Aegean Region. Annu. Rev. Earth Planet. Sci., Vol. 22, 239-271.

Jenkins, D. A. L. (1972). Structural development of western Greece. American Association of Petroleum Geologists Bulletin, Vol. 56, 128-149.

Jervey, M. T. (1988). Quantitative geological modelling of siliciclastic rock sequences and their seismic expression. In: Wilgus, C. K., Rosamentier, H. W., Ross, C. K., and Jones, W. D. V. (1968), Results of recent geological surveys in central-western Greece. Geological Society of London Proceedings, Vol. 1645, 306-310.

Jones, P. B. (1982). Oil and gas beneath east-dipping underthrust faults in the Alberta Foothills, Canada. In: Geologic Studies of the Cordilleran Thrust Belt, Vol. 1, R. B. Powers (Ed.). Rocky Mountain Association of Petroleum Geologists, Denver, 61-74.

Jones, R. E., Isserlin, B. S. J., Karastathis, V., Paramarinoplouos, S. P., Syrides, E. Uren, J., Balatsas, I., Kapopoulos, C. H., Maniatis, Y. and Facorellis, G. (2000). Exploration of the Canal of Xerxes, Northern Greece: the role of geophysical and other techniques. Archaeological Prospection, Vol. 7, Issue 3, 147-170.

Kahle, H.-G. and Müller, M. V. (1996). Trajectories of crustal deformation of Western Greece from GPS observations 1989-1994. Geophysical Research Letters, Vol.23, No. 6, 677-680.

Kallen, D., Xiang, W. and Rohn, E. D. (2006) Landslides at Qingjiang river in the downstream area of Shuibuya dam site, China. J China Univ Geosci, Vol. 17, Issue 2, 158–162.

Kamberis, E. F., Marnellis, M., Loucoyannakis, F., Maltezou, A., Hirn and Streamers Group (1996). Structure and deformation of the External Hellenides based on seismic data from offshore Western Greece. In: Wessely, G. and Liebl, W. (Eds.). Oil and Gas in Alpidic Thrustbelts and Basins of Central and Eastern Europe, EAGE, Spec. Publi., Vol. 5, 207-214.

Kayan, I. (1991). Holocene geomorphic evolution of the Besik plain and changing environment of ancient man: Studia Troica, Vol. 1, 79–92.

Kayan, I. (1995). The Troia Bay and supposed harbour sites in the Bronze Age: Studia Troica, Vol. 5, 211–235.

Kayan, I. (1996). Holocene stratigraphy of the lower Karamenderes-Dumrek plain and archaeological material in the alluvial sediments to the north of the Troia ridge: Studia Troica, Vol. 6, 239–249.

Kayan, I. (1997). Geomorphological evolution of the Ciplak Valley and archaeological material in the alluvial sediments to the south of the lower city of Troia: Studia Troica, Vol. 7, 489–507.

Kelepertsis, A. E., Alexakis, D. E., Nastos, P. T. and Kanellopoulou, E. A. (2003). The presence of volcanic ash in Western Greece and its association with the eruption of the Etna volcano, Italy: Consequence on the Environment. 8th International Conference on Environmental Science and Technology, Lemnos Island, Greece.

Kilburn, C. R. J. and Petley, D. N. (2003). Forecasting giant, catastrophic slope collapse: lessons from Vajont, Northern Italy. Geomorphology, Vol. 54, 21-23.

Knepper, D. H., Langer, W. H. and Miller, S. (1995). A Survey of Natural Aggregate Properties and Characteristics Important in Remote Sensing and Airborne Geophysics. Oxford University Press, 99 -120.

Kokinou, E., Papadimitriou, E., Karakostas, V., Kamberis, E. and Vallianatos, F. (2006). The Kefalonia Transform Zone (offshore Western Greece) with special emphasis to its prolongation towards the Ionian Abyssal Plain. Mar. Geophys Res., Vol. 27, 241-252.

Koumantakis, I. and Mimides, T. (1989). Hypersaline water in an enclosed limestone body of Kefalonia. Bulletin of Geol. Soc. Greece, Vol. 23, Issue 3, 61-76.

Kraft, J., C., Aschenbrenner, S., E. and Rapp, G. (1977). Paleogeographic Reconstructions of Coastal Aegean Archaeological Sites. Science, Vol. 195, No. 4248, 941-947.

Kraft, J., C. and Aschenbrenner, S., E. (1977). Paleogeographic Reconstructions in the Methoni Embayment in Greece, Journal of field archaeology, Vol. 4, No. 1, 19-24.

Kraft, J. C., Kayan, I., and Erol, O. (1980). Geomorphic reconstructions in the environs of ancient Troy: Science, Vol. 209, 776–782.

Kraft, J. C., Rapp, G. and Aschenbrenner, J. S. E. (1975). Late Holocene palaeogeography of the coastal plain of the Gulf of Messenia (Greece) and its

relationships to archaeological settings and coastal change. Geol. Soc. Am. Bull., Vol. 86, 1191-1208.

Kraft, J. C., Rapp, G., Kayan, I. and Luce, J. V. (2003). Harbor areas at ancient Troy: Sedimentology and geomorphology complement Homer's Iliad. Geological Society of America, Vol. 31, No. 2, 163-166.

Lagios, E., Sakkas, V., Papadimitriou, P., Parcharidis, I., Damiata, B. N., Chousianitis, K. and Vassilopoulou, S. (2007). Crustal deformation in the Central Ionian Islands (Greece): Results from DGPS and DInSAR analyses (1995-2006). Tectonophysics, Vol. 444, 119-145.

Lambeck, K. (2002). Sea level change from mid Holocene to Recent time: an Australian example with global implications. In: Ice Sheets, Sea Level and the Dynamic Earth, Geodynamics Series, Vol. 29. American Geophysical Union, Washington, DC, 33–50.

Lambeck, K. and Chappell, J. (2001). Sea level change through the last glacial cycle. Science, Vol. 292, 679-686.

Lambeck, K., Esat, T. M. and Potter, E. K. (2003). Links between climate and levels for the past three million years. Nature, Vol. 419, 199-206.

Loke, M. H. and Barker, R. D. (1996a). Rapid least-squares inversion of apparent resistivity pseudosections by a quasi-Newton method. Geophysical Prospecting, Vol. 44, 131-152.

Louvari, E., Kiratzi, A. and Papazachos, B. C. (1999). The Cephalonia Transform fault and its extension to western Lefkada Island (Greece). Tectonophysics, Vol. 308, 223–236.

Luce, J. V. (1998). Celebrating Homer's landscapes. New Haven, Connecticut, Yale University Press, 260.

Lyell, C. (1830). The Principles of Geology: Being an Attempt to Explain the Former Changes of the Earth's Surface, by Reference to Causes now in Operation. Vol. 1, 2-14.
http://darwin-online.org.uk/content/frameset?viewtype=text&itemID=A505.1&pageseq=1

Lykousis, V. and Anagnostou, C. (1992). Late Quaternary sedimentation and palaeogeography of Saronikos gulf. 6th Congr. Geol. Soc. Greece, Abstr. Vol. 63.

Maclaren, C. (1822). Dissertation on the topography of the Plain of Troy. Edinburgh, 270 pages. http://archive.org/stream/adissertationon00maclgoog#page/n6/mode/2up
Madigan, T. (2007). The Geology of the MNRRA Corridor. National Park Service, 26.

Mandl, G. (1987a). Tectonic deformation by rotating parallel faults: the “bookshelf” mechanism. Tectonophysics, Vol. 141, 277–316.

Martini, E. (1971). Standard Tertiary and Quaternary calcareous nannoplankton zonation. In: Farinacci, A. (Ed.), Proc. 2nd Int. Conf. Planktonic Microfossils Roma: Rome (Ed Tecnosci.), Vol. 2, 739-785.

McKenzie, D. P. (1972). Active tectonics of the Mediterranean region. Royal Astronomical Society Geophysical Journal, Vol. 30, 109-185.

McKenzie, D. P. (1978). Active tectonics of the Alpine-Himalayas belt: The Aegean sea and surrounding regions. Royal Astronomical Society Geophysical Journal, Vol. 55, 217-254.

Mercier, J. L., Carey, E., Philips, H. and Sorel, D. (1976) La neótectonique plio-quaternaire de l’arc ègéen externe et de la mer Egée et ses relations avec la séismicitè. Bulletin géoloigical société de la France, Vol. 18, 355-372.

Mercier, J. L., Delibassis, N., Gauthier, A., Jarrige, J., Lemeille, F., Philip, H., Sebrier, M. and Sorel, D. (1979). La néotectonique de l’arc égéen. Rév. géol. dyn. géogr. phys., Vol. 21, Issue 1, 67-92.

Mitchum Jr., R. M., Vail, P. R. and Thompson III, S. (1977). Seismic Stratigraphy and Global Changes of Sea Level: Part 2. The Depositional Sequence as a Basic Unit for Stratigraphic Analysis: Section 2. Application of Seismic Reflection Configuration to Stratigraphic Interpretation. AAPG Memoir. Seismic Stratigraphy – Applications to Hydrocarbon Exploration, 53-67.

Missiaen, T., Murphy, S., Loncke, L. and Henriet, J-P. (2002). Very high-resolution seismic mapping of shallow gas in the Belgian coastal zone. Continental Shelf Research, Vol. 22, 2291-2301.

Mix, A. C., Bard, E. and Schneider, R. (2001). Environmental processes of the ice age: land, oceans, glaciers (EPILOG). Quaternary Science Reviews, Vol. 20, 627-657.

Moernaut, J. and De Baptist, M. (2011). Frontal emplacement and mobility of sublacustrine landslides: Results from morphometric and seismostratigraphic analysis. Marine Geology, Vol. 285, Issues 1-4, 29-45.

Morley, C. K. (1986). A classification of thrust faults. American Association of Petroleum Geologists, Bulletin, Vol. 70, 12-25.

Morley, C. K. and Guerin, G. (1996). Comparison of gravity-deformation styles and behaviour associated with mobiles shales and salt. Tectonics, Vol. 15, 1154-1170.
Mueller-Miny, H. (1957). Beitrage zur morphologie der mittleren jonischen Inseln. Ann. Geol. pays Helleniques, Vol. 8, 1-28.

Nabighian, M. N, Ander, M. E., Grauch, V. J. S., Hansen, R. O., LaFehr, T. R., Li, Y., Pearson, W. C., Peirce, J. W., Philips, J. D. and Ruder, M. E. (2005). Historical development of the gravity method in exploration. Geophysics, Vol. 70, No. 6, 63-89.

Nakada, M. and Lambeck, K. (1988). The melting history of the late Pleistocene Antarctic ice sheet. Nature, Vol. 333, 36–40.

Nakada, M. and Lambeck, K. (1989). Late Pleistocene and Holocene sea level change in the Australian region and mantle rheology. Geophysical Journal, Vol. 96, Issue 3, 497–517.

de Natale, G., Troise, C., Pingue, F., Mastrolorenzo, G., Pappalardo, L., Battaglia, M. and Boschi, E. (2006). The Campi Flegrei caldera: unrest mechanisms and hazards. In: Troise, C., de Natale, G. and Kilburn, C. R. J., Mechanisms of activity and unrest at large calderas. Special Publications, Vol. 269, London: Geological Society, 26-27.

Neuendorf, K. K. E, Mehl Jr., J. P. and Jackson, J. A. (2005). Glossary of Geology (5^{th} edition). Alexandria, Virginia, Am. Geol. Int.

Ninkovich, D. and Hays, J. D. (1972). Mediterranean island arcs and origin of high potash volcanoes.: Earth and Planetary Science Letters, Vol. 16, 331-245.

le Noan, G. (2001). A la recherché d'Ithaque: Essai sur la localization de la partie d'Ulysee: Quicey-sous-Senart, Editions Tremen, 118 pages.

le Noan, G. (2003). La Ferme d'Eumee: Nouvelle recherché sur l'Ithaque Homerique: Quicey-sous-Senart, Editions Tremen, 114 pages.

le Noan, G. (2004). Le Palais l'Ulysse: Quicey-sous-Senart, Editions Tremen, 91 pages.

Papatheodorou, G., Hasiotis, T. and Ferentinos, G. (1993). Gas-charged sediments in the Aegean and Ionian Seas, Greece. Mar. Geology, Vol. 112, 171-184.

Papazachos, B. C. (1990). Seismicity of the Aegean and surrounding area. Tectonophysics, Vol. 178, 287–308.

Papazachos, B. C. (1996). Large seismic faults in the Hellenic arc. Annali Di Geofisica, Vol. 39, No. 5.

Papazachos, B. C. and Comninakis, P. E. (1971). Geophysical and Tectonics Features of the Aegean Arc. Journal of Geophysical Research, Vol. 76, No. 35, 8517-8533. DOI:10.1029/JB076i035p08517.

Papazachos B. C. and Kiratzi, A. A. (1996). A detailed study of the active crustal deformation in the Aegean and surrounding area. Tectonophysics, Vol. 253, Issues 1-2, 129-153.

Papazachos, B. C. and Papazachou, C. C. (1989). The Earthquakes of Greece. Ziti Publ. Co., Thessaloniki, 356 pages.

Papazachos, B. C. and Papazachou, C. C. (1997). The Earthquakes of Greece. P. Ziti and Co, Thessaloniki, Greece. 304 pages.

Papathanassiou, G., Pavlides, S. and Ganas, A. (2005). The 2003 Lefkada earthquake: Field observations and preliminary microzonation map based on liquefaction potential index for the town of Lafkada. Engineering Geology, Vol. 82, Issue 1, 12 – 31.

Papavasiliou, C., Konispoliatis, N., Sakelariadou, F. and Mitropoulos, D. (1988). Mineral concentrations in the recent sediments of Eastern Macedonia, Northern Greece. Geological and geochemical considerations. In: Boissonas, J. and Omenetto, P. (Eds.), Mineral Deposits within the European Union. Springer, Berlin, 530-552.

Peace, D. G., Stieglitz, T. and Spoors, R. (2012). Imaging new opportunities and play concepts in the Adriatic Sea and Levantine Basin. Petroleum Geoscience, Vol. 18, 405-416.
DOI: 10.1144/petgeo2011-066.

Pedley, R. C., Busby, J. P. and Dabek, Z. K. (1993). Gravmag User Manual: Interactive 2.5 D gravity and magnetic modelling. British Geological Survey, Technical Report WK/93/26/R.

Perissoratis, C. and Conispoliatis, N. (2003). The impacts of sea-level changes during latest Pleistocene and Holocene times on the morphology of the Ionian and Aegean seas (SE Alpine Europe). Marine Geology 196, 145-156.

Perissoratis, C., Conispoliatis, N., Zimianitis, E., Galanopoulou, S. and Zaharaki, P. (2001). Marine geological investigations in the greater area of Navarino Bay, C. Ionian Sea. 9th Int. Congress of Geol. Soc. Greece. Bull. Geol. Soc. Greece, Vol. 34, No. 2, 655-662.

Perissoratis, C. and Mitropoulos, D. (1989). Late Quaternary evolution of the North Aegean. Cont. Shelf Res. 32, 36-50.

Perissoratis, C. and Van Andel, T.H. (1991). Sea-level changes and tectonism in the formation of the Quaternary basin of the South Evvoikos Gulf, Greece. Terra Nova 3, 294-302.

Petley, D. N. and Allison, R. J. (1997). The mechanics of deep-seated landslides. Earth Surf. Processes Landf. 22, 747-758.

Petley, D. N. and Petley, D. J. (2006). On the initiation of large rockslides: perspectives from a new analysis of the Vaiont movement record. In: Evans, S. G., Scasrascia Mugnozza, G., Strom, A., and Hermanns, R., L. (Eds.), Massive Rock

Slope Failure. Kluwer, Rotterdam (NATO Science Series, Earth and Environmental Sciences 49), 77-84.

Le Pichon, X. and Angelier, J. (1979). The Hellenic arc and trench system: A key to the neotectonic evolution of the eastern Mediterranean area. Tectonophysics, Vol. 60, 1-42.

le Pichon, X. and Angelier, J. (1981).The Aegean Sea. Royal Society of London Philosophical Transactions, ser. A, Vol. 300, 357-372.

Le Pichon, X., Chamot-Rooke, N., Lallemant, S., Noomen, R. and Veis, G. (1995). Geodetic determination of the kinematics of Central Greece with respect to Europe: Implications for eastern Mediterranean tectonics. Journal of Geophysical Research, 100, 12675-12690.

Pirazzoli, P. A. (1986). The Early Byzantine tectonic paroxysm. Zeitschrift für Geomorphologie, Supplement 62, 31-49.

Pirazzoli, P. A., Stiros, S. C., Laborel, J., Laborel-Deguen, F., Arnold, M., Parageorgiou, S. and Morhange, C. (1994). Late-Holocene shorelines changes related to palaeoseismic events in the Ionian Islands, Greece. The Holocene 4, Vol. 4, 397-405.

Pollard, A. M. (1999). Geoarchaeology: exploration, environments, resources. Geological Society, London, Special Publications, Vol. 165, 7-14.

Prager, C., Krainer, K., Seidl, V. and Chwatal, W. (2006). Spatial Features of Holocene Sturzstrom-deposits inferred from subsurface investigations (Fernpass Rockslide, Tyrol, Austria). Geo. Alp., Vol. 3, 147-166.

Raffi, I., Mozzato, C., Fornaciari, E., Hilgen, F. J. and Rio, D. (2003). Late Miocene calcareous nannofossil biostratigraphy and astrobiochronology for the Mediterranean region. Micropalaeontology, Vol. 49, Issue 1, 1-26.

Rapp Jr., G. R. and Hill C. L. (1998). Geoarchaeology: The Earth-science approach to archaeological interpretation, Yale University Press, New Haven.

Rasmussen, R. and Pedersen, L. B. (1979). End Corrections in Potential Field Modelling. Geophysical Prospecting. Vol. 27, Issue 4, 749-760. DOI: 10.1111/j.1365-2478.1979.tb00994.x.

Reading, H. G. (1980). Characteristics and recognition of strike-slip fault systems. Spec. Publ. int. Ass. Sediment., Vol. 4, 7-26.

Rowan, M. G., Peel, F. J. and Vendeville, B. C. (2004). Gravity-driven fold belts on passive margins. In: McClay, K. R. (Ed.), Thrust tectonics and hydrocarbon systems, AAPG Memoir 82, 157-182.

RES2DINV ver. 3.4: Rapid 2-D Resistivity and IP inversion using the lest-squares method – Wenner (α, β, γ), dipole-dipole, inline pole-pole, pole-dipole, equatorial dipole-dipole. Schlumberger and non-conventional arrays. On land, underwater and cross-borehole surveys. Geoelectrical Imaging 2-D and 3-D. 2000-2001.

Ricci Lucchi, F. (1986). The Oligocene to Recent Foreland Basins of the northern Appenines. In: Allen, P. A. and Homewood, P. (Eds.), Foreland Basins. Special Publication of the International Association of Sedimentologists, Vol. 8, 105-140.

Rio, D., Raffi, I., and Villa, G. (1990). Pliocene-Pleistocene calcareous nannofossil distribution patterns in the Western Mediterranean. In: Kastens, K. A., Mascle, J., et al., Proceedings of the Ocean Drilling Program, Scientific Results, Vol. 107, College Station, TX (Ocean Drilling Program), 513-533.

Sacchi, M., Molisso, F., Violante, C., Esposito, E., Insgina, D., Lubritto, C., Porfido, S. and Tóth, T. (2009). Insights into flood-dominated fan-deltas: very high-resolution seismic examples off the Amalfi cliffed coasts, eastern Tyrrhenian Sea. Geological Society, London, Special Publications, Vol. 322, 33-71.
DOI: 10.1144/SP322.2

Sachpazi, M., Hirn, A., Clément, C., Haslinger. F., Laigle, M., Kissling, E., Charvis, P., Hello, Y., Lépine, J.-C., Sapin, M. and Ansorge, J. (2000). Western Hellenic subduction and Cephalonia Transform: local earthquakes and plate transport and strain. Tectonophysics, Vol. 319, 301-319.

Sasaki, Y. (1992). Resolution of resistivity tomography inferred from numerical simulation. Geophysical Prospecting, Vol. 40, 453-464.

Savage, J. C., Svarc, J. L. and Prescott, W. H. (2004). Interseismic strain and rotation rates in the northeast Mojave domain, eastern California. Journal of Geophysical Research, Vol. 109, Issue 2, B02406.
DOI:10.1029/2003JB002705

Schuster, R. L. and Alford, D. (2004). Usoi landslide dam and Lake Sarez, Pamir Mountains, Tajikistan. Environmental and Enginneering Geoscience, Vol. 10, 151-168.

Scintrex (2006). CG-5 Scintrex Autograv System: Operation Manual. Part #867700 Revision 4.

Scordilis, E., Karakaisis, G., Karakostas, B., Panagiotopoulos, D., Comninakis, P. and Papazachos, B. (1985). Evidence for transform faulting in the Ionian Sea: The Cephalonia Island earthquake sequence of 1983. Pure and Applied Geophysics, Vol. 123, 388-397.
SeisImager/2D™ Manual: Version 3.2, Pickwin v. 3.2, Plotrefa v. 2.8. Geometrics, 2006.

Shackleton, N. J., (1987). Oxygen isotopes ice volume and Sea level. Quat. Sci. Rev., Vol. 6, 183-190.

Shackleton, N. J., Sanchez-Goni, M. F., Pailler, D. & Lancelot, Y. (2003). Marine isotope Substage 5e and the Eemian Interglacial. Glob. Planet. Change, Vol. 36, 151–155.

Shang, Y., Yang, Z., Li, L., Liu, D., Liao, Q. and Yangchun. W. (2003). A super-large landslide in Tibet in 2000: Background, occurrence, disaster, and origin. Geomorphology, Vol. 54, 225–243 Sichuan Seismological Bureau (1983) Diexi earthquake in 1933. Science and Technology Press of Sichuan, Chengdu (in Chinese).

Sheriff, R. E. (1973). Encyclopedic Dictionary of Exploration Geophysics, published by the Society of Exploration Geophysics, Tulsa, Oklahoma.

Smith, R. A. (1959). Some Depth Formulae for Local Magnetic and Gravity Anomalies. Geophysical Prospecting. Vol. 7, Issue 1, 55-63.
DOI: 10.1111/j.1365-2478.1959.tb01453.x.

Smith, A. G. and Moores, E. M. (1974). Hellenides. In: Spencer, A. M. (Ed.), Mesozoic and Cenozoic orogenic belts. Geological Society of London Special Publication, Vol. 4, 159-185.

Sorel, D. (1976). Etude néotectonique des iles-Ioniennes de Cephalonie et Zanthe et de l'Etide occidentale (Grèce) [Thèse 3e cycle]: Paris, France, Université de Paris-Sud, Facultè de Science, Orsay.

Sorel, D., Nesteroff, W. D., Limond, J., Lemeille, F. and Sebrier, M. (1976). Mise en évidence de structures compressives sous-marine plio-pleistocene dans l'arc égéen externe au large de Levkas (iles Ioniennes, Grèce). Paris, Académie des Sciences Comptes Rendus, Vol. 282, 2045-2048.

Souyoudzoglou Haywood, C. (2000). Ionian Islands in the Bronze Age and Early Iron Age. Liverpool University Press, Liverpool.

Spon, J. (1678). Voyage d'Italie, de Dalmantie, de Grèce et du Levant, fait aux années 1675 and 1676 par Jacob Spon et George Wheler. A. Cellier, Lyon.

Spratt, T.A.B. (1839). Map of the Troad: London, Admiralty (British).

Stiros, S. C. (1994). Anomalous attenuation of seismic waves in the Ionian Islands (Greece). EOS, Trans. Am. geophys. Un., Vol. 75, No. 10, 117.

Stiros, S. C., Pirazzoli, P. A., Laborel, J. and Laborel-Deguen, F. (1994). The 1953 Earthquake in Cephalonia (Western Hellenic Arc): Coastal Uplift and Halotectonic Faulting. Geophysical Journal International, Vol. 117, 834-849.

Strabo. (c. 1). Geography.

Suc, J. -P., Clauzon, G., Bache, F., Cornée, J. -J., Deverchère, J., El Euch – El Koundy, N., Ferry, S., Gillet, H., Gorini, C., Lericolais, G., Lofi, J., Melinte-Dobrinescu, M. C., Popescu, S. -M., Rubino, J. -L., and Sage, F. (2008). The latest Miocene earliest Pliocene Mediterranean mega-cycle in sea-level. In: 33rd International Geological Congress (IUGS, Ed.), Oslo.

Suppe, J. (1983). Geometry and Kinematics of Fault-Bend Folding. American Journal of Science, Vol. 283, 684-721.

Supper, J. and Namson, J. (1979). Fault-bend origin of frontal folds of the western Taiwan fold-and-thrust belt: Petroleum Geology Taiwan, Vol. 16, 1-18.

Talwani, M., Wozel, J. L. and Landisman, M. (1959). Rapid gravity computations for two-dimensional bodies with application to the Mendicino submarine fracture zone. Journal of Geophysics. Res., Vol. 64, 49-59.

Talwani, M. and Ewing, M. (1960). Rapid computation of gravitational attraction of three-dimensional bodies of arbitrary shape. Geophysics, Vol. 25, 203-225.

Taylor, D. I. (1992). Near shore shallow gas around the UK coast. Continental Shelf Research, Vol. 12, Issue 10, 1135-1144.

Tchalenko, J. S. (1970). Similarities between shear zones of different magnitudes: Geol. Soc. America Bull., Vol. 81, 1625-1640.

Telford, W. M., Geldart, L. P., Sheriff, R. E. and Keys, D. A. (1976). Applied Geophysics. Cambridge University Press.

Temple, P. G. (1968). Mechanics of large-scale gravity sliding in the Greek Peloponnesus. Geological Society of American Bulletin, Vol. 79, 687-700.

Tweed, R. (2000). A History of Langstone Harbour and its environs in the County of Hampshire. Dido Publications, 16-17.

Tzedakis, P. C., Frogley, M. R. and Heaton, T. H. E. (2002). Duration of Last Interglacial Conductions in Northwestern Greece. Quat., Res., Vol. 58, 53–55.

Underhill, J. R. (1985). Neogene and Quaternary tectonics and sedimentation in western Greece [Ph.D. thesis]. Cardiff, Wales. University College, University of Wales.

Underhill, J. R. (1989). Late Cenozoic deformation of the Hellenide foreland, western Greece. Geological Society of America Bulletin, Vol. 101, No. 5, 613-634.

Underhill, J. R. (2006). Furthest towards dusk – the quest for Ithaca. Geoscientist, Vol. 16, No. 9, 4-29.

Underhill, J. R. (2008). Testing classical enigmas. Geoscientist, Vol. 18, No. 9, 20-27.

Underhill, J. R. (2009). Relocating Odysseus' homeland, Nature Geoscience, Vol. 2, 455-458.
DOI:10.1038/ngeo562.

Vafidis, A., Manakou, M., Kritikakis, G., Voganatsis, D., Sarris, A. and Kalpaxis, Th. (2003). Mapping the ancient port at the archaeological site of Itanos (Greece) using shallow seismic methods. Archaeological Prospection, Vol. 10, Issue 3, 163-173.

Vail, P. R., Mitchum Jr., R. M., and Thompson III, S. (1977). Seismic Stratigraphy and Global Changes of Sea Level, Part 3: Relative Changes of Sea Level from Coastal Onlap. Am. Assoc. Pet. Geol. Mem., Vol. 26, 49-212.

Van Andel, T. H. (1994). New Views On An Old Planet (2nd ed.). Cambridge University Press. ISBN 0-521-44243-5.

Van Dam, J. C. and Meulenkamp, J. J. (1967). Some results of the geo-electrical resistivity method in groundwater investigations in The Netherlands. Geophys. Prosp. Vol. 15, Issue 1, 92-115.

Vann, I. R., Graham, R. H. and Hayward, A. B. (1986). The structure of mountain fronts. Journal of Structural Geology, Vol. 8, 215-227.

Vearnecombe, J. R. (1982). The tectonic significance of Triassic dolomite and cargeule in the Gran Paradiso region, Western Alps. Geological Magazine. Cambridge University Press.

de Vera, J., Granado, P. and McClay, K. (2010). Structural evolution of the Orange Basin gravity-driven system offshore Namibia. Marine and Petroleum Geology, Vol. 27, Issue 1, 223-237.

Vickery, C. (2000). The Role of Geophysics in the Investigation of Contaminated Land (Ph. D. thesis). University of Edinburgh, Edinburgh.

Vita-Finzi, C. (1972). Supply of the fluvial sediment to the Mediterranean during the last 20,000 years. In: Stanley, D.J. (Ed.). The Mediterranean Sea - A Natural Sedimentation Laboratory. Dowden, Hutchinson and Ross, Stroudburg, 43-46.

Vogt, J. and Albini, P. (1992). An outstanding Ionian testimony, in Abstracts, Regional Workshop on Archaeoseismicity in the Mediterranean Region, Damascus.

Volterras, G. (1903). Kritiki Meleti peri Omerikis Ithakis (A Critical Study of Homeric Ithaca), Athens.

Vött, A. (2007). Relative sea level changes and regional tectonic evolution of seven coastal areas in NW Greece since the mid-Holocene. Quaternary Science Reviews, Vol. 26, 894-919.

Vött, A., Brücker, H., Schriever, J., L., Handl, M and Van der Borg, K. (2006). Holocene paleogeographies of the Palairos coastal plain (Akarnania, northwest Greece) and their geoarchaeological implications. Geoarchaeology. Special Issue: Eastern Mediterranean and Near Eastern Geoarchaeology: Part I, Vol. 21, Issue 7, 649-664.

Warrak, M. (1974). The petrology and origin of dedolomitised, veined or breccia ted carbonate rocks, the 'cornieules' in the Frejus region. French Alps. Q. Jl. geol. Soc. Lond., Vol. 130, 229-47.

Wessel, P. and Smith, W. H. F. (1991). Free Software Helps Map and Display Data, EOS Trans., AGU, Vol. 72, Issue 41, 441-446.

Wessel, P. and Smith, W. H. F. (1995). New Version of the Generic Mapping Tools Released, EOS Trans., AGU, Vol. 76, Issue 33, 329.
http://www.agu.org/eos_elec/95154e.html

Wessel, P. and Smith, W. H. F. (1998). New, Improved Version of Generic Mapping Tools Released, EOS Trans., AGU, Vol. 79, Issue 47, 579.
DOI:10.1029/98EO00426.

Wessel, P. and Smith, W. H. F. (2009). The Generic Mapping Tools (GMT) version 4.5.0 Technical Reference and Cookbook, SOEST/NOAA.

Widess, M. D. (1973). How thin is a thin bed? Geophysics, Vol. 38, 1176-1180.

Wilcox, R. E., Harding, T. P. and Seely, D. R. (1973). Basic Wrench Tectonics. AAPG Bulletin, Vol. 57, Issue 1, 74-96.

Witkind, I. J. (1959). The Hebgen Lake Earthquake, Geotimes, 4, No. 3.

Woldstedt, P. (1958). Das Eiszeitalter. Grundlinien einer Geologie des Quartärs. - Bd. 2: 395 S.; Stuttgart (Enke).

Woldstedt, P. (1969). Quartär. In: LOTZE, F. (Hrsg.): Handbuch der stratigraphischen Geologie. - Bd. 2: 256 S., 77 Abb., 16 Tab.; Stuttgart (Enke).

Won, I. J. and Bevis, M. (1987). Computing the gravitational and magnetic anomalies due to a polygon: Algorithms and Fortran subroutes. Geophysics, Vol. 52, No. 2, 232-238.

Yilmaz, O. (1987). Seismic Data Processing. In: Doherty, S. M. (Ed.), Investigations in Geophysics, Society of Exploration Geophysicists, No. 2. Tulsa, Oklahoma.

Zangger, E. (2001). The Future of the Past: Archaeology in the 21st Century. Orion Publishing, 288 pages.

Zappaterra, E. (1994). Source-Rock Distribution Model of the Periadriatic Region. AAPG Bulletin, Vol. 78, No. 3, 333-354.

2. Weblink References

Encyclopædia Britannica. "isthmus" Encyclopædia Britannica Online. Encyclopædia Britannica Inc., 2012. http://www.britannica.com/EBchecked/topic/297042/isthmus (accessed 17 Dec 2012)

Fugro Airborne Surveys, 2011. http://www.fugroairborne.com/services/geophysicalservices/bysurvey/electromagnetics/helicopter-electromagnetic/resolve (accessed 12 Jan 2011)

GeoExplo, 2011. http://www.geoexplo.com/airborne_survey_workshop_EM.html

“The Landslide Blog” http://www.landslideblog.org/2008/12/vaiont-vajont-landslide-of-1963.html

Southern Adriatic – Play Types, Northern Petroleum. http://oilbarrel.com/fileadmin/content/pdfs/oilbarrel/December2010/Npet%202.pdf (accessed 4 Jan 2013)

Wikipedia “Corinth Canal”: http://en.wikipedia.org/wiki/File:Corinth_Canal_2.jpg